SYNTHESIS AND CHARACTERIZATION OF 1,4-DISUBSTITUTED 1,2,3-TRIAZOLES, AS ION SENSORS, USING Cu(I) CATALYZED CLICK REACTION

Thesis Submitted for the Award of the Degree of

DOCTOR OF PHILOSOPHY (Ph.D.)

in

Chemistry

By

Gurleen Singh
Registration number: 11919636

Supervised By

Dr. Jandeep Singh (19394)
School of Chemical Engineering and Physical Sciences (Associate Professor)
Lovely Professional University, Phagwara, Punjab

Co-Supervised by

Dr. Harminder Singh (11839)
School of Chemical Engineering and Physical Sciences (Professor)
Lovely Professional University, Phagwara, Punjab

LOVELY PROFESSIONAL UNIVERSITY
PUNJAB
2024

DECLARATION

I, hereby declared that the presented work in the thesis entitled "**Synthesis and Characterization of 1,4-disubstituted 1,2,3-triazoles, as ion sensors, using Cu(I) catalyzed Click Reaction**" in fulfillment of degree of **Doctor of Philosophy (Ph.D.)** is outcome of research work carried out by me under the supervision of Dr. Jandeep Singh, working as Associate Professor in the School of Chemical Engineering and Physical Sciences and Dr. Harminder Singh, working as Professor in the School of Chemical Engineering and Physical Sciences of Lovely Professional University, Punjab, India. In keeping with general practice of reporting scientific observations, due acknowledgements have been made whenever work described here has been based on findings of other investigators. This work has not been submitted in part or full to any other University or Institute for the award of any degree.

(Signature of Scholar)

Name of the scholar: Gurleen Singh

Registration No.: 11919636

Department/school: School of Chemical Engineering and Physical Sciences,

Lovely Professional University, Punjab, India

CERTIFICATE

This is to certify that the work reported in the Ph. D. thesis entitled "**Synthesis and Characterization of 1,4-disubstituted 1,2,3-triazoles, as ion sensors, using Cu(I) catalyzed Click Reaction**" submitted in fulfillment of the requirement for the award of degree of **Doctor of Philosophy (Ph.D.)** in the School of Chemical Engineering and Physical Sciences, is a research work carried out by Gurleen Singh, Registration No. 11919636, is bonafide record of his original work carried out under mysupervision and that no part of thesis has been submitted for any other degree, diploma orequivalent course.

(Signature of Supervisor) **(Signature of Co-Supervisor)**

Dr. Jandeep Singh Dr. Harminder Singh

Associate Professor in Chemistry Professor in Chemistry

Department/school: School of Chemical Engineering and Physical Sciences, Lovely Professional University, Phagwara, Punjab-144001

ABSTRACT

In the recent two decades, the field of chemical synthesis has been revolutionized by the introduction of 'Click Chemistry', a set of remarkably efficient and precise processes that facilitate the swift construction of intricate molecular structures. The flagship transformation in 'Click Chemistry', i.e., the Copper(I)-catalyzed alkyne-azide cycloaddition (CuAAC), a has gained immense prominence due to its remarkable versatility, mild reaction conditions, and wide range of applications. The methodology has been instrumental in bridging the gap between synthetic feasibility and structural diversity, and entails the amalgamation of a terminal alkyne and an azide through a cycloaddition process, facilitated by a copper(I) catalyst, yielding the production of a 1,4-disubstituted 1,2,3-triazole functional group. The regioselectivity and tolerance of a plethora of functional groups under mild reaction conditions have made CuAAC an indispensable tool in chemical synthesis. The ability to rapidly access diverse 1,2,3-triazole derivatives through CuAAC has opened up avenues for the design and creation of structurally complex molecules, that find utility in drug discovery, material science, and chemical biology, owing to their unique electronic and steric properties. Additionally, the modular nature of click chemistry allows for facile introduction of functional groups, enabling the tailoring of the 1,2,3-triazole derivatives for specific applications including bioconjugation and drug delivery, thereby highlighting its potential in both academic and industrial settings.

Particularly, the synthesized 1,2,3-triazoles via CuAAC have found relevance in the recognition of metal ions. Metal ions play pivotal roles in various physiological and environmental processes, necessitating the development of reliable methods for their detection. The facile modification of 1,2,3-triazoles enables the design of chemosensors that exhibit enhanced metal ion binding affinity and selectivity. By judiciously introducing chelating groups onto the triazole scaffold, researchers have developed sensor platforms that undergo specific structural changes upon metal ion coordination. These changes are often accompanied by alterations in optical, electrochemical, or spectroscopic properties, allowing for sensitive and quantitative metal ion detection. Therefore, in the light of the utility of CuAAC as an efficient and robust methodology to regioselectively synthesize the 1,4-disubstituted 1,2,3-triazoles, this synthetic pathway was selected as the main approach of organic synthesis to pursue this research work, with the primary focus to develop selective, sensitive, and robust 1,2,3-triazole derivatives as chemosensors meeting the stringent criteria of analytical chemistry. The literature review conducted in relation to the CuAAC methodology and the

application of the products thereof as ion sensors, the following objectives were selected for the proposed research:

1. Synthesis of 1,4-disubstituted 1,2,3–triazole derivatives by Cu(I) catalyzed Click reaction between terminal alkyne and organic azide.

2. Characterization of synthesized compounds by spectroscopic techniques like IR, NMR (^{1}H, ^{13}C), mass spectroscopy and X-ray (wherever possible).

3. To study ion sensing behavior of synthesized 1,4-disubstituted 1,2,3–triazole derivatives using UV–Visible spectroscopy and/or fluorescence.

In accordance with these objectives, six derivatives of 1,2,3-triazole were prepared and after successful characterization via different spectroscopic techniques, these 1,2,3-triazole-linked compounds were successfully implemented as selective chemosensors for various biologically and ecologically relevant metal ions.

The selection of the starting reactant for the synthesis of the precursors for the formation of the 1,2,3-triazole functional group, i.e., the terminal alkyne was undertaken on the basis of the presence of labile protons in the parent structure, preferably with chromophoric units. Every starting molecule had a labile proton containing hydroxyl group or amino group, which was subjected to the action of a base such as K_2CO_3/Cs_2CO_3 to abstract the protons, followed by the nucleophilic substitution by a propargyl group an appropriate solvent. The addition of ice-cold water resulted in the reaction quenching, and the product was separated by filtering (for solids) or solvent extraction (for liquids). The organic azides were prepared by subjecting the starting material (benzyl chloride/ 1-chloromethylnaphthalene) to sodium azide (NaN_3) at a temperature of 85 - 90 °C for 5 hours. Subsequently, the terminal alkynes underwent Cu(I)-catalyzed cycloaddition with organic azides to yield 1,4-disubstituted 1,2,3-triazole derivatives. The characterization of the synthesized compounds was done utilizing different spectroscopic techniques such as Infrared (IR) Spectroscopy, Nuclear Magnetic Resonance (NMR) Spectroscopy (^{1}H, ^{13}C), and Mass Spectrometry.

The ion recognition potential of 1,2,3-triazole-linked probes was ascertained via absorption and/or emission spectroscopy with various biologically and ecologically relevant metal ions such as Cr(III), Mn(II), Fe(III), Co(II), Ni(II), Cu(II), Zn(II), Na(I), K(I), Mg(II), Ca(II), Ba(II), Cd(II), Hg(II), Pb(II), and Ce(III) in an appropriate solvent. To bind with a particular metal ion, the synthesized molecular assemblies have the lone-pair bearing nitrogen in the heterocyclic 1,2,3-triazole moiety in addition to the other electron rich heteroatoms like

oxygen in their structure. Since various metal ions were added in separate titrations to the solution of the molecule under study, the UV-Visible findings provided insight into the probe's specificity and selectivity towards a particular metal ion. The changes observed in the receptor unit's absorption and/or emission behaviour owing to the metal ion binding were used to identify its chemosensing capability. On that basis, a variety of graphs and figures illustrating the absorption and/or emission responses observed for the binding of different 1,2,3-triazole-linked sensor probes with particular metal ions were presented in this research work. Furthermore, the results of analytical calculations such as the stoichiometric ratio, the association constant (K_a), the limit of quantification (LoQ), and the limit of detection (LoD of the probes towards certain metal ions were also presented.

Dedication

With the hopes of this research work being one day able to contribute to the amelioration of humanity, this is dedicated to my family, teachers, and friends!

For their infinite love, persistent support, and firm belief.

ACKNOWLEDGEMENT

I am humbled to pen these acknowledgments, a mere reflection of my profound gratitude and appreciation for the multifaceted contributions that have woven the tapestry of this doctoral odyssey. Foremost, my boundless gratitude ascends to the **WAHEGURU**, as I acknowledge the benevolent guidance and inspiration bestowed upon me. It is through this connection that the vigor to explore the depths of knowledge has been nurtured and sustained.

To my erudite supervisors, **Dr. Jandeep Singh** and **Dr. Harminder Singh**, whose wisdom and perspicacity have illuminated this academic path, I extend my profound gratitude. Your discerning guidance, judicious counsel, and unerring mentorship have been instrumental in shaping not just my academic trajectory, but also my intellectual ethos. Your unwavering commitment to scholarly excellence has sculpted me into a more adept and enlightened individual.

The blessings of my parents, **S. Joginder Singh** and **Sdr. Gurmeet Kour**, have been my constant lighthouse, guiding me through the tumultuous seas of academia. Your unstinting sacrifices, unwavering belief in my abilities, and unconditional love have been the cornerstone upon which my aspirations have been erected. My gratitude extends to my sister, **Miss Gagandeep Kaur**, and the familial constellations, whose ceaseless encouragement has been invaluable. To my dear family, you have been the bedrock of my emotional sustenance, offering solace in moments of tribulation and rejoicing in the triumphs achieved in life.

To my cherished network of friends, both longstanding and newly forged, your camaraderie and unwavering encouragement have been the social nourishment that has provided equilibrium to the rigors of academia. I am profoundly grateful to my research group, **Dr. Parveen Saini**, **Miss Riddima Singh**, and **Miss Nancy George**. Your engaging discussions, intellectual debates, and shared laughter have imbued this journey with moments of resplendent vitality. I am thankful to my dear friend **Miss Gagandeep Kaur** for providing vital support and resources for my research work, as the exchange of ideas and the shared pursuit of knowledge transformed challenges into opportunities and hurdles into stepping stones. To the Almighty, my revered supervisors and staff, my beloved parents, my cherished family and friends, and my esteemed research colleagues, your indelible imprints on the canvas of my academic sojourn shall forever be etched, driving me onward in the pursuit of perpetual enlightenment.

Gurleen Singh

TABLE OF CONTENTS

Content	Page No
Chapter I: Introduction	**1-28**
1.1. Click Chemistry- a general perspective	1-2
1.2. Huisgen 1,3-dipolar cycloaddition- the precursor to 'Click Chemistry'	3-4
1.3. Cu(I)-catalyzed alkyne azide cycloaddition (CuAAC)- the prototypical 'Click Chemistry'	5-6
1.4. Mechanistic aspects of CuAAC	7-9
1.4.1. The mononuclear mechanism by Sharpless et al.	7-8
1.4.2. The binuclear mechanism by Fokin et al.	8-9
1.5. The 1,2,3-triazole ring	10-11
1.5.1. Structural aspects and properties	10
1.5.2. Potential Uses of 1,2,3-Triazoles	11
1.6. Chemical Sensor	12-15
1.6.1. Concept and classification	12-14
1.6.2. Essential components of chemosensor	14-15
1.6.3. The sensing process	15
1.7. Metal ion recognition by 1,2,3-triazoles	16
1.8. Determination of chemosensing behaviour via spectroscopic analysis	17-18
1.8.1. UV-Vis spectroscopy	17
1.8.2. Fluorescence spectroscopy	17-18
1.9. Conclusion	18-19
References	20-28
Chapter II: Review of Literature	**29-86**
2.1. Heterocycles in organic chemistry	29-32
2.1.1. A general overview	29-30
2.1.2. Applications of heterocyclic compounds	31
2.1.3. The 1,2,3-triazole	32
2.2. CuAAC 'click' methodology for 1,2,3-triazole linked derivatives	33-49
2.2.1. Synthesizing a terminal alkyne	33
2.2.1.1. α, β-eliminations	34-35
2.2.1.2. Carbene rearrangement	36-37
2.2.1.3. Miscellaneous Reactions	38-41

2.2.2. Synthesizing an organic azide 42-44
2.2.3. Synthesizing 1,2,3-triazoles via cycloaddition of a terminal alkyne with an organic azide mediated via Cu(I) catalyst 45-48
2.3. Spectroscopic analysis of the products 49-53
2.3.1. Infrared (IR) spectroscopy 49-50
2.3.2. Nuclear Magnetic Resonance (NMR) Spectroscopy 50-51
2.3.3. Mass Spectrometry 52
2.3.4. Ultraviolet-Visible (UV-Vis) Spectroscopy 52
2.3.5. Fluorescence Spectroscopy 52-53
2.4. Applications of 1,2,3-triazole linkers as chemosensors 54-70
2.5. The advantages of using 1,2,3-triazole derivatives for ion sensing 71-72
2.5.1. Tailor-made functionalities for the 1,2,3-triazole moiety 71-72
2.5.2. Lower limit of detection 72
2.5.3. Visual changes to naked eye 72
2.6. Aims and objectives of the thesis 72-74
References 75-86
Chapter III: Synthetic Procedures and Characterization Data **87-104**
3.1. Generalized synthetic route for 1,2,3-triazole synthesis 87-88
3.1.1. Synthesizing a terminal alkyne 87
3.1.2. Synthesizing an organic azide 87-88
3.1.3. Synthesizing 1,2,3-triazole 88
3.2. Synthesis of organic azides 88-89
3.2.1. Synthesis and characterization of benzyl azide (**105**) 88-89
3.2.2. Synthesis and characterization of 1-(azidomethyl)naphthalene (**137**) 89
3.3. Synthesis and characterization of maleic hydrazide-based alkyne and its corresponding 1,2,3-triazoles 90-92
3.3.1. Synthesis and characterization of terminal alkyne **139** 90
3.3.2. Synthesis and characterization of 1,2,3-triazole derivative **140** 91
3.3.3. Synthesis and characterization of 1,2,3-triazole derivative **141** 92
3.4. Synthesis and characterization of 4-tert butyl catechol-based alkyne and its corresponding 1,2,3-triazole 93-94
3.4.1. Synthesis and characterization of terminal alkyne **143** 93
3.4.2. Synthesis and characterization of 1,2,3-triazole derivative **144** 94

3.5. Synthesis and characterization of p-rosolic acid-based alkyne and its corresponding 1,2,3-triazole 95-96
3.5.1. Synthesis and characterization of terminal alkyne **146** 95
3.5.2. Synthesis and characterization of 1,2,3-triazole derivative **147** 96
3.6. Synthesis and characterization of glyoxal bis-(2-hydroxyanil)-based alkyne and its corresponding 1,2,3-triazole 97-98
3.6.1. Synthesis and characterization of terminal alkyne **149** 97
3.6.2. Synthesis and characterization of 1,2,3-triazole derivative **150** 98
3.7. Synthesis and characterization of Schiff base-derived alkyne and its corresponding 1,2,3-triazole 99-101
3.7.1. Synthesis and characterization of Schiff base **153** 99
3.7.2. Synthesis and characterization of terminal alkyne **154** 100
3.7.3. Synthesis and characterization of 1,2,3-triazole derivative **155** 101
Chapter IV: Results and discussion **105-194**
Part A: Interpretation and discussion of spectroscopic data **105-127**
4.1. Synthetic aspects in reference to the N-heterocyclic 1,2,3-triazole ring 105-106
4.1.1. Synthesis of terminal alkyne 105
4.1.2. Synthesis of organic azide 105
4.1.3. Cu(I)-catalyzed alkyne-azide cycloaddition 106
4.2. Synthesis and spectral analysis of benzyl azide (**105**) 106-107
4.2.1. Synthesis 106
4.2.2. Analysis of IR spectrum 106-107
4.2.3. Analysis of NMR spectra 107
4.3. Synthesis and spectral analysis of 1-(azidomethyl)naphthalene (**137**) 107-108
4.3.1. Synthesis 107
4.3.2. Analysis of IR spectrum 108
4.3.3. Analysis of NMR spectra 108
4.4. Synthesis and spectral analysis of terminal alkyne **139** 108-109
4.4.1. Synthesis 108
4.4.2. Analysis of IR spectrum 109
4.4.3. Analysis of NMR spectra 109
4.5. Synthesis and spectral analysis of 1,2,3-triazole derivative **140** 109-111
4.5.1. Synthesis 109-110

4.5.2. Analysis of IR spectrum 109
4.5.3. Analysis of NMR spectra 110-111
4.5.4. Analysis of mass spectrum 111
4.6. Synthesis and spectral analysis of 1,2,3-triazole derivative **141** 111-112
4.6.1. Synthesis 111
4.6.2. Analysis of IR spectrum 112
4.6.3. Analysis of NMR spectra 112
4.6.4. Analysis of mass spectrum 112
4.7. Synthesis and spectral analysis of terminal alkyne **143** 113-114
4.7.1. Synthesis 113
4.7.2. Analysis of IR spectrum 113-114
4.7.3. Analysis of NMR spectra 114
4.8. Synthesis and spectral analysis of 1,2,3-triazole derivative **144** 114-116
4.8.1. Synthesis 114-115
4.8.2. Analysis of IR spectrum 115
4.8.3. Analysis of NMR spectra 115-116
4.8.4. Analysis of mass spectrum 116
4.9. Synthesis and spectral analysis of terminal alkyne **146** 116-117
4.9.1. Synthesis 116
4.9.2. Analysis of IR spectrum 117
4.9.3. Analysis of NMR spectra 117
4.10. Synthesis and spectral analysis of 1,2,3-triazole derivative **147** 117-119
4.10.1. Synthesis 117-118
4.10.2. Analysis of IR spectrum 118
4.10.3. Analysis of NMR spectra 118-119
4.10.4. Analysis of mass spectrum 119
4.11. Synthesis and spectral analysis of terminal alkyne **149** 119-120
4.11.1. Synthesis 119
4.11.2. Analysis of IR spectrum 120
4.11.3. Analysis of NMR spectra 120
4.12. Synthesis and spectral analysis of 1,2,3-triazole derivative **150** 120-122
4.12.1. Synthesis 120-121
4.12.2. Analysis of IR spectrum 121

4.12.3. Analysis of NMR spectra 121-122
4.12.4. Analysis of mass spectrum 122
4.13. Synthesis and spectral analysis of Schiff base **153** 122-123
4.13.1. Synthesis 122-123
4.13.2. Analysis of IR spectrum 123
4.13.3. Analysis of NMR spectra 123
4.14. Synthesis and spectral analysis of terminal alkyne **154** 123-124
4.14.1. Synthesis 123-124
4.14.2. Analysis of IR spectrum 124
4.14.3. Analysis of NMR spectra 124
4.15. Synthesis and spectral analysis of 1,2,3-triazole derivative **155** 125-126
4.15.1. Synthesis 125
4.15.2. Analysis of IR spectrum 125-126
4.15.3. Analysis of NMR spectra 126
4.15.4. Analysis of mass spectrum 126
References 127
Part B: Scrutinization of Photophysical Data **128-194**
4.16. Electronic spectroscopy- mechanistic aspect and application for ion(s) sensing 128-131
4.16.1. UV-Visible spectroscopy 128-130
4.16.2. Fluorescence spectroscopy 130-131
4.17. Chemosensing analysis of maleic hydrazide based 1,2,3-triazoles **140** and **141** 131-150
4.17.1. Ion recognition analysis of 1,2,3-triazole derivative **140** 131-140
4.17.1.1. Chemosensing response of probe **140** for Pb(II) and Cr(III) via UV- Vis spectroscopy 132-138
4.17.1.2. Competitive metal ion interaction analysis 138
4.17.1.3. Time dependence analysis of probe **140**-metal ion complexation 139
4.17.1.4. Temperature dependence analysis of probe **140**-metal ion complexation 139-140
4.17.1.5. Plausible binding mode 140
4.17.2. Ion recognition analysis of 1,2,3-triazole derivative **141** 141-150

4.17.2.1. Chemosensing response of probe **141** for Pb(II) and Cr(III) via UV- Vis spectroscopy 142-147
4.17.2.2. Competitive metal ion interaction analysis 147-148
4.17.2.3. Time dependence analysis of probe **141**-metal ion complexation 148
4.17.2.4. Temperature dependence analysis of probe **141**-metal ion complexation 149
4.17.2.5. Plausible binding mode 149-150
4.18. Chemosensing analysis of 4-tert butyl catechol based 1,2,3-triazole **144** 150-160
4.18.1. Ion recognition analysis of 1,2,3-triazole derivative **144** 150-151
4.18.2. Chemosensing response of probe **144** for Hg(II) and Pb(II) via UV-Vis spectroscopy 152-154
4.18.3. Chemosensing response of probe **144** for Hg(II) and Pb(II) via fluorescence spectroscopy 154-156
4.18.4. Competitive metal ion interaction analysis 157
4.18.5. Time dependence analysis of probe **144**-metal ion complexation 157-158
4.18.6. Temperature dependence analysis of probe **144**-metal ion complexation 158-159
4.18.7. Plausible binding mode 160
4.19. Chemosensing analysis of p-rosolic acid-based 1,2,3-triazole derivative **147** 160-172
4.19.1. Ion recognition analysis of 1,2,3-triazole derivative **147** 160-161
4.19.2. Chemosensing response of probe **147** for Hg(II), Pb(II), and Cr(III) via UV-Vis spectroscopy 162-165
4.19.3. Chemosensing response of probe **147** for Hg(II), Pb(II), and Cr(III) via fluorescence spectroscopy 166-169
4.19.4. Competitive metal ion interaction analysis 169-170
4.19.5. Time dependence analysis of probe **147**-metal ion complexation 170
4.19.6. Temperature dependence analysis of probe **147**-metal ion complexation 171-172
4.19.7. Plausible binding mode 172
4.20. Chemosensing analysis of glyoxal bis-(2-hydroxyanil)-based 1,2,3-triazole derivative **150** 173-182

4.20.1. Ion recognition analysis of 1,2,3-triazole derivative 173-174
4.20.2. Chemosensing response of probe **150** for Cu(II) and Pb(II) via UV-Vis spectroscopy 174-176
4.20.3. Chemosensing response of probe **150** for Cu(II) and Pb(II) via fluorescence spectroscopy 177-180
4.20.4. Competitive metal ion interaction analysis 180
4.20.5. Time dependence analysis of probe **150**-metal ion complexation 181
4.20.6. Temperature dependence analysis of probe **150**-metal ion complexation 181-182
4.20.7. Plausible binding mode 182
4.21. Chemosensing analysis of Schiff base-derived 1,2,3-triazole derivative **155** 183-190
4.21.1. Ion recognition analysis of 1,2,3-triazole derivative **155** 183-184
4.21.2. Chemosensing response of probe **155** for Ce(III) via UV-Vis spectroscopy 184-185
4.21.3. Chemosensing response of probe **155** for Ce(III) via fluorescence spectroscopy 186-187
4.21.4. Competitive metal ion interaction analysis 187-188
4.21.5. Time dependence analysis of probe **155**-metal ion complexation 188
4.21.6. Temperature dependence analysis of probe **155**-metal ion complexation 189
4.21.7. Plausible binding mode 189-190
4.22. Conclusion 190-191
References 192-194
Summary 195-214
Annexure A: Instrumentation and Chemicals 215-216
Annexure B: Spectra 217-243
List of Publications 244-246
List of conference presentations 247
Short term courses and Workshops 248
Published papers and Certificates 249-273
List of Figures, Schemes and Tables xv-xxviii
List of Abbreviations and Chemicals xxviii-xxx

LIST OF FIGURES, SCHEMES AND TABLES

FIGURES

Contents **Page No.**

Chapter I

Figure 1.1: Distinct characteristics of 'Click Chemistry' methodology 1

Figure 1.2: Diverse reaction methodologies classified under 'Click Chemistry' 2

Figure 1.3: Proposed concerted mechanism of 1,3-dipolar cycloadditions 3

Figure 1.4: An illustrative representation of Huisgen 1,3-dipolar cycloaddition 4

Figure 1.5: An illustrative representation of Cu(I)-catalyzed alkyne-azide cycloaddition 5

Figure 1.6: Mononuclear mechanism of CuAAC as proposed by Sharpless research group 7

Figure 1.7: Binuclear mechanism of CuAAC as proposed by Finn and Fokin 9

Figure 1.8: An illustrative representation of 1H-1,2,3-triazole ring 10

Figure 1.9: Diverse applications of 1,2,3-triazoles in several research areas 11

Figure 1.10: A pie chart representation for the classification of chemical sensors into various categories based upon the technique used 13

Figure 1.11: An illustration of the indispensable components of a chemosensor and the functions thereof 15

Figure 1.12: An illustration of metal ion-binding with the ligand in accordance with the host-guest relationship and HSAB concept 16

Figure 1.13: Different types of variations exhibited in the absorption/emission spectrum of a chemosensing probe on binding with an analyte 18

Chapter II

Figure 2.1: Three, four, five, six-membered and fused heterocyclic systems 30

Figure 2.2: Applications of heterocyclic compounds 31

Figure 2.3: An illustrative categorization of 1,2,3-triazoles 32

Figure 2.4: Synthesis of terminal alkyne from 1,1-dibromo-1-alkene employing Cs_2CO_3 as the base 34

Figure 2.5: Synthesis of terminal alkynes from gem-dibromoalkenes via Na_2S mediation 34

Figure 2.6: Conversion of geminal-dibromoalkene into terminal alkyne 35

Figure 2.7: Synthesis of terminal alkyne from dibromopropanoic acid 35

Figure 2.8: Microwave-assisted one-pot synthesis of terminal alkyne 35
Figure 2.9: Synthesis of terminal alkynes from aldehydes as reported by Corey and Fuchs 36
Figure 2.10: Synthesis of terminal alkynes from aldehydes as reported by Hijfte *et al.* 36
Figure 2.11: a) synthesis of terminal alkynes via dehydrohalogenation of (Z)-1-iodo-1-alkenes with TBAF. b) synthesis of terminal alkyne directly from aldehyde 37
Figure 2.12: Synthesis of terminal alkyne from aldehyde using C-silylated-diazophosphines 37
Figure 2.13: Synthesis of terminal alkyne from acetoxynitrosamide 37
Figure 2.14: Synthesis of terminal alkynes by reacting aldehyde with Ohira–Bestmann reagent 38
Figure 2.15: Synthesis of radiofluorinated phenylacetylene from [^{18}F]-fluorobenzaldehyde 38
Figure 2.16: Synthesis of phenylacetylene from α,α-difluorophosphonate 38
Figure 2.17: Synthesis of terminal alkyne based on p-hydroxy benzaldehyde 39
Figure 2.18: Synthesis of the 3,4-dihydroxybenzaldehyde-based terminal alkyne 40
Figure 2.19: Synthesis of the cyclam based terminal alkyne 40
Figure 2.20: Synthesis of the bispropargylether containing terminal alkyne 40
Figure 2.21: Synthesis of the terminal alkyne Py-NRhB from NH_2-NRhB 41
Figure 2.22: Synthesis of salicylaldehyde and 2-(benzo[d]thiazol-2-yl)phenol based terminal alkynes 41
Figure 2.23: Synthesis of phenyl azide **59** from phenylhydrazine **58** 42
Figure 2.24: Synthesis of an organic azide **61** by using the highly toxic hydrogen azide 42
Figure 2.25: Synthesis of organic azide by reacting (a) alcohol with ADMP and DBU as the base; and (b) primary amine with ADMP and DMAP as the base 43
Figure 2.26: Synthesis of azido-thalidomide from 4-amino-substituted analogue 43
Figure 2.27: Synthesis of diaryl ether thorugh trimethylsilyl azide following 44

Ullmann reaction
Figure 2.28: Synthesis of 2,6-dimesitylphenyliodide based azide 44
Figure 2.29: Synthesis of nitrosyl-hydrazine-based azide 44
Figure 2.30: Synthesis of aromatic azide from the corresponding amine using triflyl azide 44
Figure 2.31: Synthesis of CuAAC-derived 1,2,3-triazole-coumarin derivative 45
Figure 2.32: Synthesis of carbazole-triazole-fluorene conjugated polymer 46
Figure 2.33: Synthesis of dianthracene-cyclen based 1,2,3-triazole-based conjugate 46
Figure 2.34: Synthesis of coumarin-linked 1,2,3-triazole-based probe 46
Figure 2.35: Synthesis of dual fluorophore containing 1,2,3-triazole derivative 47
Figure 2.36: Synthesis of coumarin-1,2,3-triazole based chemosensors 47
Figure 2.37: Synthesis of rhodamine 6G based 1,2,3-triazole derivative 47
Figure 2.38: Synthesis of phenylaza-15-crown-5-triazol-substituted coumarin fluoroionophore 48
Figure 2.39: Synthesis of 1,2,3-triazole probe based on fluorescein 48
Figure 2.40: Synthesis of an amphiphilic 1,2,3-triazole based probe 48
Figure 2.41: Comparative ^{1}H NMR analysis of an alkyne and a 1,2,3-triazole derivative depicting the presence of a peak at d = 2.52 ppm and δ = 7.54 ppm corresponding to the alkynyl proton and the triazole ring proton respectively 51
Figure 2.42: A representative illustration of the electronic transition corresponding absorption and emission spectroscopy 53
Figure 2.43: Quinoline-conjugated glucopyranose based 1,2,3-triazole appended chemosensor probe for the recognition of Zn(II), Cd(II), and Hg(II) 54
Figure 2.44: Rhodamine B- diarylethene based 1,2,3-triazole chemosensor for Al(III) and Cu(II) recognition 55
Figure 2.45: Bis(naphthyl)methane ‘capped’ 1,2,3- triazole-linked calix[4]arene receptor for sensing Fe(III) ions 55
Figure 2.46: Rhodamine alkyne derived 1,2,3-triazole based fluorescent chemosensor for Cu(II) and Fe(III) detection 56
Figure 2.47: Isatin-triazole-tethered rhodamine-based fluorescent probe for 57

selective Cu(II) recognition
Figure 2.48: BINOL-based cyclophane with two triazole moieties for Ag(I) sensing 57
Figure 2.49: 1,19-disubstituted ferrocene based 1,2,3-triazole derivative for the sensing of Hg(II) and Cu(II) 58
Figure 2.50: Ferrocene-naphthalene conjugate with 1,2,3-triazole linkages for detecting Hg(II) ions 58
Figure 2.51: Quinolinotriazole-b-cyclodextrin as a selective chemosensor for Cd(II) ions 59
Figure 2.52: A pyrene-linked tris-1,2,3-triazole amine based sensor for Zn(II) 59
Chapter IV
Part A
Figure 4.1: Structure of benzyl azide **105** 106
Figure 4.2: Structure of 1-(azidomethyl)naphthalene **137** 107
Figure 4.3: Structure of terminal alkyne **139** 108
Figure 4.4: Structure of 1,2,3-triazole derivative **140** 110
Figure 4.5: Structure of 1,2,3-triazole derivative **141** 111
Figure 4.6: Structure of terminal alkyne **143** 113
Figure 4.7: Structure of 1,2,3-triazole derivative **144** 114
Figure 4.8: Structure of terminal alkyne **146** 116
Figure 4.9: Structure of 1,2,3-triazole derivative **147** 118
Figure 4.10: Structure of terminal alkyne **149** 119
Figure 4.11: Structure of 1,2,3-triazole derivative **150** 121
Figure 4.12: Structure of Schiff base **153** 122
Figure 4.13: Structure of terminal alkyne **154** 124
Figure 4.14: Structure of 1,2,3-triazole derivative **155** 125
Part B
Figure 4.15: An illustrative representation of the types of electronic transitions in conjugated system and/or C=O group 129
Figure 4.16: An illustration of the relative absorption change of probe **140** for several metal ions in DMSO solvent 132
Figure 4.17: UV-Vis spectra of probe **140** (0.5 mM) upon the progressive addition of Pb(II) in DMSO as the solvent 133

Figure 4.18: Relative absorbance maxima (A_n/A_o) shifts of probe **140** according to the concentration of Pb(II) ions added 134

Figure 4.19: Correlation plot of relative absorption intensity of probe **140** (A_o-A_n)/A_o as a function of Pb(II) concentration; where A_o = initial absorption of probe **140** and A_n = absorption of probe **140** in the presence of Pb(II) 134

Figure 4.20: Benesi-Hildebrand plot for probe **140**-Pb(II) complexation 135

Figure 4.21: UV-Vis spectra of probe **140** (0.5 mM) upon the progressive addition of Cr(III) in DMSO as the solvent 136

Figure 4.22: Relative absorbance maxima (A_n/A_o) shifts of probe **140** according to the concentration of Cr(III) ions added 136

Figure 4.23: Correlation plot of relative absorption intensity of probe **140** (A_o-A_n)/A_o as a function of Cr(III) concentration; where A_o = initial absorption of probe **140** and A_n = absorption of probe **140** in the presence of Cr(III) 137

Figure 4.24: Benesi-Hildebrand plot for probe **140**-Cr(III) complexation 137

Figure 4.25: Absorption spectra of probe **140** (0.5 mM) in DMSO recognizing Cr(III) ions among several metal ions at equimolar concentrations 138

Figure 4.26: Time dependent absorption spectrum of probe **140**-Pb(II)/Cr(III) complex solution exhibiting a constant absorbance at 258 nm 139

Figure 4.27: Temperature dependent absorption spectrum of probe **140**-Pb(II)/Cr(III) exhibiting a constant absorbance over a temperature range of 20 - 50 ºC 140

Figure 4.28: Proposed interaction between probe **140** and Pb(II)/Cr(III) 140

Figure 4.29: An illustration of the relative absorption change of probe **141** for several metal ions in DMSO solvent 142

Figure 4.30: UV-Vis spectra of probe **141** (0.5 mM) upon the progressive addition of Pb(II) in DMSO as the solvent 143

Figure 4.31: Relative absorbance maxima (A_n/A_o) shifts of probe **141** according to the concentration of Pb(II) ions added 143

Figure 4.32: Correlation plot of relative absorption intensity of probe **141** (A_o-A_n)/A_o as a function of Pb(II) concentration; where A_o = initial absorption of probe **141** and A_n = absorption of probe **141** in the 144

presence of Pb(II)
Figure 4.33: Benesi-Hildebrand plot for probe **141**-Pb(II) complexation 144
Figure 4.34: UV-Vis spectra of probe **141** (0.5 mM) upon the progressive addition of Cr(III) in DMSO as the solvent 145
Figure 4.35: Relative absorbance maxima (A_n/A_o) shifts of probe **141** according to the concentration of Cr(III) ions added 146
Figure 4.36: Correlation plot of relative absorption intensity of probe **141** (A_o-A_n)/A_o as a function of Cr(III) concentration; where A_o = initial absorption of probe **141** and A_n = absorption of probe **141** in the presence of Cr(III) 146
Figure 4.37: Benesi-Hildebrand plot for probe **141**-Cr(III) complexation 147
Figure 4.38: Absorption spectra of probe **141** (0.5 mM) in DMSO recognizing Cr(III) ions among several metal ions at equimolar concentrations 148
Figure 4.39: Time dependent absorption spectrum of probe **141**-Pb(II)/Cr(III) complex solution exhibiting a constant absorbance at 260 nm 148
Figure 4.40: Temperature dependent absorption spectrum of probe **141**-Pb(II)/Cr(III) exhibiting a constant absorbance over a temperature range of 20 - 50 ºC 149
Figure 4.41: Proposed interaction between probe **141** and Pb(II)/Cr(III) 150
Figure 4.42: Absorption spectra of probe **144** (0.4 mM) solution in various solvents: (a) CH_3CN/H_2O (4:1), (b) CH_3CN, (c) DMSO, and (d) THF 151
Figure 4.43: An illustration of the relative absorption change of probe **144** for several metal ions in CH_3CN/H_2O (4:1) solvent 151
Figure 4.44: UV-Vis spectra of probe **144** (0.4 mM) upon the progressive addition of Hg(II) in CH_3CN/H_2O (4:1); the inset exhibits the relative absorbance change (A_n/A_o) vs metal ion concentration (mM) 152
Figure 4.45: UV-Vis spectra of probe **144** (0.4 mM) upon the progressive addition of Pb(II) in CH_3CN/H_2O (4:1); the inset exhibits the relative absorbance change (A_n/A_o) vs metal ion concentration (mM) 153
Figure 4.46: Benesi-Hildebrand plot for probe **144**-Hg(II) complexation 153

Figure 4.47: Benesi-Hildebrand plot for probe **144**-Pb(II) complexation 154

Figure 4.48: Fluorescence spectra of probe **144** (50 µM) upon the progressive addition of Hg(II) ions in CH_3CN/H_2O (4:1); the inset exhibits the relative emission change (I/I_o) vs metal ion concentration (µM) 155

Figure 4.49: Fluorescence spectra of probe **144** (50 µM) upon the progressive addition of Pb(II) ions in CH_3CN/H_2O (4:1); the inset exhibits the relative emission change (I/I_o) vs metal ion concentration (µM) 155

Figure 4.50: Correlation plot of relative fluorescence emission of probe **144** $(I_o\text{-}I)/I_o$ as a function of Hg(II) concentration; where I_o = initial emission of probe **144** and I = emission of probe **144** in the presence of Hg(II) 156

Figure 4.51: Correlation plot of relative fluorescence emission of probe **144** $(I_o\text{-}I)/I_o$ as a function of Pb(II) concentration; where I_o = initial emission of probe **144** and I = emission of probe **144** in the presence of Pb(II) 156

Figure 4.52: Absorption spectra of probe **144** (0.4 mM) in CH_3CN/H_2O (4:1) recognizing Hg(II) ions among several metal ions at equimolar concentrations 157

Figure 4.53: Time dependent absorption spectrum of probe **144**-Hg(II) complex solution exhibiting a successive enhancement in absorbance at 277 nm 158

Figure 4.54: Time dependent absorption spectrum of probe **144**-Pb(II) complex solution exhibiting a successive decline in absorbance at 277 nm 158

Figure 4.55: Temperature dependent absorption spectrum of probe **144-**Hg(II) exhibiting variation in absorbance over a temperature range of 20 - 50 ºC 159

Figure 4.56: Temperature dependent absorption spectrum of probe **144-**Pb(II) exhibiting variation in absorbance over a temperature range of 20 - 50 ºC 159

Figure 4.57: Proposed interaction between probe **144** and Hg(II)/Pb(II) 160

Figure 4.58: An illustration of the relative absorption change of probe **147** for several metal ions in DMSO solvent 161

Figure 4.59: UV-Vis spectra of probe **147** (0.05 mM) upon the progressive addition of Hg(II) in DMSO; the inset exhibits the relative absorbance change (A_n/A_o) vs metal ion concentration (mM) 163

Figure 4.60: UV-Vis spectra of probe **147** (0.05 mM) upon the progressive addition of Pb(II) in DMSO; the inset exhibits the relative absorbance change (A_n/A_o) vs metal ion concentration (mM) 163

Figure 4.61: UV-Vis spectra of probe **147** (0.05 mM) upon the progressive addition of Cr(III) in DMSO; the inset exhibits the relative absorbance change (A_n/A_o) vs metal ion concentration (mM) 164

Figure 4.62: Benesi-Hildebrand plot for probe **147**-Hg(II) complexation 164

Figure 4.63: Benesi-Hildebrand plot for probe **147**-Pb(II) complexation 165

Figure 4.64: Benesi-Hildebrand plot for probe **147**-Cr(III) complexation 165

Figure 4.65: Fluorescence spectra of probe **147** (0.1 µM) upon the progressive addition of Hg(II) ions in DMSO; the inset exhibits the relative emission change (I/I_o) vs metal ion concentration (µM) 166

Figure 4.66: Fluorescence spectra of probe **147** (0.1 µM) upon the progressive addition of Pb(II) ions in DMSO; the inset exhibits the relative emission change (I/I_o) vs metal ion concentration (µM) 167

Figure 4.67: Fluorescence spectra of probe **147** (0.1 µM) upon the progressive addition of Cr(III) ions in DMSO; the inset exhibits the relative emission change (I/I_o) vs metal ion concentration (µM) 167

Figure 4.68: Correlation plot of relative fluorescence emission of probe **147** $(I_o\text{-}I)/I_o$ as a function of Hg(II) concentration; where I_o = initial emission of probe **147** and I = emission of probe **147** in the presence of Hg(II) 168

Figure 4.69: Correlation plot of relative fluorescence emission of probe **147** $(I_o\text{-}I)/I_o$ as a function of Pb(II) concentration; where I_o = initial emission of probe **147** and I = emission of probe **147** in the presence of Pb(II) 168

Figure 4.70: Correlation plot of relative fluorescence emission of probe **147** $(I_o\text{-}I)/I_o$ as a function of Cr(III) concentration; where I_o = initial emission of probe **147** and I = emission of probe **147** in the presence of Cr(III) 169

Figure 4.71: Absorption spectra of probe **147** (0.05 mM) in DMSO recognizing Pb(II) ions among several metal ions at equimolar concentrations 170

Figure 4.72: Time dependent absorption spectrum of probe **147**-Hg(II)/Pb(II)/Cr(III) complex solution exhibiting a constant absorbance at 284 nm 170

Figure 4.73: Temperature dependent absorption spectrum of probe **147**-Hg(II) exhibiting a successive enhancement in absorption over a temperature range of 20 - 50 ºC 171

Figure 4.74: Temperature dependent absorption spectrum of probe **147**-Pb(II) exhibiting a successive enhancement in absorption over a temperature range of 20 - 50 ºC 171

Figure 4.75: Temperature dependent absorption spectrum of probe **147**-Cr(III) exhibiting a successive enhancement in absorption over a temperature range of 20 - 50 ºC 172

Figure 4.76: Proposed interaction between probe **147** and Hg(II)/Pb(II)/Cr(III) 172

Figure 4.77: An illustration of the relative absorption change of probe **150** for several metal ions in DMSO solvent 174

Figure 4.78: UV-Vis spectra of probe **150** (0.5 mM) upon the progressive addition of Cu(II) in DMSO; the inset exhibits the relative absorbance change (A_n/A_o) vs metal ion concentration (mM) 175

Figure 4.79: UV-Vis spectra of probe **150** (0.5 mM) upon the progressive addition of Pb(II) in DMSO; the inset exhibits the relative absorbance change (A_n/A_o) vs metal ion concentration (mM) 175

Figure 4.80: Benesi-Hildebrand plot for probe **150**-Cu(II) complexation 176

Figure 4.81: Benesi-Hildebrand plot for probe **150**-Pb(II) complexation 176

Figure 4.82: Fluorescence spectra of probe **150** (20 µM) upon the progressive addition of Cu(II) ions in DMSO; the inset exhibits the relative emission change (I/I_o) vs metal ion concentration (µM) 178

Figure 4.83: Fluorescence spectra of probe **150** (20 µM) upon the progressive addition of Pb(II) ions in DMSO; the inset exhibits the relative emission change (I/I_o) vs metal ion concentration (µM) 178

Figure 4.84: Correlation plot of relative fluorescence emission of probe **150** 179

(I_o-I)/I_o as a function of Cu(II) concentration; where I_o = initial emission of probe **150** and I = emission of probe **150** in the presence of Cu(II)

Figure 4.85: Correlation plot of relative fluorescence emission of probe **150** (I_o-I)/I_o as a function of Pb(II) concentration; where I_o = initial emission of probe **150** and I = emission of probe **150** in the presence of Pb(II) 179

Figure 4.86: Absorption spectra of probe **150** (0.5 mM) in DMSO recognizing Pb(II) ions among several metal ions at equimolar concentrations 180

Figure 4.87: Time dependent absorption spectrum of probe **150**-Cu(II)/Pb(II) exhibiting a constant absorbance at 284 nm 181

Figure 4.88: Temperature dependent absorption spectrum of probe **150**-Cu(II)/Pb(II) exhibiting constant absorbance over a temperature range of 20 - 50 ºC 182

Figure 4.89: Proposed interaction between probe **150** and Cu(II)/Pb(II) 182

Figure 4.90: An illustration of the relative absorption change of probe **155** for several metal ions in DMSO/H_2O (4:1) solvent 184

Figure 4.91: UV-Vis spectra of probe **155** (0.1 mM) upon the progressive addition of Ce(III) in DMSO/H_2O (4:1); the inset exhibits the relative absorbance change (A_n/A_o) vs metal ion concentration (mM) 185

Figure 4.92: Benesi-Hildebrand plot for probe **155**-Ce(III) complexation 185

Figure 4.93: Fluorescence spectra of probe **155** (50 µM) upon the progressive addition of Ce(III) ions in DMSO/H_2O (4:1); the inset exhibits the relative emission change (I/I_o) vs metal ion concentration (µM) 187

Figure 4.94: Correlation plot of relative fluorescence emission of probe **155** (I_o-I)/I_o as a function of Ce(III) concentration; where I_o = initial emission of probe **155** and I = emission of probe **155** in the presence of Ce(III) 187

Figure 4.95: Absorption spectra of probe **155** (0.1 mM) in DMSO/H_2O (4:1) recognizing Ce(III) ions among several metal ions at equimolar concentrations 188

Figure 4.96: Time dependent absorption spectrum of probe **155**-Ce(III) 188

exhibiting a constant absorbance at 307 nm

Figure 4.97: Temperature dependent absorption spectrum of probe **155**-Ce(III) exhibiting constant absorbance over a temperature range of 20 – 50 ºC 189

Figure 4.98: Proposed interaction between probe **140** and Ce(III) 190

Summary

Figure S1: An illustration of Cu(I)-catalyzed alkyne-azide cycloaddition 195

Figure S2: An illustration of the synthesized azides and terminal alkynes 200

Figure S3: An illustration of the synthesized 1,4-disubstituted 1,2,3-triazoles 201

Figure S4: Absorption maxima shifts of the probe **140** as a result of titration with Pb(II) solution in DMSO 202

Figure S5: Absorption maxima shifts of the probe **140** as a result of titration with Cr(III) solution in DMSO 203

Figure S6: Absorption maxima shifts of the probe **141** as a result of titration with Pb(II) solution in DMSO 204

Figure S7: Absorption maxima shifts of the probe **141** as a result of titration with Pb(II) solution in DMSO 204

Figure S8: UV-Vis spectra of probe **144** during titration with Hg(II) in CH_3CN/H_2O (4:1) 205

Figure S9: UV-Vis spectra of probe **144** during titration with Pb(II) in CH_3CN/H_2O (4:1) 206

Figure S10: Incremental enhancement in the fluorescence emission of probe **144** upon the progressive addition of Hg(II) ions in CH_3CN/H_2O (4:1) 206

Figure S11: Incremental enhancement in the fluorescence emission of probe **144** upon the progressive addition of Pb(II) ions in CH_3CN/H_2O (4:1) 207

Figure S12: Absorption spectrum of probe **147** demonstrating cumulative changes on incremental addition of Hg(II) 208

Figure S13: Absorption spectrum of probe **147** demonstrating cumulative changes on incremental addition of Pb(II) 208

Figure S14: Absorption spectrum of probe **147** demonstrating cumulative changes on incremental addition of Cr(III) 209

Figure S15: Incremental enhancement in the fluorescence emission of probe **147** upon the progressive addition of Hg(II) ions 209
Figure S16: Incremental enhancement in the fluorescence emission of probe **147** upon the progressive addition of Pb(II) ions 210
Figure S17: Incremental enhancement in the fluorescence emission of probe **147** upon the progressive addition of Cr(III) ions 210
Figure S18: Absorption spectrum of probe **150** representing collective changes on incremental addition of Cu(II) 211
Figure S19: Absorption spectrum of probe **150** representing collective changes on incremental addition of Pb(II) 212
Figure S20: Decrease in the fluorescence emission of probe **150** upon the sequential accumulation of Cu(II) ions 212
Figure S21: Increase in the fluorescence emission of probe **150** upon the sequential accumulation of Cu(II) ions 213
Figure S22: Absorption spectrum of probe **155** representing collective changes on incremental addition of Ce(III) 214
Figure S23: Increase in the fluorescence emission of probe **155** upon the sequential accumulation of Ce(III) ions 214

SCHEMES

Contents **Page No.**

Chapter III

Scheme 3.1: General reaction procedure for the synthesis of terminal alkyne 87
Scheme 3.2: General reaction procedure for the synthesis of organic azide 88
Scheme 3.3: General reaction procedure for the synthesis of 1,4-disubstituted 1,2,3-triazole from terminal alkyne and organic azide 88
Scheme 3.4: Synthesis of benzyl azide **105** from benzyl chloride 89
Scheme 3.5: Synthesis of 1-(azidomethyl)naphthalene **137** from 1-(chloromethyl)naphthalene 89
Scheme 3.6: Synthesis of maleic hydrazide-based terminal alkyne **139** 90
Scheme 3.7: Synthesis of 1,2,3-triazole derivative **140** from maleic hydrazide-based terminal alkyne 91

Scheme 3.8: Synthesis of 1,2,3-triazole derivative **141** from maleic hydrazide-based terminal alkyne 92

Scheme 3.9: Synthesis of 4-tert butyl-catechol based terminal alkyne **143** 93

Scheme 3.10: Synthesis of 1,2,3-triazole derivative **144** from 4-tert butyl-catechol based terminal alkyne 94

Scheme 3.11: Synthesis of p-rosolic acid-based terminal alkyne **146** 95

Scheme 3.12: Synthesis of 1,2,3-triazole derivative **147** from p-rosolic acid-based terminal alkyne 96

Scheme 3.13: Synthesis of glyoxal bis-(2-hydroxyanil)-based terminal alkyne **149** 97

Scheme 3.14: Synthesis of 1,2,3-triazole derivative **150** from glyoxal bis-(2-hydroxyanil)-based terminal alkyne 98

Scheme 3.15: Synthesis of Schiff base **153** from 2-amino-5-methylpyridine and vanillin 99

Scheme 3.16: Synthesis of Schiff base-derived terminal alkyne **154** 100

Scheme 3.17: Synthesis of 1,2,3-triazole derivative **155** from Schiff base-terminal alkyne 101

TABLES

Contents **Page no.**

Table 2.1: Chemosensors appended with1,2,3-triazole moiety for recognizing distinct metal ions 60-70

Table 3.1: A tabular representation of the synthesized compounds, their corresponding reaction conditions, and the percentage yield 102-104

Table 4.1: LoD, LoQ, K_{a1}, K_{a2}, and stoichiometric ratio values for probe **140** on binding with Pb(II) and Cr(III) 138

Table 4.2: LoD, LoQ, K_{a1}, K_{a2}, and stoichiometric ratio values for probe **141** on binding with Pb(II) and Cr(III) 147

Table 4.3: LoD, LoQ, K_a and stoichiometric ratio values of probe **144** on binding with Hg(II) and Pb(II) 156

Table 4.4: LoD, LoQ, K_a and stoichiometric ratio values of probe **147** on binding with Hg(II), Pb(II), and Cr(III) 169

Table 4.5: LoD, LoQ, K_a and stoichiometric ratio values of probe **150** on 180

binding with Cu(II) and Pb(II)

Table 4.6: LoD, LoQ, K_a and stoichiometric ratio values of probe **155** on binding with Ce(III) 187

LIST OF ABBREVIATIONS

STANDARD UNITS

%	Percentage
°C	Degree Celsius
Å	Angstrom
atm	Atmosphere
bp	Boiling point
cm	Centimeter
equiv.	Equivalent(s)
et al.	Latin for 'and others'
g	Gram(s)
h	Hours(s)
Hz	Hertz
in vitro	Latin for 'in glass'
in vivo	Latin for 'within the living'
K	Kelvin
Kcal/mol	Kilocalories per mole
MHz	Megahertz
min	Minute(s)
ml	Millilitre(s)
mm	Millimeter(s)
mmol	Millimole(s)
mol	Mole(s)
mp	Melting Point
nm	Nanometer(s)
ppm	Parts Per Million
W	Watt

CHEMICALS

AcOH	Acetic Acid
ADMP	2-azido-1,3-dimethylimidazolinium hexafluorophosphate
$CDCl_3$	Deuterated chloroform
DBU	1,8-Diazabicycloundec-7-ene
DCM	Dichloromethane
DIPEA	Diisopropylethylamine
DMAP	N,N-dimethyl-4-aminopyridine
DMF	N,N-Dimethylformamide
DMSO-d_6	Deuterated dimethylsulphoxide
dpy	Dipyridyl
Et	Ethyl
Et_3N/TEA	Triethylamine
Me	Methyl
MeOH	Methanol
Ph	Phenyl
TBAF	Tetrabutylammonium fluoride
TBTA	Tris(benzyltriazolylmethyl)amine
THF	Tetrahydrofuran
THPTA	Tris(hydroxypropyltriazolylmethyl)amine
TPMA	Tris(pyridylmethyl)amine
tpy	Tripyridyl

MISCELLANEOUS

µM	Micro molar
µw	Microwave
δ	Delta
εmax	Molar absorptivity coefficient
λem	Emission wavelength
λex	Excitation wavelength

λmax	Wavelength of maximum absorption
CHEF	Chelation enhanced fluorescence emission
CHEQ	Chelation enhanced fluorescence quenching
CuAAC	Copper(I) catalyzed alkyne azide cycloaddition
d	Doublet
dd	Doublet of doublet
FBW	Fritsch-Buttenberg-Wiechell
H	Hydrogen
HOMO	Highest occupied molecular orbital
HSAB	Hard-Soft acid base
IR	Infrared
J	Coupling constant
K_a	Association constant
LoD	Limit of detection
LoQ	Limit of quantification
LCMS	Liquid chromatography mass spectrum
LUMO	Lowest unoccupied molecular orbital
M	Molecular mass
m	Multiplet
MS	Mass spectrum
NMR	Nuclear magnetic resonance
rt	Room temperature
s	Singlet
stirr	Stirring
t	Triplet
TLC	Thin layer chromatography
UV	Ultraviolet
v/v	Volume/Volume

Chapter I

Let's Get Started !

Introduction

This section of the thesis pertains to the research terminologies, modus operandi, and developments till date regarding the undertaken research work that will be presented in subsequent chapters; and provides a comprehensive review of the reported literature that was conducted as part of the research. In particular, it outlines in significant detail, the factors that had to be considered for working on the proposed research gap, while arranging the same like pieces of a puzzle to successfully conclude the research work.

1.1. Click Chemistry- a general perspective

The idea of ‘click’ reactions can be traced back to the early 20th century, where the chemists began to explore reactions that were straightforward, efficient, and had broad applicability. For example, the development of the ‘click-like’ reactions like the Mannich reaction, which involves the condensation of a primary or secondary amine with an aldehyde or ketone, was an early step towards the principles of click chemistry. Dr. Karl Barry Sharpless, the two times Nobel laureate in chemistry, played a pivotal role in shaping the concept of click chemistry in 2001, wherein he and his colleagues bestowed on the global research community a novel paradigm for organic synthesis, i.e., ‘Click Chemistry’, which is a modular approach for generating novel and intricate molecular structures, meeting various essential requirements: the method should be flexible, encompass a wide scope, yields should be high, and be executable under mild conditions..[1–3] This guiding principle, inspired by the nature’s lead to preferably form carbon-heteroatom (C-X) bonds such as proteins, nucleic acids, etc. resulting in the joining of small units,[4] was magnificently accoutred to satisfy the needs of contemporary chemistry.[5] In that aspect, several methodologies are encompassed under click chemistry that share a common trajectory, which is further defined by some significant and distinct ‘click’ characteristics (**figure 1.1**) like modularity, wide scope, high product yields, inoffensive by-product generation, stereospecificity, insensitivity to oxygen and moisture, utilization of benign solvents, effortless product isolation, etc.[5–7]

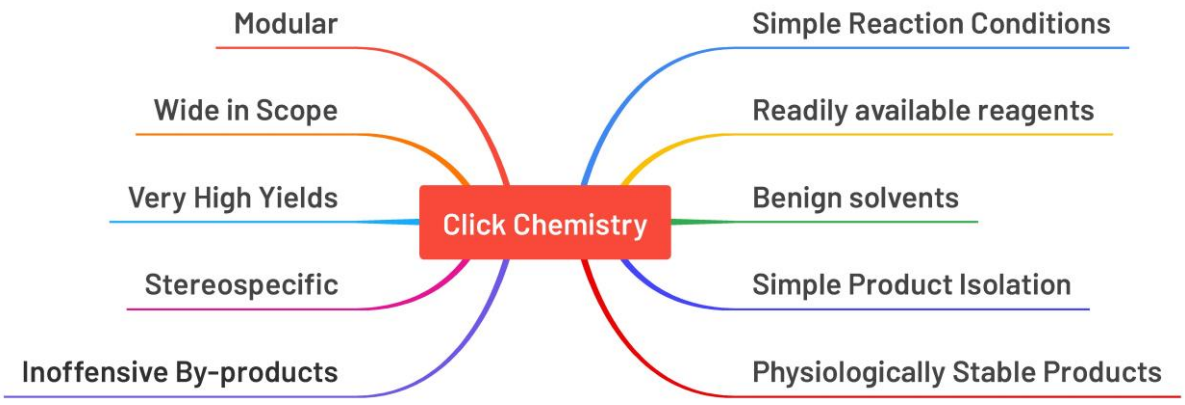

Figure 1.1: Distinct characteristics of ‘Click Chemistry’ methodology[5–7]

Over the past few years, the evolution of mechanistically discrete but conceptually similar ‘click’ approaches have equipped the researchers to increase the range of the arsenal of possible organic reactivity, by partially or fully satisfying the comprehensive set of 'click chemistry’ characteristics including Cu(I)-catalyzed alkyne azide cycloaddition (CuAAC),[8]

Inverse electron demand Diels–Alder reaction (IEDDA),[9,10] Thiol-click (thio-ene and thiol-yne) reactions,[11,12] SPAAC, i.e., Strain promoted azide-alkyne cycloaddition,[13–15] SPANC, i.e. Strain-promoted alkyne-nitrone cycloaddition,[16] and Staudinger ligation[17,18] (**figure 1.2**). Among all these methodologies, CuAAC has stood out to be the quintessential example of click chemistry, being implemented in the rapid assembly of heterocyclic molecular entities with desirable functions and hence emerging as the gold standard of click chemistry that has swiftly pushed the boundaries of previously established scientific specializations; The procedure entails the utilization of Cu(I) species as a catalyst, leading to the selective combination of an alkyne and an azide to produce 1,4-disubstituted 1,2,3-triazoles regioselectively.

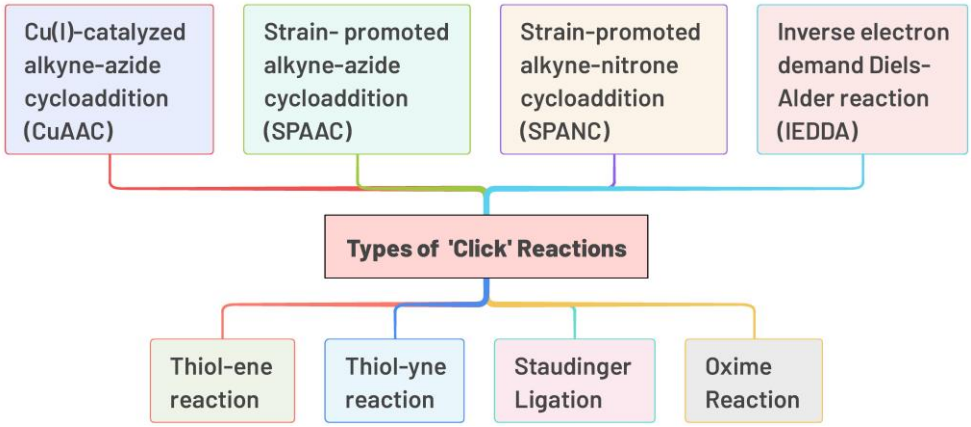

Figure 1.2: Diverse reaction methodologies classified under 'Click Chemistry'[8–20]

The 'click' methodology has found diverse applications in a vast array of research owing to its high efficiency and biocompatibility. For instance, under aqueous conditions with orthogonality, click chemistry can be performed, opening the door to the possibility of performing artificial chemical reactions in diverse biological systems such as cell surfaces and cell cytosol.[21–23] Click chemistry for post-polymerization modification is a prominent example of the functionalization strategies for polymeric product design.[24,25] Another crucial use of click chemistry is the construction of fluorogenic complexes between non-fluorescent alkynes and azides, which enables the ligation of two biomolecules with extensive applications in the developing field of cell biology and functional proteomics.[26–28] Furthermore, the synthesis of low molecular weight compounds in a single step renders *in situ* click chemistry as a target-guided synthesis (TGS) offers significant potential in drug delivery applications and can be utilized as a new method to screen building block libraries.[29–32] All these necessary utilities of 'click chemistry', in addition to many more such practical applications render this methodology a 'near ideal' approach for obtaining the desirable results in a convenient and efficient manner.

1.2. Huisgen 1,3-dipolar cycloaddition- the precursor to 'Click Chemistry'

The heterocycles synthesis involving the 1,3-dipolar addition is considered as one of the most significant routes for the synthesis of heterocyclic compounds.[33,34] The mechanism of the reaction involves the concerted formation of a cyclic compound through the combination of a 1,3-dipole (a three-atom π-electrons containing molecular entity having an atom of incomplete valency at one terminal position with the adjacent atom carrying a formal positive charge and a lone pair bearing atom at the other terminal position carrying a formal negative charge) with a dipolarophile group bearing multiple bonds. The common examples of 1,3-dipoles include nitrile imines, azomethine ylides, and diazo compounds. The electronic arrangement of these dipoles makes them highly reactive and prone to seeking out regions of high electron density in other molecules. On the other hand, the dipolarophile is typically an electron-rich species, as it contains regions of high electron density that can interact with the electron-deficient 1,3-dipole. The cyclic product is formed via cyclic electron displacement involving the formation of two new σ-bonds utilizing two available π-bonds[35,36] as shown in **figure 1.3**. The reaction follows a pericyclic process, meaning that it occurs in a single step without the formation of intermediates.

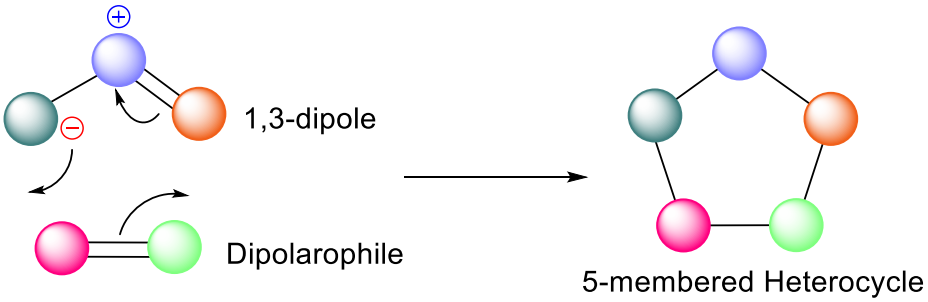

Figure 1.3: Proposed concerted mechanism of 1,3-dipolar cycloadditions[35,36]

The significance of 1,3-dipolar cycloaddition reactions lies in their versatility, efficiency, and applicability across a wide range of scientific disciplines. These reactions have revolutionized synthetic chemistry, enabled innovative material design, advanced drug discovery, and facilitated the exploration of biomolecular interactions, among other contributions to scientific and technological progress.[37,38] As a result of its efficiency and robustness, the 1,3-dipolar cycloaddition is also widely used in the synthesis of complexes of biological significance.[39]

It was Rolf Huisgen's exceptional work to organize previously disparate findings regarding the 1,3-dipolar cycloadditions into a logical progression, to go deeply into specifics, and to creatively expand on the new knowledge which was largely responsible for the direction in which this vital area of chemistry has progressed.[40,41] He focused on the reactions involving nitrile imines, azides, and diazo compounds as 1,3-dipoles and various alkynes and alkenes as dipolarophiles, highlighting the regioselectivity and stereoselectivity of these reactions and laid the groundwork for synthetically producing different five-membered heterocycles. It was proposed that these species, characterized by alternating positive and negative charges, could serve as highly reactive intermediates in cycloaddition reactions. A synthetic pathway for the synthesis of 1,2,3-triazoles, also known as the Huisgen cycloaddition was presented by him in 1963[36] wherein a terminal alkyne (acting as a dipolarophile) was subjected to thermal fusion with an organic azide (acting as a 1,3-dipole) under thermal conditions (> 100 ºC) which resulted in the production of 1,4-disubstituted as well as 1,5-disubstituted 1,2,3-triazoles[42] (ca. 1:1) as shown in **figure 1.4**.

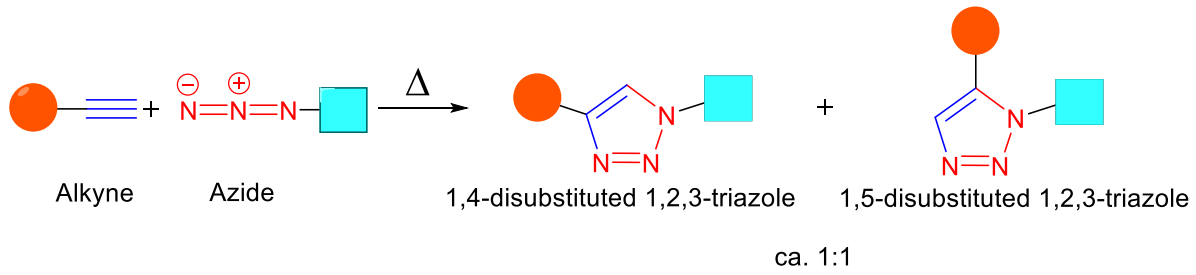

Figure 1.4: An illustrative representation of Huisgen 1,3-dipolar cycloaddition[36]

Huisgen's work was fundamental in shaping the click chemistry paradigm, as the concept of highly efficient, selective, and reliable chemical reactions aligns closely with Huisgen's emphasis on the practicality and versatility of 1,3-dipolar cycloadditions. The methodology, although an effective and robust route for the synthesis of 1,2,3-triazoles presented the following challenges resulting in the limiting of its utility:

- The reaction process involved the requirement of high temperature range (> 100 °C)
- Duration of the reaction was extremely long, ranging from a few days to a few weeks
- Due to no regiospecificity thereby resulting in the formation of a racemic mixture (ca. 1:1), the separation of the products imposed a challenge[39]

1.3. Cu(I)-catalyzed alkyne azide cycloaddition (CuAAC)- the quintessential 'Click Chemistry'

The independent investigations led by Sharpless and Meldal research groups in 2001 brought renewed interest to the 1,3-dipolar cycloadditions[43] wherein accentuating the regioselectivity and tolerance of this reaction, the findings of the conducted research evidenced that the introduction of Cu(I) species as the catalyst in Huisgen cycloaddition reaction significantly enhances the regiospecificity[44] as the 1,4-disubstituted 1,2,3-triazole is formed exclusively, and the reaction rate is accelerated by 10^7 times compared to the uncatalyzed process; while allowing the reaction to advance at relatively milder temperatures. This enhanced approach was termed as Cu(I)-catalyzed alkyne-azide cycloaddition, abbreviated as CuAAC[45] (**figure 1.5**), which since its inception, has become the flagship methodology that represents the 'click' pathway[46] with exceeding expectations, while also meeting majority of the criteria of green synthesis.[47]

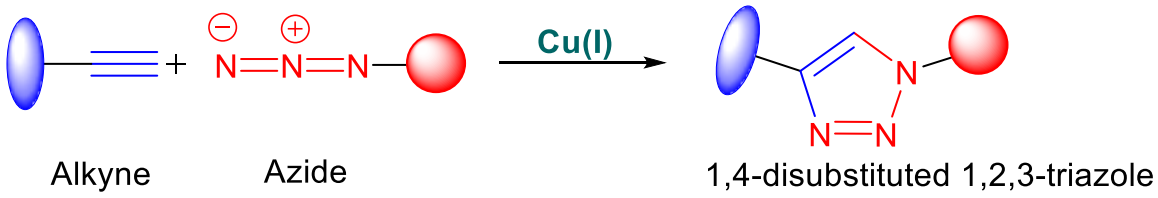

Figure 1.5: A visual depiction showcasing the Cu(I)-catalyzed alkyne-azide cycloaddition process[8]

As represented in **figure 1.5**, Cu(I) species mediates the cycloaddition of a terminal alkyne with an organic azide by acting as the catalyst, and the reaction involves the use of benign solvents like tetrahydrofuran (THF), acetonitrile, ethanol, water, etc. and providing moderately elevated temperature (55 - 60 °C). Microwave irradiation (50 - 480 W) in combination with Cu(I) in a suitable solvent is another cutting-edge technique that can be used to carry out this cycloaddition reaction. [48,49]The high yield, tolerance of reaction conditions like benign solvents, moisture and oxygen insensitivity, creation of a single product, and speed of the CuAAC reaction are all features that contribute to the method's widespread appeal.[50] The utility of CuAAC in chemical synthesis, bioconjugation, materials science, and many other areas has revolutionized the way researchers design molecules, materials, and technologies, contributing to significant advancements in science and technology. However, in contrast to the great majority of coupling systems, this reaction has a few extra properties that contribute significantly to its advantages,[51] such as:

- Under the mild conditions usually seen in CuAAC reaction, the azide and the alkyne that serve as the reactants are resistant to interaction with many other functional groups, which is remarkably useful when trying to immobilize a molecule with a lot of different functional groups.[52]

- Due to the non-availability of azide and alkyne in living organisms and hence their consequential inertness towards the biological functions, the site-specific attachment of biomolecules to surfaces is greatly facilitated by this reaction, due to which CuAAC has been dubbed 'bio-orthogonal'[53–55]

- The catalysis can be turned on and off by adjustment of the copper redox state for a wide range of catalytically active Cu(I) complexes, thereby providing control over the reaction kinetics[56]

- The final product of the reaction has good stability, with excellent resistance to hydrolysis and redox processes, compared to linkages originating from alternative couplings[57]

- Combining CuAAC with other orthogonal click reactions, such as oxime ligation or Staudinger ligation, allows for the sequential modification of a molecule with different functionalities. This can lead to the construction of intricate architectures with multiple points of attachment[58]

- Intramolecular versions of CuAAC have been developed, enabling the construction of cyclic structures through the formation of triazole linkages within a single molecule. This approach has been used in the synthesis of complex natural products and drug candidates[59]

- Advanced CuAAC products have been utilized to label and track molecular interactions *in situ*. These applications provide insights into protein-protein interactions, enzyme dynamics, and cellular signaling pathways[28]

- CuAAC is known for its high atom economy, meaning that a substantial portion of the initial materials becomes part of the product, thereby minimizing waste generation, while often avoiding the use of toxic or expensive reagents and implementing the use of benign solvents. As a result, many features of CuAAC align with the principles of green chemistry[60]

1.4. Mechanistic aspects of CuAAC

In order to improve and broaden the applications of any synthetic methodology, it is essential to comprehend the reaction pathway(s) along with the probable intermediates and various transition states. Any postulated mechanism regarding a methodology must account for the kinetic credence of the various types of components involved in the reaction such as reactants, catalysts, solvents, etc., as well as the stereoselectivity and regiospecificity.[61] The CuAAC has also remained a comprehensive subject regarding its mechanistic studies wherein it has been established that while azides and alkynes typically engage in 1,3-dipolar cycloaddition through a concerted mechanism, DFT simulations conducted on monomeric copper acetylide complexes have confirmed that a stepwise approach is considerably preferred over this mechanism.[62]

1.4.1. The mononuclear mechanism by Sharpless *et al.*

Sharpless research group initially proposed a mononuclear mechanistic pathway for CuAAC involving a six-membered mononuclear copper(III) species.[63] It is possible to think of the first proposed mechanism as a crude outline for a more veritable diagram. It clarifies why the presence of copper(I) is essential for the progression of the reaction and why the resulting triazole is regiospecific, while also emphasizing the appropriate copper-alkyne and copper-azide interactions,[64,65] as shown in **figure 1.6**.

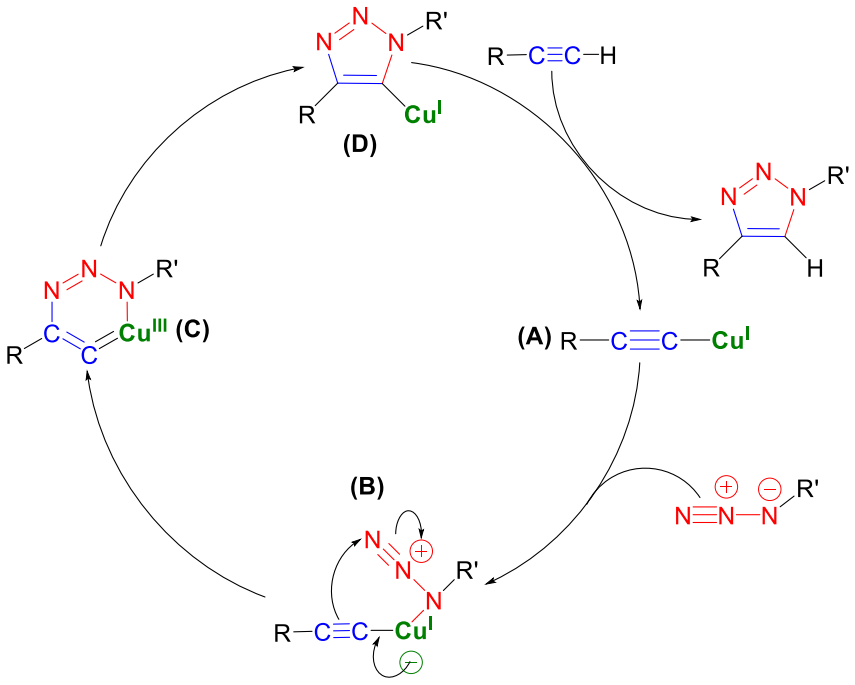

Figure 1.6: Mononuclear mechanism of CuAAC as proposed by Sharpless research group[8]

The mechanistic approach outlined in **figure 1.6** can be considered as a basic outline for a complete and more elucidated pathway. It clarifies the copper(I) dependency of the reaction and the regiospecificity of the 1,4-disubstituted 1,2,3 triazole. The σ-bonded copper(I) acetylide that must form and the azide that must coordinate with copper(I) through the alkylated nitrogen are both specified. The kinetic and structural research have revealed the refinements of this sequence since its conception.[65,66] The plausible mechanism was proposed to advance in the following sequential manner:

- Emergence of Cu(I)-acetylide complex (A) by the substitution of the labile alkynyl proton of the terminal alkyne with Cu(I)
- The coordination of azide group with the Cu(I)-acetylide complex through Cu(I) and alkylated nitrogen (B)
- Formation of a C-N bond resulting in the transformation of the azide-coordinated Cu(I) acetylide structure into a six-membered metallacycle (C) accompanied by change in the oxidation state of Cu from +1 to +3
- Generation of cuprous-triazolide complex (D) due to ring contraction in combination with the oxidation state reduction from Cu(III) to Cu(I)
- Protonation of triazolide complex to give the 1,2,3-triazole species

1.4.2. The binuclear mechanism by Fokin *et al.*

Fokin and Finn observed a rate order of two with regard to the concentration of copper(I) ions in both ligand-free and most ligand-containing CuAAC reactions, thereby suggesting that the rate-determining step involves two copper(I) ions. Molecular mechanics studies using density functional theory (DFT) agree with this concept,[66–68] predicting that a mechanistic approach involving binuclear copper(I)-acetylide complexes is preferable to a mononuclear pathway[69–71] (**figure 1.7**). The research in quantum mechanics corroborated this reaction pathway by demonstrating that the energy barrier for the reaction route using a binuclear structure is much lower than that for the reaction path including a mononuclear structure, which was found to be on the order of the noncatalyzed path. Furthermore, the conclusive evidence of the existence of bis(copper) intermediates has also been reported experimentally via isotopic labelling, separation, and electrospray ionisation mass spectrometry methods, thereby supporting the binuclear nature of the CuAAC process.[66,70]

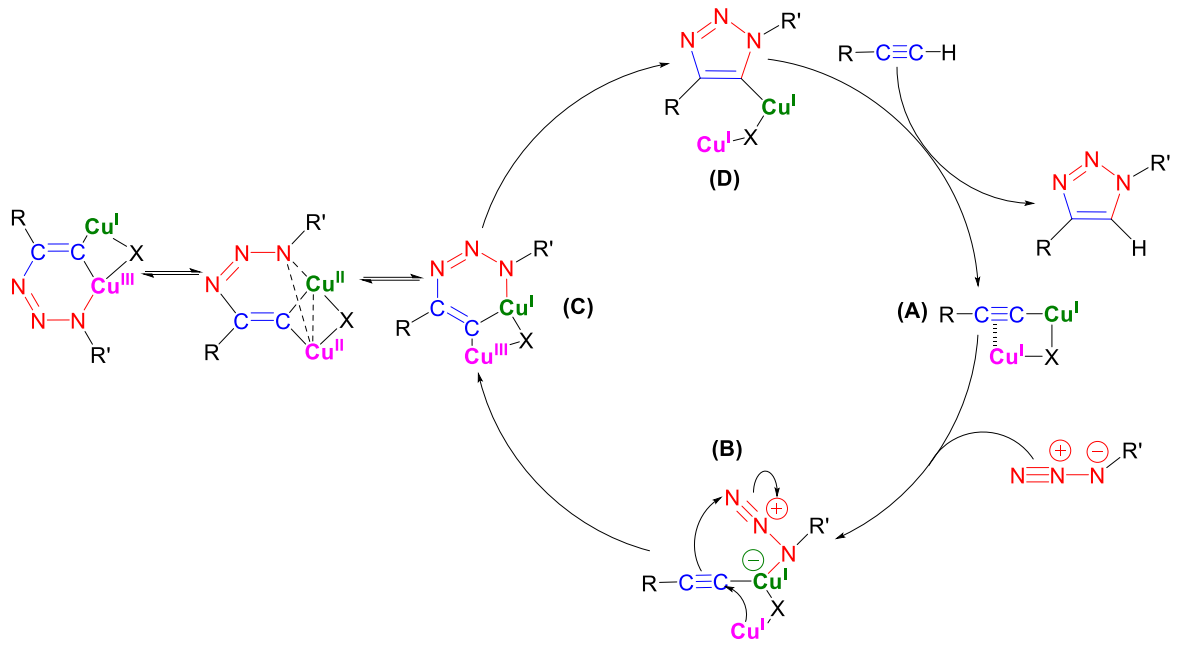

Figure 1.7: Binuclear mechanism of CuAAC as proposed by Finn and Fokin[72]

It was claimed that the conceivable mechanism would develop as follows:

- Formation of a σ, π-dicopper-acetylide complex (A)
- The coordination of azide group with the dicopper-acetylide complex (B) through one of the Cu(I) and the alkylated nitrogen leading to the formation of a ternary complex
- Oxidation of the other Cu(I) from +1 to +3 resulting in metallacycle formation (C)
- Ring contraction to yield the Cu(I)-triazolide complex (D) accompanied by the oxidation state reduction from Cu(III) to Cu(I)
- Protonation of triazolide complex to give the 1,2,3-triazole species

The activation barrier for the mononuclear mechanism is found to be greater than that of the uncatalyzed process. Furthermore, it has been established that the Cu(I) catalyst is unable to overcome the observed highest barrier for any concerted process, which stands at 23.7 kcal/mol, indicating its ineffectiveness to significantly impact the reaction rates. On the other hand, the activation barrier for the binuclear mechanism is determined to be reduced by as much as 11 kcal/mol compared to the uncatalyzed process, which explains the remarkable rate improvement observed under Cu(I) catalysis. As a result, the binuclear mechanism is strongly favoured over the mononuclear mechanism as supported by the DFT calculations and kinetic experiments.[65,72]

1.5. The 1,2,3-triazole ring

1.5.1. Structural aspects and properties

The 1,2,3-triazole is a five-membered, aromatic nitrogen heterocycle containing three nitrogen atoms in a five-membered ring[73,74] as represented in **figure 1.8**. Within a cyclic arrangement, all three nitrogen atoms are adjacently coupled with two carbon atoms and have two double bonds conjugating with the nitrogen lone pairs.[75,76] The aromatic nature of 1,4-disubstituted 1,2,3-triazoles stems from the sp^2 hybridization of all the atoms and hence the delocalization of the accessible 6π electrons of the ring.[77] The increasing demand for 1,2,3-triazoles in modern synthetic chemistry is largely due to their easy and modular synthesis using CuAAC click chemistry,[78] and the 1,2,3-triazole ring's unique structure and its significance in bioconjugation have made it a crucial building block, providing valuable tools for drug development, materials science, and biochemical research.

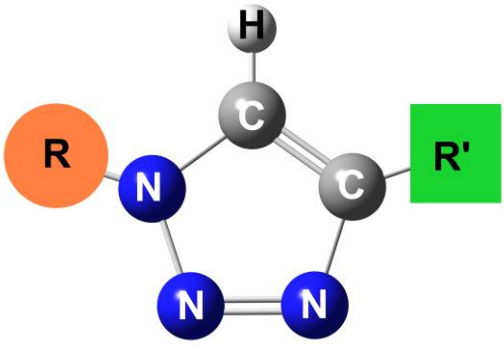

Figure 1.8: An illustration of 1H-1,2,3-triazole ring

The following are some key characteristics of 1,2,3-triazoles:

- The 1,2,3-triazole motif is intriguing in and of itself due to its strong dipole moment, hydrogen-bond donor (C-5 H) and acceptor (N-2 and N-3) sites, and cyclic nature.[79]
- The 1,2,3-triazole units have been shown to have a wide range of biological activity such as antibacterial and antiviral effects when included in synthetic compounds.[80,81]
- These moieties have the potential to function in the body at physiological pH levels without being negatively affected by protonation or changing their structure, which contrasts with the behavior of other aza-heterocycles.[82]
- The nitrogen-rich triazole is documented to implement hydrogen and halide bonding to form complexes with anions, or charge-assisted hydrogen and halogen bonds in the instance of triazolium salts.[83]

1.5.2. Potential Uses of 1,2,3-Triazoles

The CuAAC approach has been used globally to manufacture 1,2,3-triazole linked molecules having a wide variety of potential uses. It is a well-known fact that scaffolds based on 1,2,3-triazoles make up an important class of heterocycles, particularly in medicinal chemistry because 1,2,3-triazoles have demonstrated pharmacological activity[84,85] against a wide variety of pathogens. However, it is also important to note that these moieties have substantial operations in several other research zones, such as medicinal attributes,[86] proteomics,[87] polymer synthesis,[88,89] optical brightening agents,[90,91] drug discovery,[92] cellular bioimaging,[93] antimicrobial activity,[94] chemosensing,[95,96] etc. (**figure 1.9**)

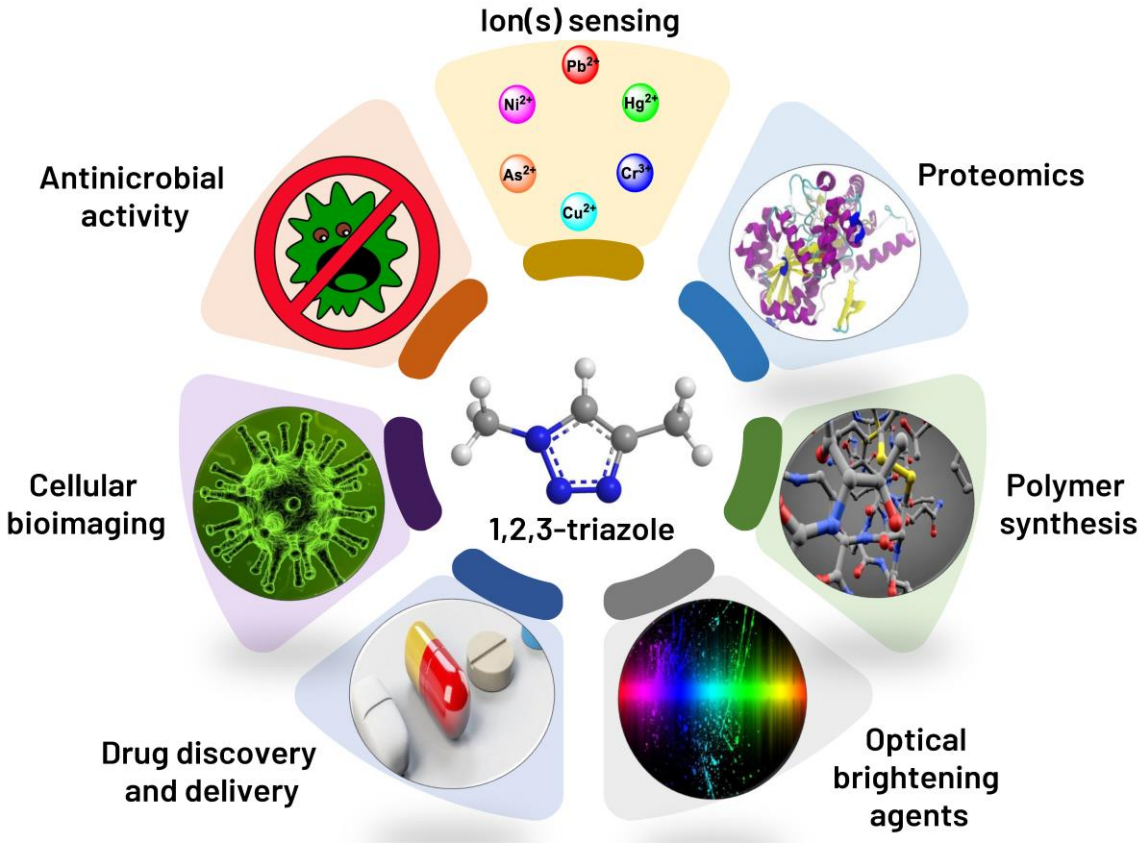

Figure 1.9: Diverse applications of 1,2,3-triazoles in several research areas[84–96]

While the uses of 1,2,3-triazoles are certainly noteworthy, chemosensing is arguably one of the most significant and extensively explored applications of 1,2,3-triazoles. Since the contamination of our environment (be it water bodies or soil/land) by the accumulation of some of the toxic heavy metal ions such as Arsenic, Chromium, Mercury, Cadmium, Lead, etc. in significantly dangerous concentrations has become a serious cause of concern,[97,98] therefore cost-effective and effectual methodology for toxic ions detection rapidly as well as efficiently has become of paramount importance and 1,2,3-triazole derivatives prepared through 'click chemistry' can substantiate to be a great asset for addressing this particular problem.[99]

1.6. Chemical Sensor

1.6.1. Concept and classification

To perform chemical sensing, a target molecule (analyte) interacts with a receptor (chemosensor), causing a readily observable change. The majority of chemical sensors rely on a binding event or chemical reaction to modify the absorption and/or emission properties of an attached fluorophore, while other chemosensors exhibit change in the redox potential or conformational changes.[100] This design principle, which leverages specific molecular interactions, has been instrumental in the development of a wide array of chemosensors tailored to identify and quantify a diverse range of substances that hold significance in both physiological and ecological contexts.[101] Chemical sensors possess the remarkable capability to transform various forms of chemical data, spanning from the precise measurement of individual components to the comprehensive characterization of an entire sample's chemical composition, into readily interpretable and actionable signals. Within an analyzer system, a chemical sensor stands as the foundational component, serving as the frontline data gatherer that interacts with the analyte. It is complemented by an array of essential components, including signal processing units for amplifying and refining the sensor's output, data processing systems for converting raw data into meaningful information, data storage capabilities for archiving valuable results, and precise sample delivery mechanisms that ensure a consistent and reliable flow of analytes to the sensor.[102]

Within meticulously controlled laboratory settings, the distinctive advantage lies in the ability to isolate and distinguish the analyte's signal from the complex matrix of other substances within the sample. This capability minimizes the necessity for extensive and often time-consuming sample pre-treatment procedures, streamlining the analytical process and providing researchers with more precise and efficient means of quantifying and characterizing target compounds, making laboratory analyses quicker and more accurate.[103] Chemical sensors are categorically classified based on the nature of their output signal and their operational principles,[104] as represented in **figure 1.10**. This systematic classification provides a structured framework for understanding and differentiating the diverse array of chemical sensors available. By grouping sensors into distinct categories, researchers can navigate the sensor landscape more effectively and select the most suitable sensor type, thereby optimizing sensor performance and analytical outcomes.

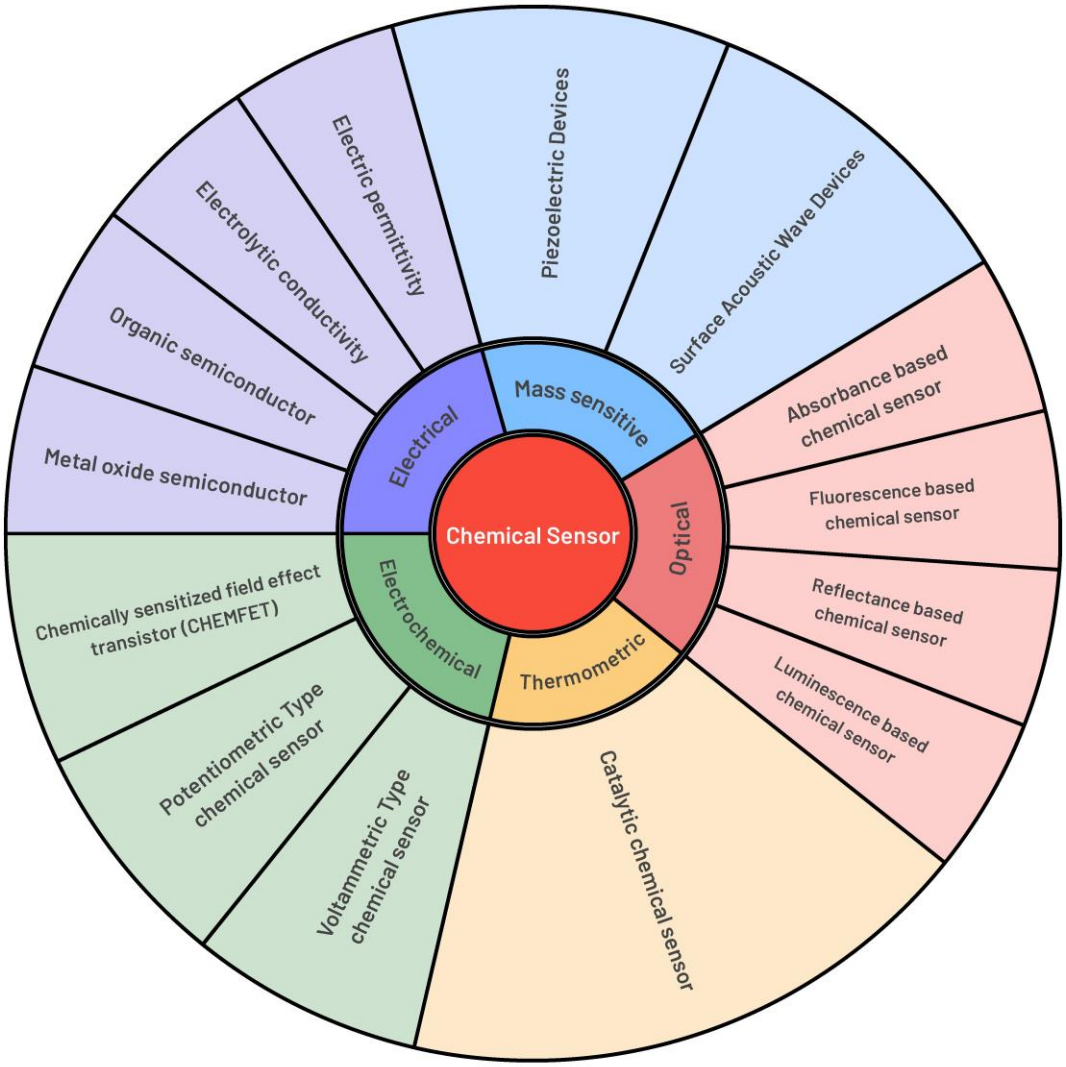

Figure 1.10: A pie chart representation for the classification of chemical sensors into various categories based upon the technique used[104]

- Optical sensors: The interlinkage between an analyte and a receptor portion of such a sensor causes changes in the overall optical phenomena, such as absorbance, fluorescence, reflectance, etc., which can be recorded by optical instruments.[100,105]

- Electrochemical sensors: An analyte and an electrode can interact electrochemically, and the resultant signal, which is essentially an effect of such electrochemical interactions can be transformed for useful interpretations.[106] Both electrical stimulation and spontaneous interaction under the zero-current state have been observed in cases of such effects and some examples include voltametric sensors, potentiometric sensors, etc.[107,108]

- Electrical sensors: No electrochemical activities take place in measurement-based electrical devices; rather, the signal is generated by the analyte's interaction with its surroundings, resulting in a change in electrical characteristics.[109]

- Mass sensitive sensors: Devices that are sensitive to mass do so by converting a variation in mass at a specifically modified surface into a variation in some other property of the substrate. The shift in mass results from the analyte's accumulation.[110]

- Thermometric sensors: Analyte-involved chemical reactions or adsorption processes that generate heat can be measured using thermometric instruments.[111]

1.6.2. Essential components of chemosensor

Any ligand designed to act as a chemosensor consists of three main parts: the receptor, which serves as the first line of interaction, not only offers a specific binding site for the target ion but also governs the chemosensor's sensitivity and selectivity. Meanwhile, the transducer or signal unit acts as the dynamic reporter, responding to the receptor-ion interaction by generating measurable photoluminescence changes. The spacer unit, a critical link between the receptor and the transducer, ensures optimal distance and flexibility, facilitating efficient molecular recognition and signal transmission within the chemosensor structure. (**figure 1.11**). Additionally, the receptor's cavity should have roughly the same size as the metal ion, allowing the ion to be precisely positioned within the cavity with no effort on the part of the ion. Using such voids for reversible ion adhesion by ionophores is a step towards modifying the chemosensor selectivity even further.[112,113] Each chemosensor has its own characteristics due to the specialized receptor unit that makes it work. The receptor, serving as the first line of interaction, not only offers a specific binding site for the target ion but also governs the chemosensor's sensitivity and selectivity. Meanwhile, the transducer or signal unit acts as the dynamic reporter, responding to the receptor-ion interaction by generating measurable photoluminescence changes. This integrated architecture forms the foundation of chemosensors, allowing them to convert molecular recognition events into easily detectable signals, making them invaluable tools in fields ranging from analytical chemistry to biomedical research.

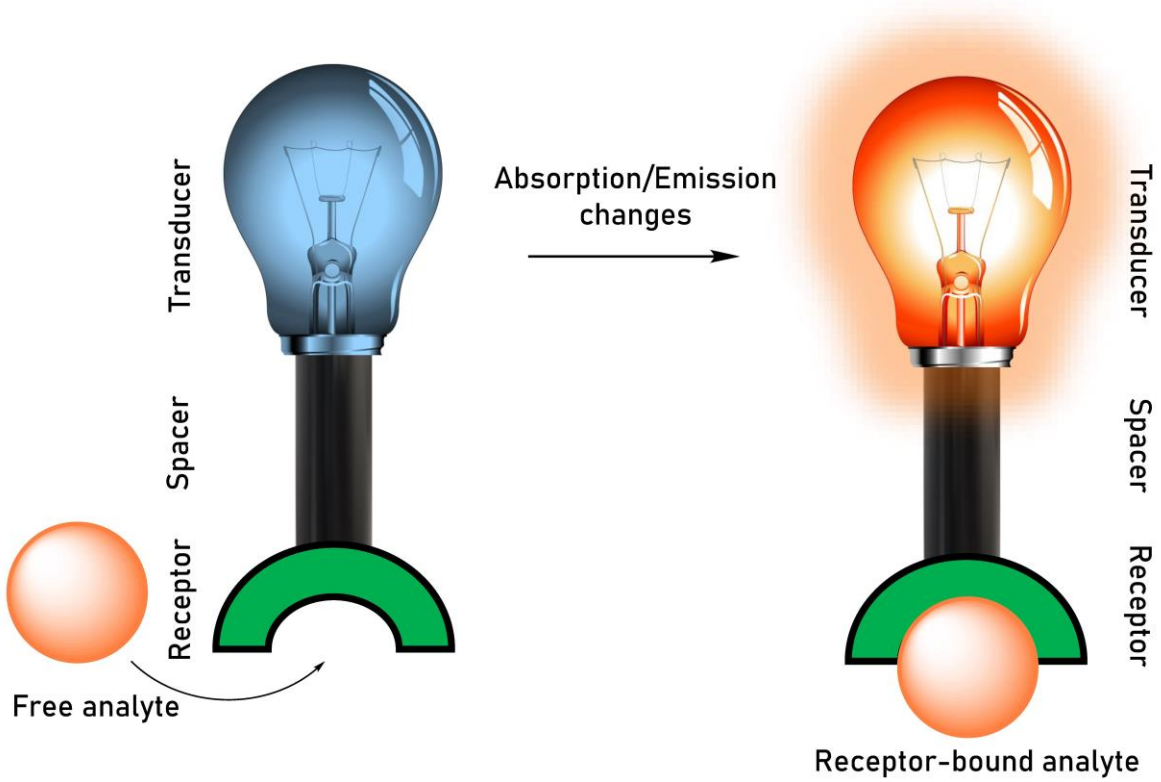

Figure 1.11: An illustration of the indispensable components of a chemosensor and the functions thereof

1.6.3. The sensing process

The whole procedure of chemosensing involves the target species, i.e., the guest connecting non-covalently with the receptor unit, i.e., the host in chemosensors, based on the host-guest relationship principle which in turn causes the transducer to exhibit photophysical changes to confirm the metal ion binding.[114,115] Additionally, the hard and soft acid-base (HSAB) concept, a fundamental principle in coordination chemistry, serves as a guiding framework for understanding how metal ions interact with chemosensors by elucidating the nuanced preferences of metal ions for certain ligands based on their electronic and structural characteristics.[116,117] In lieu of this theory, the metal ions categorized under soft acids such as Hg^{2+}, Pt^{2+}, Pd^{2+}, Ag^{+}, Au^{+} etc. preferentially bind with the ligands having donor atoms classified under soft bases such as sulphur, while the ligands having borderline bases such as nitrogen atoms have a binding appetite for borderline acids like Fe^{2+}, Co^{2+}, Cs^{2+}, Pb^{2+} etc. Molecules with chromophoric or fluorophoric units are an intriguing type of chemosensing material since they possess all the desirable characteristics of a chemosensor. These compounds can incorporate detecting features with optical transduction, i.e., an alteration in the absorbance and/or fluorescence.[118–120]

1.7. Metal ion recognition by 1,2,3-triazoles

The analytical methods for metal ions recognition have expanded over past few decades, and now include several techniques ranging from Atomic Absorption Spectroscopy (AAS)[121,122] and voltammetry to Inductively Coupled Plasma Mass Spectrometry (ICP-MS)[123,124] and electrochemical techniques. Despite their long-standing use in various fields, it is important to recognize the substantial limitations associated with these methods. These include expensive equipment, lack of precision in distinguishing similar substances, slow response times, intricate procedures, and environmental concerns.[125,126] These drawbacks collectively hinder the versatility and accessibility of these techniques, prompting the ongoing search for more efficient and cost-effective alternatives in scientific research and industrial applications. As a result of these problems, their application is constrained in achieving the desired effects. But 1,2,3-triazole moiety-containing organic compounds have remarkable success in the detection of a wide range of ions, owing to the presence of nitrogen lone pairs (the 1,2,3-triazole ring is a very electron-rich site that can be coordinated by metal electrophile). Thus, the presence of an electron-rich, non-hydrolyzable 1,2,3-triazole ring in a compound makes it possible for the positively charged metal ions to interact with the ring via several coordination strategies[127,128] as illustrated in **figure 1.12**. Furthermore, the exocyclic groups that are meant to attach with this triazole ring by exchanging the existing H- atoms can be electron rich in nature, hence improving the ring's functionality.[129] To rephrase, click chemistry allows us to consciously build molecules to have the qualities we find useful and desirable.

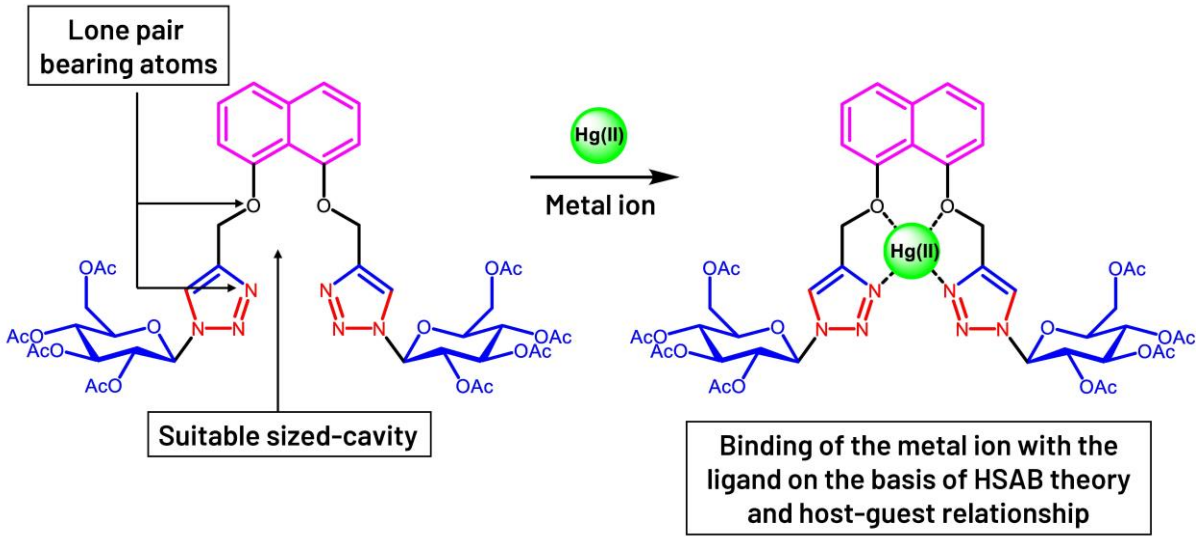

Figure 1.12: An illustration of metal ion-binding with the ligand in accordance with the host-guest relationship and HSAB concept[130]

1.8. Determination of chemosensing behaviour via spectroscopic analysis

1.8.1. UV-Vis spectroscopy

For metal ion recognition, UV-absorption spectroscopy is a fast, non-destructive, high-resolution, and low-cost alternative to conventional spectroscopic methods. In addition, recent instrumental and theoretical advancements have enhanced its usefulness, leading to a modest renaissance in its use for chemosensing purposes.[131] As UV absorption spectrophotometers are commonly found in biochemical labs, this method could be utilized to provide evidence for metal ion recognition by the chemosensors in the absence of more specialist equipment. Typically, chemosensors tend to have a pronounced peak in the UV-Vis region of the spectrum. This is made up of several bands that overlap one another and originate mostly from aromatic or conjugated residues. In great part, $n \rightarrow \pi^*$ and $\pi \rightarrow \pi^*$ transitions involving the electrons of their aromatic rings are responsible for these signals.[132] To confirm ion recognition, the changes in the absorption maxima and/or intensities are compared between the absorption spectra of the pure ligand and the metal-ligand solution (**figure 1.13**). The addition of metal ions could alter the energy difference between the ligand's ground state and its excited state, thereby resulting in a shift of the absorption peak and/or a change in the peak's intensity.[133,134] Therefore, the detection of metal ions by the ligand under observation can be understood by comparing the spectra before and after the addition of ions to the molecule.

1.8.2. Fluorescence spectroscopy

When a molecule absorbs photons of a specific wavelength, it transitions from its ground state to an excited state. Following a brief interval, the molecule emits photons upon returning to the ground state. This emitted light possesses longer wavelengths than the absorbed photons, yielding a characteristic fluorescence spectrum[135] and can be utilized to obtain information about the ion recognition ability of a ligand. The molecular entities exhibiting fluorescence emission on excitation with a suitable wavelength are referred to as fluorophores, whose emission intensity depends on three factors: the concentration of the sample, the absorbing power, i.e., extinction coefficient at the excitation wavelength, and the quantum yield.[136,137] Since the emission spectra obtained is based on fluorescence, it can be used in the same way as UV-Vis spectroscopy to estimate the metal binding ability of a ligand probe by observing any significant influence of the metal ions on the position and/or intensity of the fluorescence peak (**figure 1.13**) if metal binding with the probe occurs.[138–140]

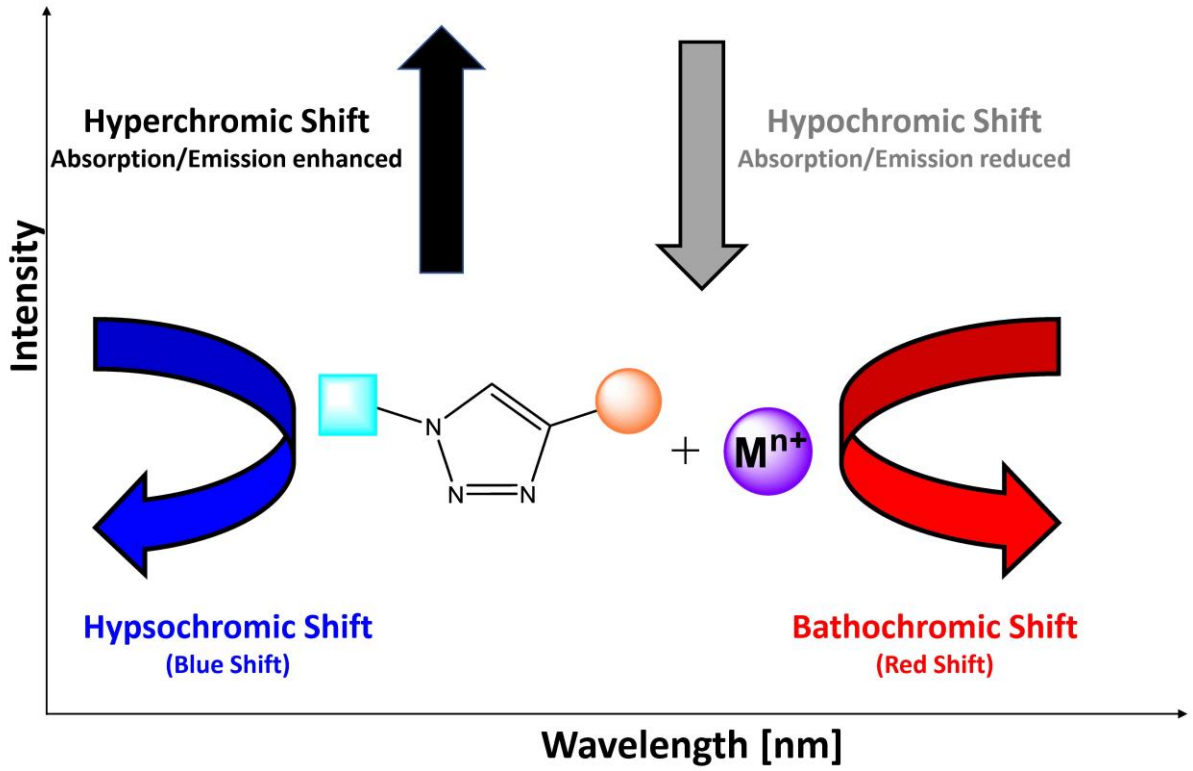

Figure 1.13: Different alterations exhibited in the absorption/emission spectrum of a chemosensing probe on binding with an analyte

1.9. Conclusion

The CuAAC 'click' methodology, known for its remarkable efficiency, affordability, and biocompatibility, stands as a paramount approach for seamlessly joining molecular entities. Beyond its role as a connector, this technique brings forth the intriguing world of 1,2,3-triazole rings, offering a myriad of practical applications. Its versatility extends to the substrates employed, enabling the creation of diverse 1,2,3-triazole-appended conjugated systems. These systems possess an inherent capability for metal-ion recognition, presenting a promising solution in the ongoing battle against the escalating menace of environmental contamination caused by toxic heavy metal ions. With CuAAC at its core, this scientific innovation not only facilitates molecular bonding but also opens doors to safeguarding our planet's ecological balance. This innovative utilization of the CuAAC 'click' reaction is paving the way for the creation of 1,2,3-triazole-based optical sensors which are engineered to excel in the precise detection of metal ions through absorption and/or emission spectroscopy techniques. This strategic fusion of click chemistry and spectroscopy promises to revolutionize the field of analytical chemistry, offering selective and sensitive tools for monitoring and mitigating the

metal ions presence in various environmental and industrial settings. The contemporary research is underway that seeks to elucidate the mechanism through which a triazole ring binds metals, while the reported literature is reminiscent that the performance of such a 1,2,3-triazole derivative is affected by several variables, including solvent, counterion, molecular, and electronic structures. The development of more sensitive and selective metal ion sensors may be made possible by future systematic research that provide light on definite patterns in metal ion binding.

References

1 J. E. Hein and V. V Fokin, *Chem. Soc. Rev.*, 2010, **39**, 1302–1315.

2 M. M. Heravi, V. Zadsirjan, M. Dehghani and T. Ahmadi, *Tetrahedron*, 2018, **74**, 3391–3457.

3 M. S. Singh, S. Chowdhury and S. Koley, *Tetrahedron*, 2016, **72**, 5257–5283.

4 J. E. Moses and A. D. Moorhouse, *Chem. Soc. Rev.*, 2007, **36**, 1249–1262.

5 H. C. Kolb, M. G. Finn and K. B. Sharpless, *Angew. Chem. Int. Ed.*, 2001, **40**, 2004–2021.

6 C. O. Kappe and E. Van Der Eycken, *Chem. Soc. Rev.*, 2010, **39**, 1280–1290.

7 S. Chassaing, V. Bénéteau and P. Pale, *Catal. Sci. Technol.*, 2016, **6**, 923–957.

8 V. V Rostovtsev, L. G. Green, V. V Fokin and K. B. Sharpless, *Angew. Chem.*, 2002, **41**, 2708–2711.

9 M. Pagel, *J. Pept. Sci.*, 2019, **25**, 1–9.

10 A. C. Knall and C. Slugovc, *Chem. Soc. Rev.*, 2013, **42**, 5131–5142.

11 C. E. Hoyle and C. N. Bowman, *Angew. Chem. Int. Ed.*, 2010, **49**, 1540–1573.

12 C. E. Hoyle, A. B. Lowe and C. N. Bowman, *Chem. Soc. Rev.*, 2010, **39**, 1355–1387.

13 J. Tummatorn, P. Batsomboon, R. J. Clark, I. V. Alabugin and G. B. Dudley, *J. Org. Chem.*, 2012, **77**, 2093–2097.

14 T. Harris and I. V. Alabugin, *Mendeleev Commun.*, 2019, **29**, 237–248.

15 N. J. Agard, J. A. Prescher and C. R. Bertozzi, *J. Am. Chem. Soc.*, 2004, **126**, 15046–15047.

16 D. A. MacKenzie, A. R. Sherratt, M. Chigrinova, L. L. W. Cheung and J. P. Pezacki, *Curr. Opin. Chem. Biol.*, 2014, **21**, 81–88.

17 F. L. Lin, H. M. Hoyt, H. Van Halbeek, R. G. Bergman and C. R. Bertozzi, *J. Am. Chem. Soc.*, 2005, **127**, 2686–2695.

18 M. Köhn and R. Breinbauer, *Angew. Chem. Int. Ed.*, 2004, **43**, 3106–3116.

19 C. Bednarek, I. Wehl, N. Jung, U. Schepers and S. Bräse, *Chem. Rev.*, 2020, **120**, 4301–4354.

20 N. J. Agard, J. A. Prescher and C. R. Bertozzi, *J. Am. Chem. Soc.*, 2004, **126**, 15046–15047.

21 E. Kim and H. Koo, *Chem. Sci.*, 2019, **10**, 7835–7851.

22 J. P. Meyer, P. Adumeau, J. S. Lewis and B. M. Zeglis, *Bioconjug. Chem.*, 2016, **27**, 2791–2807.

23 J. C. Jewett and C. R. Bertozzi, *Chem. Soc. Rev.*, 2010, **39**, 1272–1279.

24 E. Mauri and F. Rossi, in *Bioresorbable Polymers for Biomedical Applications: From Fundamentals to Translational Medicine*, eds. G. Perale and J. Hilborn, Elsevier Ltd, Amsterdam, 1st edn., 2017, pp. 303–329.

25 D. D. Díaz, S. Punna, P. Holzer, A. K. Mcpherson, K. B. Sharpless, V. V Fokin and M. G. Finn, *J. Polym. Sci. A Polym. Chem.*, 2004, **42**, 4392–4403.

26 C. Le Droumaguet, C. Wang and Q. Wang, *Chem. Sci.*, 2010, **39**, 1233–1239.

27 B. L. Oliveira, Z. Guo and G. J. L. Bernardes, *Chem. Soc. Rev.*, 2017, **46**, 4895–4950.

28 V. Hong, N. F. Steinmetz, M. Manchester and M. G. Finn, *Bioconjug. Chem.*, 2010, **21**, 1912–1916.

29 K. B. Sharpless and R. Manetsch, *Expert Opin. Drug. Discov.*, 2006, 1, 525–538.

30 R. Manetsch, A. Krasiński, Z. Radić, J. Raushel, P. Taylor, K. B. Sharpless and H. C. Kolb, *J. Am. Chem. Soc.*, 2004, **126**, 12809–12818.

31 S. K. Mamidyala and M. G. Finn, *Chem. Soc. Rev.*, 2010, **39**, 1252–1261.

32 V. P. Mocharla, B. Colasson, L. V Lee, S. Röper, K. B. Sharpless, C. Wong and H. C. Kolb, *Angew. Chem.*, 2005, **117**, 118–122.

33 R. Huisgen, *Angew. Chem. Int. Ed.*, 1963, **2**, 565–632.

34 C. Nájera, J. M. Sansano and M. Yus, *Org. Biomol. Chem.*, 2015, **13**, 8596–8636.

35 M. Kissane and A. R. Maguire, *Chem. Soc. Rev.*, 2010, **39**, 845–883.

36 R. Huisgen, *Proc. Chem. Soc.*, 1964, 101.

37 A. Ponti and G. Molteni, *European J. Org. Chem.*, 2020, **2020**, 6173–6191.

38 J. Plumet, *Chempluschem*, 2020, **85**, 2252–2271.

39 C. J. Pickens, S. N. Johnson, M. M. Pressnall, M. A. Leon and C. J. Berkland, *Bioconjug. Chem.*, 2018, **29**, 686–701.

40 M. Breugst and H. U. Reissig, *Angew. Chem. Int. Ed.*, 2020, **59**, 12293–12307.

41 A. Padwa, *Angew. Chem. Int. Ed.*, 1976, **15**, 123–180.

42 M. Danese, M. Bon, G. Piccini and D. Passerone, *Phys. Chem. Chem. Phys.*, 2019, **21**, 19281–19287.

43 M. Meldal and C. W. Tomøe, *Chem. Rev.*, 2008, **108**, 2952–3015.

44 C. Wang, D. Ikhlef, S. Kahlal, J. Y. Saillard and D. Astruc, *Coord. Chem. Rev.*, 2016, **316**, 1–20.

45 E. Haldón, M. C. Nicasio and P. J. Pérez, *Org. Biomol. Chem.*, 2015, **13**, 9528–9550.

46 E. J. Yoo, M. Ahlquist, S. H. Kim, I. Bae, V. V Fokin, K. B. Sharpless and S. Chang, *Angew. Chem. Int. Ed.*, 2007, **46**, 1730–1733.

47 M. Meldal and F. Diness, *Trends. Chem.*, 2020, **2**, 569–584.

48 P. Appukkuttan, W. Dehaen, V. V Fokin and E. Van Der Eycken, *Org. Lett.*, 2004, **6**, 4223–4225.

49 J. Totobenazara and A. J. Burke, *Tetrahedron Lett.*, 2015, **56**, 2853–2859.

50 H. Nulwala, K. Takizawa, A. Odukale, A. Khan, R. J. Thibault, B. R. Taft, B. H. Lipshutz and C. J. Hawker, *Macromolecules*, 2009, **42**, 6068–6074.

51 N. K. Devaraj and J. P. Collman, *QSAR Comb. Sci.*, 2007, **26**, 1253–1260.

52 M. G. Finn and V. V Fokin, *Chem. Soc. Rev.*, 2010, **39**, 1231–1232.

53 V. Hong, S. I. Presolski, C. Ma and M. G. Finn, *Angew. Chem.*, 2009, **121**, 10063–10067.

54 C. S. Mckay and M. G. Finn, *Chem. Biol.*, 2014, **21**, 1075–1101.

55 S. I. Presolski, V. P. Hong and M. G. Finn, *Curr. Protoc. Chem. Biol.*, 2011, **3**, 153–162.

56 S. Neumann, M. Biewend, S. Rana and W. H. Binder, *Macromol. Rapid. Commun.*, 2020, 41, 1900359.

57 Z. P. Demko and K. B. Sharpless, *Angew. Chem.*, 2002, **41**, 2110–2113.

58 X. Wang, B. Huang, X. Liu and P. Zhan, *Drug Discov. Today*, 2016, **21**, 118–132.

59 D. Núñez-Villanueva and C. A. Hunter, *Acc. Chem. Res.*, 2021, **54**, 1298–1306.

60 N. George, G. Singh, R. Singh, G. Singh, Anita Devi, H. Singh, G. Kaur and J. Singh, *Sustain. Chem. Pharm.*, 2022, **30**, 100824.

61 V. D. Bock, H. Hiemstra and J. H. Van Maarseveen, *European J. Org. Chem.*, 2006, 51–68.

62 D. Cantillo, M. Ávalos, R. Babiano, P. Cintas, J. L. Jiménez and J. C. Palacios, *Org. Biomol. Chem.*, 2011, **9**, 2952–2958.

63 V. O. Rodionov, S. I. Presolski, D. D. Díaz, V. V. Fokin and M. G. Finn, *J. Am. Chem. Soc.*, 2007, **129**, 12705–12712.

64 C. Özen and N. Ş. Tüzün, *J. Mol. Catal. A Chem.*, 2017, **426**, 150–157.

65 L. Zhu, C. J. Brassard, X. Zhang, P. M. Guha and R. J. Clark, *Chem. Rec.*, 2016, **16**, 1501–1517.

66 Y. Özkllç and N. S. Tüzün, *Organometallics*, 2016, **35**, 2589–2599.

67 Y. Fang, K. Bao, P. Zhang, H. Sheng, Y. Yun, S. X. Hu, D. Astruc and M. Zhu, *J. Am. Chem. Soc.*, 2021, **143**, 1768–1772.

68 C. Özen and N. Ş. Tüzün, *J. Mol. Graph Model*, 2012, **34**, 101–107.

69 R. S. Gomes, G. A. M. Jardim, R. L. de Carvalho, M. H. Araujo and E. N. da Silva Júnior, *Tetrahedron*, 2019, **75**, 3697–3712.

70 B. T. Worrell, J. A. Malik and V. V. Fokin, *Science*, 2013, **340**, 457–460.

71 L. Liang and D. Astruc, *Coord. Chem. Rev.*, 2011, **255**, 2933–2945.

72 V. O. Rodionov, V. V. Fokin and M. G. Finn, *Angew. Chem. Int. Ed.*, 2005, **44**, 2210–2215.

73 K. Wang, M. Chen, Q. Wang, X. Shi and J. K. Lee, *J. Org. Chem.*, 2013, **78**, 7249–7258.

74 A. De Nino, L. Maiuolo, P. Costanzo, V. Algieri, A. Jiritano, F. Olivito and M. A. Tallarida, *Catalysts*, 2021, **11**, 1–48.

75 A. E. Fernandes, A. M. Jonas and O. Riant, *Tetrahedron*, 2014, 70, 1709–1731.

76 G. Aromí, L. A. Barrios, O. Roubeau and P. Gamez, *Coord. Chem. Rev.*, 2011, **255**, 485–546.

77 H. Wamhoff, in *Comprehensive Heterocyclic Chemistry*, eds. A. R. Katritzky and C. W. Rees, Elsevier Inc., Amsterdam, 1984, vol. 5, pp. 669–732.

78 B. I. Taggert, C. Walker, D. Chen and U. Wille, *Sci. Rep.*, 2021, **11**, 1–12.

79 V. Ji Ram, A. Sethi, M. Nath and R. Pratap, in *The Chemistry of Heterocycles*, Elsevier Inc., Amsterdam, 1st edn., 2019, pp. 149–478.

80 K. Bozorov, J. Zhao and H. A. Aisa, *Bioorg. Med. Chem.*, 2019, **27**, 3511–3531.

81 A. Said Stålsmeden, A. J. Paterson, I. C. Szigyártó, L. Thunberg, J. R. Johansson, T. Beke-Somfai and N. Kann, *Org. Biomol. Chem.*, 2020, **18**, 1957–1967.

82 L. da S. M. Forezi, C. G. S. Lima, A. A. P. Amaral, P. G. Ferreira, M. C. B. V. de Souza, A. C. Cunha, F. de C. da Silva and V. F. Ferreira, *Chem. Rec.*, 2021, **21**, 2782–2807.

83 B. Schulze and U. S. Schubert, *Chem. Soc. Rev.*, 2014, **43**, 2522–2571.

84 A. Massarotti, S. Aprile, V. Mercalli, E. Del Grosso, G. Grosa, G. Sorba and G. C. Tron, *ChemMedChem*, 2014, **9**, 2497–2508.

85 S. G. Agalave, S. R. Maujan and V. S. Pore, *Chem. Asian J.*, 2011, **6**, 2696–2718.

86 D. Dheer, V. Singh and R. Shankar, *Bioorg. Chem.*, 2017, **71**, 30–54.

87 F. L. Zhan, S. Y. Gao, Y. D. Xie, J. M. Zhang, Y. Li and N. Liu, *Chin. J. Anal. Chem.*, 2020, **48**, 431–438.

88 D. Döhler, P. Michael and W. H. Binder, *Acc. Chem. Res.*, 2017, **50**, 2610–2620.

89 M. Meldal, *Macromol. Rapid Commun.*, 2008, 29, 1016–1051.

90 J. Huo, Z. Hu, D. Chen, S. Luo, Z. Wang, Y. Gao, M. Zhang and H. Chen, *ACS Omega*, 2017, **2**, 5557–5564.

91 J. P. Huo, J. C. Luo, W. Wu, J. F. Xiong, G. Z. Mo and Z. Y. Wang, *Ind. Eng. Chem. Res.*, 2013, **52**, 11850–11857.

92 C. García-Astrain and L. Avérous, *Carbohydr. Polym.*, 2018, **190**, 271–280.

93 H. Yang, L. Li, L. Wan, Z. Zhou and S. Yang, *Inorg. Chem. Commun.*, 2010, **13**, 1387–1390.

94 A. Rani, G. Singh, A. Singh, U. Maqbool, G. Kaur and J. Singh, *RSC Adv.*, 2020, **10**, 5610–5635.

95 B. xing Shen and Y. Qian, *Sens. Actuators B Chem.*, 2017, **239**, 226–234.

96 L. Yuan, W. Lin, K. Zheng and S. Zhu, *Acc. Chem. Res.*, 2013, **46**, 1462–1473.

97 J. G. Dórea, *Environ. Res.*, 2020, **188**, 109734.

98 C. Zamora-Ledezma, D. Negrete-Bolagay, F. Figueroa, E. Zamora-Ledezma, M. Ni, F. Alexis and V. H. Guerrero, *Environ. Technol. Innov.*, 2021, **22**, 101504.

99 F. Ahmed and H. Xiong, *Dyes. Pigm.*, 2021, **185**, 108905.

100 P. Gruber, M. P. C. Marques, N. Szita and T. Mayr, *Lab. Chip*, 2017, **17**, 2693–2712.

101 J. J. Bryant and U. H. F. Bunz, *Chem. Asian J.*, 2013, **8**, 1354–1367.

102 C. McDonagh, C. S. Burke and B. D. MacCraith, *Chem. Rev.*, 2008, **108**, 400–422.

103 A. P. De Silva, H. Q. N. Gunaratne, T. Gunnlaugsson, A. J. M. Huxley, C. P. McCoy, J. T. Rademacher and T. E. Rice, *Chem. Rev.*, 1997, **97**, 1515–1566.

104 A. Hulanicki, S. Glab and F. Ingman, *Pure Appl. Chem.*, 1991, **63**, 1247–1250.

105 L. Prodi, *New J. Chem.*, 2005, **29**, 20–31.

106 S. E. Zohora, A. M. Khan and N. Hundewale, *Adv. Intell. Syst. Comput.*, 2013, **178**, 177–184.

107 G. Maduraiveeran, M. Sasidharan and V. Ganesan, *Biosens. Bioelectron.*, 2018, **103**, 113–129.

108 B. J. Privett, J. H. Shin and M. H. Schoenfisch, *Anal. Chem.*, 2010, **82**, 4723–4741.

109 Q. He, S. Wu, Z. Yin and H. Zhang, *Chem. Sci.*, 2012, **3**, 1764–1772.

110 A. N. Kursunlu and E. Güler, *J. Mol. Struct.*, 2017, **1134**, 345–349.

111 H. Yukawa, M. Fujiwara, K. Kobayashi, Y. Kumon, K. Miyaji, Y. Nishimura, K. Oshimi, Y. Umehara, Y. Teki, T. Iwasaki, M. Hatano, H. Hashimoto and Y. Baba, *Nanoscale Adv.*, 2020, **2**, 1859–1868.

112 K. P. Carter, A. M. Young and A. E. Palmer, *Chem. Rev.*, 2014, **114**, 4564–4601.

113 R. Nagarajan, C. Varadaraju and K. H. Lee, *Dyes. Pigm.*, 2021, **191**, 109331.

114 X. Ma and Y. Zhao, *Chem. Rev.*, 2015, **115**, 7794–7839.

115 H. -J Schneider, *Angew. Chem. Int. Ed.*, 1991, **30**, 1417–1436.

116 R. G. Pearson, *J. Am. Chem. Soc.*, 1963, **85**, 3533–3539.

117 T. B. Kinraide, *Environ. Toxicol. Chem.*, 2009, **28**, 525–533.

118 B. Rathinam, C. C. Chien, B. C. Chen and J. H. Liu, *Tetrahedron*, 2013, **69**, 235–241.

119 S. Ast, S. Kuke, P. J. Rutledge and M. H. Todd, *Eur. J. Inorg. Chem.*, 2015, **2015**, 58–66.

120 D. Wu, A. C. Sedgwick, T. Gunnlaugsson, E. U. Akkaya, J. Yoon and T. D. James, *Chem. Soc. Rev.*, 2017, **46**, 7105–7123.

121 M. N. Oviedo, E. F. Fiorentini, A. A. Lemos, M. B. Botella and R. G. Wuilloud, *Microchem. J.*, 2020, **159**, 105386.

122 V. Zarezade, M. Behbahani, F. Omidi, H. S. Abandansari and G. Hesam, *RSC Adv.*, 2016, **6**, 103499–103507.

123 Q. Liang, H. Jing and D. C. Gregoire, *Talanta*, 2000, **51**, 507–513.

124 K. X. Yang, K. Swami and L. Husain, *Spectrochim. Acta Part B At. Spectrosc.*, 2002, **57**, 73–84.

125 G. Singh, Sanchita, A. Singh, G. Sharma, P. Kalra, Pawan, J. Singh, S. Soni and J. Kaur, *J. Mol. Struct.*, 2020, **1216**, 128220.

126 Y. Zhang, T. Ren, H. Tian, B. Jin and J. He, *ACS Appl. Mater. Interfaces*, 2018, **10**, 26705–26712.

127 S. B. Maity and P. K. Bharadwaj, *Inorg. Chem.*, 2013, **52**, 1161–1163.

128 D. Mandal, A. Thakur and S. Ghosh, *Polyhedron*, 2013, **52**, 1109–1117.

129 D. Mandal, P. Deb, B. Mondal, A. Thakur, J. Ponniah S and S. Ghosh, *RSC Adv.*, 2013, **3**, 18614–18625.

130 A. Hemamalini and T. M. Das, *New J. Chem.*, 2013, **37**, 2419–2425.

131 R. Esfandiary and C. R. Middaugh, in *Analysis of Aggregates and Particles in Protein Pharmaceuticals*, eds. H.-C. Mahler and W. Jiskoot, John Wiley & Sons, Inc., NJ, USA, 1st edn., 2012, pp. 170–200.

132 W. Mäntele and E. Deniz, *Spectrochim. Acta A Mol. Biomol. Spectrosc.*, 2017, **173**, 965–968.

133 J. Jia, A. Wu and S. Luan, *Colloids Surf. A Physicochem. Eng. Asp.*, 2014, **449**, 1–7.

134 Sudheer, V. Kumar, P. Kumar and R. Gupta, *New J. Chem.*, 2020, **44**, 13285–13294.

135 G. M. Strasburg and R. D. Ludescher, *Trends Food Sci. Technol.*, 1995, 6, 69–75.

136 N. Ramanujam, *Neoplasia*, 2000, **2**, 89–117.

137 K. R. Murphy, C. A. Stedmon, D. Graeber and R. Bro, *Anal. Methods*, 2013, **5**, 6557–6566.

138 A. Kaur, Z. Lim, K. Yang and E. J. New, in *Comprehensive Supramolecular Chemistry II*, ed. J. L. Atwood, Elsevier, Amsterdam, 2nd edn., 2017, vol. 8, pp. 295–317.

139 E. M. Carstea, J. Bridgeman, A. Baker and D. M. Reynolds, *Water Res.*, 2016, **95**, 205–219.

140 A. Rengaraj, P. Puthiaraj, Y. Haldorai, N. S. Heo, S. K. Hwang, Y. K. Han, S. Kwon, W. S. Ahn and Y. S. Huh, *ACS Appl. Mater. Interfaces*, 2016, **8**, 8947–8955.

Chapter II

Review of Literature

This section is a comprehensive review of the approaches taken into consideration and implemented in the conducted research. It provides a detailed study of the literature on Nitrogen-based heterocyclic compounds utilized for chemosensing as well as an overview of the spectroscopic techniques for characterizing the manufactured molecules; and all the stages involved in the synthesis of the molecules under investigation till their application.

2.1. Heterocycles in organic chemistry

2.1.1. A general overview

Compounds having a cyclic structure that includes elements other than carbon and hydrogen, such as oxygen, nitrogen, sulfur, etc., are referred to be heterocyclic, in the sense that the term 'heterocycle' itself refers to the presence of different atoms in a ring structure, as opposed to a homocyclic compound, where the ring consists only of carbon atoms. More than half of all organic compounds are heterocycles, making them an exceptionally significant family of molecules having wide applications.[1–3] Some heterocyclic compounds are inorganic, but the ring structure of most of the compounds often includes at least one carbon atom and other heteroatoms like sulfur, oxygen, or nitrogen, making up both aromatic and non-aromatic ring structures. The presence of heteroatoms imparts different electronic and chemical properties to the heterocycles compared to their all-carbon counterparts, as the heteroatoms can alter the reactivity, acidity/basicity, and overall chemical behavior of the compounds.[4] Heterocyclic compounds can exhibit aromaticity provided that the ring satisfies the criteria, and such compounds often have enhanced stability compared to the non-aromatic heterocycles. In contrast to the more complicated reactivity seen in non-aromatic systems, the reactivity of aromatic heterocycles is a mix of the normal non-cyclic derivatives and the effect of the heteroatoms involved, making aromatic heterocycles a more interesting class of compounds, as understanding the structural properties of heterocyclic compounds is crucial for predicting their behavior, reactivity, and interactions in various chemical and biological processes.[5–7] Heterocyclic compounds encompass a wide range of structures, including five-membered (e.g., pyrrole, furan, thiophene), six-membered (e.g., pyridine, pyrimidine, pyrazine), and larger ring systems (e.g., indole, quinoline, porphyrins). The arrangement of atoms, the number of rings, and the presence of different heteroatoms contribute to the diversity of these compounds.[2,8–10] **Figure 2.1** shows the different heterocyclic compounds, both aromatic as well as non-aromatic, grouped in accordance with the ring size, i.e., 3-membered, 4-membered, 5-membered, 6-membered, and fused heterocycles. The heterocyclic molecule of interest, the required heteroatom(s), and the accessible starting materials dictate the approach used for the synthesis of these compounds. As a result, synthetic organic chemistry is still driven by the pursuit of novel techniques and the strategic use of established methods for the synthesis of complex heterocyclic molecules.[11–17]

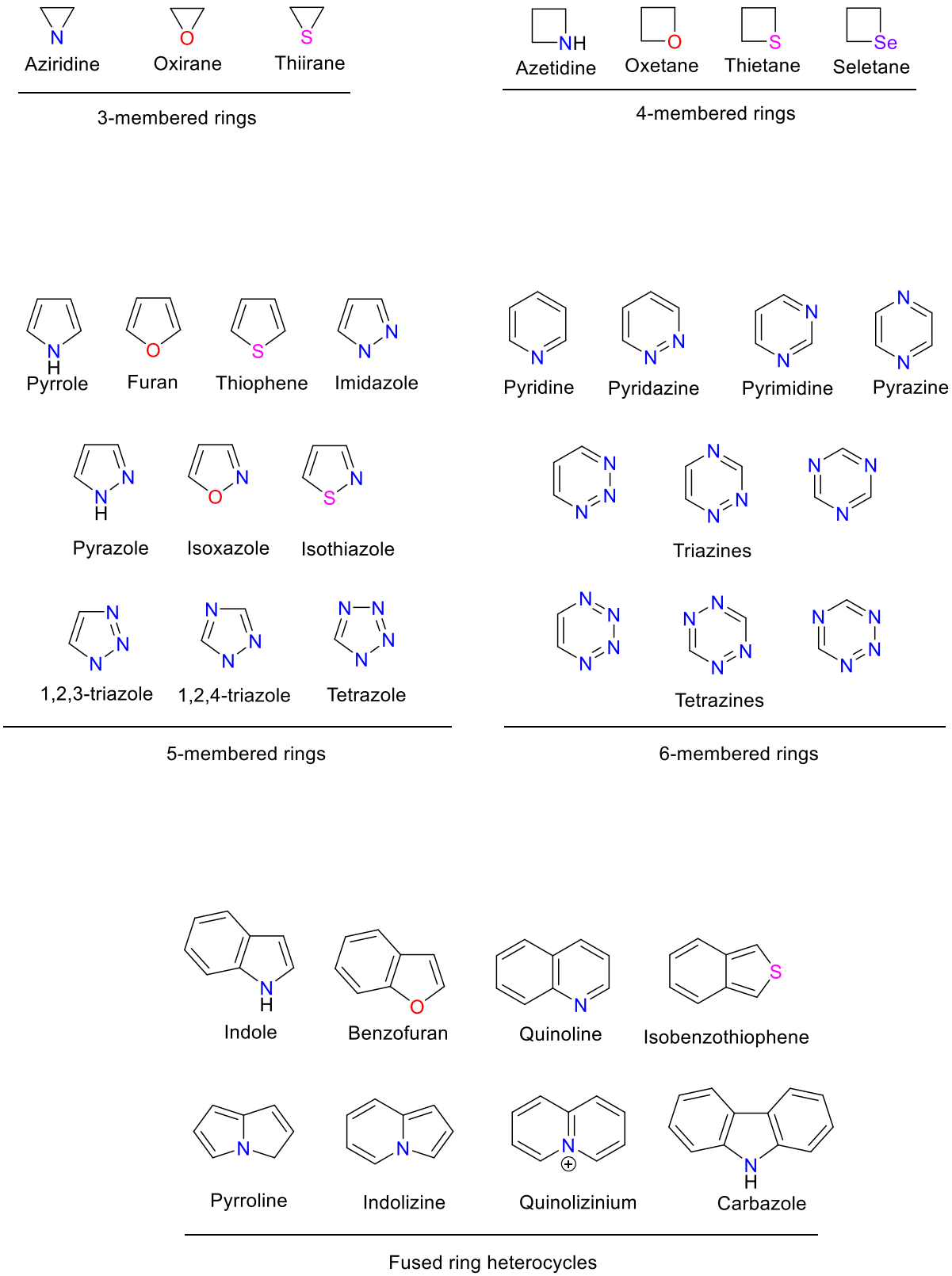

Figure 2.1: Three, four, five, six-membered and fused heterocyclic systems[2]

2.1.2. Applications of heterocyclic compounds

Being a bridge between the biological and chemical realms, where so much scientific discovery and practical application takes place, they are present in more than 90% of new medications.[18–20] Their polarity, lipophilicity, pharmacokinetics, and toxicological qualities are just a few of the physicochemical characteristics that are desirable and may be constructively manipulated. The heterocyclic compounds are the constituent structural motifs in several antidepressant, antitumor, antimalarial, anti-HIV, antidiabetic, anti-inflammatory, antibacterial, fungicidal, herbicidal, insecticidal, and synthetic drugs[21–23] found in pharmaceuticals, vitamins, natural products, biomolecules, and biologically active compounds,[8–10,24,25] while significant bio- and chemiluminescent, photochromic, and solvatochromic characteristics are seen in several of these substances.[26–31] In addition to this, these groups as linkers do show some properties like fluorescent sensors, polymers, dyes, brightening agents, and analytical reagents.[32–35] They may also be used in conjugated polymers and other supramolecular and polymer chemistry, as molecular wires, light harvesting systems, organic conductors, semiconductors, organic light-emitting diodes (OLEDs), photovoltaic cells, optical data carriers, corrosion inhibitors, etc.[36–45] In addition to their synthetic value, heterocycles are of interest due to their potential as metal ligands in chiral auxiliaries, asymmetric catalysts, organocatalysts, protecting groups in organic synthesis, and synthetic intermediates.[46–48] The applications of heterocyclic compounds as mentioned above have been illustrated in **figure 2.2**.

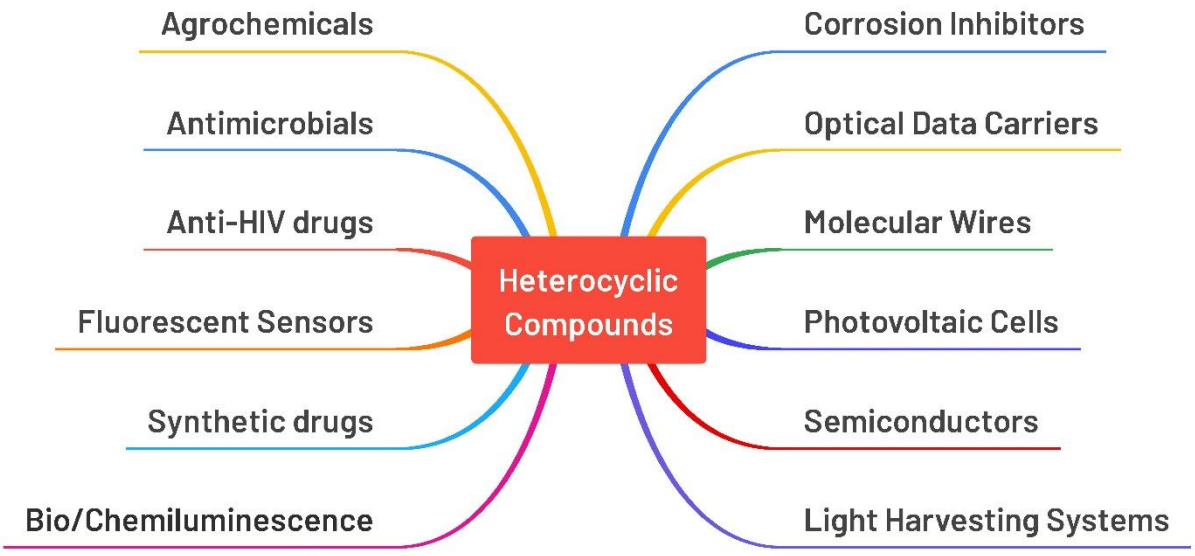

Figure 2.2: Applications of heterocyclic compounds[8–10,21–48]

2.1.3. The 1,2,3-triazole

The 1,2,3-triazoles and their derivatives are a class of N-containing, five-membered heterocyclic compounds having three nitrogen atoms and two carbon atoms constituting the heterocyclic ring, that have attracted a lot of interest from theoretical as well as experimental chemists for their potential in the modification of biologically active chemicals with applications in the chemical, biological, and medical sciences.[49,50] Since the 1,2,3-triazole core often has a number of pharmacophore properties, the hybrids that contain or are fused by a 1,2,3-triazole ring are commonly referred to as 'lead compounds' and can form hydrogen bonds with biomolecular targets, increasing their solubility and ability to interact with them. Additionally, having an electron rich core attributable to the presence of lone pair containing N atoms, they are prime moieties to be implemented as metal ion recognition agents. The 1,2,3-triazoles are broadly categorized into three main categories as monocyclic 1,2,3-triazoles, benzotriazoles, and triazolium salts (**figure 2.3**); and the position of the N-H proton allows for further subdivision of the monocyclic 1,2,3-triazoles into three distinct groups, i.e., the aromatic 1H- and 2H-1,2,3-triazoles, and the non-aromatic 4H-1,2,3-triazole which exists in equilibrium with the aromatic 1H- and 2H-1,2,3-triazoles in solution and in the gas phase.[2,51] A substantially high dipole moment of 4.18 D is observed in the 1,4-disubstituted 1,2,3-triazoles due to which the hydrogen bonds and/or π - π stacking interactions ought to be strengthened in such compounds. This is one of the quintessential features of these compounds which makes them a likely moiety for ion recognition analysis; with the additional essential ability of 1,4-disubstituted triazoles to be non-classical bioisosteres of the amide group for medicinal chemists since the amide group is one of the most often represented functional groups in medications.[52]

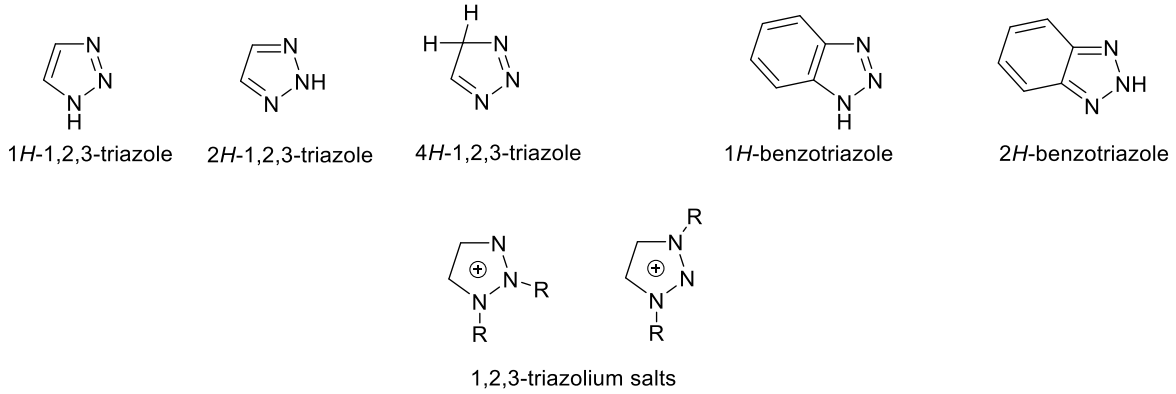

Figure 2.3: An illustrative categorization of 1,2,3-triazoles[2]

2.2. CuAAC 'click' methodology for 1,2,3-triazole linked derivatives

The literature is abundant with several methods describing the formation of 1,2,3-triazole derivatives,[53] however, the CuAAC has been the method of choice[54,55] for the past two decades due to its desirable characteristics, such as mild reaction conditions, regioselective nature, and high yields of pure products.[56] Therefore, the use of CuAAC for synthesizing the 1,2,3-triazole derivatives has been extensively done, and fruitful results have been yielded by the research community by implementing this methodology as a synthetic tool. The precursor to the 1,2,3-triazole derivative, i.e., the terminal alkyne can also be synthesized via numerous synthetic routes. While the Sonogashira coupling[57,58] has remained a conventional method for obtaining alkyne reagents, other methodologies involving *in situ* approaches like using the Bestmann-Ohira[59,60] reagent have also been devised for obtaining alkyne reagents directly from aldehyde precursors. As for the other reactant of CuAAC, i.e., the organic azides, diazonium salts[61,62] provide a convenient route from amine precursors to the resulting azides, while the conversion of diaryl ethers obtained via Ullmann reaction to yield aryl azides are also employed to obtain the desired organic azides. In addition, the remarkable ability of CuAAC to accommodate diverse functional groups enables the introduction of supplementary donor moieties at the 1- and 4-positions, thereby facilitating the synthesis of diverse chelating ligands.[63,64] The synthesis of 1,2,3-triazoles, via the CuAAC pathway, is achieved through the following three steps:

- Synthesis of a terminal alkyne
- Synthesis of an organic azide
- Synthesis of 1,2,3-triazole from terminal alkyne and organic azide

2.2.1. Synthesizing a terminal alkyne

Terminal alkynes are also called as monosubstituted alkynes (R-C≡C-H), as they consist of a single alkyl group bonded to a single sp hybridized carbon atom of the triple bond present at the very end of the carbon chain.[65] Terminal alkynes have been extensively used by the organic chemists as valuable precursors in several reactions, including the synthesis of carbocycles, heterocycles, enamines, etc. Additionally, the C≡C owing to its electronic properties and versatility has been implemented as a building block in biochemical and material science.[66,67] Several discrete pathways for synthesizing terminal alkynes from different starting materials and under different sets of reaction conditions have been reported in the literature, some of which are:

2.2.1.1. α, β-eliminations

Zhao *et al*. presented a practical and effective method to synthesize terminal alkynes **2** from 1,1-dibromo-1-alkenes **1**, wherein the reaction was conducted using Cs_2CO_3 as the base and DMSO as the solvent (**figure 2.4**). The reaction was maintained at 115 °C and progressed rapidly, while also being tolerant to several different functional groups.[68] The synthesized products were isolated with a yield of 85 - 94% via this methodology.

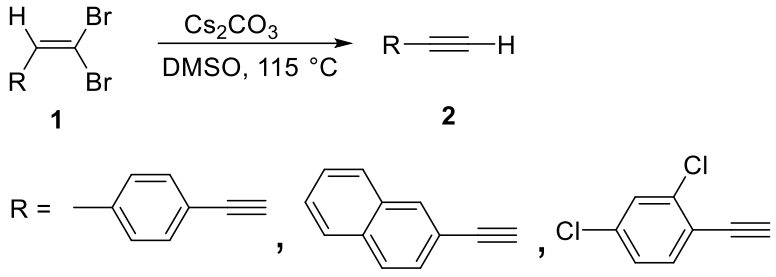

Figure 2.4: Synthesis of terminal alkyne from 1,1-dibromo-1-alkene employing Cs_2CO_3 as the base[68]

Singh and co-workers synthesized terminal alkynes **4** from gem-dibromoalkenes **3** wherein the reagent, i.e. Na_2S, being readily available in commercial quantities and at a moderate cost, the approach was considered preferable to others. With no base needed, the reaction can take place at room temperature (20 - 40 °C) and in air, with good yields of 65 - 83% (**figure 2.5**). With this approach, various heteroaromatic, aromatic, and aliphatic gem dibromoalkenes gave rise to matching terminal alkynes.[69]

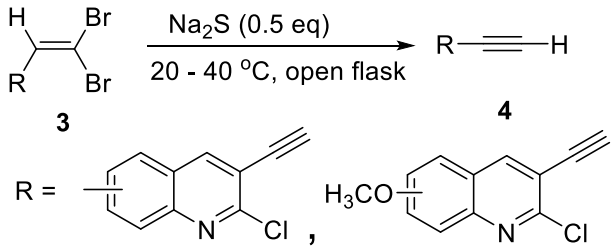

Figure 2.5: Synthesis of terminal alkynes from gem-dibromoalkenes via Na_2S mediation[69]

Morri research group reported the conversion of 1,1-dibromoolefin **5** to yield the terminal alkynes by using excess 1,8-Diazabicycloundec-7-ene (DBU), thereby taking advantage of its nucleophilicity in anhydrous conditions which resulted in the production of the terminal alkynes **6** with a high yield of 76 - 93% for substrates with electron rich moieties (**figure 2.6**).[70]

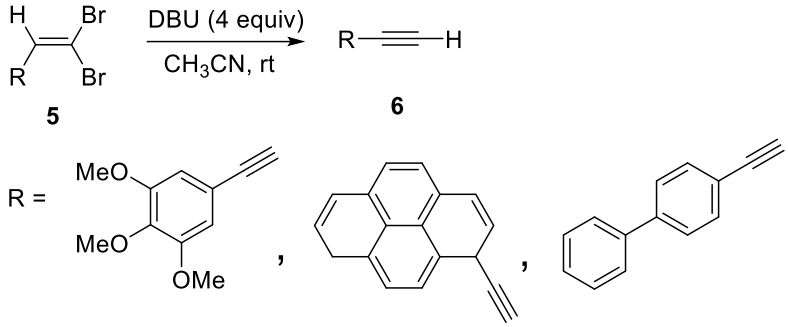

Figure 2.6: Conversion of geminal-dibromoalkene into terminal alkyne[70]

The decarboxylation and dehalogenation of 3-aryl-2,3- dibromopropanoic acid **7** was demonstrated by Kuang's group using K_2CO_3 as the base for the synthesis of terminal alkynes **8**, which was carried out at 115 °C in DMSO (**figure 2.7**). The reaction was observed to go without a hitch and was tolerant to a wide variety of heteroaryl substituents in addition to aryl groups that may either remove or donate electrons, and demonstrated high yields of 83 - 94%.[71]

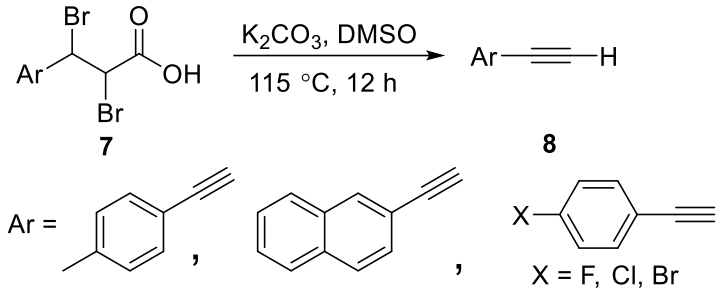

Figure 2.7: Synthesis of terminal alkyne from dibromopropanoic acid[71]

Kuang *et al.* reported the terminal alkyne synthesis from 3-aryl-2,3- dibromopropanoic acids **9** through microwave irradiation in the presence of Et_3N and DBU. Initially, a mixture of isomers of alkene **10** were produced in the presence of Et_3N. The weak basic character of Et_3N prevented the abstraction of a vinylic hydrogen and the direct synthesis of the alkyne. Then, DBU was used to carry out the elimination of the HBr form of the (Z)-aromatic alkene to get the terminal alkynes **11** with excellent yield of 88 - 99% (**figure 2.8**).[72]

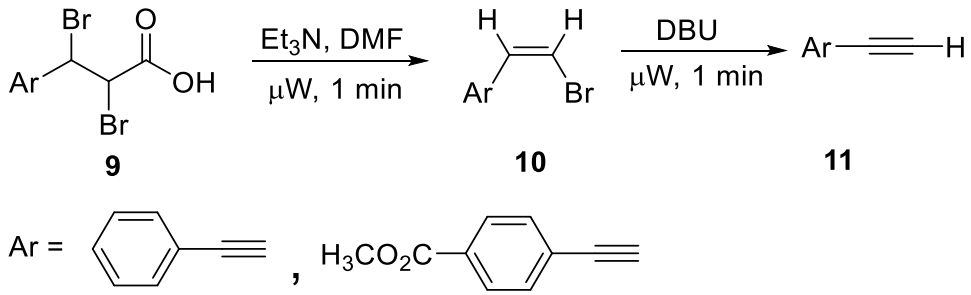

Figure 2.8: Microwave-assisted one-pot synthesis of terminal alkyne[72]

2.2.1.2. Carbene rearrangement

Corey and Fuchs presented an efficient strategy for converting aldehydes to alkynes via Ramirez olefination followed by Fritsch-Buttenberg- Wiechell (FBW) rearrangement (**figure 2.9**). The 1,1-dihaloalkene **13** obtained from the aldehyde **12** was subjected to n-BuLi to give the carbenoid **14** which subsequently gave the carbene **15**. A 1,2-shift of **15** resulted in the synthesis of the terminal alkyne **16** with good yields of 80 - 95%.[73]

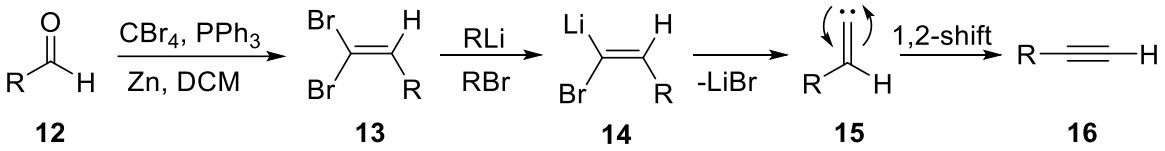

R = alkyl, phenyl, cyclohexenyl

Figure 2.9: Synthesis of terminal alkynes from aldehydes as reported by Corey and Fuchs[73]

Hijfte and colleagues observed that aldehyde **17** reacted with carbontetrabromide to form vinyl dibromide **18**, which reacted with Mg in THF during refluxing to form terminal alkynes. This reaction proceeds owing to the sufficiently negative reduction potential of magnesium to transfer electrons to vinyl dibromide (**figure 2.10**). The methodology suggested the use of magnesium as a useful alternative to a strong base, which causes many unwanted side reactions, and the terminal alkynes **19** were also in good yields of 75 - 95%.[74]

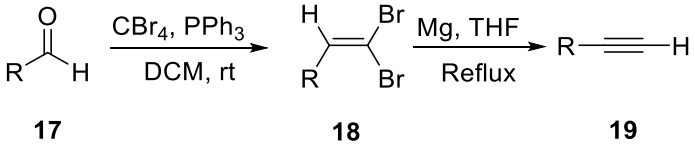

R = C_6H_5, $C_6H_5CH(CH_3)$

Figure 2.10: Synthesis of terminal alkynes from aldehydes as reported by Hijfte *et al*.[74]

Beshai group demonstrated the dehydrohalogenation of 1-iodo-1-alkenes **20** using tetrabutylammonium fluoride (TBAF) as the base, to produce terminal alkynes **21** in high yields of 81- 98% (**figure 2.11(a)**). The methodology was applicable to many functional groups, including -NO_2, C=O, aromatic halogens, and -CF_3. Also, under the usual reaction conditions, heteroaromatic groups like pyridine also posed no difficulty. Above and beyond, a one-pot direct synthesis of terminal alkynes from aldehydes **22** was also demonstrated (**figure 2.11(b)**), eliminating the need to isolate the intermediate iodoalkene. This reaction approach is a promising addition to the existing arsenal of ways to synthesis terminal alkynes **23** in good

yields of 73 - 86% from aldehydes because of its extensive substrate scope and functional group tolerance.[75]

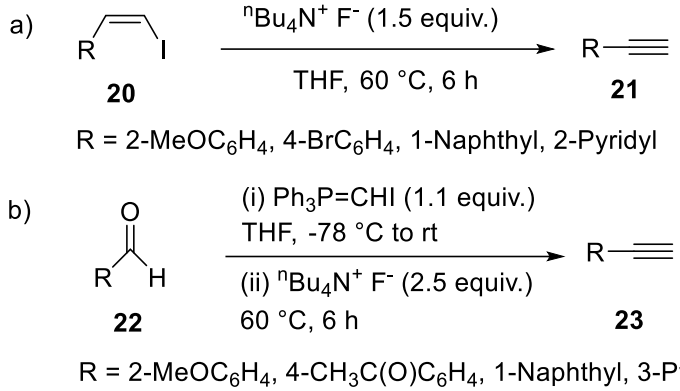

Figure 2.11: a) synthesis of terminal alkynes via dehydrohalogenation of (Z)-1-iodo-1-alkenes with TBAF. b) synthesis of terminal alkyne directly from aldehyde[75]

Illa and colleagues successfully produced several different alkynes **26** in moderate yields of 40 - 67% beginning with a carbonyl molecule **25** by using the neutral reagent C-silylated-diazophosphines **24** under relatively mild reaction conditions (**figure 2.12**).[76]

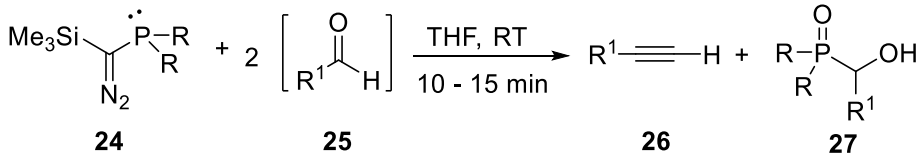

Figure 2.12: Synthesis of terminal alkyne from aldehyde using C-silylated-diazophosphines[76]

Acetoxynitrosamides **28** may be converted to terminal alkynes **32** in high yields of 77 - 97% by refluxing in THF leading to the formation of carbene **29** and subsequently undergoing a rearrangement to generate the corresponding terminal alkyne (**figure 2.13**). This strategy was applicable to the synthesis of terminal alkynes with either aryl or alkyl substituents.[77]

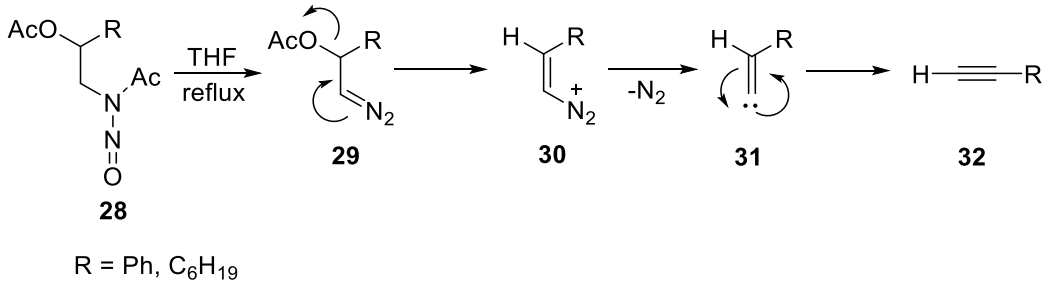

Figure 2.13: Synthesis of terminal alkyne from acetoxynitrosamide[77]

2.2.1.3. Miscellaneous Reactions

The reaction of aldehydes **33** with the Ohira–Bestmann reagent **34**, which is a phosphate derivative, in the presence of potassium carbonate and methanol was suggested by Bestmann research group as a method for the synthesis of terminal alkynes **35** with good yields of 65 - 89% (**figure 2.14**).[78]

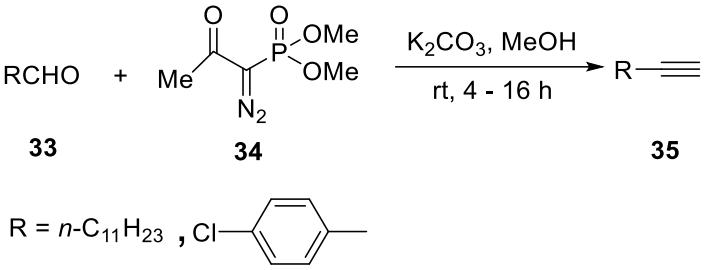

Figure 2.14: Synthesis of terminal alkynes by reacting aldehyde with Ohira–Bestmann reagent[78]

Using [^{18}F]-fluorobenzaldehyde **36**, Krapf *et al.* produced radiofluorinated phenylacetylene **37** with a yield of 40 - 60% and more than 98% radiochemical purity in under 20 minutes by treating the former with Ohira-Bestmann reagent, with K_2CO_3 as the base in CH_3CN solvent (**figure 2.15**).[79]

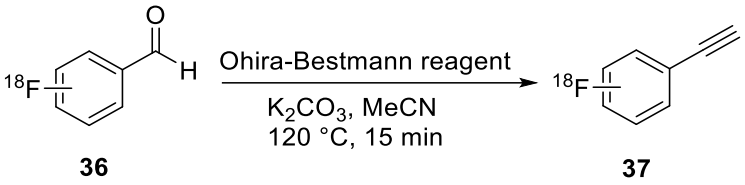

Figure 2.15: Synthesis of radiofluorinated phenylacetylene from [^{18}F]-fluorobenzaldehyde[79]

Beier group described the production of phenylacetylene **39** with a good yield of 71% via the removal of HF from α,α-difluorophosphonate **38**, mediated by t-BuOK. In addition to this, the phenylethynylphosphonate was discovered as a minor byproduct (**figure 2.16**).[80]

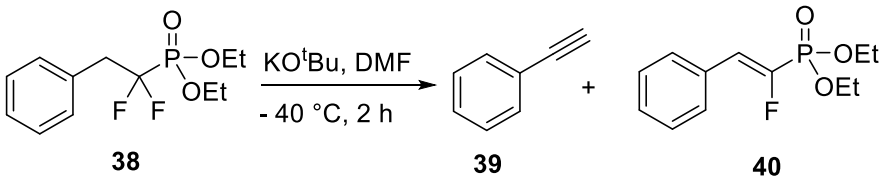

Figure 2.16: Synthesis of phenylacetylene from α,α-difluorophosphonate[80]

An examination of the pertinent literature uncovers numerous publications that describe the creation of new terminal alkynes through the utilization of different compounds that have functionalities containing at least one labile proton (-OH, -NH_2 etc.); and with the use of propargyl bromide in conjunction with various solvents such as N,N-dimethylformamide, acetone, and acetonitrile; and bases such as potassium carbonate, cesium carbonate, and sodium hydride, the successful synthesis of terminal alkynes from a wide range of compounds can be accomplished.[81–84] This method can be studied for the synthesis of new terminal alkynes with high yield since it does not necessitate robust reaction conditions or expensive experimental equipment, and can be conducted under normal laboratory conditions in an efficient and facile manner.

Ozukanar *et al.* reported the synthesis of compound **43** with 65% yield by reacting propargyl bromide **42** with p-hydroxy benzaldehyde **41** using potassium carbonate base in acetone as a solvent. This compound was then reacted with 2,7-dihydroxynaphthlane in glacial acetic acid and catalytic amount of HCl to yield the corresponding product **44**, which was further nucleophilically substituted with propynyl moieties to yield the terminal alkyne **45** as the final product (**figure 2.17**).[85]

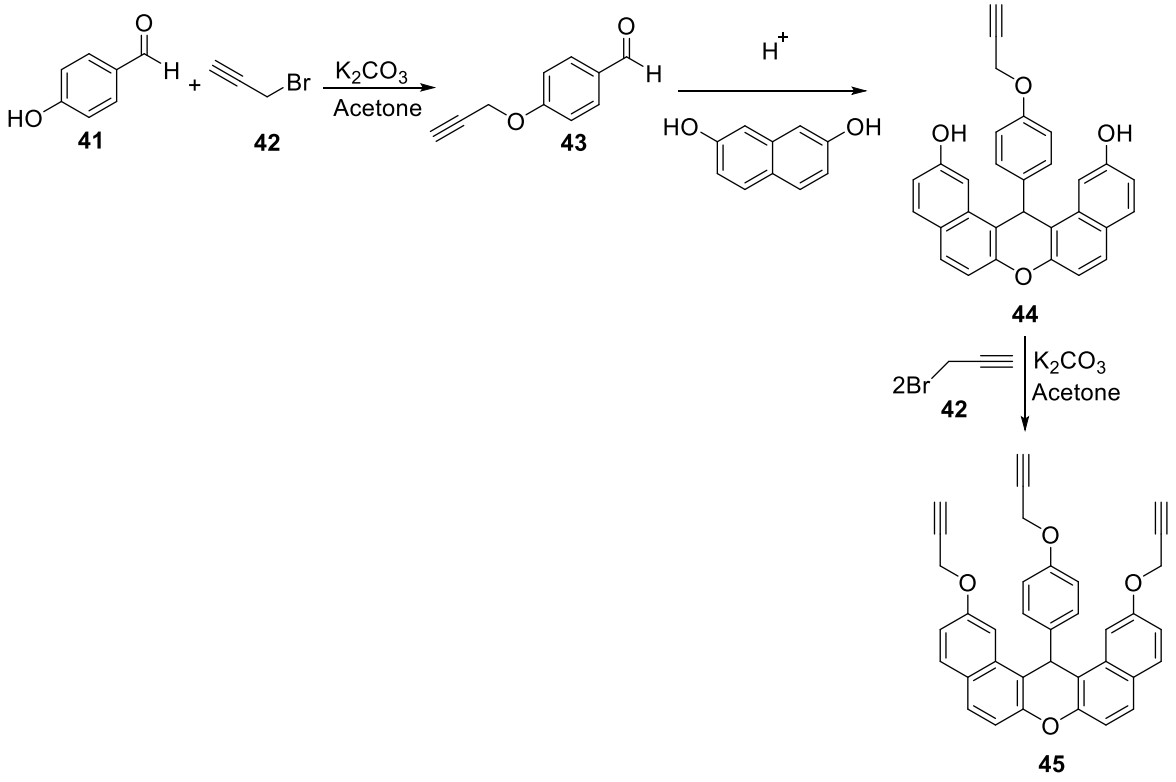

Figure 2.17: Synthesis of terminal alkyne based on p-hydroxy benzaldehyde[85]

Kursunlu research group reported the propargylation of phenolic O-H groups of compound **46** using the base potassium carbonate and solvent media dimethylformamide (DMF), leading to the formation of the molecule containing di-alkyne **47** (**figure 2.18**).[86]

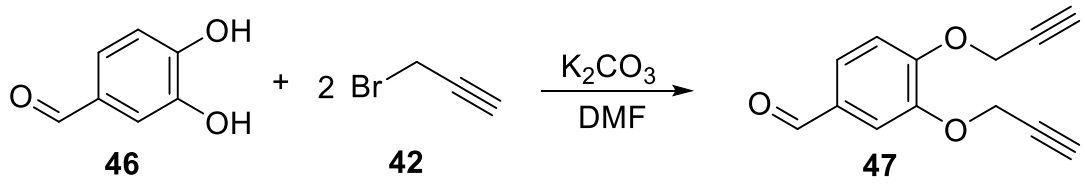

Figure 2.18: Synthesis of the 3,4-dihydroxybenzaldehyde-based terminal alkyne[86]

Tamanini and co-workers reported a synthetic procedure wherein a solution of **48** in acetonitrile (50 mL) was subjected to the addition of propargyl bromide and then stirred overnight. Subsequently, the cyclam based terminal alkyne **49** was formed with 78% yield (**figure 2.19**), which was subjected to washing with cold acetonitrile after filtration, and dried in vacuum.[87]

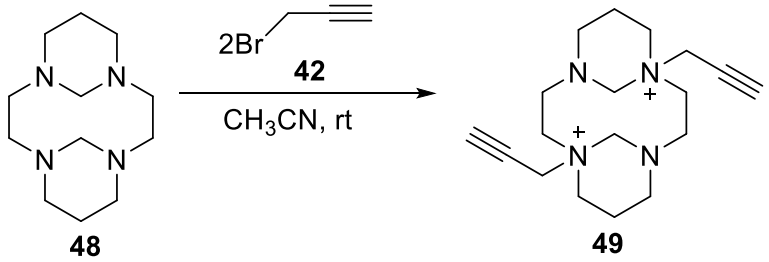

Figure 2.19: Synthesis of the cyclam based terminal alkyne[87]

Huang *et al.* presented the synthesis of a terminal alkyne wherein compound **50** was etherified using propargyl bromide using a base (potassium carbonate), potassium iodide, and acetonitrile over a period of twelve hours, which resulted in 94% yield of the bispropargylether **51** (**figure 2.20**).[88]

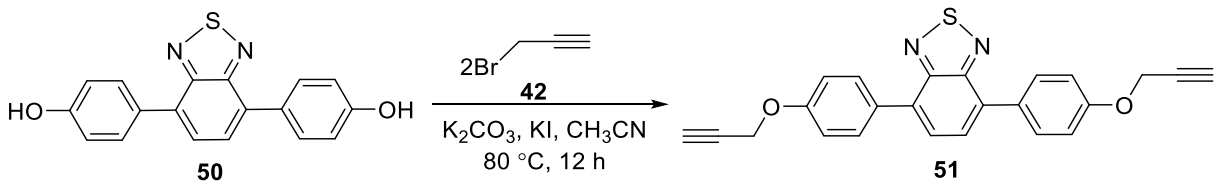

Figure 2.20: Synthesis of the bispropargylether containing terminal alkyne[88]

Shen and co-workers proposed a synthesis route in which the terminal alkyne Py-NRhB **53** was produced when NH_2-NRhB **52** was nucleophilically substituted with propargyl bromide in acetonitrile at a temperature of 60 °C (**figure 2.21**). Consequently, the labile protons of the -NH_2 group were substituted with propargyl groups, leading to the synthesis of the terminal alkyne in the form of a yellow solid.[89]

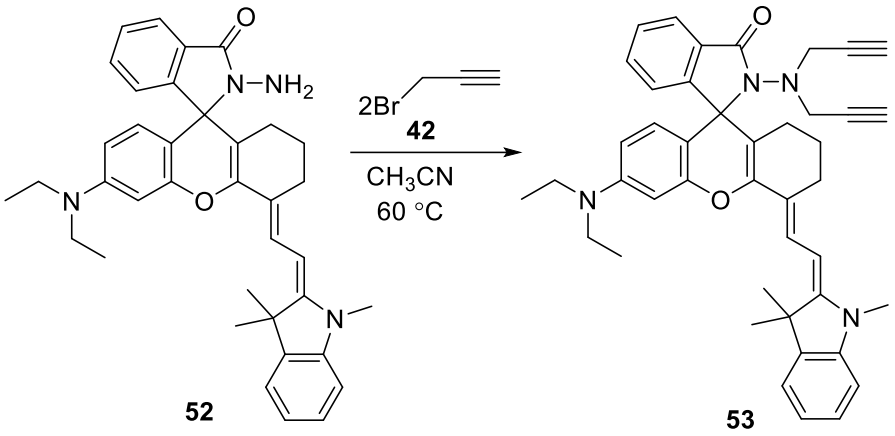

Figure 2.21: Synthesis of the terminal alkyne Py-NRhB from NH_2-NRhB[89]

Ko research group synthesized two terminal alkynes **55** and **57** via the nucleophilic substitution of the -OH groups of salicylaldehyde **54** and 2-(benzo[d]thiazol-2-yl)phenol **56** separately. The reaction conditions and solvent used for both the starting materials were the same, with the base being K_2CO_3 and the solvent being CH_3CN; refluxing the reaction mixture for 12 hours gave the corresponding terminal alkynes[81] (**figure 2.22(a)** and **2.22(b)**).

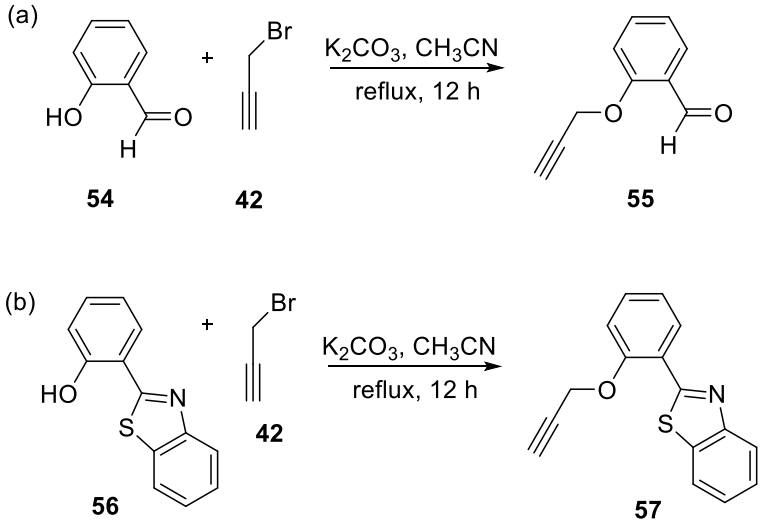

Figure 2.22: Synthesis of salicylaldehyde and 2-(benzo[d]thiazol-2-yl)phenol based terminal alkynes[81]

2.2.2. Synthesizing an organic azide

Phenyl azide **59**, which was originally synthesized by Peter Griess in 1864,[90] was the first organic azide ever to be synthesized (**figure 2.23**). Since then, researchers are interested in these highly reactive compounds owing to their possible applications in organic synthesis, medicine delivery, and other fields. Due to their usefulness in the synthesis of heterocycles including triazoles and tetrazoles, organic azides have established themselves in the realm of commercial science as well.[91] Sodium azide is often used for the SN_2-azidation of alkyl halides, acyl halides, and aryl halides. Aryl azides are crucial precursors in organic chemistry due to their high stability and high degree of conjugation. These properties have led to their widespread application in different research fields,[92–95] including biology and industry, where they are used as photoaffinity labels, cross-linkers in photoresistors, building blocks for conducting polymers, and activators of polymer surfaces when exposed to light.[96–98] Organic azides were traditionally produced using extremely volatile, poisonous, and explosive materials like hydrogen azide (**figure 2.24**)[99]; but, recently, alternative azidation techniques have been tried out that eliminate the need for these dangerous chemicals.[100]

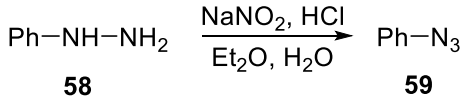

Figure 2.23: Synthesis of phenyl azide **59** from phenylhydrazine **58**[90]

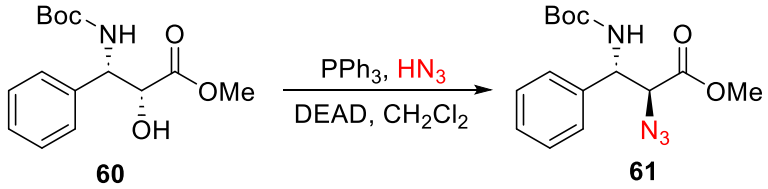

Figure 2.24: Synthesis of an organic azide **61** by using the highly toxic hydrogen azide[99]

The different methodologies reported for synthesizing organic azides are discussed below:

Organic azides have been synthesized directly using alcohols, as described by Kitamura *et al.*, who used 2-azido-1,3-dimethylimidazolinium hexafluorophosphate (ADMP) **63** for azide transfer to an alcohol **62** to obtain the desired product **64** by using 1,8-Diazabicyclo(5.4.0)undec-7-ene (DBU) as base (**figure 2.25(a)**). The whole reaction was completed in 10 minutes at room temperature, with high product yield (65 - 96%).[101] Similar results were also reported when primary amine **65** was used as the starting material to react

with ADMP **63** using N,N-dimethyl-4-aminopyridine (DMAP) as base to yield the products **66** with yields of 63 - 94% (**figure 2.25(b)**).[102]

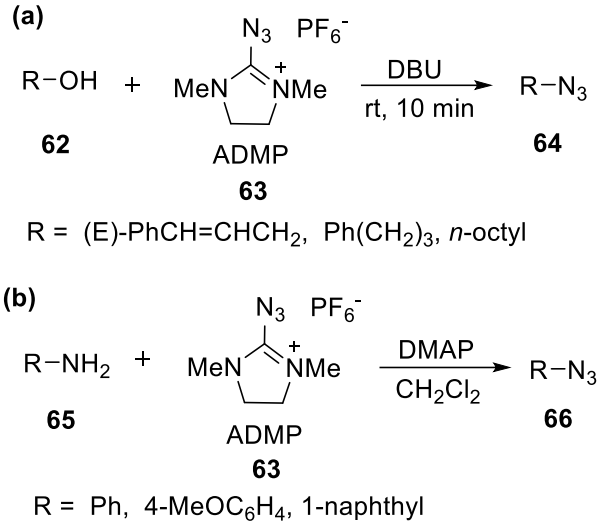

Figure 2.25: Synthesis of organic azide by reacting (a) alcohol with ADMP and DBU as the base; and (b) primary amine with ADMP and DMAP as the base[101,102]

An alternative approach to produce aromatic azides includes the diazotization of aromatic amines, and their subsequent a nucleophilic substitution using sodium azide. Capitosti and co-workers reported a procedure for azide synthesis wherein the nitro group of the heterocyclic reactant **67** was efficiently reduced using 10% Pd/C and H_2, resulting in 80% yield of the 4-amino-substituted analogue. The corresponding 4-azido-substituted thalidomide analogue **69** was obtained in 35% yield through diazotization of **68** by using sodium nitrite in aqueous HCl, and subsequently adding sodium azide (**figure 2.26**).[103]

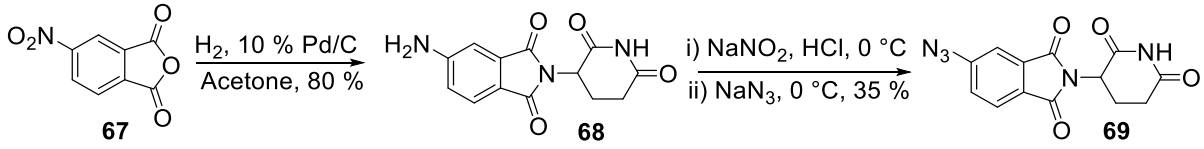

Figure 2.26: Synthesis of azido-thalidomide from 4-amino-substituted analogue[103]

Knepper *et al.* reported the synthesis of diaryl ethers **73** in varying yields of 34 - 95% via Ullmann reaction through the cleavage of polymer-bound aryl triazenes **72**, which provided a combinatorial route to aryl azides, wherein in the presence of trimethylsilyl azide, the aryl triazenes underwent conversion to yield the corresponding azides (**figure 2.27**).[104]

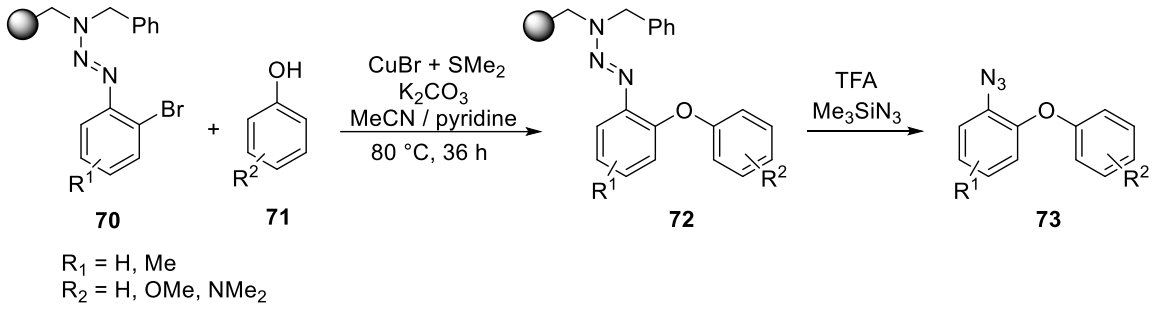

Figure 2.27: Synthesis of diaryl ether thorugh trimethylsilyl azide following Ullmann reaction[104]

Gavenonis research group proposed the conversion of 2,6-dimesitylphenyliodide **74** to its corresponding azide **75** with 96% yield by reacting the former with n-BuLi at 0 °C in hexane and then subjecting p-toluenesulfonyl azide to the resulting lithium salt with to yield the azide (**figure 2.28**) as red-orange crystals in 96% yield.[105]

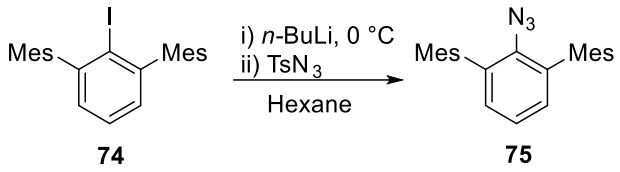

Figure 2.28: Synthesis of 2,6-dimesitylphenyliodide based azide[105]

The utilization of hydrazines **76** in conjunction with nitrosyl ions or their precursors is a recognized procedure that is applicable in the production of different aromatic and aliphatic azides. **77** with excellent yields (84 - 95%) as described by Kim *et al.* (**figure 2.29**).[106]

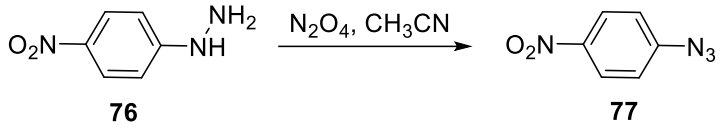

Figure 2.29: Synthesis of nitrosyl-hydrazine-based azide[106]

Liu and Tor described that the reaction of anilines **78** with triflyl azide **79** yielded aryl azides and heteroaryl azides **80** with good yields (78 - 96%) (**figure 2.30**). These transformations are the go-to for preparing a wide variety of aromatic azides due to their low reaction temperatures, good yields, and ease of use.[107]

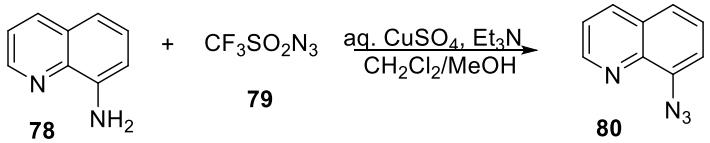

Figure 2.30: Synthesis of aromatic azide from the corresponding amine using triflyl azide[107]

2.2.3. Synthesizing 1,2,3-triazoles via cycloaddition of a terminal alkyne with an organic azide mediated via Cu(I) catalyst

The Huisgen cycloaddition, which yielded 1,2,3-triazoles as a racemic mixture (1,4- and 1,5-disubstituted, ca. 1:1), was further improved independently by Sharpless and Meldal by introducing Cu(I) salt as the catalyst and since its inception, the methodology has been extensively explored to synthesize several 1,2,3-triazole derivatives, owing to the desirable characteristics of this pathway including modularity, high yields, stereospecific nature, benign solvents, etc. in addition to the overlapping features with green synthesis such as atom economy, energy efficient, less hazardous, waste prevention, etc. The 1,3-dipolar nature of the organic azide makes it possible to undergo [3+2] cycloaddition with the unsaturated alkyne mediated via Cu(I) catalytic system to yield the 1,4-disubstituted 1,2,3-triazole. Some of the reports of synthesizing 1,2,3-triazole derivatives via the cycloaddition of a terminal alkyne with an organic azide have been enlisted as under:

Puthiyedath and Bahulayan demonstrated the successful formation of a 1,2,3-triazole-linked compound **83** consisting of two different coumarin derivatives by reacting an equimolar amount of 4-azidomethyl umbeliferone **82** and the coumarin based alkyne **81** in the presence of $CuSO_4$/Na ascorbate catalyst for 12 h at room temperature following the CuAAC methodology (**figure 2.31**).[108]

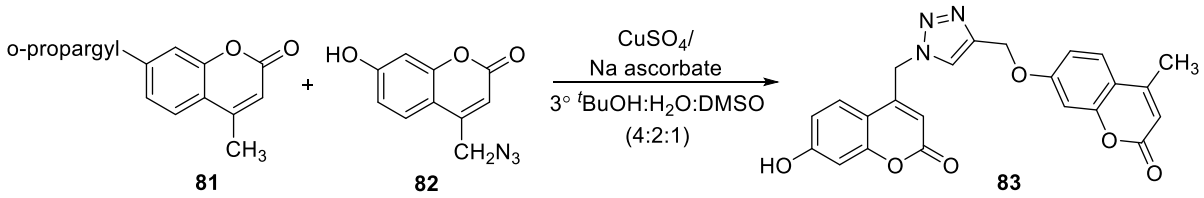

Figure 2.31: Synthesis of CuAAC-derived 1,2,3-triazole-coumarin derivative[108]

Tane and Michinobu demonstrated that by combining the monomeric 1,8-diethynylcarbazole **84** with counter monomer 2,7-diazidofluorene **85** via the CuAAC pathway, the polymeric systems based on 1,8-carbazole **86** were produced, by employing $CuSO_4.5H_2O$/Na ascorbate as the catalytic system and THF/t-BuOH/H_2O (5:1:1) as the solvent media (**figure 2.32**).[109]

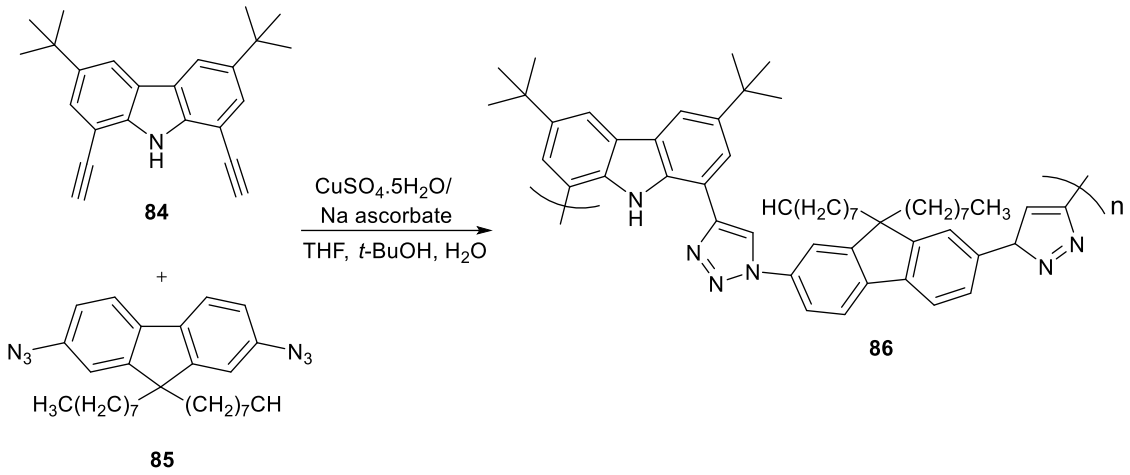

Figure 2.32: Synthesis of carbazole-triazole-fluorene conjugated polymer[109]

Xu research group designed 1,2,3-triazole-tethered cyclen-functionalized anthracene conjugates **89** via 'click' reaction between anthracene azide **88** and boc-cyclen alkyne **87** using CuI catalytic system in acidic medium (**figure 2.33**).[110]

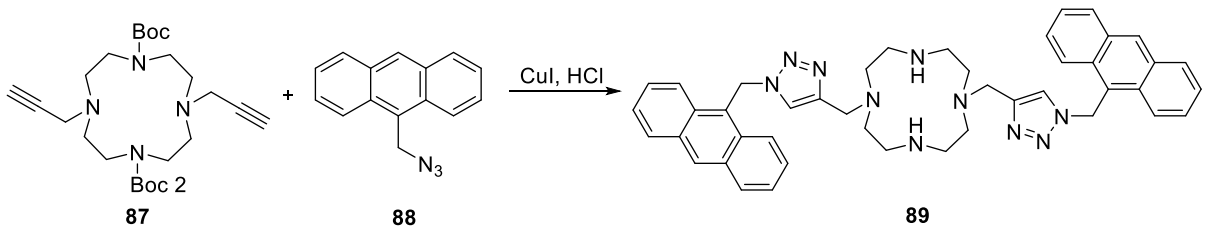

Figure 2.33: Synthesis of 1,2,3-triazole-linked dianthracene-cyclen based conjugate[110]

Shaily research group synthesized a 1,2,3-triazole tethered compound **92** by converting 4-hydroxycoumarin into its corresponding alkyne **90** as well as azide **91** in separate reactions, and then combining the two precursors via the cycloaddition process in the presence of $CuSO_4.5H_2O$/Na ascorbate catalyst to produce the final product, having two coumarin moieties connected via a 1,2,3-triazole moiety (**figure 2.34**).[111]

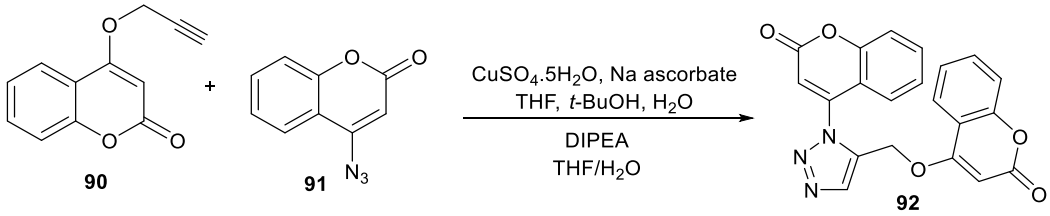

Figure 2.34: Synthesis of coumarin-linked 1,2,3-triazole-based probe[111]

According to the work of Dwivedi *et al.*, a 1,2,3-linked compound **94** was synthesized by connecting naphthalimide-based alkyne **93** and anthracene-based azide **88** via a molecular bridge comprising piperazine and triazole units via the click reaction, utilizing the $CuSO_4$/Na ascorbate catalytic system in DMSO/H_2O solvent (4:1, v/v) (**figure 2.35**).[112]

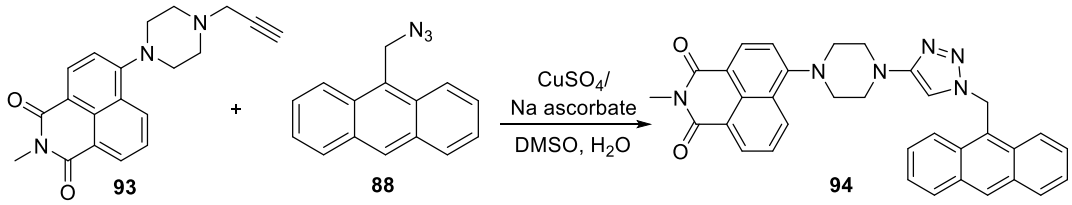

Figure 2.35: Synthesis of dual fluorophore containing 1,2,3-triazole derivative[112]

Joshi and coworkers demonstrated the successful formation of two coumarin-1,2,3-triazole based chemosensor probes **97** by stitching together protected amino acyl O-propargyl esters **95** with 4-azidomethyl-7-hydroxycoumarin **96** via cycloaddition mediated by Cu(I) catalyst (**figure 2.36**).[113]

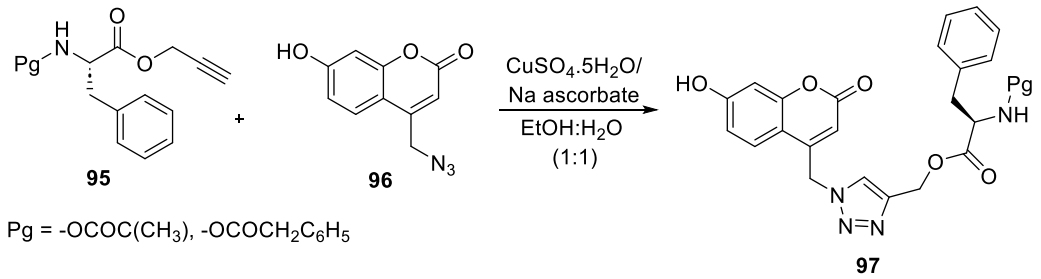

Figure 2.36: Synthesis of coumarin-1,2,3-triazole based chemosensors[113]

Kang and co-workers demonstrated the development of a 1,2,3-triazole-linked derivative **100** via the cycloaddition of **98** and **99**. The catalytic system used for the cycloaddition reaction was $CuSO_4$/Na ascorbate in EtOH/H_2O (1:1) solvent system (**figure 2.37**).[114]

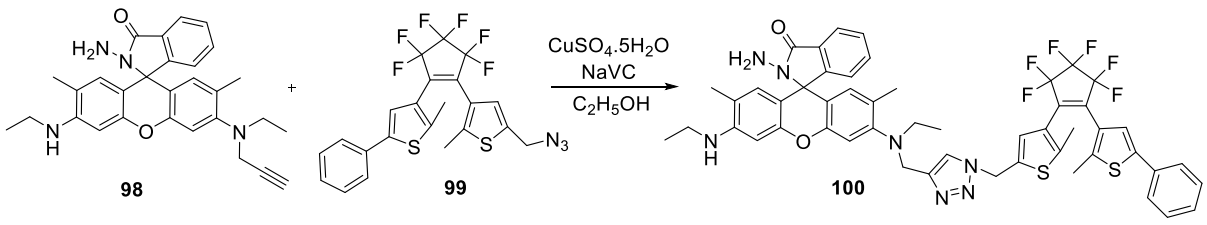

Figure 2.37: Synthesis of rhodamine 6G based 1,2,3-triazole derivative[114]

Zhang *et al.* reported the cycloaddition of N-phenylaza-15-crown-5 ether **101** with coumarin fluorophore **102** to synthesize a 1,2,3-triazole-linked compound **103** using $CuSO_4.5H_2O$/Na ascorbate as the catalyst in partial aqueous solvent system (THF/H_2O, 1:1) with 65% yield (**figure 2.38**).[115]

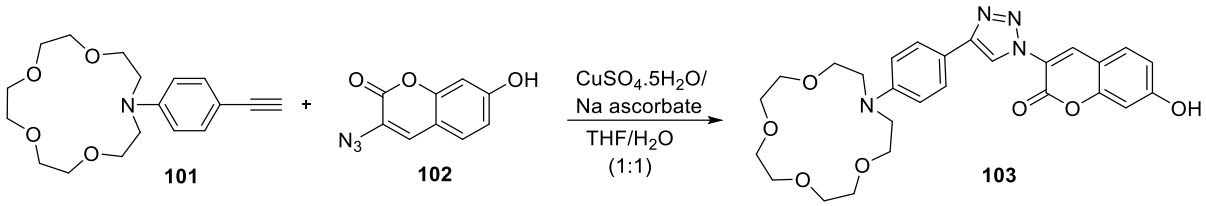

Figure 2.38: Synthesis of phenylaza-15-crown-5-triazol-substituted coumarin fluoroionophore[115]

Kaur group reported a fluorescein based 1,2,3-triazole derivative **106** obtained via CuAAC reaction between fluorescein based moiety **104** and benzyl azide **105** using $Cu(PPh_3)_3Br$ as the Cu(I) source and THF/TEA (1:1) as the solvent media with a high yield of 81% (**figure 2.39**).[116]

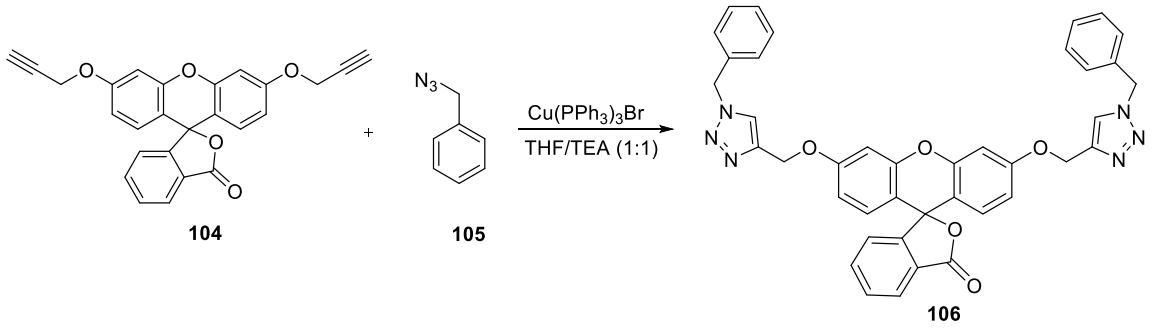

Figure 2.39: Synthesis of 1,2,3-triazole probe based on fluorescein[116]

Liu and co-workers designed an amphiphilic 1,2,3-triazole based probe **109** by the cycloaddition of a hydroxylquinoline ring **107** with a hydrophobic cetyl chain **108**, while using $CuSO_4.5H_2O$/ NaVc as the Cu(I) source in DMF as the solvent with 80% yield (**figure 2.40**).[117]

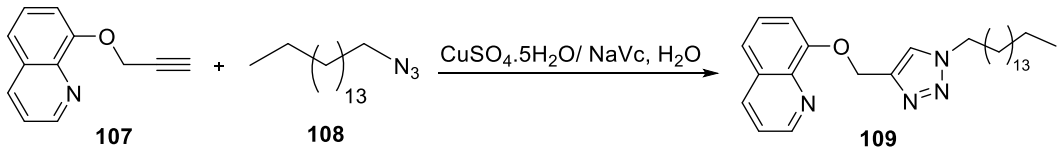

Figure 2.40: Synthesis of an amphiphilic 1,2,3-triazole based probe[117]

The aforementioned examples demonstrate the emergence of CuAAC as a versatile and efficient methodology in the realm of organic chemistry. It has revolutionized the production of 1,4-disubstituted 1,2,3-triazoles, thereby offering an exceptionally efficient, selective, and adaptable approach for constructing heterocyclic compounds. These reactions further underscore the substantial benefits offered by CuAAC, such as its ability to work effectively with a wide range of functional groups and under various reaction conditions. This flexibility serves diverse 1,2,3-triazoles with tailored properties, making it a valuable methodology in drug discovery, materials science, and analytical chemistry. The simplicity of the reaction setup, relatively low cost of copper catalysts, and high yields further contribute to the widespread adoption of CuAAC in academic and industrial laboratories.

2.3. Spectroscopic analysis of the products

The products of every synthesis must undergo critical characterization, which irrefutably proves the product formation and is thus of the highest significance. In the characterization of 1,2,3-triazole-based probes, various analytical techniques such as IR spectroscopy, NMR spectroscopy (^{1}H and ^{13}C), mass spectrometry, etc. can be employed. The additional studies to understand the photophysical properties of the synthesized molecules can be performed using UV-Vis and fluorescence spectroscopy. In addition to these spectroscopic techniques, some basic analytical methods can also help us to confirm the product formation that include melting/boiling point determination, CHNS analysis, etc. Apart from these, physical inspection can also help a researcher to evaluate the product by looking at the color, texture, and odour of the compound.

2.3.1. Infrared (IR) spectroscopy

IR spectroscopy provides information about the vibrational modes of molecules, thereby allowing for the identification of functional groups and structural characterization. The shifts in a molecular dipole are due to the vibrations and can provide a detailed understanding of the interaction of IR radiations with the product, especially the functional groups present in a synthesized molecule/compound.[118] The interaction of IR radiations with a sample is measured as a function of frequency using an infrared spectrometer, yielding an IR spectrum. The absorption of the IR radiations by distinct functional groups at a particular frequency causes vibrations in various bonds in the molecule,[119] and the strength of vibration determines the specific frequencies at which the bonds vibrate.[120] Several important distinguishing peaks

and regions in IR spectroscopy provide valuable information for the structure elucidation of organic compounds. These peaks correspond to specific functional groups or structural features, allowing chemists to identify and characterize different bonds and groups within a molecule. Here are some notable peaks and regions in IR spectroscopy:

- O-H Stretch: A broad peak around 3600 - 3200 cm^{-1} indicates the presence of hydroxyl groups (alcohols, phenols, carboxylic acids) or water molecules.
- C=O Stretch: The carbonyl group (C=O) shows characteristic peaks around 1750 - 1650 cm^{-1}. The position of the peak can vary depending on the specific type of carbonyl compound: ketones (~1715 cm^{-1}), aldehydes (~1735 cm^{-1}), amides (~1670 - 1650 cm^{-1}), carboxylic acids (~1725 - 1710 cm^{-1}), and esters (~1750 - 1740 cm^{-1}).
- C=C Stretch: Double bonds (C=C) typically exhibit peaks in the range of 1680 - 1600 cm^{-1}. The exact position of the peak can depend on factors such as conjugation and substitution patterns.
- C-H Stretch: The aromatic C-H stretch generally appears above 3000 cm^{-1} whereas the aliphatic C-H stretch lies in the range of 3000 - 2850 cm^{-1}. The presence of other functional groups can cause shifts or splitting of these peaks.
- N-H Stretch: Amine groups (primary, secondary, and tertiary) exhibit peaks in the range of 3300-3500 cm^{-1}, which can vary depending on the degree of substitution and hydrogen bonding.
- C≡C Stretch: The triple bond (C≡C) stretching frequency typically appears around 2250 - 2100 cm^{-1} and is characteristic of alkynes.
- Fingerprint Region: The region below 1500 cm^{-1}, known as the fingerprint region, contains a complex pattern of peaks that can provide additional information about the molecule's overall structure and functional groups present.

2.3.2. Nuclear Magnetic Resonance (NMR) Spectroscopy

Nuclear Magnetic Resonance (NMR) spectroscopy is an indispensable technique for the structure elucidation of organic compounds, as it provides detailed information about the connectivity, hybridization, and environment of atoms within a molecule, allowing chemists to determine the structure and identify functional groups. Thus, the newly synthesized compounds are often characterized using ^{1}H and ^{13}C NMR spectroscopy to get insights into their structures.[121,122] The recent innovations in magnet technologies, equipment gear, pulse sequences, data collecting and processing, and sample preparation have led to a significant

upsurge in the quality of information regarding the structure and dynamics of chemical as well as biological systems owing to the exceptional increase in the accuracy of the acquired data.[123–125] The signals from chemical shifts at various magnetic field strengths shown by the magnetically non-equivalent protons help to deduce the molecular structure. For instance, looking at the ^{1}H NMR of a terminal alkyne, a signal in the region of δ = 1.7 - 2.7 ppm corresponds to an alkynyl proton, whereas the peaks emerging at δ = 6.5 - 8.0 ppm are suggestive of protons attached to a 1,2,3-triazole ring and/or aromatic groups (**figure 2.41**). The proton of the aldehyde (-CHO) group usually gives a signal at δ = 10 ppm. Moreover, since the magnetic field of a proton combines with field of neighbouring protons to induce splitting of signal, the number of neighbouring protons for each observed proton can be validated. To a similar extent, the ^{13}C NMR spectrum displays signals that correspond to various forms of carbon in a molecule, for example, the proton decoupled ^{13}C NMR spectrum exhibits the C_5 signal of a 1,4-disustituted 1,2,3-triazole at around δ = 120 ppm, whereas the C_4 signal appears at δ = 133 ppm.

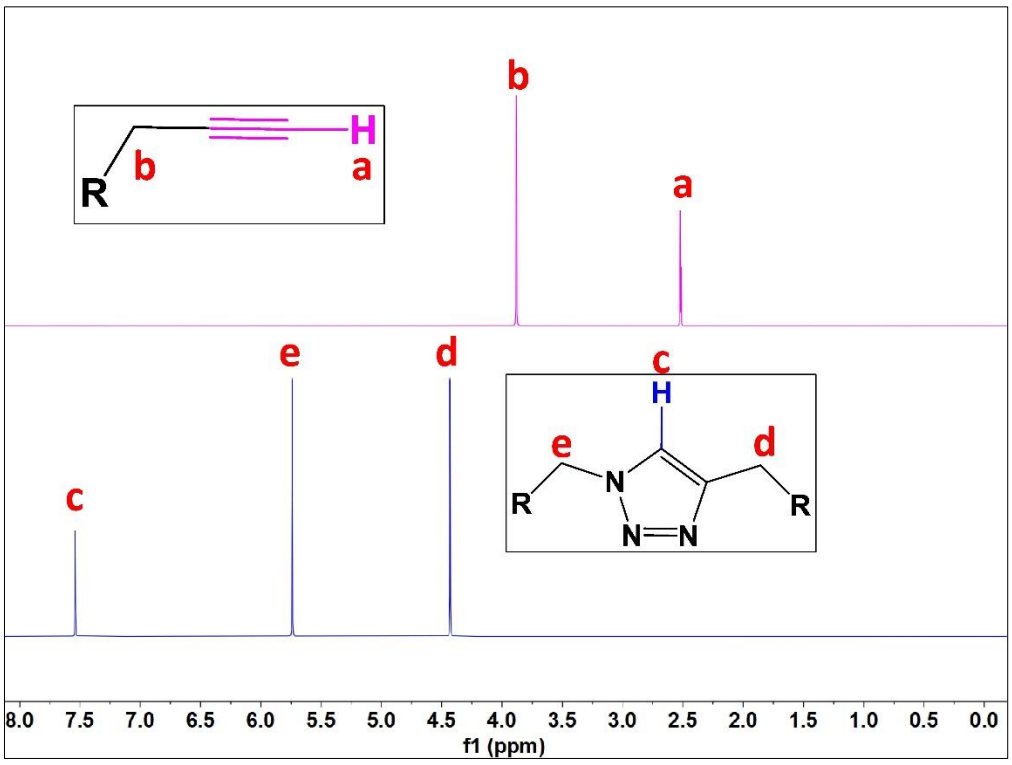

Figure 2.41: Comparative ^{1}H NMR analysis of an alkyne and a 1,2,3-triazole derivative depicting the presence of a peak at δ = 2.52 ppm and δ = 7.54 ppm corresponding to the alkynyl proton and the triazole ring proton respectively

2.3.3. Mass Spectrometry

Mass spectrometry is used for a wide variety of applications, including reaction monitoring and optimization, library compound quality evaluation, and structural characterization of library products[126,127] as well as for determining the molecular mass of unidentified substances. The process begins with the vaporization of the product molecules, which is followed by their ionization by electrons, and finally their fragmentation into smaller ions. The mass spectrometer is used to calculate the mass-to-charge ratio of ions, and peaks are produced in the corresponding spectrum for a range of mass-to-charge ratios and ion abundances.[128,129] In order to determine the molecular mass, the peak is read against the ratio of mass to charge that is the highest. By coupling mass spectrometry with chromatographic techniques such as Gas chromatography (GC) or Liquid chromatography (LC), the resulting hybrid technique provides a highly comprehensive analysis of complex samples owing to the detection and quantification of trace-level analytes in addition to providing structural information about the analytes, such as molecular weight and fragmentation patterns.

2.3.4. Ultraviolet-Visible (UV-Vis) Spectroscopy

The excitation of electrons from the ground state to an excited state and their instantaneous reversion to the ground state by emitting energy occurs when ultraviolet light passes through a solution of a compound and some of the photons of the radiation have energy equal to the difference in energies of the ground state and the excited state of an electron are absorbed by the molecules of the compound (**figure 2.42**).[130,131] In general, UV may be used to describe compounds that are conjugated, aromatic, or have unpaired electrons on O, N, or S atoms connected through double or triple bonds, e.g., a single low-intensity band between 250 nm and 360 nm represents $n \rightarrow \pi^*$ transitions, suggestive of functional groups like -N=N, -C=O, -COOR, $-NO_2$, -COOH, etc, whereas two medium-intensity bands above 200 nm are indicative of the presence of an aromatic system.[132,133]

2.3.5. Fluorescence Spectroscopy

Fluorescence spectroscopy is a powerful analytical technique used to study the fluorescent properties of molecules. It involves the absorption of light energy by a molecule, followed by its subsequent re-emission at a longer wavelength (**figure 2.42**). This phenomenon, known as fluorescence, occurs due to the molecule's transition from an excited electronic state to a lower energy state. The emitted fluorescence light is characterized by its intensity,

spectrum (wavelength distribution), and lifetime (duration of fluorescence emission).[134,135] By measuring and analyzing these properties, one can gain insights into various aspects of the molecule under investigation. Fluorescence spectroscopy offers several advantages over other analytical techniques, as it is highly sensitive, capable of detecting extremely low concentrations of fluorescent molecules, making it suitable for trace analysis.[136] Secondly, it has a wide dynamic range, allowing the quantification of both weak and strong fluorescence signals. Additionally, fluorescence spectroscopy is highly selective, as the emitted light is specific to the molecule of interest, enabling selective detection in complex mixtures. Lastly, it is a non-destructive technique, allowing for repeated measurements and sample reusability.[137–139]

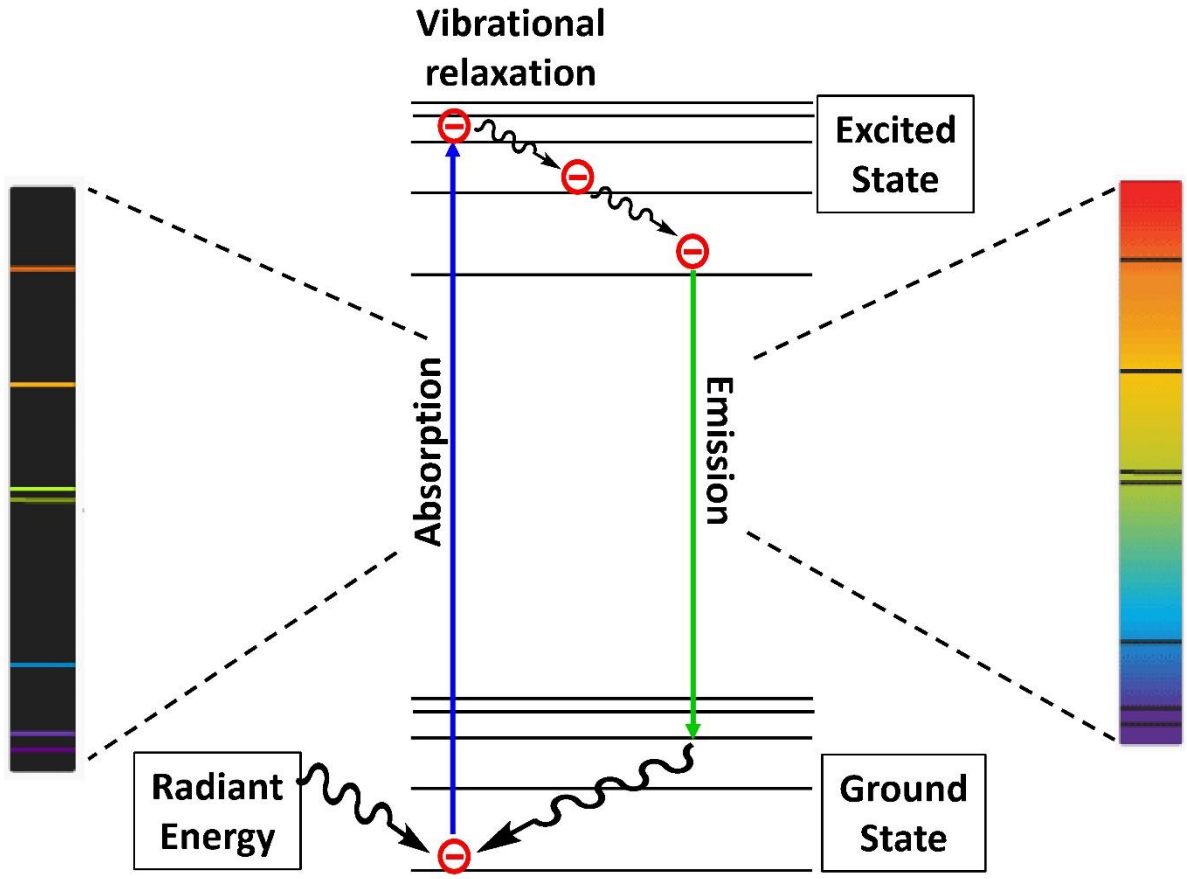

Figure 2.42: A representative illustration of the electronic transition corresponding absorption and emission spectroscopy

2.4. Applications of 1,2,3-triazole linkers as chemosensors

Click-generated 1,2,3-triazole derivatives have emerged as significant structural motifs in the area of chemical sensing owing to the ease with which they can be synthesized and the great selectivity they exhibit toward certain analytes of interest like heavy metal ions, anions, and neutral analytes.[140,141] Because of this ability, click-generated triazoles are considered to be one among the many essential classes of chemosensors.[142,143] Beyond serving as a bridge between the binding site and the reporter, the 1,2,3-triazole component often plays an additional role as an integral part of a conjugated fluorophore which in turn aids in the binding of the target analyte.[144,145] Numerous studies have documented the use of chemosensors wherein the 1,2,3-triazole establishes connections, either directly or indirectly, between the binding unit and the reporter unit (the chromophore).[146–149]

Areti and coworkers presented the synthesis of a quinoline-conjugated glucopyranose based 1,2,3-triazole appended chemosensor probe **110** via 'click' cycloaddition of 8-propargyloxyquinoline and tetra acetyl-β-glucopyranosyl azide which was subsequently utilized for selectively recognizing Hg(II) , Cd(II), and Zn(II) ions (**figure 2.43**). The probe exhibited fluorescence enhancement on the introduction of Zn(II) and Cd(II) ions whereas fluorescence quenching was observed on the introduction of Hg(II) ions.[150]

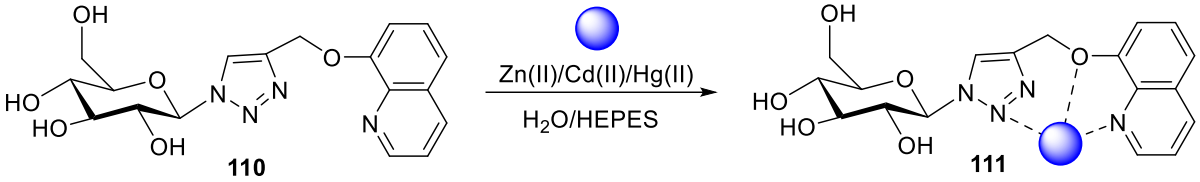

Figure 2.43: Quinoline-conjugated glucopyranose based 1,2,3-triazole-linked sensor for the recognition of Hg(II), Cd(II), and Zn(II)[150]

Pu and co-workers presented a naked eye chemosensor **112** for Al(III) and Cu(II) which consisted of a rhodamine B unit linked with triazole along with diarylethene (**figure 2.44**). The diarylethene unveiled significant change in fluorescence for Al(III), converting to yellow color from dark in acetonitrile as the solvent, whereas for Cu(II) recognition, the observed phenomenon involved a transition in fluorescence intensity, shifting from a low intensity, dark yellow color to a high intensity, bright yellow color in CH_3CN/H_2O (2:3 v/v ratio).[151]

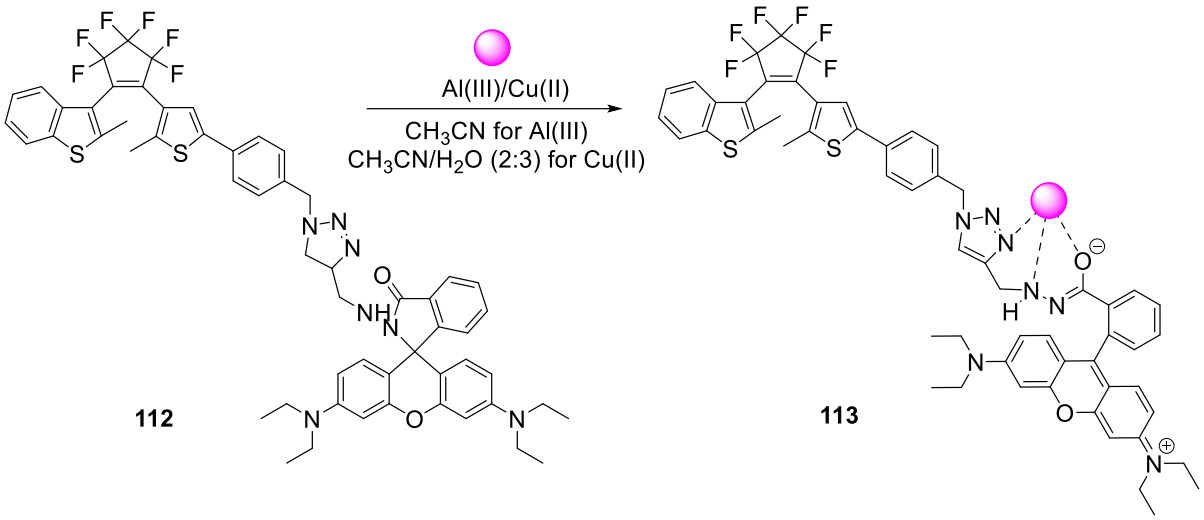

Figure 2.44: Rhodamine B- diarylethene based 1,2,3-triazole-linked chemosensor for Al(III) and Cu(II) recognition[151]

Aljabri *et al.* analyzed the binding characteristics of a newly synthesized substituted-bis(naphthyl)methane 'capped' calix[4]arene-based 1,2,3-triazole receptor **114** (**figure 2.45**) toward several clinically relevant metal ions via fluorescence spectroscopy titrations, wherein the sensitivity and selectivity of the probe for Fe(III) ions were confirmed by the quenched fluorescence spectrum shifts upon successive addition of Fe(III) ions.[152]

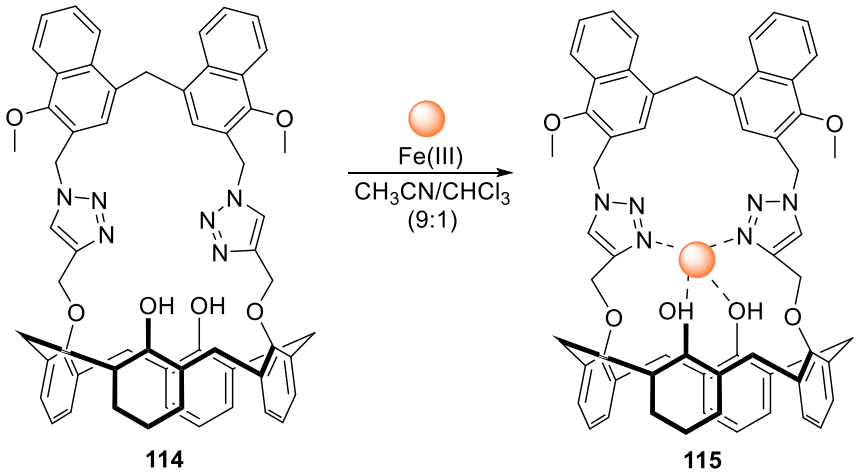

Figure 2.45: Bis(naphthyl)methane 'capped' 1,2,3- triazole-based calix[4]arene receptor for sensing Fe(III) ions[152]

Rathinam and colleagues reported the click reaction of rhodamine alkyne derivative with 11- aziodoundecan-1-ol in $CuSO_4$/Na ascorbate catalytic system and $^tBuOH/H_2O$ (3:1) which yielded the 1,2,3-triazole derived receptor **116** (**figure 2.46**). An increase in the

fluorescence by 20-fold compared to the free probe is achieved by adding Cu(II), while an increase of 14-fold is achieved by adding Fe(III).[153]

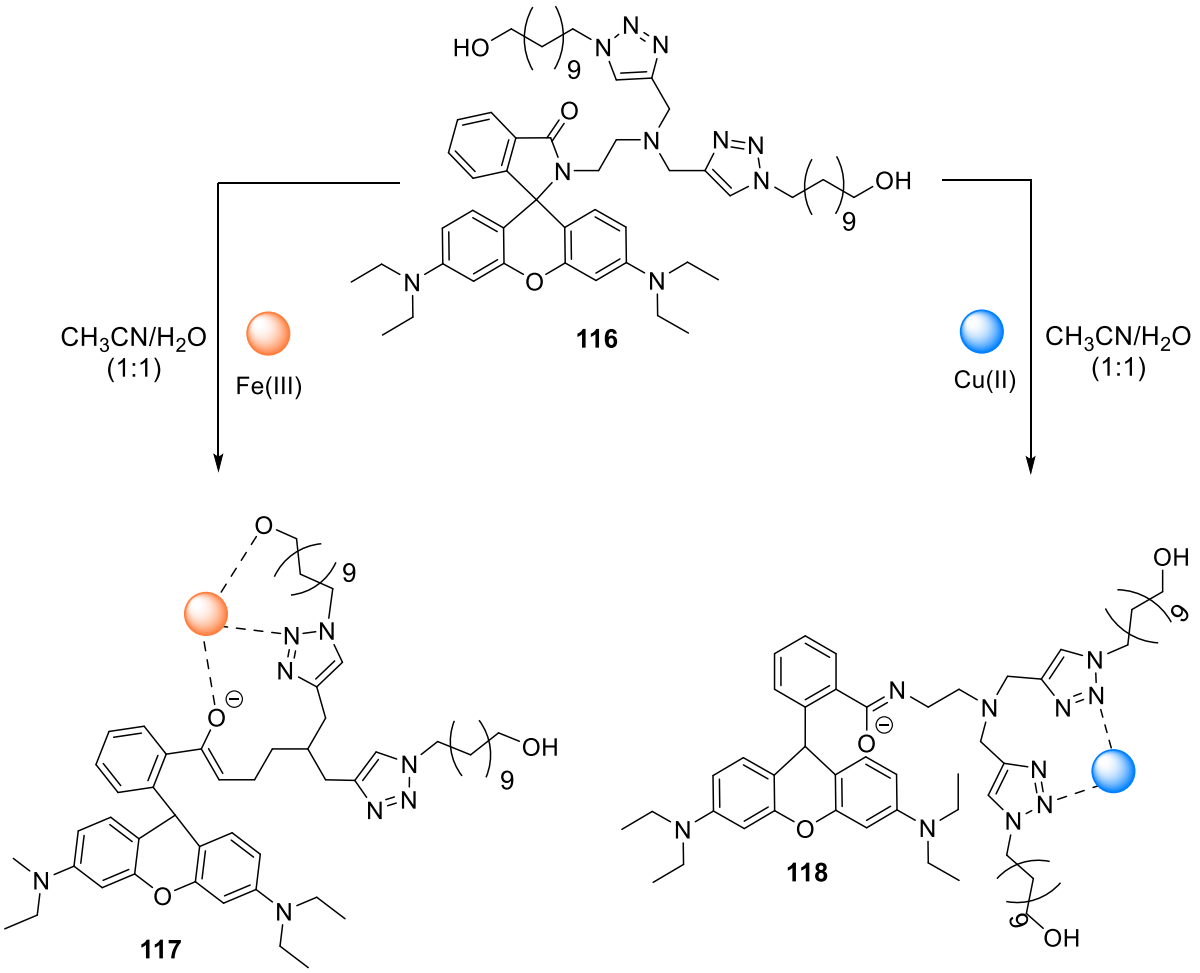

Figure 2.46: Rhodamine alkyne derived fluorescent sensor for Cu(II) and Fe(III) detection[153]

Gahlyan group described a novel isatin triazole-tethered rhodamine-based fluorescent probe **119** using the click chemistry technique. The fluorescence of the probe was enhanced on successive introduction of both Cu(II) and Fe(III) ions, making it a useful dual-sensor (**figure 2.47**). These metal ions were visually recognizable due to the distinctive color shift of the probe solution, changing to pink from colorless. The selective recognition of Cu(II)/Fe(II) ions was confirmed by strong bands at 585 nm on Cu(II)/Fe(II) ions addition and a faint band for Fe(II) at 583 nm in the fluorescence spectrum, while other metal ions did not induce any such shift.[154]

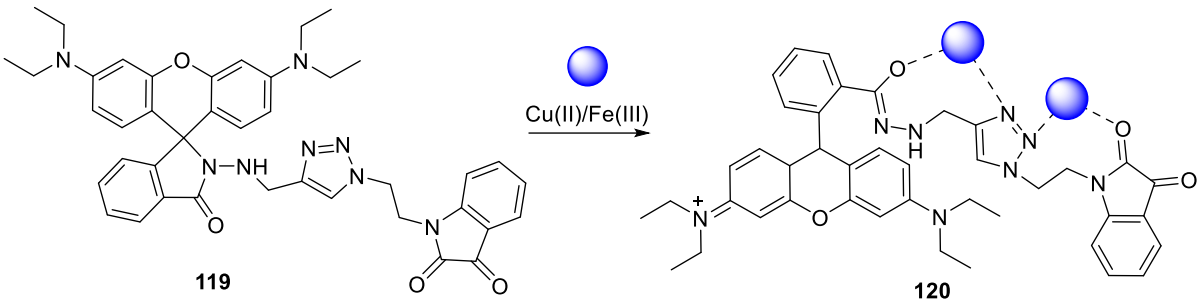

Figure 2.47: Isatin-triazole-tethered rhodamine-based fluorescent probe for selective Cu(II) recognition[154]

Hou and colleagues presented a BINOL-based cyclophane with two triazole moieties **121**. The emission of the sensor probe was selectively decreased by Ag(I) ions among various metal ions screened, in methanol solution (**figure 2.48**). The probe was conceptualized keeping in mind the Stokes shift of roughly 70 nm due to the BINOL moiety, possibility of the O atom of the BINOL taking part in binding with the metal ion, and the preorganized cavity of the cyclophane formed via click chemistry to enhance the metal ion selectivity of the probe.[155]

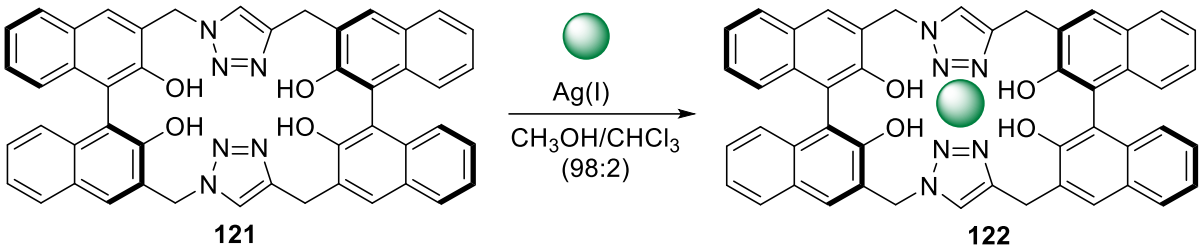

Figure 2.48: BINOL-based cyclophane with two triazole moieties for Ag(I) sensing[155]

Mandal *et al.* synthesized unsymmetrically 1,19-disubstituted ferrocene based 1,2,3-triazole derivative **123** with successive functionalization at the cyclopentadienyl rings, wherein a cholesterol moiety was connected to the first position of the ferrocene center through a 1,2,3-triazole ring. Additionally, a fluorescent moiety, i.e., pyrene unit was attached to the 19-position of the same core using another 1,2,3-triazole-ether linkage. (**figure 2.49**); these were the unique structural features present in these ligands. A colorimetric response was seen from the probe, and it was able to selectively exhibit 'turn off' fluorescence response on adding Hg(II) and Cu(II).[156]

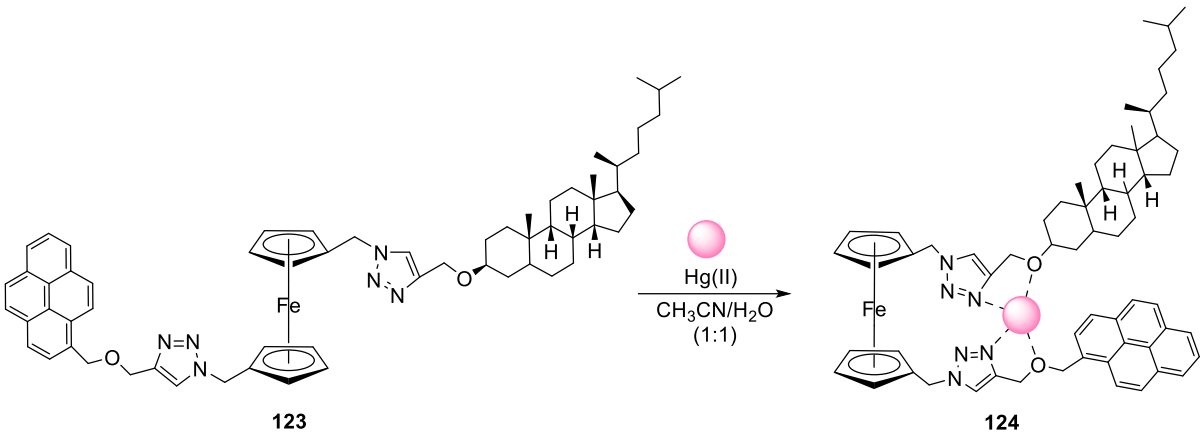

Figure 2.49: 1,19-disubstituted ferrocene-appended 1,2,3-triazole-linked compound for the sensing of Hg(II) and Cu(II)[156]

The synthesis of a ferrocene-naphthalene conjugate **125** with 1,2,3-triazole linkages (**figure 2.50**) was described by Bhatta and coworkers. The conjugate was employed as a simple colorimetric, electrochemical, and fluorescent chemosensor. The strong binding affinity towards Hg(II) ions was demonstrated by the significant quenching of the probe's fluorescence on introducing the metal ions, accompanied by color change from yellow to greenish blue rapidly, proving its naked-eye detectability of Hg(II).[157]

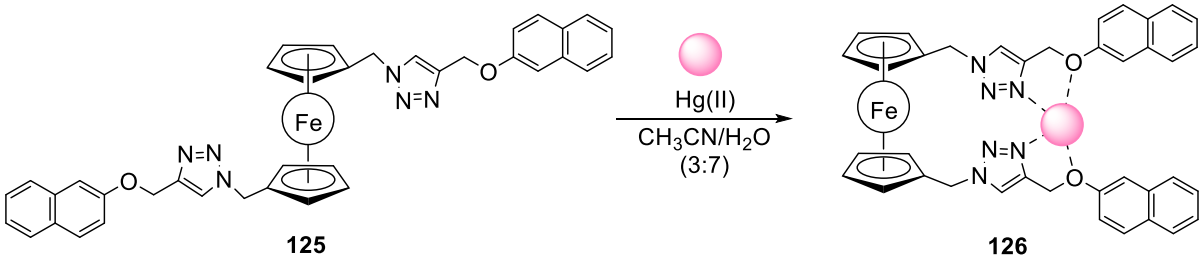

Figure 2.50: Ferrocene-naphthalene conjugate with 1,2,3-triazole linkages for detecting Hg(II) ions[157]

Zhang group produced a new b-cyclodextrin derivative chemosensor **127** with 8-hydroxyquinolino and 1,2,3-triazole group. The probe showed a strong switch-on fluorescence response to Cd(II) relative to other common metal ions under physiological conditions, and it was water soluble up to 0.03 mol/L. **(figure 2.51)**.[158]

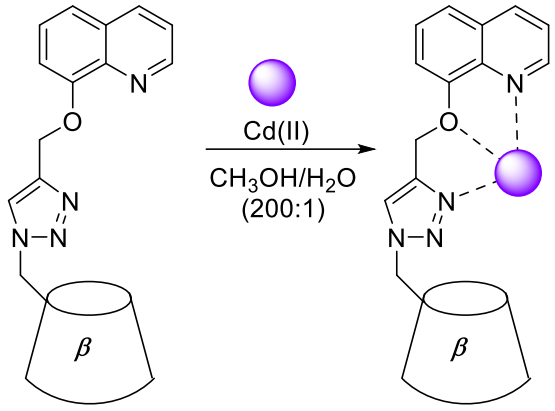

Figure 2.51: Quinolinotriazole-b-cyclodextrin as a selective sensor probe for Cd(II) ions[158]

Ingale and co-workers described a tripropargylamine pyrene azide click adduct-based ratiometric fluorescent 'on-off' Zn(II) chemosensor **129**. The ratiometric shift in emission, wherein the monomer emission displayed an enhancement whereas the excimer emission displayed quenching, was indicative of Zn(II) selectivity in the fluorescence 'on-off' sensor **(figure 2.52).**[159]

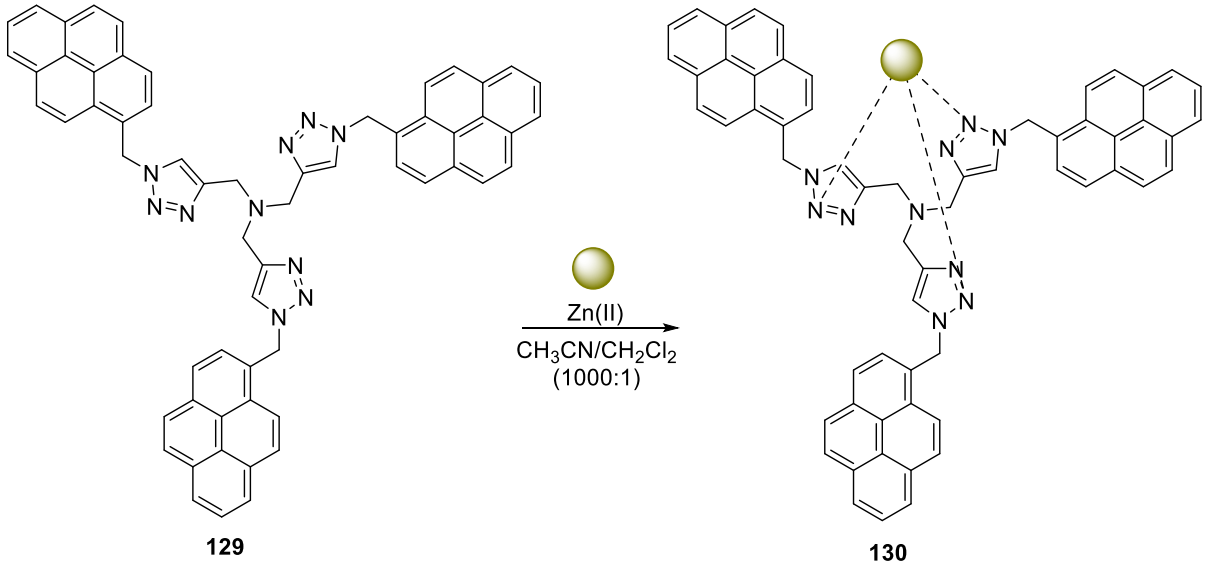

Figure 2.52: A pyrene-linked tris-1,2,3-triazole amine based sensor for Zn(II)[159]

Entry	Sensor probe	Metal ion(s)	Spectroscopy		Solvent media	Detection Limit (LoD)	Stoichiometry (L:M)	Ref
			UV-Vis	Fluorescence				
01	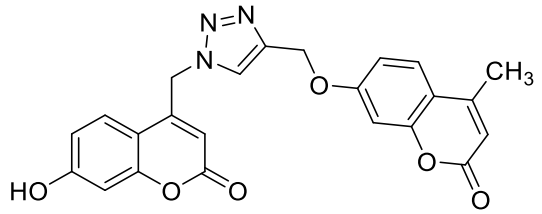 **83**	Ca^{2+}	✓	✓	DMSO	2.61 µM	1:1	[108]
		Fe^{3+}	✓	✓		3.81 µM		
02	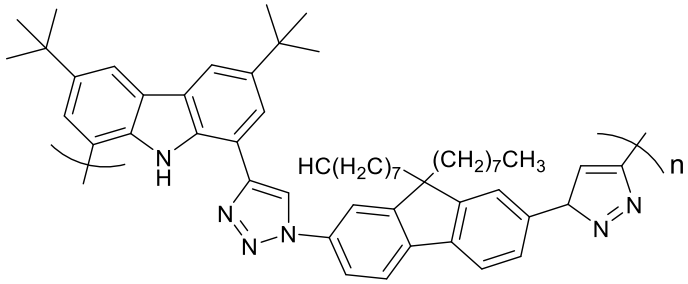 **86**	Sn^{2+}	×	✓	$CHCl_3$	N/A	1:1	[109]
03	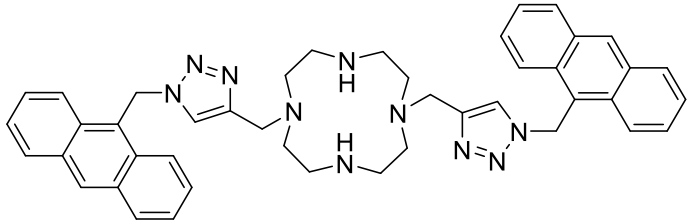 **89**	Pb^{2+}	×	✓	H_2O (with HEPES Buffer)	N/A	1:1	[110]

Entry	Sensor probe	Metal ion(s)	Spectroscopy		Solvent media	Detection Limit (LoD)	Stoichiometry (L:M)	Ref
			UV-Vis	Fluorescence				
04	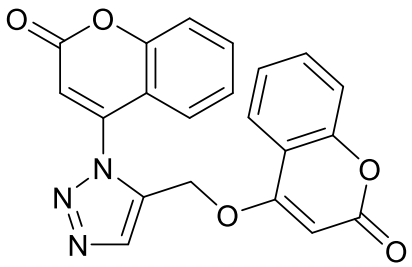 **92**	Pb^{2+}	✓	✓	DMSO/H_2O (1:9)	1.9 × 10^{-3} µM	1:1	[111]
05	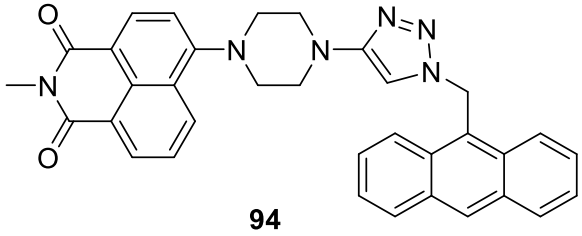 **94**	Cr^{3+}	✓	✓	THF/H_2O (4:6)	5.567 ×10^{-2} µM	1:1	[112]

Entry	Sensor probe	Metal ion(s)	Spectroscopy		Solvent media	Detection Limit (LoD)	Stoichiometry (L:M)	Ref
			UV-Vis	Fluorescence				
06	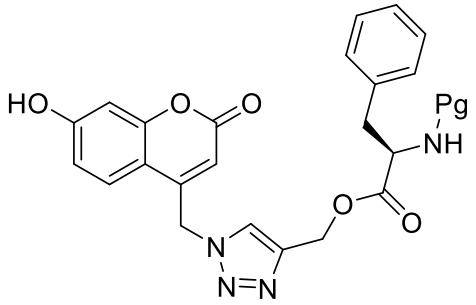 **97**	Fe^{3+}	×	✓	DMF	7.65 µM	1:1	113
07	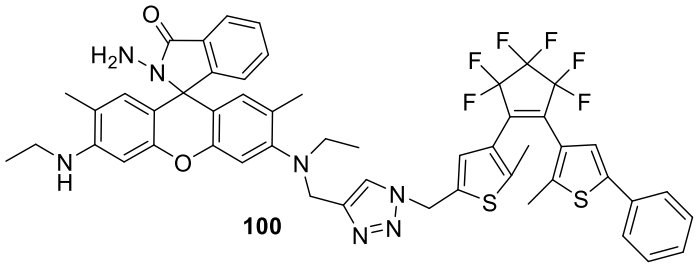 **100**	Fe^{3+}	✓	✓	aq. CH_3CN (1:1)	0.77 µM	1:1	114
		Cu^{2+}	×	✓		0.76 µM		

Entry	Sensor probe	Metal ion(s)	Spectroscopy		Solvent media	Detection Limit (LoD)	Stoichiometry (L:M)	Ref
			UV-Vis	Fluorescence				
08	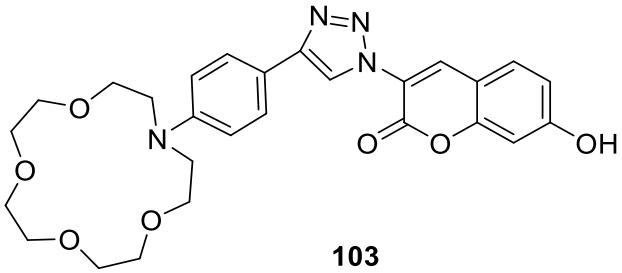 **103**	Fe^{3+}	×	✓	H_2O	3.6 µM	1:1	115
		Hg^{2+}	×	✓		1.0 µM		
09	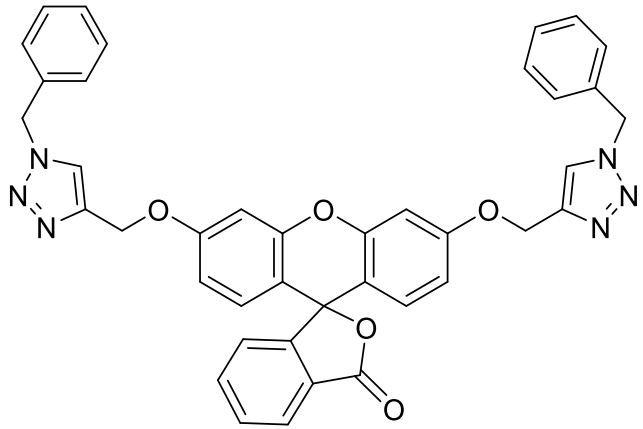 **106**	Co^{2+}	✓	×	C_2H_5OH/H_2O (1:1)	10 µM	1:1	116
		Cd^{2+}	✓	×		10 µM		

Entry	Sensor probe	Metal ion(s)	Spectroscopy		Solvent media	Detection Limit (LoD)	Stoichiometry (L:M)	Ref
			UV-Vis	Fluorescence				
10	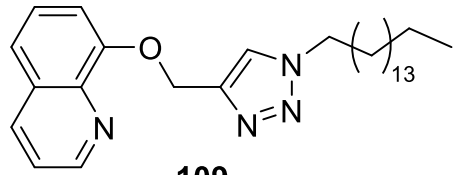 **109**	Hg^{2+}	×	✓	H_2O	4.42 nM	1:1	[117]
11	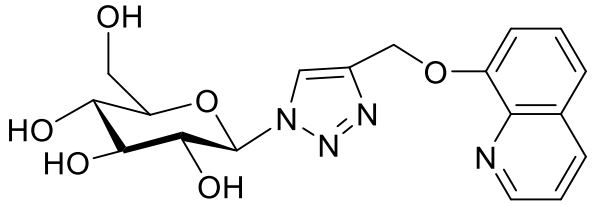 **110**	Zn(II)	✓	✓	H_2O (with HEPES buffer)	$(24\pm2)\times 10^{-3}$ µM	1:2	[150]
		Cd(II)	✓	✓		$(38\pm3) \times 10^{-3}$ µM		
		Hg(II)	✓	✓		$(34\pm3) \times 10^{-3}$ µM	1:1	
12		Al(III)	×	✓	CH_3CN	N/A	N/A	[151]

Entry	Sensor probe	Metal ion(s)	Spectroscopy		Solvent media	Detection Limit (LoD)	Stoichiometry (L:M)	Ref
			UV-Vis	Fluorescence				
	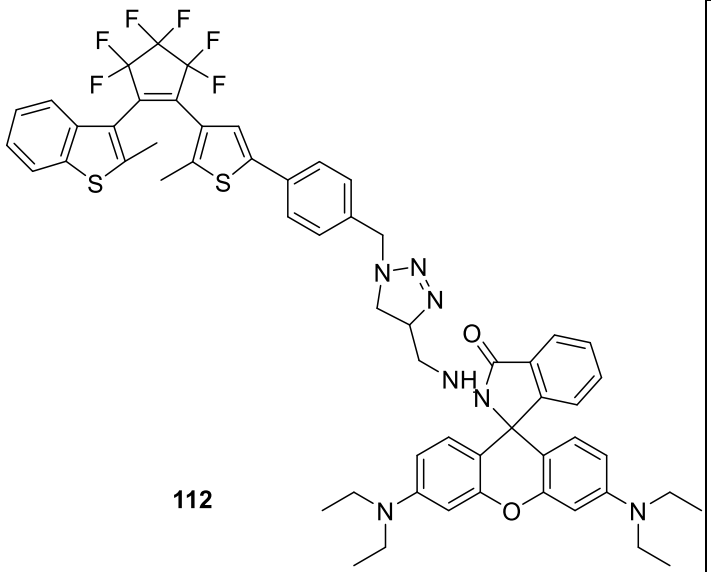 112	Cu(II)	×	✓	CH_3CN/H_2O (2:3)	N/A		

Entry	Sensor probe	Metal ion(s)	Spectroscopy		Solvent media	Detection Limit (LoD)	Stoichiometry (L:M)	Ref
			UV-Vis	Fluorescence				
13	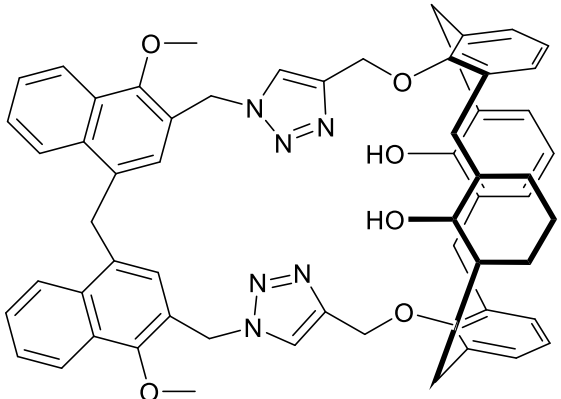 **114**	Fe(III)	×	✓	$CH_3CN/CHCl_3$ (9:1)	N/A	1:1	[152]
14	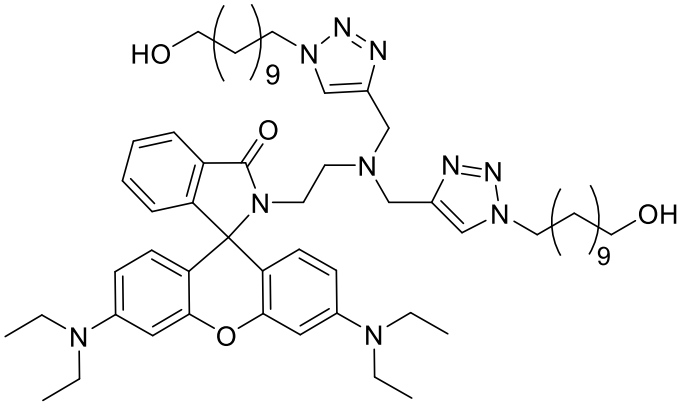 **116**	Fe(III)	✓	✓	CH_3CN/H_2O (1:1)	250 µM	1:1	[153]
		Cu(II)	✓	✓		100 µM		

Entry	Sensor probe	Metal ion(s)	Spectroscopy		Solvent media	Detection Limit (LoD)	Stoichiometry (L:M)	Ref
			UV-Vis	Fluorescence				
15	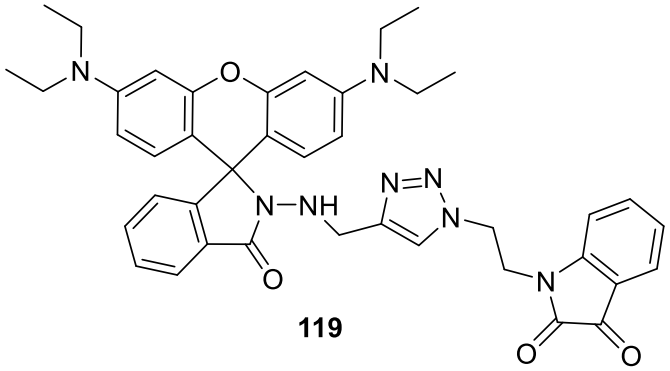 **119**	Cu(II)	✓	✓	N/A	12.2×10^{-3} µM	1:2	[154]
		Fe(III)	✓	✓		0.33 µM		
16	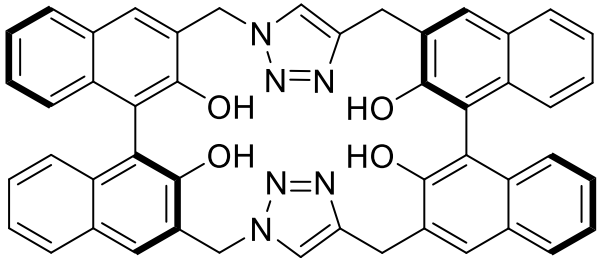 **121**	Ag(I)	×	✓	$CH_3OH/CHCl_3$ (98:2)	N/A	1:1	[155]

Entry	Sensor probe	Metal ion(s)	Spectroscopy		Solvent media	Detection Limit (LoD)	Stoichiometry (L:M)	Ref
			UV-Vis	Fluorescence				
17	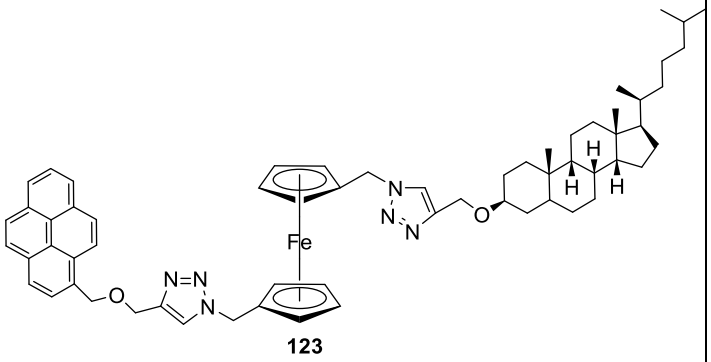 123	Hg(II)	✓	✓	CH_3CN/H_2O (1:1)	2 ppb	1:1	[156]

Entry	Sensor probe	Metal ion(s)	Spectroscopy		Solvent media	Detection Limit (LoD)	Stoichiometry (L:M)	Ref
			UV-Vis	Fluorescence				
18	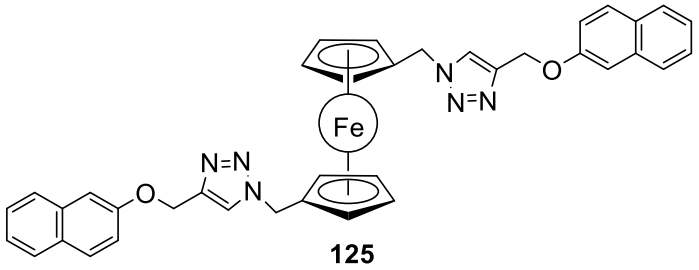 125	Hg(II)	✓	✓	CH_3CN/H_2O (3:7)	4.5 ppb	1:1	[157]
19	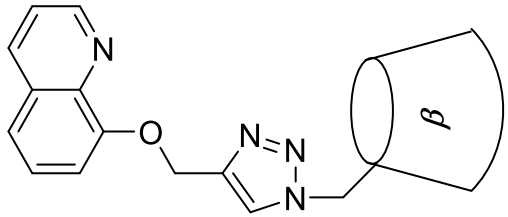 127	Cd(II)	×	✓	CH_3OH/H_2O (200:1)	1.89×10^{-3} M	1:1	[158]

Entry	Sensor probe	Metal ion(s)	Spectroscopy		Solvent media	Detection Limit (LoD)	Stoichiometry (L:M)	Ref
			UV-Vis	Fluorescence				
20	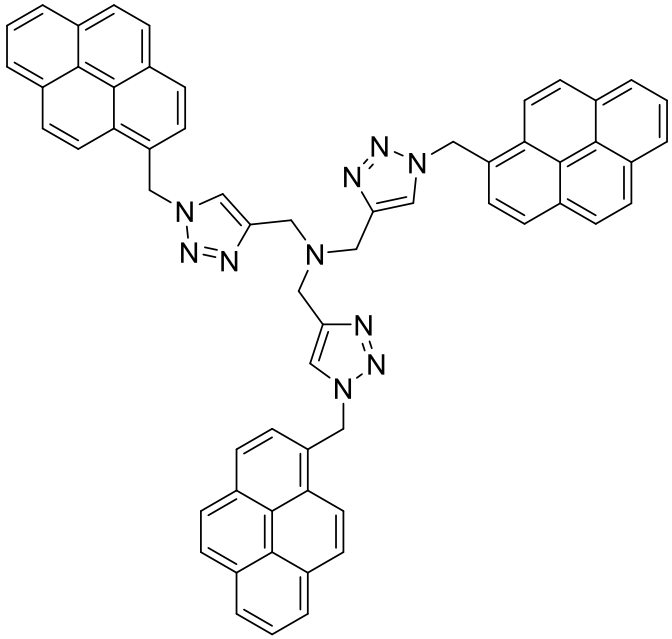 **129**	Zn(II)	×	✓	CH_3CN/CH_2Cl_2 (1000:1)	0.2 µM	1:1	[159]

Entry	Sensor probe	Metal ion(s)	Spectroscopy		Solvent media	Detection Limit (LoD)	Stoichiometry (L:M)	Ref
			UV-Vis	Fluorescence				
21	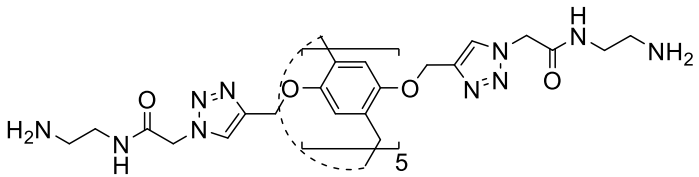 **130**	Fe^{3+}	✓	✓	D_2O/CD_3OD (9.2:0.8)	689 ppm	---	[160]
22	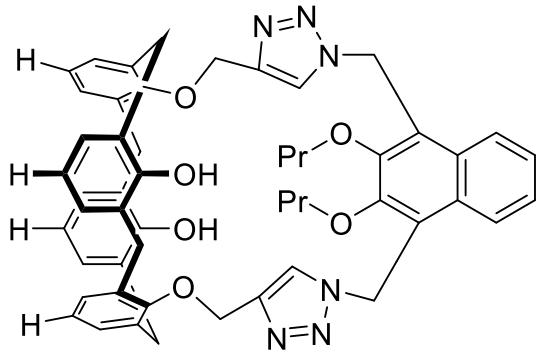 **131**	Fe^{3+}	×	✓	$CH_3CN/CHCl_3$ (9:1)	N/A	1:1	[161]
		Hg^{2+}	×	✓		N/A		

Entry	Sensor probe	Metal ion(s)	Spectroscopy		Solvent media	Detection Limit (LoD)	Stoichiometry (L:M)	Ref
			UV-Vis	Fluorescence				
23	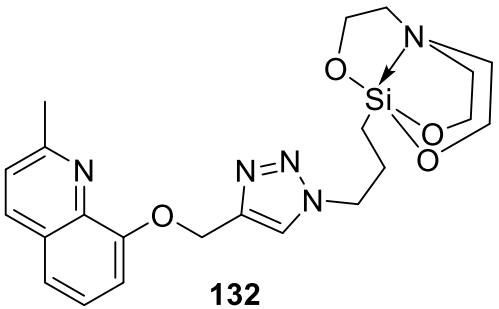 **132**	Fe^{2+}	✓	✓	CH_3OH	N/A	1:2	[162]
		Fe^{3+}	✓	✓		N/A		
24	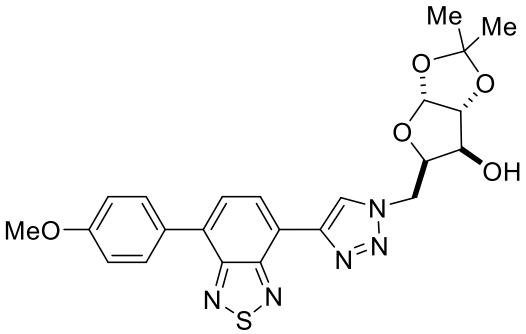 **133**	Ni^{2+}	×	✓	CH_3CN	N/A	N/A	[163]

Entry	Sensor probe	Metal ion(s)	Spectroscopy		Solvent media	Detection Limit (LoD)	Stoichiometry (L:M)	Ref
			UV-Vis	Fluorescence				
25	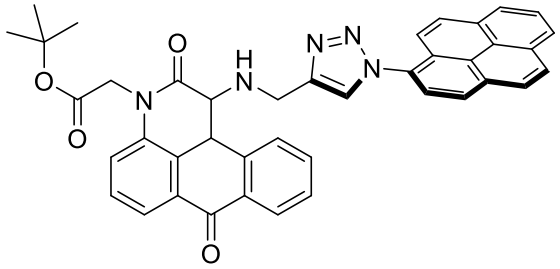 **134**	Ni^{2+}	✓	✓	C_2H_5OH	0.5 µM	1:1	164
		Cu^{2+}	✓	✓		0.2 µM		

Table 2.1: Chemosensors appended with 1,2,3-triazole moiety for recognizing distinct metal ions

2.5. The advantages of using 1,2,3-triazole derivatives for ion sensing

As the widespread heavy metal ion build-up in the environment, which is harmful to terrestrial and aquatic life, posing a serious worldwide environmental threat, therefore it is essential that their presence be detected as quickly and accurately as possible.[165] Many methods and approaches have been developed specifically for this objective, out of which one of the most common approaches of metal ion sensing is Atomic Absorption Spectroscopy (AAS),[166–169] which involves the utilization of metal atom absorption and emission spectra, capitalizing on their distinct and robust spectral lines. Additionally, Inductively Coupled Plasma-Mass Spectrometry (ICP-MS) stands out as a well-regarded technique, offering multi-elemental detection capabilities at ultratrace levels. It has proven particularly valuable in geological material analysis, leveraging the selectivity of mass spectrometry and ICP in atomizing and ionizing samples.[170–172] Despite their remarkable sensitivity, these methods present several drawbacks, including the requirement for expensive instrumentation, extensive sample preparation, intricate sample pre-treatment procedures, the need for skilled personnel to operate the equipment, and the inability to perform on-site analyses.[173,174] Recognizing these limitations, the scientific community has been exploring alternative methodologies, Notably, 1,2,3-triazole-linked chemosensors synthesized through CuAAC have shown promise, as these probes offer distinct advantages, including , rapid reaction times, high sensitivity, and in some cases, the possibility of on-site analysis, all of which may be achieved by their simple laboratory synthesis without the utilization of sophisticated equipment and/or instruments.[175–177] The following features of ion sensing ligands are of special relevance in terms of their effectiveness and selectivity:

2.5.1. Tailor-made functionalities for the 1,2,3-triazole moiety

The flexibility of organic chemistry allows for the precise design of an unlimited variety of host compounds including numerous centres capable of interacting with one another in mutually beneficial ways. In turn, this allows for comprehensive experimental studies predicated on binding increments, which may be demonstrated to be highly additive.[178] Researchers now have the option of producing a wide range of 1,2,3-triazole-based ligands by means of ‘click chemistry’, which facilitates the efficient stitching of substituted alkynes and azides.[179–182] These ligands act as selective recognition agents for many different cations and anions. According to the HSAB principle,[183] exocyclic moieties linked to the 1,2,3-triazole component may display high electron density, like F^-, Cl^-, -OH, -OR, and similar species (often

referred to as hard bases), or in some cases the exocyclic moieties may exhibit low electron density, such as -H, -RS, -PR_3, and similar species (referred to as soft bases) that demonstrate selective binding with the corresponding cations. To further enhance selective ion identification, the 1,2,3-triazole ring includes aza atoms that facilitate metal ion attachment to the ring.

2.5.2. Lower limit of detection

It is generally agreed that chemosensing probes with a lower metal ion detection limit[184] than the allowable value in the environment as stated by the EPA are superior examples of their kind.[185,186] The limit of detection (LOD) for metal ion sensing using 1,2,3-triazole derivatives can vary depending on the specific functional groups, the metal ion being detected, and the sensing method used. In this endeavor, sensor probes that exhibit fluorescence upon interacting with metal ions demonstrate exceptional sensitivity, capable of detecting concentrations as low as parts per billion (ppb).

2.5.3. Visual changes to naked eye

Many studies on 1,2,3-triazole derivatives that are able to display colour changes following complexation with metal ions can be found in the published scientific literature. These visual changes can be useful for rapid and easy detection of metal ions, especially in field applications or scenarios where complex instrumentation is not readily available. One common approach is the development of colorimetric sensors based on 1,2,3-triazole derivatives. These sensors undergo specific interactions with metal ions, leading to changes in their molecular structure or conformation. As a result, their absorption properties in visible region are altered, leading to changes in color.[187–189]

2.6. Aims and objectives of the thesis

The extensive research shows that novel 1,2,3-triazole derivatives may be synthesized from simple alkynes and azides using the CuAAC technique, and this potential spans a broad range of structures. To create novel 1,2,3-triazole linked compounds, a wide variety of organic molecules, including those with excellent fluorophoric units, may be used by first changing their functional groups using straightforward procedures, yielding new terminal alkynes and organic azides. A method of ion sensing may be used to the newly synthesized compounds once they have been characterized. The following aims for this study were developed in light of this realization:

1. Synthesis of 1,4-disubstituted 1,2,3–triazole derivatives by Cu(I) catalyzed Click reaction between terminal alkyne and organic azide.
2. Characterization of synthesized compounds by spectroscopic techniques like IR, NMR (^{1}H, ^{13}C), mass spectroscopy and X-ray (wherever possible).
3. To study ion sensing behavior of synthesized 1,4-disubstituted 1,2,3–triazole derivatives using UV–Visible spectroscopy and/or fluorescence.

The aim of this thesis titled 'SYNTHESIS AND CHARACTERIZATION OF 1,4-DISUBSTITUTED 1,2,3−TRIAZOLES, AS ION SENSORS, USING Cu(I) CATALYZED CLICK REACTION' was to design and test novel 1,2,3-triazole-appended probes with the hope of using them as optical sensors for the detection of certain metal ions such as Cr(III), Pb(II), Cu(II), Hg(II), Ce(III), etc.

The identification of harmful analytes that have an adverse effect on the environment and the development of living systems has received a great deal of attention globally in recent years and is now regarded as one of the most important areas of study in the discipline of chemistry. For instance, humans are susceptible to the harmful effects of cadmium, which may have an adverse impact on their skeletons, lungs, kidneys, and reproductive systems, and even cause cancer. Because of its tenacious nature, it may build up in several human organs. Every chemical form of mercury is neurotoxic, but it is particularly dangerous for developing brains. Many organs are susceptible to Hg poisoning, but the CNS is particularly vulnerable on both the high and low end of the scale. The non-biodegradable nature of lead is a major contributor to its long-lasting presence in the environment, including the soil, the air, and the water. Lead is a likely human carcinogen and has been linked to memory and intellectual functioning deficiencies in both adults and children who have been exposed to it at high levels.

Hence, the synthesis of novel and selective chemosensors is a fundamental endeavour, wherein the 1,2,3-triazole-tethered sensors have made great strides in the past decade, with one major aim being the detection and sensing of physiologically and ecologically relevant metal ions. In that realm, UV-Vis and fluorescence spectroscopy are two important analytical instruments because of their high detection limit, instantaneous results, and ability to be used in bioimaging. Consequently, over the past decade, 1,2,3-triazole-based chemosensors generated through click chemistry have proven to be versatile functional structures, exhibiting remarkable selectivity and binding capabilities. It has become common practice to employ click reactions in the production of extremely sensitive and selective sensors for metal cations

because of their adaptability, efficiency, and durability. As an added bonus, click chemistry allows for the preparation of photoactive materials with highly adjustable and fascinating sensing capabilities, as well as the use of a broad variety of substrates, which opens the door to exploring a vast array of ligand structures for a variety of purposes.

References

1 J. Alvárez-Builla and J. Barluenga, in *Modern Heterocyclic Chemistry*, eds. Julio Alvarez-Builla, J. J. Vaquero and J. Barluenga, Wiley, 1st edn., 2011, vol. 1, pp. 1–9.

2 V. Ji Ram, A. Sethi, M. Nath and R. Pratap, in *The Chemistry of Heterocycles*, Amsterdam, 1st edn., 2019, pp. 149–478.

3 Q. Li, L. Han, L. Zhao, Y. Hou and R. Sharma, *Synth. Commun.*, 2021, **51**, 2754–2781.

4 P. Zahl and Y. Zhang, *Energy Fuels*, 2019, **33**, 4775–4780.

5 H. Szatylowicz, O. A. Stasyuk and T. M. Krygowski, in *Advances in Heterocyclic Chemistry*, eds. E. F. V. Scriven and C. A. Ramsden, Elsevier Ltd, 2016, vol. 120, pp. 301–327.

6 A. T. Balaban, D. C. Oniciu and A. R. Katritzky, *Chem. Rev.*, 2004, **104**, 2777–2812.

7 J. Toldo, O. El Bakouri, M. Solà, P. O. Norrby and H. Ottosson, *Chempluschem*, 2019, **84**, 712–721.

8 J. Bergman and T. Janosik, in *Modern Heterocyclic Chemistry*, eds. J. Alvarez-Builla, J. J. Vaquero and J. Barluenga, Wiley, 1st edn., 2011, vol. 1, pp. 269–375.

9 J. Barluenga and C. Valdés, in *Modern Heterocyclic Chemistry*, eds. J. Alvarez-Builla, J. J. Vaquero and J. Barluenga, Wiley, 1st edn., 2011, vol. 1, pp. 377–531.

10 L. Yet, in *Modern Heterocyclic Chemistry*, eds. J. Alvarez-Builla, J. J. Vaquero and J. Barluenga, Wiley, 1st edn., 2011, vol. 2, pp. 989–1045.

11 Y. Volkova, S. Baranin and I. Zavarzin, *Adv. Synth. Catal.*, 2021, **363**, 40–61.

12 D. Yadagiri, M. Rivas and V. Gevorgyan, *J. Org. Chem.*, 2020, **85**, 11030–11046.

13 L. L. Anderson, *Asian J. Org. Chem.*, 2016, **5**, 9–30.

14 A. Z. Halimehjani, I. N. N. Namboothiri and S. E. Hooshmand, *RSC Adv.*, 2014, **4**, 51794–51829.

15 A. Z. Halimehjani, I. N. N. Namboothiri and S. E. Hooshmand, *RSC Adv.*, 2014, **4**, 48022–48084.

16 S. K. Bur and A. Padwa, *Chem. Rev.*, 2004, **104**, 2401–2432.

17 Y. Sun, M. Hu, S. Fu and B. Liu, *Org. Biomol. Chem.*, 2020, **18**, 6443–6466.

18 E. Kabir and M. Uzzaman, *Results Chem.*, 2022, **4**, 100606.

19 A. Lauria, R. Delisi, F. Mingoia, A. Terenzi, A. Martorana, G. Barone and A. M. Almerico, *Eur. J. Org. Chem.*, 2014, **2014**, 3289–3306.

20 J. Jampilek, *Molecules*, 2019, **24**, 3839.

21 P. N. Kalaria, S. C. Karad and D. K. Raval, *Eur. J. Med. Chem.*, 2018, **158**, 917–936.

22 A. Mermer, T. Keles and Y. Sirin, *Bioorg. Chem.*, 2021, **114**, 105076.

23 S. A. Khanum, S. Shashikanth, S. Umesha and R. Kavitha, *Eur. J. Med. Chem.*, 2005, **40**, 1156–1162.

24 C. A. Malapit and A. R. Howell, *J. Org. Chem.*, 2015, **80**, 8489–8495.

25 J. T. Yu and C. Pan, *ChemComm.*, 2016, **52**, 2220–2236.

26 C. C. Woodroofe, P. L. Meisenheimer, D. H. Klaubert, Y. Kovic, J. C. Rosenberg, C. E. Behney, T. L. Southworth and B. R. Branchini, *Biochemistry*, 2012, **51**, 9807–9813.

27 M. Kuse, in *Marine Natural Products*, ed. H. Kiyota, Springer Singapore, 1st edn., 2020, pp. 85–103.

28 N. M. W. Wu, M. Ng, W. H. Lam, H. L. Wong and V. W. W. Yam, *J. Am. Chem. Soc.*, 2017, **139**, 15142–15150.

29 S. Helmy and J. Read de Alaniz, in *Advances in Heterocyclic Chemistry*, eds. E. F. V. Scriven and C. A. Ramsden, Elsevier Ltd, Amsterdam, 2015, vol. 117, pp. 131–177.

30 B. D. Stringer, L. M. Quan, P. J. Barnard, D. J. D. Wilson and C. F. Hogan, *Organometallics*, 2014, **33**, 4860–4872.

31 H. J. Park, S. Yoo, I. S. Shin, Y. K. Chung and J. Kim, *Electroanalysis*, 2013, **25**, 1111–1115.

32 S. Khaghaninejad and M. M. Heravi, in *Advances in Heterocyclic Chemistry*, ed. A. R. Katritzky, Elsevier, 1st edn., 2014, vol. 111, pp. 95–146.

33 M. E. Cinar and T. Ozturk, *Chem. Rev.*, 2015, **115**, 3036–3140.

34 A. R. Kennedy, J. Klett, R. E. Mulvey and S. D. Robertson, *Eur. J. Inorg. Chem.*, 2011, 4675–4679.

35 S. Shaun Murphree, in *Progress in Heterocyclic Chemistry*, eds. G. Gribble and J. A. Joule, Elsevier Ltd, 2011, vol. 22, pp. 21–58.

36 L. K. M. O. Goni, M. A. J. Mazumder, M. A. Quraishi and M. M. Rahman, *Chem. Asian J.*, 2021, **16**, 1324–1364.

37 B. Eftekhari-Sis, M. Zirak and A. Akbari, *Chem. Rev.*, 2013, **113**, 2958–3043.

38 A. K. Pal and G. S. Hanan, *Chem. Soc. Rev.*, 2014, **43**, 6184–6197.

39 V. S. Kumar, Y. S. Mary, K. Pradhan, D. Brahman, Y. S. Mary, R. Thomas, M. S. Roxy and C. Van Alsenoy, *J. Mol. Struct.*, 2020, **1199**, 127035.

40 J. M. Tour, A. M. Rawlett, M. Kozaki, Y. Yao, R. C. Jagessar, S. M. Dirk, D. W. Price, M. A. Reed, C. W. Zhou, J. Chen, W. Wang and I. Campbell, *Chem. Eur. J.*, 2001, **7**, 5118–5134.

41 A. Pizarro, G. Abarca, C. Gutiérrez-Cerón, D. Cortés-Arriagada, F. Bernardi, C. Berrios, J. F. Silva, M. C. Rezende, J. H. Zagal, R. Onate and I. Ponce, *ACS Catal.*, 2018, **8**, 8406–8419.

42 L. Leontie, R. Danac, I. Druta, A. Carlescu and G. I. Rusu, *Synth. Met.*, 2010, **160**, 1273–1279.

43 J. Huang and G. Yu, *Chem. Mater.*, 2021, **33**, 1513–1539.

44 K. S. Son, M. Yahiro, T. Imai, H. Yoshizaki and C. Adachi, *Chem. Mater.*, 2008, **20**, 4439–4446.

45 M. A. Quraishi, D. S. Chauhan and V. S. Saji, *J. Mol. Liq.*, 2021, **341**, 117265.

46 M. Yusuf and P. Jain, *Arab. J. Chem.*, 2014, **7**, 553–596.

47 S. A. Raw, C. D. Wilfred and R. J. K. Taylor, *Org. Biomol. Chem.*, 2004, **2**, 788–796.

48 D. Guianvarc'h, J. L. Fourrey, M. E. T. H. Dau, V. Guérineau and R. Benhida, *J. Org. Chem.*, 2002, **67**, 3724–3732.

49 C. R. Kella, C. Balachandran, Y. Arun, E. Kaliyappan, S. M. Mahalingam, S. Ignacimuthu, N. Arumugam, A. I. Almansour, R. Suresh Kumar and P. T. Perumal, *Arab. J. Chem.*, 2020, **13**, 9047–9057.

50 W. Yao, Y. Xue, L. Qian, H. Yang and G. Cheng, *Energ. Mater. Front.*, 2021, **2**, 131–138.

51 J. Dai, S. Tian, X. Yang and Z. Liu, *Front. Chem.*, 2022, **10**, 1–24.

52 M. Abboud, R. Notario, R. E. Trifonov, A. P. Volovodenko, V. A. Ostrovskii and I. Alkorta, *Eur. J. Org. Chem.*, 2001, 3013–3024.

53 B. R. Nemallapudi, D. R. Guda, N. Ummadi, B. Avula, G. V. Zyryanov, C. S. Reddy and S. Gundala, *Polycycl. Aromat. Compd.*, 2022, **42**, 3874–3892.

54 Z. Chen, Q. Yan, Z. Liu, Y. Xu and Y. Zhang, *Angew. Chem. Int. Ed.*, 2013, **52**, 13324–13328.

55 K. Harju, M. Vahermo, I. Mutikainen and J. Yli-Kauhaluoma, *J. Comb. Chem.*, 2003, **5**, 826–833.

56 A. K. Feldman, B. Colasson and V. V. Fokin, *Org. Lett.*, 2004, **6**, 3897–3899.

57 D. Wang and S. Gao, *Org. Chem. Front.*, 2014, **1**, 556–566.

58 M. Bakherad, *Appl. Organomet. Chem.*, 2013, **27**, 125–140.

59 M. F. Jamali, N. K. Vaishanv and K. Mohanan, *Chem. Rec.*, 2020, **20**, 1394–1408.

60 M. Dhameja and J. Pandey, *Asian J. Org. Chem.*, 2018, **7**, 1502–1523.

61 F. Mo, G. Dong, Y. Zhang and J. Wang, *Org. Biomol. Chem.*, 2013, **11**, 1582–1593.

62 A. Roglans, A. Pla-Quintana and M. Moreno-Mañas, *Chem. Rev.*, 2006, **106**, 4622–4643.

63 C. Yang, J. P. Flynn and J. Niu, *Angew. Chem. Int. Ed.*, 2018, **57**, 16194–16199.

64 N. V. Sokolova and V. G. Nenajdenko, *RSC Adv.*, 2013, **3**, 16212–16242.

65 R. J. Ouelette and J. D. Rawn, in *Organic Chemistry*, Elsevier Inc., Amsterdam, 2nd edn., 2018, pp. 195–211.

66 A. M. Jones and S. P. Stanforth, in *Rodd's Chemistry of Carbon Compounds*, ed. M. Sainsbury, Elesvier B.V., Amsterdam, 1991, vol. IA/B, pp. 156–213.

67 R. J. Ouellette and J. D. Rawn, in *Principles of Organic Chemistry*, Elsevier Inc., Amsterdam, 1st edn., 2015, pp. 95–132.

68 M. Zhao, C. Kuang, Q. Yang and X. Cheng, *Tetrahedron Lett.*, 2011, **52**, 992–994.

69 R. M. Singh, D. Nandini, K. C. Bharadwaj, T. Gupta and R. P. Singh, *Org. Biomol. Chem.*, 2017, **15**, 9979–9982.

70 A. K. Morri, Y. Thummala and V. R. Doddi, *Org. Lett.*, 2015, **17**, 4640–4643.

71 X. Cheng, J. Jia and C. Kuang, *Chin. J. Chem.*, 2011, **29**, 2350–2354.

72 C. Kuang, Q. Yang, H. Senboku and M. Tokuda, *Tetrahedron*, 2005, **61**, 4043–4052.

73 E. J. Corey and P. L. Fuchs, *Tetrahedron Lett.*, 1972, **13**, 3769–3772.

74 L. Van Hijfte, M. Kolb and P. Witz, *Tetrahedron Lett.*, 1989, **30**, 3655–3656.

75 M. Beshai, B. Dhudshia, R. Mills and A. N. Thadani, *Tetrahedron Lett.*, 2008, **49**, 6794–6796.

76 O. Illa, X. Bagan, A. M. Cazorla, C. Lyon, A. Baceiredo, V. Branchadell and R. M. Ortuño, *J. Org. Chem.*, 2006, **71**, 5320–5327.

77 A. G. Godfrey and B. Ganem, *J. Am. Chem. Soc.*, 1990, **112**, 3717–3718.

78 G. J. Roth, B. Liepold, S. G. Müller and H. J. Bestmann, *Synthesis*, 2004, 59–62.

79 P. Krapf, R. Richarz, E. A. Urusova, B. Neumaier and B. D. Zlatopolskiy, *Eur. J. Org. Chem.*, 2016, **2016**, 430–433.

80 P. Cherkupally, A. Slazhnev and P. Beier, *Synlett*, 2011, 331–334.

81 Y. G. Ko, W. S. Na, Mayank, N. Singh and D. O. Jang, *J. Fluoresc.*, 2019, **29**, 945–952.

82 W. J. Shi, J. Y. Liu, P. C. Lo and D. K. P. Ng, *Chem. Asian J.*, 2019, **14**, 1059–1065.

83 M. Vedamalai and S. P. Wu, *Eur. J. Org. Chem.*, 2012, 1158–1163.

84 K. Wechakorn, S. Prabpai, K. Suksen, P. Kanjanasirirat, Y. Pewkliang, S. Borwornpinyo and P. Kongsaeree, *Luminescence*, 2018, **33**, 64–70.

85 O. Ozukanar, H. Gunduz, C. Unlu and V. Kumbaraci, *Opt. Mater.*, 2021, **119**, 111370.

86 A. N. Kursunlu and E. Güler, *J. Mol. Struct.*, 2017, **1134**, 345–349.

87 E. Tamanini, K. Flavin, M. Motevalli, S. Piperno, L. A. Gheber, M. H. Todd and M. Watkinson, *Inorg. Chem.*, 2010, **49**, 3789–3800.

88 D. Huang, M. Prehm, H. Gao, X. Cheng, Y. Liu and C. Tschierske, *RSC Adv.*, 2016, **6**, 21387–21395.

89 B. Shen, Y. Qian, Z. Qi, C. Lu and Y. Cui, *ChemistrySelect*, 2017, **2**, 9970–9976.

90 P. Griess, *Phil. Trans. R. Soc.*, 1864, **154**, 667–731.

91 E. F. V. Scriven and K. Turnbull, *Chem. Rev.*, 1988, **88**, 297–368.

92 L. Li, P. S. Lopes, V. Rosa, C. A. Figueira, M. A. N. D. A. Lemos, M. T. Duarte, T. Avilés and P. T. Gomes, *Dalton. Trans.*, 2012, **41**, 5144–5154.

93 S. H. Kim, S. H. Park, J. H. Choi and S. Chang, *Chem. Asian J.*, 2011, **6**, 2618–2634.

94 M. Minozzi, D. Nanni and P. Spagnolo, *Chem. Eur. J.*, 2009, **15**, 7830–7840.

95 X. Kang, X. Cai, L. Yi and Z. Xi, *Chem. Asian J.*, 2020, **15**, 1420–1429.

96 A. Schulz, A. Stocco, A. Bethry, J. P. Lavigne, J. Coudane and B. Nottelet, *Adv. Funct. Mater.*, 2018, **28**, 1–7.

97 K. A. Schnapp, R. Poe, E. Leyva, N. Soundararajan and M. S. Platz, *Bioconjug. Chem.*, 1993, **4**, 172–177.

98 L. Godoy Prieto, M. J. Lo Fiego, A. B. Chopa and M. T. Lockhart, *J. Organomet. Chem.*, 2017, **830**, 26–32.

99 S. H. Lee, J. Yoon, S. H. Chung and Y. S. Lee, *Tetrahedron*, 2001, **57**, 2139–2145.

100 S. Bräse, C. Gil, K. Knepper and V. Zimmermann, *Angew. Chem. Int. Ed.*, 2005, **44**, 5188–5240.

101 M. Kitamura, T. Koga, M. Yano and T. Okauchi, *Synlett*, 2012, **23**, 1335–1338.

102 M. Kitamura, M. Yano, N. Tashiro, S. Miyagawa, M. Sando and T. Okauchi, *Eur. J. Org. Chem.*, 2011, 458–462.

103 S. M. Capitosti, T. P. Hansen and M. L. Brown, *Org. Lett.*, 2003, **5**, 2865–2867.

104 K. Knepper, M. E. P. Lormann and S. Bräse, *J. Comb. Chem.*, 2004, **6**, 460–463.

105 J. Gavenonis and T. D. Tilley, *Organometallics*, 2002, 5549–5563.

106 Y. H. Kim, K. Kim and S. B. Shim, *Tetrahedron Lett.*, 1986, **27**, 4749–4752.

107 Q. Liu and Y. Tor, *Org Lett*, 2003, **5**, 2571–2572.

108 T. Puthiyedath and D. Bahulayan, *Sens. Actuators B Chem.*, 2018, **272**, 110–117.

109 S. Tane and T. Michinobu, *Polym. Int.*, 2020, 2–12.

110 H. R. Xu, K. Li, Q. Liu, T. M. Wu, M. Q. Wang, J. T. Hou, Z. Huang, Y. M. Xie and X. Q. Yu, *Analyst*, 2013, **138**, 2329–2334.

111 Shaily, A. Kumar, I. Parveen and N. Ahmed, *Luminescence*, 2018, **33**, 713–721.

112 S. K. Dwivedi, R. C. Gupta, P. Srivastava, P. Singh, B. Koch, B. Maiti and A. Misra, *Anal. Chem.*, 2018, **90**, 10974–10981.

113 S. Joshi, S. Kumari, R. Bhattacharjee, A. Sarmah, R. Sakhuja and D. D. Pant, *Sens. Actuators B Chem.*, 2015, **220**, 1266–1278.

114 H. Kang, C. Fan, H. Xu, G. Liu and S. Pu, *Tetrahedron*, 2018, **74**, 4390–4399.

115 Z. Zhang, H. Wang, H. Zhang and Y. Liu, *Chin. J. Chem.*, 2013, **31**, 598–602.

116 P. Kaur, B. Lal, N. Kaur, G. Singh and A. Singh, *J. Photochem. Photobiol. A Chem.*, 2019, **382**, 111847.

117 L. N. Liu, L. He, Y. Qu, N. Lu, Q. Y. Cao and Z. Yan, *Inorganica Chim. Acta*, 2018, **474**, 128–133.

118 B. Stuart, *Kirk-Othmer Encyclopedia of Chemical Technology*, 2015, 30, 570–579.

119 K. B. Beć, J. Grabska and C. W. Huck, *Molecules*, 2020, **25**, 2948.

120 T. Hong, J. Y. Yin, S. P. Nie and M. Y. Xie, *Food Chem. X*, 2021, **12**, 100168.

121 U. Holzgrabe, *Prog. Nucl. Magn. Reson. Spectrosc.*, 2010, 57, 229–240.

122 J. C. Lindon, J. K. Nicholson, E. Holmes and J. R. Everett, *Concepts Magn. Reson.*, 2000, **12**, 289-320.

123 A. M. Gronenborn and T. Polenova, *Chem. Rev.*, 2022, **122**, 9265–9266.

124 U. Holzgrabe, R. Deubner, C. Schollmayer and B. Waibel, *J. Pharm. Biomed. Anal.*, 2005, **38**, 806–812.

125 D. Marion, *Mol. Cell Proteomics*, 2013, **12**, 3006–3025.

126 G. L. Glish and R. W. Vachet, *Nat. Rev. Drug. Discov*, 2003, **2**, 140–150.

127 L. V. Schaffer, R. J. Millikin, R. M. Miller, L. C. Anderson, R. T. Fellers, Y. Ge, N. L. Kelleher, R. D. LeDuc, X. Liu, S. H. Payne, L. Sun, P. M. Thomas, T. Tucholski, Z. Wang, S. Wu, Z. Wu, D. Yu, M. R. Shortreed and L. M. Smith, *Proteomics*, 2019, **19**, 1–15.

128 G. T. H. Nguyen, T. N. Tran, M. N. Podgorski, S. G. Bell, C. T. Supuran and W. A. Donald, *ACS Cent. Sci.*, 2019, **5**, 308–318.

129 A. C. Leney and A. J. R. Heck, *J. Am. Soc. Mass. Spectrom.*, 2017, **28**, 5–13.

130 A. A. Edwards and B. D. Alexander, in *Encyclopedia of Spectroscopy and Spectrometry*, eds. J. C. Lindon, G. E. Tranter and D. W. Koppenaal, Elsevier Ltd., 3rd edn., 2016 pp 511-519.

131 G. E. Tranter, in *Encyclopedia of Spectroscopy and Spectrometry*, eds. J. C. Lindon, G. E. Tranter, D. W. Koppenaal, Elsevier Ltd., Amsterdam, 3rd edn., 2016 pp. 488-490.

132 B. M. Tissue, in *Characterization of Materials*, ed. E. N. Kaufmann, John Wiley & Sons Inc, NJ, USA, 2nd edn., 2012, pp. 353–380.

133 R. Esfandiary and C. R. Middaugh, in *Analysis of Aggregates and Particles in Protein Pharmaceuticals*, eds. H.-C. Mahler and W. Jiskoot, John Wiley & Sons Inc., NJ, USA, 1st edn., 2012, pp. 170–200.

134 G. Misra, in *Data Processing Handbook for Complex Biological Data Sources*, Elsevier Inc., Amsterdam, 2019 pp. 31-37.

135 A. P. Demchenko, in *Introduction to Fluorescence Sensing*, Springer, Berlin, 2009.

136 K. Vishwanath and N. Ramanujam, in *Encyclopedia of Analytical Chemistry*, John Wiley & Sons Inc., NJ, USA, 2011.

137 F. V. Bright, *Anal. Chem.*, 1988, **60**, 1031A-1039A.

138 K. R. Murphy, C. A. Stedmon, D. Graeber and R. Bro, *Anal. Methods*, 2013, **5**, 6557–6566.

139 R. Karoui, in *Modern Techniques for Food Authentication*, ed. D. W. Sun, Elsevier Inc., Amsterdam, 2nd edn., 2018 ch. 7, pp. 219-252.

140 J. D. Crowley and D. A. McMorran, in *Click Triazoles*, ed. J. Košmrlj, Springer-Verlag, Switzerland, 1st edn., 2012, vol. 28, pp. 31–84.

141 F. Ahmed and H. Xiong, *Dyes Pigm.*, 2021, **185**, 108905.

142 H. H. Qazi, A. B. Bin Mohammad and M. Akram, *Sensors*, 2012, **12**, 16522–16556.

143 Y. Jeong and J. Yoon, *Inorganica Chim. Acta*, 2012, **381**, 2–14.

144 P. A. Scattergood, A. Sinopoli and P. I. P. Elliott, *Coord. Chem. Rev.*, 2017, **350**, 136–154.

145 X. Creary, A. Anderson, C. Brophy, F. Crowell and Z. Funk, *J. Org. Chem.*, 2012, **77**, 8756–8761.

146 G. Singh, S. S. Mangat, J. Singh, A. Arora and M. Garg, *J. Organomet. Chem.*, 2014, **769**, 124–129.

147 C. Y. Wang, J. F. Zou, Z. J. Zheng, W. S. Huang, L. Li and L. W. Xu, *RSC Adv.*, 2014, **4**, 54256–54262.

148 D. Ghosh, S. Rhodes, D. Winder, A. Atkinson, J. Gibson, W. Ming, C. Padgett, S. Landge and K. Aiken, *J. Mol. Struct.*, 2017, **1134**, 638–648.

149 S. B. Maity and P. K. Bharadwaj, *Inorg. Chem.*, 2013, **52**, 1161–1163.

150 S. Areti, S. Bandaru and C. P. Rao, *ACS Omega*, 2016, **1**, 626–635.

151 and H. X. Shouzhi Pu, Haichang Ding, Gang Liu, Chunhong Zheng, *J. Phys. Chem. C*, 2014, **118**, 7010–7017.

152 M. D. Aljabri, S. Rahman and P. E. Georghiou, *ChemistrySelect*, 2017, **2**, 1214–1218.

153 B. Rathinam, C. C. Chien, B. C. Chen and J. H. Liu, *Tetrahedron*, 2013, **69**, 235–241.

154 P. Gahlyan, R. Bawa, H. Jain, M. Dalela, A. Joshi, C. N. Ramachandran, A. K. Prasad, A. Kaur and R. Kumar, *ChemistrySelect*, 2019, **4**, 7532–7540.

155 J. T. Hou, Q. F. Zhang, B. Y. Xu, Q. Sen Lu, Q. Liu, J. Zhang and X. Q. Yu, *Tetrahedron Lett.*, 2011, **52**, 4927–4930.

156 D. Mandal, P. Deb, B. Mondal, A. Thakur, J. Ponniah S and S. Ghosh, *RSC Adv.*, 2013, **3**, 18614–18625.

157 S. R. Bhatta, V. Bheemireddy, G. Vijaykumar and A. Thakur, *Sens. Actuators B Chem.*, 2017, **240**, 640–650.

158 Y. M. Zhang, Y. Chen, Z. Q. Li, N. Li and Y. Liu, *Bioorg. Med. Chem.*, 2010, **18**, 1415–1420.

159 S. A. Ingale and F. Seela, *J. Org. Chem.*, 2012, **77**, 9352–9356.

160 R. Joseph, *ACS Omega*, 2020, **5**, 6215–6220.

161 S. Rahman, Y. Assiri, A. N. Alodhayb, L. Y. Beaulieu, A. K. Oraby and P. E. Georghiou, *New. J. Chem.*, 2016, **40**, 434–440.

162 G. Singh, J. Singh, J. Singh and S. S. Mangat, *J. Lumin.*, 2015, **165**, 123–129.

163 A. V. Moro, P. C. Ferreira, P. Migowski, F. S. Rodembusch, J. Dupont and D. S. Lüdtke, *Tetrahedron*, 2013, **69**, 201–206.

164 A. Kumar, P. S. Chae and S. Kumar, *Dyes Pigm.*, 2020, **174**, 108092.

165 Kiran, R. Bharti and R. Sharma, *Mater. Today Proc.*, 2021, **51**, 880–885.

166 P. R. M. Correia, E. Oliveira and P. V. Oliveira, *Anal. Chim. Acta*, 2000, **405**, 205–211.

167 R. Oikarl, L. Botti and R. Hernberg, *Appl. Spectrosc.*, 2002, **56**, 1453–1457.

168 V. Zarezade, M. Behbahani, F. Omidi, H. S. Abandansari and G. Hesam, *RSC Adv.*, 2016, **6**, 103499–103507.

169 M. N. Oviedo, E. F. Fiorentini, A. A. Lemos, M. B. Botella and R. G. Wuilloud, *Microchem. J.*, 2020, **159**, 105386.

170 Q. Liang, H. Jing and D. C. Gregoire, *Talanta*, 2000, **51**, 507–513.

171 K. X. Yang, K. Swami and L. Husain, *Spectrochim. Acta Part B At. Spectrosc.*, 2002, **57**, 73–84.

172 D. Beauchemin, *Anal. Chem.*, 2009, **80**, 4455–4486.

173 B. Situ, J. Zhao, W. Lv, J. Liu, H. Li, B. Li, Z. Chai, N. Cao and L. Zheng, *Sens. Actuators B Chem.*, 2017, **240**, 560–565.

174 Y. Zhang, T. Ren, H. Tian, B. Jin and J. He, *ACS Appl. Mater. Interfaces*, 2018, **10**, 26705–26712.

175 M. Sulak, A. N. Kursunlu, B. Girgin, Ö. Ö. Karakuş and E. Güler, *J. Photochem. Photobiol. A Chem.*, 2017, **349**, 129–137.

176 G. Wu, M. Li, J. Zhu, K. W. C. Lai, Q. Tong and F. Lu, *RSC Adv.*, 2016, **6**, 100696–100699.

177 Y. Wu, Y. Dong, J. Li, X. Huang, Y. Cheng and C. Zhu, *Chem. Asian J*, 2011, **6**, 2725–2729.

178 H. J. Schneider, *Angew. Chem. Int. Ed.*, 1991, **30**, 1417–1436.

179 B. Schulze and U. S. Schubert, *Chem. Soc. Rev.*, 2014, **43**, 2522–2571.

180 S. Martens, J. O. Holloway and F. E. Du Prez, *Macromol. Rapid. Commun.*, 2017, **38**, 1–15.

181 C. D. Hein, X. M. Liu and D. Wang, *Pharm. Res.*, 2008, **25**, 2216–2230.

182 J. Totobenazara and A. J. Burke, *Tetrahedron Lett.*, 2015, **56**, 2853–2859.

183 R. G. Pearson, *J. Am. Chem. Soc.*, 1963, **85**, 3533–3539.

184 G. L. Long and J. D. Winefordner, *Anal. Chem.*, 1983, **55**, 712A–724A.

185 A. Thakur, D. Mandal and S. Ghosh, *Anal. Chem.*, 2013, **85**, 1665–1674.

186 V. V. S. Mummidivarapu, A. Nehra, V. K. Hinge and C. P. Rao, *Org. Lett.*, 2012, **14**, 2968–2971.

187 L. Wang, G. Fang, D. Ye and D. Cao, *Sens. Actuators B Chem.*, 2014, **195**, 572–580.

188 D. Mandal, A. Thakur and S. Ghosh, *Polyhedron*, 2013, **52**, 1109–1117.

189 S. Çetindere, S. O. Tümay, A. Kılıç, M. Durmuş and S. Yeşilot, *J. Fluoresc.*, 2016, **26**, 1173–1181.

Chapter III

Synthetic Procedures and Characterization Data

This section contains detailed information regarding the synthetic routes for the experimental work that was carried out for several novel molecules, as well as the comprehensive structural characterization of these molecules, which includes various studies such as colour, yield, melting point, Infrared (IR) Spectroscopy, Nuclear Magnetic Resonance (NMR) Spectroscopy, and Mass Spectrometry.

3.1. Generalized synthetic route for 1,2,3-triazole synthesis

The typical technique for synthesizing 1,2,3-triazole-appended compounds involves the sequential steps as described in subsections 3.1.1 to 3.1.3 below. Additionally, the reaction conditions and the specific azide and alkyne precursors used can vary depending on the desired outcome and the substrates being used.

3.1.1. Synthesizing a terminal alkyne

The starting material consisting of labile protons (1.00 mmol) was completely dissolved in DMF followed by adding anhydrous potassium carbonate/cesium carbonate (5.00 mmol). Subsequently, the slow and dropwise addition of propargyl bromide (1.30 mmol) was done, with constant stirring at room temperature within 5 minutes (**scheme 3.1**). Thin layer chromatography (TLC) with hexane and ethyl acetate solvent mixtures was implemented for monitoring the progress. After completion of reaction, the mixture was subjected to chilled water for reaction quenching and stirred to separate out the desired product. The resulting product, if in the form of precipitates, was filtered and subsequently washed with plentiful distilled water to eliminate the residual solvent, then air-dried until consistent weight. In case of oily product, the solvent extraction technique was used, wherein the organic compound was isolated by ethyl acetate or diethyl ether, and the combined organic phases were desiccated using sodium sulphate (anhydrous) and afterwards vacuum evaporation was used to eliminate the solvent to yield the pure product.

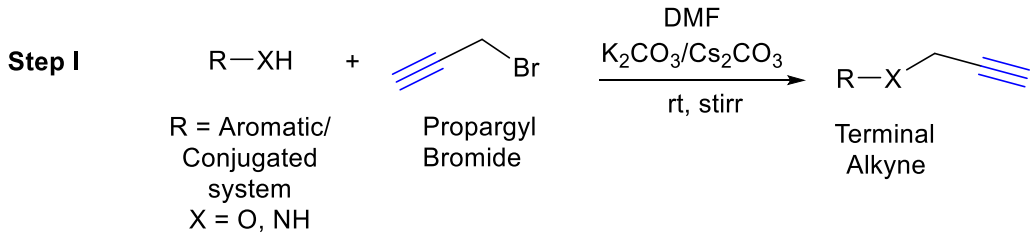

Scheme 3.1: General reaction procedure for the synthesis of terminal alkyne

3.1.2. Synthesizing an organic azide

Caution! Sodium azide must be handled with extra precaution and care as it is heat and shock sensitive.

As a preliminary step, the sodium azide was subjected to vacuum drying in order to completely remove any traces of moisture. Subsequently, the dried sodium azide (5.00 mol) was added to a solution of benzyl azide/ 1-chloromethyl naphthalene (1.00 mol) in 25 mL of DMF and the reaction temperature was maintained at 85 - 90 °C with continuous stirring for 4 - 5 h (**scheme 3.2**). Subsequently, the reaction was allowed to come to room temperature and

then terminated employing ice-cold water. The product was isolated by the solvent extraction process utilizing ethyl acetate, wherein the organic layers underwent drying with sodium sulphate (anhydrous) and vacuum evaporated to yield the pure product.

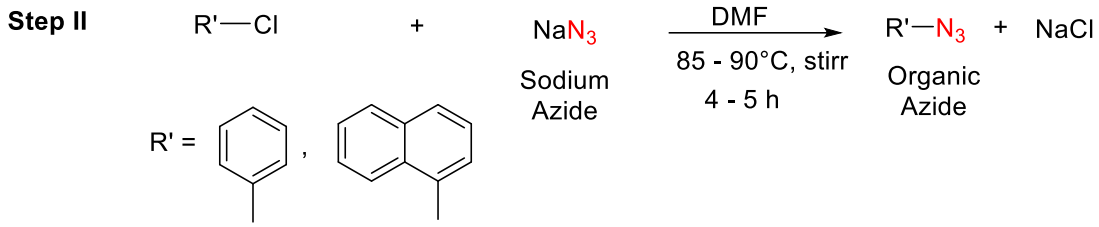

Scheme 3.2: General reaction procedure for the synthesis of organic azide

3.1.3. Synthesizing 1,2,3-triazole

The terminal alkyne (1.00 mol) was completely dissolved in THF/TEA solution, and subsequently the organic azide (1.00 mol) was added. The reaction mixture was then stirred at 55 - 60 °C after the addition of a catalytic quantity of [$CuBr(PPh_3)_3$] (0.001 mmol) complex (**scheme 3.3**). TLC determined the reaction progress and after confirming the reaction completion, the product was separated from the mixture by first quenching the reaction using ice cold water, and then filtering the solid precipitates followed by their washing with distilled water and air-drying, until the weight remained constant. **Scheme 3.1** depicts the overall reaction procedure including all the steps.

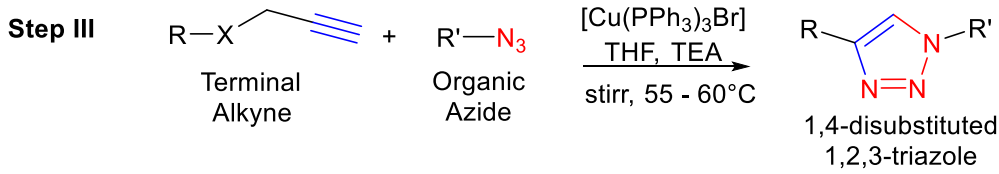

Scheme 3.3: General reaction procedure for synthesizing 1,4-disubstituted 1,2,3-triazole from terminal alkyne and organic azide

3.2. Synthesis of organic azides

3.2.1. Synthesis and characterization of benzyl azide (105)

After dissolving benzyl chloride **135** (5.5 g, 47.8 mmol (1 equiv)) in DMF (25 mL), sodium azide (15.5 g, 238.9 mmol (5 equiv)) was added. After 5 hours of stirring the mixture at 85 - 90 °C, the product **105** was extracted via the solvent extraction process using ethyl acetate. After combining the organic layers, they were desiccated using sodium sulphate (anhydrous), filtered, and then evaporated under vacuum for solvent elimination (**scheme 3.4.**).

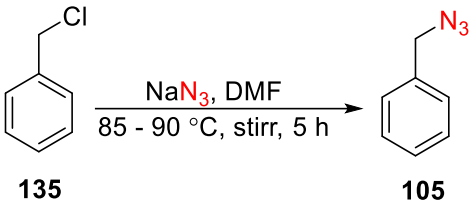

Scheme 3.4: Synthesis of benzyl azide **105** from benzyl chloride

Yield: 60 %

Colour/texture: light yellow oil

Molecular formula: $C_7H_7N_3$

IR (neat, cm^{-1}): 3032, 2930, 2089, 1452, 1252

^{1}H NMR (500 MHz, $CDCl_3$): δ = 7.22 (d, *J* = 7.5 Hz, 2H), 7.19 (d, *J* = 7.2 Hz, 1H), 7.17 - 7.13 (m, 2H), 4.14 (s, 2H)

^{13}C NMR (126 MHz, $CDCl_3$): δ = 135.53, 128.91, 128.37, 128.31, 54.82

3.2.2. Synthesis and characterization of 1-(azidomethyl)naphthalene (137)

After dissolving 1-(chloromethyl)naphthalene **136** (6.0 g, 34.0 mmol, 1 equiv) in DMF (25 mL), sodium azide (11.0 g, 170.0 mmol, 5 equiv) was added. After 5 hours of refluxing the reaction mixture at 85 - 90 °C, the product **137** was extracted with ethyl acetate via the solvent extraction process. After combining the organic layers, they were desiccated over sodium sulphate (anhydrous), filtered, and then evaporated under vacuum to remove the solvent (**scheme 3.5**).

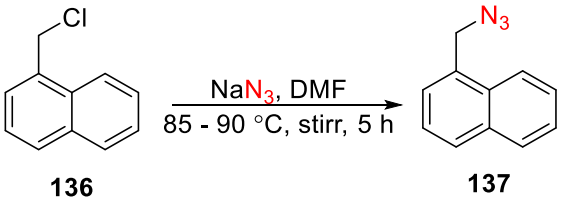

Scheme 3.5: Synthesis of 1-(azidomethyl)naphthalene **137** from 1-(chloromethyl)naphthalene

Yield: 61 %

Colour/texture: light yellow oil

Molecular formula: $C_{11}H_9N_3$

IR (neat, cm^{-1}): 3051, 2938, 2091, 1510, 1229

^{1}H NMR (500 MHz, $CDCl_3$): δ = 8.10 (d, *J* = 9.0 Hz, 1H), 7.96 (d, *J* = 8.1 Hz, 1H), 7.90 (d, *J* = 6.9 Hz, 1H), 7.68 - 7.58 (m, 2H), 7.53 - 7.48 (m, 2H), 4.76 (s, 2H)

^{13}C NMR (126 MHz, $CDCl_3$): δ = 134.05, 131.50, 131.15, 129.53, 128.97, 127.37, 126.86, 126.31, 125.37, 123.64, 53.02

3.3. Synthesis and characterization of maleic hydrazide-based alkyne and its corresponding 1,2,3-triazoles

3.3.1. Synthesis and characterization of terminal alkyne 1,2-di(prop-2-yn-1-yl)-1,2-dihydropyridazine-3,6-dione (139)

Maleic hydrazide **138** was treated with propargyl bromide, as per the procedure described in **section 3.1.1**, to generate the terminal alkyne (**scheme 3.6**). After dissolving maleic hydrazide (1.0 g, 8.92 mmol) in DMF, potassium carbonate (anhydrous) (6.16 g, 44.6 mmol) was added, subsequently the dropwise addition of propargyl bromide **42** (2.44 g, 20.5 mmol) was done. The mixture was stirred for 74 hours and the reaction progress was monitored by using TLC (hexane: ethyl acetate:: 4:1). The desired product **139** was obtained by first quenching the reaction with chilled water and then proceeding with the solvent extraction process using ethyl acetate. The solvent was removed by evaporating the mixed organic layers in vacuum, after they had been dried on anhydrous sodium sulphate. Upon the complete removal of the solvent, the product solidified.

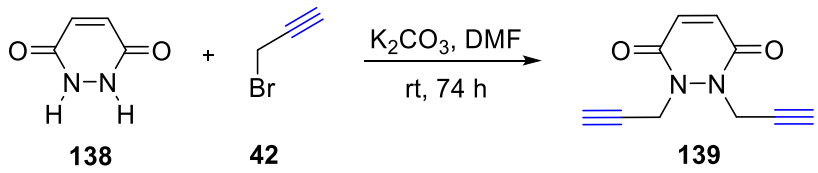

Scheme 3.6: Synthesis of maleic hydrazide-based terminal alkyne **139**

Yield: 74 %

Colour/texture: dark brown powder

mp: 69 - 71 °C

MF: $C_{10}H_8N_2O_2$

Elem. Anal. Calculated (%): C = 63.83, H = 4.29, N = 14.89; **Found (%):** C = 63.79, H = 4.31, N = 14.91

IR (neat, cm^{-1}): 3289, 3059, 2930, 2125, 1665, 1586, 1433, 1276, 1197, 1149, 839, 646

^{1}H NMR (500 MHz, $CDCl_3$): δ = 7.01 (d, *J* = 9.8 Hz, 1H), 6.95 (d, *J* = 9.8 Hz, 1H), 4.83 (d, *J* = 2.4 Hz, 2H), 4.80 (d, *J* = 2.5 Hz, 2H), 2.59 (t, *J* = 2.4 Hz, 1H), 2.35 (t, *J* = 2.4 Hz, 1H)

^{13}C NMR (126 MHz, $CDCl_3$): δ = 159.27, 133.15, 75.56, 72.74, 40.56

3.3.2. Synthesis and characterization of 1,2-bis((1-benzyl-1H-1,2,3-triazol-4-yl)methyl)-1,2-dihydropyridazine-3,6-dione (140)

The maleic hydrazide-based alkyne **139** (0.7 g, 3.72 mmol) was dissolved in minimal volume of THF:TEA (v/v, 3:2) to get a clear solution. Afterwards, freshly synthesized benzyl azide **105** (1.0 g, 7.44 mmol) was added, along with a catalytic quantity of $[CuBr(PPh_3)_3]$ (0.001 mmol). After 5 hours of stirring at 55 - 60 °C (Scheme 3.5), the reaction was completed, as confirmed by TLC (hexane: ethyl acetate:: 4:1). The addition of chilled water into the mixture led to reaction quenching, and a solid product **140**, identified by its characteristic dark brown appearance, was obtained by filtering the reaction mixture, rinsing multiple times with distilled water, and drying the final product till constant yield (**scheme 3.7**).

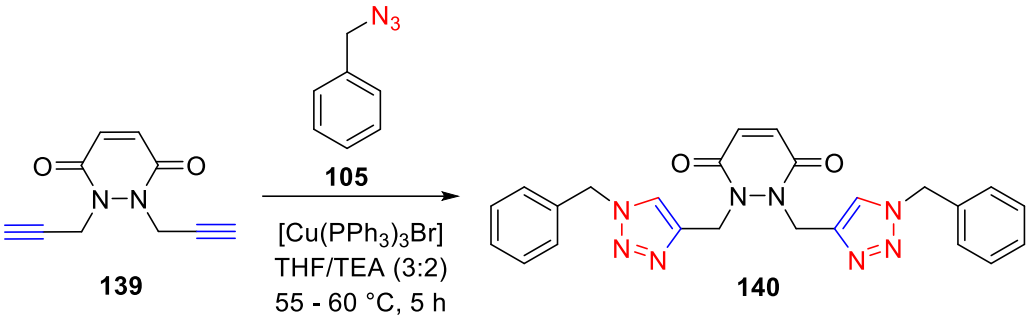

Scheme 3.7: Synthesis of 1,2,3-triazole derivative **140** from maleic hydrazide-based terminal alkyne

Yield: 85 %

Colour/texture: light brown solid

mp: 136 - 138 °C

MF: $C_{24}H_{22}N_8O_2$

Elem. Anal. Calculated (%): C = 63.43, H = 4.88, N = 24.66; **Found (%):** C = 63.34, H = 4.34, N = 14.97

IR (neat, cm^{-1}): 3134, 3061, 2970, 1660, 1576, 1527, 1439, 1281, 1145, 1026, 949, 776, 658

^{1}H NMR (500 MHz, $CDCl_3$): δ = 7.69 (s, 2H), 7.39 (d, *J* = 6.2 Hz, 4H), 7.37 - 7.28 (m, 6H), 6.89 - 6.79 (m, 2H), 5.51 (d, *J* = 21.3 Hz, 4H), 5.29 (d, *J* = 17.2 Hz, 4H).

^{13}C NMR (126 MHz, $CDCl_3$): δ = 158.52, 142.72, 130.10, 129.76, 129.03, 128.82, 127.21, 125.39, 52.27, 46.66

Molar Mass Calculated: 454.49; **Observed (m/z):** 454.25

3.3.3. Synthesis and characterization of 1,2-bis((1-(naphthalen-1-ylmethyl)-1H-1,2,3-triazol-4-yl)methyl)-1,2-dihydropyridazine-3,6-dione (141)

The maleic hydrazide-based alkyne **139** (0.7 g, 3.72 mmol) was dissolved in a minimum amount of THF:TEA (v/v, 3:2). Thereafter, [$CuBr(PPh_3)_3$] (0.001 mmol) and freshly prepared 1-(azidomethyl)naphthalene **137** (1.36 g, 7.44 mmol) were added. TLC (hexane: ethyl acetate:: 4:1) verified the reaction completion after the reaction mixture was stirred for 5 hours at 55 - 60 °C. After subjecting the reaction mixture to ice-cold water, it was filtered to produce a solid product **141** with a distinctive dark brown colour. After many washes in distilled water, the product was dried at room temperature till a steady yield was maintained (**scheme 3.8**).

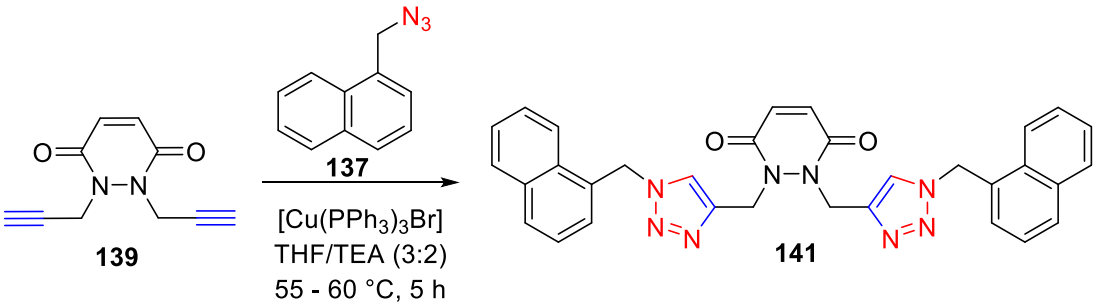

Scheme 3.8: Synthesis of 1,2,3-triazole derivative **141** from maleic hydrazide-based terminal alkyne

Yield: 80 %

Colour/texture: light brown solid

mp: 152 - 154 °C

MF: $C_{32}H_{26}N_8O_2$

Elem. Anal. Calculated (%): C = 69.30, H = 4.73, N = 20.20; **Found (%):** C = 69.64, H = 4.20, N = 14.77

IR (neat, cm^{-1}): 3140, 3059, 2960, 1660, 1585, 1437, 1274, 1149, 1039, 925, 840, 776

^{1}H NMR (500 MHz, $CDCl_3$): δ = 8.13 (d, *J* = 4.4 Hz, 2H), 8.01 (d, *J* = 5.7 Hz, 2H), 7.89 (d, *J* = 4.0 Hz, 2H), 7.63 - 7.58 (m, 2H), 7.55 - 7.47 (m, 4H), 7.47 - 7.42 (m, 2H), 7.39 (dd, *J* = 7.5, 3.8 Hz, 2H), 6.79 (q, *J* = 9.7 Hz, 2H), 5.85 (d, *J* = 2.0 Hz, 4H), 5.17 (d, *J* = 5.0 Hz, 4H)

^{13}C NMR (126 MHz, $CDCl_3$): δ = 159.18, 142.42, 133.79, 132.52, 129.89, 129.50, 129.17, 129.09, 128.76, 128.12, 127.94, 126.86, 126.05, 125.42, 124.79, 54.11, 43.86

Molar Mass Calculated: 554.61; **Observed (m/z):** 555.40 (M+1)

3.4. Synthesis and characterization of 4-tert butyl catechol-based alkyne and its corresponding 1,2,3-triazole

3.4.1. Synthesis and characterization of terminal alkyne 4-(tert-butyl)-1,2-bis(prop-2-yn-1 yloxy)benzene (143)

With constant stirring, 4-tert butyl catechol **142** (1.0 g, 6.0 mmol, 1 equiv) was completely dissolved in DMF (15.0 mL). Thereafter, cesium carbonate (anhydrous) (6.84 g, 21.0 mmol, 3.5 equiv.) was added to this solution, followed by adding propargyl bromide **42** (2.05 g, 13.8 mmol, 2.3 equiv.) dropwise over the course of 10 minutes at room temperature. TLC (hexane: ethyl acetate:: 4:1) analysis confirmed the reaction completion in 88 hours. Ice-cold water was used for reaction quenching, and ethyl acetate was used to extract the oily product **143**. The solvent was removed by drying the mixed organic layers over anhydrous sodium sulphate, filtering, and then evaporating under vacuum (**scheme 3.9**).

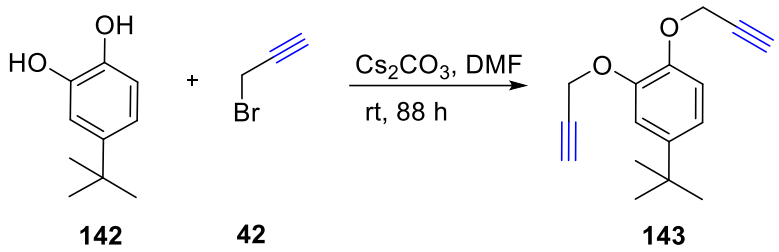

Scheme 3.9: Synthesis of 4-tert butyl-catechol based terminal alkyne **143**

Yield: 95 %

Colour/texture: dark brown viscous oil

MF: $C_{16}H_{18}O_2$

Elem. Anal. Calculated (%): C = 79.31, H = 7.49; **Found (%):** C = 79.44, H = 7.41

IR (neat, cm^{-1}): 3290, 3054, 2961, 2869, 2121, 1756, 1590, 1505, 1453, 1366, 1261, 1199, 1142, 1016, 924, 852, 808

^{1}H NMR (500 MHz, $CDCl_3$): δ = 7.12 (s, 1H), 6.97 (s, 2H), 4.74 (dd, *J* = 7.0, 2.4 Hz, 4H), 2.50 (dt, *J* = 6.9, 2.3 Hz, 2H), 1.31 (s, 9H)

^{13}C NMR (126 MHz, $CDCl_3$): δ = 146.94, 145.48, 145.30, 118.72, 114.50, 113.62, 78.85, 75.71, 75.68, 57.14, 56.90, 34.35, 31.39

3.4.2. Synthesis and characterization of 4,4'-(((4-(tert-butyl)-1,2-phenylene)bis(oxy))bis(methylene))bis(1-benzyl-1H-1,2,3-triazole) (144)

THF: Et_3N (1:1) solution was used to dissolve 4-tertbutyl catechol-based alkyne **143** (0.7 g, 2.9 mmol). The reaction mixture was then supplemented with benzyl azide **105** (0.77 g, 5.8 mmol), followed by 0.001 mmol Cu(I) catalyst. Stirring of the reaction mixture at 55 - 60 °C for 5.5 hours resulted in completion and ascertained by TLC (ethyl acetate: hexane, 1:4). The reaction was quenched by using ice-cold water, and the solid product **144** was filtered, and washed with distilled water (3×5 mL), and then air-dried till constant weight (**scheme 3.10**).

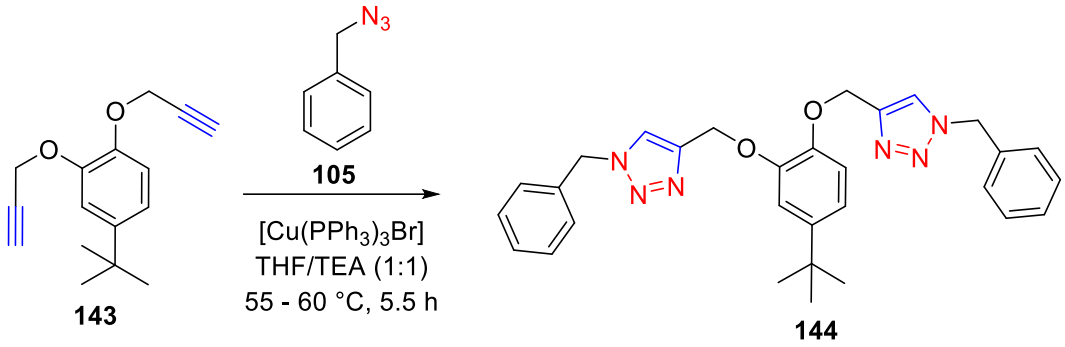

Scheme 3.10: Synthesis of 1,2,3-triazole derivative **144** from 4-tert butyl-catechol based terminal alkyne

Yield: 81 %

Colour/texture: light brown fine powder

mp: 120 - 122 °C

MF: $C_{30}H_{32}N_6O_2$

Elem. Anal. Calculated (%): C = 70.84, H = 6.34, N = 16.52; **Found (%):** C = 70.75, H = 6.36, N = 16.59

IR (neat, cm^{-1}): 3134, 3062, 2956, 2862, 1591, 1511, 1460, 1384, 1315, 1255, 1200, 1145, 1013, 917, 800, 694

^{1}H NMR (500 MHz, $CDCl_3$): δ = 7.58 (d, *J* = 5.6 Hz, 2H), 7.32 (dt, *J* = 4.3, 2.2 Hz, 4H), 7.28 - 7.19 (m, 6H), 7.04 (d, *J* = 2.0 Hz, 1H), 6.93 - 6.89 (m, 2H), 5.45 (s, 4H), 5.19 (d, *J* = 2.2 Hz, 4H), 1.24 (s, 9H)

^{13}C NMR (126 MHz, $CDCl_3$): δ = 147.86, 146.41, 145.50, 134.69, 129.09, 128.71, 128.12, 128.08, 123.15, 123.10, 118.88, 115.10, 114.05, 63.92, 63.68, 54.11, 34.40, 31.46

Molar Mass Calculated: 508.63; **Observed (m/z):** 509.50 (M+1)

3.5. Synthesis and characterization of p-rosolic acid-based alkyne and its corresponding 1,2,3-triazole

3.5.1. Synthesis and characterization of terminal alkyne 4-(bis(4-(prop-2-yn-1-yloxy)phenyl)methylene)cyclohexa-2,5-dien-1-one (146)

The constant stirring of p-rosolic acid **145** (1.0 g, 3.4 mmol) in DMF (10 mL) resulted in a clear solution, which was subjected to the addition of potassium carbonate (anhydrous) (2.4 g, 17 mmol), and then propargyl bromide **42** (0.8 g, 6.8 mmol) was added drop by drop over the course of 15 minutes. TLC (ethyl acetate: hexane, 2:3) was employed to observe the reaction progress; the reaction was finished after 30 hours. Adding ice-cold water led to the reaction quenching, and afterwards, the oily product **146** was extracted using ethyl acetate via solvent extraction process. The solvent was removed by drying the combined organic layers using sodium sulphate (anhydrous), filtering them, and then evaporating them in a vacuum (**scheme 3.11**).

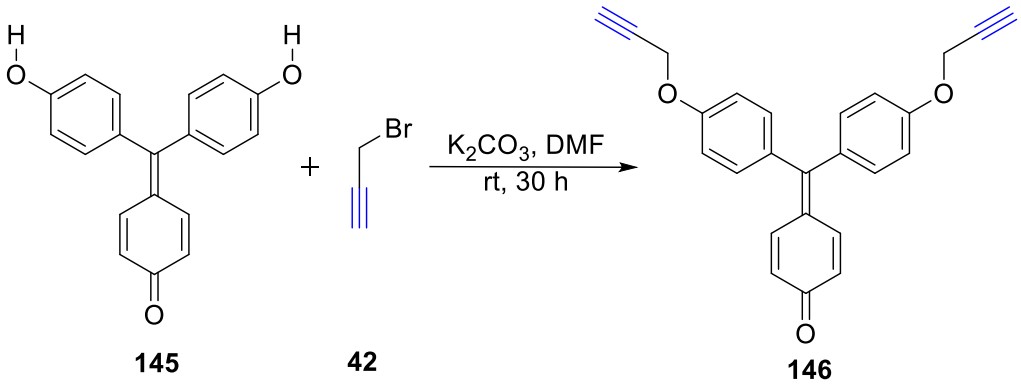

Scheme 3.11: Synthesis of p-rosolic acid-based terminal alkyne **146**

Yield: 93 %

Colour/texture: dark brown viscous oil

MF: $C_{25}H_{18}O_3$

Elem. Anal. Calculated (%): C = 81.95, H = 4.95; **Found (%):** C = 81.88, H = 4.99

IR (neat, cm^{-1}): 3286, 3047, 2923, 2121, 1754, 1603, 1503, 1218, 1021, 923, 827, 641

^{1}H NMR (500 MHz, $CDCl_3$): δ = 7.19 - 7.14 (m, 2H), 7.03 (d, *J* = 9.0 Hz, 4H), 6.91 - 6.85 (m, 4H), 6.71 (d, *J* = 9.4 Hz, 2H), 4.65 (d, *J* = 2.2 Hz, 4H), 2.51 (t, *J* = 2.4 Hz, 2H)

^{13}C NMR (126 MHz, $CDCl_3$): δ = 185.26, 157.76, 139.14, 135.72, 131.47, 130.48, 129.18, 114.19, 78.67, 75.70, 55.90

3.5.2. Synthesis and characterization of 4-(bis(4-((1-(naphthalen-1-ylmethyl)-1H-1,2,3-triazol-4-yl)methoxy)phenyl)methylene)cyclohexa-2,5-dien-1-one (147)

The p-rosolic acid-based alkyne **146** (1.0 g, 2.73 mmol) was thoroughly dissolved in a THF:Et_3N (2:1) solution. To the preceding solution, 1-(azidomethyl)naphthalene **137** (1.0 g, 5.46 mmol) was added, and then Cu(I) catalyst (0.001 mmol) was introduced. For 12 hours, the reactants were stirred at 55 - 60 °C. TLC (ethyl acetate: hexane, 1:4) was used to determine reaction completion. Adding ice-cold water led to reaction quenching, and the solid product **147** was filtered, rinsed with water (3×5 mL), and air-dried till constant yield (**scheme 3.12**).

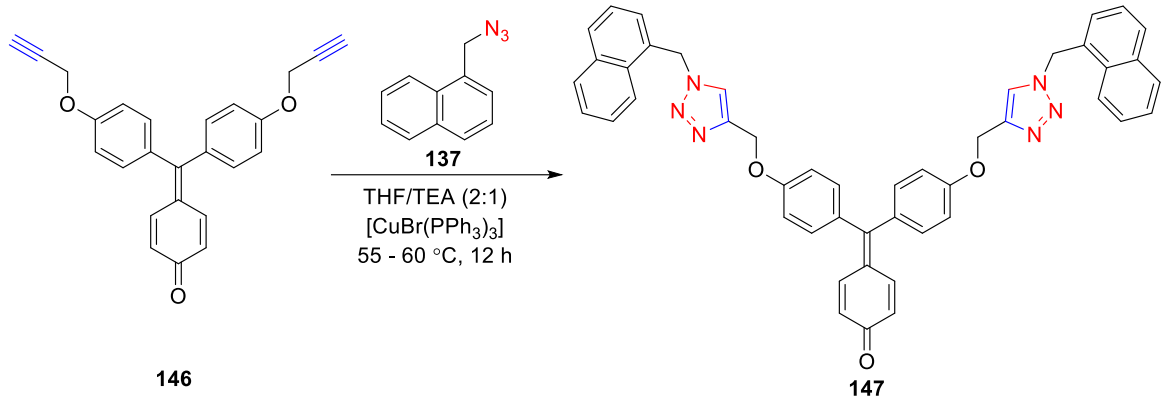

Scheme 3.12: Synthesis of 1,2,3-triazole derivative **147** from p-rosolic acid-based terminal alkyne

Yield: 83 %

Colour/texture: Golden yellow fine powder

mp: 113 - 115 °C

MF: $C_{47}H_{36}N_6O_3$

Elem. Anal. Calculated (%): C = 77.03, H = 4.95, N = 11.47; **Found (%):** C = 77.15, H = 4.87, N = 11.44

IR (neat, cm^{-1}): 3142, 3057, 2951, 1602, 1504, 1462, 1300, 1240, 1172, 1120, 1009, 785

^{1}H NMR (500 MHz, $CDCl_3$): δ = 7.97 - 7.91 (m, 2H), 7.91 - 7.84 (m, 4H), 7.53 - 7.47 (m, 4H), 7.45 (dd, *J* = 11.1, 5.7 Hz, 4H), 7.38 (dd, *J* = 12.0, 6.2 Hz, 6H), 7.32 (d, *J* = 6.5 Hz, 2H), 7.05 (d, *J* = 8.8 Hz, 4H), 6.78 (d, *J* = 9.0 Hz, 2H), 5.94 (s, 4H), 5.04 (s, 4H)

^{13}C NMR (126 MHz, $CDCl_3$): δ = 185.52, 158.40, 149.41, 138.31, 133.94, 131.16, 130.13, 129.65, 129.02, 128.55, 127.97, 127.35, 126.44, 125.36, 124.08, 121.72, 113.97, 62.07, 52.42

Molar Mass Calculated: 732.28; **Observed (m/z):** 733.30 (M+1)

3.6. Synthesis and characterization of glyoxal bis-(2-hydroxyanil)-based alkyne and its corresponding 1,2,3-triazole

3.6.1. Synthesis and characterization of terminal alkyne (1*E*,2*E*)-*N*$_1$,*N*$_2$-bis(2-(prop-2-yn-1-yloxy)phenyl)ethane-1,2-diimine (149)

Glyoxal bis-(2-hydroxyanil) **148** (1.0 g, 4.16 mmol) was dissolved in DMF (15.0 mL), subsequently adding caesium carbonate (anhydrous) (4.74 g, 14.5 mmol) and the addition of propargyl bromide (anhydrous) **42** (0.98 g, 8.32 mmol) over the course of 10 minutes. The progress of reaction was monitored by TLC (hexane: ethyl acetate:: 1:4), which confirmed the completion after 40 hours. The reaction was quenched with chilled water and the product **149** was extracted using ethyl acetate. The combined organic layers were dried using sodium sulphate (anhydrous). The product was precipitated on the addition of n-hexane, which was then filtered, washed, and dried till constant yield (**scheme 3.13**).

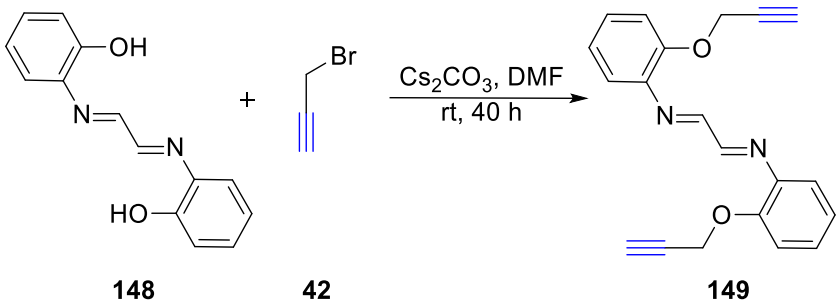

148 **42** **149**

Scheme 3.13: Synthesis of glyoxal bis-(2-hydroxyanil)-based terminal alkyne **149**

Yield: 95 %

Colour/texture: dark brown fine powder

mp: 112 - 114 °C

MF: $C_{20}H_{16}N_2O_2$

Elem. Anal. Calculated (%): C = 75.93, H = 5.10, N = 8.86; **Found (%):** C = 75.81, H = 5.15, N = 8.92

IR (neat, cm^{-1}): 3283, 2967, 2907, 2120, 1670, 1596, 1498, 1452, 1372, 1246, 1198, 1109, 1018, 924, 801, 741, 634

^{1}H NMR (500 MHz, $CDCl_3$): δ = 7.05 - 7.00 (m, 2H), 7.00 - 6.94 (m, 2H), 6.92 - 6.87 (m, 2H), 6.82 (td, *J* = 7.3, 1.4 Hz, 2H), 6.75 - 6.72 (m, 2H), 4.73 (dd, *J* = 5.9, 2.5 Hz, 4H), 2.51 (t, *J* = 6.2 Hz, 2H)

^{13}C NMR (126 MHz, $CDCl_3$): δ = 159.20, 145.42, 136.69, 122.35, 122.21, 118.47, 115.71, 112.76, 78.88, 75.55, 56.68, 56.58

3.6.2. Synthesis and characterization of (1*E*,2*E*)-N_1,N_2-bis(2-((1-(naphthalen-1-ylmethyl)-1H-1,2,3-triazol-4-yl)methoxy)phenyl)ethane-1,2-diimine (150)

Glyoxal bis-(2-hydroxyanil)-based alkyne **149** (0.7 g, 2.2 mmol) was dissolved in THF:Et_3N (3:2). This reaction mixture was then supplemented with 1-(azidomethyl)naphthalene **137** (0.8 g, 4.4 mmol), subsequently incorporating Cu(I) catalyst (0.001 mmol). For six hours, the reactants were heated between 55 and 60 °C. The end of the reaction (ethyl acetate: hexane, 1:4) was determined by TLC. Addition of ice-cold water led to reaction quenching, and the solid product **150** was filtered, washed with water (3×5 mL), and finally air-dried till constant yield (**scheme 3.14**).

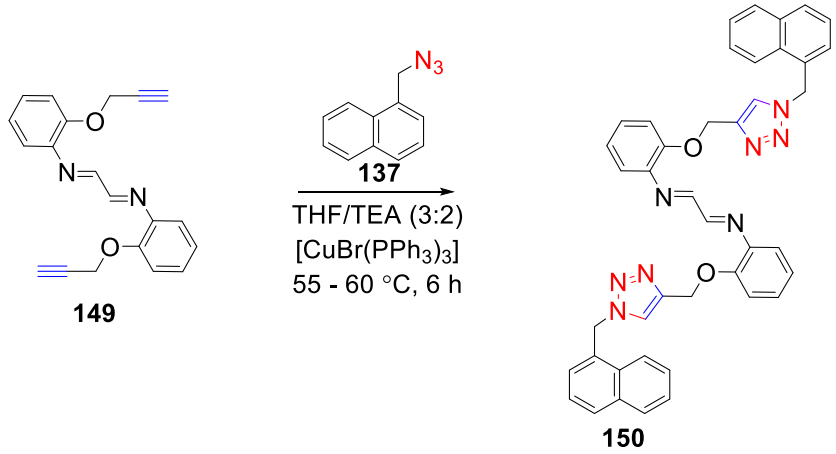

Scheme 3.14: Synthesis of 1,2,3-triazole derivative **150** from glyoxal bis-(2-hydroxyanil)-based terminal alkyne

Yield: 86 %

Colour/texture: dark brown fine powder

mp: 130 - 132 °C

MF: $C_{42}H_{34}N_8O_2$

Elem. Anal. Calculated (%): C = 73.88, H = 5.02, N = 16.41; **Found (%):** C = 73.82, H = 5.05, N = 16.44

IR (neat, cm^{-1}): 3138, 3051, 2963, 1667, 1654, 1596, 1499, 1454, 1396, 1258, 1212, 1162, 1093, 1044, 1012, 859, 787, 743

^{1}H NMR (500 MHz, DMSO-d_6): δ = 8.31 - 8.21 (m, 6H), 7.82 (d, *J* = 16.4 Hz, 2H), 7.59 (d, *J* = 7.0 Hz, 4H), 7.46 (d, *J* = 8.1 Hz, 4H), 7.34 (d, *J* = 6.7 Hz, 2H), 7.18 (dd, *J* = 22.2, 13.9 Hz, 4H), 6.97 (dd, *J* = 21.4, 12.9 Hz, 4H), 5.98 (d, *J* = 13.5 Hz, 4H), 5.15 (d, *J* = 11.7 Hz, 4H)

^{13}C NMR (126 MHz, DMSO-d_6): δ = 143.27, 140.50, 133.31, 131.37, 130.57, 128.98, 128.62, 127.55, 126.75, 126.13, 125.49, 124.57, 123.15, 121.51, 116.09, 112.77, 61.97, 50.79

Molar Mass Calculated: 682.28; **Observed (m/z):** 683.28 (M+1)

3.7. Synthesis and characterization of Schiff base-derived alkyne and its corresponding 1,2,3-triazole

3.7.1. Synthesis and characterization of Schiff base (*E*)-2-methoxy-4-(((5-methylpyridin-2-yl)imino)methyl)phenol (153)

2-amino-5-methylpyridine (1.0 g, 9.26 mmol) **151** was dissolved in ethanol with continuous stirring and to this solution, 4-hydroxy-3-methoxybenzaldehyde **152** (1.4 g, 9.26 mmol) was intorduced. The reaction mixture was then subjected to refluxing and TLC (ethyl acetate: hexane, 1:4) ascertained reaction completion after 30 hours. The product **153** was obtained by adding ice-cold water to the reaction mixture, which resulted in precipitates formation, which were subsequently filtered, whased with water (3×5 mL) and dried till constant weight (**scheme 3.15**)

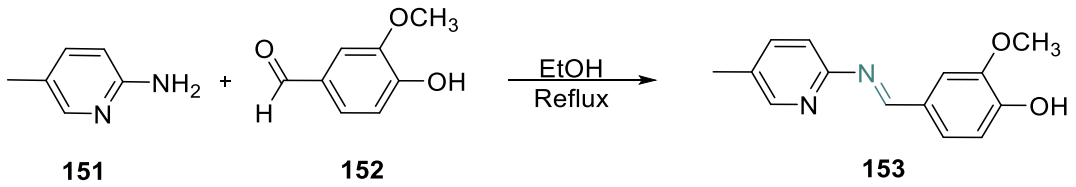

151 **152** **153**

Scheme 3.15: Synthesis of Schiff base **153** from 2-amino-5-methylpyridine and vanillin

Yield: 93 %

Colour/texture: golden yellow fine powder

mp: 152 - 153 °C

MF: $C_{14}H_{14}N_2O_2$

Elem. Anal. Calculated (%): C = 69.41, H = 5.82, N = 11.56; **Found (%):** C = 69.28, H = 5.86, N = 11.62

IR (neat, cm^{-1}): 3367, 2934, 2837, 1672, 1613, 1587, 1498, 1457, 1392, 1282, 1144, 1062, 1030, 856, 814, 728, 633

^{1}H NMR (500 MHz, $CDCl_3$): δ = δ 9.68 (s, 1H), 7.90 (d, J = 25.7 Hz, 2H), 7.59 - 7.32 (m, 4H), 6.85 (d, J = 25.2 Hz, 1H), 3.91 (s, 3H), 2.12 (s, 3H)

^{13}C NMR (126 MHz, $CDCl_3$): δ = 163.66, 160.46, 149.81, 149.23, 133.23, 129.29, 127.19, 124.97, 114.56, 110.87, 59.53, 14.13

3.7.2. Synthesis and characterization of terminal alkyne (*E*)-1-(3-methoxy-4-(prop-2-yn-1-yloxy)phenyl)-N-(5-methylpyridin-2-yl)methanimine (154)

The newly synthesized Schiff base **153** (1.0 g, 4.13 mmol) was dissolved in DMF (5.0 mL). This solution was augmented with potassium carbonate (anhydrous) (2.85 g, 20.65 mmol), and subsequently, propargyl bromide **42** (0.5 g, 4.13 mmol) was added dropwise over a period of 10 minutes with continuous stirring at room temperature. The reaction was observed for its progress using thin-layer chromatography (TLC) with a solvent mixture of hexane: ethyl acetate:: 1:4, which confirmed its completion after 24 hours. The product **154** was extracted using ice-cold water, which resulted in precipitates formation which were subsequently filtered, washed with water (3×5 mL) and dried till constant weight (**scheme 3.16**).

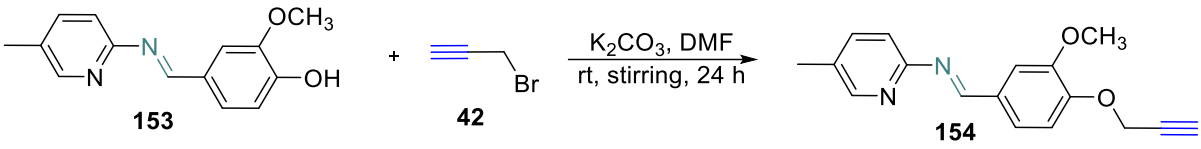

Scheme 3.16: Synthesis of Schiff base-derived terminal alkyne **154**

Yield: 94 %

Colour/texture: light brown fine powder

mp: 165 °C (decomp.)

MF: $C_{17}H_{16}N_2O_2$

Elem. Anal. Calculated (%): C = 72.84, H = 5.75, N = 9.99; **Found (%):** C = 72.87, H = 5.74, N = 9.97

IR (neat, cm^{-1}): 3282, 3007, 2937, 2867, 2117, 1684, 1608, 1497, 1460, 1383, 1299, 1209, 1141, 1065, 992, 924, 858, 809

^{1}H NMR (500 MHz, $CDCl_3$): δ = 7.96 (s, 1H), 7.90 (s, 1H), 7.54 (s, 1H), 7.47 (d, *J* = 1.2 Hz, 1H), 7.44 (d, *J* = 1.9 Hz, 2H), 6.78 (d, *J* = 8.0 Hz, 1H), 4.70 (d, *J* = 2.5 Hz, 2H), 3.90 (s, 3H), 2.57 (t, *J* = 2.4 Hz, 1H), 2.12 (s, 3H)

^{13}C NMR (126 MHz, $CDCl_3$): δ = 163.80, 160.53, 150.96, 149.22, 133.65, 129.09, 127.37, 124.18, 114.60, 110.61, 79.56, 75.74, 56.79, 55.74, 17.36

3.7.3. Synthesis and characterization of (*E*)-1-(4-((1-benzyl-1H-1,2,3-triazol-4-yl)methoxy)-3-methoxyphenyl)-*N*-(5-methylpyridin-2-yl)methanimine (155)

A solution of Schiff base alkyne **154** (0.8 g, 2.86 mmol) was prepared by dissolving it in a mixture of THF and Et_3N in a ratio of 2:1. Subsequently, benzyl azide **105** (0.38 g, 2.86 mmol) and 0.001 mmol Cu(I) catalyst were introduced. The reactants were stirred at 55 to 60 °C for a duration of six hours. The completion of the reaction was ascertained through thin-layer chromatography (TLC) (ethyl acetate/hexane, 1:4). Ice-cold water was utilized to terminate the process, and subsequently the resultant solid product **155** was filtered, washed water (3×5 mL), and subsequently air-dried until constant yield was achieved (**scheme 3.17**).

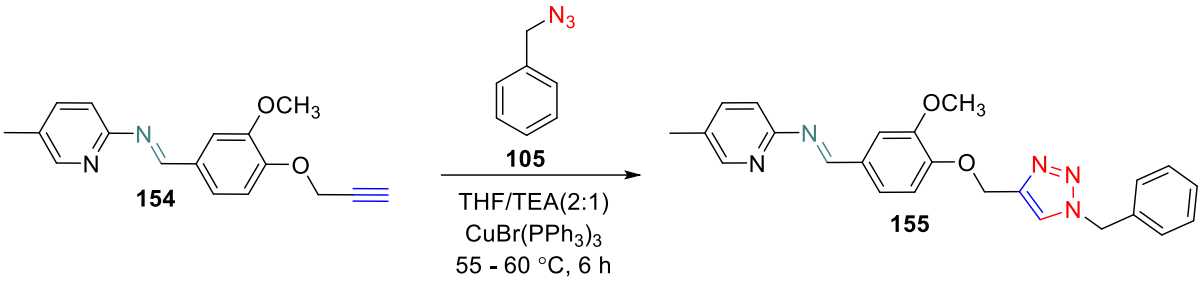

Scheme 3.17: Synthesis of 1,2,3-triazole derivative **155** from Schiff base-terminal alkyne

Yield: 91 %

Colour/texture: dark brown fine powder

mp: 184 °C (decomp.)

MF: $C_{24}H_{23}N_5O_2$

Elem. Anal. Calculated (%): C = 69.72, H = 5.61, N = 16.94; **Found (%):** C = 69.77, H = 5.58, N = 16.92

IR (neat, cm^{-1}): 3137, 3007, 2964, 2811, 1690, 1610, 1498, 1459, 1385, 1301, 1261, 1216, 1140, 1026, 800, 718

^{1}H NMR (500 MHz, $CDCl_3$): δ = 7.96 (s, 1H), 7.90 (s, 1H), 7.67 (s, 1H), 7.54 (s, 1H), 7.50 - 7.42 (m, 8H), 6.79 (d, *J* = 4.8 Hz, 1H), 5.84 (s, 2H), 5.09 (s, 2H), 3.90 (s, 3H), 2.13 (s, 3H)

^{13}C NMR (126 MHz, $CDCl_3$): δ = 163.24, 160.34, 151.25, 150.05, 149.79, 149.49, 149.26, 133.98, 131.08, 129.58, 128.95, 128.60, 127.44, 126.88, 126.05, 124.16, 114.88, 114.34, 110.94, 58.55, 54.94, 52.14, 18.16

Molar Mass Calculated: 413.19; **Observed (m/z):** 414.19 (M+1)

To summarize, different compounds including organic azides, terminal alkunes, and 1,2,3-triazole derivatives have been synthesized and characterized via elemental analysis, IR, NMR (^{1}H, ^{13}C), and mass spectrometry. **Table 3.1** illustrates the various compounds synthesized, the reaction conditions utilized, and the percentage yield obtained.

Entry	**Compound**	**Reactions conditions**	**% yield**
01	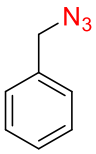 **105**	NaN_3, DMF 85 - 90 °C, stirr, 5 h	60
02	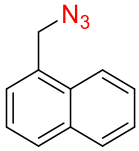 **137**	NaN_3, DMF 85 - 90 °C, stirr, 5 h	61
03	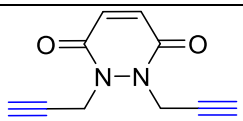 **139**	K_2CO_3, DMF rt, 74 h	74
04	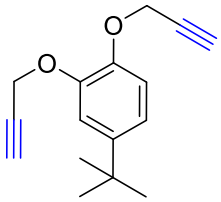 **143**	Cs_2CO_3, DMF rt, 88 h	95
05	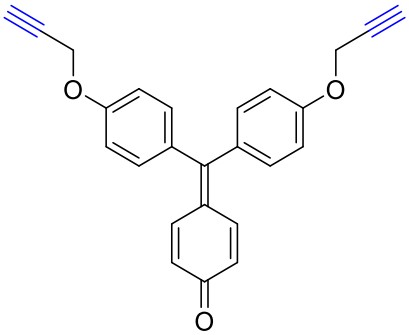 **146**	K_2CO_3, DMF rt, 30 h	93

Entry	Compound	Reactions conditions	% yield
06	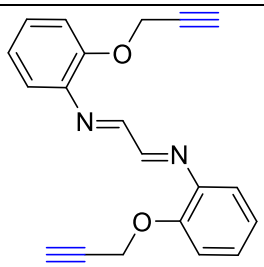 **149**	Cs_2CO_3, DMF rt, 40 h	95
07	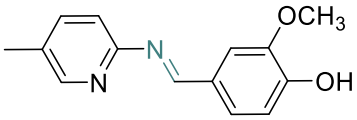 **153**	EtOH, Reflux, 4 h	93
08	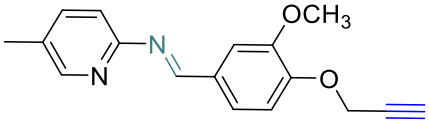 **154**	K_2CO_3, DMF rt, stirr, 24 h	94
09	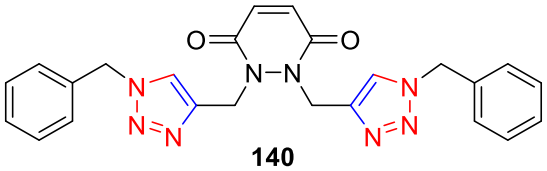 **140**	$[Cu(PPh_3)_3Br]$ THF/TEA (3:2) 55 - 60 °C, 5 h	85
10	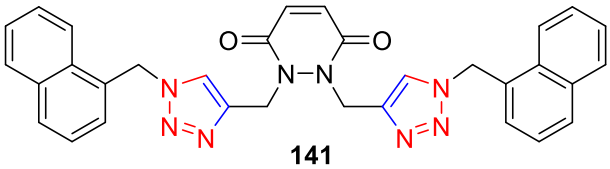 **141**	$[Cu(PPh_3)_3Br]$ THF/TEA (3:2) 55 - 60 °C, 5 h	80
11	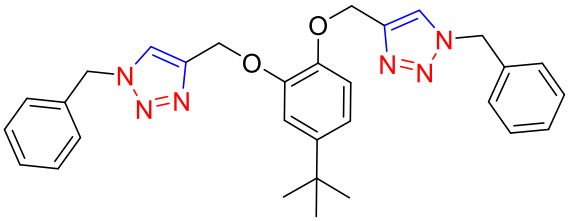 **144**	$[Cu(PPh_3)_3Br]$ THF/TEA (1:1) 55 - 60 °C, 5.5 h	81

Entry	Compound	Reactions conditions	% yield
12	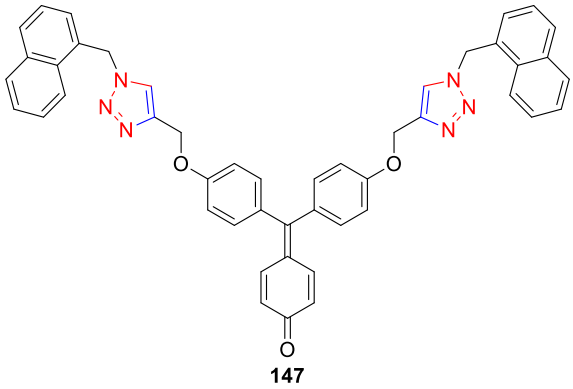 147	[Cu(PPh$_3$)$_3$Br] THF/TEA (2:1) 55 - 60 °C, 12 h	83
13	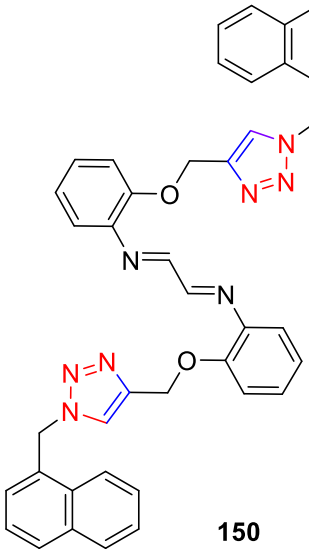 150	[Cu(PPh$_3$)$_3$Br] THF/TEA (3:2) 55 - 60 °C, 6 h	86
14	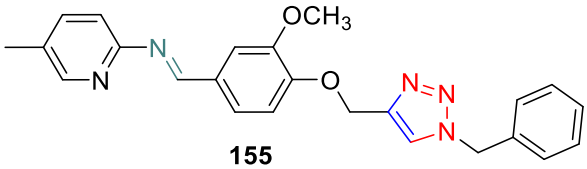 155	[Cu(PPh$_3$)$_3$Br] THF/TEA (2:1) 55 - 60 °C, 6 h	91

Table 3.1: A tabular representation of the synthesized compounds, their corresponding reaction conditions, and the percentage yield

Chapter IV

Results and Discussion

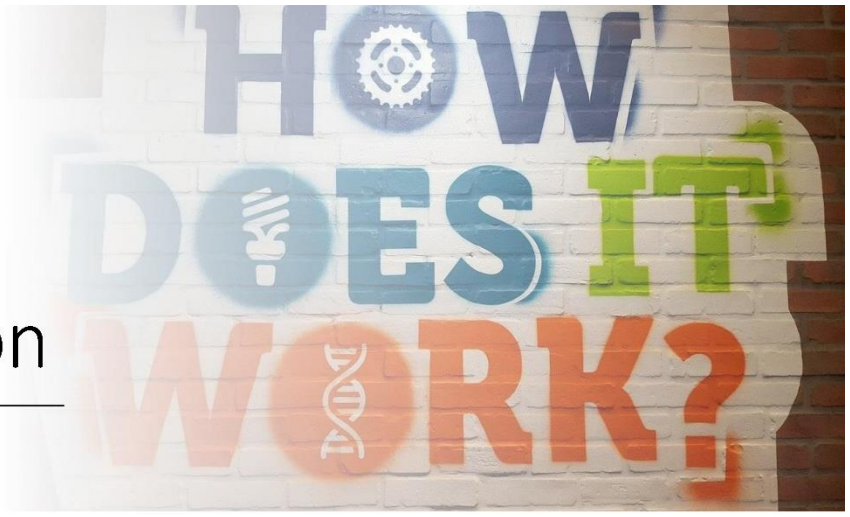

Results and Discussion

This chapter provides a detailed interpretation of the spectroscopic and photophysical data, giving the conceptions about the synthetic as well as spectroscopic aspects of the compounds while explaining the outcomes of the photophysical data thereof.

Chapter IV

Part A

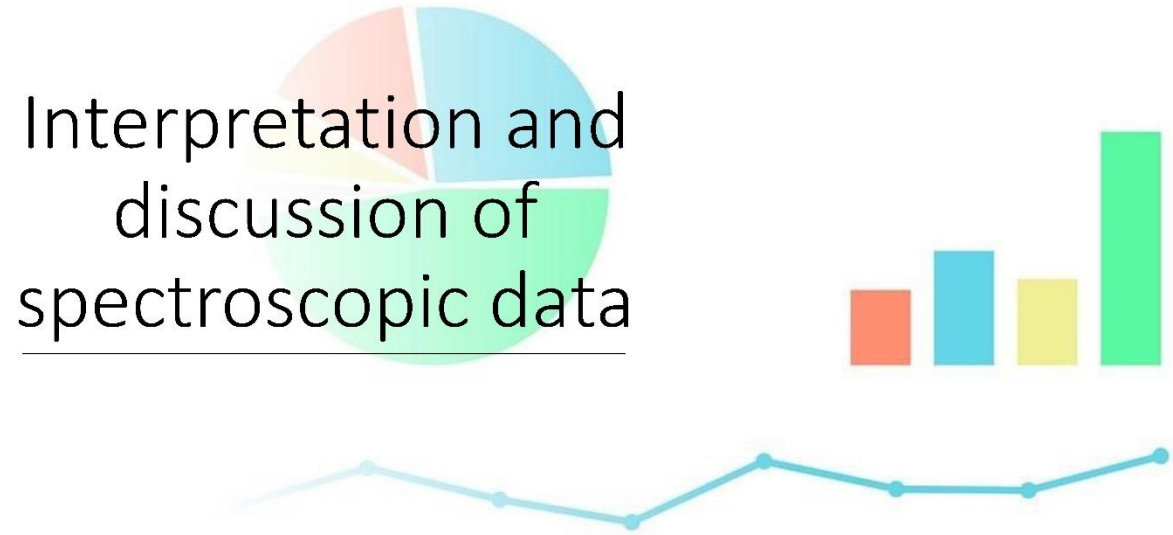

Interpretation and discussion of spectroscopic data

This section presents a detailed discussion of the spectroscopic analysis of the synthesized compounds and the findings and outcomes of the analysis as well as the causes for those specific results are presented in the form of text and figures in this chapter of the thesis.

4.1. Synthetic aspects in reference to the N-heterocyclic 1,2,3-triazole ring

The 1,2,3-triazoles, owing to their 'click' features such as regioselectivity, high yields, benign nature in addition to orthogonality enhancement, and processing ease, etc., have been frequently used as a linker and a functional moiety in several disparate compounds throughout the last several decades.[1,2] Consequently, being one of the most important nitrogen-containing compounds, 1,2,3-triazoles have been extensively investigated and have found their use in a wide variety of organic synthesis, supramolecular chemistry, drug discovery, polymer chemistry, cell biology, chemosensing, and material science applications[3–6] mainly attributable to their aromaticity, polarity, thermal and chemical stability, and inertness to oxidation and reduction conditions.[7,8] Since 1,2,3-triazole derivatives can be used in a wide variety of contexts, their synthesis has been a subject of intensive study. Among the many methods utilised to create these extraordinary compounds, the CuAAC is considered a major advancement in synthetic organic chemistry.[9,10] The CuAAC reaction is notable for its great regioselectivity, i.e., its ability to generate 1,2,3-triazole molecules: its outstanding yield of product and its scope under moderate circumstances, and its relatively low toxicity.[11–14] This study focused on the CuAAC reaction for synthesising of different 1,2,3-triazole derivatives, with the stages being as follows:

4.1.1. Synthesis of terminal alkyne

The terminal alkynes were synthesised by reacting a labile proton(s) bearing substrate with propargyl bromide and a suitable base. Stirring the reaction mixture using a base at room temperature in DMF as the solvent resulted in the extraction of the labile protons from starting material and subsequent substitution by the propynyl groups. Using TLC, the reaction progress was monitored. Since the propensity to lose a proton differs between substrates, the reaction time varied accordingly for different substrates. If the synthesised alkyne was a solid, it was filtered out of the reaction mixture, and if it is was oily/liquid, then solvent extraction process was implemented for its extraction using ethyl acetate.

4.1.2. Synthesis of organic azide

Organic azides were synthesised using the process described by Lourdes *et al.,* [15] by nucleophilic replacement of an aralkyl halide with dried sodium azide. The reaction was conducted in DMF while being heated at 85 - 90 °C for 5 hours. All the necessary precautions were followed to handle sodium azide as it is sensitive to heat and shock.

4.1.3. Cu(I)-catalyzed alkyne-azide cycloaddition

The cycloaddition between terminal alkynes and organic azides was catalysed by utilising the Cu(I) species with THF as the solvent and Et_3N base. Maintaining the reaction at 55 - 60 °C ranging from 5 - 12 hours (depending on the reactants) resulted in the formation of 1,2,3-triazole derivates by 'click' cycloaddition. The Cu(I) catalyst not only accelerated the reaction, but also imparted stereospecificity.

4.2. Synthesis and spectral analysis of benzyl azide (105)

4.2.1. Synthesis

Benzyl azide **105** was synthesized via the combination of benzyl chloride **135** with dried sodium azide (NaN_3) in DMF as the solvent, wherein the reaction proceeded via nucleophilic substitution. The reaction came to completion after 5 hours of stirring the reaction mixture at 85-90 °C. The reaction conditions were carefully monitored and managed to prevent any mishaps from occurring, which was necessary due to the extreme reactivity and explosiveness of sodium azide under these circumstances. After following solvent extraction process, benzyl azide was dried to eliminate any traces of the solvent before being analysed by infrared (IR) and nuclear magnetic resonance (NMR) spectroscopy to establish its successful synthesis.

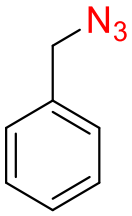

105

Figure 4.1: Structure of benzyl azide **105**

4.2.2. Analysis of IR spectrum

The IR spectrum of the newly synthesised benzyl azide **105** was reported as neat in the range 4000 - 500 cm^{-1}, wherein a significant signal at 2089 cm^{-1} distinctive of azide group was observed, thereby suggesting the replacement of the chloro group of benzyl chloride with the azide group to form benzyl azide. The aromatic C-H bond stretching signal was at 3032 cm^{-1},

whereas the aliphatic C-H bond symmetric stretch signal was at 2930 cm^{-1} for the protons of the benzylic carbon.

4.2.3. Analysis of NMR spectra

The ^{1}H NMR spectrum of benzyl azide **105** was recorded at 500 MHz in $CDCl_3$ relative to tetramethylsilane, wherein it showed a singlet at δ = 4.14 ppm, which was due to the two protons on the benzylic carbon, and the multiplet in the region of δ = 7.22 - 7.13 ppm corresponded to five aromatic protons on the benzene ring.

The ^{13}C NMR spectrum was also obtained for benzyl azide **105** in $CDCl_3$, providing further evidence in support of the successful synthesis of the product. The C atoms in the benzene ring provided the signals at δ = 135.53 - 128.31 ppm, whereas benzylic carbon contributed the signal at δ = 54.82 ppm.

4.3. Synthesis and spectral analysis of 1-(azidomethyl)naphthalene (137)

4.3.1. Synthesis

The aromatic organic azide 1-(azidomethyl)naphthalene **137** (**figure 4.2**) was synthesised by the nucleophilic substitution reaction of 1-(chloromethyl)naphthalene with the highly reactive sodium azide. The light yellow coloured oily product was obtained by stirring at 85-90 °C in DMF and then extracting it via solvent extraction process. Thereafter, the combined organic layers containing the extracted product were first dried using sodium sulphate (anhydrous) and then implementing vacuum evaporation to completely remove the solvent. Finally, IR and NMR spectroscopic methods were used to characterize the pure product and verify its formation.

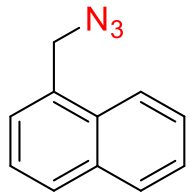

137

Figure 4.2: Structure of 1-(azidomethyl)naphthalene **137**

4.3.2. Analysis of IR spectrum

The IR spectrum of 1-(azidomethyl)naphthalene **137** was measured in the region of 4000 - 500 cm^{-1} (neat), and the obtained results verified the formation of the desired product. A sharp signal of high intensity at 2091 cm^{-1} evidenced the presence of a N_3 group, whereas a signal at 3051 cm^{-1} was due to the vibrational frequency of the aromatic C-H groups. In addition, the signal at 2938 cm^{-1} corresponded to the C-H stretching of the benzylic carbon.

4.3.3. Analysis of NMR spectra

In the 500 MHz ^{1}H NMR spectrum of 1-(azidomethyl)naphthalene **137** in $CDCl_3$, the aromatic protons of the naphthyl group were represented by the multiplet at δ = 8.10 - 7.48 ppm, while the benzylic protons were represented by the singlet at δ = 4.76 ppm.

Similarly, the ^{13}C NMR findings were also consistent with what was hypothesised. The carbon atoms in the aromatic ring contributed to the signals at δ = 134.05 - 123.64 ppm, while the singlet at δ = 53.02 ppm corresponded to the methylene carbon in the synthesized molecule.

4.4. Synthesis and spectral analysis of terminal alkyne 1,2-di(prop-2-yn-1-yl)-1,2-dihydropyridazine-3,6-dione (139)

4.4.1. Synthesis

The nucleophilic substitution reaction of the starting material (maleic hydrazide) **138** with 80% propargyl bromide solution **42** (in toluene) was used to synthesise the terminal alkyne **139** (**figure 4.3**). By continuous stirring of the mixture while using K_2CO_3 as the base, the labile protons of the secondary amino groups on the starting material were abstracted, and subsequently replaced by the propargyl group to synthesize the terminal alkyne derivative of maleic hydrazide. Thereafter, the brown coloured oily product was obtained by employing solvent extraction process and further evaporating the combined organic layers through vacuum evaporation to get the final product, which eventually solidified.

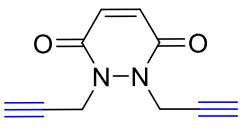

139

Figure 4.3: Structure of terminal alkyne **139**

4.4.2. Analysis of IR spectrum

IR spectrum in the range of 4000 - 500 cm^{-1} (neat) was used to characterize the maleic hydrazide-based terminal alkyne **139**, and the findings were consistent with those that were predicted. The signal observed at 3289 cm^{-1} is attributed to C≡*C-H* bond. Similarly, the signal observed at 2125 cm^{-1} is attributed to C≡C bond, thereby confirming the successful synthesis of terminal alkyne. The signal at 3059 cm^{-1} was because of the alkenyl C-H stretching, 2930 cm^{-1} was attributable to C-H stretching of methylene group, 1665 cm^{-1} was owing to the carbonyl stretch, 1586 cm^{-1} was due to C=C stretching and 1276 cm^{-1} was due to C-N stretching. In addition to this, the absence of signal at about 3400 cm^{-1} corresponding to the N-H stretching confirmed the successful conversion of the NH groups to form the terminal alkyne.

4.4.3. Analysis of NMR spectra

The predicted terminal alkyne **139** synthesis was ascertained owing to the presence of two triplets at δ = 2.35 ppm and δ = 2.59 ppm, which was attributable to the alkynyl protons (C≡*C–H*). The signal at δ = 4.80 ppm corresponded to the methylene protons, whereas the alkenyl protons exhibited doublets at δ = 6.95 ppm and δ = 7.01 ppm.

The ^{13}C NMR spectrum of the terminal alkyne **139** also confirmed its successful synthesis, wherein the signals at δ = 72.74 ppm and δ = 75.56 ppm corresponded to the C atoms of the C≡C moiety and a singlet at δ = 40.56 ppm corresponded to the methylene C atoms. The signal at δ = 133.15 ppm was due to the alkenyl C atoms, whereas the signal at δ = 159.27 was due to the carbonyl C atoms.

4.5. Synthesis and spectral analysis of 1,2-bis((1-benzyl-1H-1,2,3-triazol-4-yl)methyl)-1,2-dihydropyridazine-3,6-dione (140)

4.5.1. Synthesis

The maleic hydrazide-based 1,2,3-triazole derivative **140** (**figure 4.4**) was regioselectively synthesized by the combination of maleic hydrazide-based terminal alkyne **139** and benzyl azide **105** via CuAAC carried out in in a THF:TEA (v/v, 3:2) solvent media and in the presence of $[CuBr(PPh_3)_3]$ (0.001 mmol) complex serving as the catalyst. The reaction was facilitated by the triethylamine base, which allowed for the simple abstraction of the terminal proton, whereas the stereoselectivity of the cycloaddition to get exclusively the 1,4-disubstituted product was determined by the presence of Cu(I)-complex as catalyst. The

reaction reached completion after 5 hours of stirring at 55-60 °C. The product was produced by treating the reaction mixture with ice-cold water, and its comprehensive characterization was accomplished via standard spectroscopic techniques.

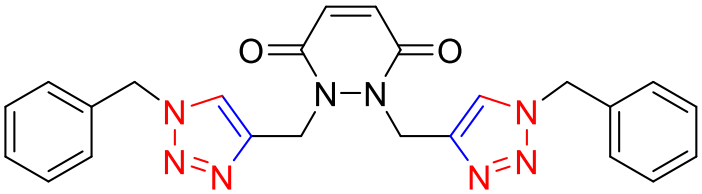

140

Figure 4.4: Structure of 1,2,3-triazole derivative **140**

4.5.2. Analysis of IR spectrum

The measurement of the IR spectrum (neat) of compound **140** between 4000 - 500 cm^{-1} provided conclusive evidence of the production of the target compound. The absence of signals due to the C≡*C*-*H* and C≡C stretching at 3289 cm^{-1} and 2126 cm^{-1} respectively, and -N=N=N stretching at 2090 cm^{-1} indicated the modification of C≡C-H and N_3 groups to form 1,2,3-triazole ring. Furthermore, the signal at 3134 cm^{-1} was due to the aromatic C-H stretching, 3061 cm^{-1} was due to the C-H stretching of the 1,2,3-triazole moiety, 2970 cm^{-1} was due to the C-H stretching of the methylene groups, 1660 cm^{-1} corresponded to the carbonyl stretching, and 1281 cm^{-1} was due to C-N stretching.

4.5.3. Analysis of NMR spectra

The ^{1}H NMR spectrum of compound **140** was observed in comparison to tetramethylsilane at 500 MHz, wherein the absence of triplets at δ = 2.35 ppm and δ = 2.59 ppm indicated the conversion of the alkyne moieties into 1,2,3-triazole rings. Due to this, the signal of the erstwhile alkynyl proton was observed in aromatic range of ^{1}H NMR spectrum of **140**. Furthermore, the doublet at δ = 5.29 ppm corresponded to the methylene protons adjoining the 1,2,3-triazole ring and the N atoms of parent structure, whereas the doublet at δ = 5.51 ppm resulted from the benzylic protons. The alkenyl protons gave the multiplet at δ = 6.89 - 6.79 ppm, whereas the multiplet at δ = 7.39 - 7.28 ppm were due to the aromatic protons.

The confirmation of effective synthesis of compound **140** was also provided by ^{13}C NMR spectroscopy. The methylene C atoms in the ^{13}C NMR of maleic hydrazide-based terminal alkyne **139** exhibiting signal at δ = 40.55 ppm was shifted downfield to δ = 46.66 ppm, due to their presence near the 1,2,3-triazole moiety in the ^{13}C NMR of the 1,2,3-triazole

derivative **140**. Also, the signals at δ = 72.74 ppm and δ = 75.55 ppm corresponding to the C≡C moiety in the ^{13}C NMR of maleic hydrazide-based terminal alkyne were absent in the ^{13}C NMR of **140**, thereby indicating their conversion to form the 1,2,3-triazole ring. The signal at δ = 52.27 ppm was due to the benzylic C atoms, whereas the signals at δ = 142.72 - 125.39 ppm corresponded to the aromatic C atoms. Furthermore, the signal at δ = 158.52 ppm corresponded to the C atoms of the carbonyl groups.

4.5.4. Analysis of mass spectrum

The synthesised 1,2,3-triazole derivative **140** had a predicted molecular mass peak (m/z) of 454.49 and its mass spectrum (GC-MS) revealed a prominent peak at m/z = 454.25, thereby verifying its successful synthesis.

4.6. Synthesis and spectral analysis of 1,2-bis((1-(naphthalen-1-ylmethyl)-1H-1,2,3-triazol-4-yl)methyl)-1,2-dihydropyridazine-3,6-dione (141)

4.6.1. Synthesis

The regioselective synthesis of the maleic hydrazide-based 1,2,3-triazole derivative **141** (**figure 4.5**) was achieved by reacting the terminal alkyne **139** derived from maleic hydrazide with 1-(azidomethyl)naphthalene **137** in the presence of [$CuBr(PPh_3)_3$] (0.001 mmol) complex in THF:TEA (v/v, 3:2) solvent media. The triethylamine base assisted the reaction by allowing for the easy abstraction of the terminal protons, while the presence of Cu(I)-complex as a catalyst regulated the stereoselectivity of the cycloaddition, resulting in the selective formation of the 1,4-disubstituted product. The reaction completion was achieved after 5 hours of stirring at 55-60 °C. Using chilled water, the solid product was obtained from the reaction mixture, and conventional spectroscopic methods were used to characterize it.

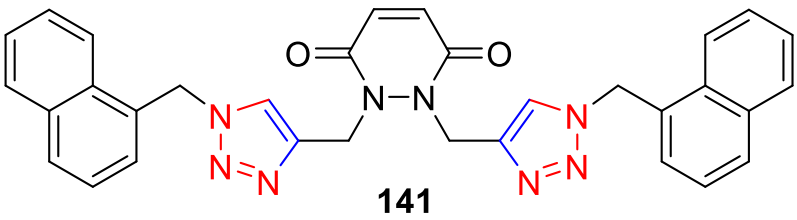

141

Figure 4.5: Structure of 1,2,3-triazole derivative **141**

4.6.2. Analysis of IR spectrum

The 1,2,3-triazole derivative of maleic hydrazide **141** was shown to have been synthesised by measuring its infrared spectrum (neat) between 4000 - 500 cm^{-1}. The synthesis

of the 1,2,3-triazole was verified by the elimination of the signals at 3289 cm^{-1} owing to C≡*C*-*H* stretching, 2126 cm^{-1} due to C≡C stretching, and 2091 cm^{-1} due to -N=N=N stretching of 1-(azidomethyl)naphthalene. The signal due to aromatic C-H stretching was observed at 3140 cm^{-1}, and the C-H stretching of the 1,2,3-triazole moiety was attributed to 3059 cm^{-1}, 2960 cm^{-1} for C-H stretching of the methylene groups, 1660 cm^{-1} for carbonyl stretching, and 1274 cm^{-1} for C-N stretching.

4.6.3. Analysis of NMR spectra

The ^{1}H NMR spectrum of compound **141** was obtained in $CDCl_3$ at 500 MHz in reference to tetramethylsilane. The absence of triplets at δ = 2.35 ppm and δ = 2.59 ppm suggested that the alkyne moieties had been converted into 1,2,3-triazole rings. As a consequence of this, the signal of the alkynyl proton manifested itself in aromatic range. In addition, the doublet at δ = 5.17 ppm belonged to the methylene protons, whilst the doublet at δ = 5.85 ppm was due to the benzylic protons. The signal at δ = 6.79 ppm was caused by the alkenyl protons, whilst the multiplet at δ = 8.13 - 7.39 ppm was caused by the aromatic protons.

The ^{13}C NMR spectroscopy also presented evidence for the successful synthesis of compound **141**. Due to their proximity to the aromatic 1,2,3-triazole ring, the methylene C atoms in the ^{13}C NMR of the terminal alkyne **139**, displaying signal at δ = 40.55 ppm, were shifted downfield to δ = 43.86 ppm in the ^{13}C NMR of the 1,2,3-triazole derivative **141**. Additionally, the ^{13}C NMR of the terminal alkyne **139** showed signals at δ = 72.74 ppm and δ = 75.55 ppm corresponding to the C≡C moiety; these signals were missing in the ^{13}C NMR of the 1,2,3-triazole derivative **141**, confirming their conversion to create the 1,2,3-triazole ring. Besides, the benzylic C atoms contributed the signal at δ = 54.11 ppm, whereas the aromatic C atoms were responsible for the signals at δ = 142.42 - 124.79 ppm. The carbonyl C atoms exhibited the signal at δ = 159.18 ppm.

4.6.4. Analysis of mass spectrum

The synthesised 1,2,3-triazole derivative **141** had a predicted molecular mass peak (m/z) = 554.61 and its mass spectrum (GC-MS) revealed a prominent peak at m/z = 555.40 corresponding to M+1, thereby verifying its successful synthesis.

4.7. Synthesis and spectral analysis of terminal alkyne 4-(tert-butyl)-1,2-bis(prop-2-yn-1-yloxy)benzene (143)

4.7.1 Synthesis

The terminal alkyne **143** (**figure 4.6**) was synthesised by reacting 4-tert butyl catechol **142** with a solution of propargyl bromide **42** in toluene at a concentration of 80%. The reaction proceeded with the abstraction of the labile protons of the hydroxyl groups on the starting material via Cs_2CO_3 as the base, and replacing them with the propargyl groups. Ice-cold distilled water was used to quench the reaction, and ethyl acetate was used to extract the final product. The organic layers were combined and desiccated over sodium sulphate (anhydrous), and the solvent was evaporated using vacuum evaporation to obtain the dark brown oily product. Subsequently, IR and NMR spectroscopy were used to determine the precise structure of the terminal alkyne, thereby proving its effective synthesis.

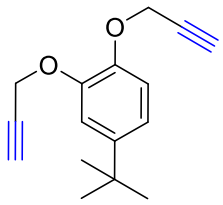

143

Figure 4.6: Structure of terminal alkyne **143**

4.7.2. Analysis of IR spectrum

The characterization of 4 tert-butyl catechol-based terminal alkyne **143** was done by infrared spectroscopy in the region of 4000 - 500 cm^{-1} (neat), and the findings agreed with those expected. The synthesis of terminal alkyne was verified by the signal at 2121 cm^{-1}, attributable to C≡C stretching and the signal at 3290 cm^{-1}, owing to C≡*C-H* stretching. At the same time disappearance of a broad signal at 3341 cm^{-1} indicated the modification of -OH functional group on starting compound. The methylene C-H stretching contributed to the signal at 3054 cm^{-1}, whereas the methyl C-H stretching contributed to the signal at 2961 cm^{-1}. The aromatic C=C stretching contributed the signals at 1590 cm^{-1} and 1505 cm^{-1} and the signals at 1453 cm^{-1} and 1366 cm^{-1} were attributed to methylene groups and the methyl groups respectively (bending vibrations). In addition to this, the absence of a broad signal at about 3400 cm^{-1} corresponding to the O-H stretching confirmed the successful conversion of the OH group to form the terminal alkyne.

4.7.3. Analysis of NMR spectra

The signal at δ = 2.50 ppm in the ^{1}H NMR spectrum of **143**, which corresponded to the alkynyl protons, provided evidence that the terminal alkyne synthesis that had been anticipated was successfully achieved. Additionally, the singlet at δ = 1.31 ppm was due to the methyl protons. The methylene protons were responsible for the signal at δ = 4.74 ppm, whereas the signals at δ = 6.97 ppm and δ = 7.12 ppm corresponded the aromatic protons.

The ^{13}C NMR spectrum of compound **143** further validated the successful synthesis of the compound. In this spectrum, the signals at δ = 75.71 ppm and δ = 78.85 ppm belonged to the C atoms of the C≡C moiety, while the signals at δ = 31.39 ppm and δ = 34.35 ppm were due to the C atoms of the methyl groups and the quaternary C atom attached to them respectively. Also, the signals at δ = 56.90 ppm and δ = 57.14 ppm were due to the methylene C atoms. The signals that appeared at δ = 146.94 - 113.62 ppm were due to the aromatic C atoms.

4.8. Synthesis and spectral analysis of 4,4'-(((4-(tert-butyl)-1,2-phenylene)bis(oxy))bis(methylene))bis(1-benzyl-1H-1,2,3-triazole) (144)

4.8.1. Synthesis

The 4-tert butyl catechol-based 1,2,3-triazole derivative **144** (**figure 4.7**) was synthesised by reacting the terminal alkyne **143** with benzyl azide **105** using [$CuBr(PPh_3)_3$] (0.001 mmol) catalytic system in THF:TEA (v/v, 1:1) solvent medium. By facilitating the abstraction of the terminal protons, the triethylamine base aided the reaction, while the Cu(I)-complex controlled the stereoselectivity of the cycloaddition. After 5.5 hours of stirring at 55 - 60 °C, the reaction reached completion. The solid product was separated from reaction mixture using ice-cold water, and then characterized using traditional spectroscopic techniques.

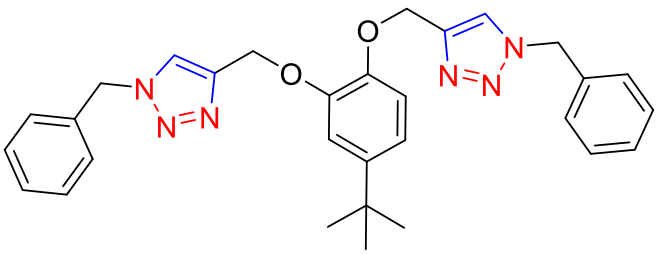

144

Figure 4.7: Structure of 1,2,3-triazole derivative **144**

4.8.2. Analysis of IR spectrum

The measurement of the IR spectrum (neat) of compound **144** between 4000 - 500 cm^{-1} gave strong evidence of the target compound's synthesis. The absence of signals at 3290 cm^{-1} owing to C≡*C*-*H* stretching, 2121 cm^{-1} due to C≡C stretching, and 2089 cm^{-1} due to -N=N=N stretching suggested that the C≡C-H and N_3 groups were modified to produce the triazole moiety. Furthermore, the signal at 3134 cm^{-1} was caused by aromatic C-H stretching, 3062 cm^{-1} by C-H stretching of the 1,2,3-triazole moiety, 2956 cm^{-1} by C-H stretching of the methyl groups, 1591 cm^{-1} and 1511 cm^{-1} by aromatic C=C stretching, and the signals at 1460 cm^{-1} and 1384 cm^{-1} were attributable to the methylene groups and the methyl groups respectively (bending vibrations).

4.8.3. Analysis of NMR spectra

The ^{1}H NMR spectrum of compound **144** was observed at 500 MHz in $CDCl_3$, with tetramethylsilane as the reference. The lack of triplet at δ = 2.50 ppm indicated the conversion of alkyne moieties into the 1,2,3-triazole rings. The methyl protons caused the singlet at δ = 1.24 ppm, while the methylene protons exhibited the signal at δ = 5.19 ppm. In addition, the benzylic protons caused the signal at δ = 5.45 ppm. The aromatic protons provided the multiplet at δ = 7.32 - 6.89 ppm, and the protons of the 1,2,3-triazole rings were represented by the singlet at δ = 7.58 ppm.

The ^{13}C NMR spectroscopy also confirmed the successful synthesis of compound **144**. The signals at δ = 75.71 ppm and δ = 78.85 ppm owing to the C≡C moiety of the terminal alkyne were absent in the ^{13}C NMR of the 1,2,3-triazole derivative **144**, showing their conversion to the 1,2,3-triazole ring. Also, the methylene C atoms in the ^{13}C NMR spectrum of the terminal alkyne **143** displaying signals at δ = 56.90 ppm and δ = 57.14 ppm were displaced downfield to δ = 63.68 ppm and δ = 63.92 ppm due to their presence in the proximity of the aromatic 1,2,3-triazole ring in the ^{13}C NMR of the 1,2,3-triazole derivative **144**. The benzylic C atoms were responsible for the signal at δ = 54.11 ppm, whereas the aromatic C atoms were responsible for the signals at δ = 147.86 - 114.05 ppm.

4.8.4. Analysis of mass spectrum

The 1,2,3-triazole derivative **144** had a predicted molecular mass peak (m/z) of 508.63, and its mass spectrum (GC-MS) showed a strong peak at m/z = 509.50 corresponding to M+1, thereby confirming that the synthesis was successful.

4.9. Synthesis and spectral analysis of terminal alkyne 4-(bis(4-(prop-2-yn-1-yloxy)phenyl)methylene)cyclohexa-2,5-dien-1-one (146)

4.9.1. Synthesis

The terminal alkyne **146** (**figure 4.8**) was synthesised by combining p-rosolic acid **145** with an 80% propargyl bromide solution **42** in toluene. Using K_2CO_3 as the base, the labile protons of the starting material were removed and replaced with propargyl groups. The reaction was quenched with ice-cold water, and the product was isolated using ethyl acetate. The dark brown viscous product was obtained by removing the solvent by dehydrating the combined organic layers over sodium sulphate (anhydrous), filtering them, and then evaporating them under vacuum. IR and NMR spectroscopy were then used to ascertain the precise structure of the terminal alkyne, thereby demonstrating its successful synthesis.

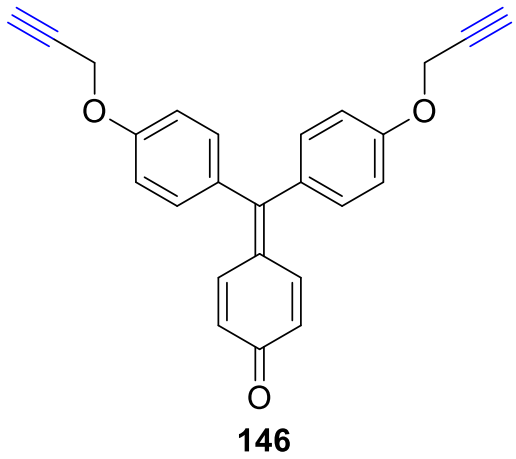

146

Figure 4.8: Structure of terminal alkyne **146**

4.9.2. Analysis of IR spectrum

The terminal alkyne **146** was characterized by infrared spectroscopy (4000 - 500 cm^{-1}) with expected results. A signal at 2121 cm^{-1}, attributed to the C≡C stretching, and an additional signal at 3286 cm^{-1}, owing to the C≡*C*-*H* stretching, confirmed the synthesis of the terminal alkyne. The aromatic C-H stretching corresponded to the signal at 3047 cm^{-1}, whereas the C-H stretching of the methylene groups contributed to the signal at 2923 cm^{-1}. The aromatic C=C

stretching contributed the signals at 1603 cm^{-1} and 1503 cm^{-1}. In addition to this, the absence of a broad signal at about 3400 cm^{-1} corresponding to the O-H stretching confirmed the successful conversion of the OH group to form the terminal alkyne.

4.9.3. Analysis of NMR spectra

The ^{1}H NMR spectrum of the terminal alkyne **146** was obtained at 500 MHz in $CDCl_3$ using tetramethylsilane as the reference. The presence of a triplet at δ = 2.51 ppm, which corresponded to the alkynyl protons, was evidence that the anticipated terminal alkyne synthesis was successful. Additionally, methylene protons were responsible for the doublet at δ = 4.65 ppm, and the aromatic protons corresponded the multiplets at δ = 7.19 - 6.71 ppm.

The ^{13}C NMR spectrum of the terminal alkyne **146** further validated the effective synthesis of the compound. The signals at δ = 75.70 ppm and δ = 78.67 ppm in this spectrum belonged to the C atoms of the C≡C moiety, whereas the signal at δ = 55.90 ppm was caused by the C atoms of the methylene groups. The signals at δ = 157.76 - 114.19 ppm were caused by aromatic C atoms, whereas the carbonyl C atom gave the signal at 185.26.

4.10. Synthesis and spectral analysis of 4-(bis(4-((1-(naphthalen-1-ylmethyl)-1H-1,2,3-triazol-4-yl)methoxy)phenyl)methylene)cyclohexa-2,5-dien-1-one (147)

4.10.1. Synthesis

The p-rosolic acid-based 1,2,3-triazole derivative **147** (**figure 4.9**) was synthesized by reacting the terminal alkyne **146** with 1-(azidomethyl)naphthalene **137** in the presence of $[CuBr(PPh_3)_3]$ (0.001 mmol) in a solvent medium of THF:TEA (v/v, 2:1). The triethylamine base helped the reaction by enabling the abstraction of the terminal protons, while the Cu(I)-complex regulated the stereoselectivity of the cycloaddition, resulting in the selective synthesis of the 1,4-disubstituted product. The reaction was complete after 12 hours of stirring at 55-60 °C. Using chilled water, the solid product was obtained from the reaction mixture and subsequently characterized using standard spectroscopic methods.

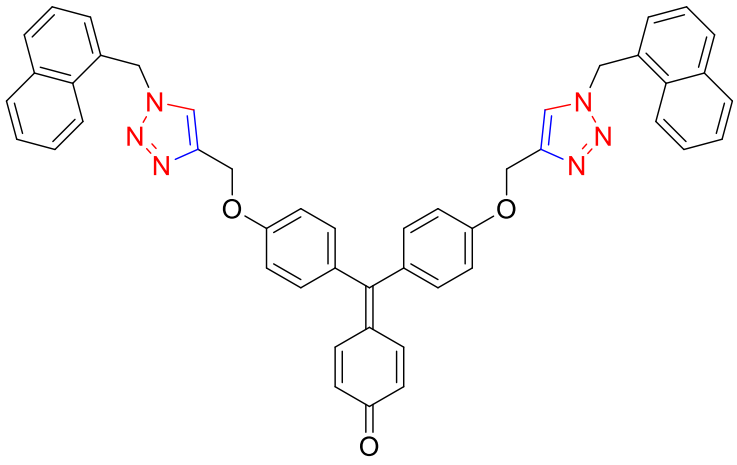

147

Figure 4.9: Structure of 1,2,3-triazole derivative **147**

4.10.2. Analysis of IR spectrum

The infrared spectrum (neat) between 4000 and 500 cm^{-1} of compound **147** provided conclusive evidence that the compound had been synthesised. The disappearance of $-N_3$ stretching signal at 2091 cm^{-1} from 1-(azidomethyl)naphthalene, C≡C stretching signal at 2126 cm^{-1}, and C≡*C*-*H* stretching signal at 3289 cm^{-1} due to the alkyne group confirmed the successful conversion of these moieties to synthesize the 1,2,3-triazole ring. Additional signals were seen at 3142 cm^{-1} for aromatic C-H stretching, 3059 cm^{-1} for C-H stretching of the 1,2,3-triazole moiety, and 2951 cm^{-1} for C-H stretching of the methylene groups. The signals for the aromatic C=C stretching were present at 1602 cm^{-1} and 1504 cm^{-1}, while the C-H bending of the methylene groups corresponded to the signal at 1462 cm^{-1}.

4.10.3. Analysis of NMR spectra

The ^{1}H NMR spectrum of compound **147** was measured in $CDCl_3$ at a frequency of 500 MHz relative to tetramethylsilane wherein the lack of a triplet at δ = 2.51 ppm evidenced that the alkyne moieties had been transformed into 1,2,3-triazole rings. Because of this, the signal from the alkynyl protons appeared in the aromatic range of the ^{1}H NMR spectrum of the 1,2,3-triazole derivative **147**. In addition, the singlets that appeared at δ = 5.04 ppm and δ = 5.94 ppm were attributed to the methylene protons and the benzylic protons respectively. The aromatic protons were responsible for the multiplets that appeared at δ = 7.97 - 6.78 ppm.

The effective synthesis of compound **147** was also validated by ^{13}C NMR spectroscopy. The signals at δ = 75.70 ppm and δ = 78.67 ppm owing to the C≡C moiety were absent in the

^{13}C NMR of the 1,2,3-triazole derivative **147**, indicating their conversion to the 1,2,3-triazole ring. Furthermore, the methylene C atoms in the alkyne ^{13}C NMR spectrum with signal at δ = 55.90 ppm were displaced downfield to δ = 62.07 ppm due to their proximity to the aromatic 1,2,3-triazole ring in the ^{13}C NMR of compound **147**. The signal at δ = 52.42 ppm was attributed to the benzylic C atoms, whereas the signals at δ = 185.52 - 113.97 ppm were caused by aromatic C atoms.

4.10.4. Analysis of mass spectrum

The mass spectrum (LC-MS) of the synthesised 1,2,3-triazole derivative **147** displayed a prominent peak at m/z = 733.30, matching to M+1, verifying the accuracy of the expected molecular mass peak (m/z) of 732.28.

4.11. Synthesis and spectral analysis of terminal alkyne (1*E*,2*E*)-*N*^{1},*N*^{2}-bis(2-(prop-2-yn-1-yloxy)phenyl)ethane-1,2-diimine (149)

4.11.1. Synthesis

By reacting glyoxal bis-(2-hydroxyanil) **148** with propargyl bromide solution **42** in toluene at a concentration of 80%, the terminal alkyne **149** (**figure 4.10**) was synthesised. The Cs_2CO_3 acting as the base led to the removal of the labile protons which were substituted with propargyl groups. The adding ice-cold water resulted in the quenching of the reaction, and ethyl acetate was used to separate the product. The drying of the combined organic layers was done over sodium sulphate (anhydrous) and then filtered. The final product was obtained after the addition of n-hexane, which precipitated the product, followed by filtration, washing, and drying.

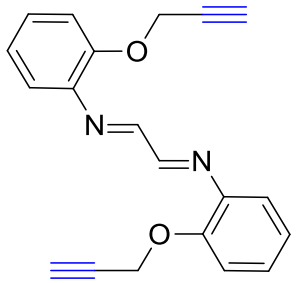

149

Figure 4.10: Structure of terminal alkyne **149**

4.11.2. Analysis of IR spectrum

Infrared spectroscopy was used in the region of 4000 - 500 cm^{-1} (neat) in order to characterize the terminal alkyne **149**, and the findings were as anticipated. The synthesis of the

terminal alkyne was validated by the appearance of a signal at 3283 cm^{-1}, which corresponded to the C≡*C-H* stretching, as well as an additional signal at 2120 cm^{-1}, which was attributable to the C≡C stretching. The C-H stretching of the aromatic groups contributed to the signal that was seen at 3062 cm^{-1}, while the C-H stretching of the methylene groups was responsible for the signal that was observed at 2967 cm^{-1}. The signal at 1670 cm^{-1} was attributed to the C=N stretching, whereas the 1596 cm^{-1} and the 1498 cm^{-1} signals were due to the aromatic C=C stretching. In addition to this, the absence of a broad signal at about 3400 cm^{-1} corresponding to the O-H stretching confirmed the successful conversion of the OH group to form the terminal alkyne.

4.11.3. Analysis of NMR spectra

Using tetramethylsilane as a standard, the ^{1}H NMR spectrum of the terminal alkyne **149** was recorded at 500 MHz in $CDCl_3$. The terminal alkyne synthesis was confirmed owing to the observation of a triplet at δ = 2.51 ppm in the ^{1}H NMR spectrum of the alkyne, corresponding to the alkynyl protons. The methylene protons were attributable to the signal at δ = 4.73 ppm, whereas aromatic protons showed up as multiplet at δ = 7.05 - 6.72 ppm.

The ^{13}C NMR spectrum of the terminal alkyne **149** provided additional validation of the effective synthesis. The C atoms that make up the C≡C moiety were ascribed to the signals that appeared at δ = 75.55 ppm and δ = 78.88 ppm. On the other hand, the methylene C atoms were responsible for the signal at δ = 56.58 ppm. The presence of aromatic C atoms was the origin of the signals that were observed between δ = 159.20 - 112.76 ppm.

4.12. Synthesis and spectral analysis of (1*E*,2*E*)-N^1,N^2-bis(2-((1-(naphthalen-1-ylmethyl)-1H-1,2,3-triazol-4-yl)methoxy)phenyl)ethane-1,2-diimine (150)

4.12.1. Synthesis

Figure 4.11 shows the glyoxal bis-(2-hydroxyanil)-based 1,2,3-triazole derivative **150**, which was synthesized by reacting the previously synthesized terminal alkyne **149** with 1-(azidomethyl)naphthalene **137** in the presence of 0.001 mmol of $[CuBr(PPh_3)_3]$ in a THF:TEA (v/v, 3:2) solvent media. The triethylamine base helped the reaction by allowing the terminal alkynyl protons to be removed; while the Cu(I)-complex acted as a catalyst to control the stereoselectivity of the cycloaddition, which made it possible to make only the desired 1,4-disubstituted product. After 6 hours of stirring at 55 to 60 °C, the process was completed, as

ascertained via TLC. The solid product was separated from the reaction mixture with ice-cold water and then analyzed with standard spectral methods.

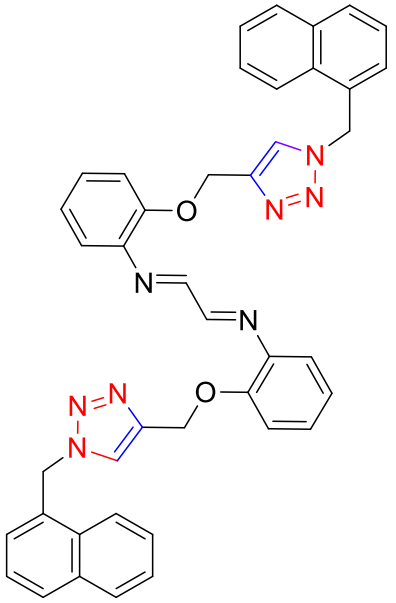

150

Figure 4.11: Structure of 1,2,3-triazole derivative **150**

4.12.2. Analysis of IR spectrum

The synthesis of compound **150** was shown by its characteristic infrared spectrum (neat) between 4000 and 500 cm^{-1}. The effective formation of the 1,2,3-triazole ring was verified by the absence of -N=N=N stretching signal at 2091 cm^{-1}, C≡*C-H* stretching signal at 3283 cm^{-1}, and C≡C stretching signal at 2120 cm^{-1}, owing to the alkyne group. C-H stretching signals were also seen at 3138 cm^{-1} for aromatic C-H stretching, 3051 cm^{-1} for the 1,2,3-triazole moiety, and 2963 cm^{-1} for the methylene groups. The signals at 1596 and 1499 cm^{-1} were suggestive of aromatic C=C stretching and the signal at 1454 cm^{-1} corresponded the C-H bending in methylene groups.

4.12.3. Analysis of NMR spectra

The ^{1}H NMR spectrum of compound **150** was measured in DMSO as the solvent at a frequency of 500 MHz relative to tetramethylsilane. It was shown that the alkyne moieties had been converted into 1,2,3-triazole rings as a result of the absence of a triplet at δ = 2.51 ppm. As a result of this, one of the signals in the aromatic section of the ^{1}H NMR spectrum of the 1,2,3-triazole derivative **150** was caused by the protons that were previously connected to the alkynyl group. In addition, the doublets that manifested at δ = 5.15 ppm and 5.98 ppm were

assigned to the methylene protons and the benzylic protons, respectively. The multiplets that emerged at δ = 8.31 - 6.94 ppm was caused by aromatic protons.

The ^{13}C NMR spectroscopy was also used to demonstrate the effective synthesis of compound **150**. In the spectrum, the absence of signals at δ = 75.55 ppm and δ = 78.88 ppm corresponding to the C≡C moiety of the terminal alkyne indicated that the moiety was converted to the 1,2,3-triazole ring. Furthermore, the methylene C atoms of the terminal alkyne **149**, which had a signal at δ = 56.58 ppm, were displaced downfield to δ = 61.97 ppm in the ^{13}C NMR spectrum of **150** because of their proximity to the aromatic ring. The benzylic C atoms were responsible for the signal at δ = 50.79 ppm, whilst the aromatic C atoms were the source of the signals at δ = 143.27 - 112.77 ppm.

4.12.4. Analysis of mass spectrum

The mass spectrum (LC-MS) of the synthetic 1,2,3-triazole derivative **150** showed a peak at m/z = 683.28, which corresponded to the theoretically calculated [M+1] peak (theoretical m/z = 682.28). This verified that the desired 1,2,3-triazole derivative was successfully synthesized.

4.13. Synthesis and spectral analysis of Schiff base (*E*)-2-methoxy-4-(((5-methylpyridin-2-yl)imino)methyl)phenol (153)

4.13.1. Synthesis

The Schiff base **153** was synthesized by subjecting the reaction mixture containing equimolar concentration of 2-amino-5-methylpyridine **151** and 4-hydroxy-3-methoxybenzaldehyde **152** (vanillin) to refluxing in ethanol as the solvent, wherein the two reactants underwent nucleophilic addition to get connected via a newly formed imine moiety. A TLC analysis confirmed the reaction completion after 40 hours. After separating the solid product from the reaction mixture using ice-cold water, it was examined using conventional spectroscopic techniques.

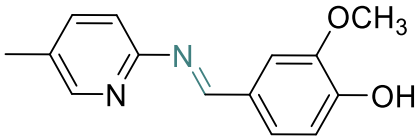

153

Figure 4.12: Structure of Schiff base **153**

4.13.2. Analysis of IR spectrum

The IR spectrum (neat) analyzed for the Schiff base **153** in the range of 4000 - 500 cm^{-1} was suggestive of its successful synthesis. The broad signal corresponding to the -OH moiety appeared at 3367 cm^{-1}, whereas the signal at 1672 cm^{-1} was suggestive of the formation of a C=N bond. In addition to this, the absence of signals at 3450 cm^{-1} and 3300 cm^{-1} corresponding to the NH_2 stretching confirmed the successful conversion of the NH_2 group to form the Schiff base.

4.13.3. Analysis of NMR spectra

The ^1H NMR spectrum of compound **153** was measured in $CDCl_3$ as the solvent at a frequency of 500 MHz relative to tetramethylsilane. The methyl protons were attributable to the singlet at δ = 2.12 ppm, while the methoxy protons were responsible for the singlet at δ = 3.91 ppm. The aromatic protons appeared as multiplets at δ = 7.93 - 6.82 ppm. The proton of the hydroxyl group was attributed to the singlet at δ = 9.68 ppm.

The ^{13}C NMR spectroscopy was also used to demonstrate the effective synthesis of compound **153**. The C atom of the methyl group was assigned to the signal at δ = 14.13 ppm, whereas the C atom of the methoxy group was responsible for the signal at δ = 59.53 ppm. The aromatic C atoms were marked by the presence of the signals between δ = 160.46 - 110.87 ppm, and the C atom of the C=N group was attributed to the signal at δ = 163.66 ppm.

4.14. Synthesis and spectral analysis of terminal alkyne (*E*)-1-(3-methoxy-4-(prop-2-yn-1-yloxy)phenyl)-N-(5-methylpyridin-2-yl)methanimine (154)

4.14.1. Synthesis

The terminal alkyne **154** (**figure 4.13**) was synthesized by reacting the synthesized Schiff base **153** with propargyl bromide solution **42** in toluene at an 80% concentration. Stirring the reaction mixture with K_2CO_3 as the base at room temperature resulted in the removal of labile protons from the hydroxyl group on the Schiff base and their replacement with propargyl groups. Following the addition of ice-cold water to terminate the reaction, the resultant solid product was subjected to filtration, further washing with water, and subsequent drying until a constant weight was achieved. The structure of the terminal alkyne was then determined using infrared (IR) and nuclear magnetic resonance (NMR) spectroscopy, thereby evidencing that the synthesis was successful.

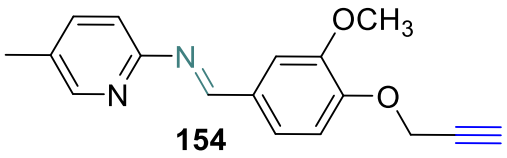

154

Figure 4.13: Structure of terminal alkyne **154**

4.14.2. Analysis of IR spectrum

The terminal alkyne **154** was characterized using infrared spectroscopy (4000 - 500 cm^{-1}), and the findings corroborated the anticipated outcomes. A sharp signal at 3282 cm^{-1}, corresponding to the C≡*C-H* stretching, and an additional signal at 2117 cm^{-1}, related to the C≡C stretching, confirmed the terminal alkyne synthesis. The signal at 3007 cm^{-1} was due to the aromatic C-H stretching, and the signal at 2937 cm^{-1} corresponded to the C-H stretching of the aliphatic groups. Furthermore, the absence of a broad signal at 3367 cm^{-1} due to the O-H stretching was absent, which confirmed the successful conversion of the O-H moiety into the terminal alkyne.

4.14.3. Analysis of NMR spectra

The ^{1}H NMR spectrum of the terminal alkyne **154** was attained at 500 MHz in $CDCl_3$ using tetramethylsilane as a reference, and the results were suggestive of successful synthesis of the product. The detection of a triplet at δ = 2.57 ppm, corresponding to the alkynyl proton, validated the terminal alkyne synthesis. Also, the methylene protons were responsible for the singlet at δ = 4.70 ppm. The methyl protons were attributable to the singlet at δ = 2.12 ppm, while the methoxy protons were responsible for the singlet at δ = 3.90 ppm. The aromatic protons appeared as multiplet at δ = 7.96 - 6.78 ppm.

The ^{13}C NMR spectrum of the terminal alkyne **154** gave further confirmation of the successful synthesis. The C atoms that comprised the C≡C moiety were assigned to the signals at δ = 75.74 ppm and δ = 79.56 ppm, while the methylene C atom was attributed to the signal at δ = 56.79 ppm. Additionally, the C atom of the methyl group was assigned to the signal at δ = 17.36 ppm, whereas the C atom of the methoxy group was responsible for the signal at δ = 55.74 ppm. The aromatic C atoms were marked by the presence of the signals between δ = 160.53 - 110.61 ppm, and the C atom of the C=N group was attributed to the signal at δ = 163.80 ppm.

4.15. Synthesis and spectral analysis of (*E*)-1-(4-((1-benzyl-1H-1,2,3-triazol-4-yl)methoxy)-3-methoxyphenyl)-*N*-(5-methylpyridin-2-yl)methanimine (155)

4.15.1. Synthesis

The 1,2,3-triazole derivative **155** of the Schiff base alkyne is shown in **figure 4.14**, which was prepared by reacting the previously synthesized terminal alkyne **154** with benzyl chloride **105** in THF:TEA (v/v, 2:1) solvent medium containing 0.001 mmol of [$CuBr(PPh_3)_3$]. The removal of the terminal alkynyl protons was facilitated by the triethylamine base, and the Cu(I)-complex worked as a catalyst to maintain stereoselectivity throughout the cycloaddition, allowing for the production of solely the required 1,4-disubstituted product. TLC confirmed completion of reaction after 6 hours of stirring at 55 to 60 °C. The solid product was extracted from the reaction mixture using ice-cold water, and then conventional spectrum techniques were applied to it for analysis.

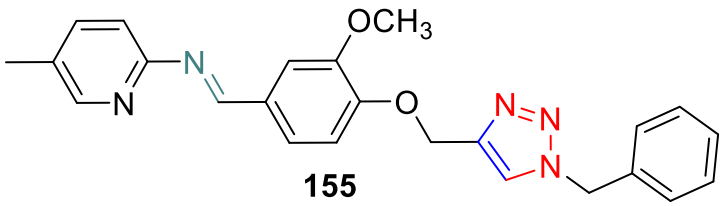

155

Figure 4.14: Structure of 1,2,3-triazole derivative **155**

4.15.2. Analysis of IR spectrum

The successful synthesis of compound **155** was demonstrated by its infrared spectrum (neat) between 4000 and 500 cm^{-1}. The absence of -N=N=N stretching signal at 2089 cm^{-1} due to the azide group, the C≡C stretching signal at 2117 cm^{-1}, and C≡*C*-*H* stretching signal at 3282 cm^{-1} due to the alkyne group confirmed the efficient synthesis of 1,2,3-triazole moieties to create the 1,2,3-triazole ring. The signals for aromatic C-H stretching were seen at 3137 cm^{-1} for the C-H stretching of the 1,2,3-triazole moiety, 3007 cm^{-1} for the aromatic C-H stretching, and 2964 cm^{-1} for the methylene groups. The signals at 1610 and 1498 cm^{-1} indicated aromatic C=C stretching, while the signals at 1459 cm^{-1} and 1385 cm^{-1} indicated C-H bending of the methylene and methyl groups respectively.

4.15.3. Analysis of NMR spectra

The ^1H NMR spectrum of compound **155** was measured in $CDCl_3$ at a frequency of 500 MHz relative to tetramethylsilane, wherein the results obtained were suggestive of successful

synthesis of the product. The absence of a triplet at δ = 2.57 ppm demonstrated that the alkyne moiety had been converted into the 1,2,3-triazole moiety. Therefore, the aromatic region of the ^{1}H NMR spectrum of **155** showed a signal from the proton that was originally connected to the alkynyl group. Furthermore, the singlets at δ = 5.09 ppm and δ = 5.84 ppm were assigned to methylene protons and benzylic protons, respectively. Additionally, the methyl protons were attributable to the singlet at δ = 2.13 ppm, while the methoxy protons were attributed to the singlet at δ = 3.90 ppm. The aromatic protons were responsible for the multiplet at δ = 7.96 - 6.79 ppm.

The successful synthesis of compound **155** was also confirmed via ^{13}C NMR spectrum, which was also obtained in $CDCl_3$ in reference to tetramethylsilane. The spectrum displayed no signal at δ = 75.74 ppm and δ = 79.56 ppm, which were due to the C≡C moiety in the ^{13}C NMR spectrum of terminal alkyne, thereby indicating the conversion of this group into the 1,2,3-triazole ring. Additionally, two signals at δ = 58.55 ppm and δ = 52.14 ppm were assigned to the methylene C atom and the benzylic C atom, respectively. Furthermore, the methyl C atom was attributable to the signal at δ = 18.16 ppm, while the methoxy C atom was attributed to the signal at δ = 54.94 ppm. The aromatic C atoms were marked by the presence of the signals between δ = 160.34 - 110.94 ppm, and the C atom of the C=N group was attributed to the signal at δ = 163.24 ppm.

4.15.4. Analysis of mass spectrum

The mass spectrum (LC-MS) of the synthesised 1,2,3-triazole derivative **155** revealed a prominent peak at m/z = 414.19 (M+1), which corresponded to the theoretically calculated peak (413.19). This confirmed the effective synthesis of the required 1,2,3-triazole derivative.

References

1 Y. Bourne, K. B. Sharpless, P. Taylor and P. Marchot, *J. Am. Chem. Soc.*, 2016, **138**, 1611–1621.

2 W. Zhai, B. M. Chapin, A. Yoshizawa, H. C. Wang, S. A. Hodge, T. D. James, E. V. Anslyn and J. S. Fossey, *Org. Chem. Front.*, 2016, **3**, 918–928.

3 H. J. Park, S. Yoo, I. S. Shin, Y. K. Chung and J. Kim, *Electroanalysis*, 2013, **25**, 1111–1115.

4 K. S. Son, M. Yahiro, T. Imai, H. Yoshizaki and C. Adachi, *Chem. Mater.*, 2008, **20**, 4439–4446.

5 P. N. Kalaria, S. C. Karad and D. K. Raval, *Eur. J. Med. Chem.*, 2018, **158**, 917–936.

6 E. Kabir and M. Uzzaman, *Results Chem.*, 2022, **4**, 100606.

7 A. T. Balaban, D. C. Oniciu and A. R. Katritzky, *Chem. Rev.*, 2004, **104**, 2777–2812.

8 F. Feixas, J. Poater, E. Matito and M. Solà, in *Structure, Bonding and Reactivity of Heterocyclic Compounds*, eds. F. De Proft and P. Geerlings, Springer-Verlag, 1st edn., 2014, pp. 129–160.

9 V. V Rostovtsev, L. G. Green, V. V Fokin and K. B. Sharpless, *Angew. Chem.*, 2002, **41**, 2708–2711.

10 S. Neumann, M. Biewend, S. Rana and W. H. Binder, *Macromol. Rapid. Commun.*, 2020, **41**, 1900359.

11 S. Chassaing, V. Bénéteau and P. Pale, *Catal. Sci. Technol.*, 2016, **6**, 923–957.

12 M. Meldal and F. Diness, *Trends Chem.*, 2020, **2**, 569–584.

13 C. Özen and N. Ş. Tüzün, *J. Mol. Catal. A Chem.*, 2017, **426**, 150–157.

14 Y. Özkllç and N. S. Tüzün, *Organometallics*, 2016, **35**, 2589–2599.

15 M. De Lourdes G. Ferreira, L. C. S. Pinheiro, O. A. Santos-Filho, M. D. S. Peçanha, C. Q. Sacramento, V. Machado, V. F. Ferreira, T. M. L. Souza and N. Boechat, *Med. Chem. Res.*, 2014, **23**, 1501–15.

Chapter IV

Part B

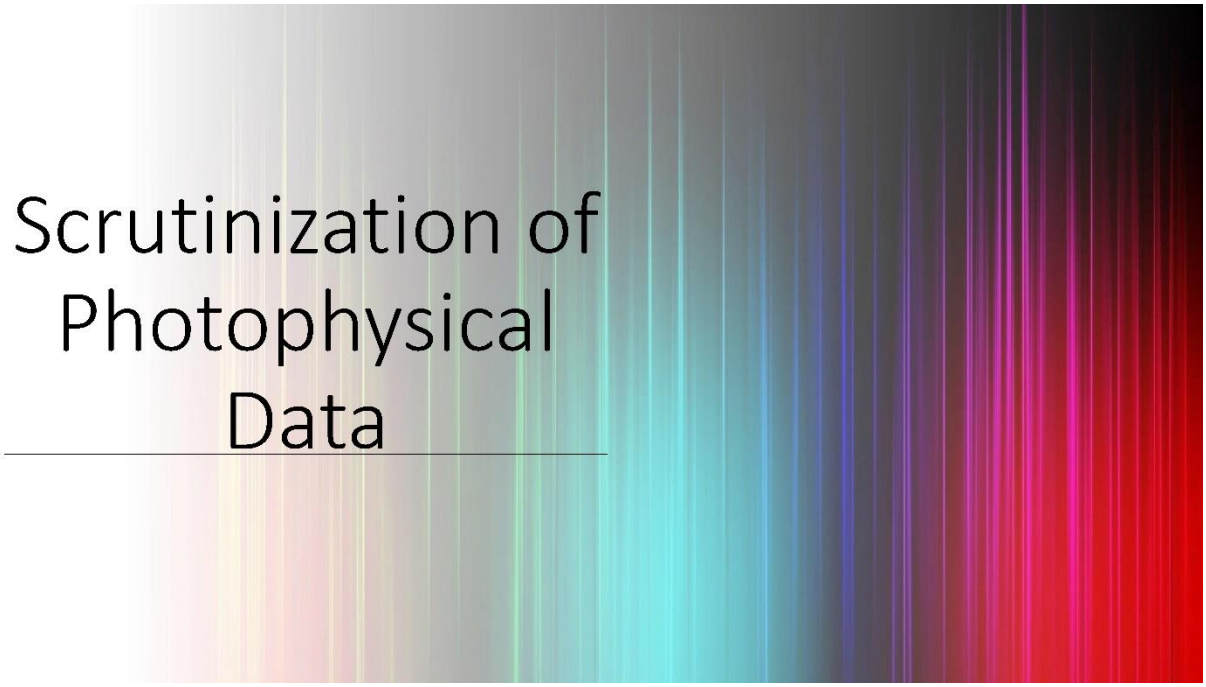

Scrutinization of Photophysical Data

In this part of chapter 4, the photophysical properties of the newly synthesised 1,4-disubstituted 1,2,3-triazole-appended compounds are described in detail. UV-Visible and fluorescence spectroscopy were used to investigate the photophysical behaviour of these compounds, on the basis of which the selective chemosensing behaviour of the 1,2,3-triazole appended probes is established.

4.16. Electronic spectroscopy- mechanistic aspect and application for ion(s) sensing

4.16.1. UV-Visible spectroscopy

Lambert-Beer's law is the foundation of early spectroscopic observations involving UV-Vis spectroscopy and many current analytical procedures in the environment and the laboratory.[1,2] The principle i.e., "in a medium of uniform transparency the light remaining in a collimated beam is an exponential function of the length of the path in the medium" was originally described by Bouguer,[3] which forms the foundation of UV-Vis spectroscopy. In comparison to other typical spectroscopic methods employed for analysis, UV-Vis spectroscopy has the advantages of being quick, non-destructive, high-resolution, and low-cost, due to which it has found widespread applications in qualitative and quantitative analysis, such as pharmaceutical analysis, pollution monitoring, DNA and RNA analysis, nanoparticle characterization, etc.[4–8]

Electronic transitions occur when a molecule absorbs UV-Visible light, with the most likely transition involving excitation of an electron from the HOMO, i.e., the highest occupied molecular orbital to the LUMO, i.e., the lowest unoccupied molecular orbital, thereby resulting in the attenuation of the incident light which is subsequently measured by the UV-Vis spectrophotometer. Due to the presence of different types of molecular orbitals in a compound (bonding, antibonding and non-bonding), the electronic transitions occurring are also of several types depending on the type of electrons present, as represented in **figure 4.15**.

- Molecules such as alkanes which possess only single bonds are able to exhibit only $\sigma \rightarrow \sigma^*$ transitions, owing to the exclusive presence of σ electrons. Such transitions are extremely energetic, absorbing ultraviolet light at wavelengths that are too short to be measured by conventional spectrophotometers in experiments and hence it is not feasible to deduce much information about such compounds through UV.
- $n \rightarrow \sigma^*$ transitions are observed in saturated molecules having atoms with lone pairs of electrons, such as alcohols, amines, ethers, etc. Although being high-energy transitions like $\sigma \rightarrow \sigma^*$, these are observed in experimentally accessible range, with alcohols and amines exhibiting such transitions in the range of 175-200 nm whereas sulfides and thiols demonstrate these transitions in the range of 200-225 nm. However, most of these transitions are below the cut-off value for the solvents used in UV-Vis spectroscopy and hence are not observed.

- Unsaturated molecules having π electrons demonstrate π→π* transitions, such as the alkenes show absorption at 175 nm, whereas alkynes show absorption at 170 nm. Furthermore, the positions of such transitions are highly sensitive to the presence of substitution, despite their relatively high energy.
- Unsaturated molecules having lone pair bearing heteroatoms such as oxygen or nitrogen exhibit n→π* transitions. When it comes to carbonyl compounds, these are the transitions that have received the greatest attention and study, and the changes are also rather sensitive to substitutions made to the chromophoric structure. Transition occurs at 280-290 nm for the typical carbonyl compound. Because most n→π* transitions are forbidden, they are relatively weak in intensity.

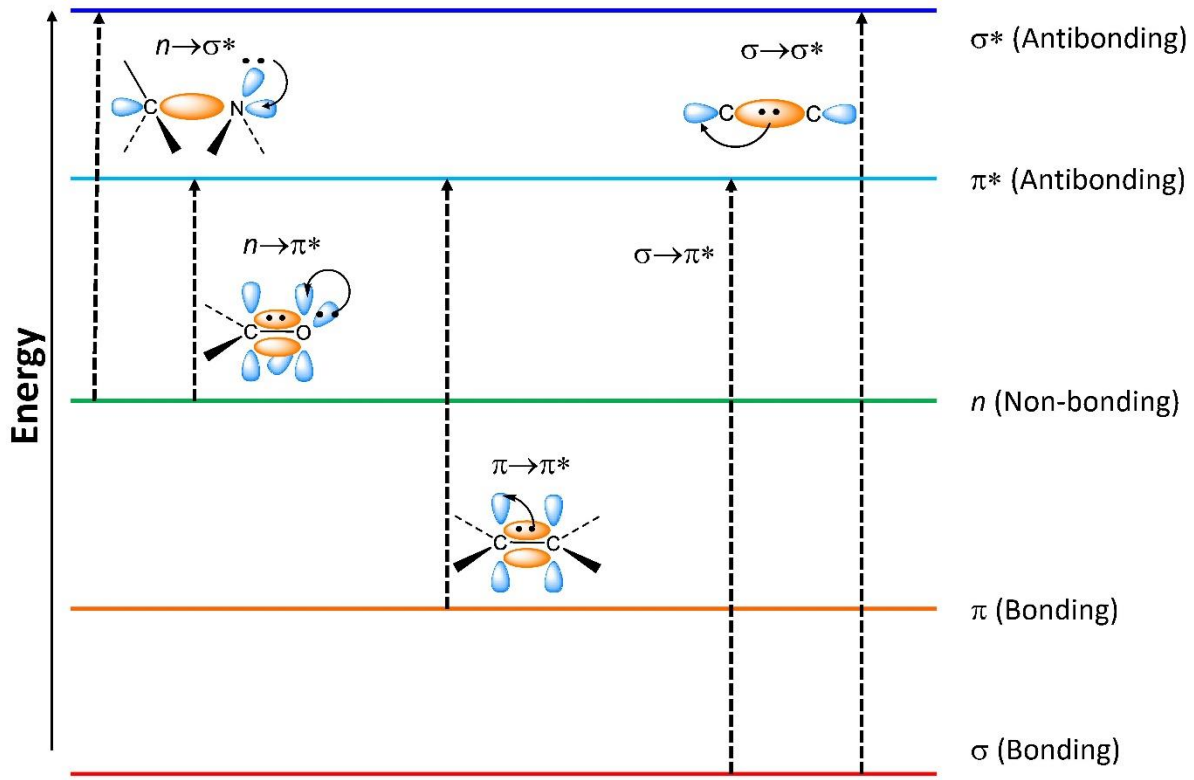

Figure 4.15: An illustrative representation of the types of electronic transitions in conjugated system and/or C=O group[1-3]

UV-vis spectroscopy is still the standard spectroscopic technique for many niche applications, especially those involving distinctive chromophoric compounds like dyes, indicators, and filters,[9,10] but it is not as commonly used as other spectroscopies like nuclear

magnetic resonance for initial structural analysis. An analyte possessing chromophoric group(s) and absorptions typical of a certain family of functional groups can be investigated by UV-vis spectroscopy.[11] Taking direction from this idea, the analysis of new compounds with chemosensing applications using UV-Vis spectroscopy was the focus of this research. Therefore, in this research work, using aromatic compounds as building blocks, novel chemosensing compounds were synthesized, and their ability to detect various metal ions was analyzed through UV-Vis and/or fluorescence spectroscopic techniques.

The transition metal ions in their solution state exist as cations due to their electropositive nature. These cationic species are also capable of exhibiting electronic transitions by absorbing radiations in the UV-Vis region. Their positive charge is mainly responsible for their interaction with electron rich species, thereby potentially altering the electron density on both the interacting species due to the potential for different types of electronic transitions to occur during this interaction.[12–14] The metal ion or its binding ligands (other ions or molecules that coordinate with the metal ion) may be involved in these excitations. In case of the metal ion, these are the d-d transitions, and they are unique to transition metals, whereas for the ligands, the type of electrons present is responsible for the different transitions as discussed above. In any case, if the electronic arrangement of a free ligand gets transformed due to its interaction with an analyte in the solution state (in this case a metal ion) then there is a distinctive change in the absorbance of the sensor probe after metal-ion binding, which provides evidence for the successful interaction of the ligand and the metal ion which can be established by comparing the UV-Vis spectrum before and after the addition of the metal ions.[15–18]

4.16.2. Fluorescence spectroscopy

The theory and practice of fluorescence spectroscopy have been widely used in the fields of chemistry and biochemistry to examine molecular structure and function.[19] The electron density of a chromophore is redistributed upon absorption of light of visible and ultraviolet wavelengths, inducing an electronic transition.[20] Some organic compounds, such as those with a system of conjugated double bonds, can radiate the absorbed energy as fluorescence, which is typically the rapid emission of the photons from the singlet state.[21] There are a number of benefits unique to fluorescence spectroscopy that make it ideal for studying molecular interactions and reactions. To begin, its sensitivity is 100-1000 times higher than that of conventional spectrophotometric methods. Second, the environment has a profound

effect on the sensitivity of fluorescent compounds.[22] Therefore, fluorescence spectroscopy in the light of such desirable advantages is employed in a diverse range of applications, ranging from *in vivo* analysis to wastewater monitoring.[23–27]

Regarding the recognition of metal ions by electron-rich ligands, fluorescence spectroscopy is employed in a manner akin to UV-Vis spectroscopy. The synthesized ligands in this research work contain fluorophores, which are the functionalities that emit fluorescence when excited by light of a certain wavelength.[28,29] On binding with a metal ion, the electronic rearrangement within the metal-ligand complex induces substantial changes in the fluorescence spectrum, which on comparison with the fluorescence of the free sensor confirms the recognition of metal ions.[30,31]

4.17. Chemosensing analysis of maleic hydrazide based 1,2,3-triazoles 140 and 141

4.17.1. Ion recognition analysis of 1,2,3-triazole derivative 140

Utilizing UV-Vis spectroscopy, the ion recognition potential of the synthesized 1,2,3-triazole derivative **140** was analyzed utilizing a variety of metal chlorides. The molecule was designed by modifying the parent maleic hydrazide moiety in such a way that it was connected to a benzyl group (acting as the transducer group) via a 1,2,3-triazole bridge, which in addition to serving as the spacer unit, also had the potential to provide the receptor sites for the electron-deficient metal ions due to the presence of lone pair bearing N atoms. As a result, an overall strong molecular framework accompanied by aromaticity presented the synthesized probe as a robust molecule to possess chemosensing potential.

Dimethylsulfoxide (DMSO) was chosen as the solvent for UV-Vis investigations of the 1,2,3-triazole derivative **140** owing to its good solubility and favourable spectral data. Following the completion of the optimization for the solution concentration in the UV-vis examinations of the probe, a concentration of 0.5 mM was established to be employed for monitoring the sensing behaviour because of the presence of interpretable absorption band. The probe **140** exhibited an absorption peak at 312 nm, along with a slight shoulder peak at 258 nm, characterized by respective intensities of 1.7 and 0.8. Subsequently, the chemosensing potential of the probe were evaluated using 1 mM chlorides of Ca(II), Mg(II), Ba(II), Cr(III), Mn(II), Co(II), Ni(II), Zn(II), and Pb(II) dissolved in DMSO. When the probe solution was subjected to titration with 1 mM solutions of the metal chlorides, the absorption spectrum of the probe exhibited negligible alterations in absorption maxima and/or absorption intensity,

except for Pb(II) and Cr(III), which displayed the most significant changes in absorbance peaks. **Figure 4.16** is a graphical representation of the relative chemosensing behavior of the probe **140** for several metal ions, where it can be seen that the probe has a relatively higher recognition potential for Pb(II) and Cr(III) over other metal ions.

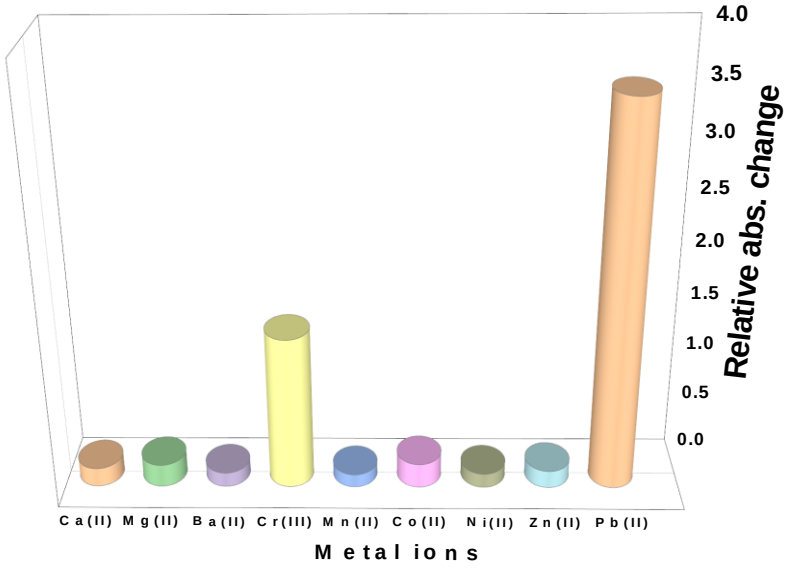

Figure 4.16: An illustration of the relative absorption change of probe **140** for several metal ions in DMSO solvent

4.17.1.1. Chemosensing response of probe 140 for Pb(II) and Cr(III) via UV-Vis spectroscopy

In order to investigate the interaction between probe **140** and Pb(II) and Cr(III) ions, an analysis was performed by UV-Vis spectroscopy wherein titration of a 0.5 mM solution of probe **140** was undertaken with 1 mM solutions of Pb(II) and Cr(III) ions. The results of these titrations are shown in **figure 4.17**, wherein the incremental introduction of Pb(II) ions resulted in a significant hyperchromic shift at 258 nm in probe **140**, surpassing the shift observed in Cr(III) by more than twofold. A bathochromic shift of 4-5 nm was also observed in addition to the hyperchromic response. On the contrary, the absorption peak at 312 nm exhibited a decrease in intensity, resulting in the appearance of an isosbestic point around 288 nm. The relative change in the maximum absorbance (A_n/A_o) for peaks at 258 nm and 312 nm is displayed in **figure 4.18**, wherein A_n = absorption maxima with succeeding addition of Pb(II) ions, and A_o = absorption maxima of the probe. Furthermore, the correlation plot as depicted in **figure 4.19** was utilized to determine the limit of detection (LoD) and limit of quantification

(LoQ) of the probe for Pb(II), which came out to be 58 µM and 195 µM respectively, whereas the binding ratio calculated from the plot was established to be 2:1 (M:L). In addition to this, the Benesi-Hildebrand (B-H) equations (A) and (B) were implemented to calculate the first association constant K_{a1} and second association constant K_{a2} for 1:1 and 1:2 host-guest complexation respectively, and the corresponding B-H plot for the complexation of the probe for Pb(II) is represented in **figure 4.20**. The first association constant (K_{a1}) of **140** for Pb(II) was determined to be 0.22×10^4 M^{-1}; whereas the second association constant (K_{a2}) was 0.61×10^5 M^{-1}.

$$\frac{1}{A - Ao} = \frac{1}{A' - Ao} + \frac{1}{Ka(A' - Ao)[M^{n+}]} \qquad (A)$$

$$\frac{1}{A - Ao} = \frac{1}{A' - Ao} + \frac{1}{Ka(A' - Ao)[M^{n+}]^2} \qquad (B)$$

Where *Ao* = initial absorption intensity

A = absorption intensity with a specific metal ion concentration

A' = final absorption intensity

$[M^{n+}]$ = metal ion concentration, and

Ka = association constant

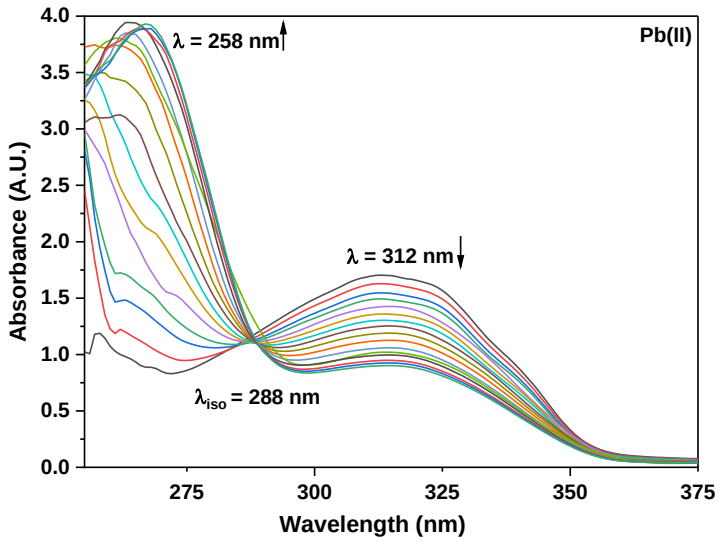

Figure 4.17: UV-Vis spectra of probe **140** (0.5 mM) upon the progressive addition of Pb(II) in DMSO as the solvent

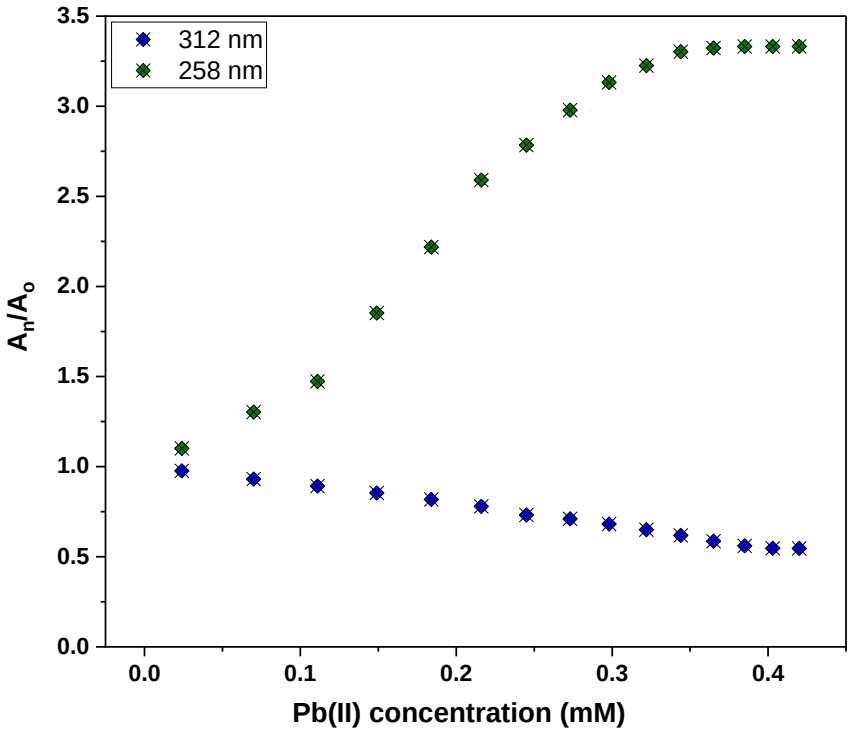

Figure 4.18: Relative absorbance maxima (A_n/A_o) shifts of probe **140** according to the concentration of Pb(II) ions added

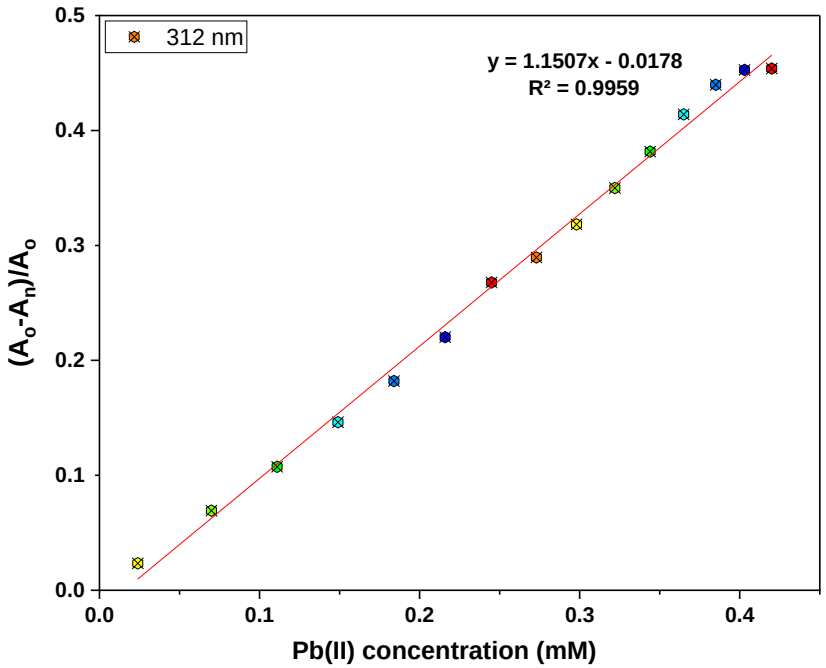

Figure 4.19: Correlation plot of relative absorption intensity of probe **140** $(A_o-A_n)/A_o$ as a function of Pb(II) concentration; where A_o = initial absorption of probe **140** and A_n = absorption of probe **140** in the presence of Pb(II)

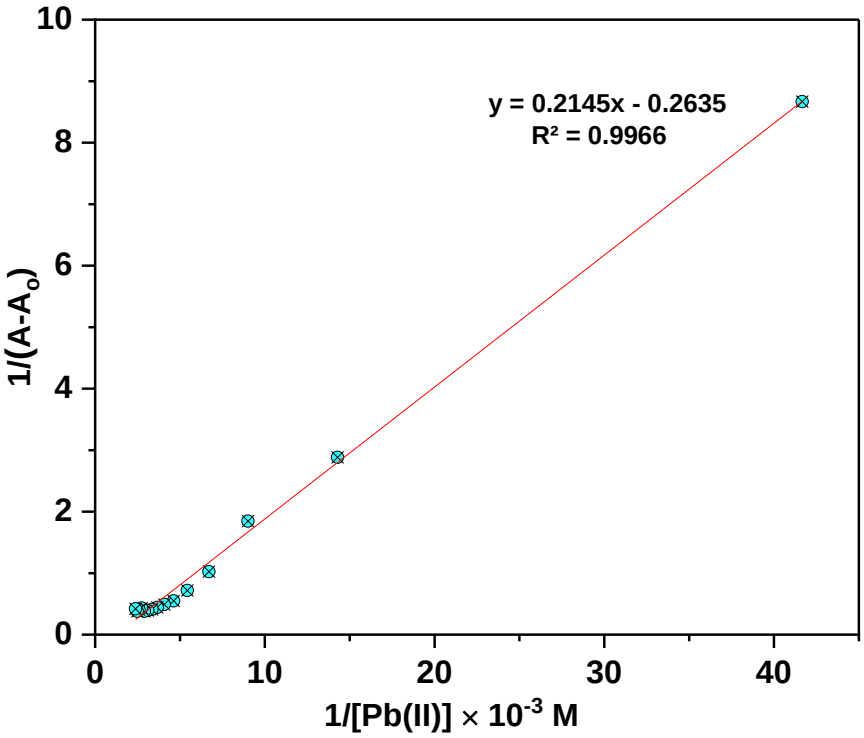

Figure 4.20: Benesi-Hildebrand plot for probe **140**-Pb(II) complexation

The probe **140** showed a consistent hyperchromic change in the absorbance intensity measured at 258 nm when Cr(III) ions were utilized in the titration procedure. In addition to this, a hypochromic shift of equivalent magnitude was seen in the absorbance at 312 nm, thereby resulting in an isosbestic point located at 279 nm (**figure 4.21**). The relative absorption change (A_n/A_o) for the peaks at 258 nm and 312 nm is shown in **figure 4.22**, where A_n denotes the absorption maxima with further addition of Cr(III) ions and A_o denotes the maximum absorption of the probe. Additionally, the correlation plot shown in **figure 4.23** was used to calculate the binding ratio, which was established to be 2:1 (M:L), as well as the limit of detection (LoD) and limit of quantification (LoQ) of the probe for Cr(III), which turned out to be 79 µM and 263 µM, respectively. Moreover, the B-H equations (A) and (B) were used to calculate the first association constant K_{a1} and second association constant K_{a2} for 1:1 and 1:2 host-guest complexation respectively, and the corresponding B-H plot for the complexation of the probe for Cr(III) is shown in **figure 4.24**. In the case of a 1:1 host-guest complex, the first association constant (K_{a1}) for the probe for Cr(III) was found to be 0.55×10^4 M^{-1}; whereas, with a 1:2 stoichiometry, the second association constant (K_{a2}) was found to be 0.20×10^6 M^{-1}. The values of LoD, LoQ, stoichiometric ratio, and association constants of the probe for Pb(II) as well as Cr(III) have been compiled in **table 4.1**.

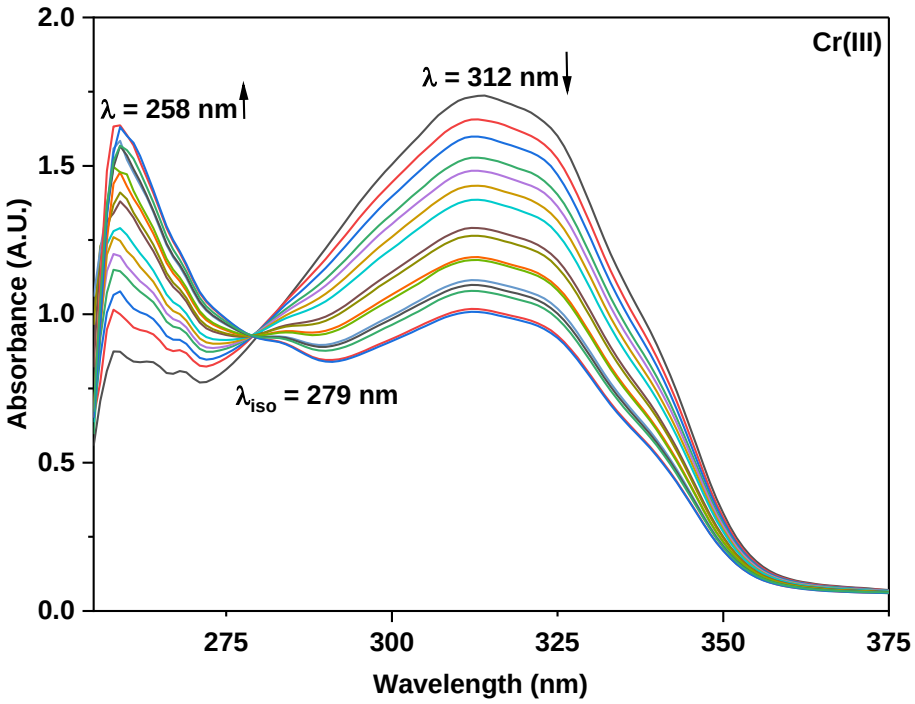

Figure 4.21: UV-Vis spectra of probe **140** (0.5 mM) upon the progressive addition of Cr(III) in DMSO as the solvent

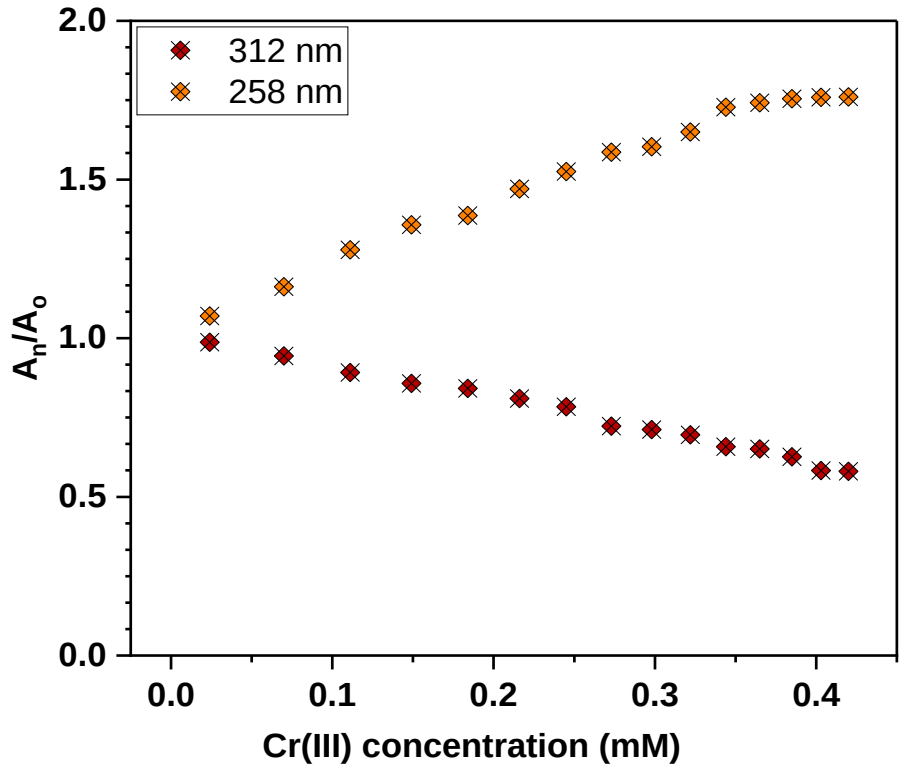

Figure 4.22: Relative absorbance maxima (A_n/A_o) shifts of probe **140** according to the concentration of Cr(III) ions added

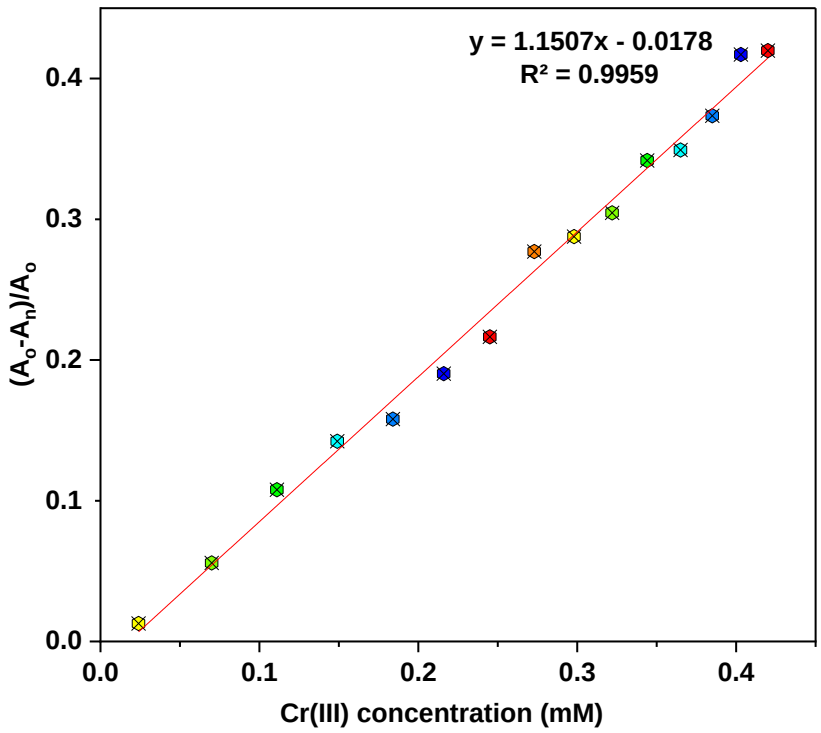

Figure 4.23: Correlation plot of relative absorption intensity of probe **140** $(A_o-A_n)/A_o$ as a function of Cr(III) concentration; where A_o = initial absorption of probe **140** and A_n = absorption of probe **140** in the presence of Cr(III)

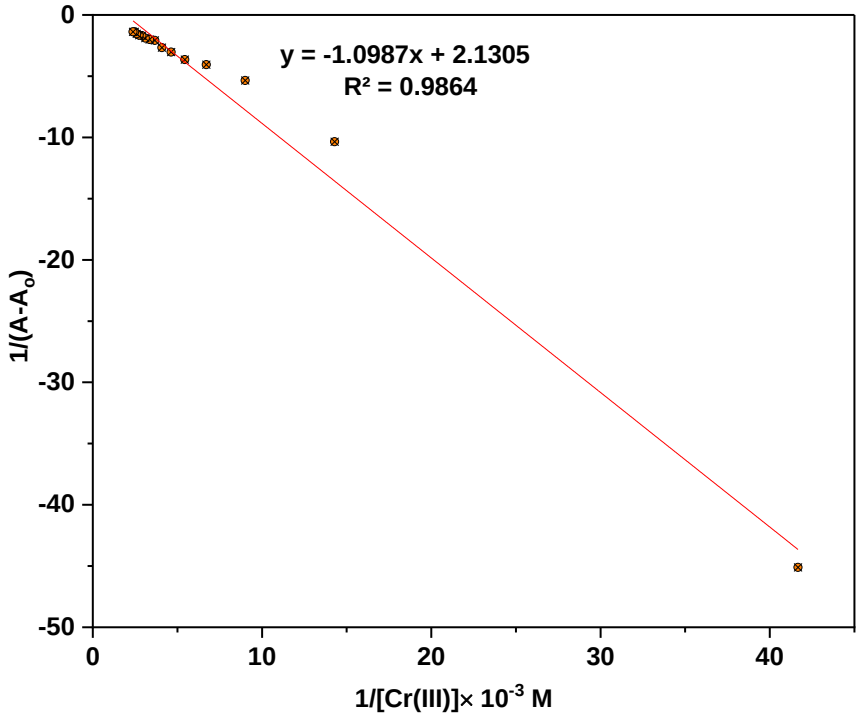

Figure 4.24: Benesi-Hildebrand plot for probe **140**-Cr(III) complexation

Entry	Metal ion	LoD (µM)	LoQ (µM)	Ist association constant (K_{a1})	IInd association constant (K_{a2})	Stoichiometry (M:L)
140	Pb(II)	58	195	$0.22 \times 10^4\ M^{-1}$	$0.61 \times 10^5\ M^{-1}$	2:1
	Cr(III)	79	263	$0.55 \times 10^4\ M^{-1}$	$0.20 \times 10^6\ M^{-1}$	2:1

Table 4.1: LoD, LoQ, K_{a1}, K_{a2}, and stoichiometric ratio values for probe **140** on binding with Pb(II) and Cr(III)

4.17.1.2. Competitive metal ion interaction analysis

In addition to the analysis focused on selective ion recognition, the probe **140**'s selectivity was also assessed when all the metal ions were present in equimolar concentrations, and the titration carried out of a 0.5 mM probe solution in DMSO with a solution comprising equimolar ratio of all the metal ions produced a UV-Vis spectrum that closely resembled the one observed for pure Cr(III) as shown in **figure 4.25**. This experiment effectively showcased the probe's specificity for Cr(III) and established that other metal ions did not impact the chemosensing capabilities of the probe.

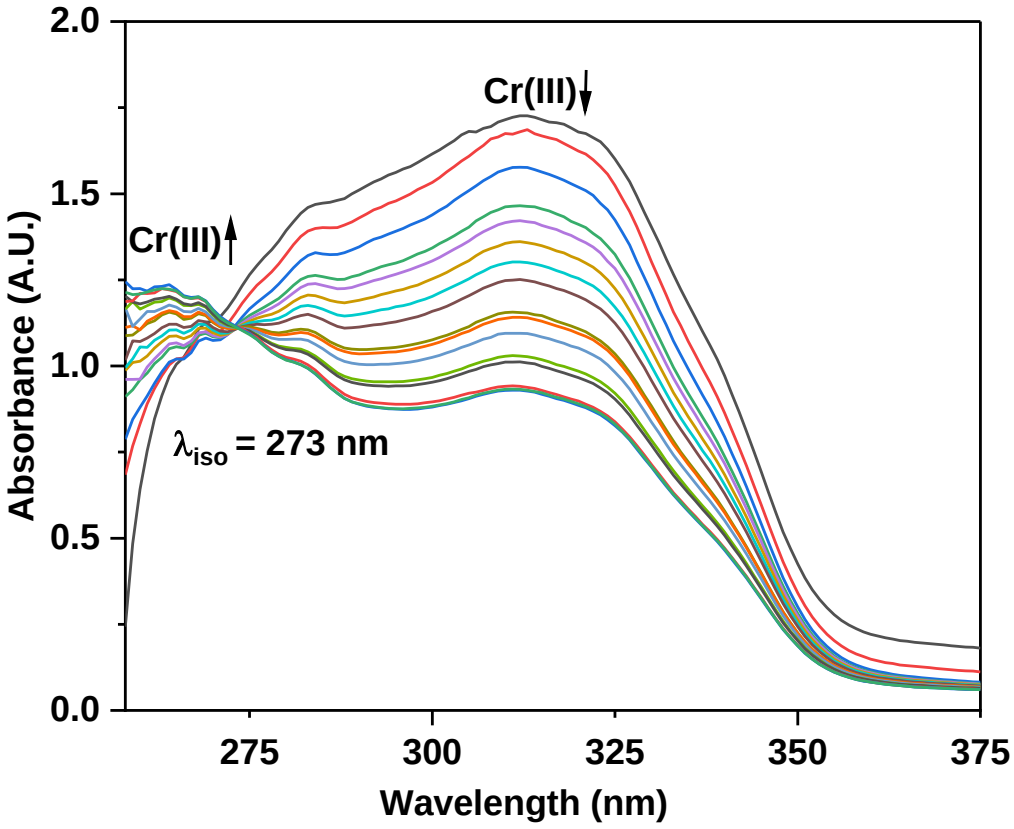

Figure 4.25: Absorption spectra of probe **140** (0.5 mM) in DMSO recognizing Cr(III) ions among several metal ions at equimolar concentrations

4.17.1.3. Time dependence analysis of probe 140-metal ion complexation

The examination of the response of the probe **140**-metal ion complex to variations in time provides valuable insights about its susceptibility for the analytes (metal ions). The impact of time on the behavior of metal-bound probe **140** by the utilization of absorption spectroscopy was carried out, and the results (**figure 4.26**) indicated that the absorbance of Pb(II)-bound and Cr(III)-bound probe solutions displayed no significant change despite being left to stand for long periods of time. This demonstrated a very stable and robust affinity of the probe **140** for metal ions.

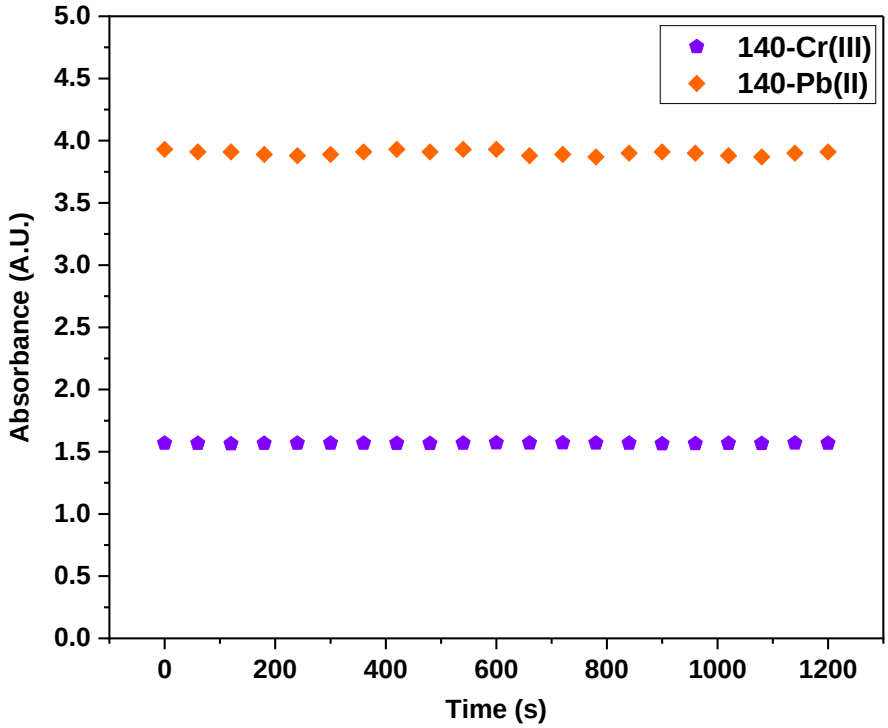

Figure 4.26: Time dependent absorption spectrum of probe **140**-Pb(II)/Cr(III) complex solution exhibiting a constant absorbance at 258 nm

4.17.1.4. Temperature dependence analysis of probe 140-metal ion complexation

The temperature effect on the binding capability of probe **140** was also studied throughout a range of temperatures, complementing the time-dependent study. Absorption spectra were recorded at 2 °C intervals from 20 °C up to 50 °C, wherein the investigation revealed that variations in temperature did not have a substantial impact on the binding capacity of probe **140**, as illustrated in **figure 4.27**. This suggests a strong and stable binding interaction between the probe and the metal ions.

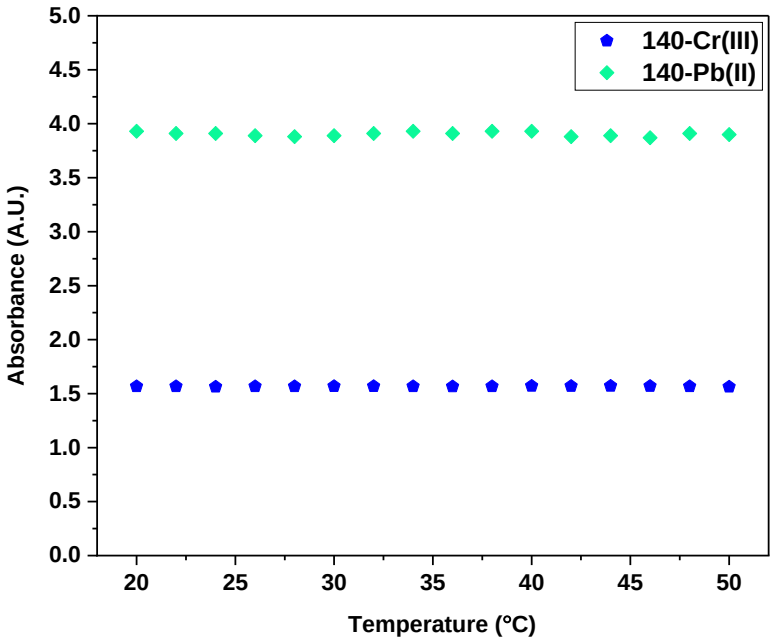

Figure 4.27: Temperature dependent absorption spectrum of probe **140**- Pb(II)/Cr(III) exhibiting a constant absorbance over a temperature range of 20 - 50 ºC

4.17.1.5. Plausible binding mode

Pb(II) is classified as a borderline acid in accordance with the HSAB hypothesis, but Cr(III) is regarded as a hard acid. Both ions have the ability to form bonds with the lone-pair containing N, O or S. The synthetic probe **140** contains 1,2,3-triazole moieties with lone pair-bearing N atoms, and O atoms on the parent structure, which can be attributed for binding with the ions mentioned above. This is attained through the regulation of the orientation of the 1,2,3-triazole moieties, resulting in the formation of a binding core designed to have a cavity of appropriate size to accept Pb(II) and Cr(III) ions through coupling with the nitrogen and oxygen atoms. Consequently, a ligand-metal stoichiometry of 1:2 is observed. (**figure 4.28**). Rest of the coordination sites are expected to be filled by the solvent molecules.

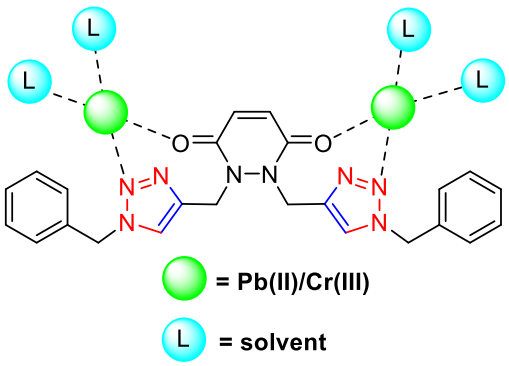

Figure 4.28: Proposed interaction between probe **140** and Pb(II)/Cr(III)

4.17.2. Ion recognition analysis of 1,2,3-triazole derivative 141

The ion sensing potential of the synthesised 1,2,3-triazole derivative based on maleic hydrazide **141** was studied using UV-Vis spectroscopy in a similar manner as that of probe using a number of metal chlorides. The synthesis of this molecule was carried out to achieve relatively more aromaticity on the transducer moiety in order to get better UV-Vis spectral results. For this, the parent maleic hydrazide moiety was modified so that it was linked to a naphthyl group (the transducer group) via a 1,2,3-triazole bridge, thereby providing higher aromaticity to the transducer in comparison to the previous 1,2,3-triazole derivative. Similar to the probe, the 1,2,3-triazole moiety not only served as a spacer unit, but also had the potential to provide receptor sites for electron-deficient metal ions owing to the presence of electron-rich N atoms. Therefore, the synthesised probe was presented as a strong molecule with relatively better chemosensing potential due to its overall strong molecular framework and high aromaticity.

Dimethylsulfoxide (DMSO) was chosen as the solvent medium for the UV-Vis examinations of the 1,2,3-triazole derivative **141** in this case also due to its admirable solubility and good spectrum data. Because of the existence of an interpretable absorption band, a concentration of 0.5 mM was chosen to be used for monitoring the sensing behaviour after optimizing the solution concentration for the UV-Vis examinations of the probe. The probe's absorption peak was found at 284 nm, with additional smaller peaks at 274 nm and 294 nm. The absorption intensities corresponding to these peaks were 1.5, 1.3, and 1.2 respectively. Thereafter, the probe's ion sensing capabilities were tested using 1 mM chlorides of Ca(II), Mg(II), Ba(II), Cr(III), Mn(II), Co(II), Ni(II), Zn(II), and Pb(II) dissolved in DMSO. With the exception of Pb(II) and Cr(III), which showed the greatest changes in absorbance peaks when the probe solution was titrated with the aforementioned metal chlorides, no appreciable change was observed in the former's absorption spectrum. **Figure 4.29** shows a graphical depiction of the probe's relative chemosensing behaviour for several metal ions of equimolar concentration, with Pb(II) and Cr(III) showing a significantly stronger behavioural response than the other metal ions.

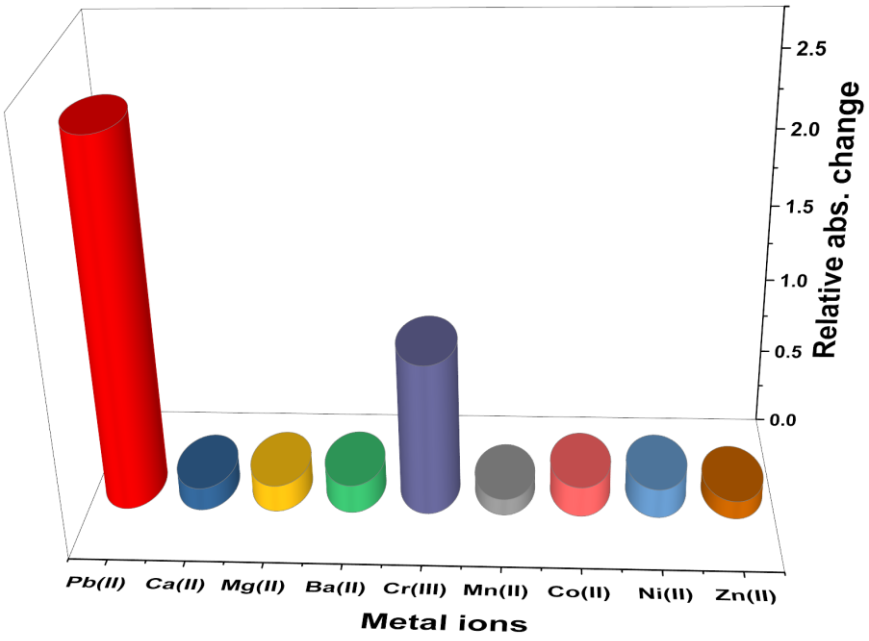

Figure 4.29: An illustration of the relative absorption change of probe **141** for several metal ions in DMSO solvent

4.17.2.1. Chemosensing response of probe 141 for Pb(II) and Cr(III) via UV-Vis spectroscopy

Similar to the experiments to establish the chemosensing potential of probe, UV-Vis analysis for probe **141** was conducted wherein 0.5 mM of the probe solution was titrated with 15 equiv. of 1mM of Pb(II) solution, to analyze the UV-Vis spectrum for evidence of the interaction of the probe with Pb(II) ions. The titration outcomes shown in **figure 4.30** reveal that the peak at 294 nm was shown to undergo a hypochromic shift when Pb(II) ions were successively added to the probe solution, whereas the peaks at 274 nm and 284 nm underwent an immense hyperchromic shift, eventually merging at about 270 nm and giving rise to a broad band. The emergence of an isosbestic point was observed at about 287 nm. **Figure 4.31** illustrates the relative variation in maximum absorption intensity (A_n/A_o) for the peaks at 270 nm and 294 nm, wherein A_n represents the maximum absorption with the addition of Pb(II) ions, while A_o denotes the absorption maximum of the probe. The correlation plot (**figure 4.32**) was employed to determine the limit of detection (LoD) and limit of quantification (LoQ), and was found to be 142 µM and 473 µM respectively, with the binding ratio of probe with Pb(II) being 2:1 (M:L). Moreover, the B-H equations (A) and (B) were employed to determine the first association constant (K_{a1}) and second association constant (K_{a2}) respectively, and the

values were 0.18 × 10^5 M^{-1} for K_{a1} and 0.46 × 10^6 M^{-1} for K_{a2} in case of binding with Pb(II). The B-H plot for the same has been represented in **figure 4.33**.

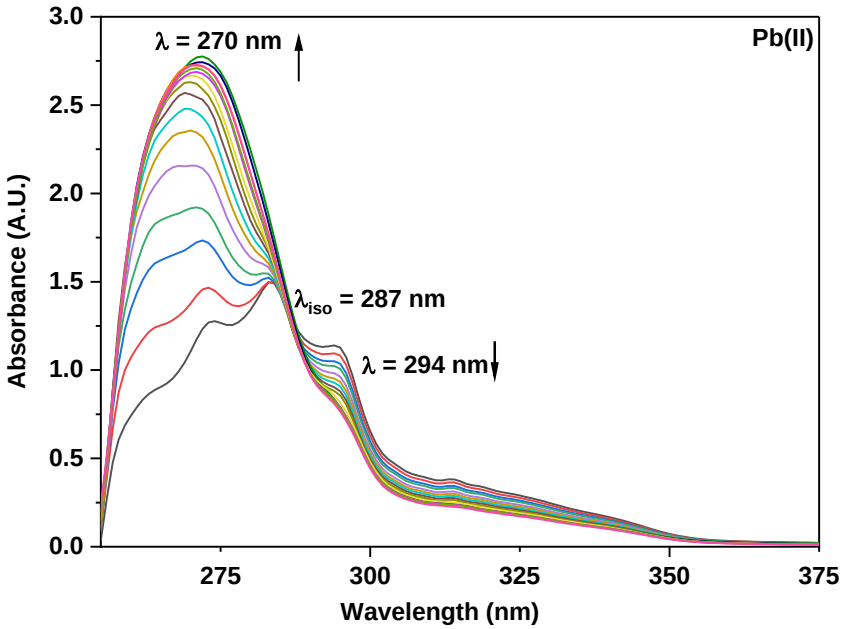

Figure 4.30: UV-Vis spectra of probe **141** (0.5 mM) upon the progressive addition of Pb(II) in DMSO as the solvent

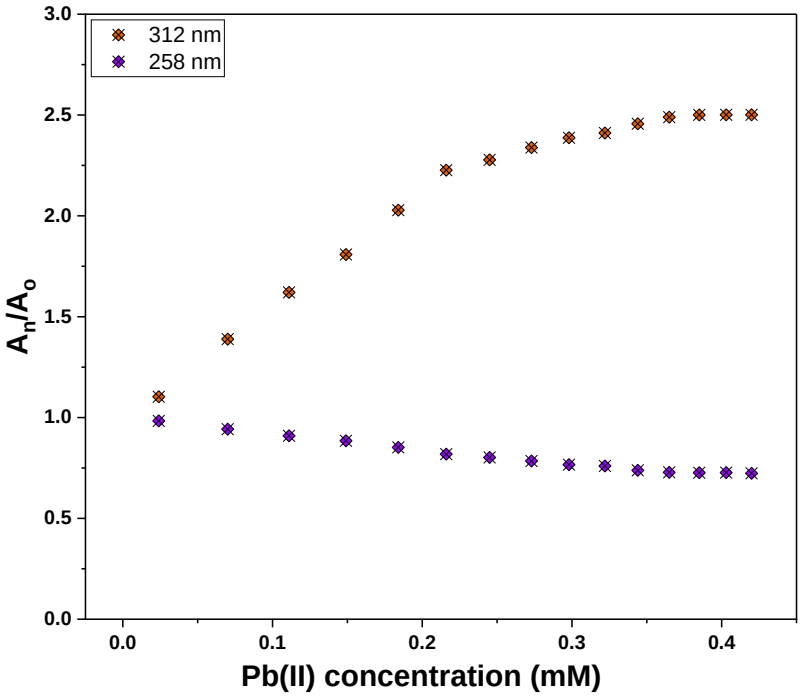

Figure 4.31: Relative absorbance maxima (A_n/A_o) shifts of probe **141** according to the concentration of Pb(II) ions added

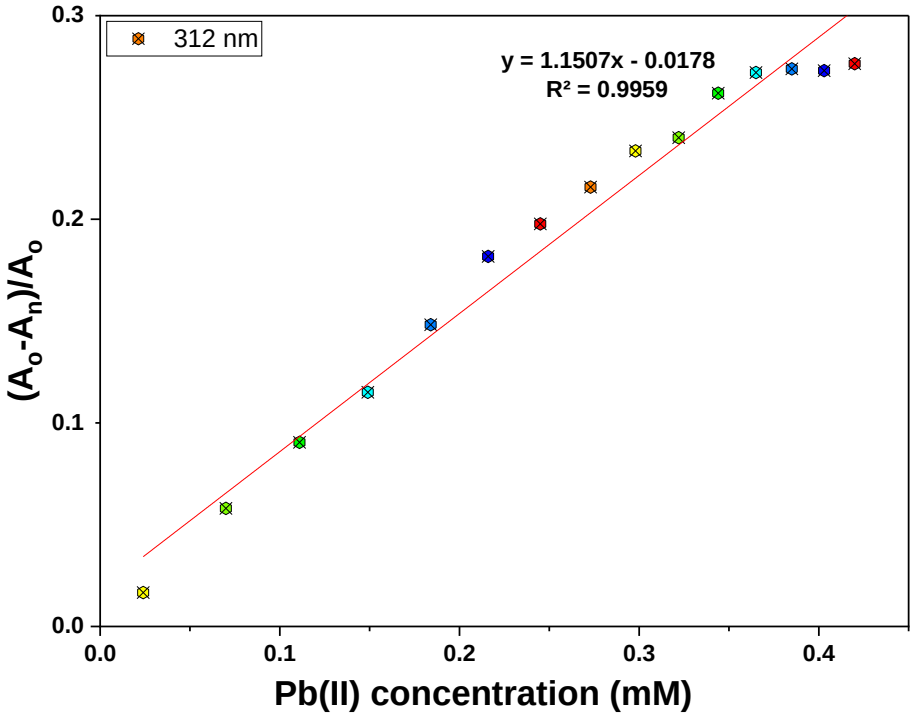

Figure 4.32: Correlation plot of relative absorption intensity of probe **141** $(A_o-A_n)/A_o$ as a function of Pb(II) concentration; where A_o = initial absorption of probe **141** and A_n = absorption of probe **141** in the presence of Pb(II)

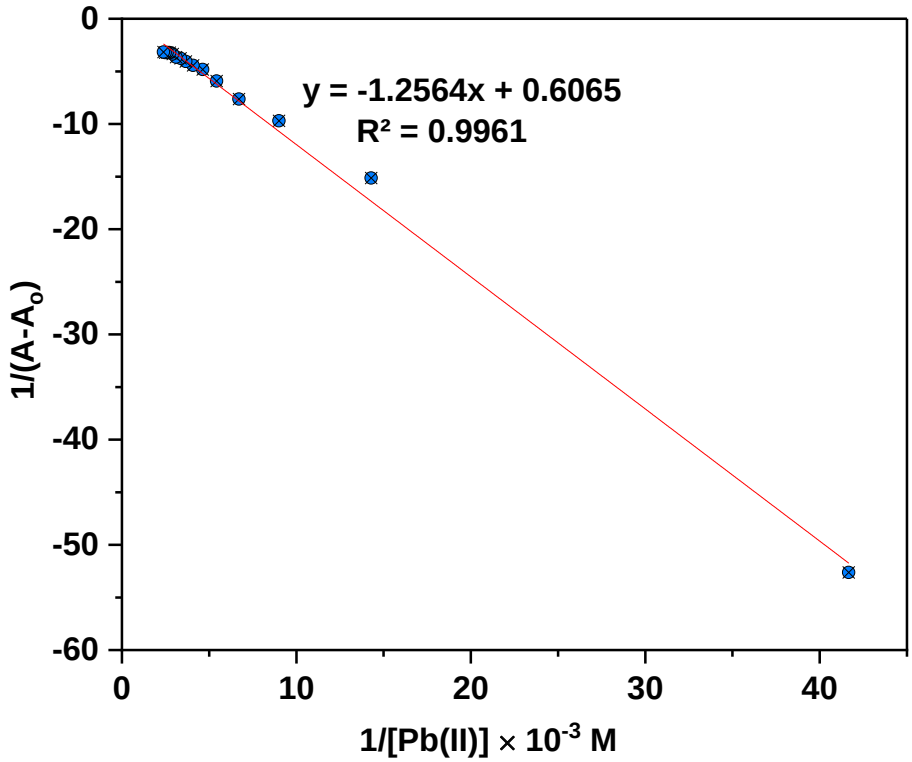

Figure 4.33: Benesi-Hildebrand plot for probe **141**-Pb(II) complexation

A hypochromic shift was seen in the absorption peaks at 274 nm, 284 nm, and 294 nm for probe **141** when Cr(III) ions were employed in the titration experiment. Furthermore, an additional spectral peak was detected at a wavelength of 260 nm, accompanied by the appearance of an isosbestic point at 270 nm (**figure 4.34**). The relative absorption change (A_n/A_o) is shown in **figure 4.35** for the peaks at 260 nm, 274 nm, 284 nm and 294 nm, wherein the absorption maxima with subsequent accumulation of Cr(III) ions are denoted by the symbol A_n, whereas the maximum absorbance of the probe is denoted by the symbol A_o. The limit of detection (LoD) and limit of quantification (LoQ) of the probe for Cr(III) were determined to be 87 µM and 290 µM, respectively, and the binding ratio was shown to be 2:1 (M:L) using the correlation plot given in **figure 4.36**. Furthermore, the complexation of the probe **141** for Cr(III) is depicted in a B-H plot (**figure 4.37**), and the association constants K_{a1} and K_{a2} for 1:1 and 1:2 host-guest complexation were calculated using the B-H equations (A) and (B), respectively. The first association constant (K_{a1}) for the probe for Cr(III) was determined to be 0.30×10^5 M^{-1} for a 1:1 host-guest complex, while the second association constant (K_{a2}) was determined to be 0.76×10^6 M^{-1} for a 1:2 stoichiometry. The values of LoD, LoQ, stoichiometric ratio, and association constants of the probe for Pb(II) ans well as Cr(III) have been compiled in **table 4.2**.

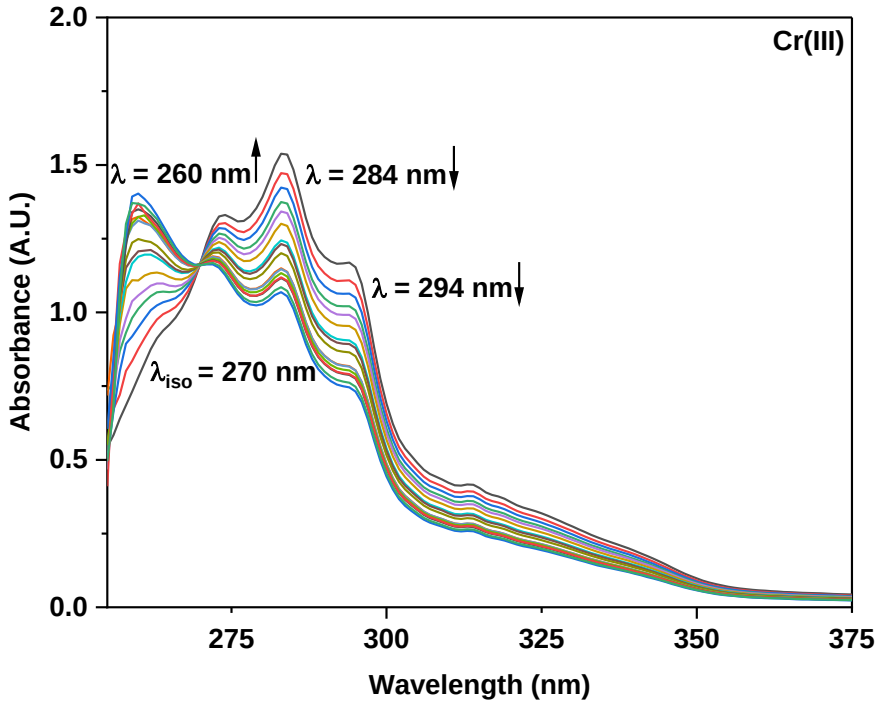

Figure 4.34: UV-Vis spectra of probe **141** (0.5 mM) upon the progressive addition of Cr(III) in DMSO as the solvent

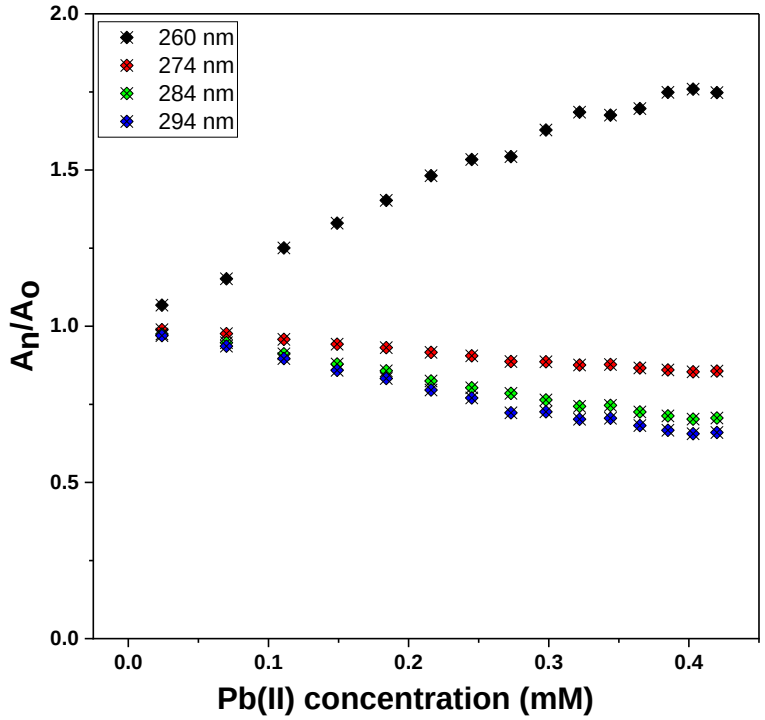

Figure 4.35: Relative absorbance maxima (A_n/A_o) shifts of probe **141** according to the concentration of Cr(III) ions added

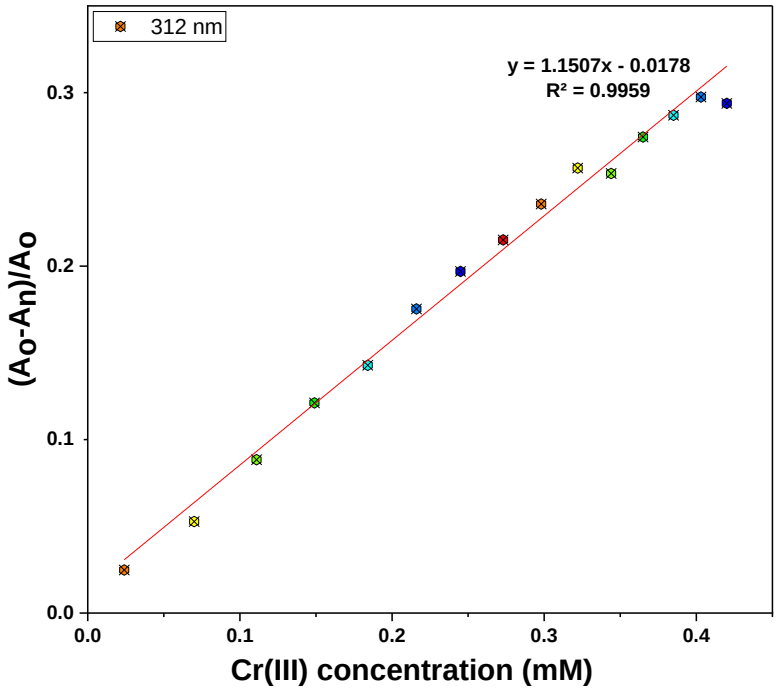

Figure 4.36: Correlation plot of relative absorption intensity of probe **141** $(A_o-A_n)/A_o$ as a function of Cr(III) concentration; where A_o = initial absorption of probe **141** and A_n = absorption of probe **141** in the presence of Cr(III)

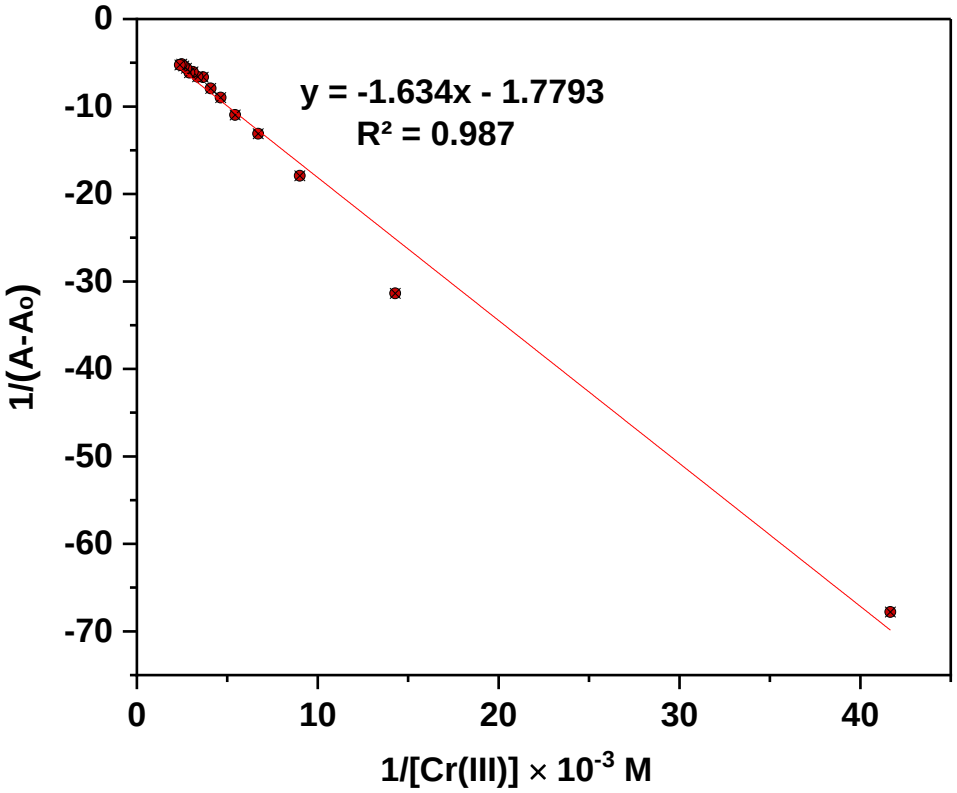

Figure 4.37: Benesi-Hildebrand plot for probe **141**-Cr(III) complexation

Entry	Metal ion	LoD (µM)	LoQ (µM)	Ist association constant (K_{a1})	IInd association constant (K_{a2})	Stoichiometry (M:L)
141	Pb(II)	142	473	0.18×10^5 M^{-1}	0.46×10^6 M^{-1}	2:1
	Cr(III)	87	290	0.30×10^5 M^{-1}	0.76×10^6 M^{-1}	2:1

Table 4.2: LoD, LoQ, K_{a1}, K_{a2}, and stoichiometric ratio values for probe **141** on binding with Pb(II) and Cr(III)

4.17.2.2. Competitive metal ion interaction analysis

In addition to the analysis focused on selective ion recognition, the probe **141**'s selectivity was also evaluated when all the metal ions were present in equimolar proportions. The titration carried out of a 0.5 mM probe **141** solution in DMSO with a solution comprising equimolar ratio of all the metal ions yielded UV-Vis spectrum similar as in the case of pure Cr(III), thereby proving the selectivity of the probe **141** for Cr(III) (**figure 4.38**).

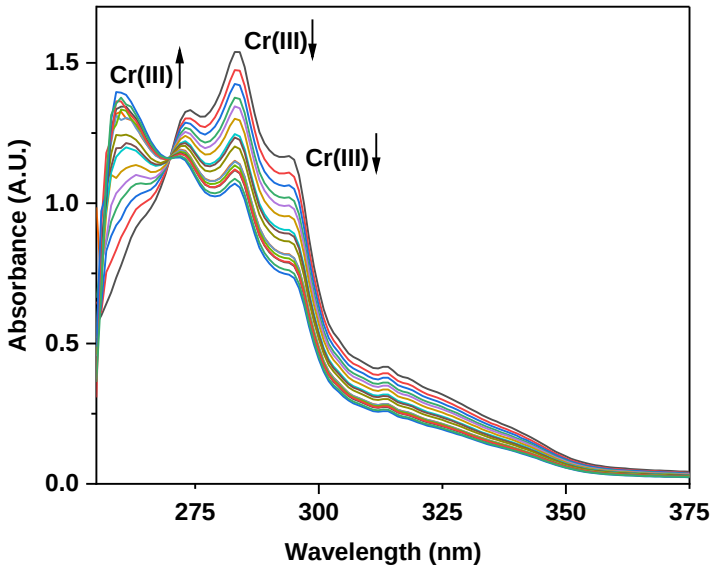

Figure 4.38: Absorption spectra of probe **141** (0.5 mM) in DMSO recognizing Cr(III) ions among several metal ions at equimolar concentrations

4.17.2.3. Time dependence analysis of probe 141-metal ion complexation

The effects of time on metal-bound probe **141** were also explored using absorption spectroscopy, and the results (**figure 4.39**) indicated that the absorbance of Pb(II)-bound and Cr(III)-bound probe solutions displayed no significant change despite being left to stand for long periods of time. This demonstrated that the probe **141** had a very stable and robust affinity for metal ions.

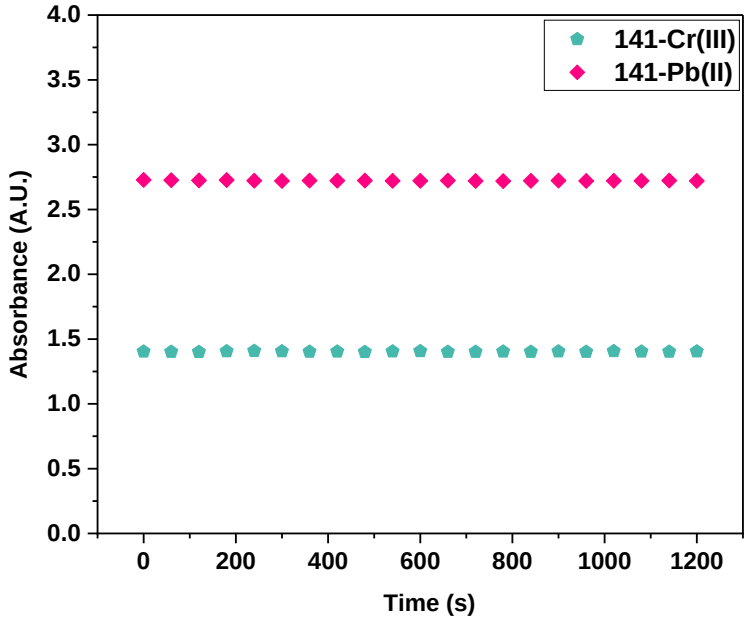

Figure 4.39: Time dependent absorption spectrum of probe **141**-Pb(II)/Cr(III) complex solution exhibiting a constant absorbance at 260 nm

4.17.2.4. Temperature dependence analysis of probe 141-metal ion complexation

The study of the binding ability of probe **141** influenced by temperature was conducted across a spectrum of temperatures, complementing the time-dependent investigation. Absorption spectra were recorded at 2 °C intervals from 20 °C up to 50 °C, wherein it was observed that the A variation in temperature did not produce any noteworthy impact on the binding capacity of probe **141**, as shown in **figure 4.40**, thereby suggesting a strong and consistent binding between the probe and the metal ions.

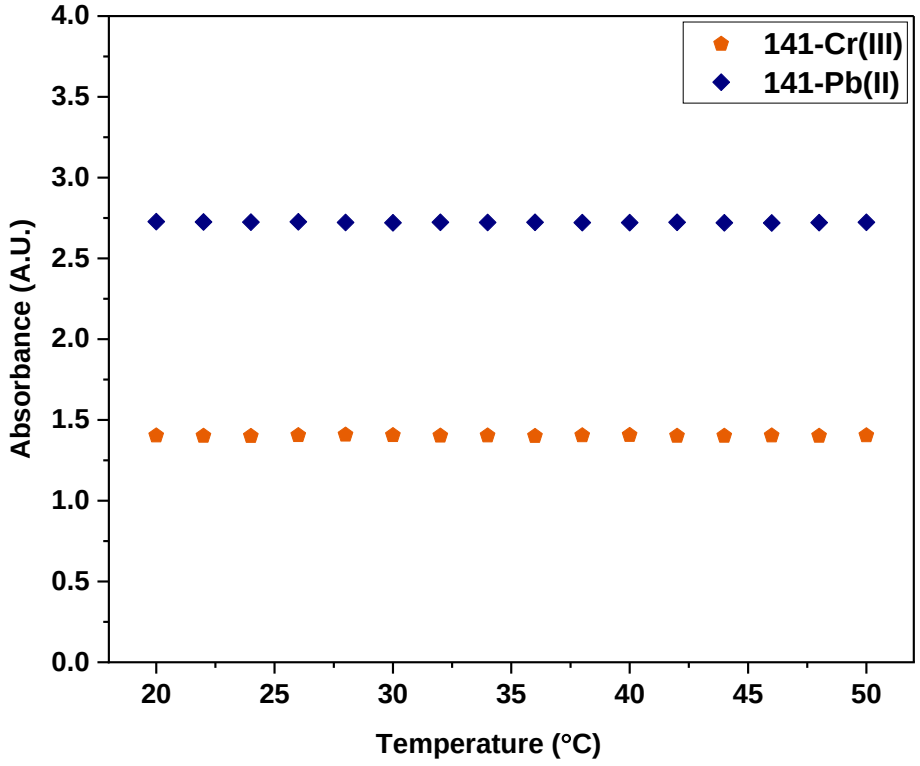

Figure 4.40: Temperature dependent absorption spectrum of probe **141**-Pb(II)/Cr(III) exhibiting a constant absorbance over a temperature range of 20 - 50 ºC

4.17.2.5. Plausible binding mode

Since the structure of the probe **141** is similar to that of probe, with the only difference being the transducer, therefore, the binding of the probe to the metal ions was achieved in a manner analogous to the probe **140**, through the manipulation of the arrangement of the 1,2,3-triazole groups to create a binding core structured to allow for the accommodation of Pb(II) and Cr(III) ions through interaction with the nitrogen and oxygen atoms, thereby exhibiting a 1:2 ligand-metal stoichiometry (**figure 4.41**). Rest of the coordination sites are expected to be filled by the solvent molecules.

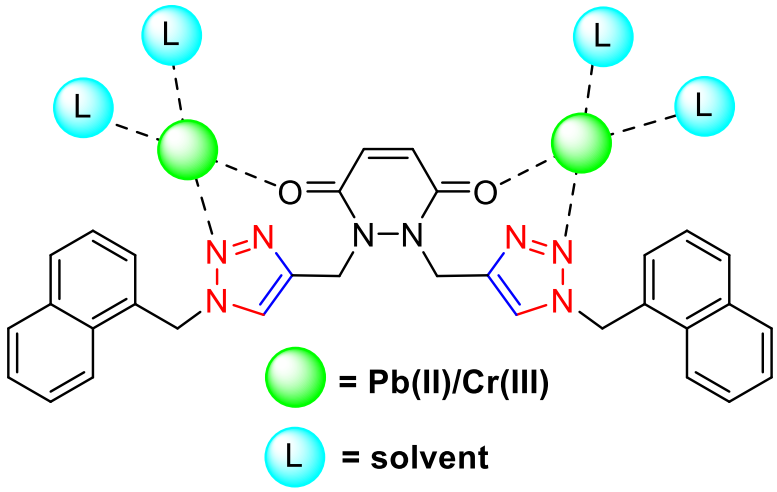

Figure 4.41: Proposed interaction between probe **141** and Pb(II)/Cr(III)

4.18. Chemosensing analysis of 4-tert butyl catechol based 1,2,3-triazole 144

4.18.1. Ion recognition analysis of 1,2,3-triazole derivative 144

Analysis of the ion recognition potential of 4-tert butyl catechol-based 1,2,3-triazole derivative **144** was carried out using UV-Vis spectroscopy, and a number of different metal chlorides were used in the analysis. The molecule was designed by modifying the 4-tert butyl catechol moiety in such a way that it was connected to a benzyl group (which acted as the transducer group) via a 1,2,3-triazole bridge. This bridge, in addition to serving as the spacer unit, also had the potential to provide the receptor sites for the metal ions due to the presence of N atoms having lone pairs of electrons. As a consequence of this, the synthesised probe was a robust molecule that had chemosensing potential.

For the purposes of sensing, the probe **144** displayed fine quality and interpretable spectral data. The solvatochromic evaluation of probe **144** resulted in the identification of acetonitrile and water in a ratio of 4:1 as the preferred solvent system for conducting UV-Vis analysis after considering other solvents such as DMSO, THF, acetonitrile, and acetonitrile/water (4:1). The selection was based on the solvent's effective solubility properties and the high quality of the obtained spectral data, as shown in **figure 4.42**. Following the completion of an optimization process aimed at determining the optimal solution concentration for conducting UV-Vis experiments, the concentration of the probe **144** solution was adjusted to 0.4 mM. The probe exhibited an absorption peak at 277 nm, which was equivalent to a 1.5 magnitude intensity.

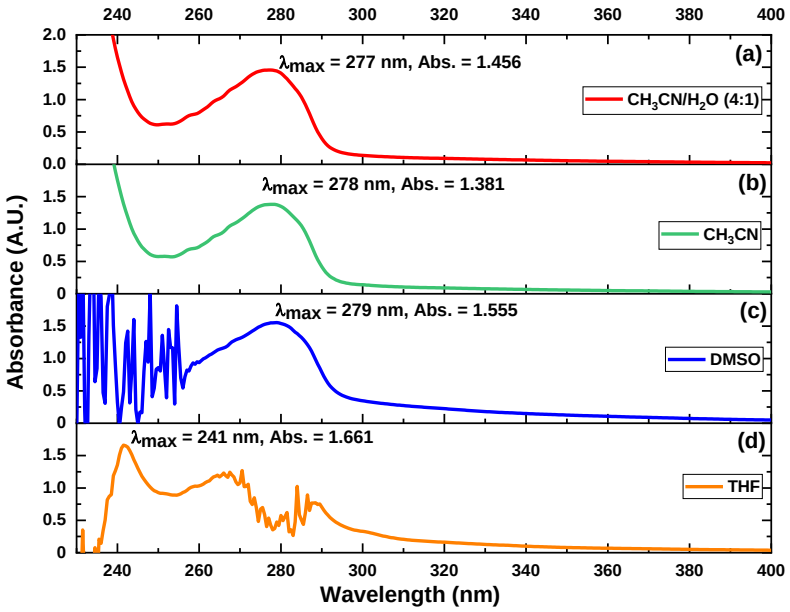

Figure 4.42: Absorption spectra of probe **144** (0.4 mM) solution in various solvents: (a) CH_3CN/H_2O (4:1), (b) CH_3CN, (c) DMSO, and (d) THF

Thereafter, the ion sensing capabilities of the probe **144** were tested by utilizing 1 mM chlorides dissolved in CH_3CN/H_2O (4:1) of the ions Na(I), Mg(II), Ba(II), Cr(III), Mn(II), Co(II), Ni(II), Cu(I), Zn(II), Cd(II), Hg(II), and acetate of Pb(II), wherein the metal ions were put through their paces in terms of sensing experiments using the probe solution. It was found that only the metal ion solutions of Pb(II) and Hg(II) (1mM) were able to effectively generate significantly large changes in the absorption spectra of probe **144**, as represented in **figure 4.43** as relative absorption change.

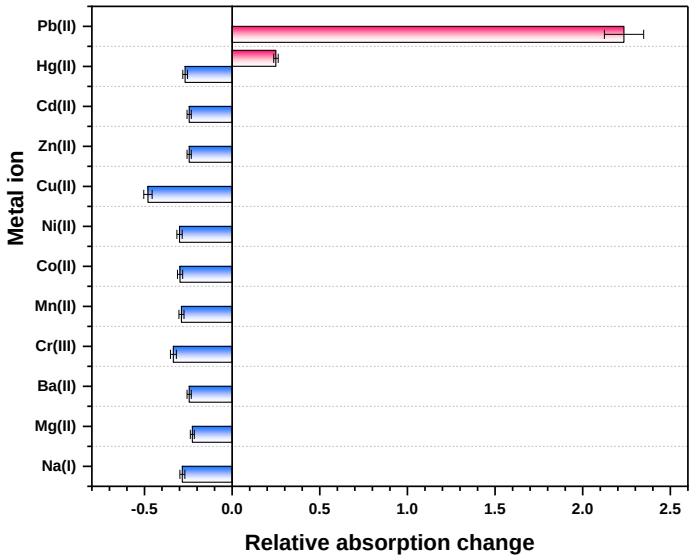

Figure 4.43: An illustration of the relative absorption change of probe **144** for several metal ions in CH_3CN/H_2O (4:1) solvent

4.18.2. Chemosensing response of probe 144 for Hg(II) and Pb(II) via UV-Vis spectroscopy

The assessment of probe **144**'s ability to detect Pb(II) and Hg(II) ions involved conducting a titration using a 0.4 mM solution of probe **144** and 1 mM solutions of Pb(II) and Hg(II). During this process, absorption spectra for every titration were recorded, wherein the concentration of the probe was kept constant at 0.4 mM while incrementally increasing the concentration of the metal ions from 0 to 15 equivalents. In **figure 4.44**, it is evident that the binding of Hg(II) ions to the probe solution was confirmed as indicated by a gradual decrease in absorption intensity at 277 nm (hypochromic shift) and a slight increase at 249 nm (hyperchromic response), and an isosbestic point at 255 nm was also observed. An inset graph displaying the ratio of the absorbance maxima (A_n/A_o) at 277 nm as a function of the molar concentration of Hg(II) ions, where A_n represents the absorption maxima with incremental Hg(II) ions and A_o represents the absorption maxima of the probe, is included. While progressively titrating the ligand solution with Pb(II), the probe **144** displayed a strong hyperchromic response at 277 nm, with a blue shift of roughly 22 nm as shown in **figure 4.45**. Furthermore, the association constant (K_a) of probe **144** was calculated using the B-H equation, yielding values of $2.46 \times 10^3\ M^{-1}$ and $0.71 \times 10^3\ M^{-1}$ in the case of interaction with Hg(II) and Pb(II) respectively; **figure 4.46** and **figure 4.47** depict the B-H plot for the same.

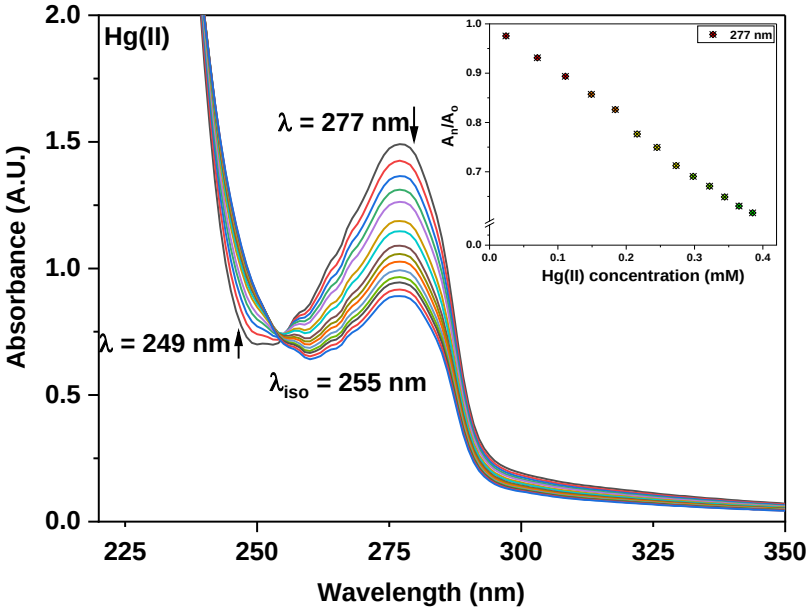

Figure 4.44: UV-Vis spectra of probe **144** (0.4 mM) upon the progressive addition of Hg(II) in CH_3CN/H_2O (4:1); the inset exhibits the relative absorbance change (A_n/A_o) vs metal ion concentration (mM)

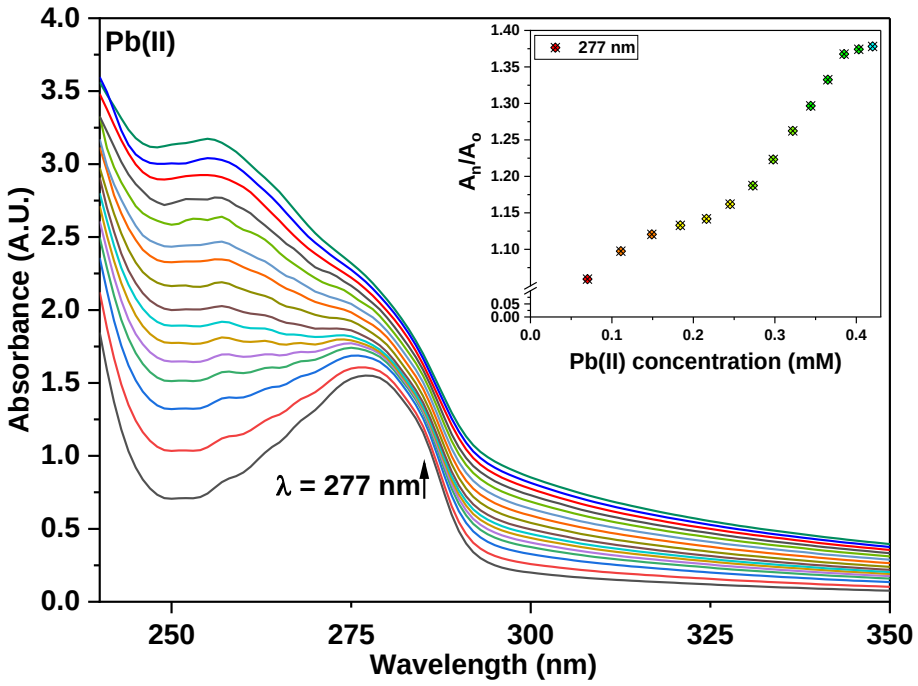

Figure 4.45: UV-Vis spectra of probe **144** (0.4 mM) upon the progressive addition of Pb(II) in CH_3CN/H_2O (4:1); the inset exhibits the relative absorbance change (A_n/A_o) vs metal ion concentration (mM)

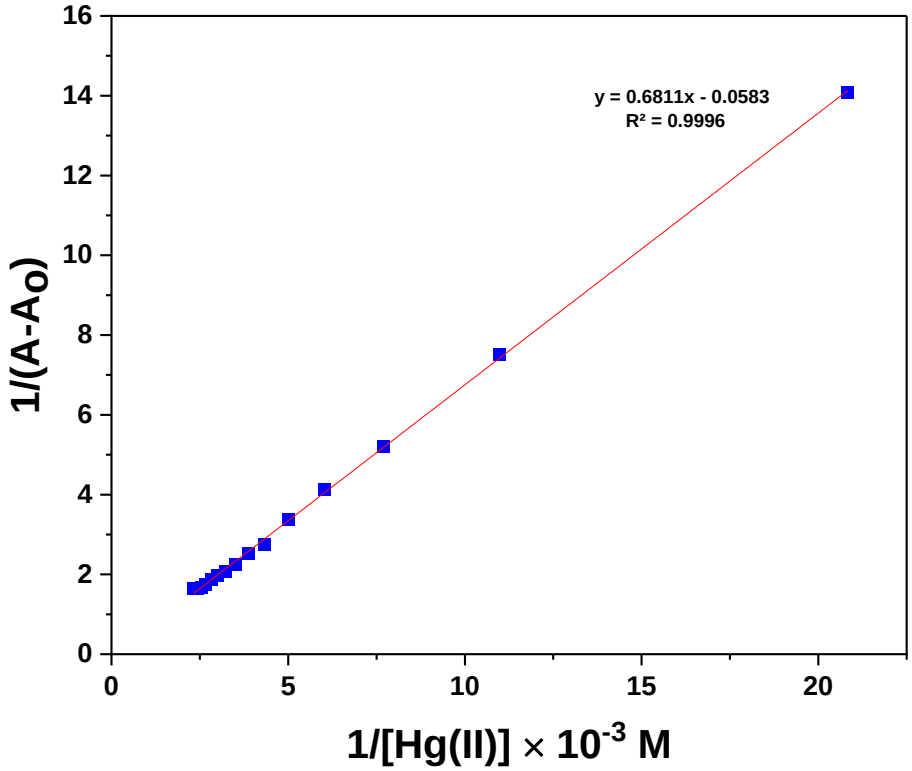

Figure 4.46: Benesi-Hildebrand plot for probe **144**-Hg(II) complexation

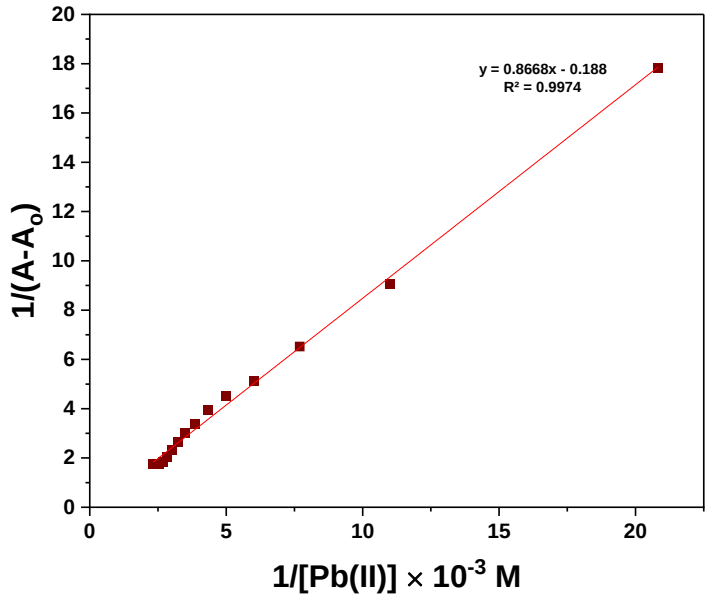

Figure 4.47: Benesi-Hildebrand plot for probe **144**-Pb(II) complexation

4.18.3. Chemosensing response of probe 144 for Hg(II) and Pb(II) via fluorescence spectroscopy

Fluorescence spectroscopy was also used to analyze the sensing behaviour of the probe **144** for different metal ions. When excited at a wavelength of 280 nm (λ_{ex}), probe **144** displayed a peak emission (λ_{ems}) characterized by a prominent peak at 340 nm and a secondary peak at 653 nm, which exhibited a relatively lower intensity. The excimer formation accounts for the 653 nm emission peak, whereas the monomer emission is responsible for the 340 nm emission peak, wherein it is possible for the benzyl groups of distinct molecules to undergo π-π stacking, thereby allowing for the formation of the excimer. The ratio of the relative intensities of the monomer and excimer bands for the free probe **144** (M_{340}/E_{653}) was 2.45, which went up to 2.53 when either of the metal ions was added, which signifies that a probe **144**-metal complex was formed. The successive introduction of Hg(II) and Pb(II) ions in distinct analytical titrations to probe **144** resulted in an enhanced fluorescence emission at the peaks at 340 nm and 653 nm, with the emergence of an isosbestic point at about 630 nm, as shown in **figure 4.48** and **figure 4.49** respectively; and the insets on both plots show the relative fluorescence emission (I/I_o) plotted against metal ion concentration, wherein I is the intensity of the fluorescence emission of probe **144** when metal ions are added, and I_o is the intensity of fluorescence emission of pure probe **144**. Also, the correlation plot (I_o-I)/I_o vs. Pb(II) concentration (**figure 4.50**) revealed that the probe's limit of detection (LoD) and limit of quantification (LoQ) were 8.6 µM and 28.7 µM, respectively, while the metal-to-ligand

binding ratio was 2:1 (**table 4.3**). In the same way, the correlation plot for Hg(II) (**figure 4.51**) showed that the probe's limit of detection (LoD) and limit of quantification (LoQ) were 11 µM and 38 µM, respectively, and the ratio of metal to ligand binding was 2:1 (**table 4.3**).

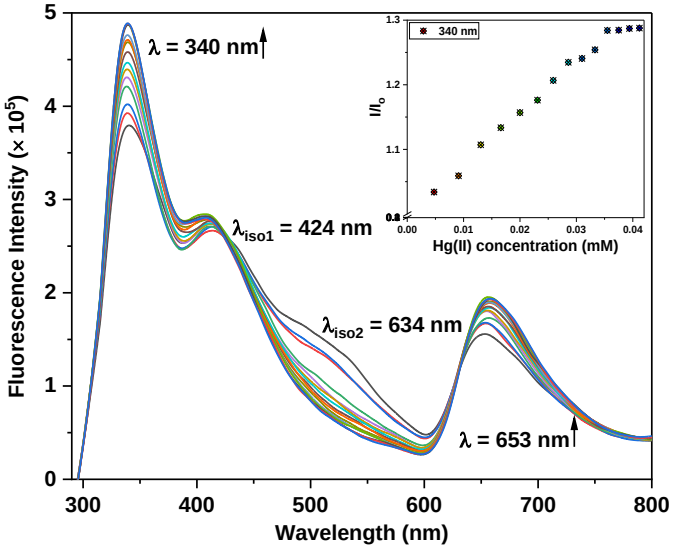

Figure 4.48: Fluorescence spectra of probe **144** (50 µM) upon the progressive addition of Hg(II) ions in CH_3CN/H_2O (4:1); the inset exhibits the relative emission change (I/I_o) vs metal ion concentration (µM)

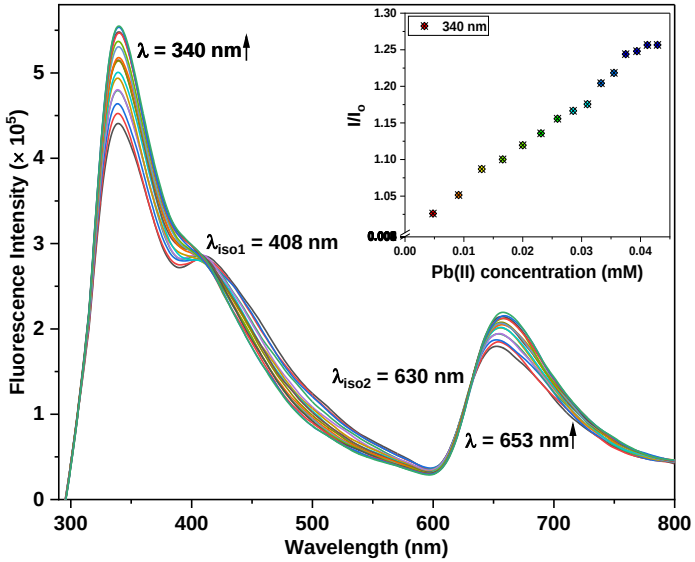

Figure 4.49: Fluorescence spectra of probe **144** (50 µM) upon the progressive addition of Pb(II) ions in CH_3CN/H_2O (4:1); the inset exhibits the relative emission change (I/I_o) vs metal ion concentration (µM)

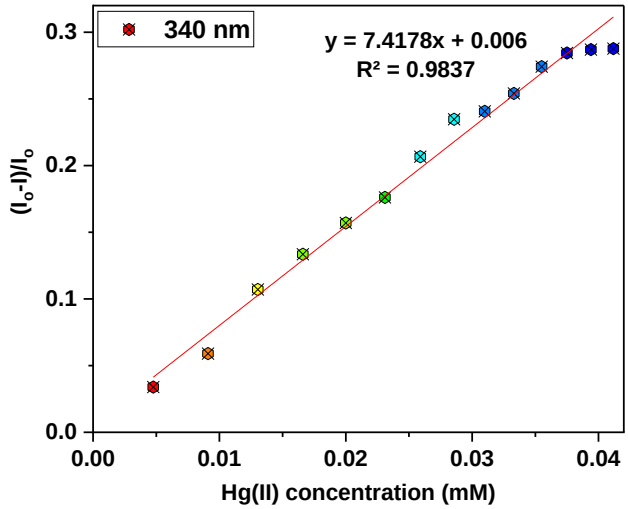

Figure 4.50: Correlation plot of relative fluorescence emission of probe **144** $(I_o\text{-}I)/I_o$ as a function of Hg(II) concentration; where I_o = initial emission of probe **144** and I = emission of probe **144** in the presence of Hg(II)

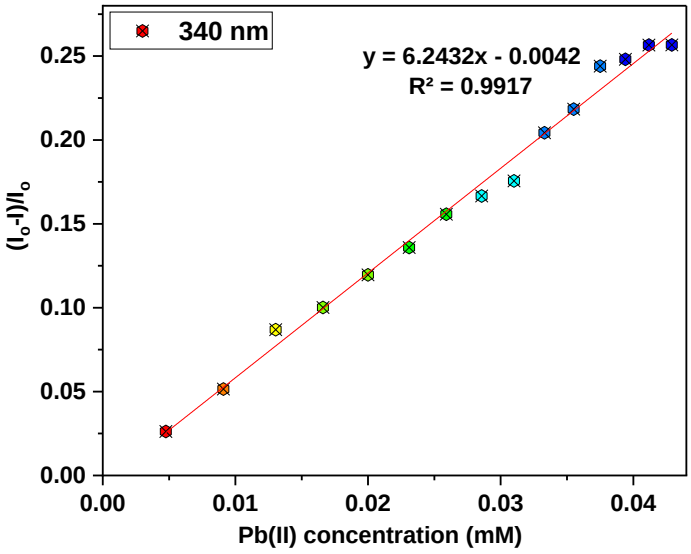

Figure 4.51: Correlation plot of relative fluorescence emission of probe **144** $(I_o\text{-}I)/I_o$ as a function of Pb(II) concentration; where I_o = initial emission of probe **144** and I = emission of probe **144** in the presence of Pb(II)

Entry	**Metal ion**	**LoD (µM)**	**LoQ (µM)**	**Association constant (K_a)**	**Stoichiometry (M:L)**
144	Hg(II)	11	38	$2.46 \times 10^3\ M^{-1}$	2:1
	Pb(II)	8.6	28.7	$0.71 \times 10^3\ M^{-1}$	2:1

Table 4.3: LoD, LoQ, K_a and stoichiometric ratio values of probe **144** on binding with Hg(II) and Pb(II)

4.18.4. Competitive metal ion interaction analysis

A solution of 0.4 mM probe **144** in CH_3CN/H_2O (4:1) was subjected to a competitive titration with the aim of determining whether the probe could selectively detect either Hg(II) or Pb(II) when other metal ions were present. This involved titrating the 0.4 mM probe solution with a solution containing an equivalent quantity of all the metal ions in an equimolar ratio. The absorption spectra obtained after the titrations closely resembled those observed during Hg(II) complexation, indicating that the sensor probe **144**'s ability to detect Hg(II) remained unaffected by the presence of other metal ions (**figure 4.52**).

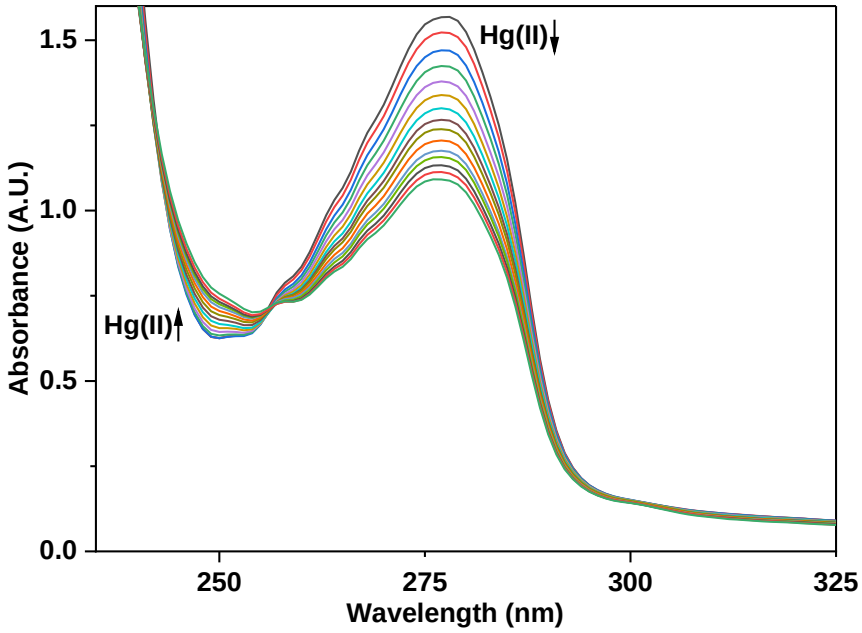

Figure 4.52: Absorption spectra of probe **144** (0.4 mM) in CH_3CN/H_2O (4:1) recognizing Hg(II) ions among several metal ions at equimolar concentrations

4.18.5. Time dependence analysis of probe 144-metal ion complexation

The time-dependent binding of probe **144** to Pb(II) and Hg(II) ions was examined by monitoring changes in the absorbance of probe **144**-Pb(II) and **144**-Hg(II) complex solutions over a period of one hour. As illustrated in **figure 4.57**, the spectral data suggests a gradual reduction in the absorption intensity of the **144**-Pb(II) complex over time, while the absorption intensity of the **144**-Hg(II) complex increases towards the end of the spectrum (**figure 4.53** and **4.54**). Furthermore, immediate changes in absorbance and fluorescence intensity were observed upon the addition of these metal ions to the probe solution, indicating that probe **144** serves as an efficient and "no-wait" sensor for Pb(II) and Hg(II).

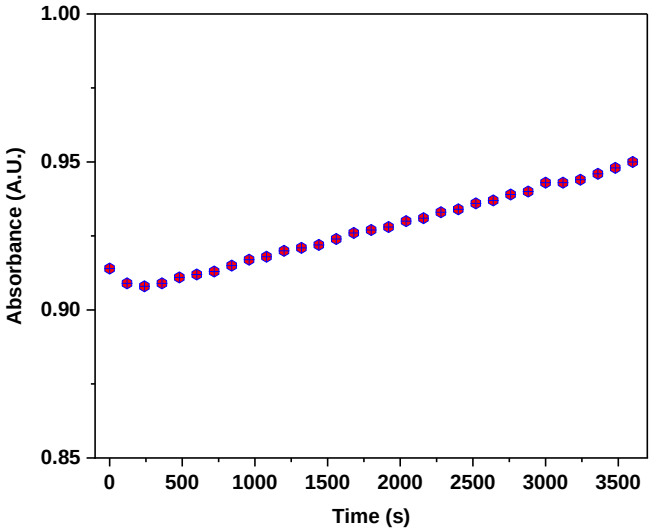

Figure 4.53: Time dependent absorption spectrum of probe **144**-Hg(II) complex solution exhibiting a successive enhancement in absorbance at 277 nm

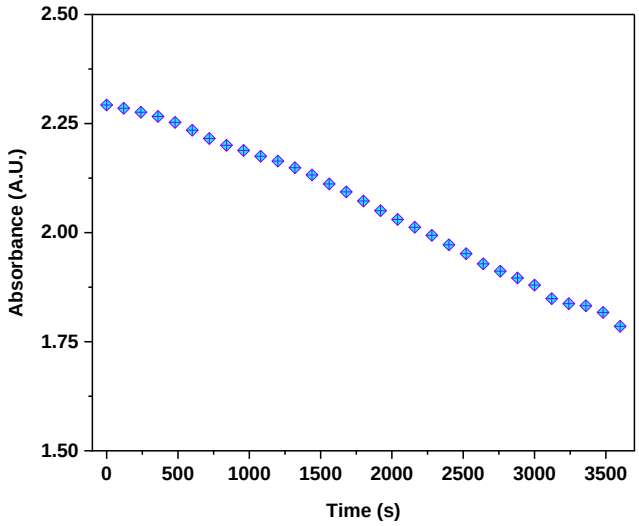

Figure 4.54: Time dependent absorption spectrum of probe **144**-Pb(II) complex solution exhibiting a successive decline in absorbance at 277 nm

4.18.6. Temperature dependence analysis of probe 144-metal ion complexation

The probe's potential for recognizing metal ions was also evaluated over a spectrum of temperature range, from 30 °C to 50 °C. The resulting absorbance of solutions of probe **144**-Hg(II) and probe **144**-Pb(II) were recorded at intervals of 2 °C. The **144**-Hg(II) combination showed a temperature-dependent rise in absorption strength in the spectra (**figure 4.55**), however this trend might just as well be explained by the behavior of the probe with respect to change in time. Absorption intensity for the **144**-Pb(II) complex diminishes with decreasing temperature, as shown in **figure 4.56**. This observed decrease in absorption intensity with

increasing temperature is attributed to the time dependency, as the delayed recording of the absorption intensity values of **144**-Pb(II) complex at temperatures of 34 °C and 36 °C provides further confirmation of this. Consequently, it was determined that the interaction between probe **144** and Hg(II) and Pb(II) was not influenced by changes in temperature.

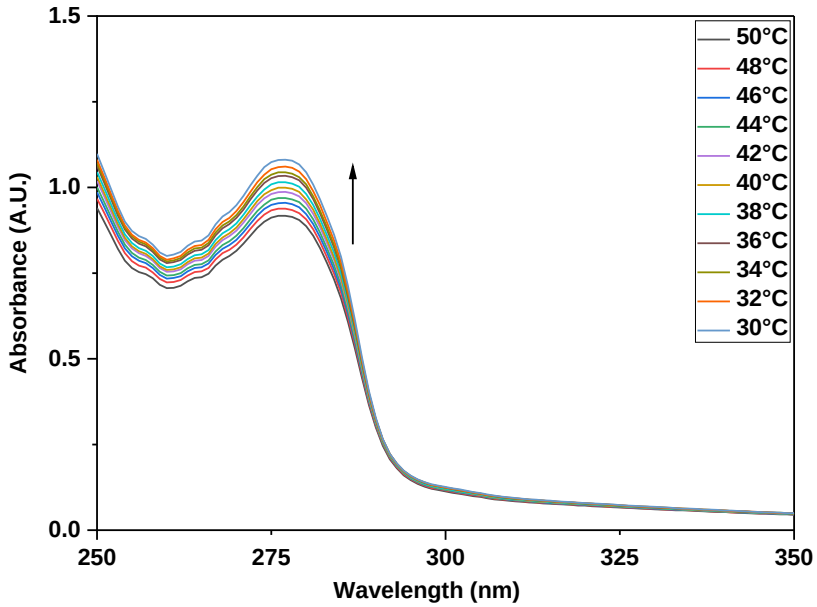

Figure 4.55: Temperature dependent absorption spectrum of probe **144**-Hg(II) exhibiting variation in absorbance over a temperature range of 20 - 50 ºC

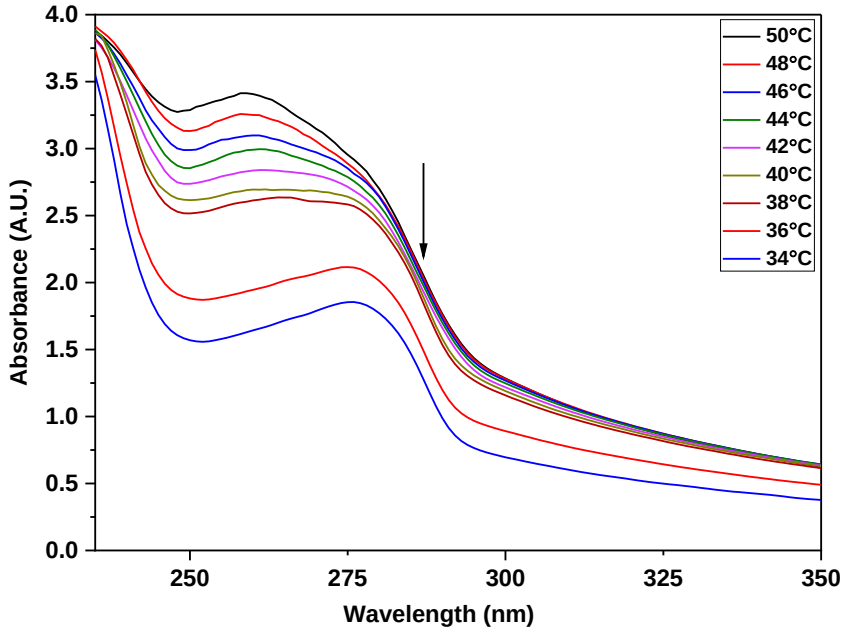

Figure 4.56: Temperature dependent absorption spectrum of probe **144**-Pb(II) exhibiting variation in absorbance over a temperature range of 20 - 50 ºC

4.18.7. Plausible binding mode

The HSAB concept recognizes Pb(II) to be a borderline acid whereas Hg(II) is a soft acid. Interactions can be established between these metal ions and groups that possess atoms carrying lone pairs like N, O, and S. The probe **144** may attach to the incoming metal ions via the 1,2,3-triazole moiety, as it contains the lone pairs present on the N atoms. The probe **144** formed a 2:1 metal-ligand combination with both Pb(II) and Hg(II), as confirmed by the correlation plot. Based on the foregoing, **figure 4.57** depicts a possible mode of interaction of the receptor **144** with the metal ions; wherein it is hypothesized that the triazole moiety's arms adjust such that the the N atom of the triazole ring bind with the metal ions on either side of the molecule. Rest of the coordination sites are expected to be filled by the solvent molecules.

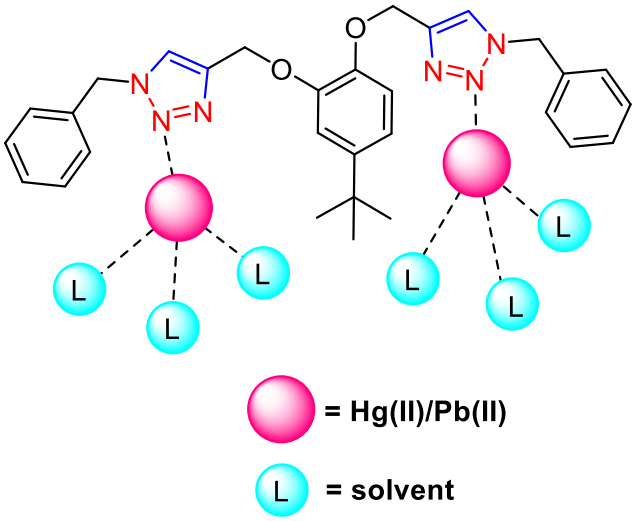

Figure 4.57: Proposed interaction between probe **144** and Hg(II)/Pb(II)

4.19. Chemosensing analysis of p-rosolic acid-based 1,2,3-triazole derivative 147

4.19.1. Ion recognition analysis of 1,2,3-triazole derivative 147

Using UV-Vis spectroscopy, an evaluation of the ion recognition potential of the newly synthesized p-rosolic acid-based 1,2,3-triazole derivative **147** was performed employing a variety of various metal chlorides. The evaluation was carried out in order to determine whether or not the ion recognition potential was present. The molecule was selected on the basis of the presence of labile protons which could be replaced to synthesize the corresponding alkyne, thereby subsequently subjecting it to cycloaddition with organic azide to form the 1,2,3-triazole derivative, Besides, the high aromaticity of the parent structure could be useful for better spectroscopic investigations. p-rosolic acid was likewise changed in the same way as the other compounds mentioned, with a 1,2,3-triazole bridge connecting it to a naphthyl moiety (the

transducer group). The 1,2,3-triazole bridge had electron-rich receptor sites for electron-deficient metal ions in addition to serving as the spacer unit, thanks to the presence of lone pair carrying N atoms. As a result, the synthesized probe was a robust molecule that had the ability to exhibit chemosensing potential.

The probe **147** showed fine quality and interpretable spectrum data, making it a good candidate for usage in sensing applications. For the spectral study of PRT, DMSO was chosen as the solvent of choice due to its solvability and fine spectrum data. Once the optimal concentration of probe **147** for UV-Vis studies was established, the concentration was set at 50 µM. Absorption maximum for the probe was observed at 284 nm, with two additional smaller peaks at 274 nm and 294 nm. Assessment for the recognition ability of probe **147** towards 0.5 mM chlorides of Cr(III), Mn(II), Co(II), Ni(II), Zn(II), Na(I), K(I), Mg(II), Ca(II), Ba(II), Cd(II), Hg(II), and Pb(II) prepared in DMSO, via UV-Vis analysis resulted in substantial changes in the UV-Vis spectrum exclusively for Cr(III), Hg(II) and Pb(II), whereas in the case of the remaining metal ions, no significant changes were observed (**figure 4.58**).

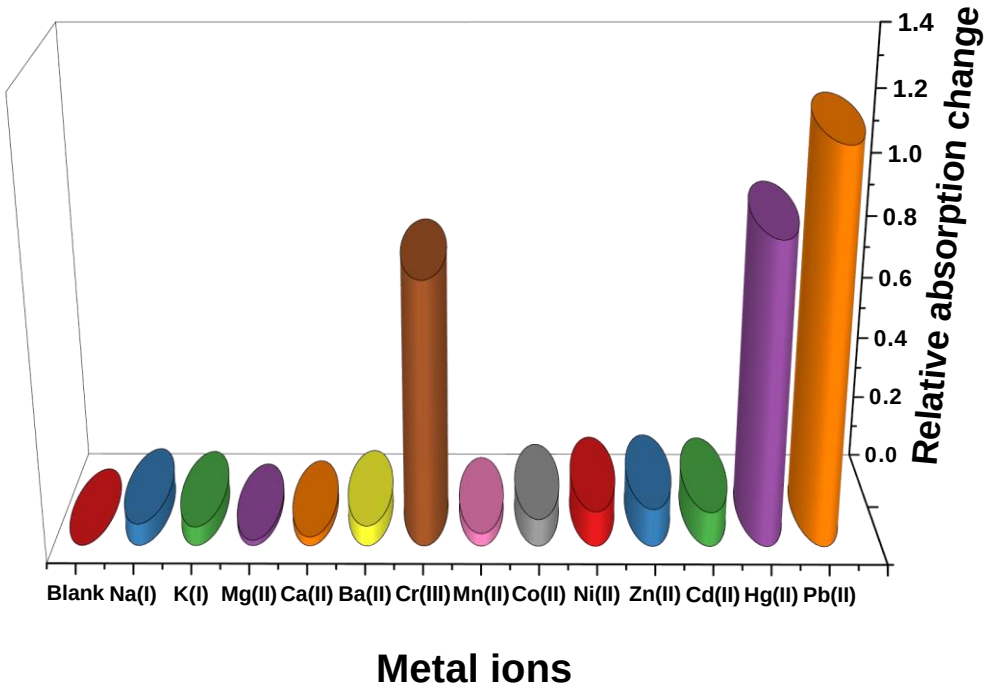

Figure 4.58: An illustration of the relative absorption change of probe **147** for several metal ions in DMSO solvent

4.19.2. Chemosensing response of probe 147 for Hg(II), Pb(II), and Cr(III) via UV-Vis spectroscopy

To assess the remarkable selectivity of probe **147** in detecting the metal ions Hg(II), Pb(II), and Cr(III), a comprehensive investigation was conducted employing UV-Vis spectral analysis. This analytical approach involved titrating a solution of probe **147** with solutions containing each of these metal ions individually at a concentration of 0.5 mM. Throughout all UV-Vis analyses, the probe's concentration was consistently maintained at 50 µM, while the metal ions concentration was systematically raised from 0 to 15 equivalents. The titration process was methodically executed by incrementally increasing the metal ions concentration from an initial concentration of 0 mM, representing the absence of metal ions, to a maximum of 15 equiv. This gradual increment in metal ion concentration enabled the monitoring of spectral changes in the probe's UV-Vis absorption profile as the metal ion concentration increased.

When 15 equivalents of Hg(II) ions were introduced into the solution of probe **147**, all three peaks at 274 nm, 284 nm, and 294 nm significantly exhibited hypochromic shift, and a concomitant hyperchromic effect resulting in the emergence of a peak at 262 nm was observed, thereby creating an isosbestic point at 271 nm (**figure 4.59**). For Pb(II) ions, the peak at 294 nm was barely impacted, but the peaks at 274 nm and 284 nm exhibited an immense hyperchromic response, leading to their merging into a single peak with a simultaneous hypsochromic shift to around 266 nm (**figure 4.60**).

Titration of the probe solution with Cr(III) ions yielded a hypochromic response at 274 nm, 284 nm, and 294 nm, with a new peak observed at 262 nm exhibiting a significant hyperchromic response (**figure 4.61**). The insets in all the absorption spectra demonstrate the relative change in the absorption intensity (A_n/A_o) as a function of the metal ion concentration; A_o = absorbance maxima of probe **147** and A_n = absorbance maxima of probe **147** with successive addition of metal ions. Additionally, the association constant (K_a) of probe **147** was calculated using the B-H equation (A), yielding values of $1.312 \times 10^4\ M^{-1}$, $1.527 \times 10^4\ M^{-1}$, $4.94 \times 10^4\ M^{-1}$ in the case of interaction with Hg(II), Pb(II), and Cr(III) respectively; **figure 4.62 - 4.64** depict the B-H plot for the same respectively.

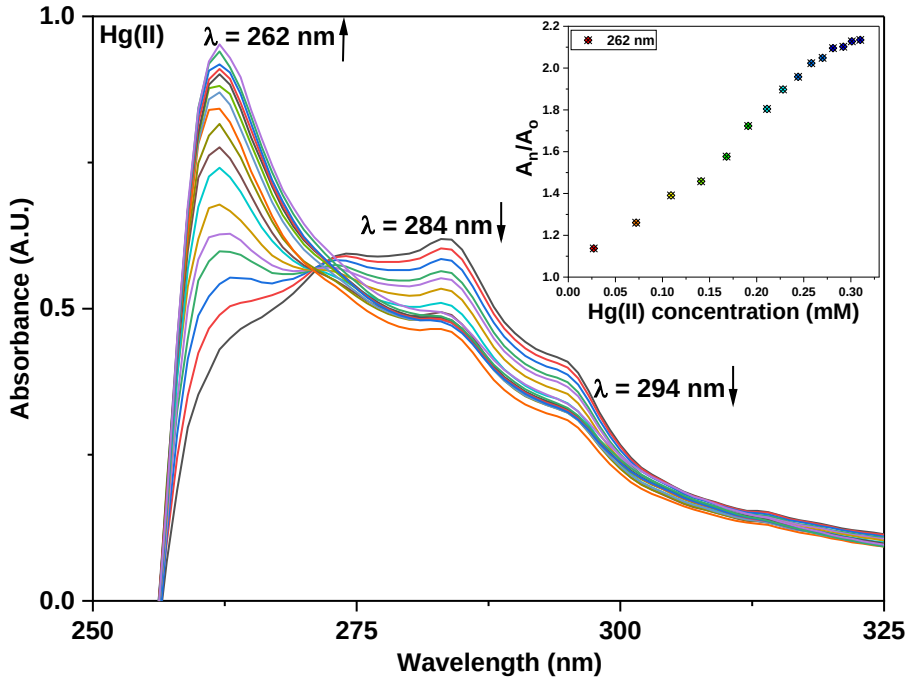

Figure 4.59: UV-Vis spectra of probe **147** (0.05 mM) upon the progressive addition of Hg(II) in DMSO; the inset exhibits the relative absorbance change (A_n/A_o) vs metal ion concentration (mM)

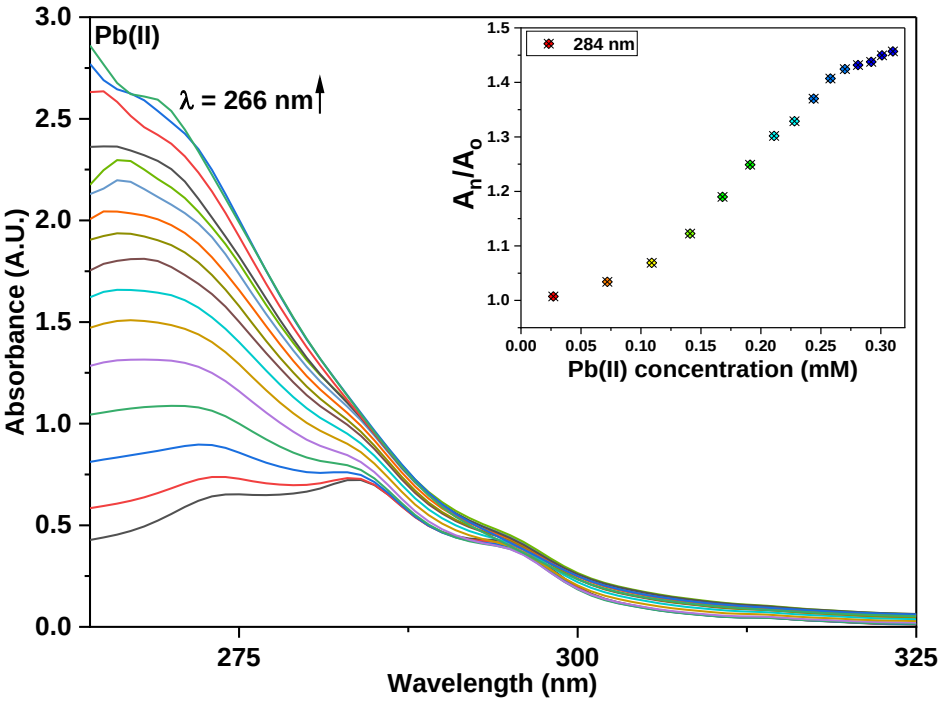

Figure 4.60: UV-Vis spectra of probe **147** (0.05 mM) upon the progressive addition of Pb(II) in DMSO; the inset exhibits the relative absorbance change (A_n/A_o) vs metal ion concentration (mM)

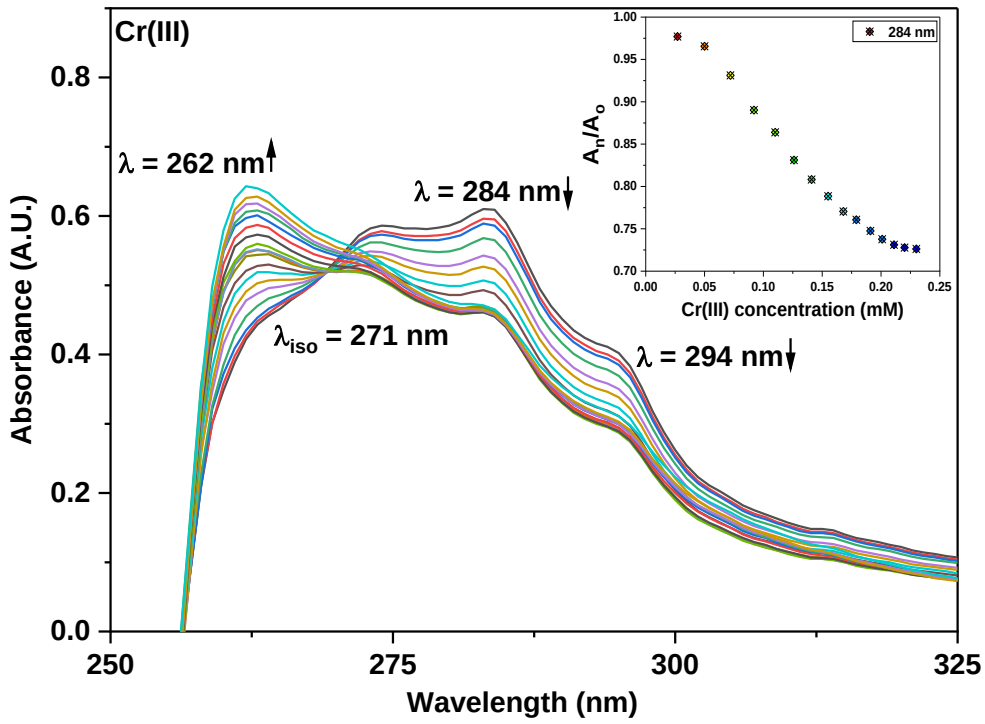

Figure 4.61: UV-Vis spectra of probe **147** (0.05 mM) upon the progressive addition of Cr(III) in DMSO; the inset exhibits the relative absorbance change (A_n/A_o) vs metal ion concentration (mM)

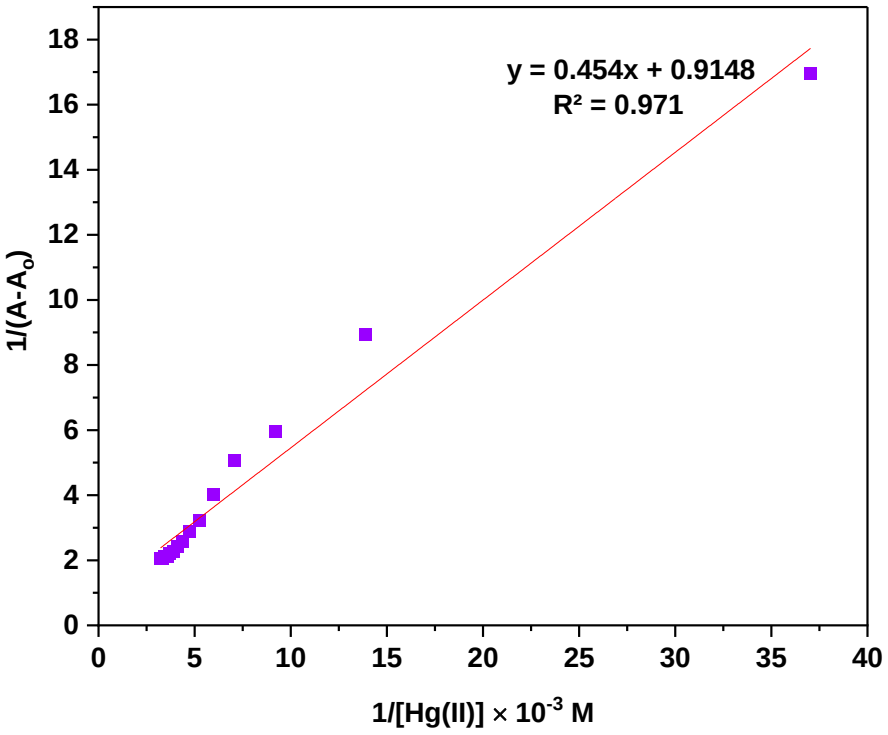

Figure 4.62: Benesi-Hildebrand plot for probe **147**-Hg(II) complexation

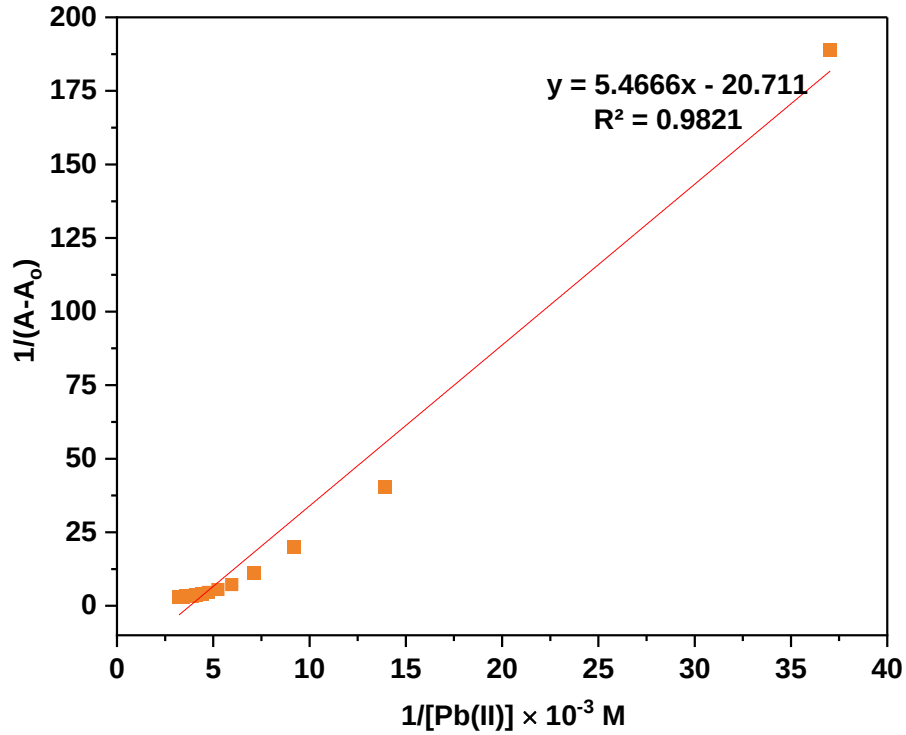

Figure 4.63: Benesi-Hildebrand plot for probe **147**-Pb(II) complexation

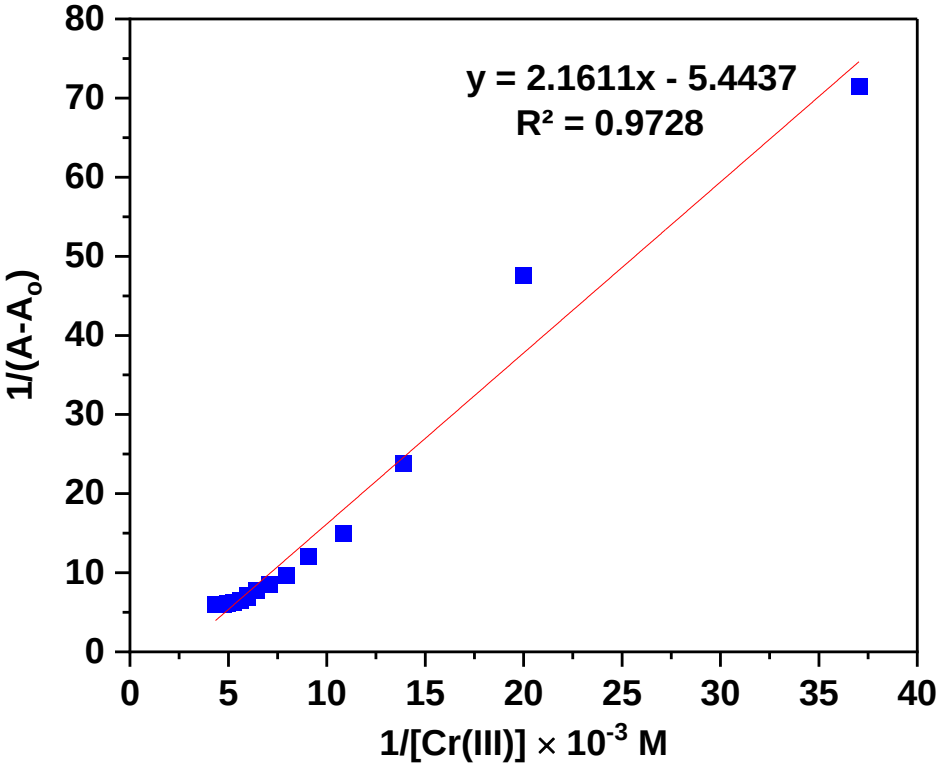

Figure 4.64: Benesi-Hildebrand plot for probe **147**-Cr(III) complexation

4.19.3. Chemosensing response of probe 147 for Hg(II), Pb(II), and Cr(III) via fluorescence spectroscopy

The complexation of the sensor probe **147** with the aforementioned metal ions was also investigated using fluorescence spectroscopy. Intense fluorescence emission (λ_{em}) at 365 nm and a comparatively weak emission at 657 nm, attributable to excimer emission were observed in the fluorescence spectrum of the probe **147** when excitation wavelength (λ_{ex}) was set to 290 nm. The effect of the three distinct metal ions on probe **147** solution was done at a concentration of 0.1 µM, it was observed that the fluorescence emission peaks at 365 nm and 657 nm experienced an increase in intensity as the metal ions concentration increased from 0.5 µM to 4 µM (**figures 4.65 - 4.67**), the inset illustrates the relative change in emission (I/I_o) plotted against metal ion concentration. Furthermore, **figure 4.68 - 4.70** show the correlation plot of $(I-I_o)/I_o$ against $[M^{n+}]$, and the LoD and LoQ values calculated using these plots for all three metal ions were determined to be 0.09 µM and 0.29 µM for Hg(II), 0.10 µM and 0.33 µM for Pb(II), and 0.12 µM and 0.41 µM for Cr(III). Additionally, the binding ratio as calculated from the correlation plots was determined to be 1:1 in all three cases. The values of LoD, LoQ, binding ratio, and association constant have been compiled in **table 4.4**.

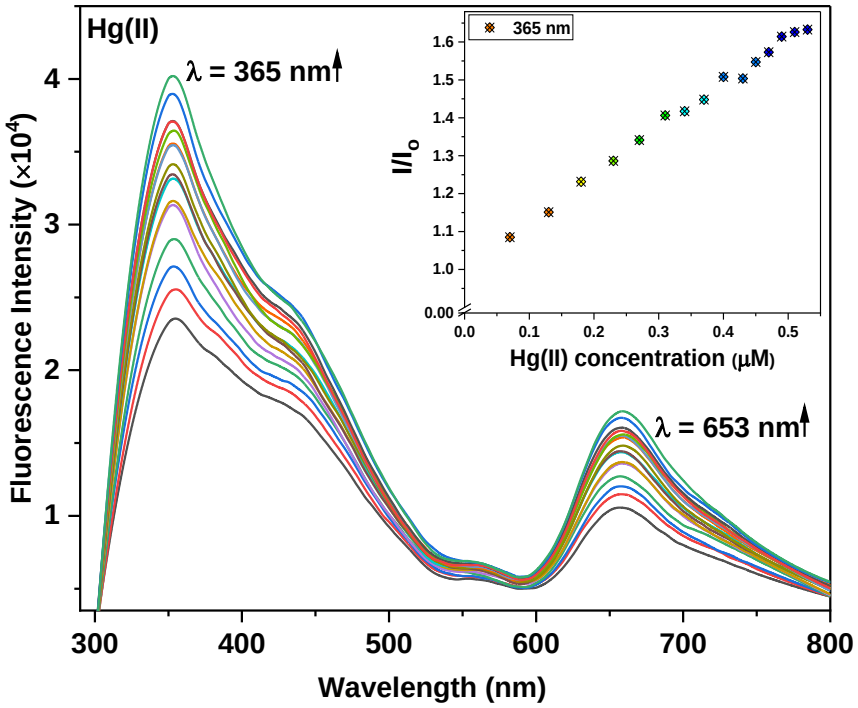

Figure 4.65: Fluorescence spectra of probe **147** (0.1 µM) upon the progressive addition of Hg(II) ions in DMSO; the inset exhibits the relative emission change (I/I_o) vs metal ion concentration (µM)

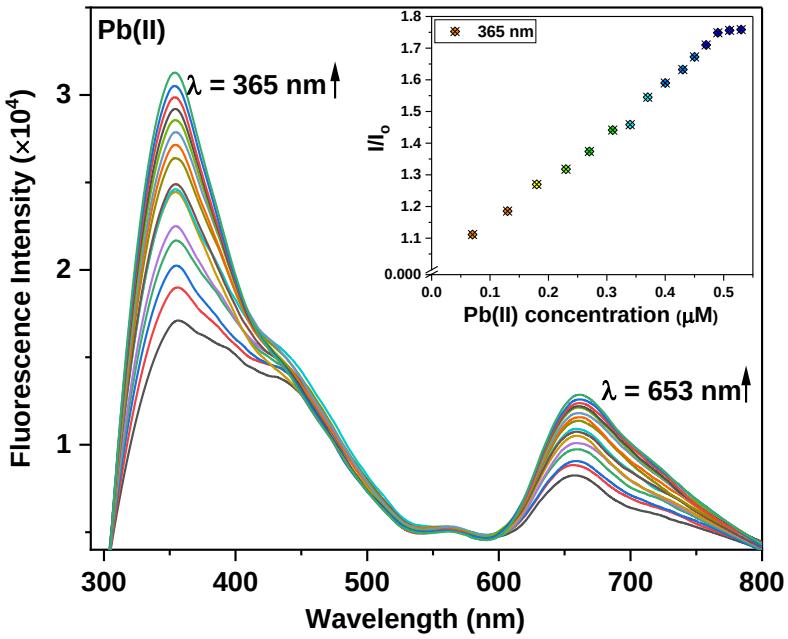

Figure 4.66: Fluorescence spectra of probe **147** (0.1 μM) upon the progressive addition of Pb(II) ions in DMSO; the inset exhibits the relative emission change (I/I_o) vs metal ion concentration (μM)

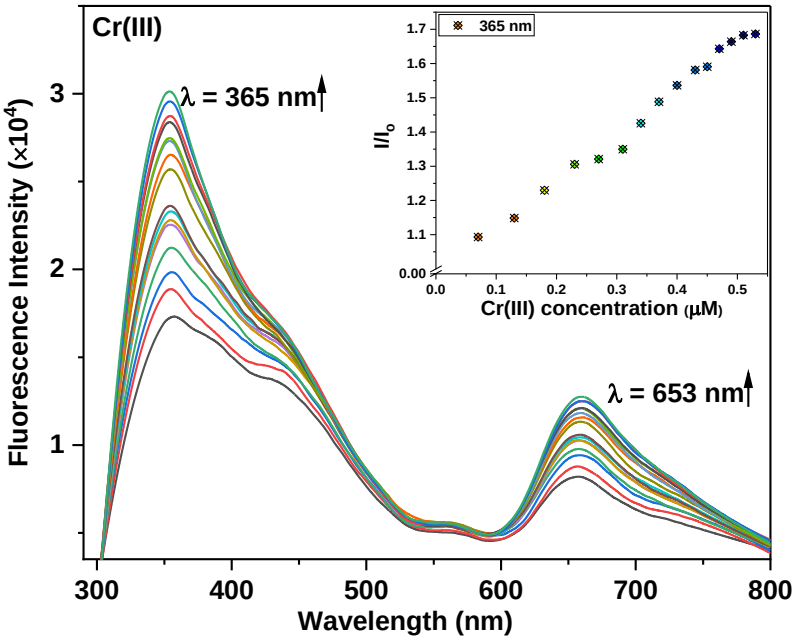

Figure 4.67: Fluorescence spectra of probe **147** (0.1 μM) upon the progressive addition of Cr(III) ions in DMSO; the inset exhibits the relative emission change (I/I_o) vs metal ion concentration (μM)

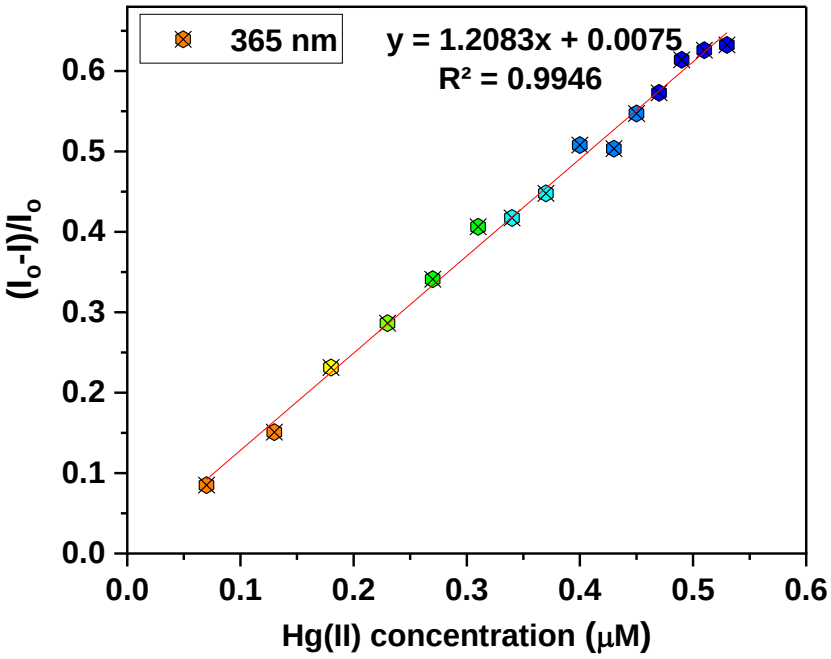

Figure 4.68: Correlation plot of relative fluorescence emission of probe **147** $(I_o\text{-}I)/I_o$ as a function of Hg(II) concentration; where I_o = initial emission of probe **147** and I = emission of probe **147** in the presence of Hg(II)

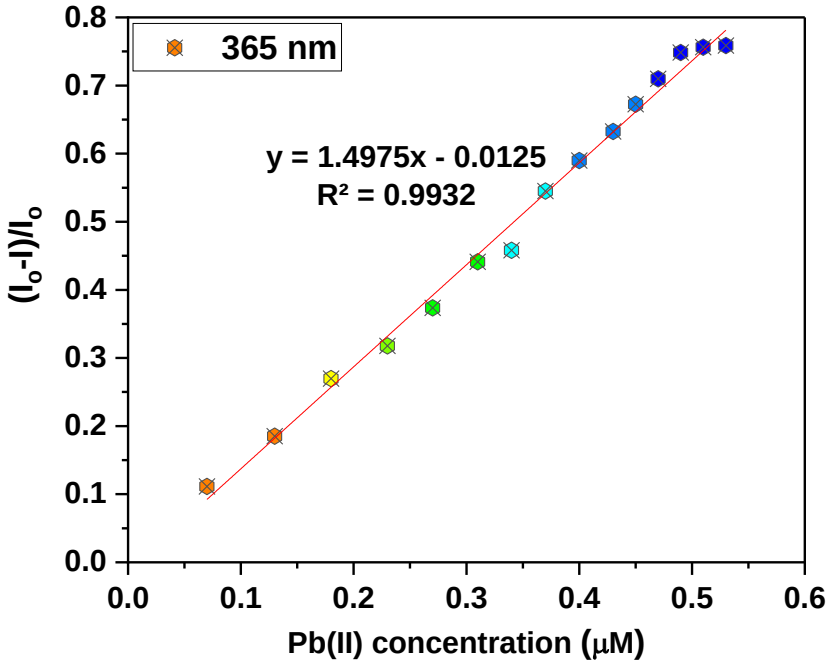

Figure 4.69: Correlation plot of relative fluorescence emission of probe **147** $(I_o\text{-}I)/I_o$ as a function of Pb(II) concentration; where I_o = initial emission of probe **147** and I = emission of probe **147** in the presence of Pb(II)

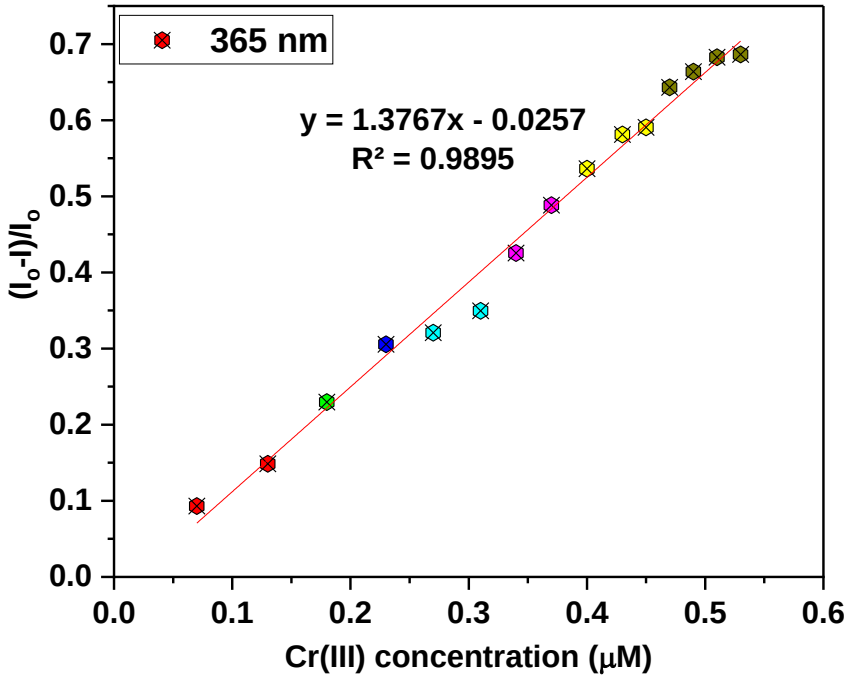

Figure 4.70: Correlation plot of relative fluorescence emission of probe **147** $(I_o\text{-}I)/I_o$ as a function of Cr(III) concentration; where I_o = initial emission of probe **147** and I = emission of probe **147** in the presence of Cr(III)

Probe	**Metal ion**	**LoD (μM)**	**LoQ (μM)**	**Association Constant (K_a)**	**Stoichiometry (M:L)**
147	Cr(III)	0.12	0.41	$4.94 \times 10^4\ M^{-1}$	1:1
	Pb(II)	0.10	0.33	$1.527 \times 10^4\ M^{-1}$	1:1
	Hg(II)	0.09	0.29	$1.312 \times 10^4\ M^{-1}$	1:1

Table 4.4: LoD, LoQ, K_a and stoichiometric ratio values of probe **147** on binding with Hg(II), Pb(II), and Cr(III)

4.19.4. Competitive metal ion interaction analysis

The probe **147**'s ability to selectively detect a particular metal ion, regardless of the presence of other metal ions, was demonstrated through a competitive titration. In this experiment, probe **147** was titrated with a solution containing equal concentrations of various metal ions. The absorption spectrum shown in **figure 4.71**, obtained after the titration, displayed an identical pattern to that of probe **147**-Pb(II). This observation suggests that probe **147**'s capacity to identify Pb(II) remained unaffected, even when other metal ions were present.

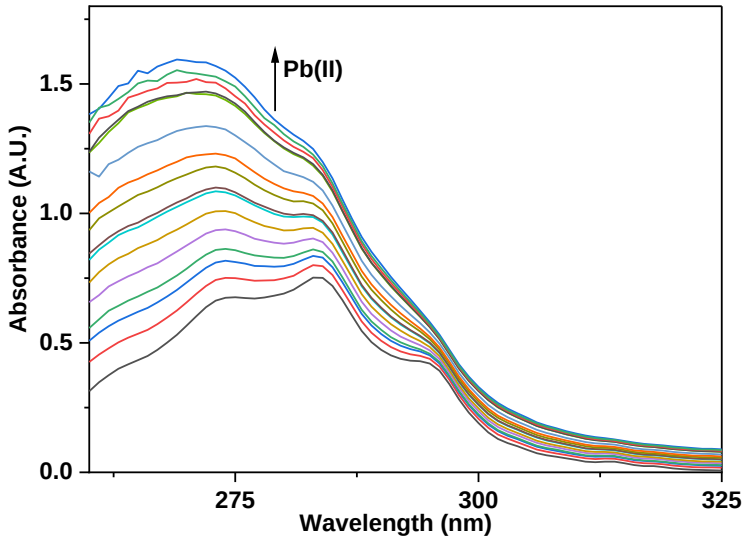

Figure 4.71: Absorption spectra of probe **147** (0.05 mM) in DMSO recognizing Pb(II) ions among several metal ions at equimolar concentrations

4.19.5. Time dependence analysis of probe 147-metal ion complexation

The time dependent study investigated the impact of time on the metal-bound probe **147**, aiming to understand the contributions to sensing and to gain insights into the probe's capability for detecting metal ions. The absorption spectroscopy technique was employed to analyze the time dependence of metal-bound probe **147**. The spectra of the probe in case of distinct metal ions, depicted in **figure 4.72**, indicated that the absorbance remained unchanged even after an extended period of time. This observation indicates a significant level of stability and a strong attraction between the probe and the metal ions.

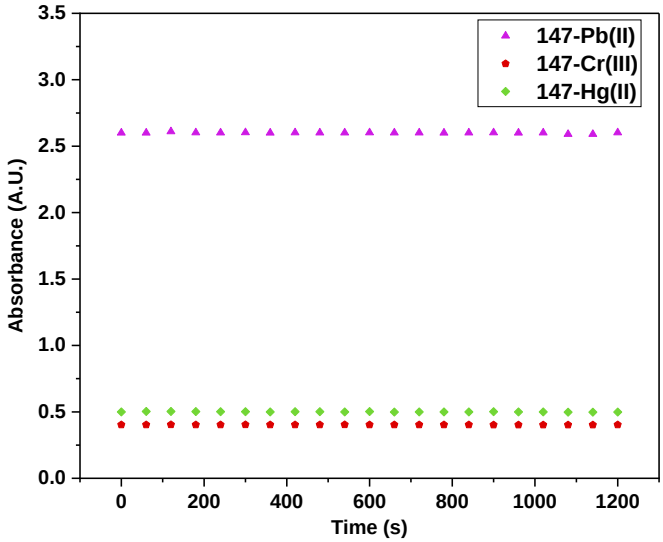

Figure 4.72: Time dependent absorption spectrum of probe **147**-Hg(II)/Pb(II)/Cr(III) complex solution exhibiting a constant absorbance at 284 nm

4.19.6. Temperature dependence analysis of probe 147-metal ion complexation

In addition to the time-dependent analysis, an investigation was carried out to assess how the probe's binding capacity was affected by the variations in temperature over a range of values. The temperature of the solutions containing probe **147** bound to metal ions was systematically increased from 20 °C to 50 °C, with absorbance being recorded at 2 °C intervals during this temperature escalation. Because of this progressive increase in temperature, the findings that were obtained showed that all the solutions had increased absorbance, as seen in **figure 4.73 - 4.75**.

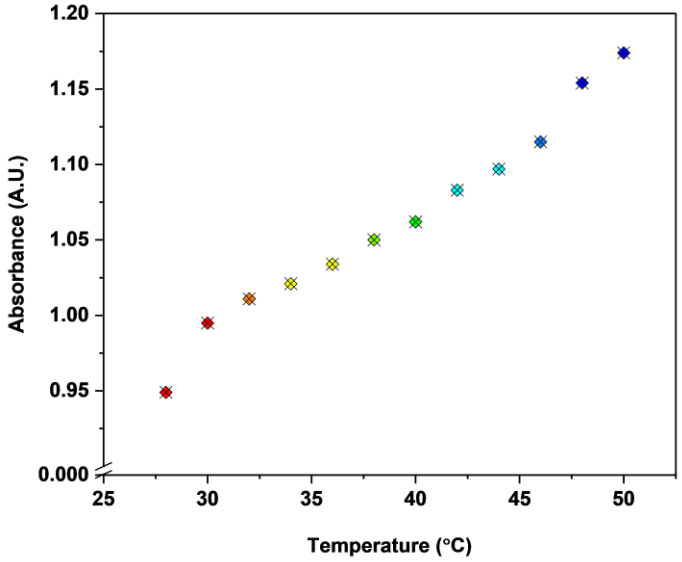

Figure 4.73: Temperature dependent absorption spectrum of probe **147**-Hg(II) exhibiting a successive enhancement in absorption over a temperature range of 20 - 50 ºC

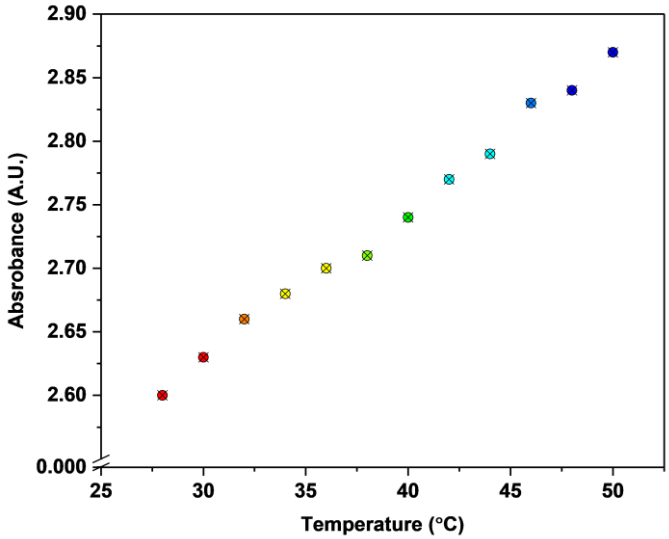

Figure 4.74: Temperature dependent absorption spectrum of probe **147**-Pb(II) exhibiting a successive enhancement in absorption over a temperature range of 20 - 50 ºC

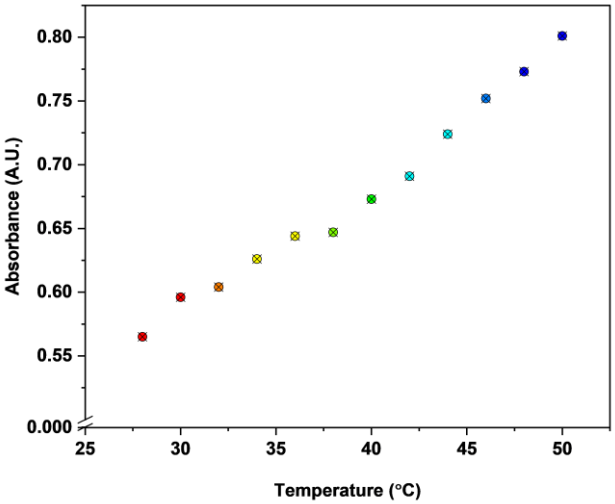

Figure 4.75: Temperature dependent absorption spectrum of probe **147**-Cr(III) exhibiting a successive enhancement in absorption over a temperature range of 20 - 50 ºC

4.19.7. Plausible binding mode

The interaction between probe **147** and the electron-deficient metal ions can be elucidated using the HSAB approach, according to which Hg(II) is classified as a soft acid, Pb(II) enacts as a borderline acid, and Cr(III) is a hard acid. Based on the observation that the Job plot of the probe corresponds to a 1:1 (M:L) complex, and taking into account that the nitrogen atoms within the 1,2,3-triazole moiety and the oxygen atoms within the ligand are likely responsible for interacting with the metal ions, a proposed binding mode between probe **147** and the metal ions is illustrated in **figure 4.76**. Rest of the coordination sites are expected to be filled by the solvent molecules.

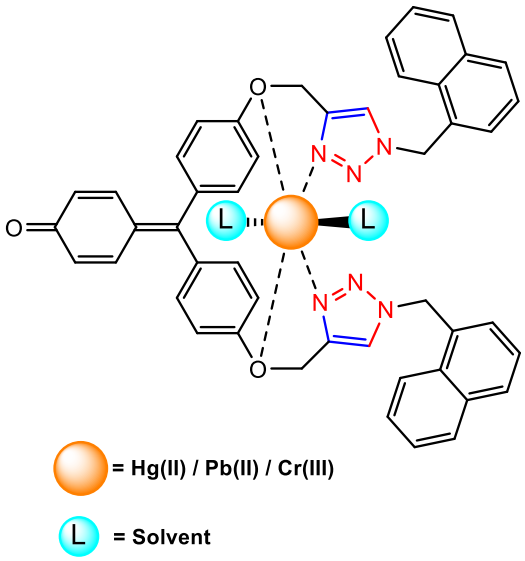

Figure 4.76: Proposed interaction between probe **147** and Hg(II)/Pb(II)/Cr(III)

4.20. Chemosensing analysis of glyoxal bis-(2-hydroxyanil)-based 1,2,3-triazole derivative 150

4.20.1. Ion recognition analysis of 1,2,3-triazole derivative 150

The newly synthesised glyoxal bis-(2-hydroxyanil)-based 1,2,3-triazole derivative **150** was tested for its ion recognition potential using UV-Vis spectroscopy and fluorescence spectroscopy for different metal chlorides. The molecule was chosen owing to its high aromaticity and the presence of labile protons which are easily replaceable, allowing for the synthesis of the appropriate alkyne and subsequent cycloaddition with organic azide, yielding the 1,2,3-triazole derivative. Like the other compounds discussed, glyoxal bis-(2-hydroxyanil) underwent a similar transformation by adding a 1,2,3-triazole bridge to its naphthyl moiety (the transducer group). Due to the existence of lone pair carrying N atoms, the 1,2,3-triazole bridge not only served as the spacer unit, but also as electron-rich receptor sites for electron-deficient metal ions. The resulting synthetic probe was a robust molecule with chemosensing capabilities.

The 1,2,3-triazole-linked probe **150** demonstrated fine spectrum data when used as a sensing probe. For the ion recognition investigations of the probe, DMSO was selected as the solvent due to its high solubility and fine quality spectrum data. The optimal concentration of probe **150** solution was set at 50 µM and subsequently employed for UV-Vis studies. The maximum absorption (λ_{max}) was observed at 284 nm, with two additional bands at 274 nm and 294 nm. The metal ions including Na(I), K(I), Mg(II), Ca(II), Ba(II), Mn(II), Co(II), Ni(II), Cu(II), Zn(II), Cd(II), Pb(II), and Ce(III) were solubilized in dimethyl sulfoxide (DMSO) at a concentration of 1 mM. These metal ion solutions, which are of physiological and environmental importance, were subsequently subjected to analysis in order to evaluate the sensing characteristics of the probe. Substantial shifts in the absorption spectrum of the probe were seen when metal ion solutions of Cu(II) and Pb(II) were progressively added, whereas no significant change was observed for the rest of the ions as shown in the **figure 4.77**.

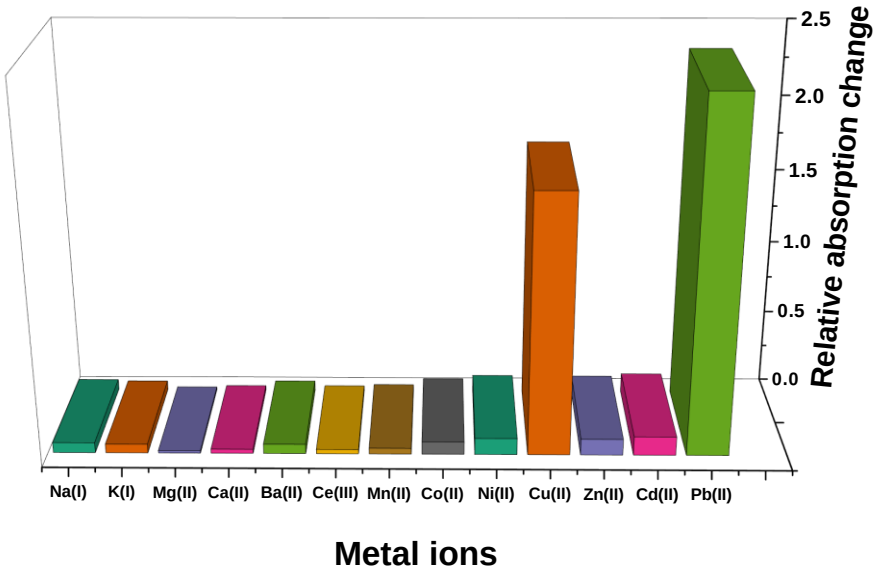

Figure 4.77: An illustration of the relative absorption change of probe **150** for several metal ions in DMSO solvent

4.20.2. Chemosensing response of probe 150 for Cu(II) and Pb(II) via UV-Vis spectroscopy

Titrations of a 0.05 mM probe **150** solution with 0.5 mM solutions of Cu(II) and Pb(II) were performed separately to examine the ion detection potential of probe **150** with these metal ions by UV-Vis spectral analysis. The probe showed a hyperchromic shift with the incremental addition of Cu(II) ions to the ligand solution, confirming the binding of Cu(II) to the probe as shown in **figure 4.78**, with an inset showing the relative maximum absorbance change (A_n/A_o) as a function of the increase in Cu(II) molar concentration. In the case of Pb(II) ions, a hypochromic shift in the 294 nm peak was observed, as well as a hyperchromic shift in the 274 nm and 284 nm peaks, with the latter two peaks merging into a single peak at about 270 nm as shown in **figure 4.79**, the inset exhibits the relationship between the relative change in the absorption intensity (A_n/A_o) and the increase in Pb(II) molar concentration at, where A_o = maximum absorbance of the probe, and A_n = maximum absorbance upon progressive addition of Pb(II) ions. In addition, the association constant (K_a) for the 1:1 probe **150**-metal complexation in respect to both metal ions was calculated using the B-H equation (A), and the related B-H graphs are shown in **figure 4.80** and **figure 4.81**, wherein the K_a values for Cu(II) and Pb(II) were determined to be 1.16×10^3 M^{-1} and 1.10×10^3 M^{-1} respectively.

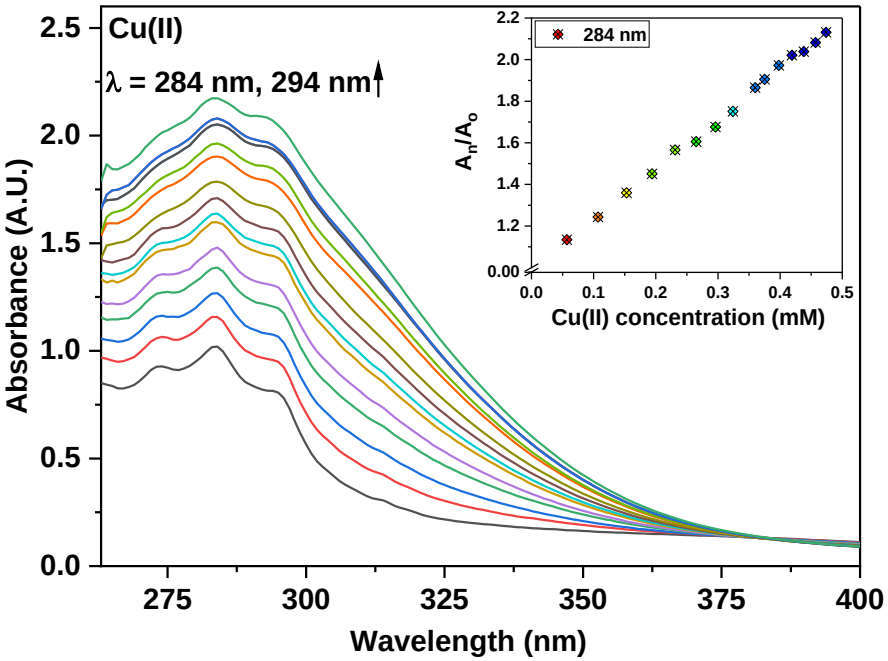

Figure 4.78: UV-Vis spectra of probe **150** (0.5 mM) upon the progressive addition of Cu(II) in DMSO; the inset exhibits the relative absorbance change (A_n/A_o) vs metal ion concentration (mM)

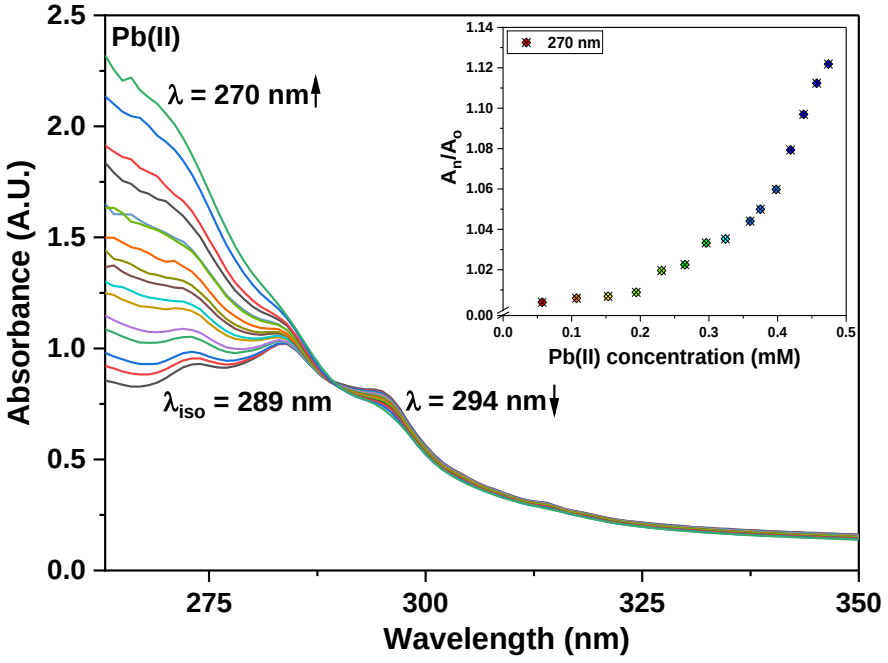

Figure 4.79: UV-Vis spectra of probe **150** (0.5 mM) upon the progressive addition of Pb(II) in DMSO; the inset exhibits the relative absorbance change (A_n/A_o) vs metal ion concentration (mM)

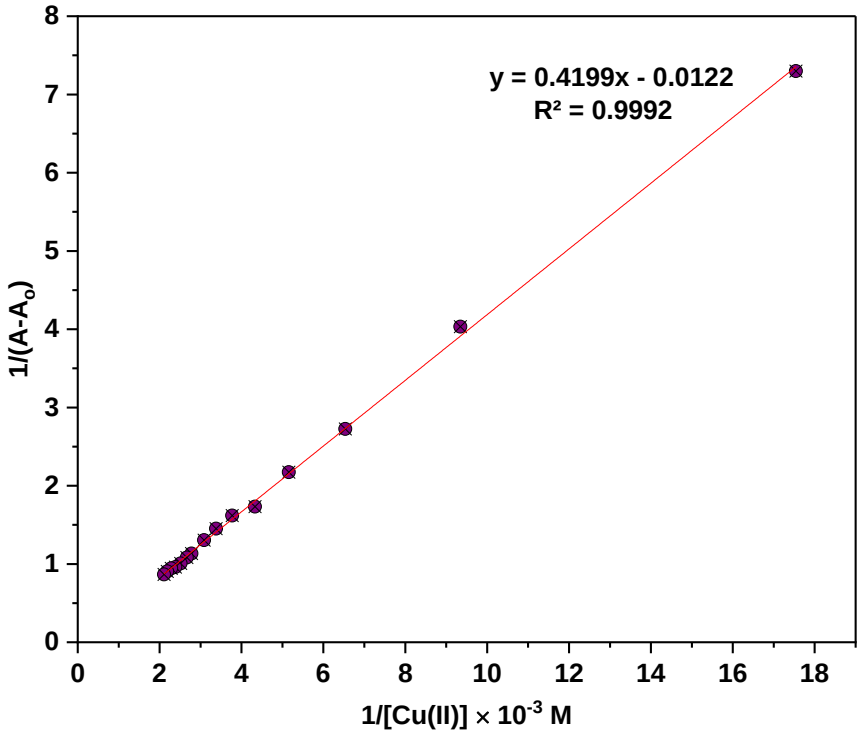

Figure 4.80: Benesi-Hildebrand plot for probe **150**-Cu(II) complexation

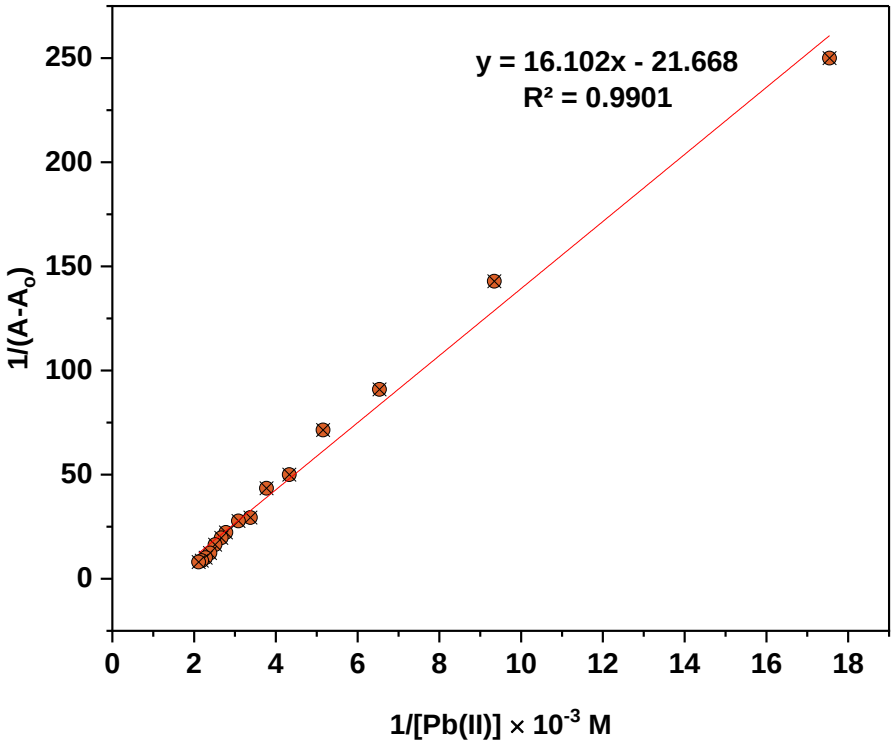

Figure 4.81: Benesi-Hildebrand plot for probe **150**-Pb(II) complexation

4.20.3. Chemosensing response of probe 150 for Cu(II) and Pb(II) via fluorescence spectroscopy

To further investigate the ion-binding properties of probe **150**, the fluorescence emission of a 20 μM probe **150** solution was monitored, wherein the probe when excited at 270 nm, showed a monomer emission at about 324 nm and a weak excimer emission at about 617 nm, attributed to the π-π interactions of the naphthyl moieties. When testing probe **150**'s selective ion recognition behaviour for Cu(II), it was observed that the emission intensity of the probe decreased dramatically as more and more Cu(II) ions were added, reaching a minimum at 15 equiv. of Cu(II). The development of the probe **150**-Cu(II) complex was accountable for the drop in fluorescence intensity since it resulted in a charge transfer from the metal to the ligand. The d^9 electronic structure of Cu(II) often results in chelation-enhanced fluorescence quenching (CHEQ) effect throughout the formation of its metal complex, and the results obtained in this case were in line with expectations.

When it came to Pb(II) ions, their gradual introduction into solution of probe **150** resulted in a modest red shift of the λ_{em} and an intense enhancement of the fluorescence emission, suggesting the formation of a probe **150**-Pb(II) complex. In the presence of Pb(II), the amplification of the monomer emission as well as the excimer emissions of the probe were ascribable to chelation-enhanced fluorescence (CHEF). **Figure 4.82** and **figure 4.83** represent the fluorescence spectra of the probe on incrementally adding Cu(II) and Pb(II) ions respectively, wherein the inset displays the relative emission change against metal ion concentration. Moreover, from the correlation plots exhibiting relative emission intensity $(I-I_o)/I_o$ against the metal ion concentration, the LoD and LoQ were calculated for Cu(II) and Pb(II) ions, using the widely used criteria of LoD = 3σ/S and LoQ = 10σ/S, where σ is the blank standard deviation and S is the slope of the calibration curve, as shown in **figure 4.84** and **figure 4.85** respectively. It was found that the LoD for Cu(II) was 3.16 μM and for Pb(II) it was 2.52 μM, whereas the LoQ was 10.53 μM and 8.40 μM. In addition, the correlation plots showed that the stoichiometric ratio was 1:1 in both instances. The stoichiometric ratio, K_a, and the values for LoD and LoQ have been tabulated in **table 4.5**

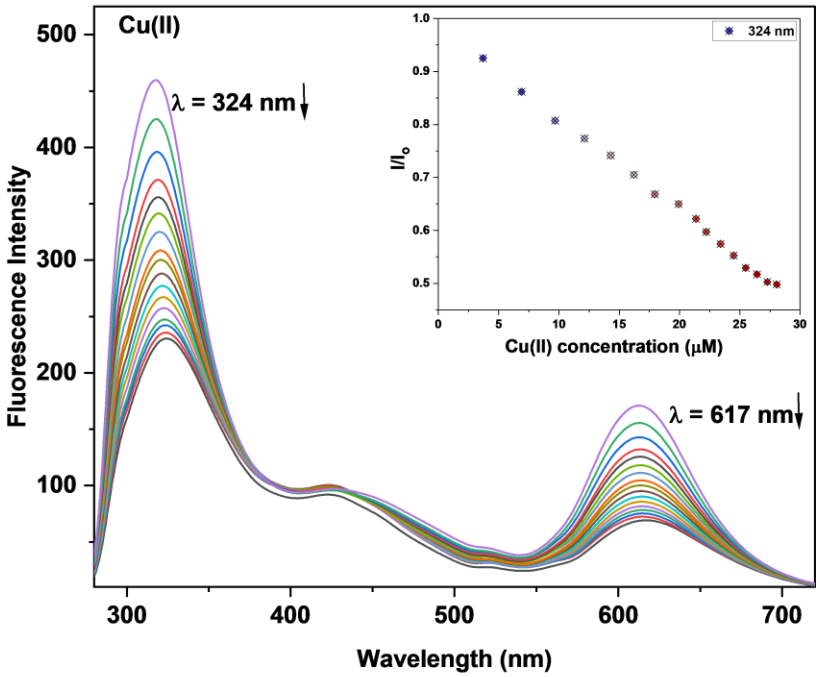

Figure 4.82: Fluorescence spectra of probe **150** (20 μM) upon the progressive addition of Cu(II) ions in DMSO; the inset exhibits the relative emission change (I/I_o) vs metal ion concentration (μM)

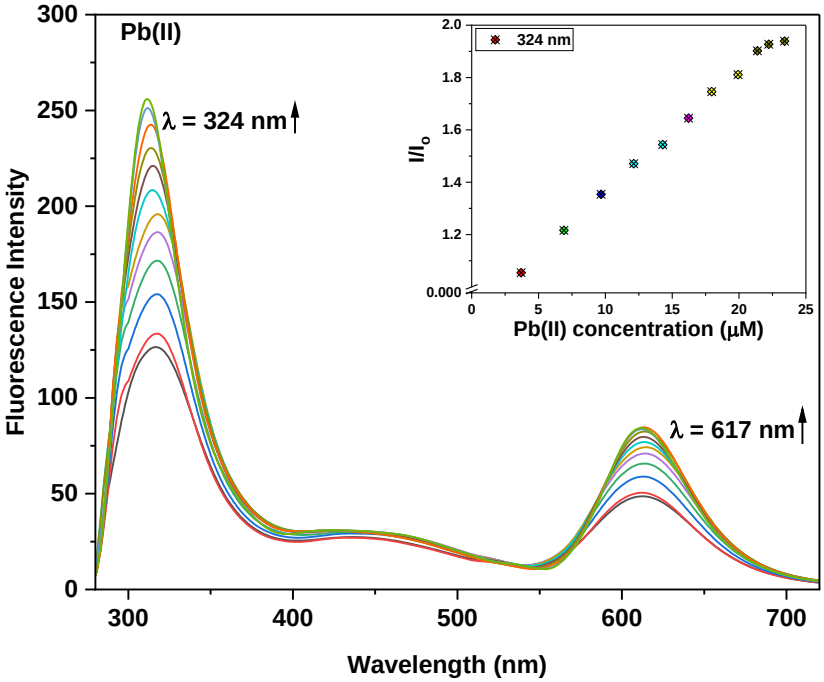

Figure 4.83: Fluorescence spectra of probe **150** (20 μM) upon the progressive addition of Pb(II) ions in DMSO; the inset exhibits the relative emission change (I/I_o) vs metal ion concentration (μM)

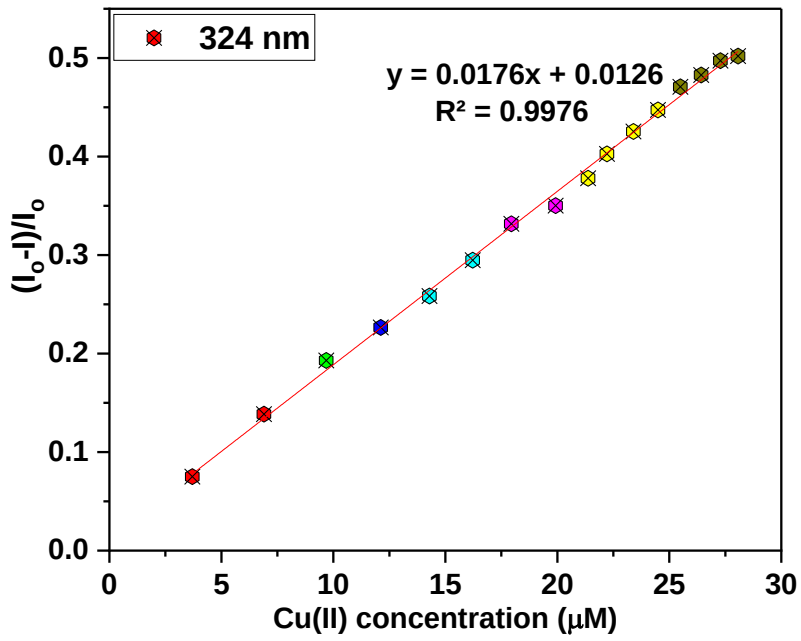

Figure 4.84: Correlation plot of relative fluorescence emission of probe **150** $(I_o\text{-}I)/I_o$ as a function of Cu(II) concentration; where I_o = initial emission of probe **150** and I = emission of probe **150** in the presence of Cu(II)

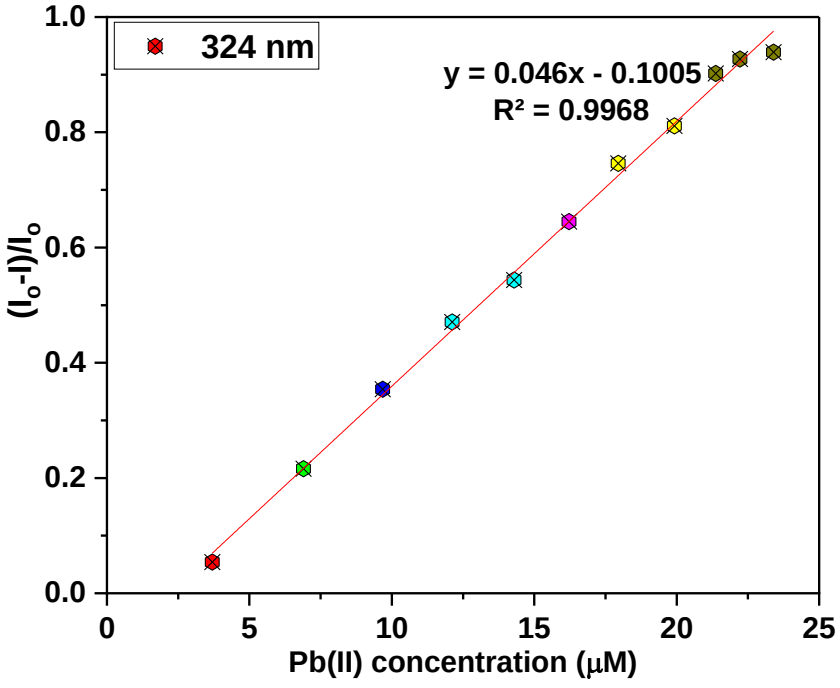

Figure 4.85: Correlation plot of relative fluorescence emission of probe **150** $(I_o\text{-}I)/I_o$ as a function of Pb(II) concentration; where I_o = initial emission of probe **150** and I = emission of probe **150** in the presence of Pb(II)

Probe	Metal ion	LoD (µM)	LoQ (µM)	Association Constant (K_a)	Stoichiometry (M:L)
150	Cu(II)	3.16	10.53	$1.16 \times 10^3\ M^{-1}$	1:1
	Pb(II)	2.52	8.40	$1.10 \times 10^3\ M^{-1}$	1:1

Table 4.5: LoD, LoQ, K_a and stoichiometric ratio values of probe **150** on binding with Cu(II) and Pb(II)

4.20.4. Competitive metal ion interaction analysis

An essential characteristic exhibited by some potential metal ion sensors is their capacity to selectively detect specific metal ions among other competing metal ions. In the presence of other metal ions, the chemosensor **150** was shown to be effective using competitive ions titration for specifically detecting Pb(II). The process of ion titration involved the incremental introduction of a solution containing multiple metal ions at equimolar concentrations into the probe solution at a concentration of 50 µM, dissolved in DMSO. Absorption spectrum observed after titrations (**figure 4.86**) revealed that the ability of the sensor probe to selectively detect Pb(II) was unaffected by the presence of other metal ions.

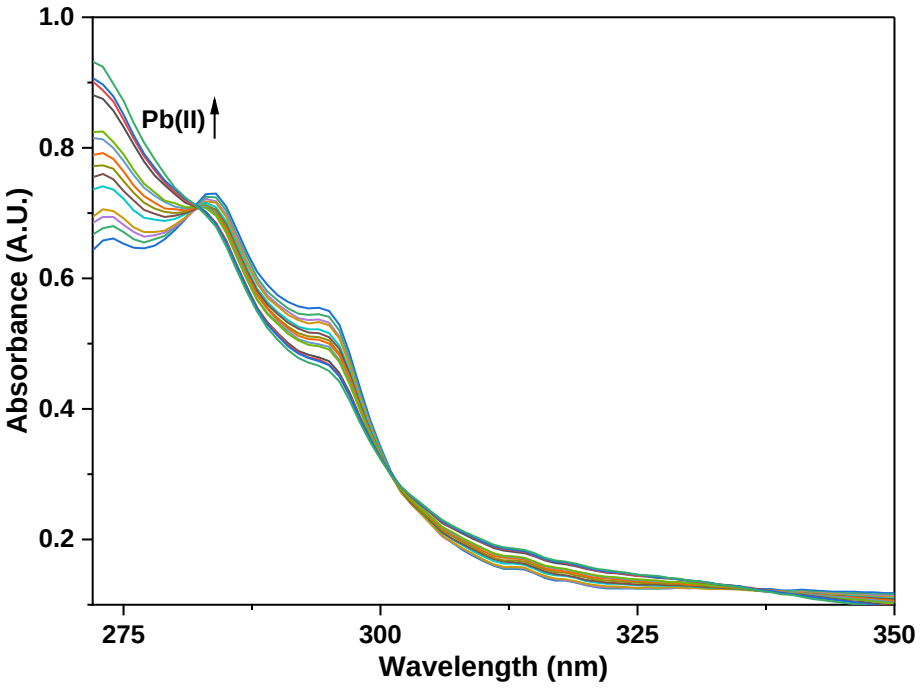

Figure 4.86: Absorption spectra of probe **150** (0.5 mM) in DMSO recognizing Pb(II) ions among several metal ions at equimolar concentrations

4.20.5. Time dependence analysis of probe 150-metal ion complexation

To comprehend the probe's sensitivity towards metal ions, it is necessary to examine its reaction to temporal fluctuations. The technique of absorption spectroscopy was employed to investigate the temporal evolution of the metal-bound probe **150**, and the findings (**figure 4.87**) were suggestive of the fact that the absorbance of Cu(II)-bound and Pb(II)-bound probe **150** solutions exhibited no substantial change despite keeping them undisturbed for long periods of time. This established that the binding of the chemosensor with the metal ions was stable and strong.

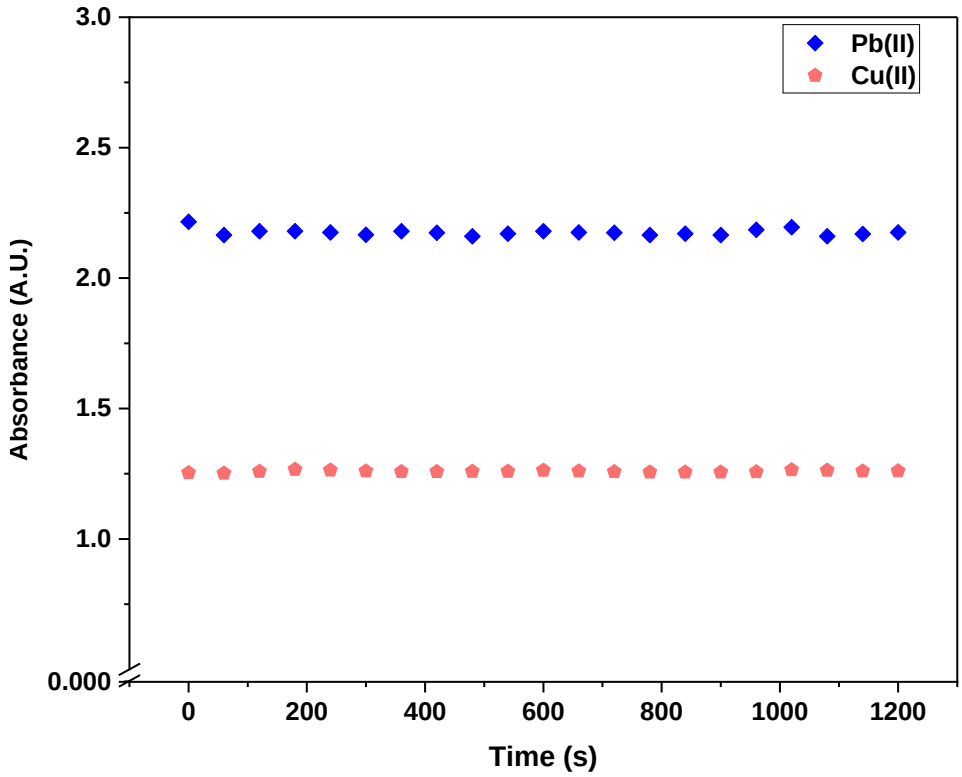

Figure 4.87: Time dependent absorption spectrum of probe **150**-Cu(II)/Pb(II) exhibiting a constant absorbance at 284 nm

4.20.6. Temperature dependence analysis of probe 150-metal ion complexation

The efficiency of binding of the probe with the metal ions was also assessed at various temperature levels to observe the impact of the latter on the ion sensing potential of the probe. To demonstrate that the Cu(II) and Pb(II) binding to the probe was temperature-insensitive, the absorption spectra of metal-bound probe **150** solutions at 2 °C intervals from 20 °C up to 50 °C (**figure 4.88**) was obtained, wherein it was observed that the absorption of metal-bound probe **150** solution was insensitive to temperature variation across these temperature ranges.

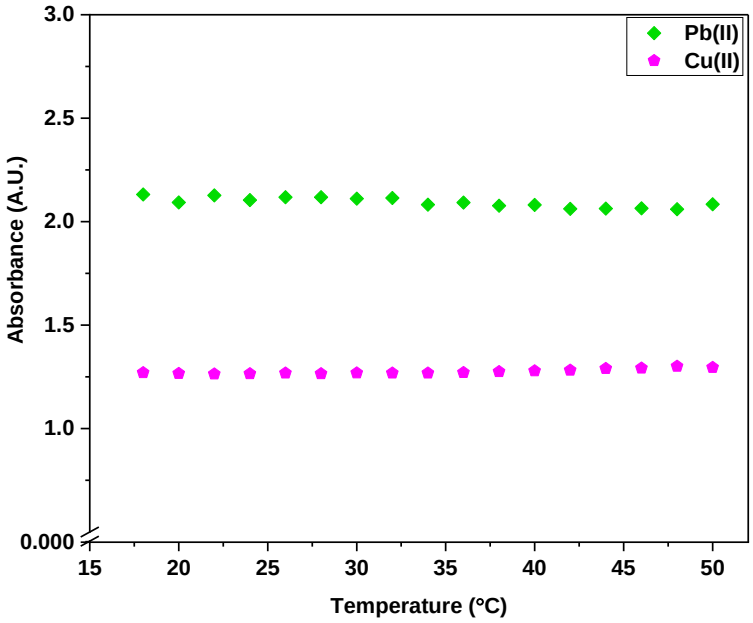

Figure 4.88: Temperature dependent absorption spectrum of probe **150**-Cu(II)/Pb(II) exhibiting constant absorbance over a temperature range of 20 - 50 ºC

4.20.7. Plausible binding mode

The HSAB theory states that Cu(II) is a borderline acid whereas Pb(II) is a weak acid. Coordination bonds can be established between metal ions and atomic groups that possess lone pairs, including N, O, and S. The probe **150** can be ascribed to be able to capture the incoming metal ions because of the presence of lone pairs of N atoms on the 1,2,3-triazole moiety incorporated within its structure. As expected from the probe's Job plot, it forms a 1:1 metal-ligand combination with Cu(II) and Pb(II). From these findings, the manner of interaction of the receptor **150** with the metal ions can be inferred, as shown in **figure 4.89**. Rest of the coordination sites are expected to be filled by the solvent molecules.

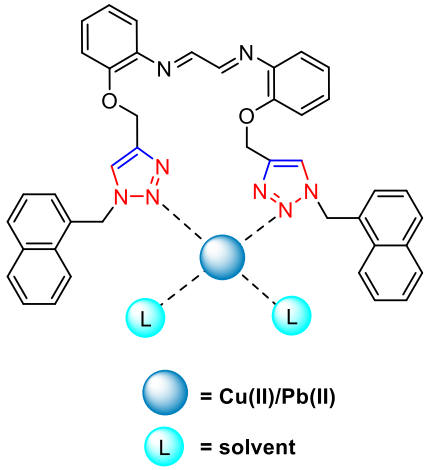

Figure 4.89: Proposed interaction between probe **150** and Cu(II)/Pb(II)

4.21. Chemosensing analysis of Schiff base-derived 1,2,3-triazole derivative 155

4.21.1. Ion recognition analysis of Schiff base-derived 1,2,3-triazole derivative 155

The newly synthesised Schiff base-derived 1,2,3-triazole derivative **155** was examined for its chemosensing potential against a variety of metal chlorides using UV-Vis and fluorescence spectroscopy. The molecule was synthesized starting from the combination of an aldehyde and an amine to form a Schiff base, which possesses C=N functionality in addition to the aromatic functionalities of the parent compounds, thereby imparting it the ability to exhibit $\pi \rightarrow \pi^*$ as well as $n \rightarrow \pi^*$ transitions which in turn yields fine quality absorption and/or emission spectrum.

Besides, other fluorophore moieties attached to this compound by subjecting it to the CuAAC methodology further improved the molecular design to obtain the desirable results. Above and beyond, the 1,2,3-triazole moiety attached to the Schiff base functionality also acted as an electron-rich receptor sites owing to the N atoms, thereby enhancing the probability of the probe to act as a selective metal ion recognition agent. As a result, the end product was a robust molecule with chemosensing capabilities.

When utilized as a sensing probe, the Schiff base-derived 1,2,3-triazole derivative **155** produced fine and interpretable spectrum data. For determining the ion sensing potential of the probe, DMSO/H_2O (4:1) was chosen as the solvent as it exhibited good solubility and spectral results.. The ideal concentration of probe **155** solution was determined to be 0.1 mM and was then used for UV-Vis investigations. The greatest absorption (λ_{max}) was measured at 284 nm, corresponding to an intensity of 0.76. Subsequently, chlorides of Mg(II), Ca(II), Ba(II), Cr(III), Mn(II), Co(II), Ni(II), Zn(II), Cd(II), Hg(II), Pb(II), Na(I), K(I), and Ce(III) were prepared in DMSO/H_2O (4:1) (0.5 mM) and the probe was examined for sensing behaviour with these physiologically and ecologically relevant metal ion solutions. Significant changes in the probe's absorption spectra were seen when metal ion solution of Ce(III) was gradually introduced, whereas no significant change was found for the other ions, as indicated in the **figure 4.90**.

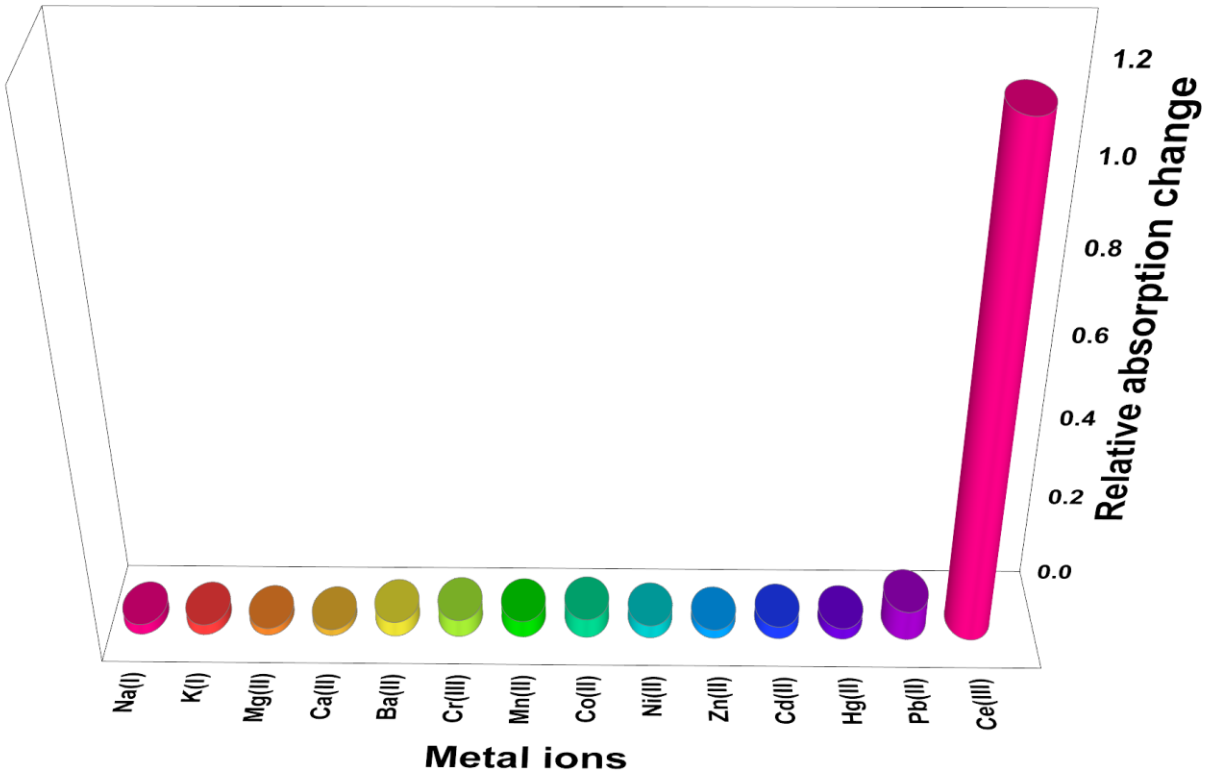

Figure 4.90: An illustration of the relative absorption change of probe **155** for several metal ions in DMSO/H_2O (4:1) solvent

4.21.2. Chemosensing response of probe 155 for Ce(III) via UV-Vis spectroscopy

The metal ion recognition potential of probe **155** with Ce(III) ions was investigated by successively adding a solution of Ce(III) ions (0.5 mM) to a 0.1 mM probe **155** solution and observing the absorption spectra after every addition. The binding of Ce(III) to the probe was confirmed by a substantial hyperchromic shift, concomitant with a red shift of about 23 nm, thereby leading to the shifting of λ_{max} from 284 nm to 307 nm when Ce(III) ions were progressively intorduced to the ligand solution, as depicted in the **figure 4.91**; the inset depicts the relative maximum absorbance change (A_n/A_o) as a function of the increase in Ce(III) molar concentration. Additionally, the K_a value for the 1:1 probe **155**-Ce(III) complexation was calculated using the B-H equation (A), which came out to be 3.55×10^3 M^{-1}, while the B-H graph is depicted in **figure 4.92**.

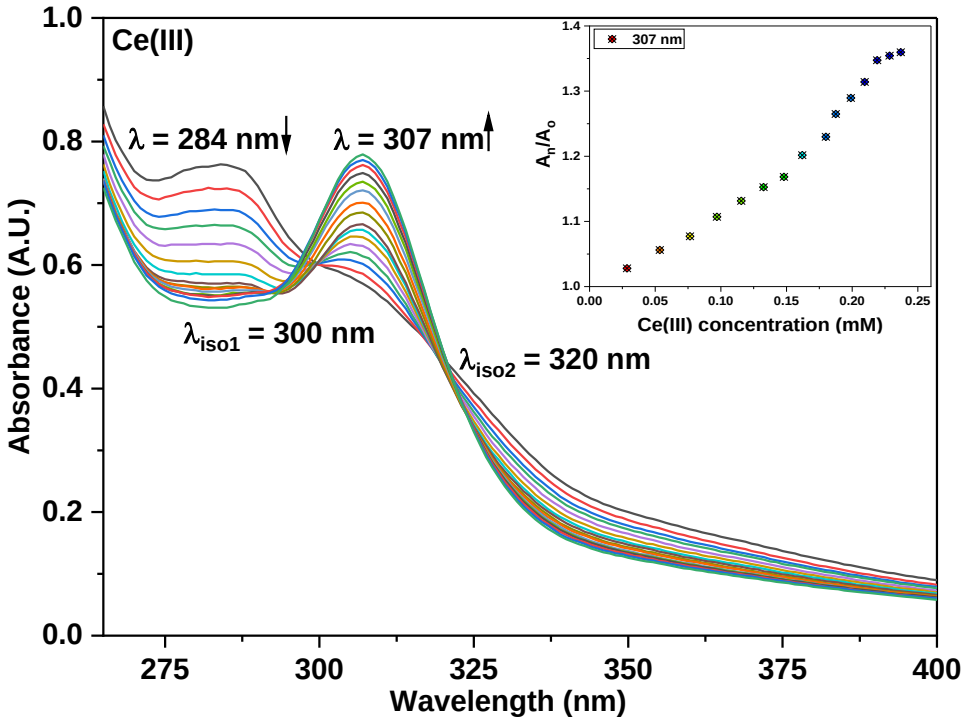

Figure 4.91: UV-Vis spectra of probe **155** (0.1 mM) upon the progressive addition of Ce(III) in DMSO/H_2O (4:1); the inset exhibits the relative absorbance change (A_n/A_o) vs metal ion concentration (mM)

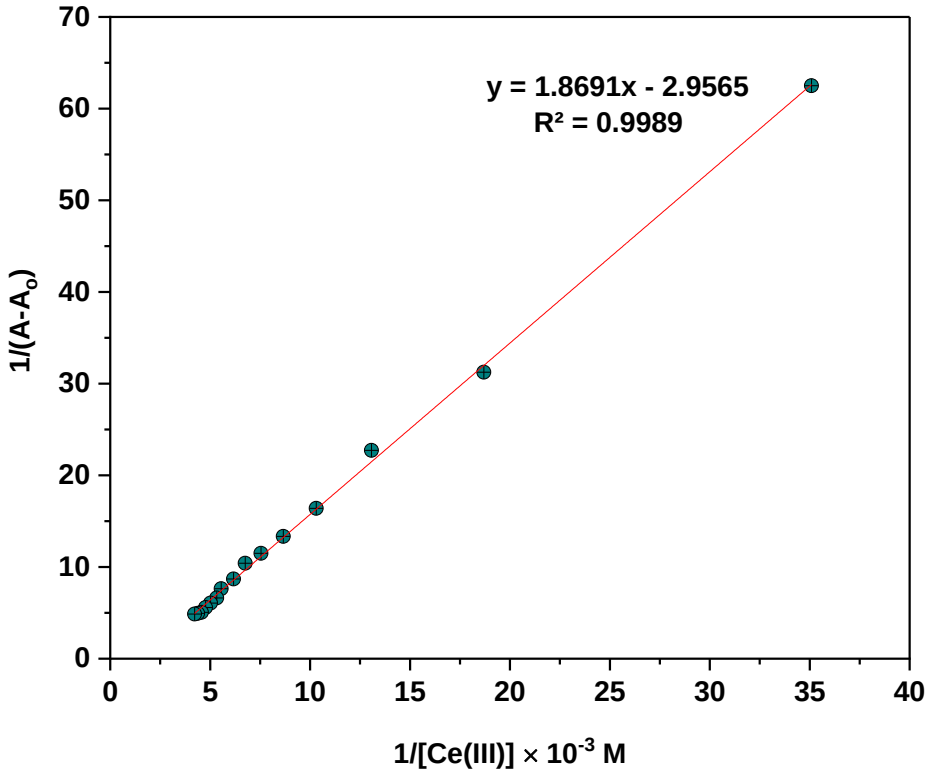

Figure 4.92: Benesi-Hildebrand plot for probe **155**-Ce(III) complexation

4.21.3. Chemosensing response of probe 155 for Ce(III) via fluorescence spectroscopy

The ion-binding properties of probe **155** were further studied by monitoring the fluorescence emission of a 50 µM probe **155** solution, which revealed a monomer emission at around 313 nm and a weak excimer emission at around 611 nm, ascribable to π-π interactions of the benzyl moieties. The emission of the solution of probe **155** significantly enhanced when Ce(III) ions were incrementally introduced into the probe **155** solution, reaching a maximum intensity at 15 equiv. of Ce(III). The relative emission change vs the concentration of metal ions is shown in the inset of the **figure 4.93** depicting the probe's fluorescence spectrum after incremental addition of Ce(III) ions. LoD = 3σ/S and LoQ = 10σ/S, where σ is the standard deviation of blank and S is the slope of the calibration curve, were applied to the correlation plot (**figure 4.94**) displaying relative emission intensity $(I_o\text{-}I)/I_o$ versus Ce(III) concentration to determine the LoD and LoQ for Ce(III) ions. It was determined that the LoD was 9.53 µM, whereas the LoQ value was 31.75 µM. The stoichiometric ratio was also shown to be 1:1 using the correlation plot. The values for LoD and LoQ as well as the stoichiometric ratio, Ka, are reported in **table 4.6**

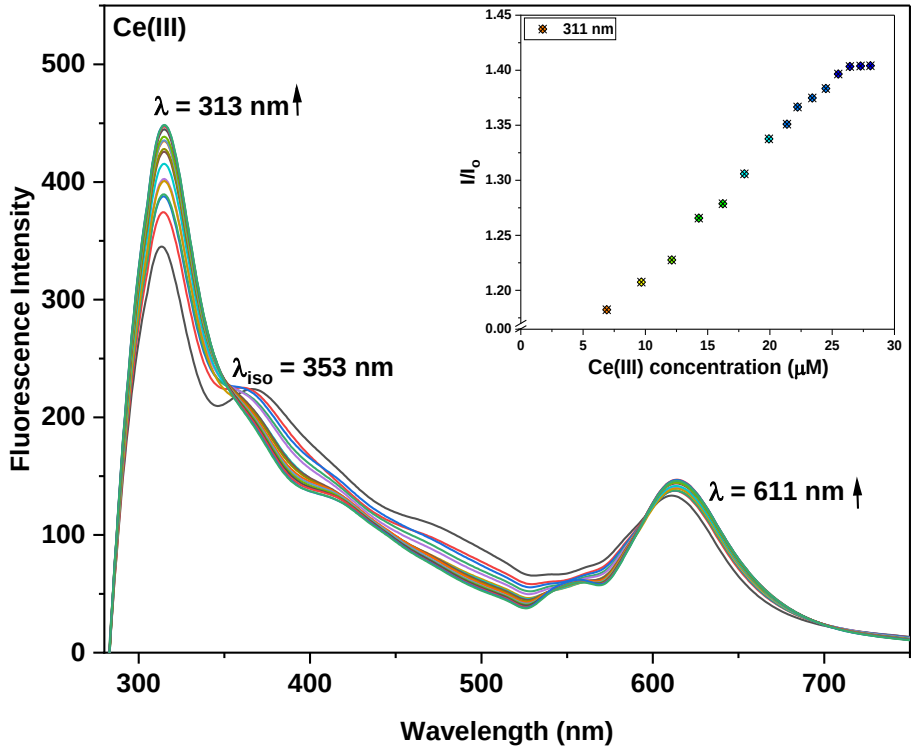

Figure 4.93: Fluorescence spectra of probe **155** (50 µM) upon the progressive addition of Ce(III) ions in DMSO/H_2O (4:1); the inset exhibits the relative emission change (I/I_o) vs metal ion concentration (µM)

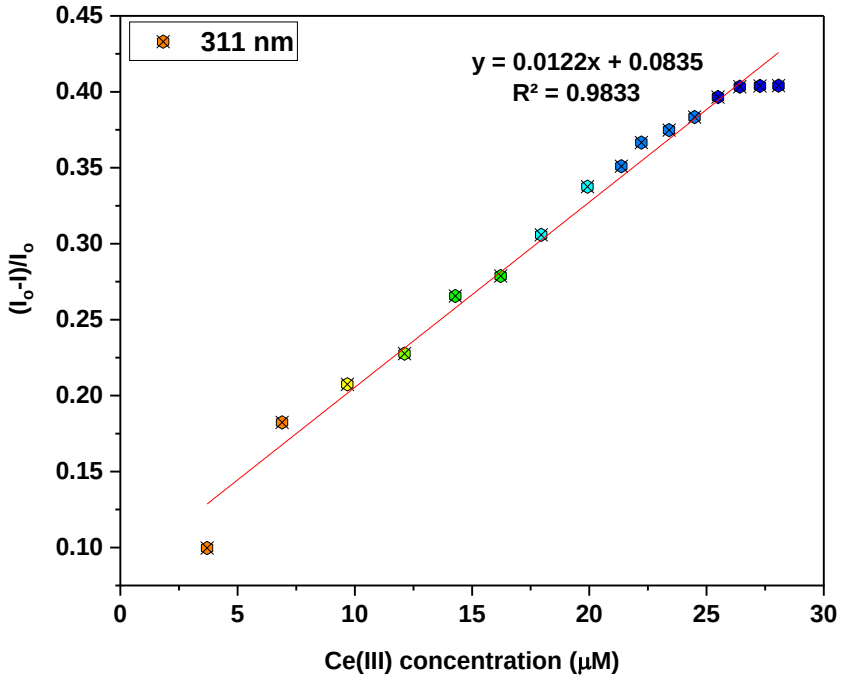

Figure 4.94: Correlation plot of relative fluorescence emission of probe **155** $(I_o\text{-}I)/I_o$ as a function of Ce(III) concentration; where I_o = initial emission of probe **155** and I = emission of probe **155** in the presence of Ce(III)

Probe	Metal ion	LoD (μM)	LoQ (μM)	Association Constant (K_a)	Stoichiometry (M:L)
155	Ce(III)	9.53	31.75	$3.55 \times 10^3\ M^{-1}$	1:1

Table 4.6: LoD, LoQ, K_a and stoichiometric ratio values of probe **155** on binding with Ce(III)

4.21.4. Competitive metal ion interaction analysis

The selective detection capability of various potential metal ion sensors, distinguishing specific metal ions from competing ones, represents a fundamental attribute. In the presence of other metal ions, the probe **155** was proven to be effective for precisely detecting Ce(III) utilizing competitive ions titration, which was performed by progressively adding an equimolar quantity of several metal ions to the 0.1 mM probe solution. The absorption spectrum, as depicted in Figure 4.95, obtained subsequent to the titration experiments, revealed that the presence of alternative metal ions did not exert any influence on the sensor probe's capacity to detect Ce(III).

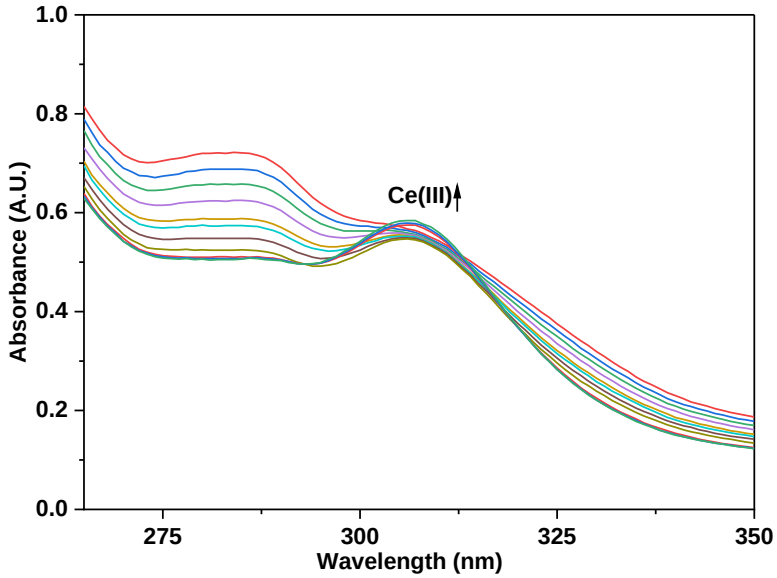

Figure 4.95: Absorption spectra of probe **155** (0.1 mM) in DMSO/H_2O (4:1) recognizing Ce(III) ions among several metal ions at equimolar concentrations

4.21.5. Time dependence analysis of probe 155-metal ion complexation

Investigating the way in which the metal ions-appended probe behaves with variations in time might offer useful information on the sensitivity of the probe to metal ions. The influence of time on the metal-bound probe **155** was investigated through absorption spectroscopy, and the results (**figure 4.96**) indicated that the absorbance of Ce(III)-bound probe **155** solution did not display any significant change despite being left to stand for extended periods of time. This demonstrated that the probe has a great affinity for Ce(III) as well as a high degree of stability of the complexation.

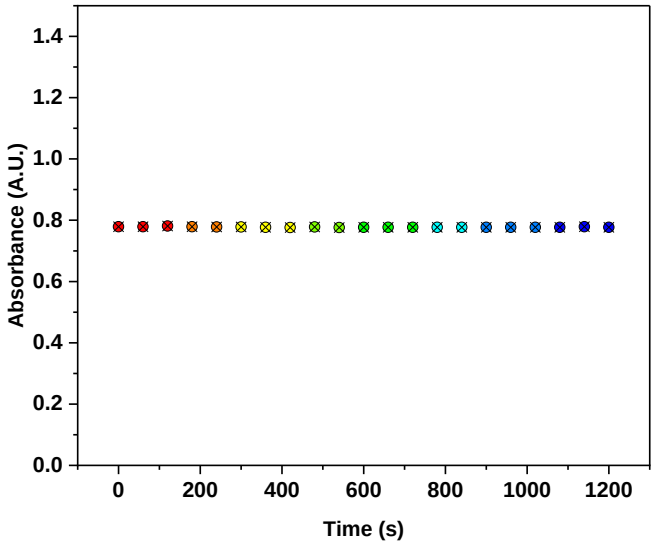

Figure 4.96: Time dependent absorption spectrum of probe **155**-Ce(III) exhibiting a constant absorbance at 307 nm

4.21.6. Temperature dependence analysis of probe 155-metal ion complexation

The influence that varying temperatures had on the effectiveness with which the sensor probe bound with the metal ion was investigated. After obtaining the absorption spectra of metal-bound probe **155** solutions from 20 °C up to 50 °C at every 2 °C intervals (**figure 4.97**), it was observed that the absorption of metal-bound probe **155** solution was insensitive to temperature variation across these temperature ranges. The results corroborated that the probe-metal ions interaction exhibited temperature insensitivity.

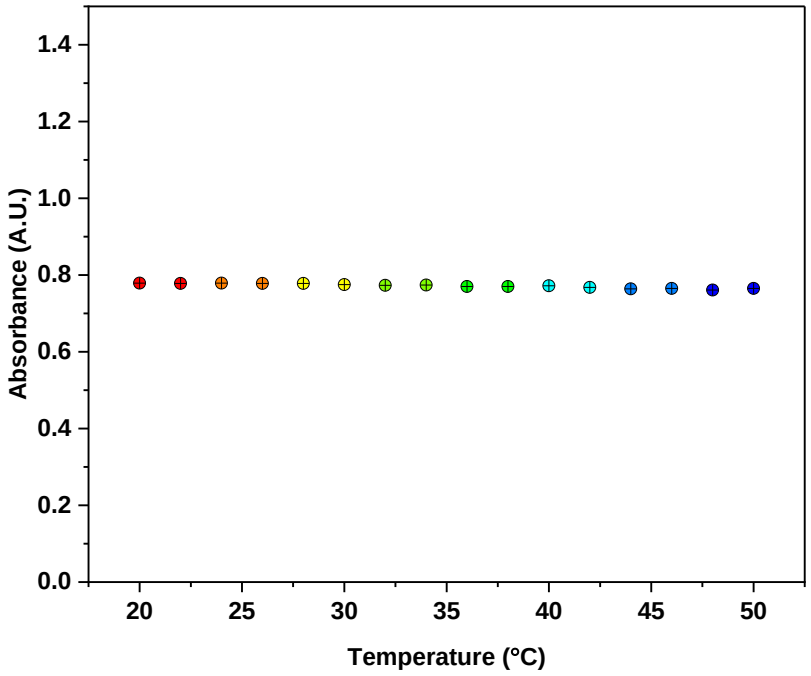

Figure 4.97: Temperature dependent absorption spectrum of probe **155**-Ce(III) exhibiting constant absorbance over a temperature range of 20 - 50 ºC

4.21.7. Plausible binding mode

Ce(III) is regarded as a hard acid in accordance with the HSAB hypothesis. The metal ion may form coordination bonds with atomic groups including N, O, and S which carry lone-pair electrons. Owing to the presence of lone pairs of N atoms within the 1,2,3-triazole moiety included in the structure of probe **155**, it is hypothesised that probe **155** is able to grab the incoming metal ions via these receptor sites. The Job plot shows that the probe forms a 1:1 metal-ligand complex with Ce(III), and therefore, these results allowed us to deduce, as seen in **figure 4.98**, how the receptor probe **155** might be able to bind to the metal ions. Rest of the coordination sites are expected to be filled by the solvent molecules.

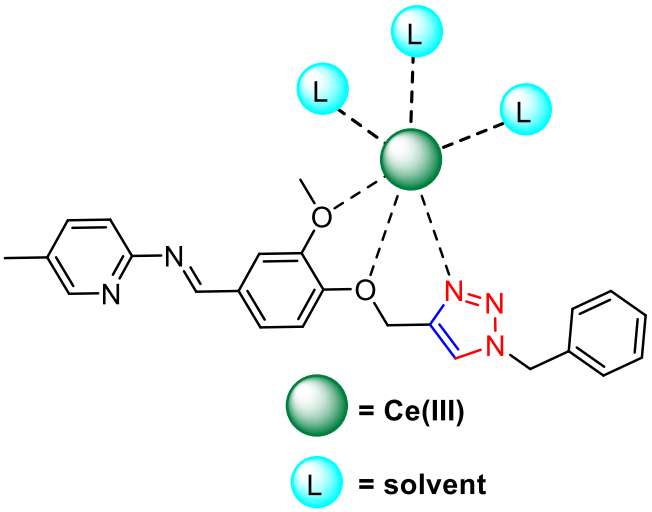

Figure 4.98: Proposed interaction between probe **155** and Ce(III)

Concluding from the observed results, in the specific context of metal ion sensing, 1,2,3-triazole derivatives stand out as promising ligands, leveraging the HSAB concept and host-guest relationship for the selective recognition of metal ions. The nitrogen atoms within the triazole ring facilitate multifaceted interactions with the metal ions, as the nitrogen and/or oxygen atoms bearing lone pair of electrons act as lewis bases whereas the metal ions which are electron deficient act as lewis acids. Furthermore, the host-guest relationship involves 1,2,3-triazole derivatives providing a suitable sized cavity for the meal ions as hosts and metal ions as the guests, yielding stable complexes characterized by discernible electronic configurations. Through deliberate molecular design, these 1,2,3,-triazole-based ligands serve as effective sensors, demonstrating heightened sensitivity and specificity in detecting targeted metal ions. These findings affirm the efficacy of 1,2,3-triazole derivatives as sensors, showcasing their potential as robust tools in analytical chemistry, which further contributes significantly to the advancement of analytical chemistry methodologies, particularly in the realm of metal ion detection.

4.22. Conclusion

In conclusion, the interpretation of spectroscopic data for the synthesized compounds through spectroscopic methods such as Infrared spectroscopy, Nuclear Magnetic Resonance (NMR) spectroscopy, and Mass spectrometry discussed in this chapter has provided invaluable insights into the structural and chemical properties of these compounds, aiding in the identification of functional groups, and unravelling the intricate details of molecular structures. The IR spectroscopic data revealed vital information about the functional groups present in the compounds under investigation. The absorption peaks in the IR spectra provided evidence of

the presence of key chemical bonds and allowed for the determination of compound purity. Moreover, the identification of characteristic peaks aided in confirming the success of the synthesis process. NMR spectroscopy played a pivotal role in elucidating the molecular structure of the compounds. By examining chemical shifts, coupling patterns, and integration values, a deeper understanding of the connectivity of atoms within the molecules was established. Mass spectrometry provided valuable data regarding the molecular weight and fragmentation patterns of the synthesized compounds. It offered insights into the stability of the molecules and allowed for the identification of specific fragments, aiding in the determination of their structural components.

Additionally, the synthesized N-heterocyclic 1,2,3-tethered ensembles, were explored as selective recognition agents for different ecologically and physiologically significant metal ions. The molecules were designed from commercially available compounds having labile protons and fine aromaticity which were subjected to 'click' pathway after converting them to terminal alkynes via nucleophilic substitution with propargyl groups. The resulting 1,2,3-triazole derivatives were well equipped with chromogenic/fluorogenic units, thereby allowing for better absorption/emission results which were interpreted, after metal ion addition, to analyze their selective ion recognition behaviour. The selectivity of the sensing probes was observed to diversify with the variation in the structural arrangement of the probe, thereby resulting in the alteration of the size and/or flexibility of the receptor cavity which was responsible for distinct selectivity in every compound. The probes were also scrutinized for the robustness of their binding with the metal ions by subjecting them to absorption analysis over prolonged durations of time as well as different temperature ranges. The analytical determination of the limit of detection (LoD), limit of quantification (LoQ), association constant (K_a), and stoichiometric ratio of the probe-metal ion complexation was also performed to elucidate the interaction between the metal ions and the recognition probes.

References

1 H. Mach, D. B. Volkin, C. J. Burke and C. R. Middaugh, *Methods. Mol. Biol.*, 1995, **40**, 91–114.

2 W. Mäntele and E. Deniz, *Spectrochim. Acta A Mol. Biomol. Spectrosc.*, 2017, **173**, 965–968.

3 U. Platt and J. Stutz, in *Differential Optical Absorption Spectroscopy*, Springer Berlin Heidelberg, 2008, vol. 174, pp. 135–174.

4 J. W. Farley, W. C. Brumley and D. L. Eastwood, in *Encyclopedia of Spectroscopy and Spectrometry*, eds. J. C. Lindon, G. E. Tranter and D. W. Koppenaal, Elsevier Ltd., Amsterdam, 3rd edn., 2016, pp. 452–458.

5 A. A. Edwards and B. D. Alexander, in *UV-visible absorption spectroscopy, organic applications*, Elsevier Ltd., 3rd edn., 2016.

6 G. E. Tranter, in *UV-visible absorption and circular dichroism spectroscopy, inorganic chemistry applications*, Elsevier Ltd., 3rd edn., 2016.

7 G. A. Rance, D. H. Marsh, R. J. Nicholas and A. N. Khlobystov, *Chem. Phys. Lett.*, 2010, **493**, 19–23.

8 B. P. Kafle, in *Chemical Analysis and Material Characterization by Spectrophotometry*, Elsevier Ltd., 1st edn., 2020, 17–38.

9 R. Nagarajan, C. Varadaraju and K. H. Lee, *Dyes Pigm.*, 2021, **191**, 109331.

10 T. Förster, *Zeitschrift fur Physikalische Chemie*, 1957, **11**, 406.

11 G. Singh, J. Singh, S. S. Mangat and A. Arora, *RSC Adv.*, 2014, **4**, 60853–60865.

12 K. Gupta, P. Joshi, R. Gusain and O. P. Khatri, *Coord. Chem. Rev.*, 2021, **445**, 214100.

13 A. Kaur, Z. Lim, K. Yang and E. J. New, in *Comprehensive Supramolecular Chemistry II*, ed. J. L. Atwood, Elsevier, Amsterdam, 2nd edn., 2017, vol. 8, pp. 295–317.

14 Y. Jeong and J. Yoon, *Inorganica Chim. Acta*, 2012, **381**, 2–14.

15 M. Formica, V. Fusi, L. Giorgi and M. Micheloni, *Coord. Chem. Rev.*, 2012, **256**, 170–192.

16 B. Pedras, V. Rosa, R. Welter, C. Lodeiro and T. Avilés, *Inorganica Chim. Acta*, 2012, **381**, 143–149.

17 R. Joseph, *ACS Omega*, 2020, **5**, 6215–6220.

18 G. C. Midya, S. Paladhi, S. Bhowmik, S. Saha and J. Dash, *Org. Biomol. Chem.*, 2013, **11**, 3057–3063.

19 K. Vishwanath and N. Ramanujam, in *Encyclopedia of Analytical Chemistry*, 2011 John Wiley & Sons, NJ, USA.

20 C. A. Royer, in *Methods in Molecular Biology*, ed. B. A. Shirley, Humana Press Inc., Totowa, NJ, ch. 3, pp. 65-89.

21 R. Karoui, in *Modern Techniques for Food Authentication*, ed. D. W. Sun, Elsevier Inc., 2nd edn., 2018, ch. 7, pp. 219-252.

22 G. M. Strasburg and R. D. Ludescher, *Trends Food Sci. Technol.*, 1995, **6**, 69–75.

23 N. Boens, W. Qin, N. Basarić, J. Hofkens, M. Ameloot, J. Pouget, J. P. Lefèvre, B. Valeur, E. Gratton, M. VandeVen, N. D. Silva, Y. Engelborghs, K. Willaert, A. Sillen, G. Rumbles, D. Phillips, A. J. W. G. Visser, A. Van Hoek, J. R. Lakowicz, H. Malak, I. Gryczynski, A. G. Szabo, D. T. Krajcarski, N. Tamai and A. Miura, *Anal. Chem.*, 2007, **79**, 2133–2149.

24 F. V. Bright, *Anal. Chem.*, 1988, **60**, 1031A-1039A.

25 S. Weiss, *Science*, 1999, **283**, 1676–1683.

26 K. R. Murphy, C. A. Stedmon, D. Graeber and R. Bro, *Anal. Methods*, 2013, **5**, 6557–6566.

27 E. M. Carstea, J. Bridgeman, A. Baker and D. M. Reynolds, *Water Res.*, 2016, **95**, 205–219.

28 B. N. Dai, Q. Y. Cao, L. Wang, Z. C. Wang and Z. Yang, *Inorganica Chim. Acta*, 2014, **423**, 163–167.

29 B. xing Shen and Y. Qian, *Sens. Actuators B Chem.*, 2017, **239**, 226–234.

30 J. H. Zhu, X. T. Fan and Q. Y. Cao, *Inorganica Chim. Acta*, 2016, **451**, 111–115.

31 X. Huang, J. Meng, Y. Dong, Y. Cheng and C. Zhu, *Polymer*, 2010, **51**, 3064–3067.

Thesis overview

Summary

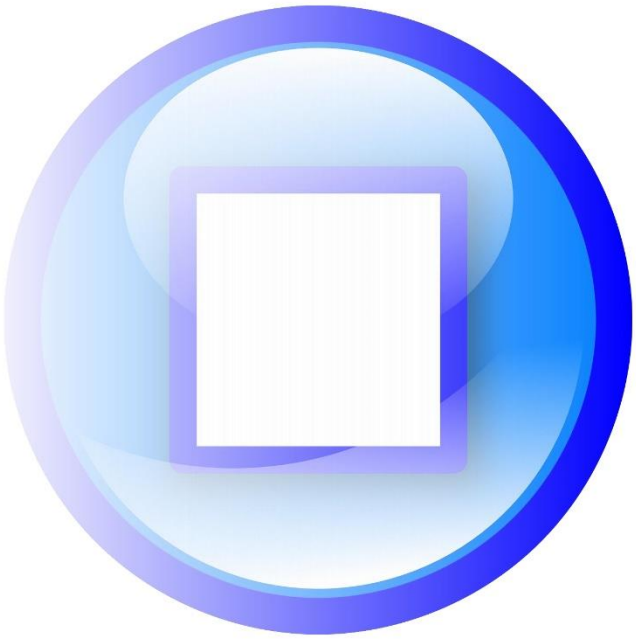

This chapter summarises the whole thesis in a few concise paragraphs, providing an overview of the methodology, experimental data, and outcomes.

Dr. M. Meldal's invention of the CuAAC reaction in 2001, which nicely coincided with Dr. K.B. Sharpless's broad characterization of the need for such click chemistry, was a case in point. The prevalence of the quintessential CuAAC click reaction, which is employed extensively across all fields of chemistry to synthesize molecules of inconceivable chemical complexity, may be attributed to the fact that it complies with the laws that govern click chemistry. The current study activity covers the implementation of CuAAC 'click' methodology to synthesize 1,2,3-triazole-appended molecules, their subsequent characterization using standard spectroscopic methods, and their application as selective metal ion recognition agents via absorption and emission spectroscopy. The whole thesis may be broken down into four primary sections: The first chapter is the **introduction**, the second chapter is a **review of literature**, the third chapter describes the **synthetic procedures and characterization data**, and the fourth chapter presents the **interpretation and discussion of spectroscopic and photophysical data**.

Chapter I: Introduction

This chapter provides a comprehensive analysis of the key class of 'click chemistry' known as the Cu(I)-catalyzed alkyne-azide cycloaddition reaction (CuAAC) (**figure S1**) and its further application in the synthesis of 1,4-disubstituted 1,2,3-triazoles as potential ion recognition agents. The chapter is divided into subsections that detail the many features as well as mechanistic characteristics of the CuAAC reaction, followed by the significance of the 1,4-disubstituted 1,2,3-triazole derivatives formed via this cycloaddition. Initiating by providing a general prespective of 'click chemistry' and the distinct reaction pathways that share this common trajectory, the major focus of this chapter is the description of 1,3-dipolar cycloaddition processes, which were first explored in the late 19th and early 20th centuries when a variety of 1,3-dipoles were developed. After Dr. K. B. Sharpless achieved the same reaction in 2001 using Cu(I) as catalyst, it became a major scientific breakthrough worldwide, owing to the enhanced reaction rate, and regioselective production of 1,4-disubstituted 1,2,3-triazole in high yield and purity, under modest reaction conditions.

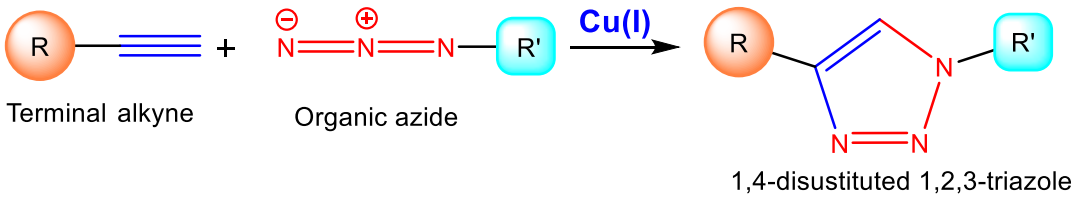

Figure S1: An illustration of Cu(I)-catalyzed alkyne-azide cycloaddition

A description of the mechanistic aspects of CuAAC, discussing both the mononuclear as well as binuclear reaction pathways in support of the regioselective nature of the methodology has also been provided in the subsequent subsections. The succeeding subsections lay emphasis on the fact that the relevance of 1,2,3-triazole ring and its derivatives at physiological pH is considerable because they are aromatic with low basicity, very stable to small thermal and chemical changes. Most pharmaceuticals include the heterocyclic ring 1,2,3-triazole, which has several important pharmacological functions (including antiviral, anticancer, antibacterial, anti-HIV, and antifungal properties). However, the N heteroatoms in the ring provide these compounds a strong propensity to coordinate with a wide variety of metal ions, and due to this quality, they may be used as chemosensors for a variety of toxic heavy metal ions, thereby providing a substantial solution to tackle the escalating problem of environmental contamination. In fields such as drug development, environmental research, and process control, these chemosensors prove to be a useful analytical tool for situations in which constant monitoring and up-to-the-moment data are necessary. The final subsections include the categorization of chemical sensors and the criteria for a molecular ensemble to have chemosensing abilities, followed by the recognition of metal ions by the 1,4-disubstituted 1,2,3-triazole derivatives decorated with chromophoric/fluorophoric units. The chapter concludes with a brief discussion of UV-Visible and fluorescence spectroscopy and its applications in evaluating the chemosensing capability of 1,2,3-triazole based molecules.

Chapter II: Review of Literature

The literature review begins with an overview of heterocyclic compounds, their primary applications as significant pharmacophoric agents including antibiotic, antidepressant, antitumor, antimalarial, anti-HIV, antimicrobial, antidiabetic, anti-inflammatory, antibacterial, etc. Apart from that, their secondary applications such as conjugated polymers, molecular wires, light harvesting systems, organic conductors, etc. have also been mentioned. The literature on the methods used to synthesise the predicted heterocyclic compounds is discussed in the next part, divided into the three categories below:

- Synthesis of a terminal alkyne
- Synthesis of an organic azide
- Synthesis of 1,2,3-triazole from alkyne and azide

The different chemical approaches to the synthesis of terminal alkynes are described, along with the wide range of reactants and reaction conditions used in each synthetic pathway,

such as α,β-eliminations, carbene rearrangement, Ohira–Bestmann reagent, etc. These methods are discussed in terms of the practicality and feasibility of the reaction conditions, both economically and experimentally. In a similar manner, the next section details the various synthetic approaches implemented in the synthesis of both aliphatic and aromatic organic azides. Subsequently, a description of the [3+2] cycloaddition reaction of organic azide with terminal alkyne to yield 1,4-disubstituted 1,2,3-triazoles reported in various instances with different Cu(I) catalytic systems and solvent media has been presented. Research contributions involving direct use of Cu(I) salts as catalyst have also been reported in the literature, alongside multicomponent catalytic systems that involve generation of Cu(I) from Cu(II) salts; however, the stability/existence of Cu(I) in a particular solvent system is generally questioned, owing to the observed low yields of Cu(II) since the Cu(I) readily oxidises to Cu(II) form, a stable oxidation state of copper. For this, the usage of exogenous ligands that include donor atoms like N, O, S, or P in combination with Cu(I) salt has been proposed as a solution to the oxidation state-conversion problem, with the latest addition of bulky organic moieties containing coordination complexes of Cu(I) to stabilize the Cu(I) state. Therefore, this study reports the use of the $[CuBr(PPh_3)_3]$ complex as a Cu(I) catalyst for the synthesis of new 1,2,3-triazole derivatives.

The next subsection of this chapter provides a short overview of the different spectroscopic methods, including infrared (IR) spectroscopy, nuclear magnetic resonance (NMR) spectroscopy, and mass spectrometry (MS), that are used to characterize the synthesised compounds. The last section focuses on the practical uses of 1,2,3-triazole derivatives, with particular attention paid to their potential in chemosensing via presenting the reported examples of 1,2,3-triazole based molecular sensors used to analyse a wide range of toxic heavy metal ions. In conclusion, the literature review on 1,2,3-triazoles as ion sensors highlights the potential of these compounds for the development of highly sensitive and selective ion sensors. These sensors can detect a range of metal ions in various solvent media, with high selectivity and sensitivity. The incorporation of chromophoric and/or fluorophoric groups onto the 1,2,3-triazole moiety enhances their absorption/emission response, thereby improving the spectral responses for easy interpretation. Future research in this field is expected to focus on the development of new 1,2,3-triazole-based ion sensors with improved properties, such as distinct visible changes to the naked eye, increased sensitivity and selectivity, applications in biosensing, etc.

Chapter III: Synthetic procedures and characterization data

This chapter provides a full account of the experimental work carried out to complete the research objectives. It provides a comprehensive explanation of all the experimental procedures to synthesize the novel 1,2,3-triazole-tethered compounds, in addition to the necessary analytical measurements for supporting the synthesis. The chapter starts with a detailed description of the general synthetic procedures implemented for the terminal alkyne, the organic azide, and the 1,2,3-triazole derivative. The subsequent section provides a description of the actual experimental work that was done to synthesise two different organic azides, i.e., benzyl azide and 1-(azidomethyl)naphthalene, accompanied by the analytical data such as yield, color/texture, and characterization data of IR and NMR (^{1}H, ^{13}C) of the synthesised azides. Thereafter, a description of the synthesis of novel terminal alkynes from starting materials is demonstrated, and the structures of the synthesized azides and terminal alkynes are shown in **figure S2**. The experimental conditions for each synthesis are also mentioned, while the characterization data such as the yield, colour, and melting point is provided following every reaction scheme. The IR and NMR (^{1}H and ^{13}C) data values of each individual alkyne is provided in order to confirm their successful synthesis.

The [3+2] cycloaddition procedure to obtain the 1,2,3-triazole-appended molecules (**figure S3**) from their preceding alkynes are described in the individual subsections subsequent to the subsections describing the terminal alkyne synthesis, along with the necessary experimental conditions. Each 1,2,3-triazole derivative was analyzed for its product yield, melting point, color/texture, IR, NMR (^{1}H, ^{13}C), and mass spectrum using appropriate instrumentation, and the data values are provided immediately following the reaction schemes. In appendix A, the materials, procedures, and instruments employed in the analysis of the synthesized compounds have been provided. Infrared (IR), nuclear magnetic resonance (^{1}H, ^{13}C), and mass spectra are all included as appendices B, C, and D, respectively.

Chapter IV: Interpretation and discussion of spectroscopic and photophysical data

This chapter compiles the interpretation and scrutiny of the data obtained from the standard spectroscopic analysis and provides a detailed discussion about the successful synthesis of the proposed terminal alkynes, the organic azides and the 1,2,3-triazole derivatives. Furthermore, the UV-Vis and fluorescence analysis performed to establish the chemosensing potential of the synthesized 1,2,3-triazole derivatives is also discussed in detail to confirm the metal ion sensing by these compounds. On the basis of the type of spectral

results, the chapter is divided into two parts: part A consists the IR, NMR and mass analysis to establish the successful synthesis of the desirable products, whereas part B presents the UV-Vis and fluorescence analysis which explores the selective ion recognition response of the synthesized probes.

Part A

Benzyl chloride **135** and 1-(chloromethyl)naphthalene **136** were substituted with sodium azide by stirring the mixture while heating at 85-90 °C in DMF to produce the corresponding azides **105** and **137** respectively. Both the azides were oily at room temperature, and their synthesis was corroborated by infrared and nuclear magnetic resonance spectroscopy. The IR spectra of both azides recorded as neat in the 4000 - 450 cm^{-1} range revealed the characteristic peak around 2090 cm-1 for the $-N_3$ group, while the other peaks were also in good accord with the synthesised azide structures. Both the azides were characterized via 1H NMR spectra at 500 MHz in $CDCl_3$; the singlet at δ = 4.78 - 4.14 ppm is the result of the $-CH_2$ group linked to the azide functionality, and the peaks in the range δ = 8.12 - 7.14 ppm correspond to aromatic protons. Since the naphthyl group is more effective at deshielding than the phenyl group, the signal from the $-CH_2$ protons is somewhat further deshielded in 1-(azidomethyl)naphthalene than in benzyl azide. Like ^{1}H NMR spectra, the ^{13}C NMR data is in well agreement with the hypothesised structures. The C atoms belonging to the aromatic rings contribute to signals between δ = 135.53 - 123.64 ppm, while the methylene C atoms in both the azides contributes to signals between δ = 54.82 ppm and δ = 53.02 ppm.

To generate the terminal alkynes, 1 mol of the starting material containing labile proton(s) was treated with 1.30 mol of an 80% propargyl bromide solution in toluene and a suitable base. At room temperature with DMF as the solvent, stirring the reaction mixture with the base causes the labile proton(s) of the starting material to be extracted and replaced by the propynyl group(s) via the nucleophilic substitution reaction. As the propensity to lose a proton differs amongst substrates, the time required for a reaction to occur also varies accordingly. Using IR spectroscopy in the 4000 - 450 cm^{-1} region, the characterization and comparison of the newly formed alkynes with their respective starting materials, and the recorded results have thoroughly validated the formation of the predicted output. The -C≡*C-H* group contributes an IR peak at about 3287-3280 cm^{-1} to the spectra of various alkynes, whereas the -C≡C moiety of alkynes contributes a peak at around 2120-2100 cm^{-1}. The alkyne proton (≡C-H), is ascribed in the ^{1}H NMR spectra of compounds as a peak at δ = 2.47 - 2.40 ppm, and the benzylic group

(-CH_2) is confirmed as a peak at δ = 4.57 - 4.52 ppm. The production of alkyne from the reactants having hydroxyl groups is also confirmed by the absence of a signal at δ = 5.00 - 3.00 ppm for the proton of the -OH group, which is suggestive of their replacement by the propynyl group, while the aromatic protons are ascribed to the peaks between δ = 7.20 - 6.95 ppm. Peaks at δ = 78.70 - 76.65 ppm in ^{13}C NMR spectra of alkynes are attributable to C≡C, whereas peaks at δ = 60.02 - 55.23 ppm belong to -CH_2O moiety, thereby demonstrating the effective synthesis of alkyne.

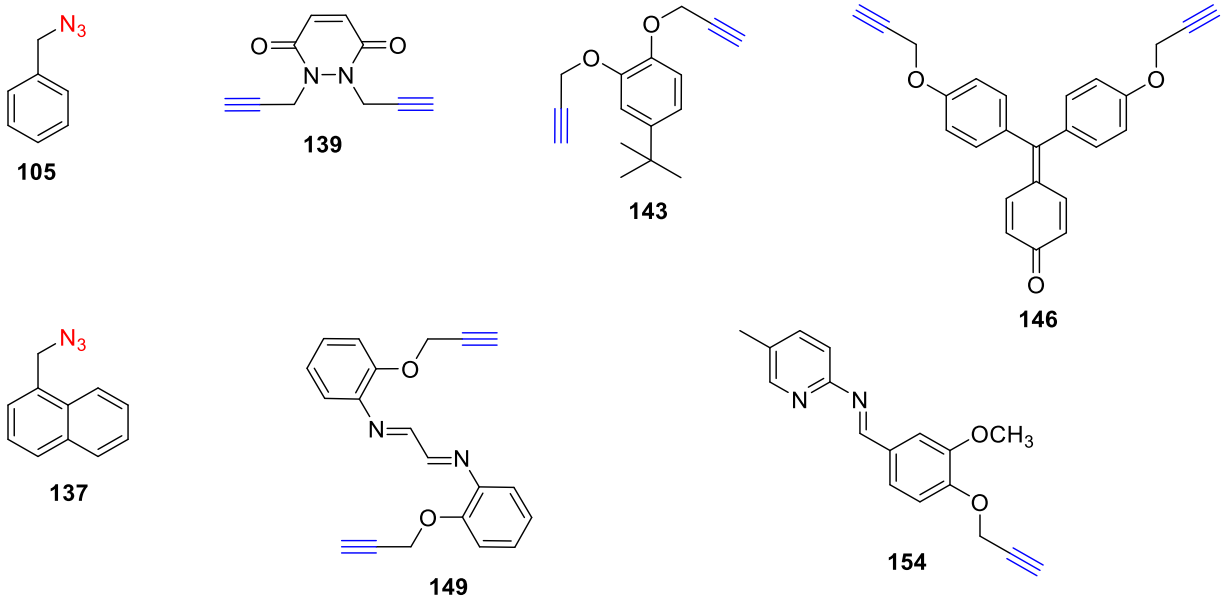

Figure S2: An illustration of the synthesized azides and terminal alkynes

To synthesize the 1,2,3-triazole-derived chemosensor probes, the preceding alkynes were subjected to [3+2] cycloaddition with the organic azide in small amounts of [$CuBr(PPh_3)_3$] complex as the catalytic system in THF:TEA (v/v, 1:1) as a solvent media. The IR, NMR, and mass analysis performed on all these heterocyclic compounds demonstrate the efficacy of the cycloaddition process. A strong peak observed in the IR spectrum of the azides at 2090 cm^{-1} and in the area of 2120-2100 cm^{-1} for terminal alkynes vanished entirely from the IR spectra of the products after the cycloaddition process, demonstrating that the alkyne and azide precursors had been fully cyclized. The NMR experiments corroborated this behaviour by showing that the 1,2,3-triazole derivatives were successfully synthesized, as shown by the disappearance of a peak at δ = 2.59 - 2.35 ppm for the proton of the alkyne group (C≡*C*-*H*). Due to the creation of the 1,2,3-triazole ring, which has a considerable deshielding effect, the peaks at δ= 4.83 - 4.65 ppm, caused by the -CH_2 of the methylene protons in every alkyne

molecule, were pushed downfield. As the C atoms of the terminal alkyne and organic azide have formed the triazole ring during cyclization, the peaks at δ = 78.91 - 72.75 ppm in the ^{13}C NMR spectra of the alkynes were displaced downfield in the spectra of 1,2,3-triazole derivatives. In addition, the mass spectrum information strongly suggested that the heterocyclic compounds resulted from CuAAC reactions. All the 1,2,3-triazole-based compounds had mass spectra in accordance with their structures.

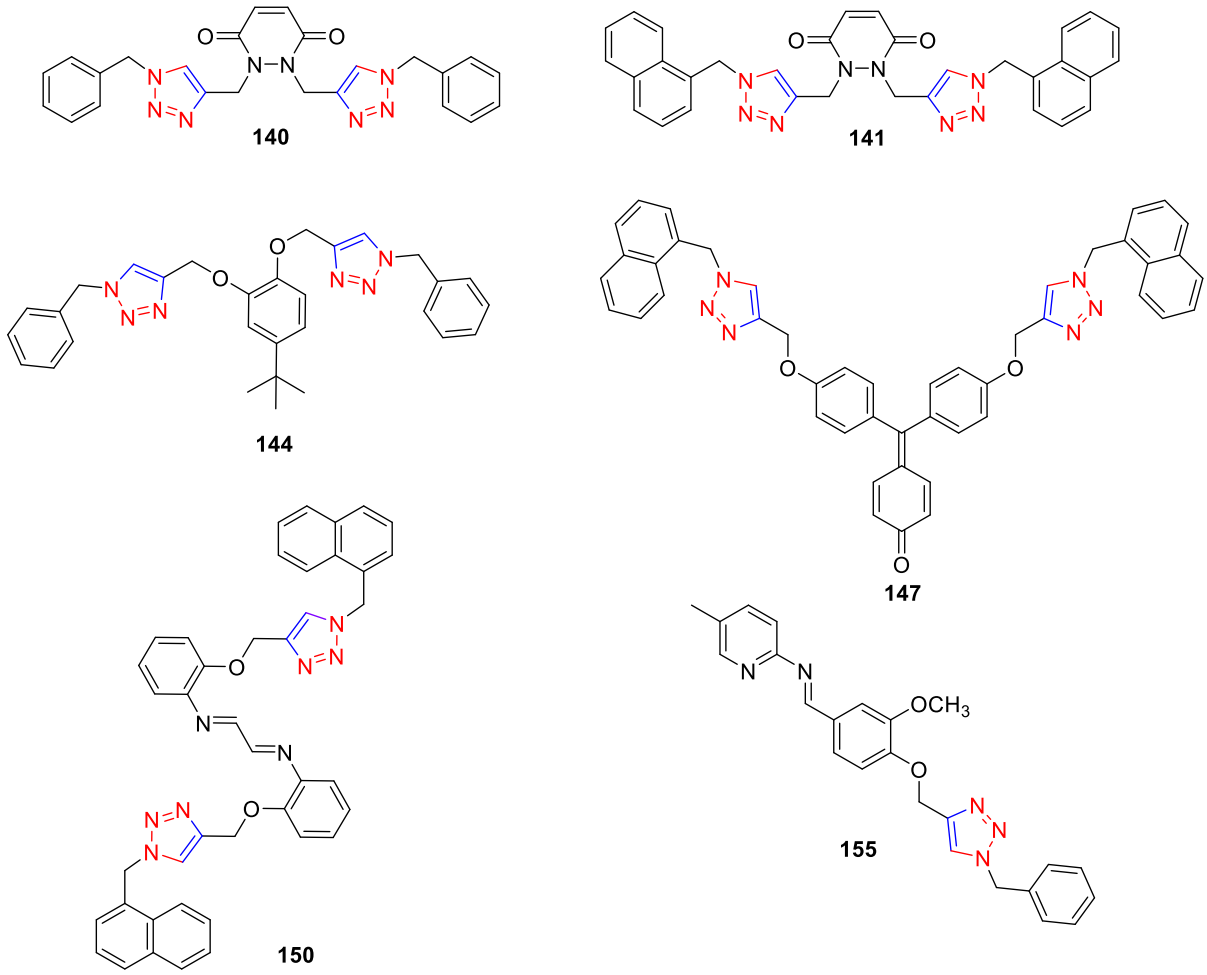

Figure S3: An illustration of the synthesized 1,4-disubstituted 1,2,3-triazoles

Part B

In order to investigate the ion sensing behaviour of the synthesized 1,2,3-triazole derivatives, their photophysical characteristics were investigated in detail by UV-Vis and fluorescence spectroscopy, as exhibited in part B of Chapter IV. Having 1,2,3-triazole moieties incorporated in their structure with N atoms that are the ideal coordinating sites for certain metal ions, the synthesized chemosensor probes were explored for their ion recognition potential via UV-Vis and/or fluorescence titrations carried out towards specific metal ions.

The selectivity of the 1,2,3-triazole-appended maleic hydrazid-based probes **140** and **141** for Pb(II) and Cr(III) ions was analyzed by their respective responses to different metal ions in their absorption spectra. As can be seen in **figure S4** and **figure S5**, a discernible hyperchromic shift at 258 nm, and a hypochromic shift at 312 nm is shown by the probe **140** in response to an increase in the concentration of Pb(II) as well as Cr(III) ions respectively. As a result, this selective chemosensor a qualified for a direct quantitative measurement of Pb(II) and Cr(III) ions by UV-Visible spectroscopy, with LoD of 58 µM and 79 µM respectively, while having LoQ 195 µM and 263 µM respectively, as determined by the correlation plots for probe a. The association constants calculated from the Benesi - Hildebrand equation were 0.61 × 10^5 M^{-1} for Pb(II) and 0.20 × 10^6 M^{-1} for Cr(III) for 2:1 (M:L) complexation, and the stoichiometry was deduced to be 2:1 (M:L) in both cases.

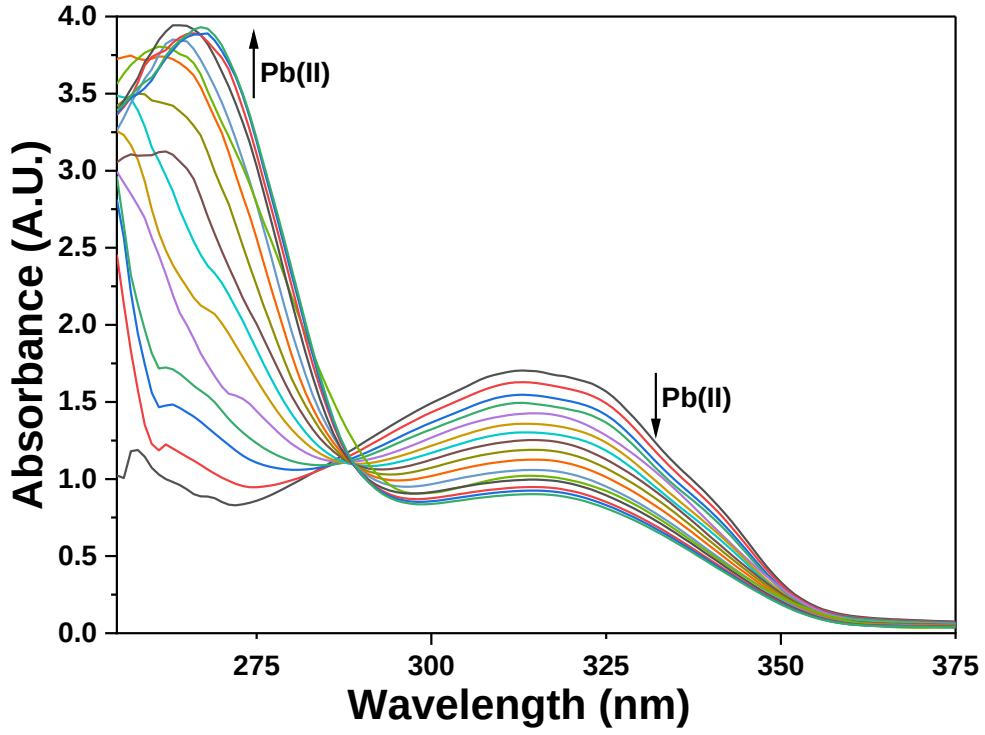

Figure S4: Absorption maxima shifts of the probe **140** as a result of titration with Pb(II) solution in DMSO

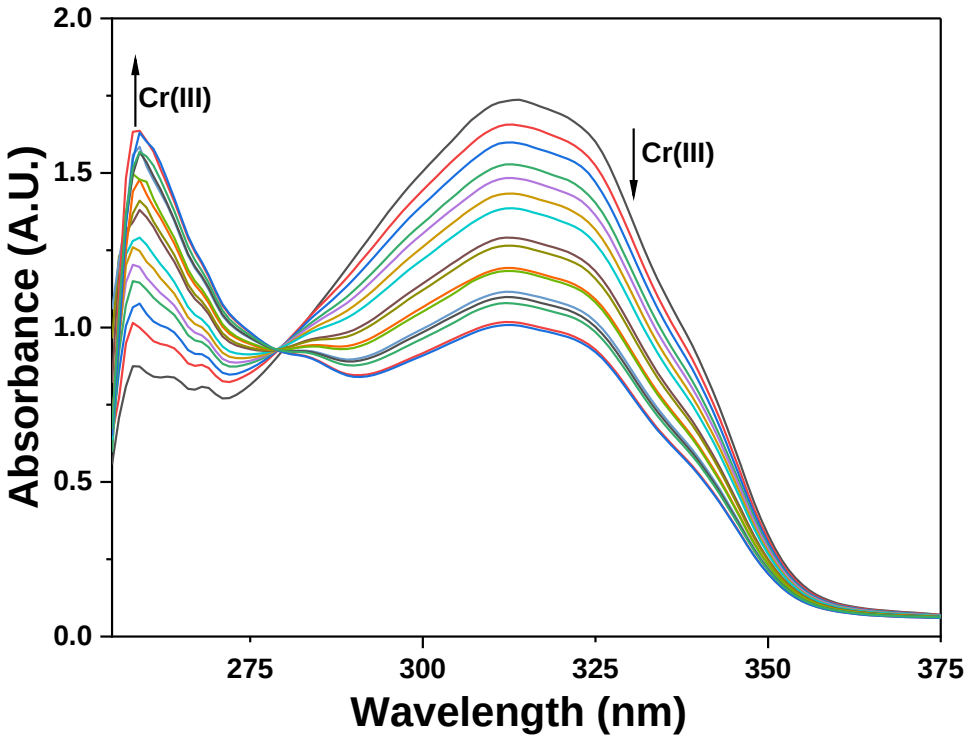

Figure S5: Absorption maxima shifts of the probe **140** as a result of titration with Cr(III) solution in DMSO

For the probe **141**, the peak at 294 nm displayed a hypochromic shift whereas the peaks at 274 nm and 284 nm displayed an intense hyperchromic shift, ultimately merging into a single broad band around 270 nm on the addition of Pb(II) ions (**figure S6**). However, addition of Cr(III) resulted in a hypochromic shift in the peaks at 274 nm, 284 nm,, and 294 nm, with a concomitant hyperchromic shift at 260 nm, leading to the emergence of an isosbestic point at 270 nm (**figure S7**). Therefore, probe b like its counterpart probe a also qualified for a direct quantitative measurement of Pb(II) and Cr(III) ions, with LoD of 142 µM and 87 µM respectively, while having LoQ 473 µM and 290 µM respectively, as determined by the correlation plots for probe a. The association constants calculated from the Benesi - Hildebrand equation were 0.46×10^6 M^{-1} for Pb(II) and 0.76×10^6 M^{-1} for Cr(III) for 2:1 (M:L) complexation, and the stoichiometry was deduced to be 2:1 (M:L) in both cases.

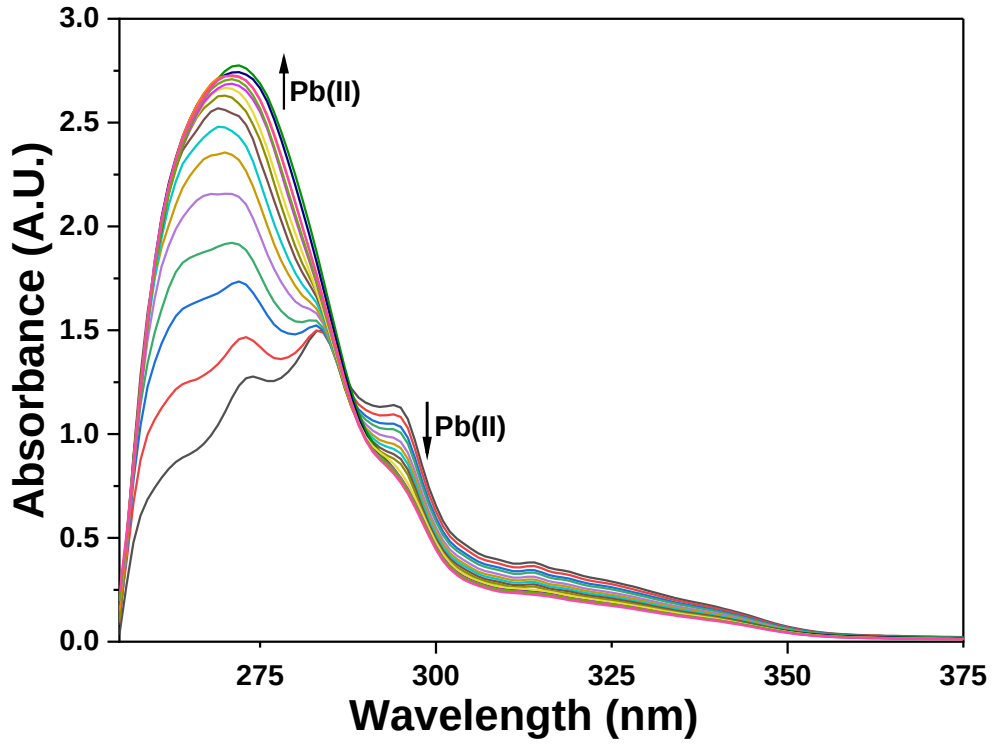

Figure S6: Absorption maxima shifts of the probe **141** as a result of titration with Pb(II) solution in DMSO

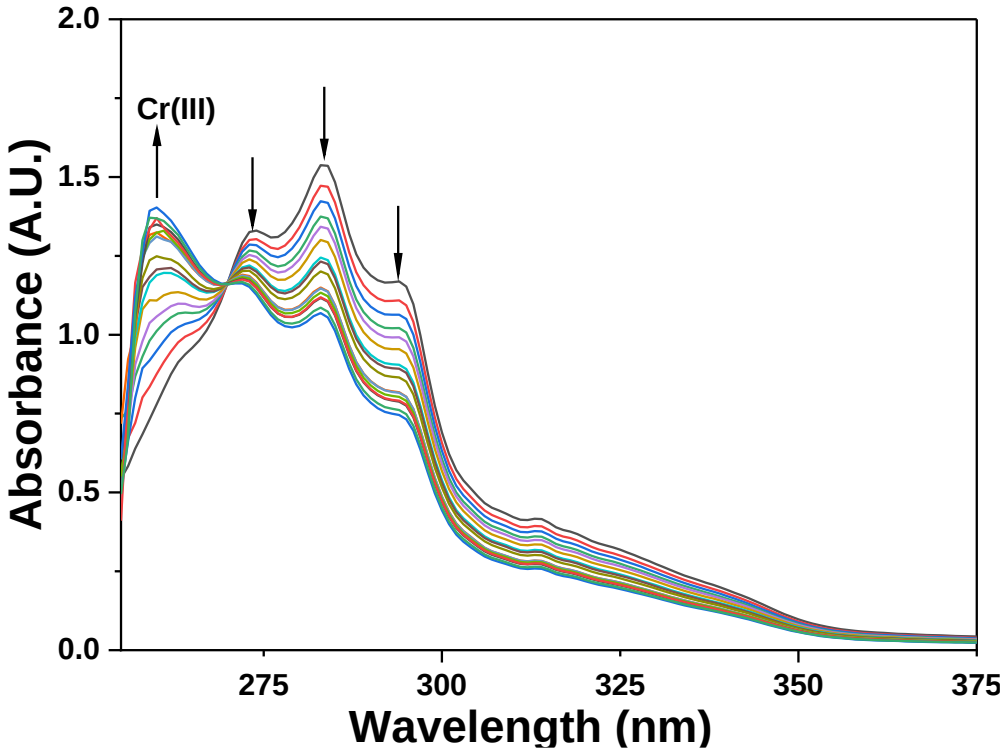

Figure S7: Absorption maxima shifts of the probe **141** as a result of titration with Pb(II) solution in DMSO

UV-Vis and fluorescence spectroscopy were used to analyze the response of the 1,2,3-triazole-appended 4-tert butyl catechol-based probe **144** for different metal ions and determine the probe's selectivity and sensitivity for Hg(II) and Pb(II) ions. As illustrated in **figure S8**, the probe **144** displayed a hypochromic shift at 277 nm in response to Hg(II) addition, with an isosbestic point at 255 nm, whereas for Pb(II) addition, an intense hyperchromic shift in addition to a blue shift of about 22 nm was observed (**figure S9**). Additionally, the fluorescence spectra of the probe **144** in separate titrations with Hg(II) and Pb(II) yielded similar results, exhibiting hyperchromic response at both the monomer and excimer peaks at 340 nm and 653 nm respectively (**figure S10** and **figure S11**). The correlation plots deduced from the fluorescence spectroscopic data were employed to determine the LoD, LoQ, and stoichiometric ratio of the probe for both the metal ions; the LoD was 11 µM and 8.6 µM for Hg(II) and Pb(II), while the LoQ was 38 µM and 28.7 µM respectively. Additionally, the association constant (K_a) determined from the Benesi - Hildebrand equation was $2.46 \times 10^3\ M^{-1}$ and $0.71 \times 10^3\ M^{-1}$ for Hg(II) and Pb(II) respectively, while the stoichiometric ratio for both the metal ions was 2:1 (M:L).

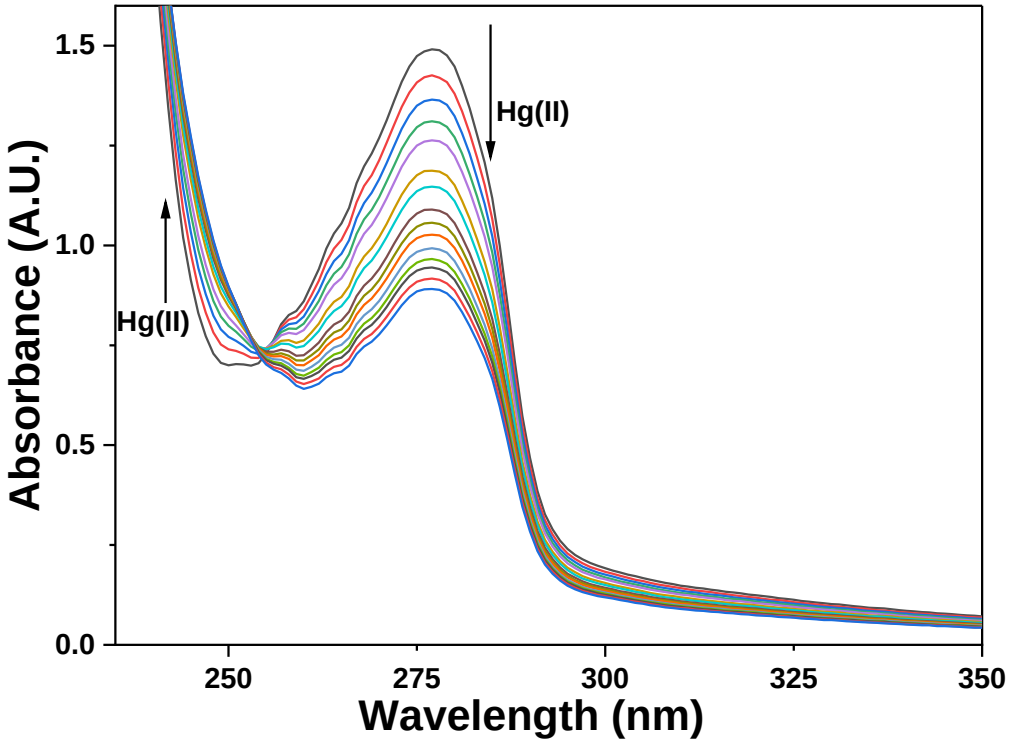

Figure S8: UV-Vis spectra of probe **144** during titration with Hg(II) in CH_3CN/H_2O (4:1)

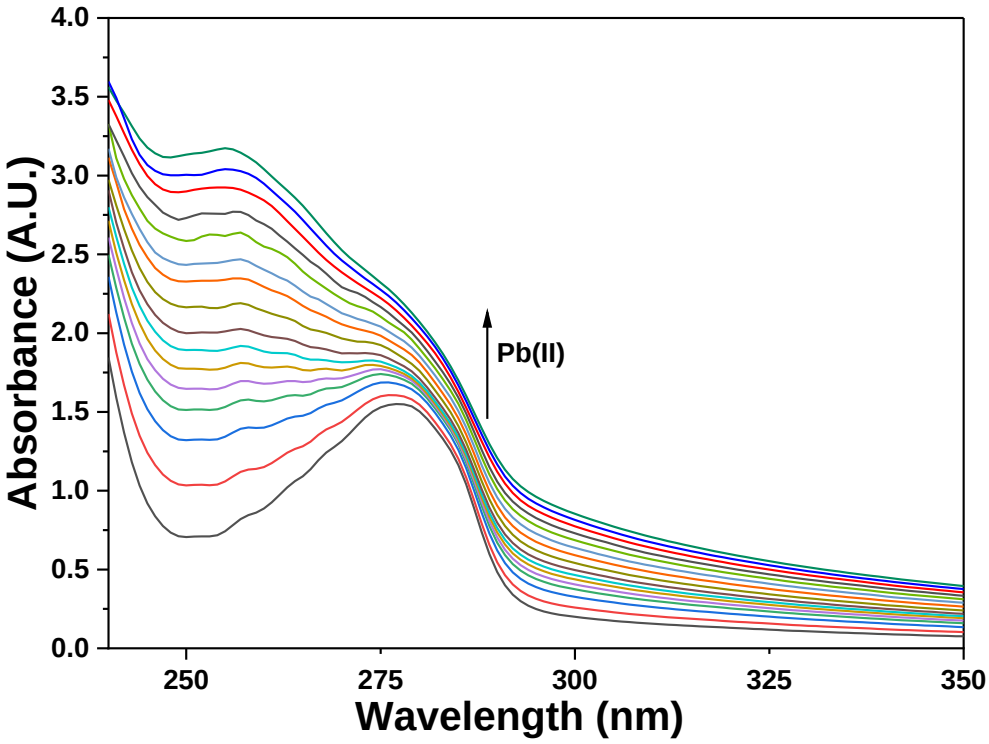

Figure S9: UV-Vis spectra of probe **144** during titration with Pb(II) in CH_3CN/H_2O (4:1)

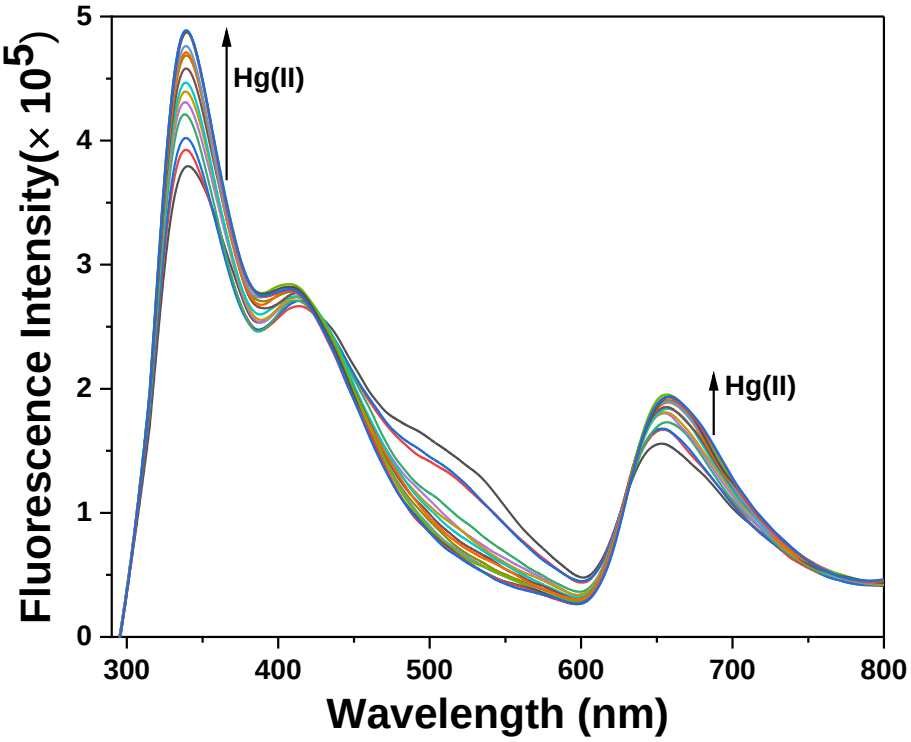

Figure S10: Incremental enhancement in the fluorescence emission of probe **144** upon the progressive addition of Hg(II) ions in CH_3CN/H_2O (4:1)

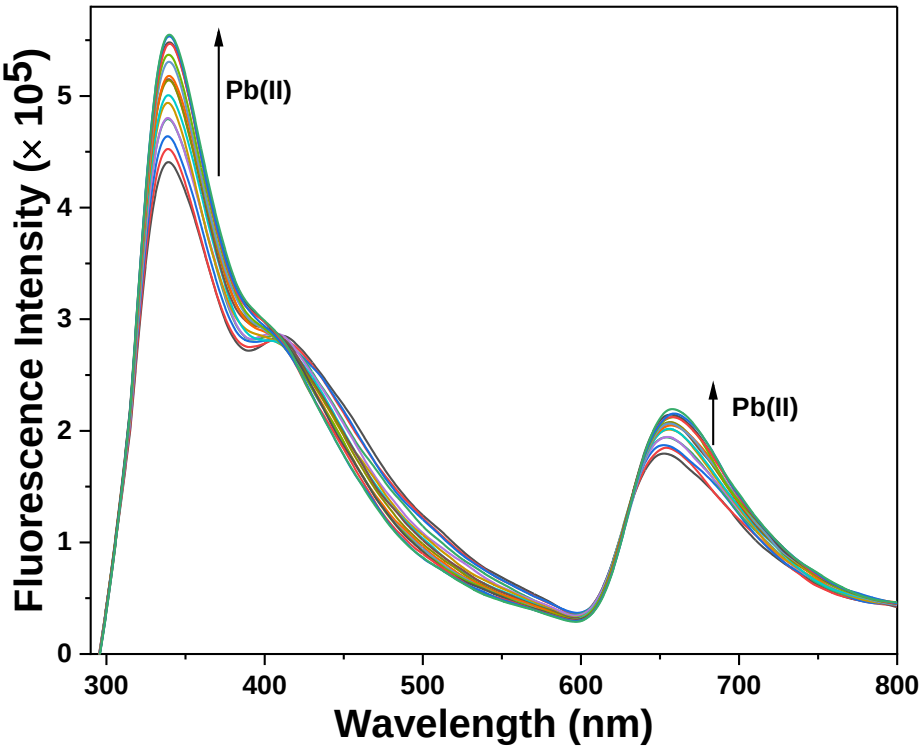

Figure S11: Incremental enhancement in the fluorescence emission of probe **144** upon the progressive addition of Pb(II) ions in CH_3CN/H_2O (4:1)

The selectivity and sensitivity of the 1,2,3-triazole-appended p-rosolic acid-based probe **147** for Hg(II), Pb(II), and Cr(III) ions was determined by analyzing the probe's spectral response to various metal ions using UV-Vis and fluorescence spectroscopy. Addition of Hg(II) ions to the probe solution led to a hypochromic shift at 274 nm, 284 nm, and 294 nm, with the concomitant hyperchromic shift at 262 nm leading to an isosbestic point around 271 nm (**figure S12**). Addition of Pb(II) ions led to hyperchromic shift at 274 nm and 284 nm, with their merging into a single broad peak at 270 nm (**figure S13**). Cr(III) ions had similar effect on the probe's absorption spectrum as in the case of Hg(II) ions, however, the hyperchromic shift was less intense in this case (**figure S14**). In fluorescence spectral analysis, addition of any of the three metal ions led to hyperchromic shift at monomer emission at 356 nm as well as excimer emission at 657 nm (**figure S15, S16, S17**). The correlation plots were employed for the determination of LoD and LoQ; the LoD was calculated to be 0.09 µM, 0.10 µM, and 0.12 µM for Hg(II), Pb(II), and Cr(III) respectively, while the LoQ was calculated to be 0.29 µM, 0.33 µM, and 0.41 µM for Hg(II), Pb(II), and Cr(III) respectively. Furthermore, the Benesi - Hildebrand equation was used to calculate the association constant (K_a), which had the values 1.312×10^4 M^{-1} for Hg(II), 1.527×10^4 M^{-1} for Pb(II), and 4.94×10^4 M^{-1} for Cr(III). The stoichiometric ratio of the complexation of the probe with all the metal ions was 1:1.

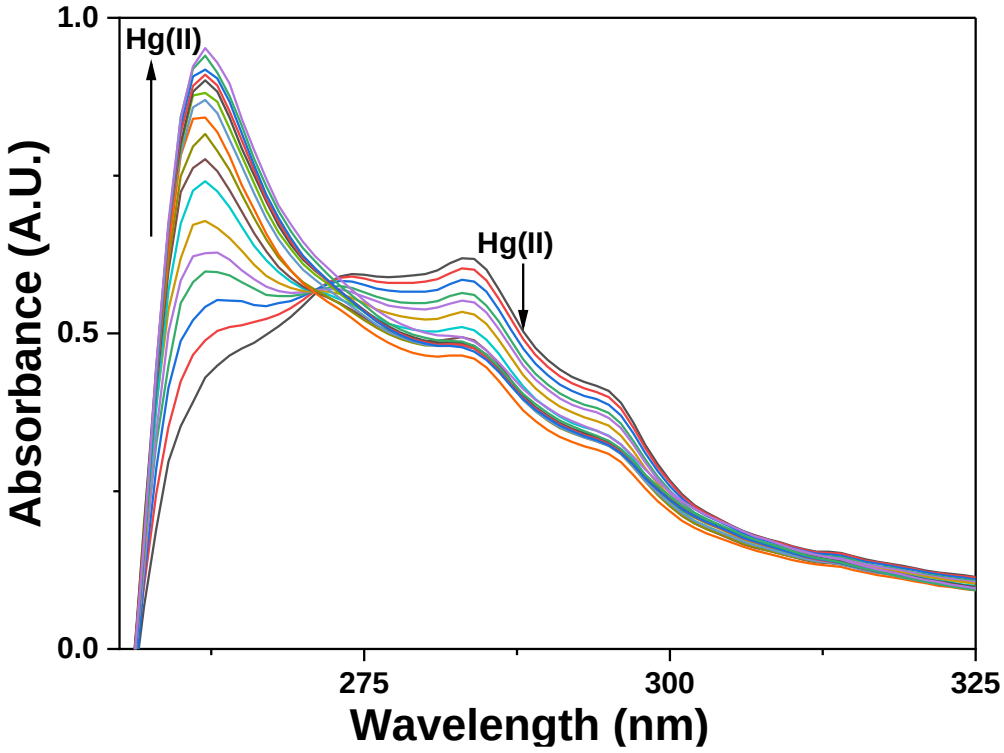

Figure S12: Absorption spectrum of probe **147** demonstrating cumulative changes on incremental addition of Hg(II)

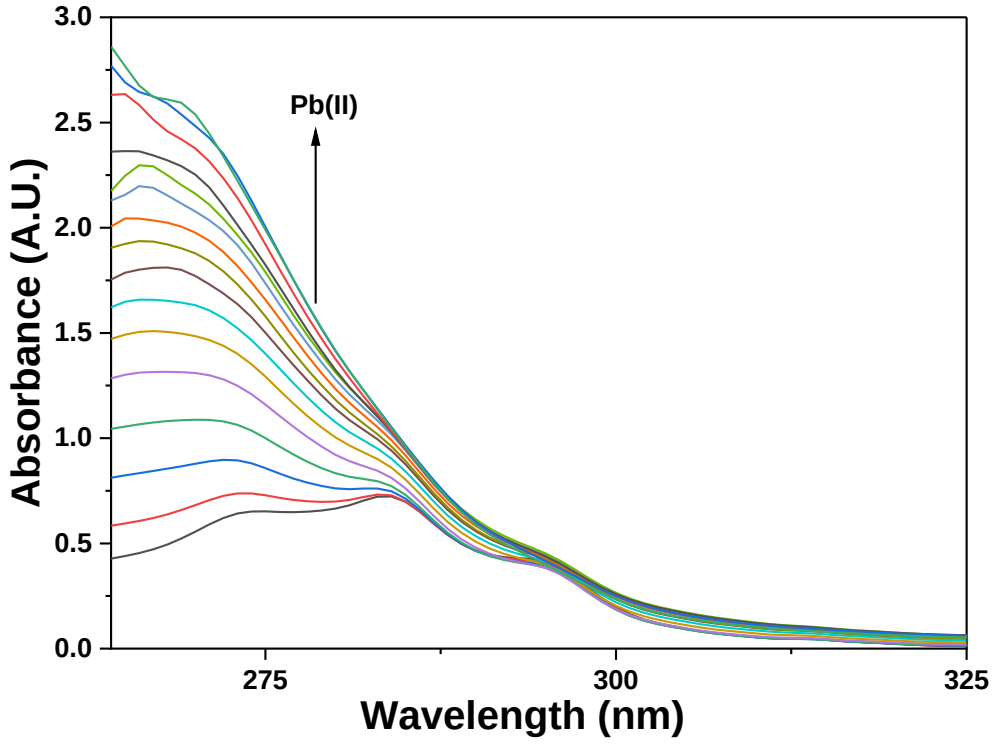

Figure S13: Absorption spectrum of probe **147** demonstrating cumulative changes on incremental addition of Pb(II)

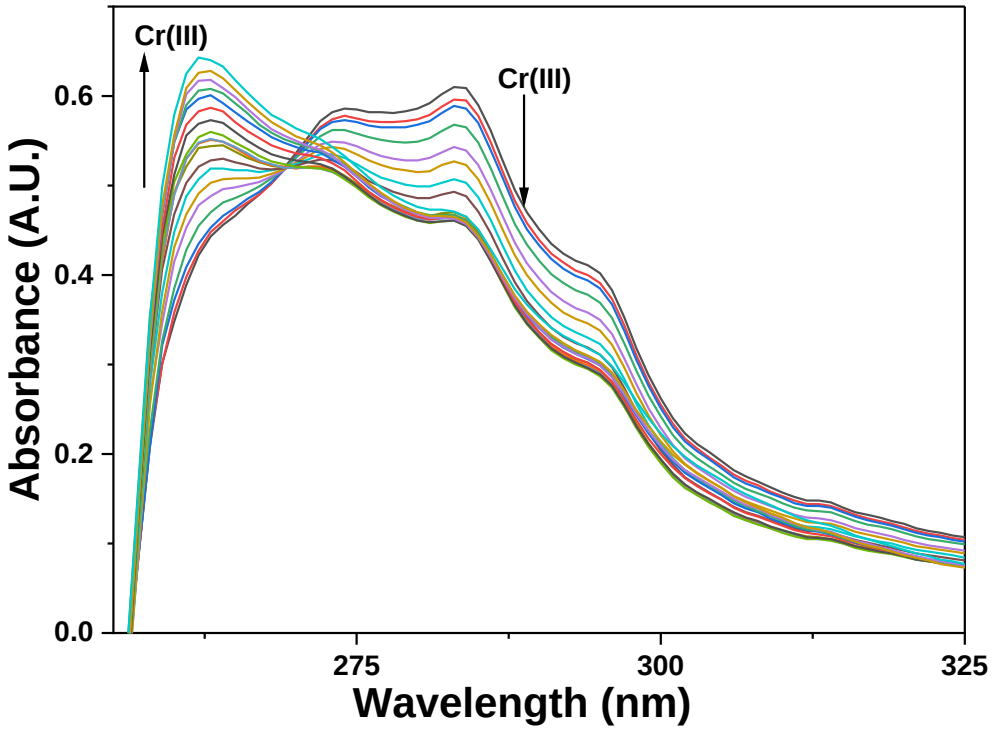

Figure S14: Absorption spectrum of probe **147** demonstrating cumulative changes on incremental addition of Cr(III)

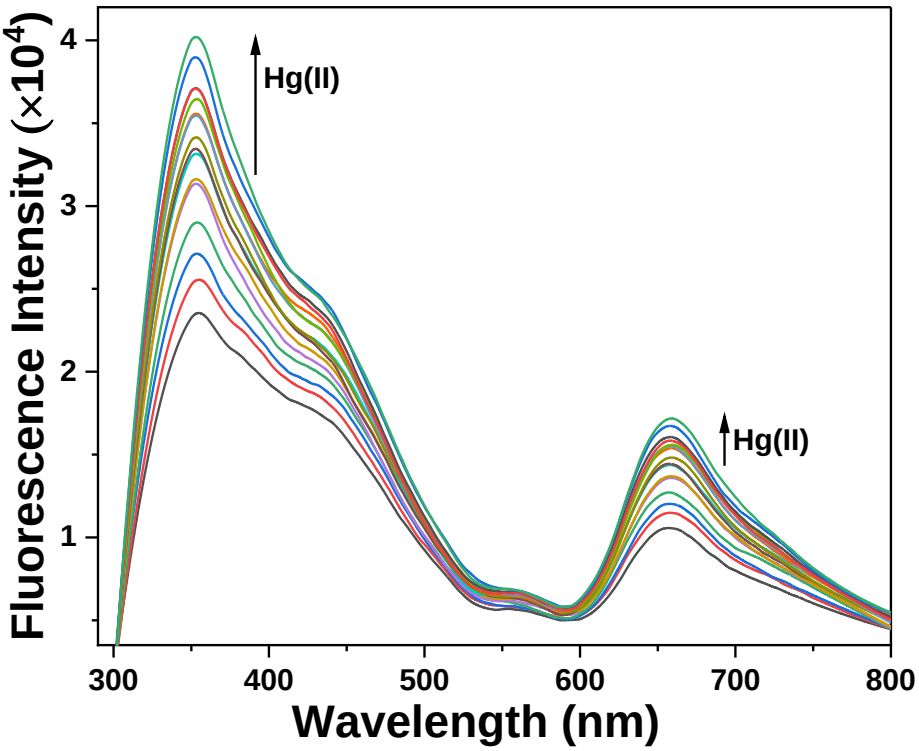

Figure S15: Incremental enhancement in the fluorescence emission of probe **147** upon the progressive addition of Hg(II) ions

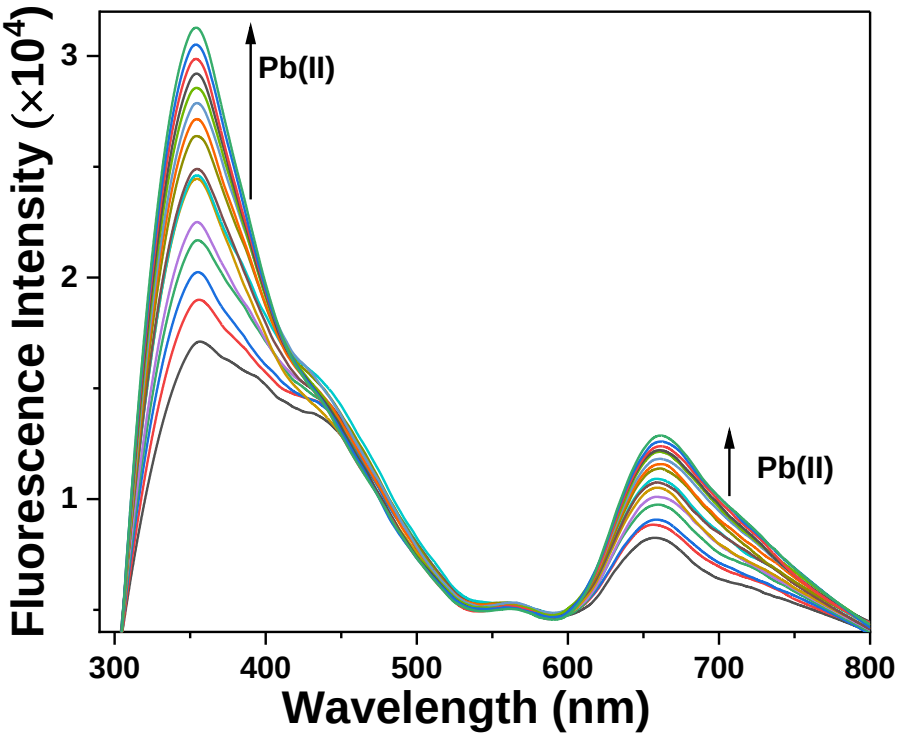

Figure S16: Incremental enhancement in the fluorescence emission of probe **147** upon the progressive addition of Pb(II) ions

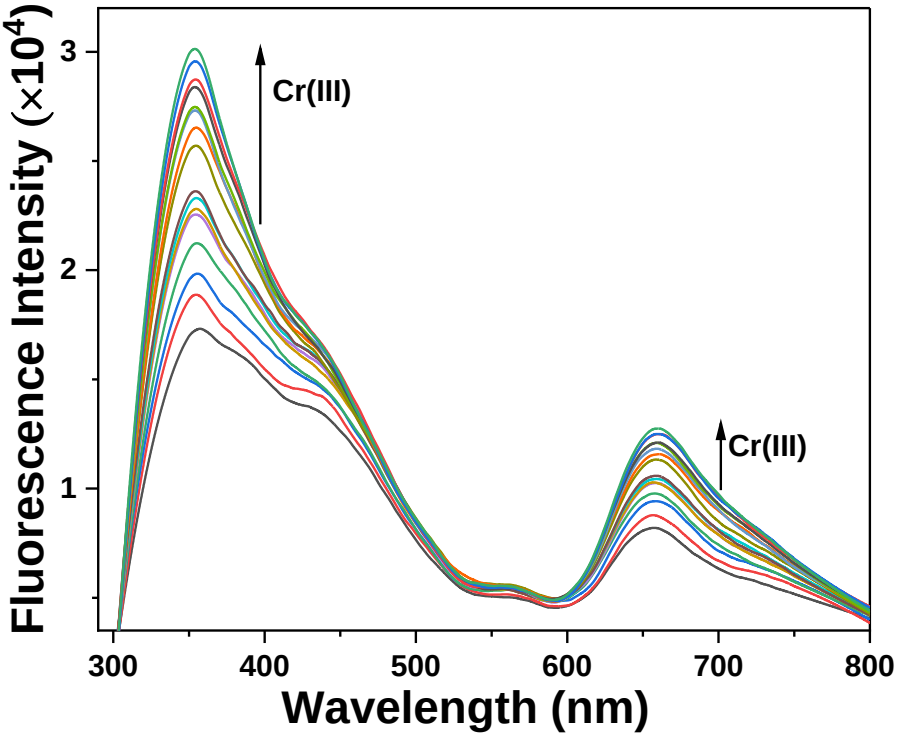

Figure S17: Incremental enhancement in the fluorescence emission of probe **147** upon the progressive addition of Cr(III) ions

The selectivity and sensitivity of the 1,2,3-triazole-appended glyoxal bis-(2-hydroxyanil)-based probe **150** for Cu(II) and Pb(II) ions were assessed utilising UV-Vis and fluorescence spectroscopy on the probe's spectrum response to different metal ions. Addition of Cu(II) ions to the probe solution showed a hyperchromic shift at 274 nm, 284 nm and 294 nm, confirming the binding of Cu(II) to the probe solution (**figure S18**). Pb(II) ions resulted into a hypochromic shift in the 294 nm peak, as well as a hyperchromic shift in the 274 nm and 284 nm peaks, with the latter two peaks merging into a single peak at about 270 nm (**figure S19**). In fluorescence spectral analysis of probe **150**, adding Cu(II) ions to the probe solution caused a gradual decrease in the emission intensity for both the monomer emission at 324 nm and excimer emission at 617 nm (**figure S20**), whereas Pb(II) ions led to enhancement in the intensity of both the peaks (**figure S21**). The LoD and LoQ as determined by the correlation plots for the complexation of the probe with Cu(II) ions was 4.35 µM and 14.52 µM respectively; while for Pb(II) ions, the LoD and LoQ was 3.10 µM and 10.34 µM respectively. Also, the Benesi - Hildebrand equation resulted in the association constant (K_a) being 1.16×10^3 M^{-1} for Cu(II) and 1.10×10^3 M^{-1} for Pb(II). The stoichiometric ratio for the probe complexation with either of the metal ions was 1:1.

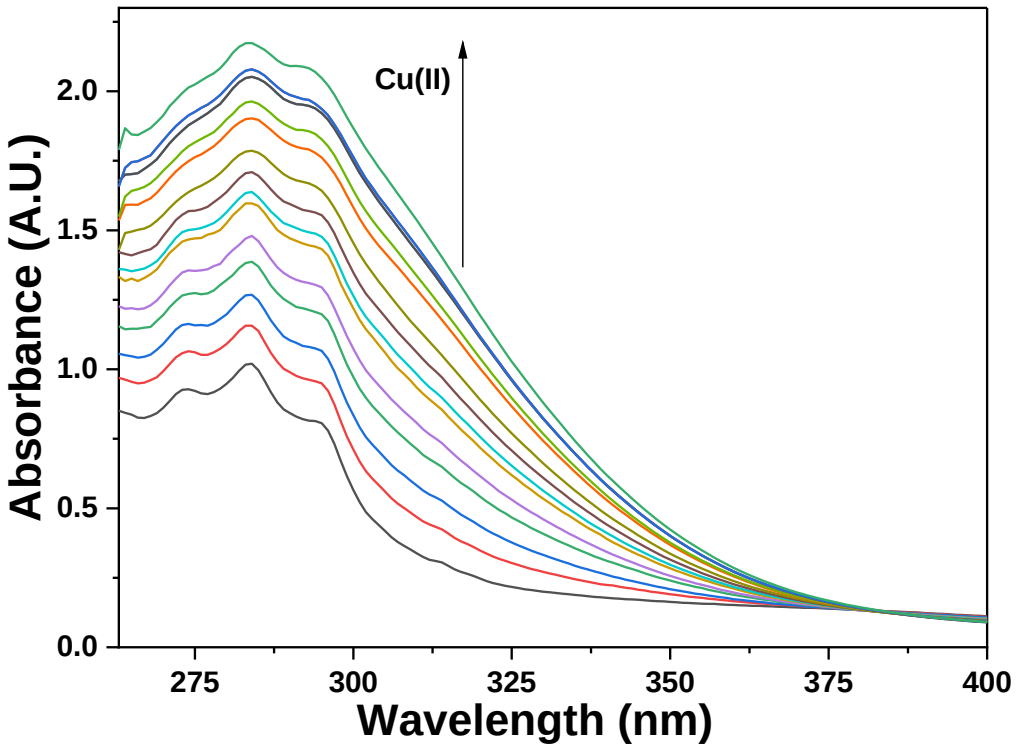

Figure S18: Absorption spectrum of probe **150** representing collective changes on incremental addition of Cu(II)

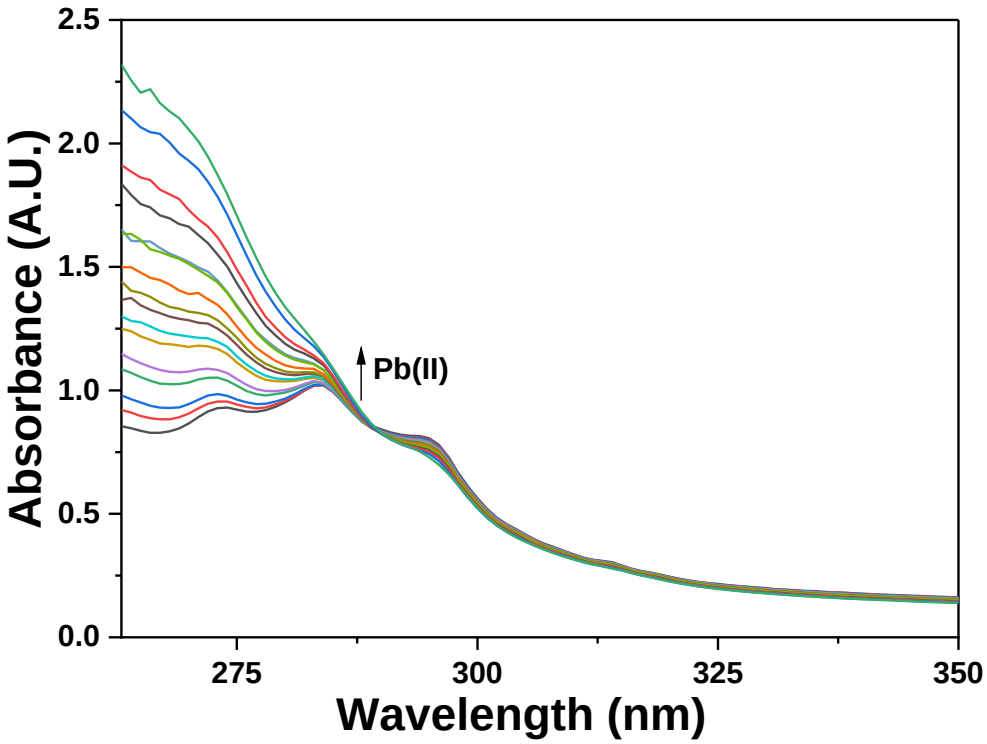

Figure S19: Absorption spectrum of probe **150** representing collective changes on incremental addition of Pb(II)

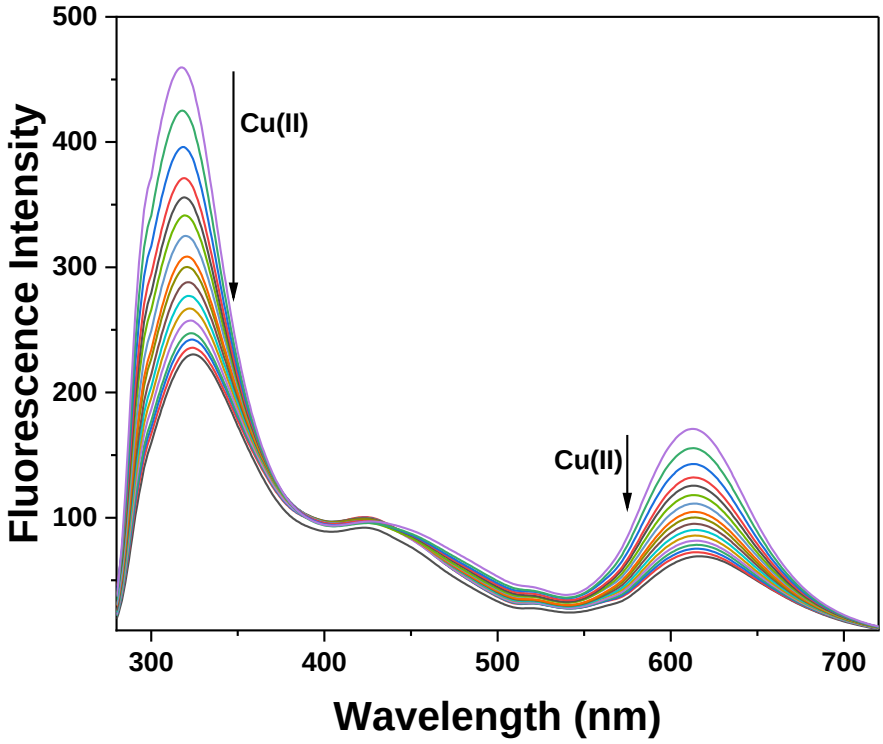

Figure S20: Decrease in the fluorescence emission of probe **150** upon the sequential accumulation of Cu(II) ions

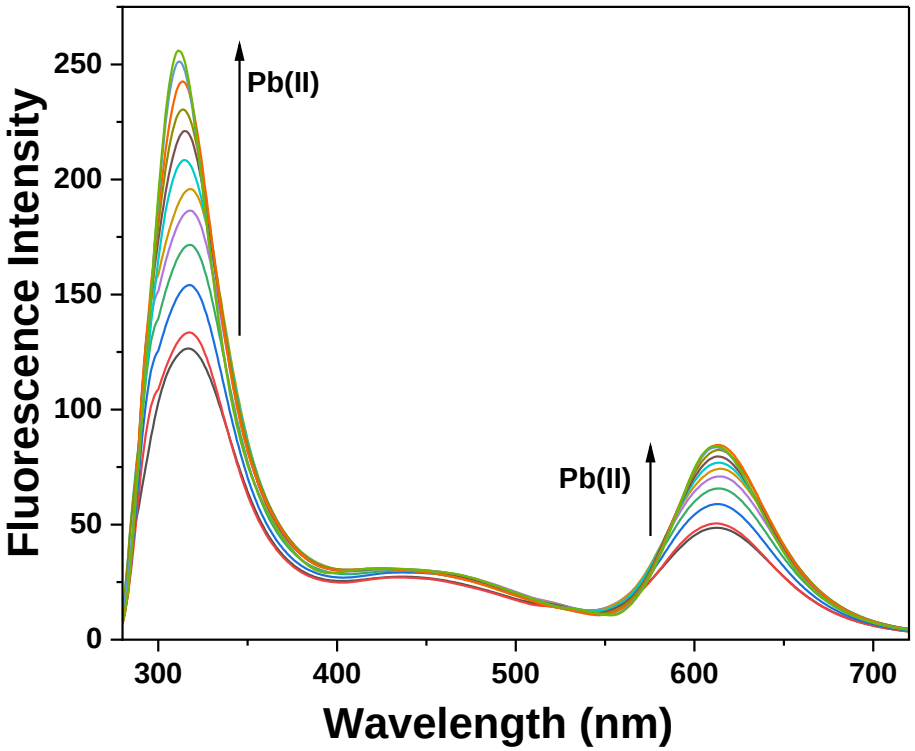

Figure S21: Increase in the fluorescence emission of probe **150** upon the sequential accumulation of Cu(II) ions

The 1,2,3-triazole-appended probe **155**'s reaction to various metal ions was studied using UV-Vis and fluorescence spectroscopy, and the probe's selectivity and sensitivity for Ce(III) ions were determined. The probe **155** revealed a hyperchromic shift at 307 nm in response to Ce(III) addition, accompanied by a red shift of roughly 23 nm (**figure S22**). Furthermore, the probe's fluorescence spectra during titrations with Ce(III) ions showed a hyperchromic response at both the monomer and excimer peaks at 313 nm and 611 nm, respectively (**figure S23**). The correlation plots derived from the fluorescence spectroscopic data were used to calculate the LoD, LoQ, and stoichiometric ratio of the probe; the LoD was 9.53 µM while the LoQ was 31.75 µM. Furthermore, the association constant (Ka) derived using the Benesi - Hildebrand equation was 3.55×10^3 M^{-1}, whereas the stoichiometric ratio was 1:1 (M:L).

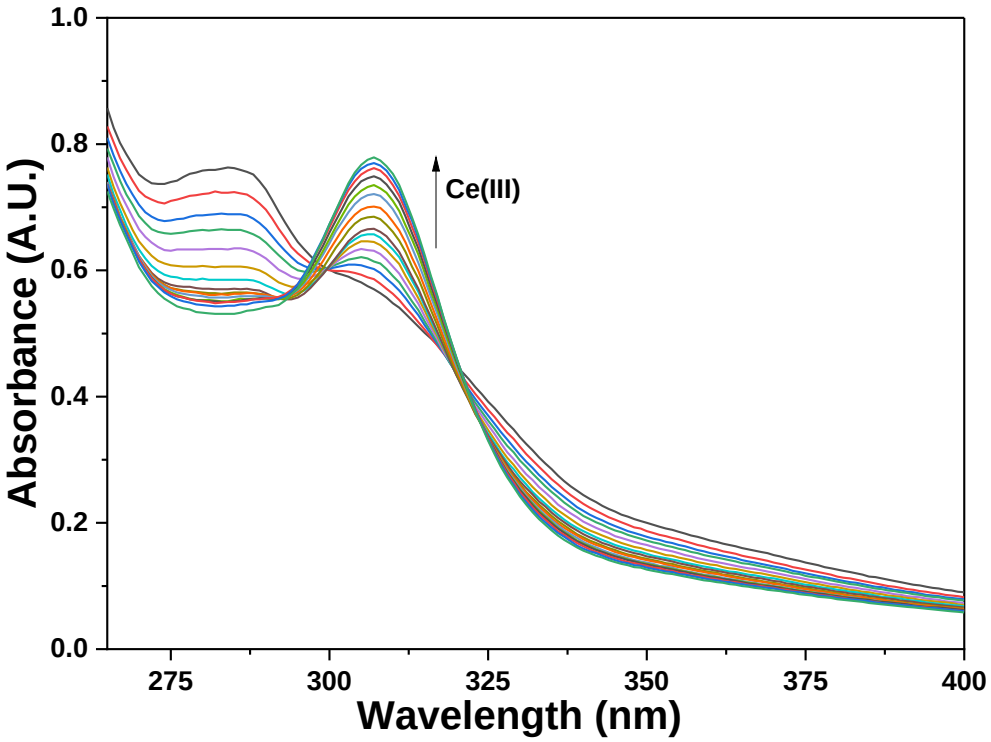

Figure S22: Absorption spectrum of probe **155** representing collective changes on incremental addition of Ce(III)

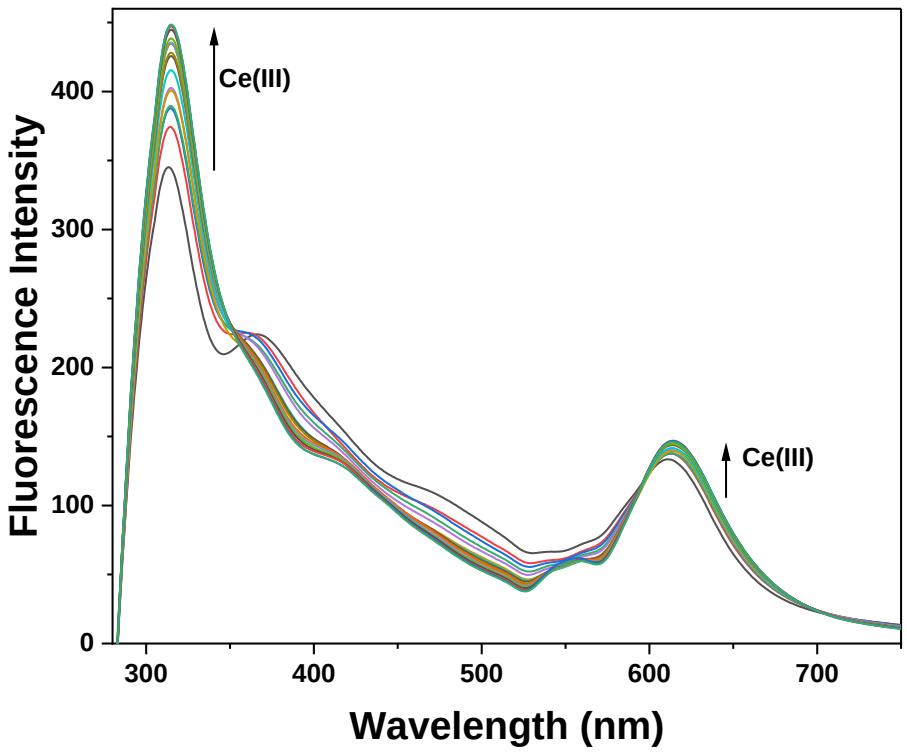

Figure S23: Increase in the fluorescence emission of probe **155** upon the sequential accumulation of Ce(III) ions

Annexure A

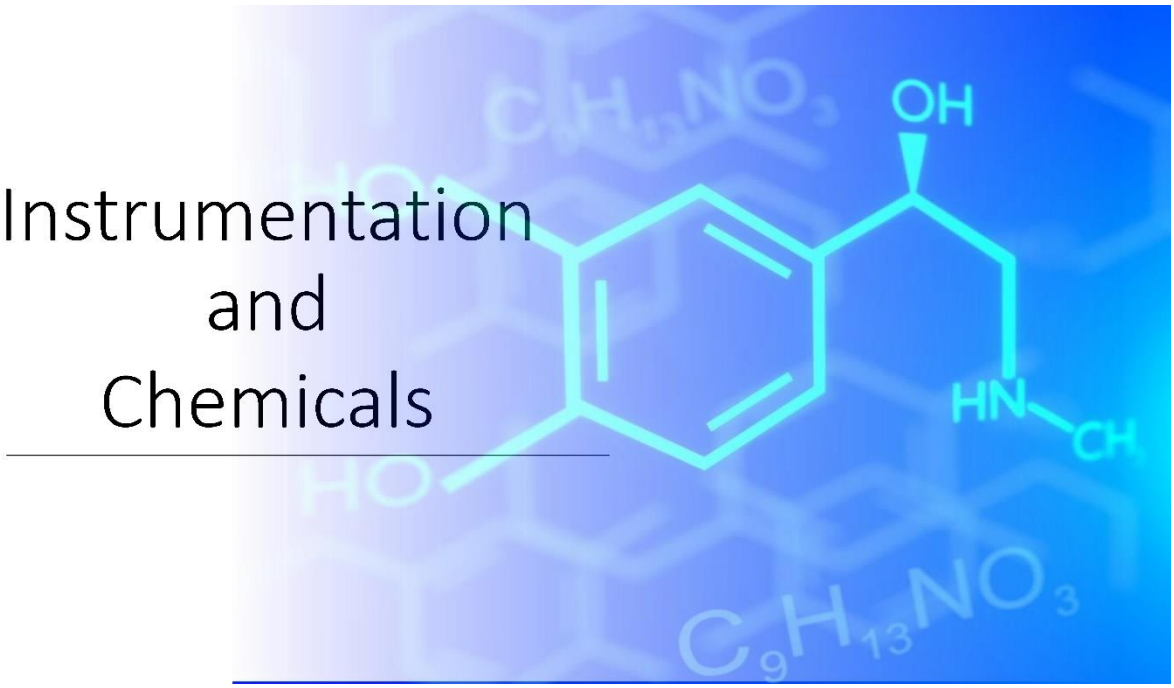

Instrumentation and Chemicals

Annexure A provides all the instruments implemented for spectroscopic analysis of the synthesized compounds, and enlists the different reagents, catalysts, and solvents used in the chemical synthesis and analytical examination of the synthesised molecules.

General experimental techniques

1. Infrared spectra

The infrared spectra of the synthesized compounds were recorded in the range of 4000 - 450 cm^{-1} using SHIMADZU FTIR-8400S, availed at Central Instrumentation Facility (CIF), Lovely Professional University, Phagwara, Punjab.

2. NMR spectra

The ^{1}H and ^{13}C NMR spectra of all the synthesized compounds were recorded utilizing a Bruker Advance Neo FT NMR spectrophotometer, with tetramethylsilane (TMS) as the internal reference, and $CDCl_3$ and DMSO-d_6 as the solvents. The facility was availed at Sophisticated Analytical Instrumentation Facility (SAIF), Panjab University, Chandigarh.

3. Mass spectra

The mass spectrometric analysis (LCMS) of the synthesized 1,2,3-triazoles was obtained through Bruker Esquire 3000 mass spectrometer, availed at Sophisticated Analytical Instrumentation Facility (SAIF), Panjab University, Chandigarh.

4. UV-Vis spectra

UV-Vis spectroscopic investigations were carried out on SHIMADZU UV-1900 spectrophotometer, availed at School of Chemical Engineering and Physical Sciences, Lovely Professional University, Phagwara, Punjab.

5. Fluorescence spectra

The fluorescence spectroscopic investigations were carried out on a Perkin Elmer FL 6500 spectrophotometer, availed at the Central Instrumentation Facility (CIF), Lovely Professional University, Phagwara, Punjab.

6. Melting Point

The melting points of the synthesized substances were determined through the Mel Temp II apparatus using sealed capillaries at School of Chemical Engineering and Physical Sciences, Lovely Professional University, Phagwara, Punjab.

7. General materials

Bromotris(triphenylphosphine)copper(I) [$CuBr(PPh_3)_3$] (Aldrich), propargyl bromide (80% by weight in toluene) (spectrochem), N,N-dimethylformamide (DMF) (LOBA Chemie), benzyl

chloride (LOBA Chemie), 1-naphthyl chloride (LOBA Chemie), sodium azide (LOBA Chemie), tetrahydrofuran (THF) (SDFCL), triethylamine (TEA) (LOBA Chemie), potassium carbonate (LOBA Chemie), cesium carbonate (LOBA Chemie), ethyl acetate (LOBA Chemie), n-hexane (LOBA Chemie), dimethyl sulfoxide (LOBA Chemie), acetonitrile (SDFCL), maleic hydrazide (LOBA Chemie), 4-tert butyl catechol (LOBA Chemie), p-rosolic acid (LOBA Chemie), glyoxal bis-(2-hydroxyanil) (LOBA Chemie), 2-amino-5-methylpyridine (LOBA Chemie), 4-hydroxy-3-methoxybenzaldehyde (vanillin) (LOBA Chemie).

Annexure B

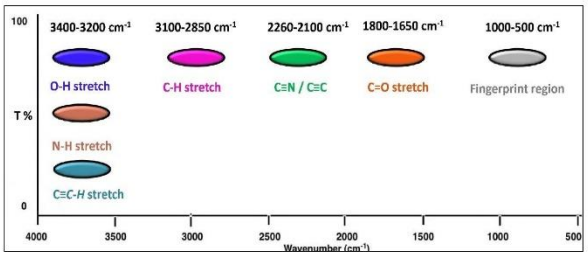

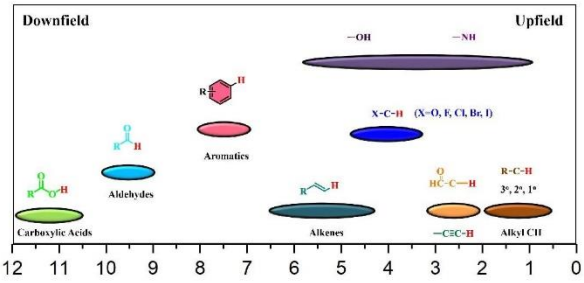

Annexure B contains all the IR, NMR (^{1}H and ^{13}C), and mass spectra of all the synthesized terminal alkynes, organic azides, and the 1,2,3-triazole derivatives.

IR spectrum of benzyl azide 105

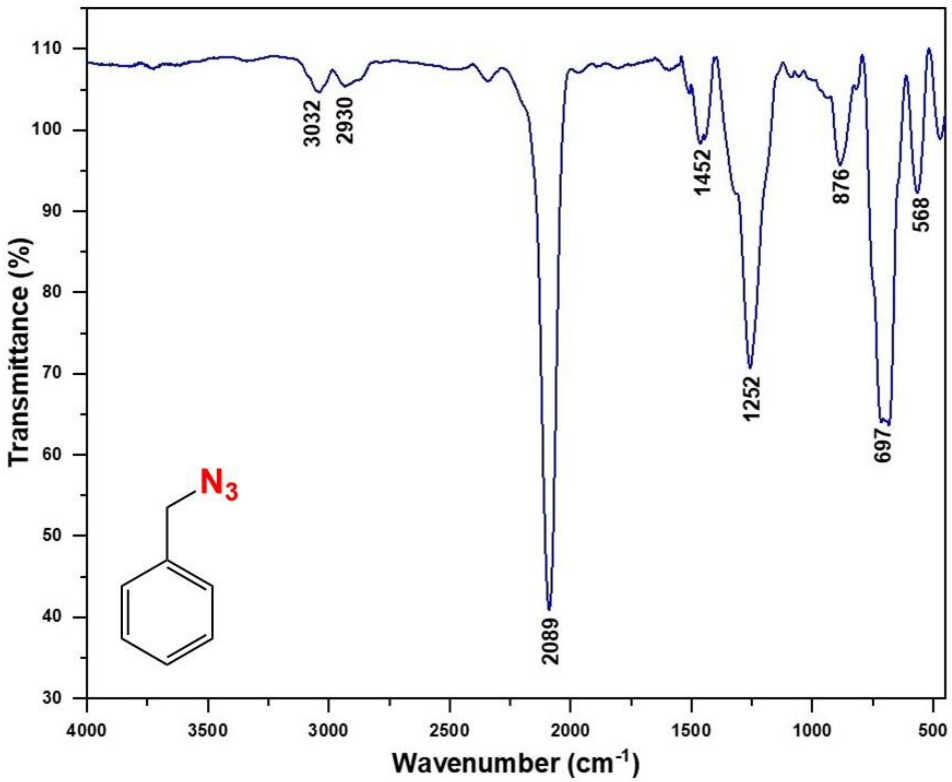

IR spectrum of 1-(azidomethyl)naphthalene 137

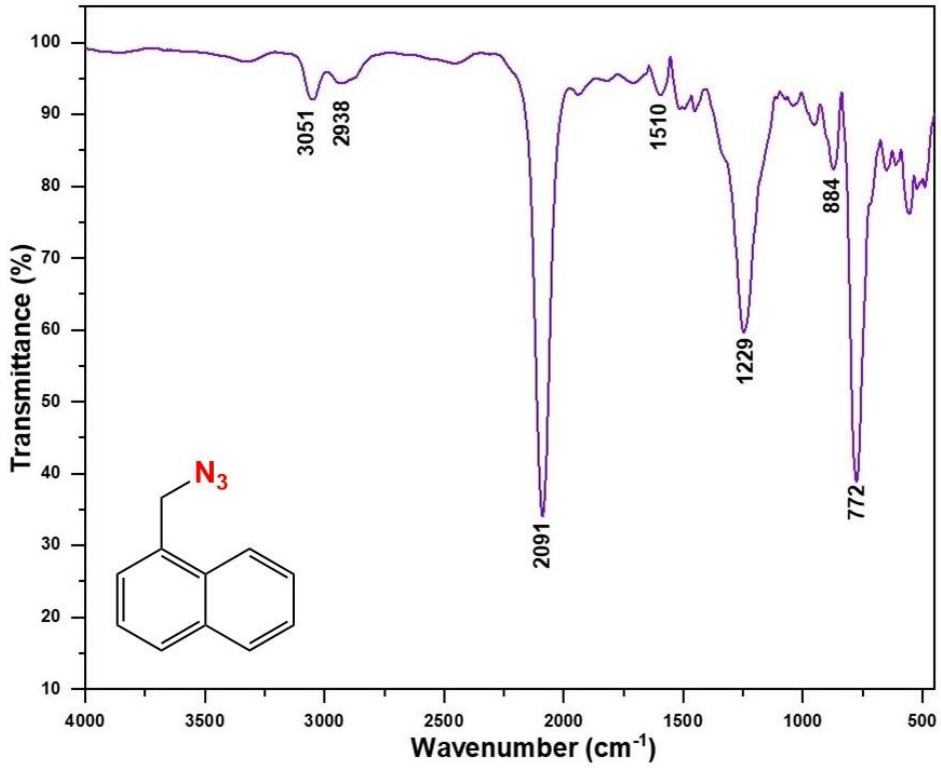

IR spectrum of alkyne 139

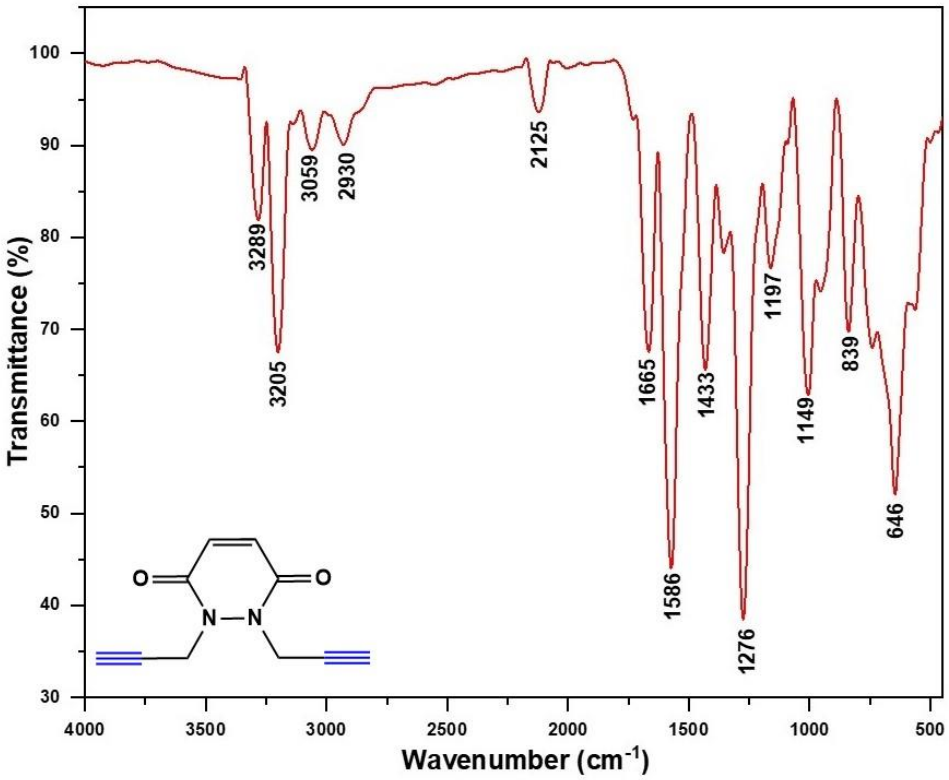

IR spectrum of 1,2,3-triazole derivative 140

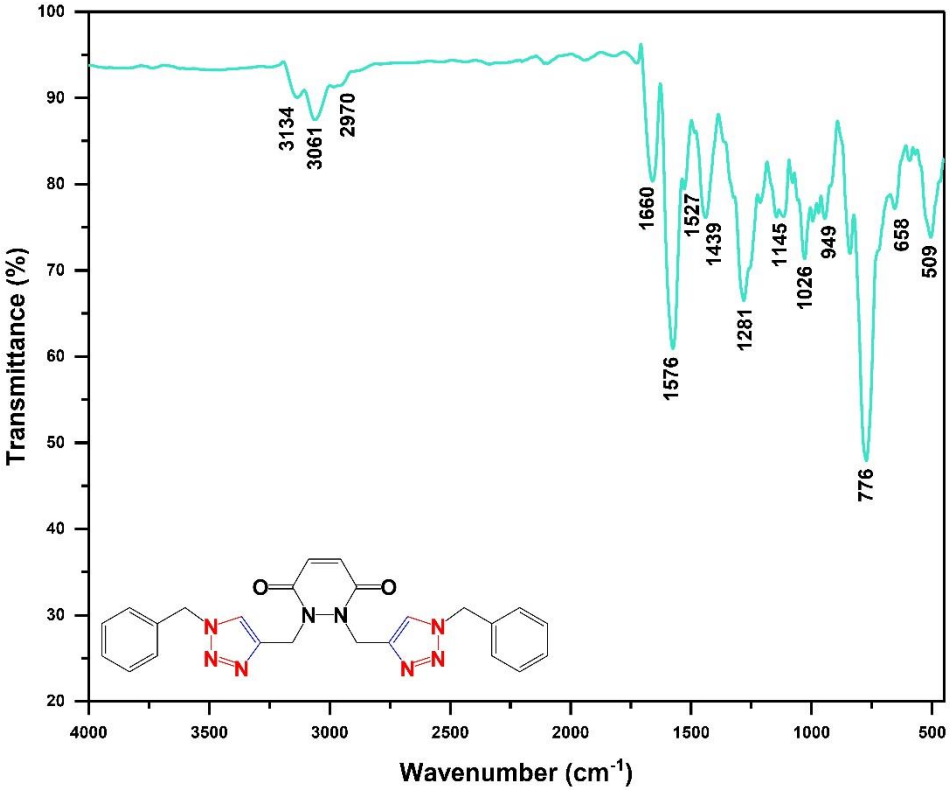

IR spectrum of 1,2,3-triazole derivative 141

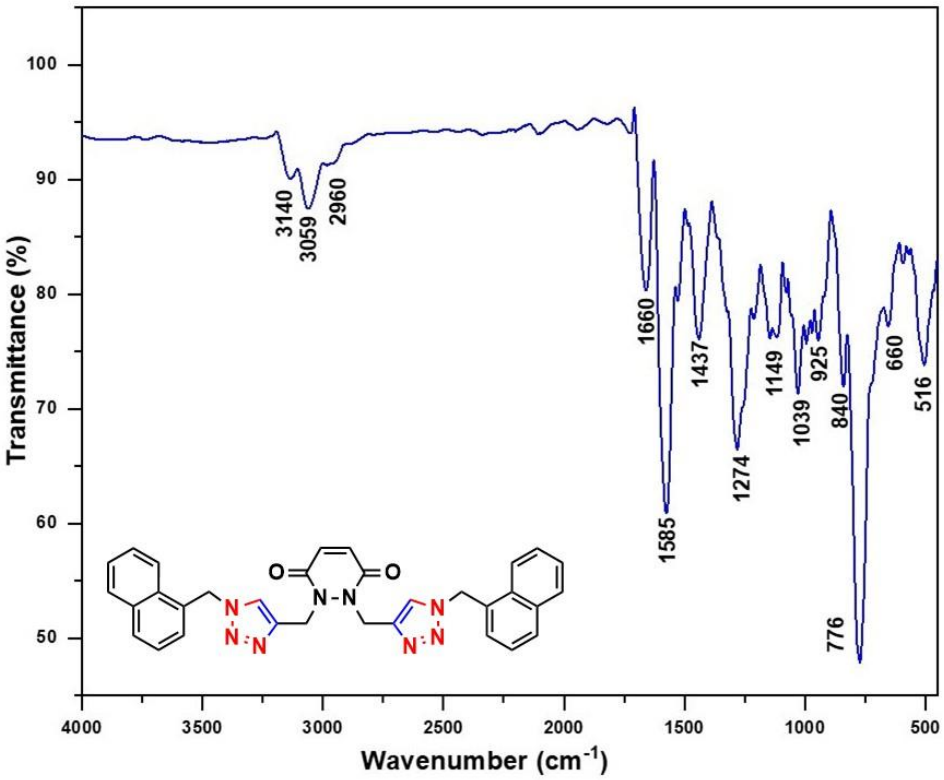

IR spectrum of alkyne 143

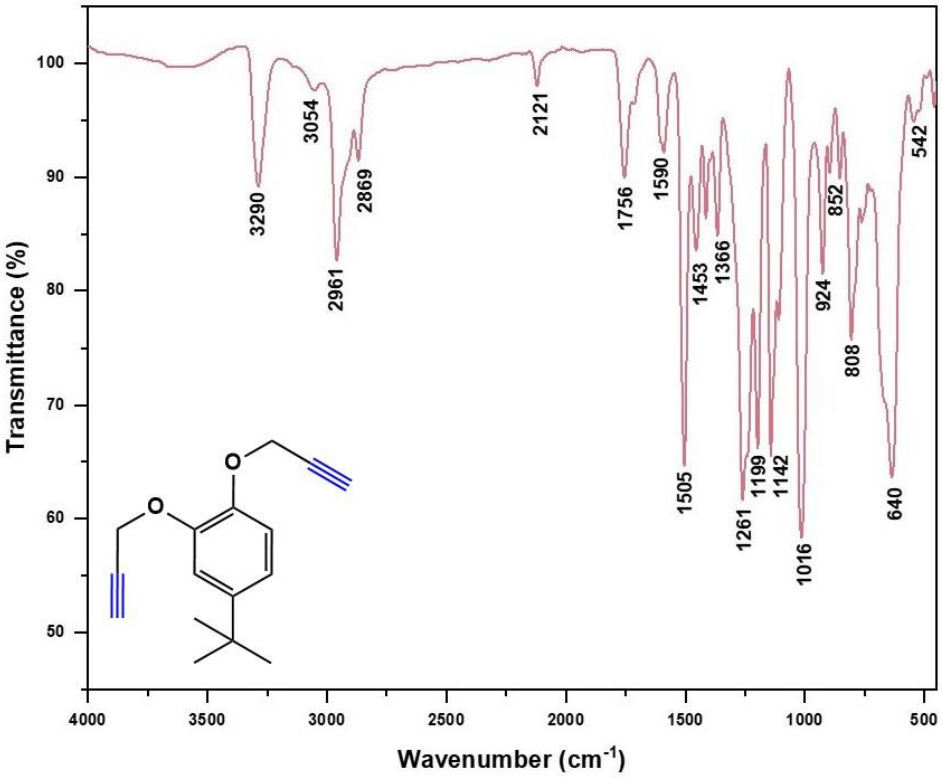

IR spectrum of 1,2,3-triazole derivative 144

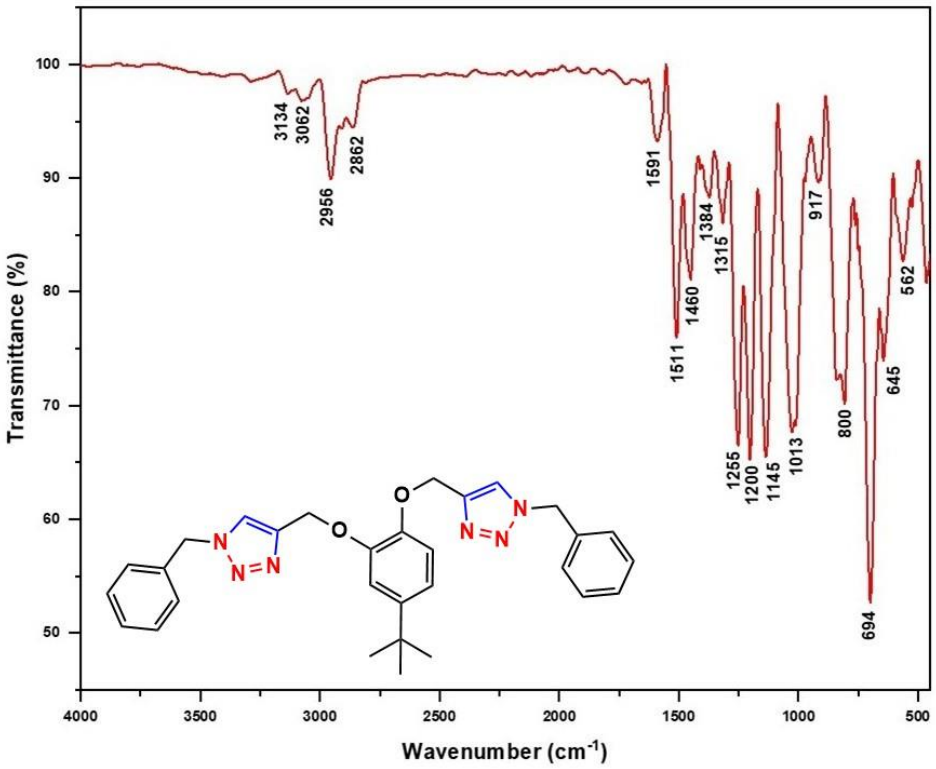

IR spectrum of alkyne 146

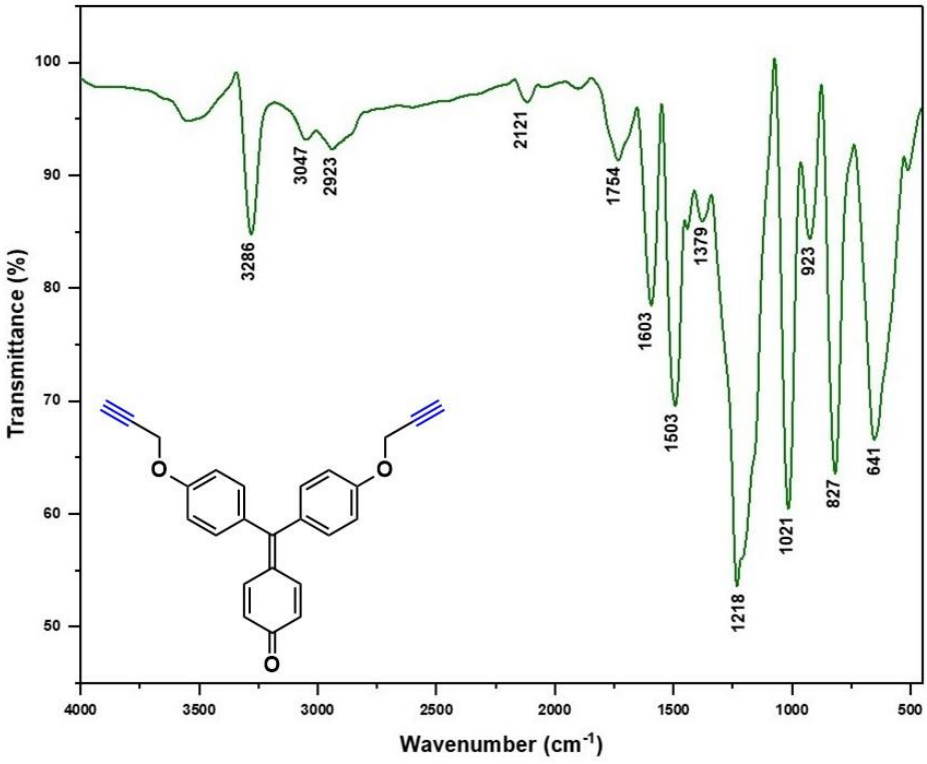

IR spectrum of 1,2,3-triazole derivative 147

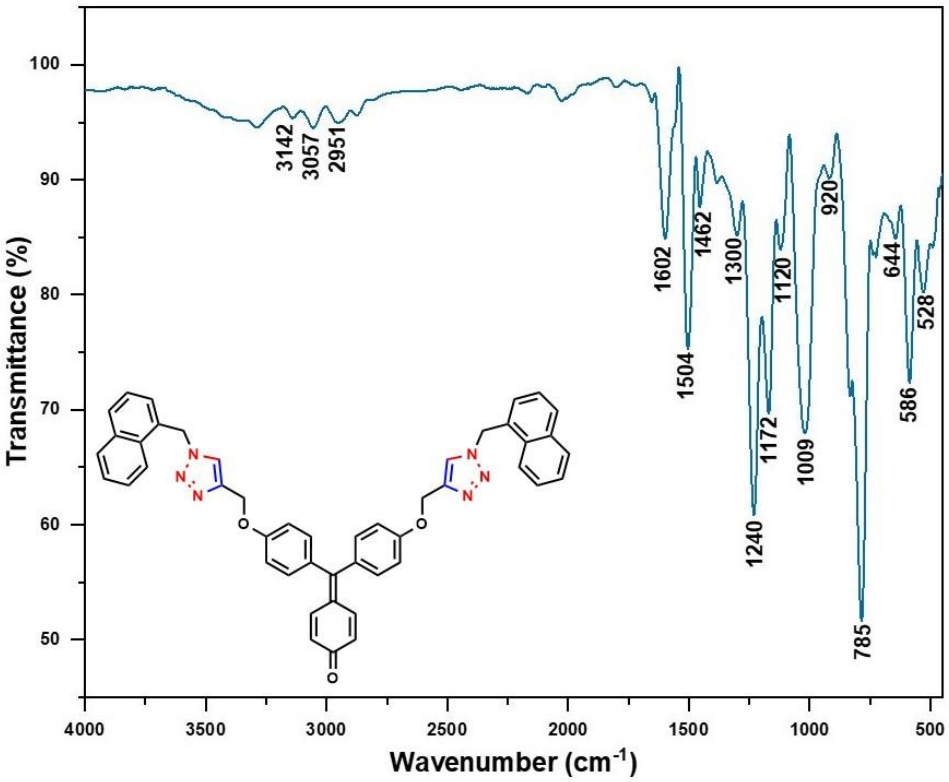

IR spectrum of alkyne 149

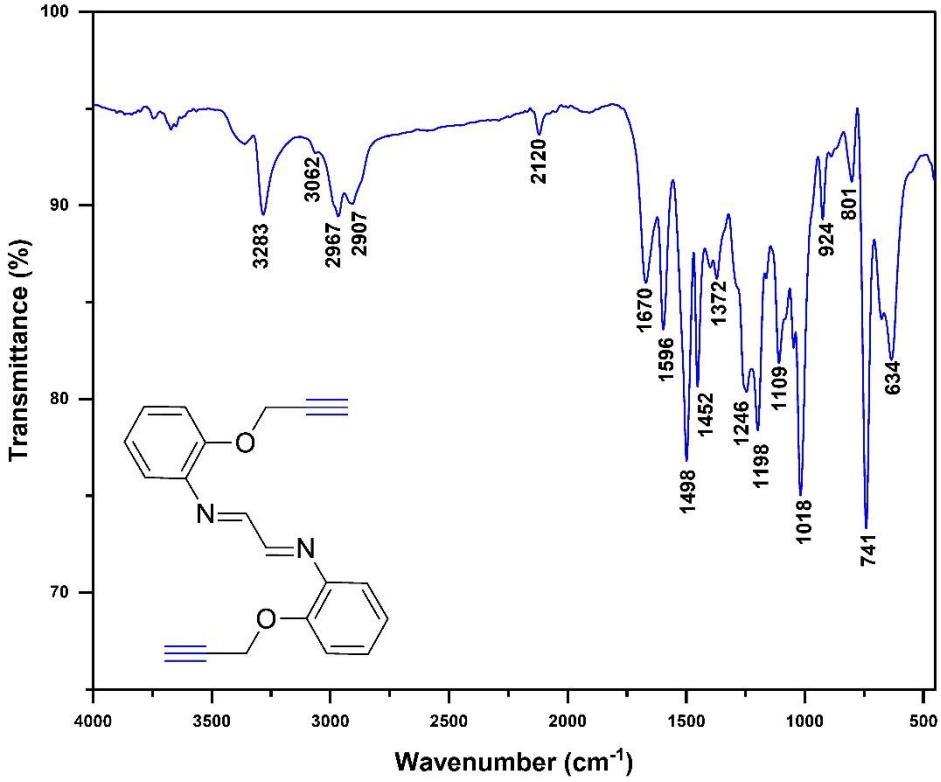

IR spectrum of 1,2,3-triazole derivative 150

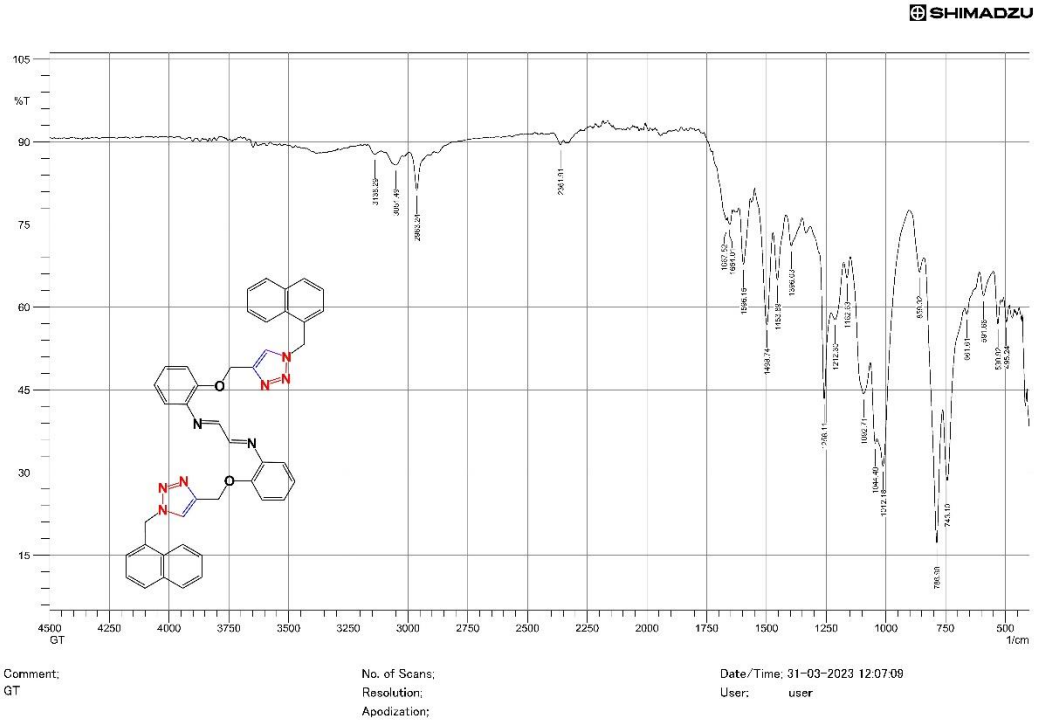

IR spectrum of Schiff base 153

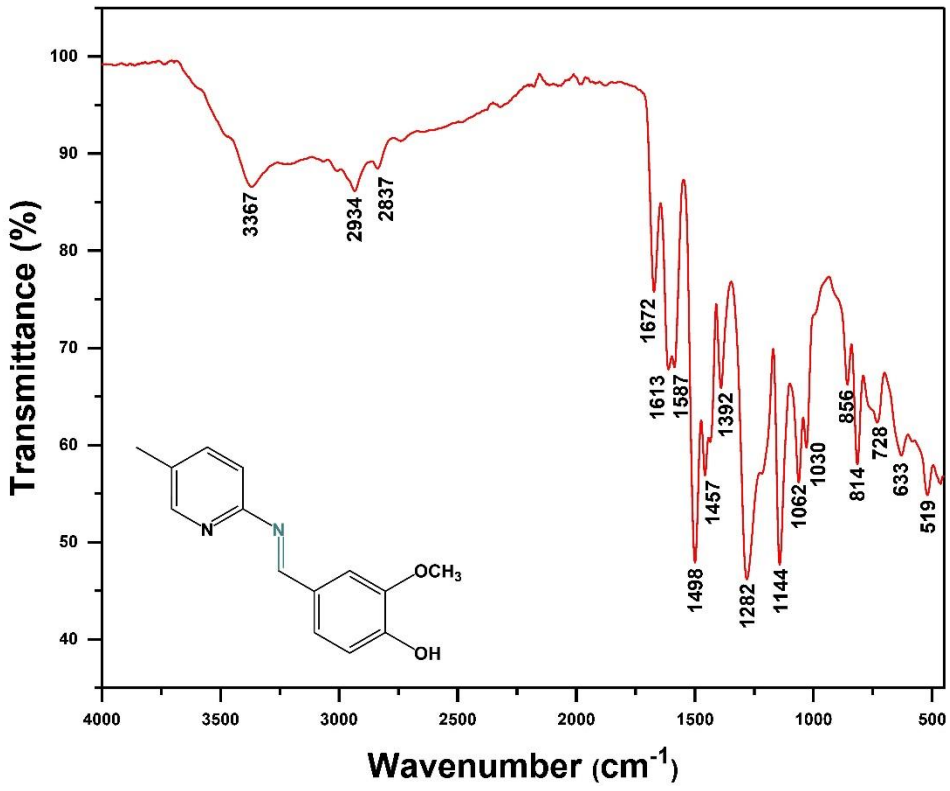

IR spectrum of alkyne 154

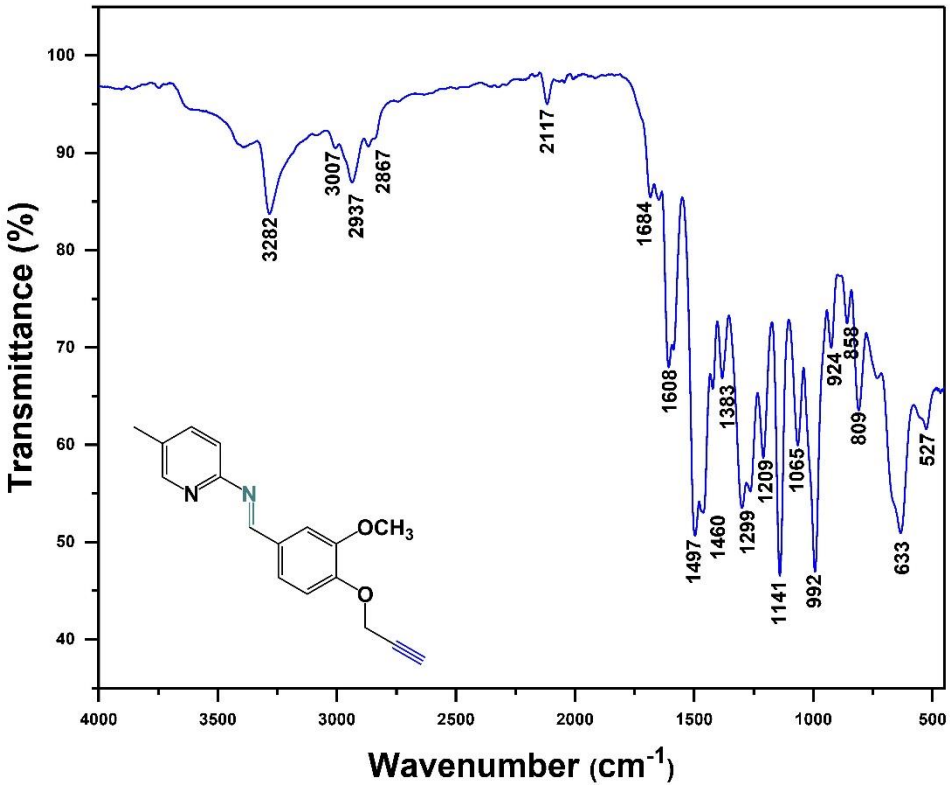

IR spectrum of 1,2,3-triazole derivative 155

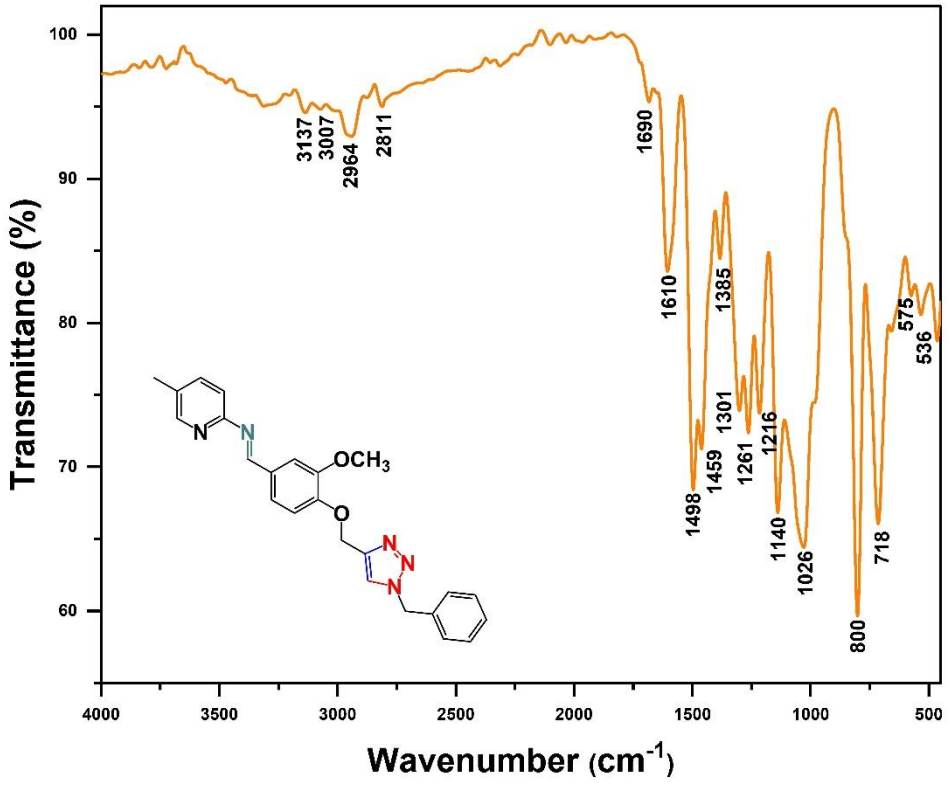

^{1}H NMR spectrum of benzyl azide 105

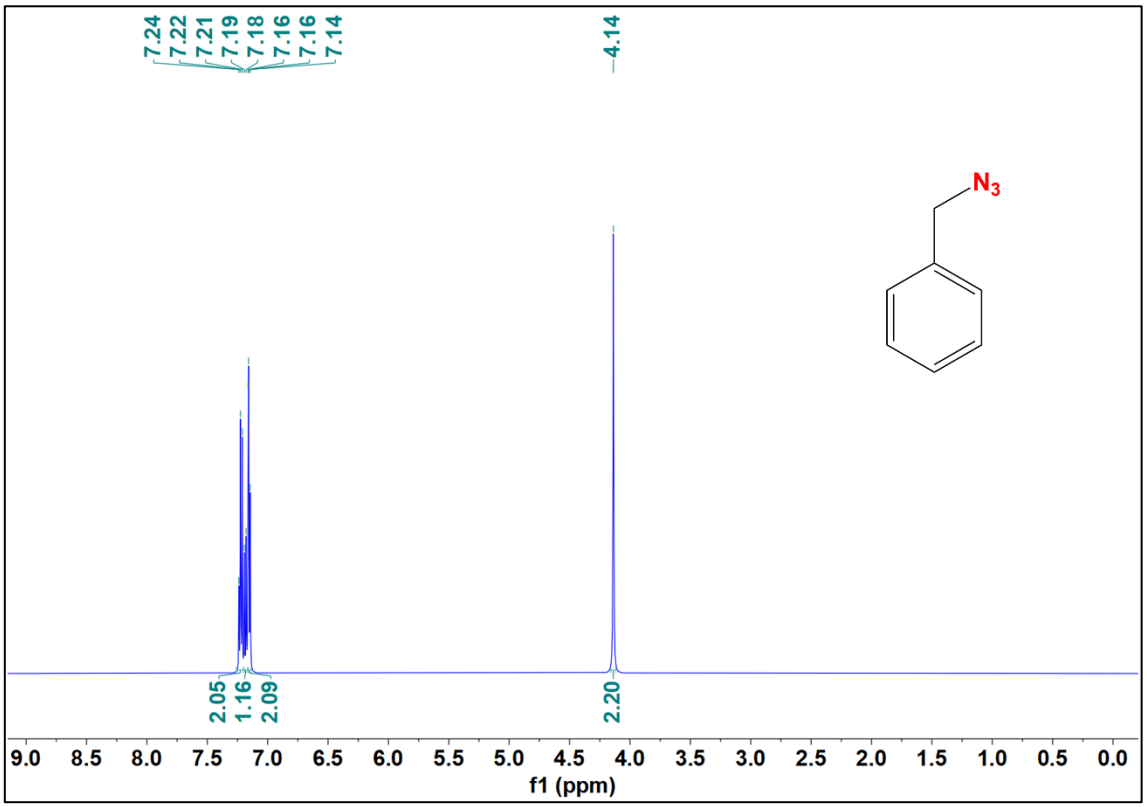

^{13}C NMR spectrum of benzyl azide 105

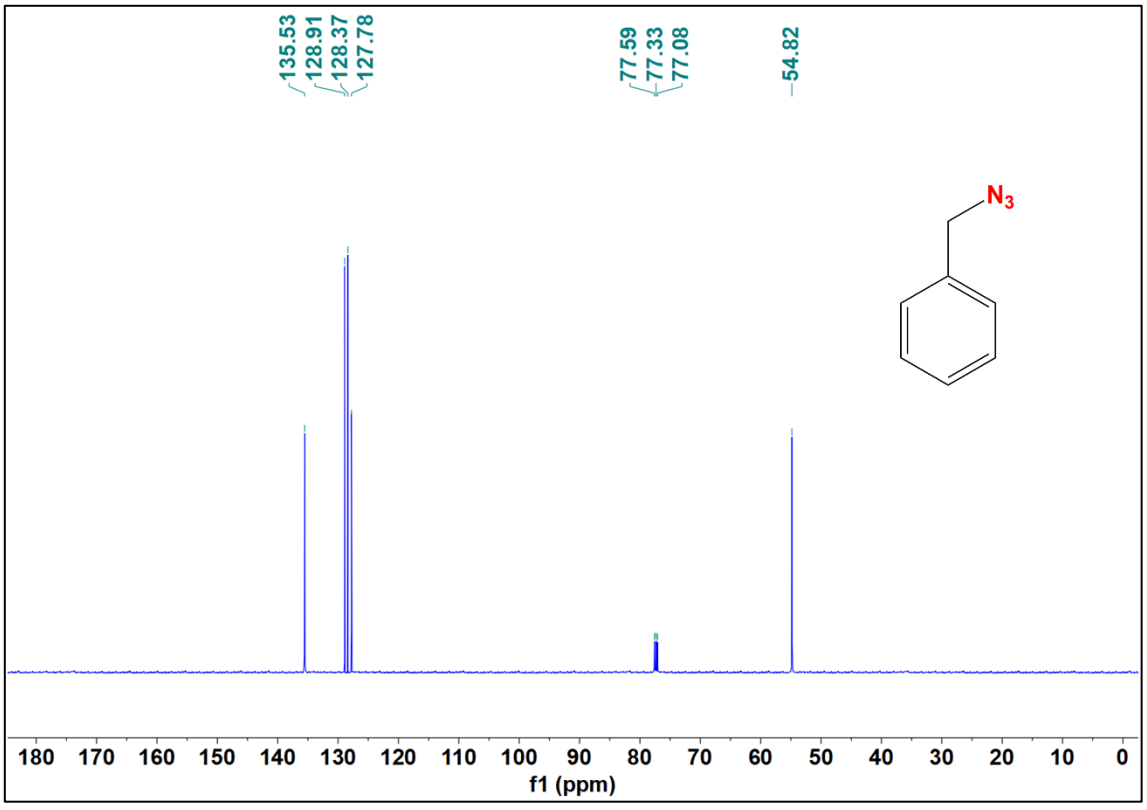

^{1}H NMR spectrum of 1-(azidomethyl)naphthalene 137

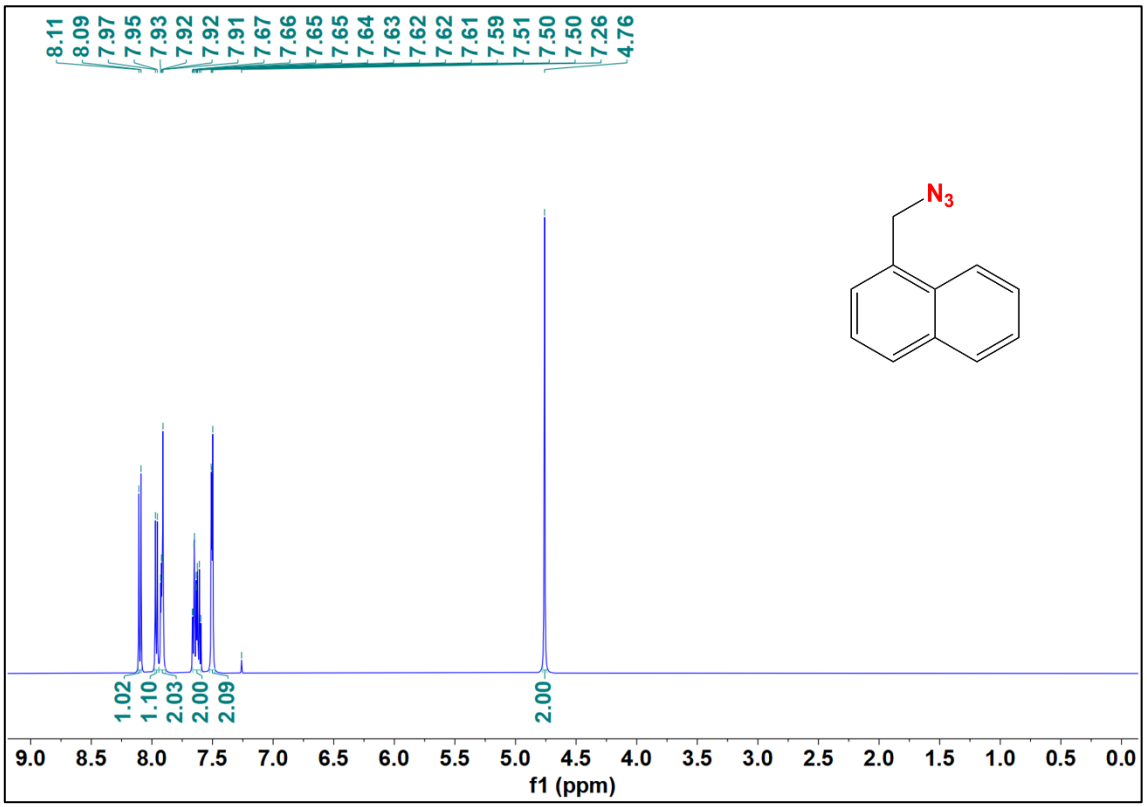

^{13}C NMR spectrum of 1-(azidomethyl)naphthalene 137

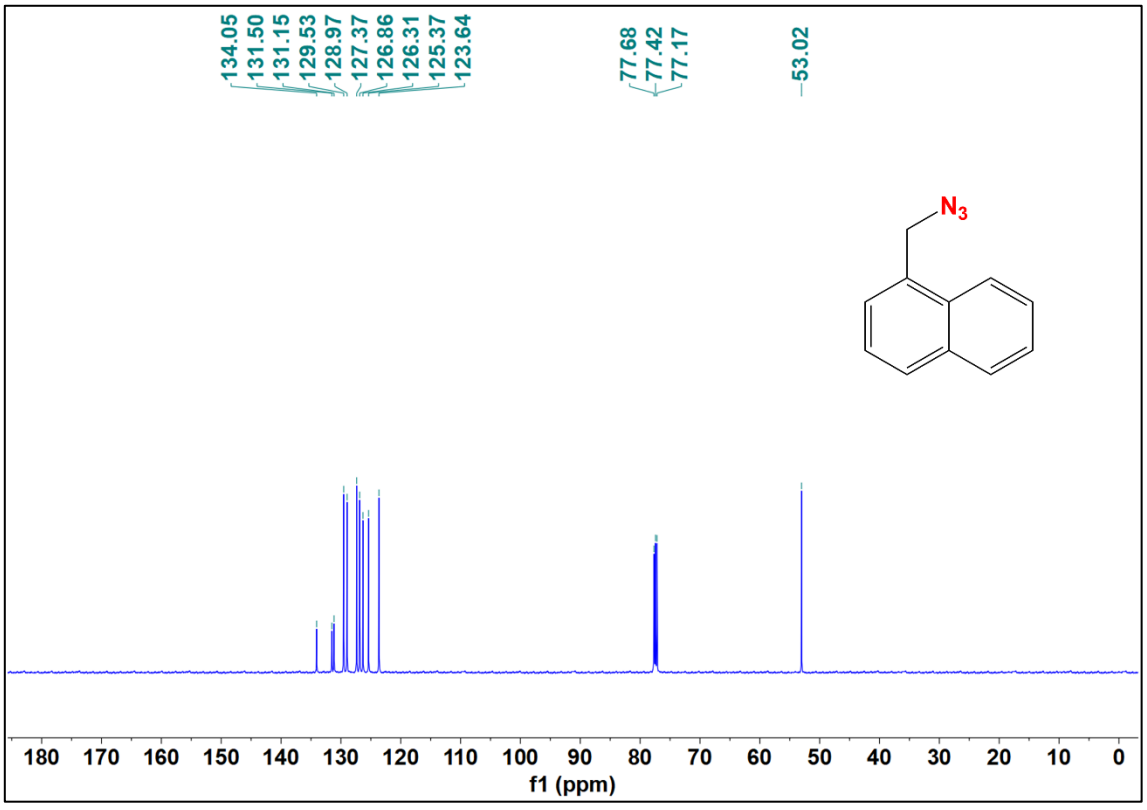

^{1}H NMR spectrum of alkyne 139

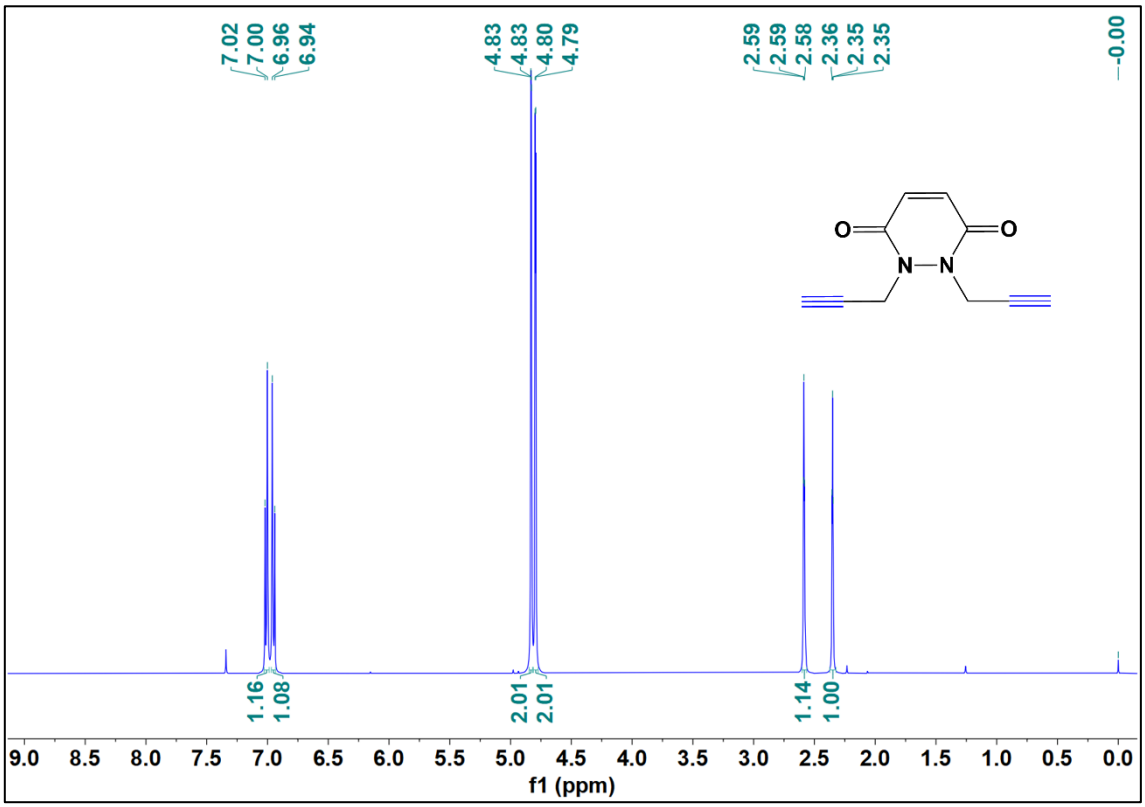

^{13}C NMR spectrum of alkyne 139

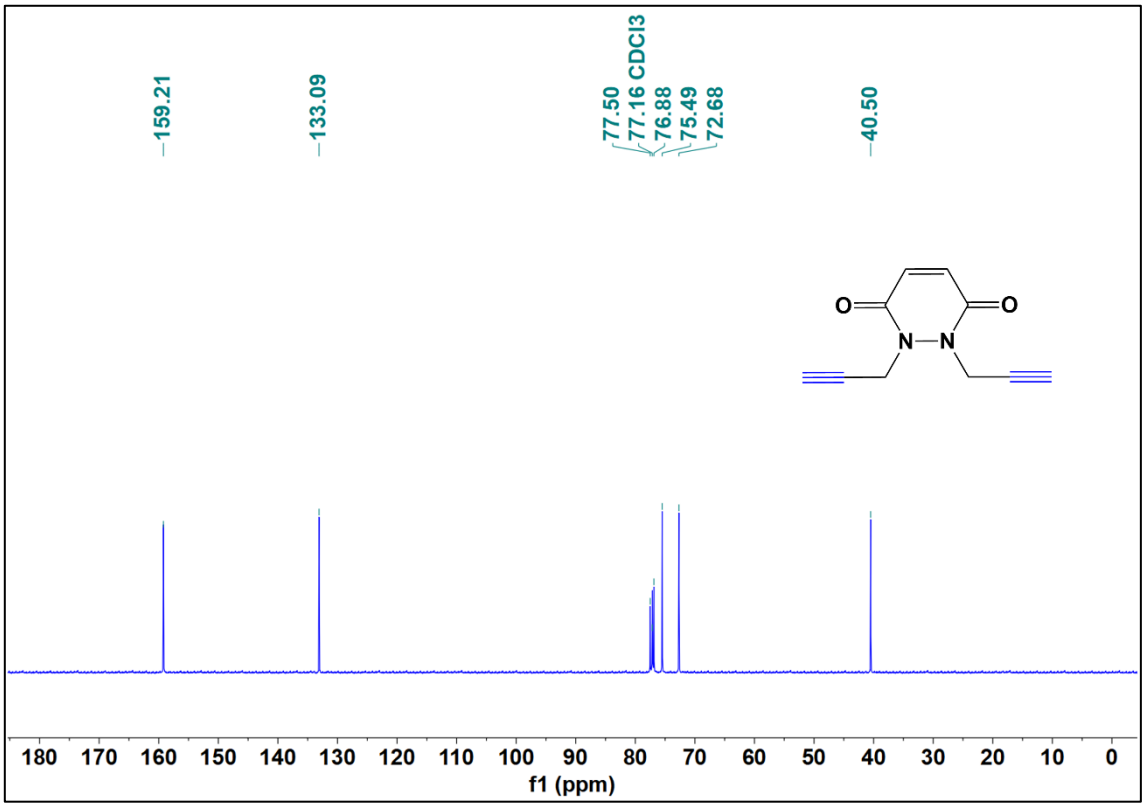

^{1}H NMR spectrum of 1,2,3-triazole derivative 140

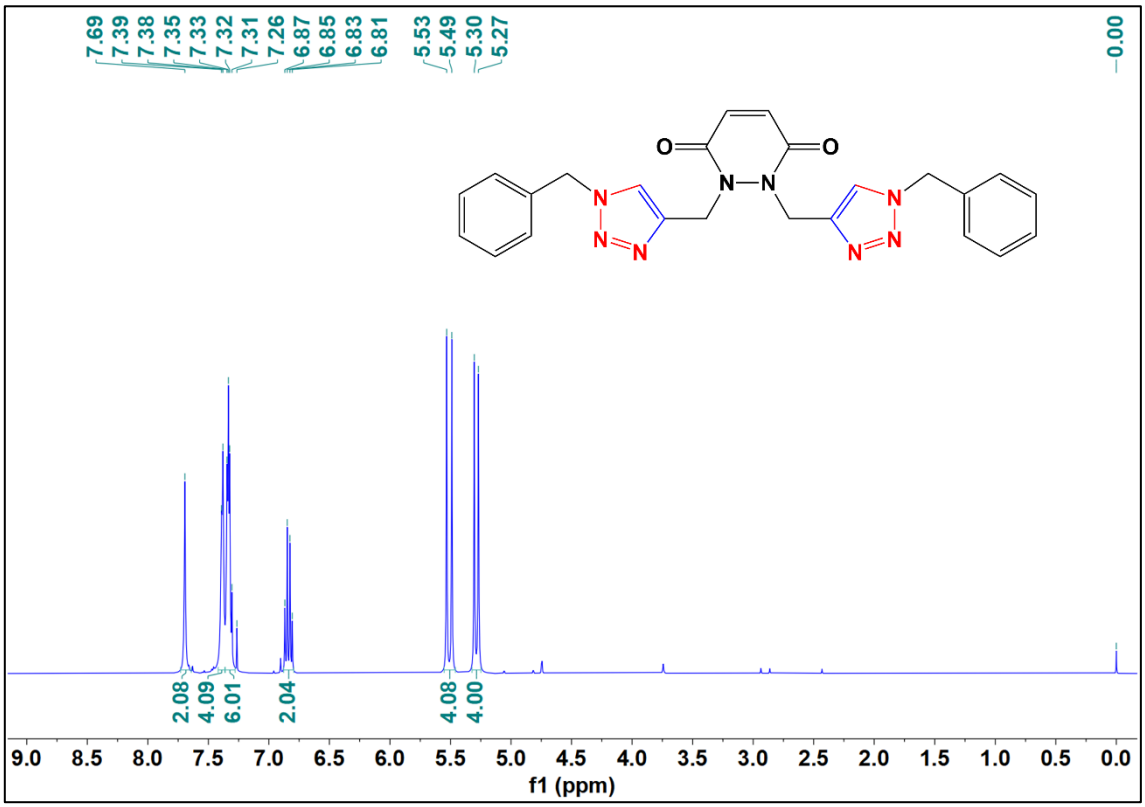

^{13}C NMR spectrum of 1,2,3-triazole derivative 140

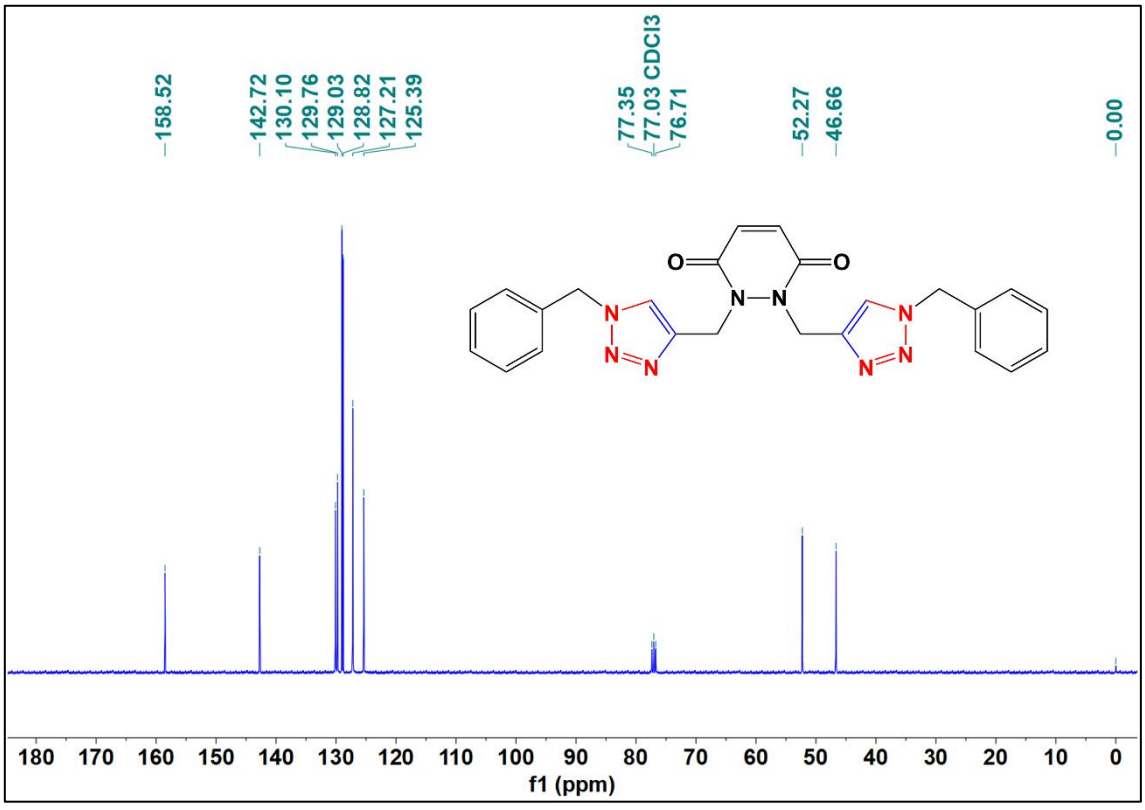

^{1}H NMR spectrum of 1,2,3-triazole derivative 141

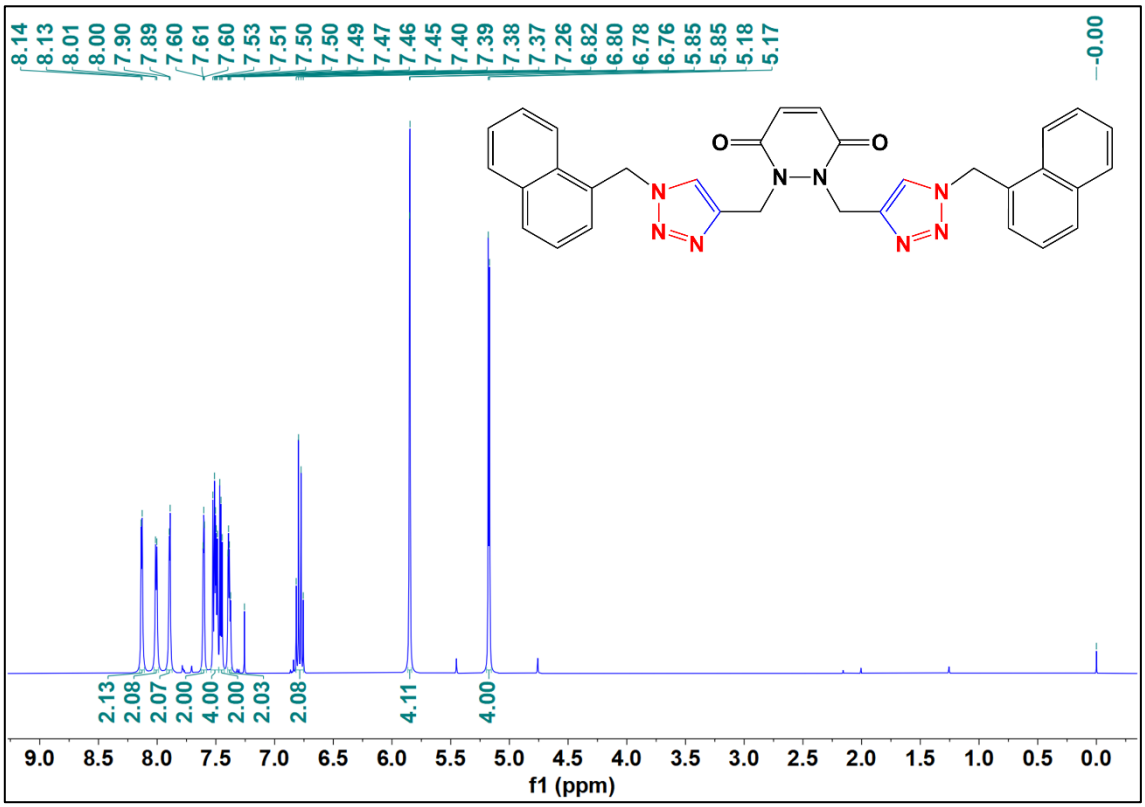

^{13}C NMR spectrum of 1,2,3-triazole derivative 141

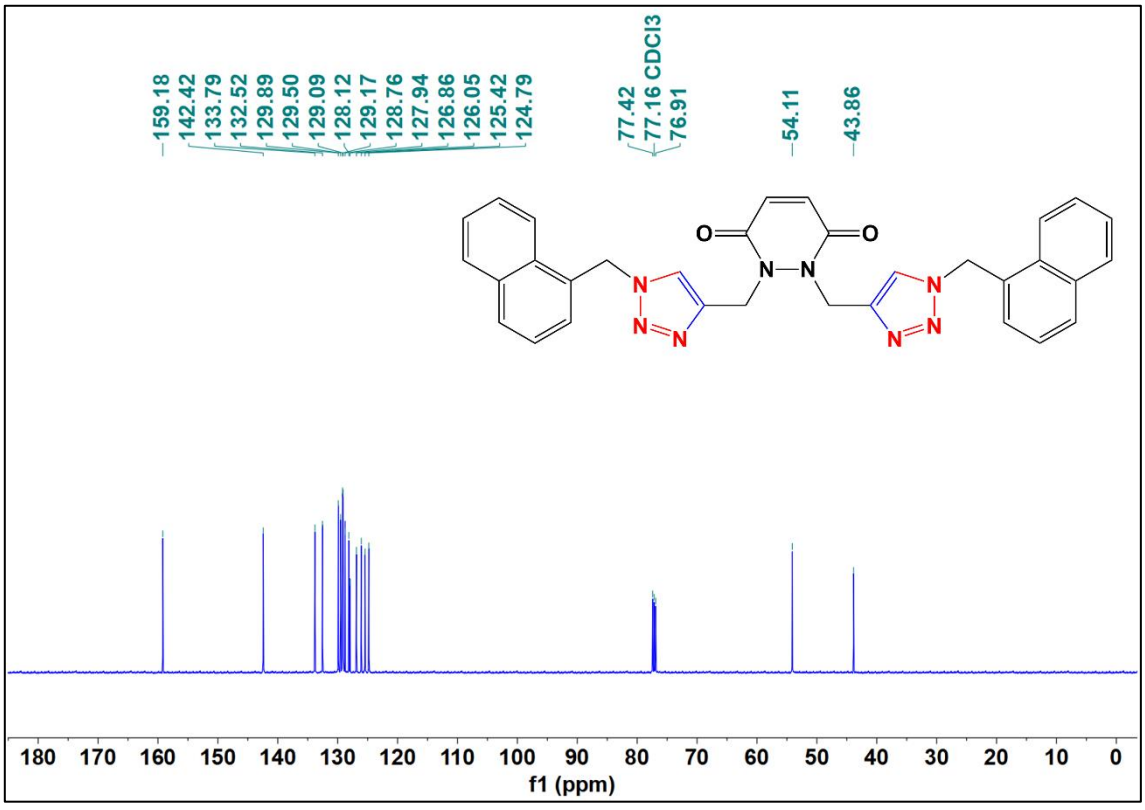

^{1}H NMR spectrum of alkyne 143

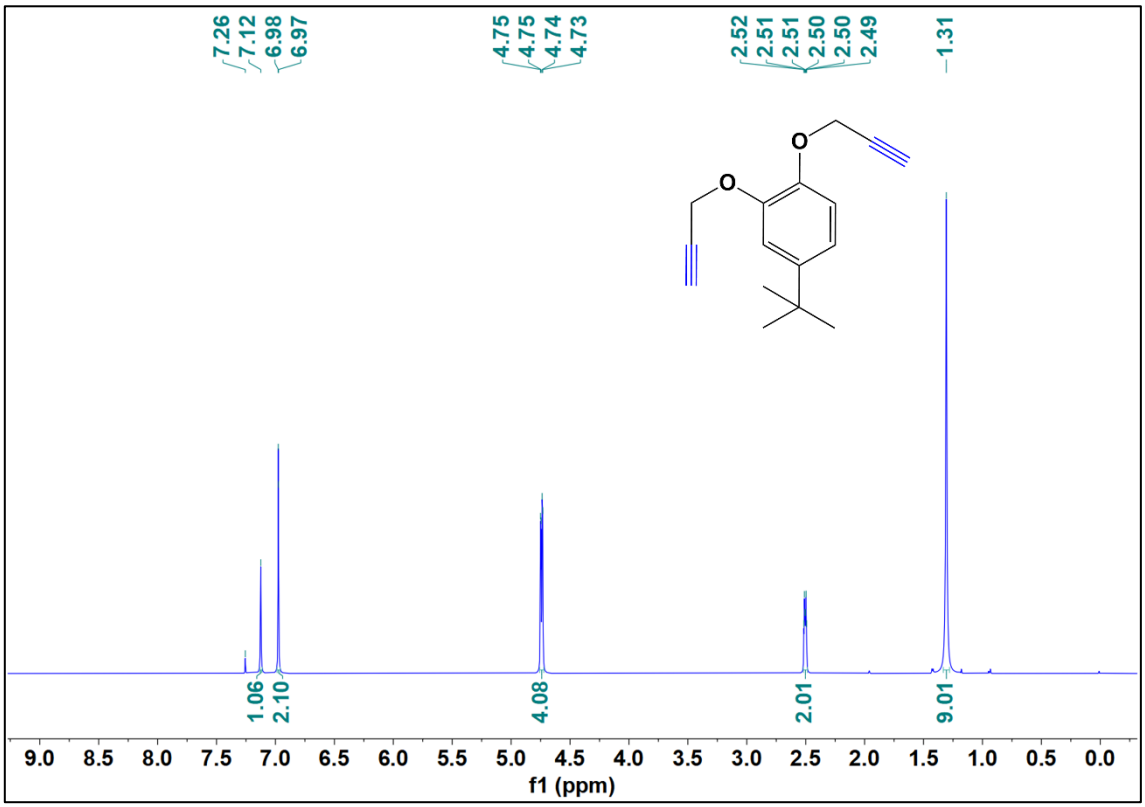

^{13}C NMR spectrum of alkyne 143

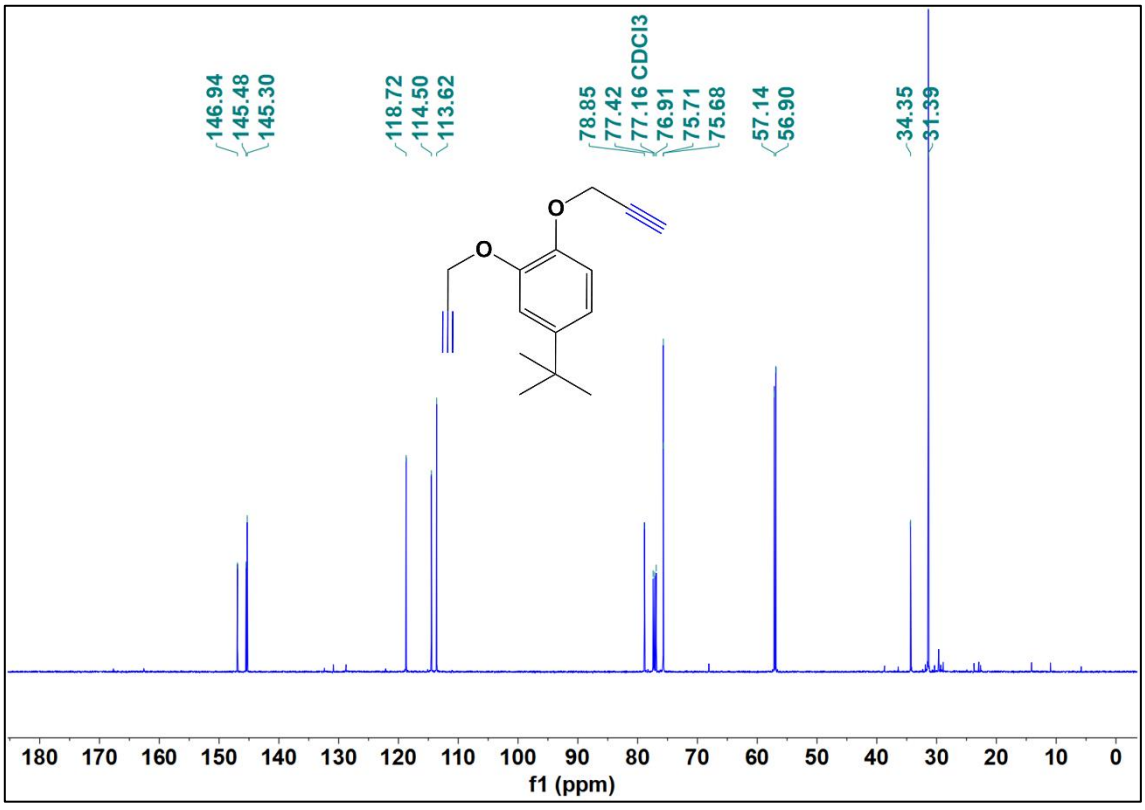

^{1}H NMR spectrum of 1,2,3-triazole derivative 144

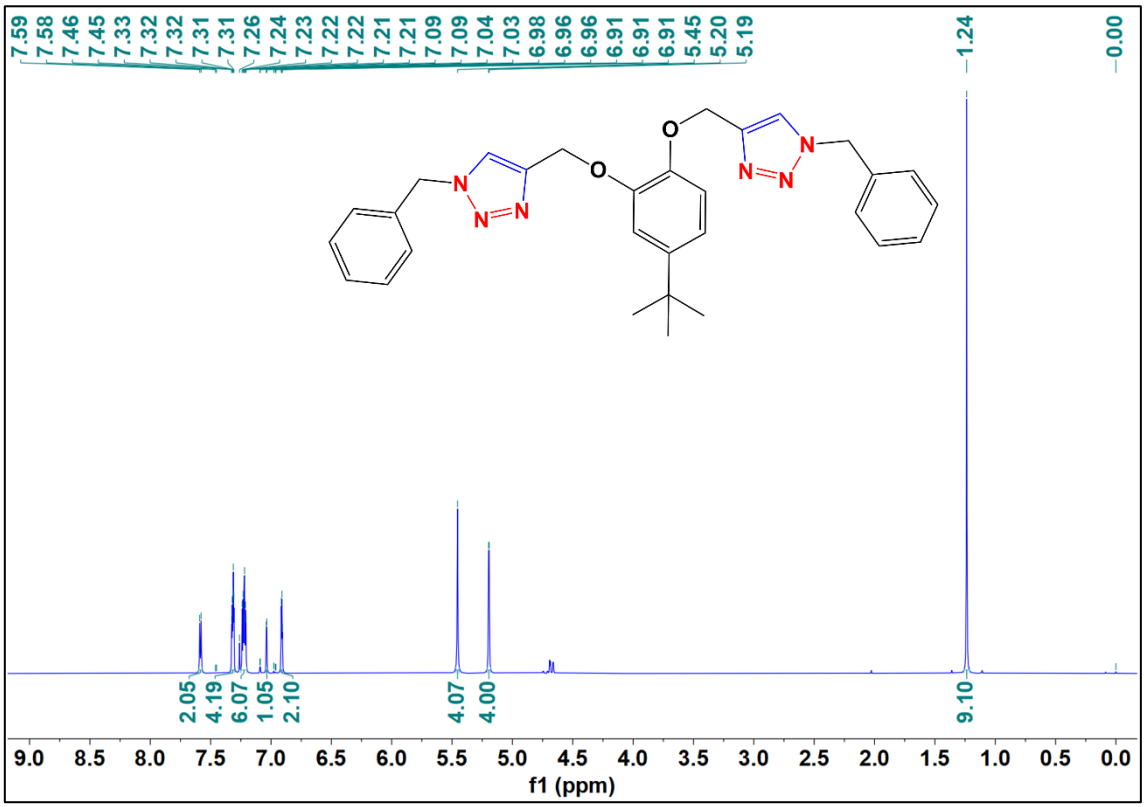

^{13}C NMR spectrum of 1,2,3-triazole derivative 144

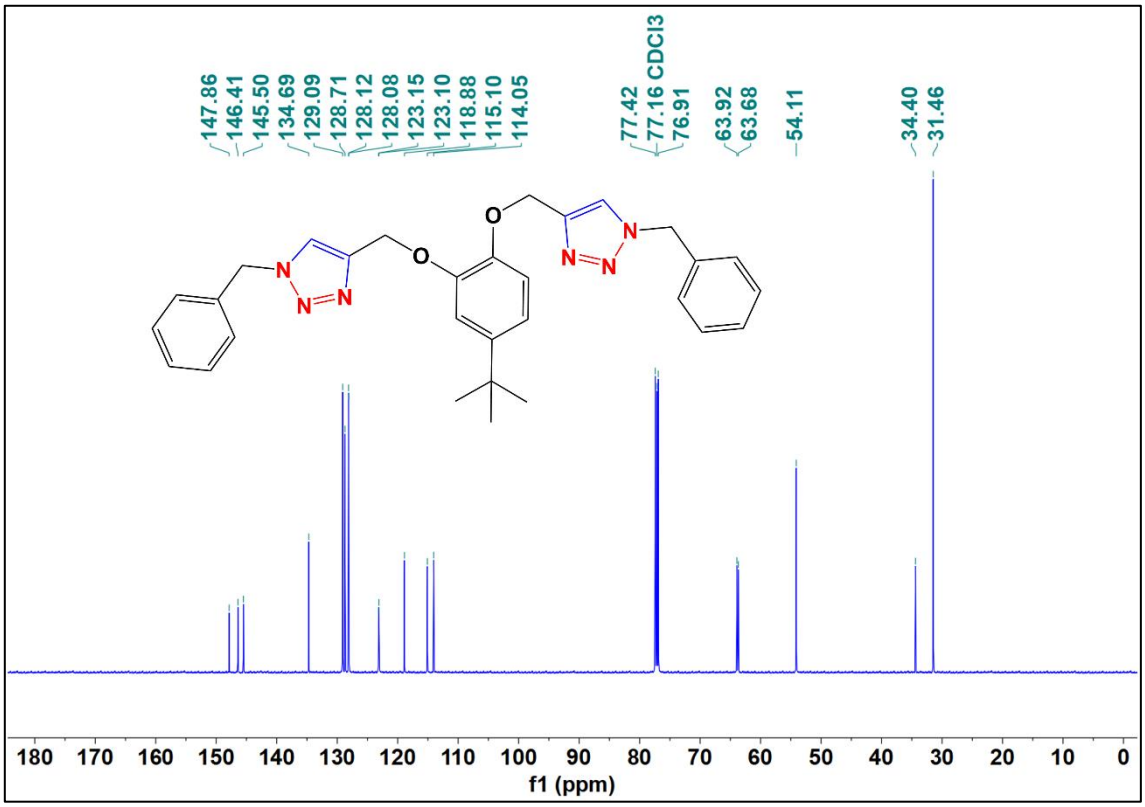

^{1}H NMR spectrum of alkyne 146

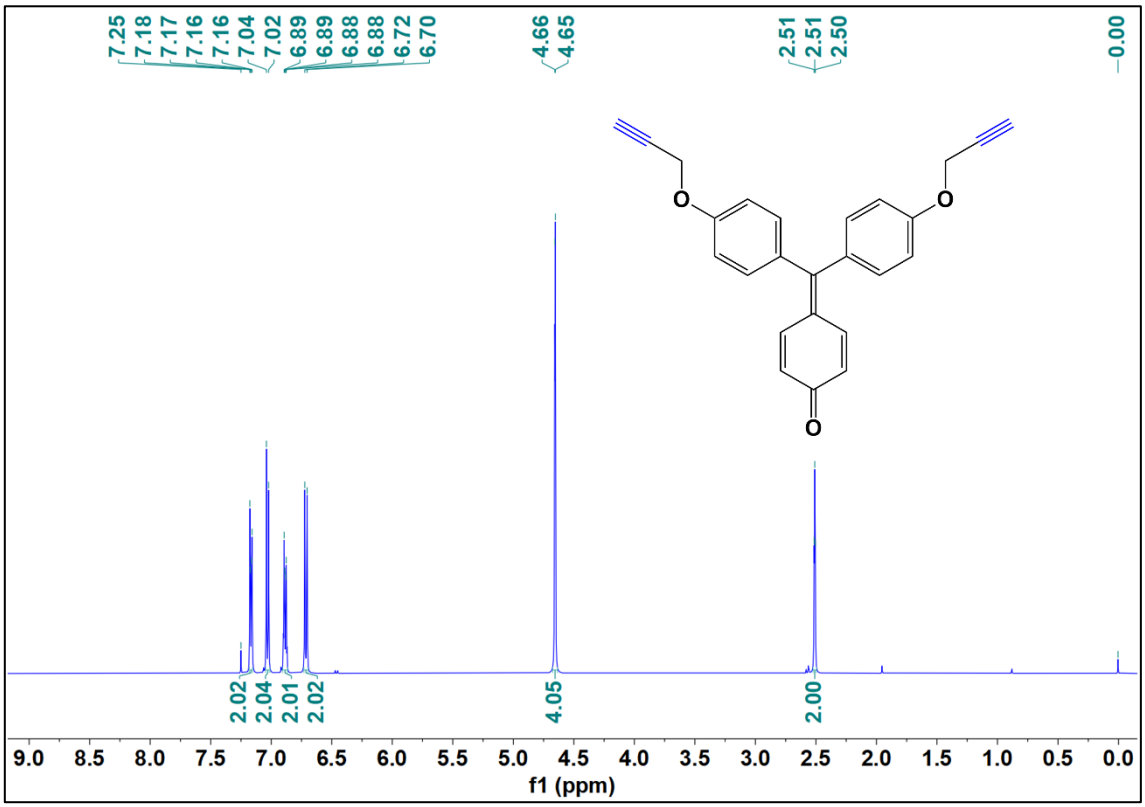

^{13}C NMR spectrum of alkyne 146

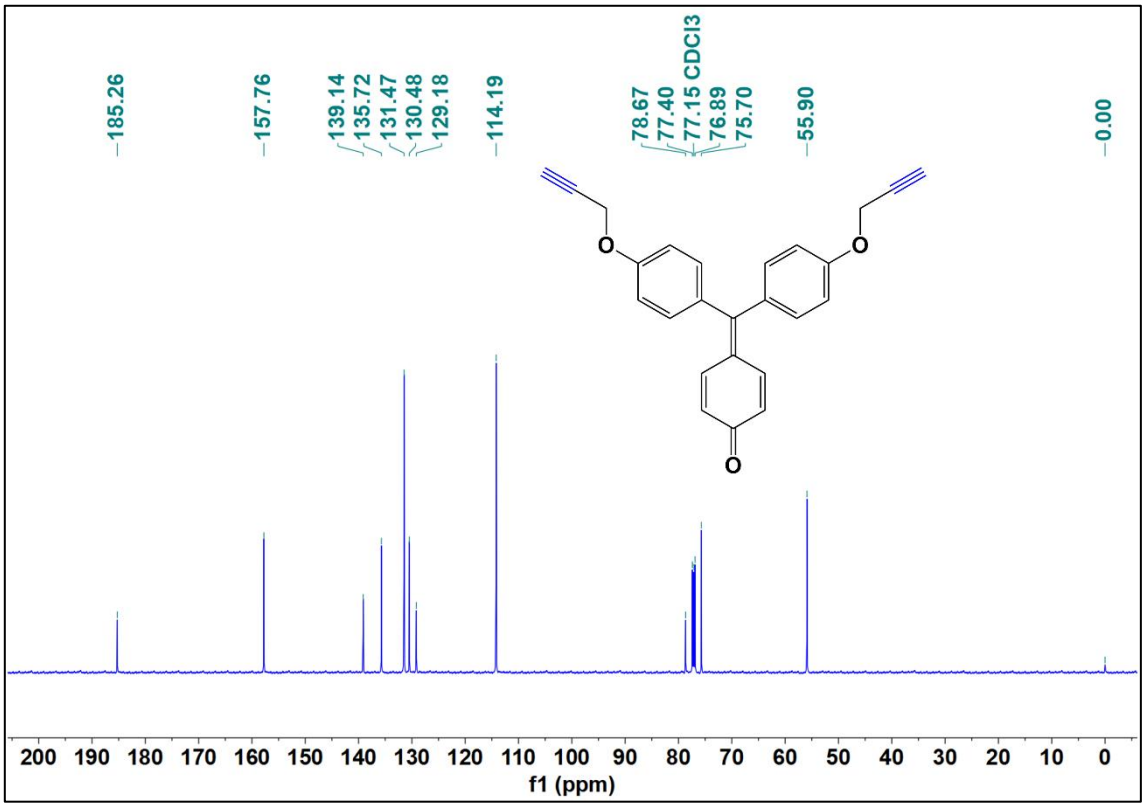

^{1}H NMR spectrum of 1,2,3-triazole derivative 147

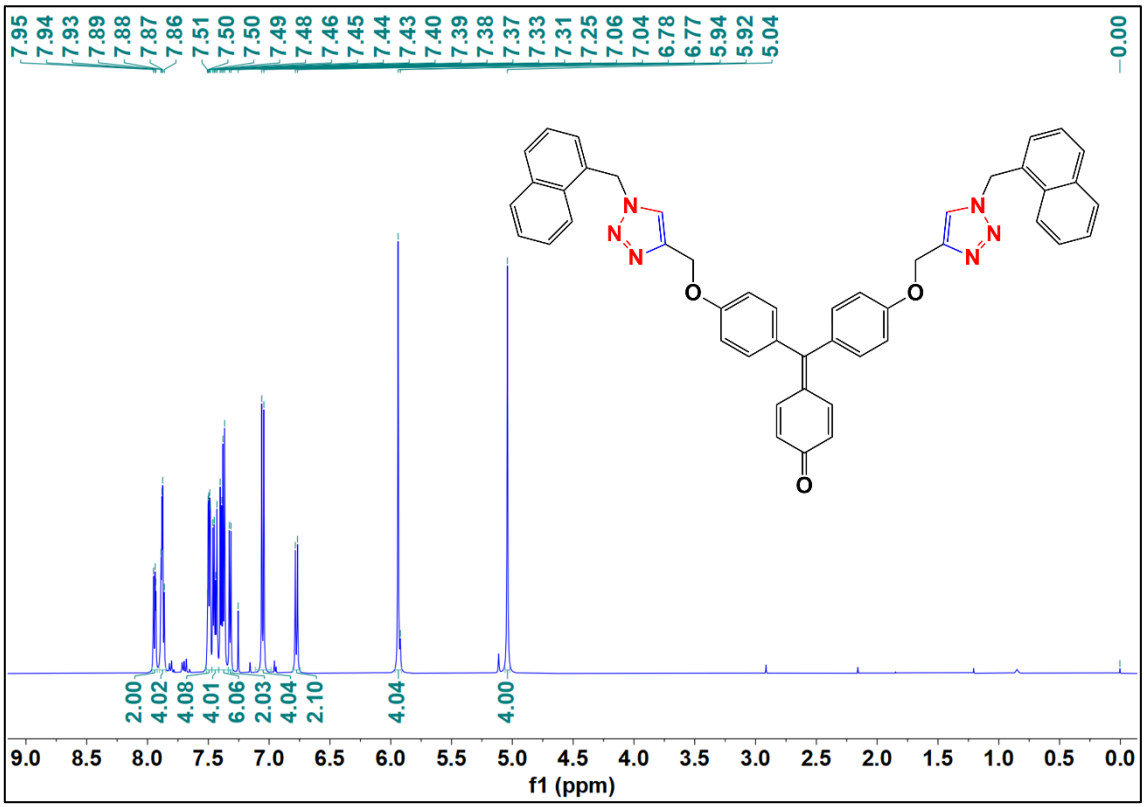

^{13}C NMR spectrum of 1,2,3-triazole derivative 147

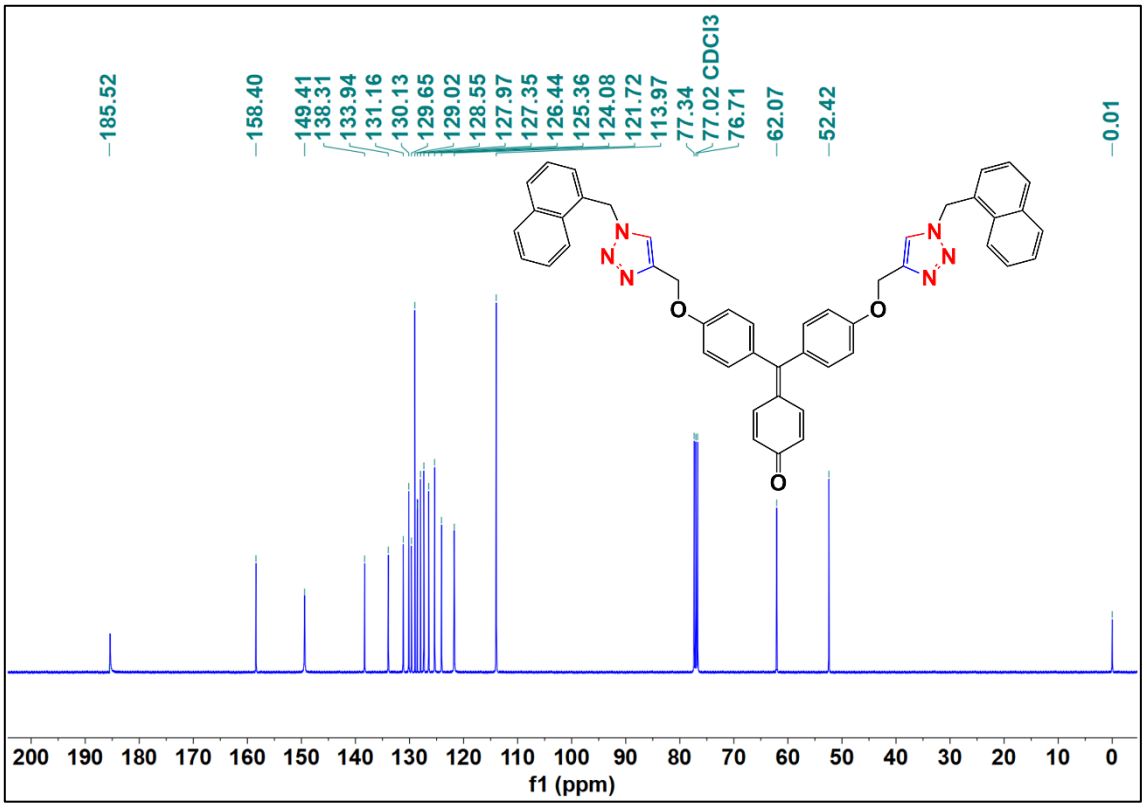

^{1}H NMR spectrum of alkyne 149

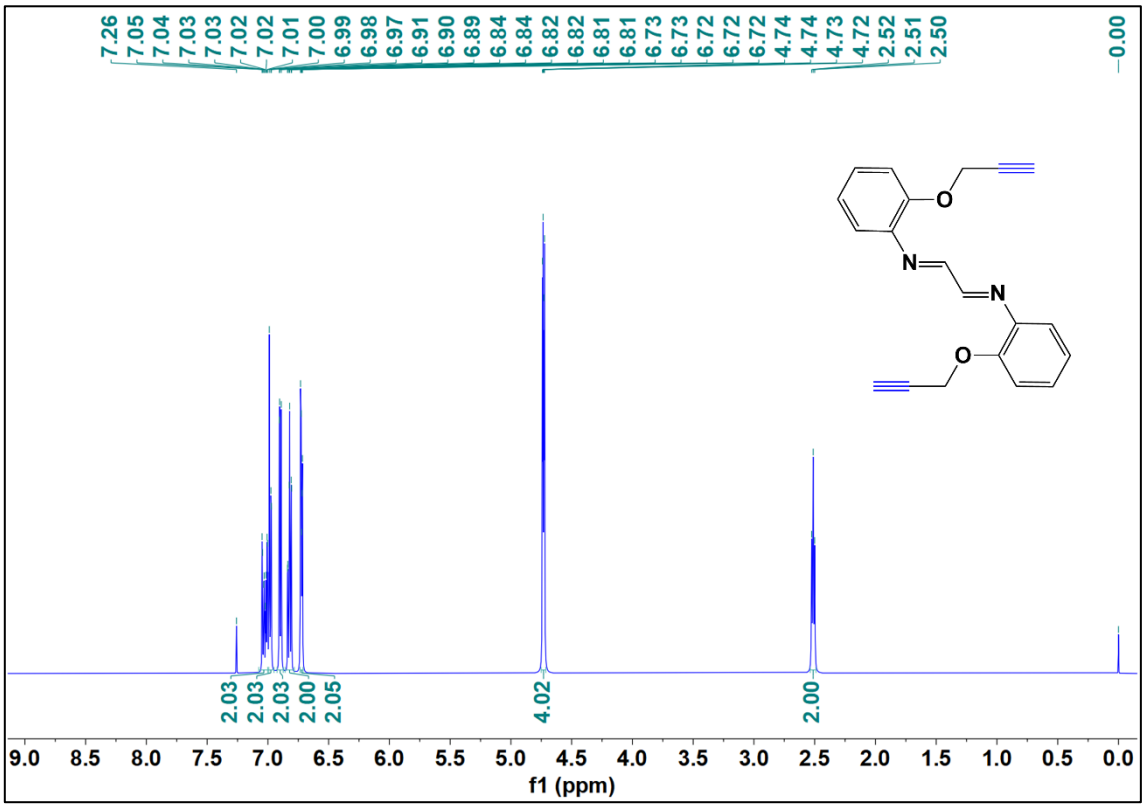

^{13}C NMR spectrum of alkyne 149

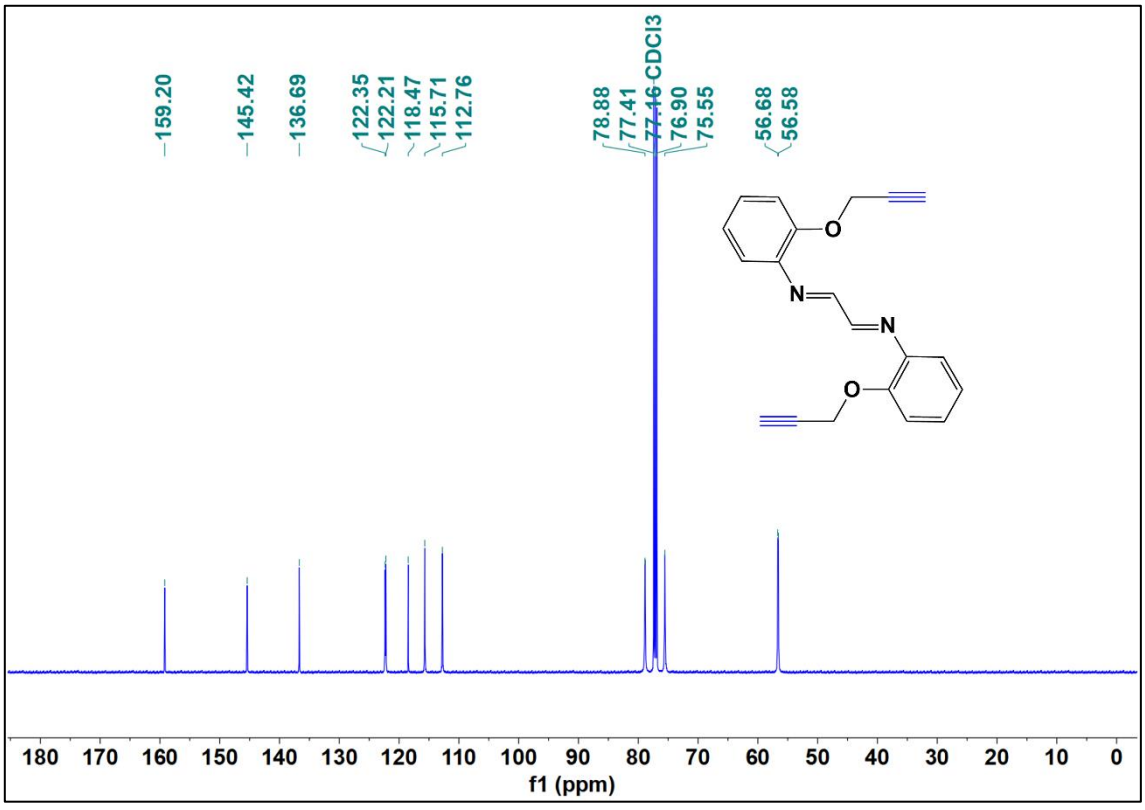

^{1}H NMR spectrum of 1,2,3-triazole derivative 150

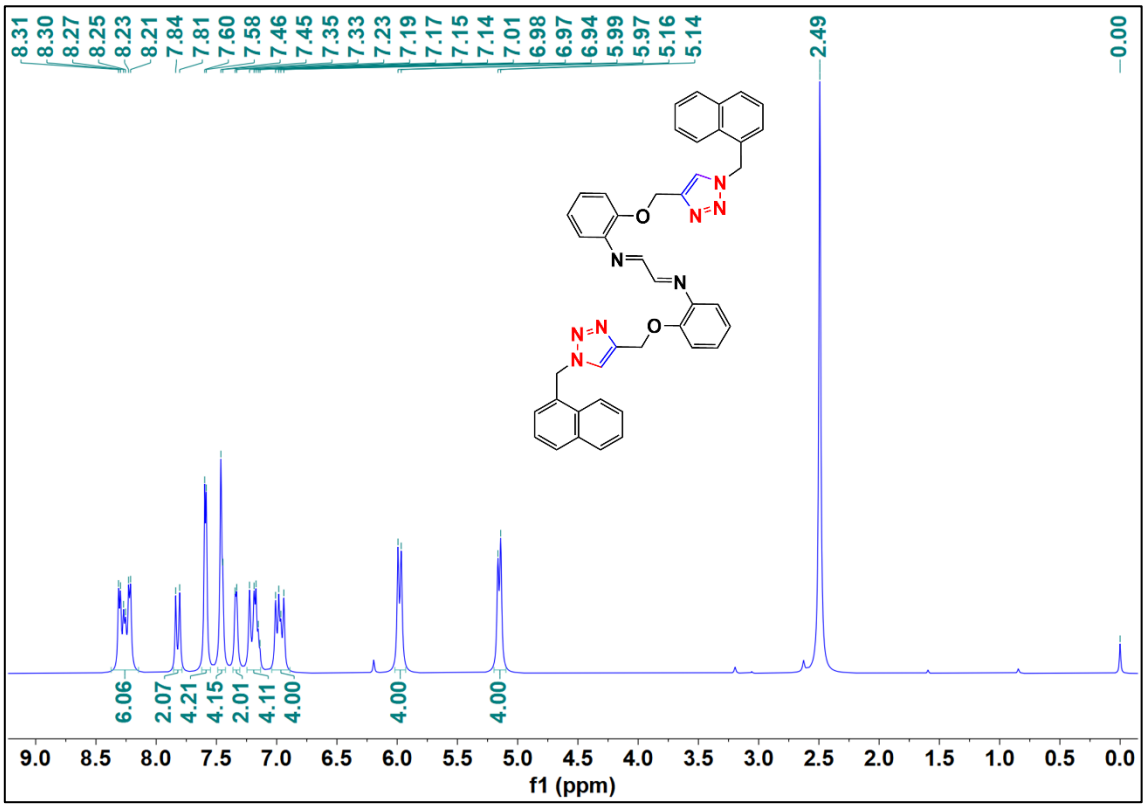

^{13}C NMR spectrum of 1,2,3-triazole derivative 150

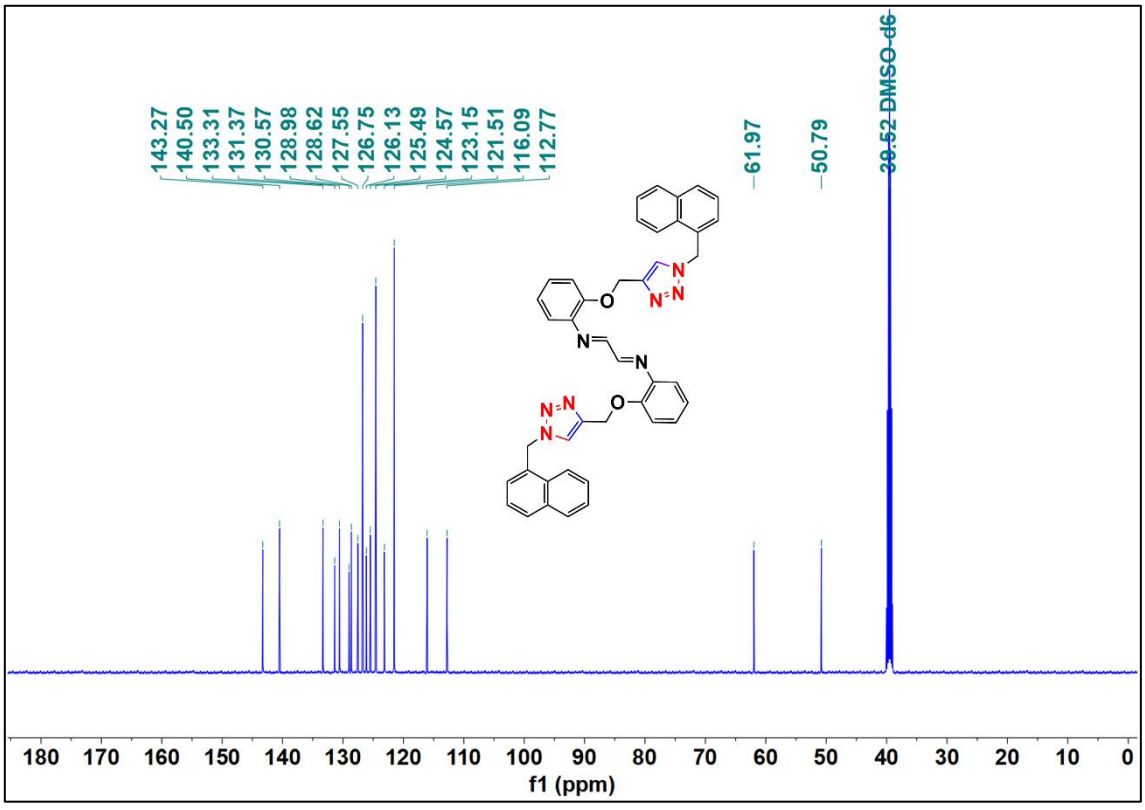

^{1}H NMR spectrum of Schiff base 153

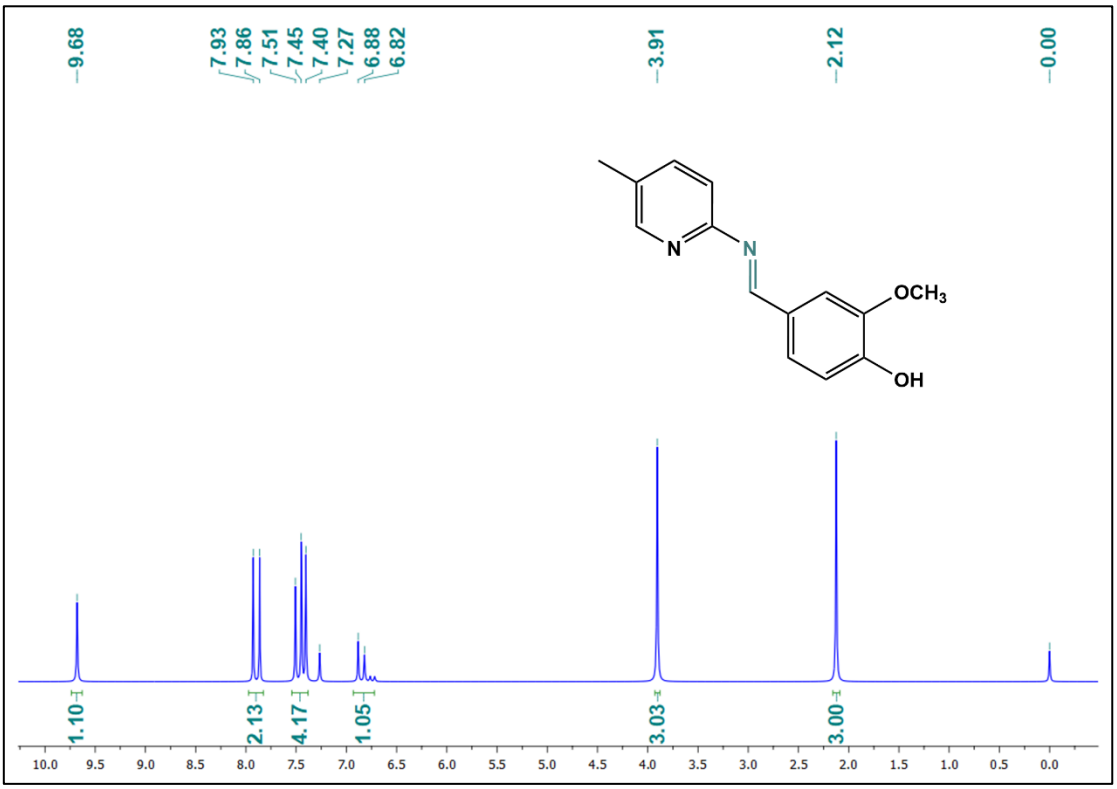

^{13}C NMR spectrum of Schiff base 153

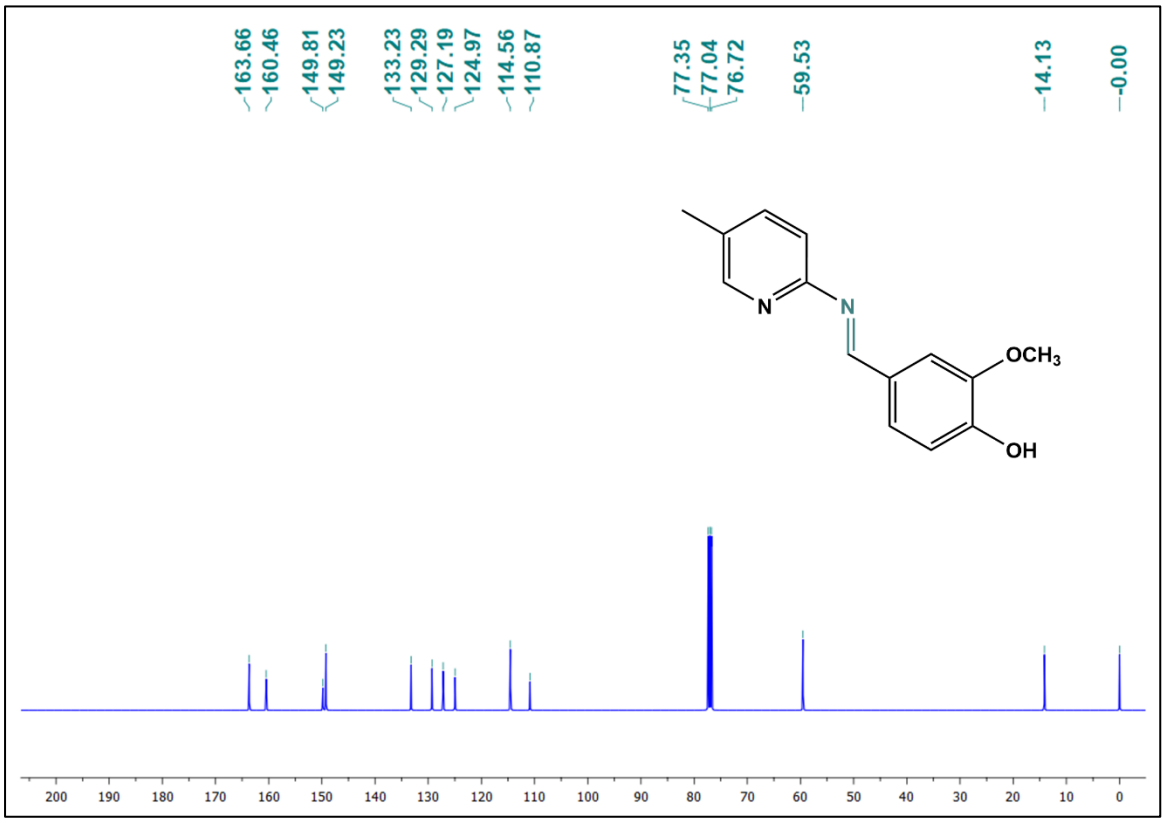

^{1}H NMR spectrum of alkyne 154

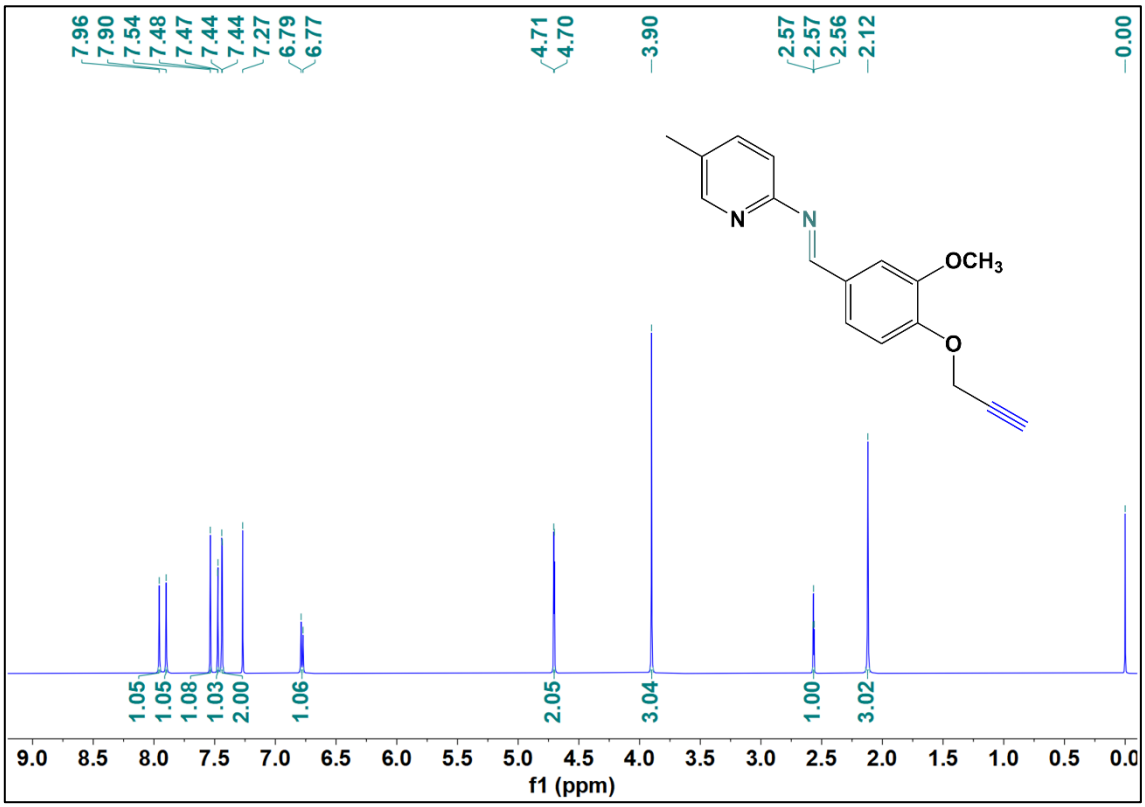

^{13}C NMR spectrum of alkyne 154

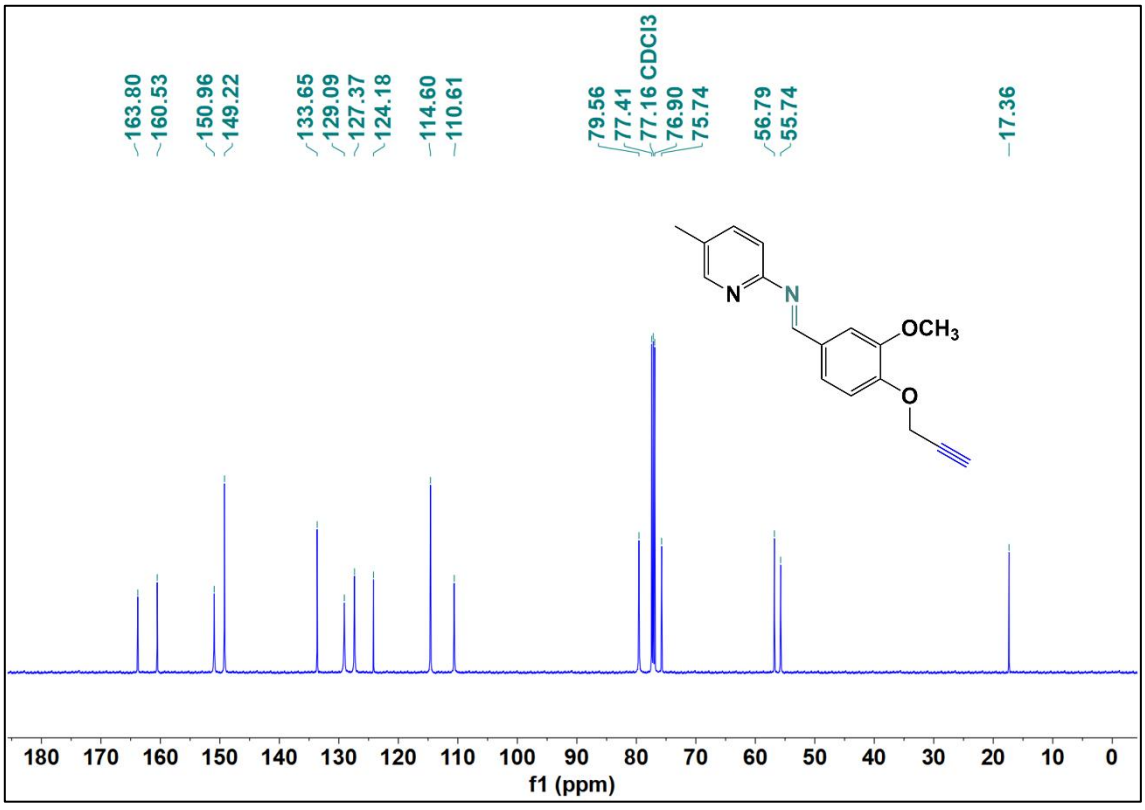

^{1}H NMR spectrum of 1,2,3-triazole derivative 155

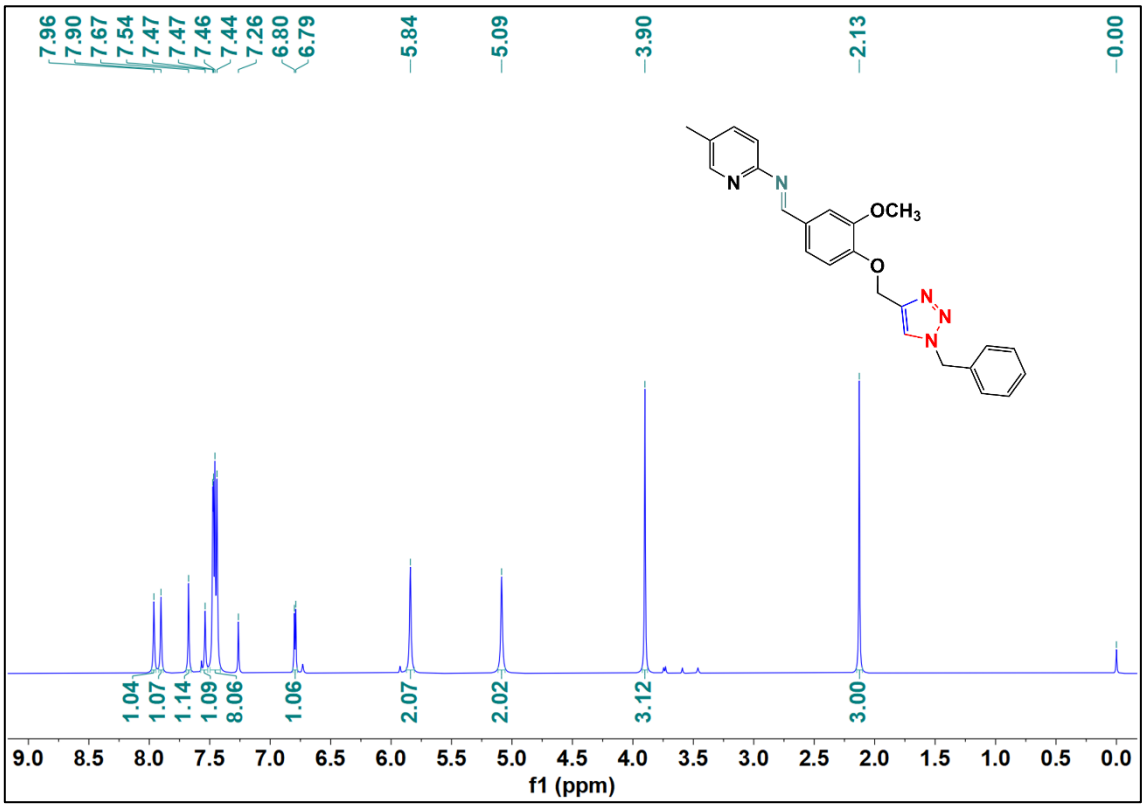

^{13}C NMR spectrum of 1,2,3-triazole derivative 155

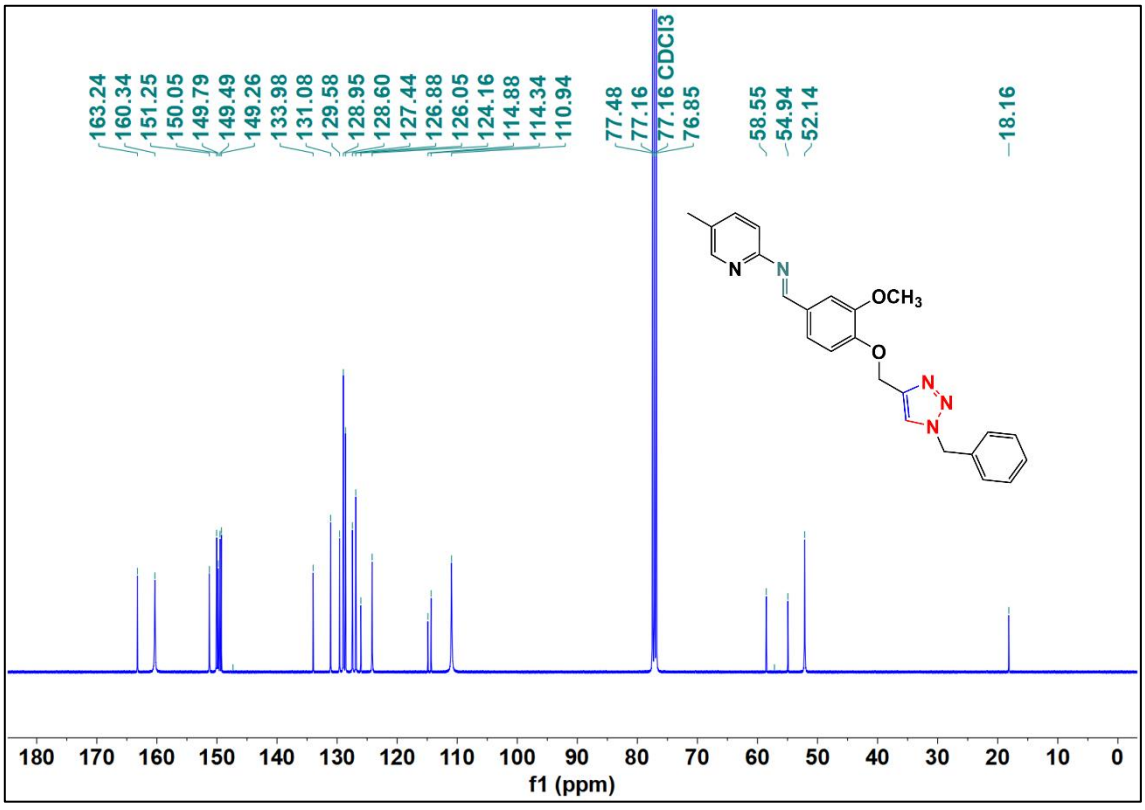

Mass spectrum of 1,2,3-triazole derivative 140

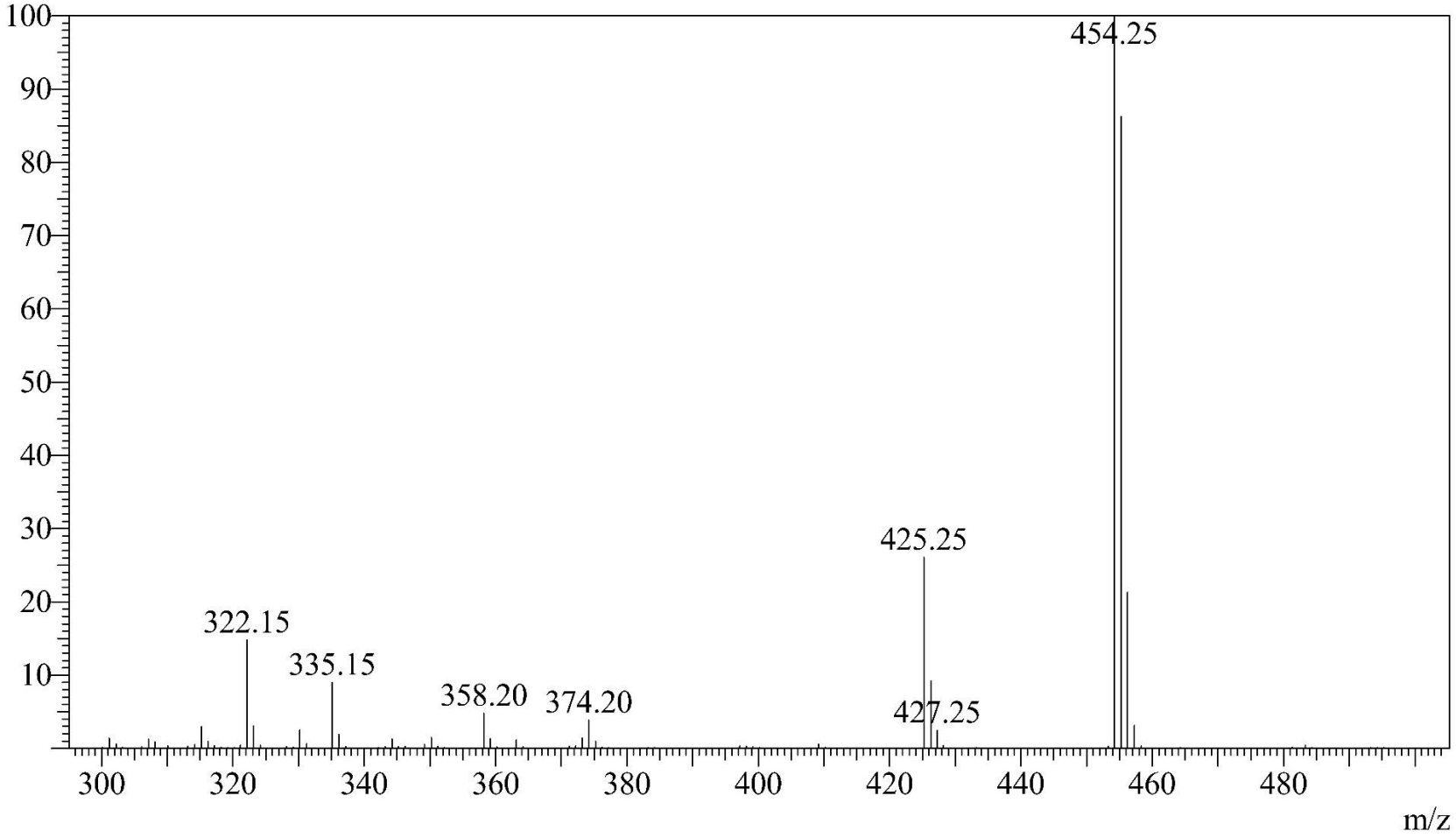

Mass spectrum of 1,2,3-triazole derivative 141

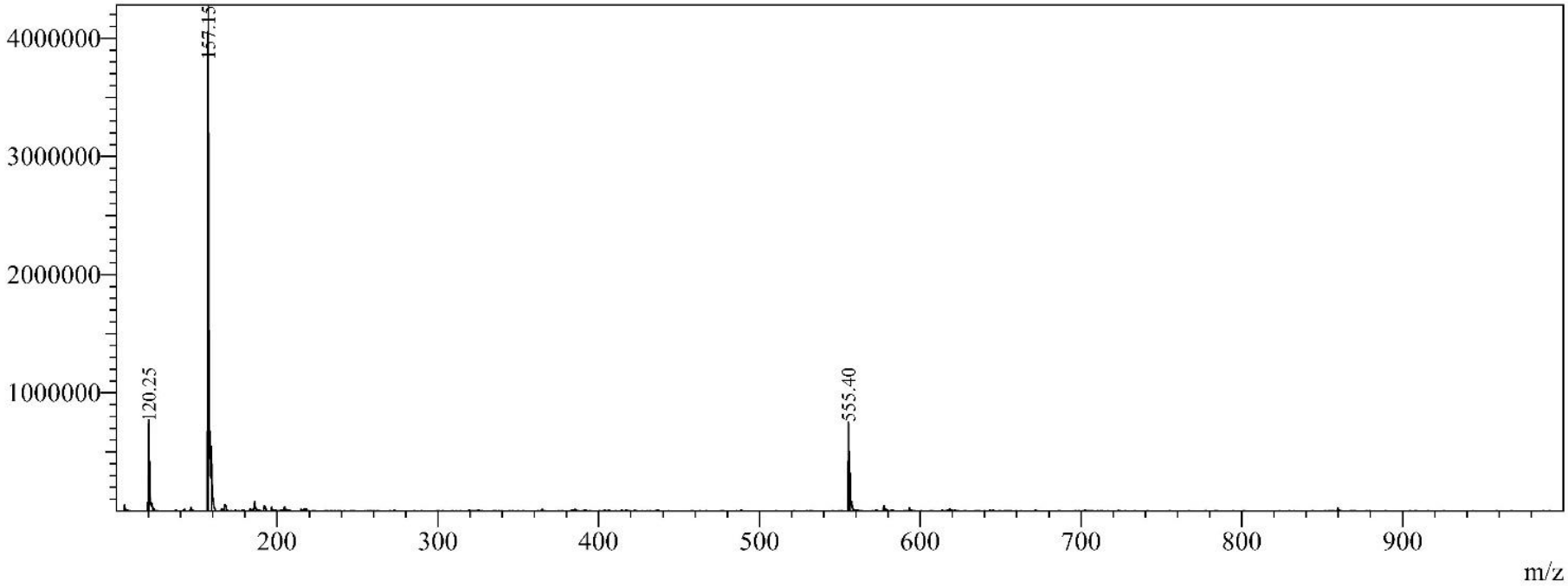

Mass spectrum of 1,2,3-triazole derivative 144

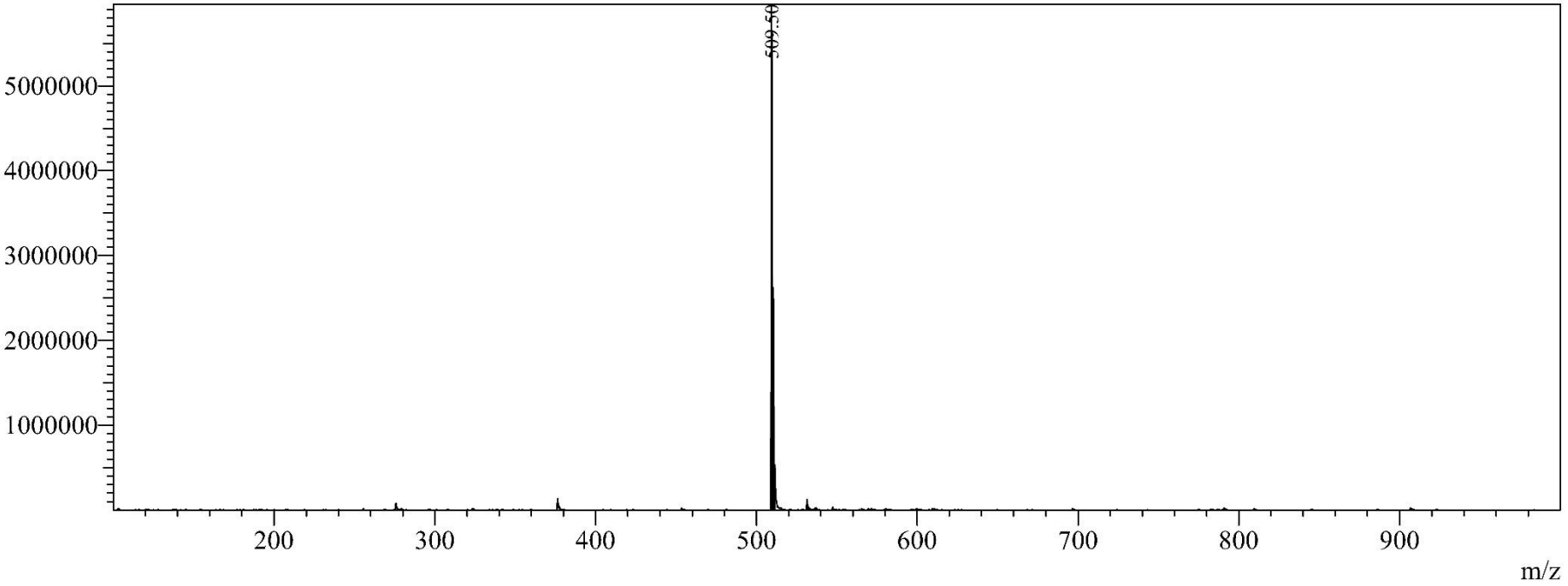

Mass spectrum of 1,2,3-triazole derivative 147

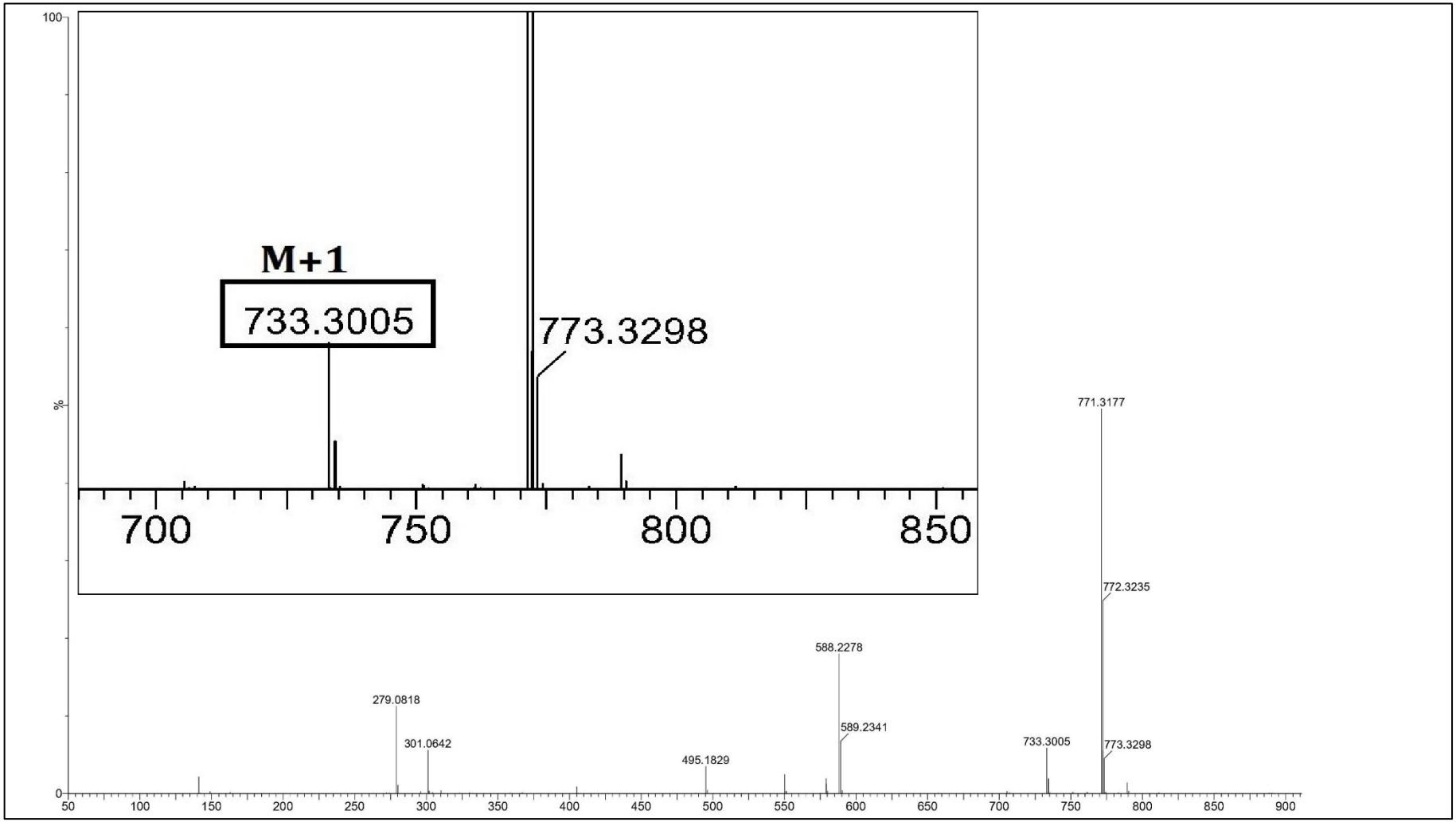

Mass spectrum of 1,2,3-triazole derivative 150

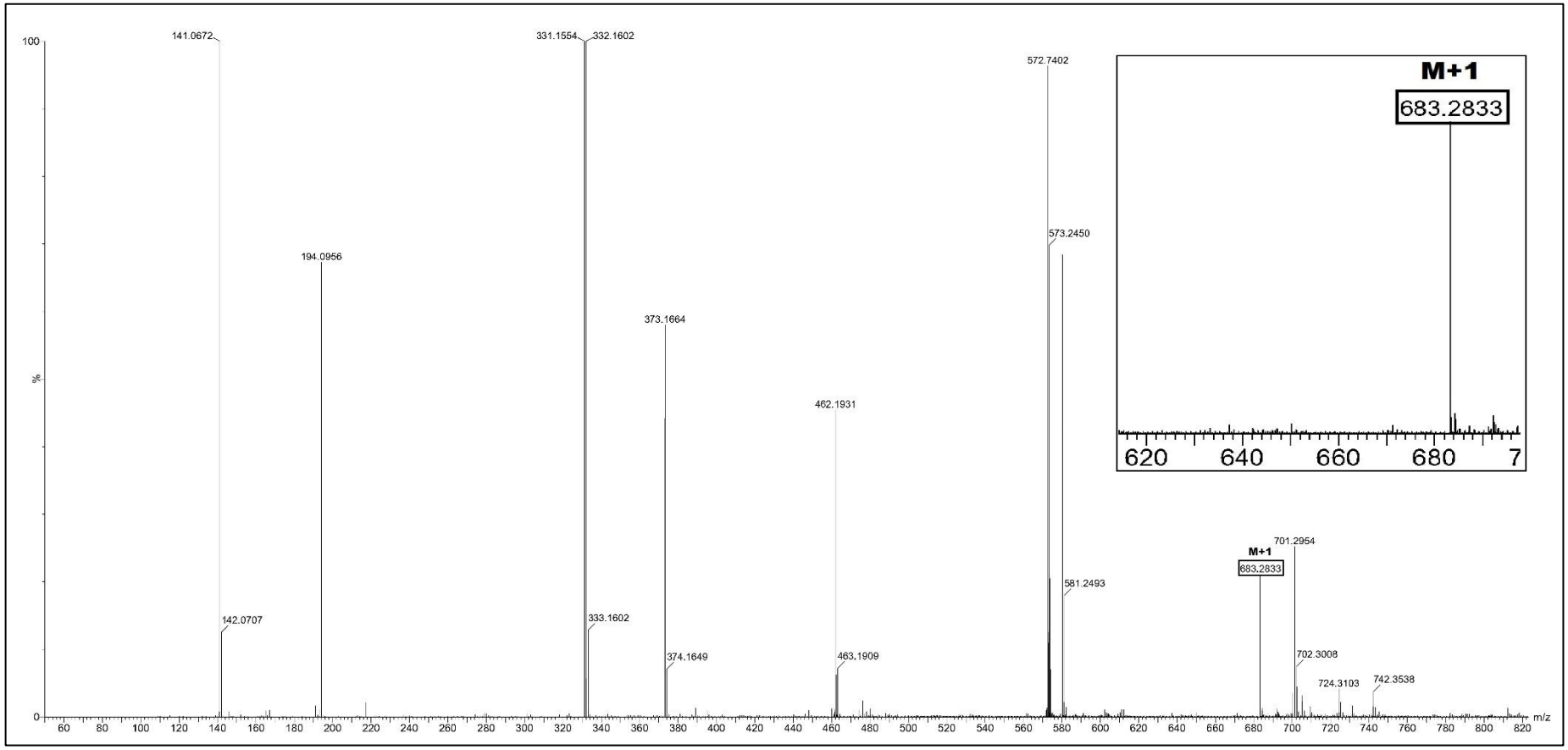

Mass spectrum of 1,2,3-triazole derivative 155

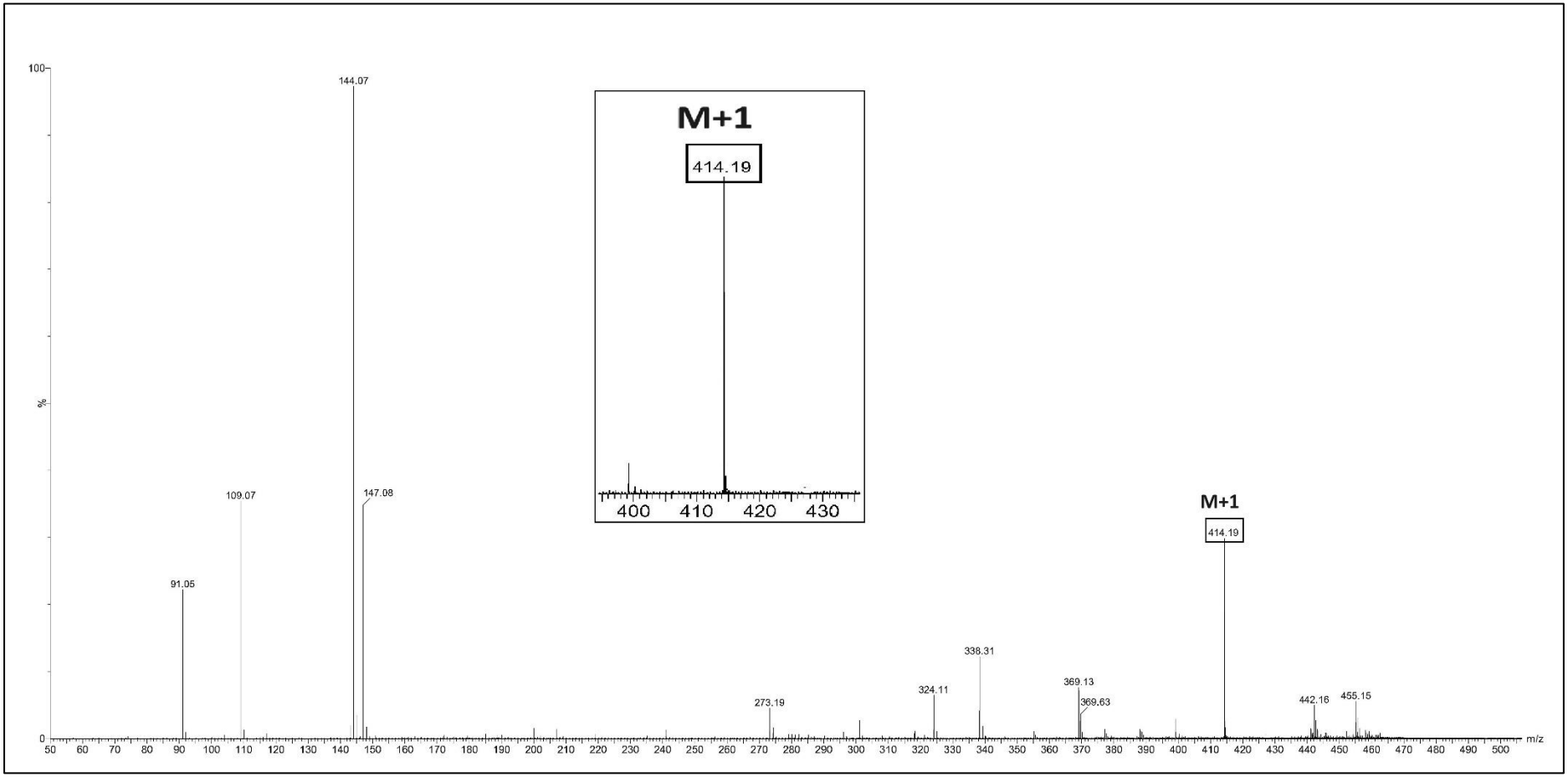

List of Publications

1. **Singh, G.**; George, N.; Singh, R.; Singh, G.; Kaur, J. D.; Kaur, G.; Singh, H.; Singh, J. CuAAC-Derived Selective Fluorescent Probe as a Recognition Agent for Pb(II) and Hg(II): DFT and Docking Studies. *ACS Omega* **2022**, *7*, 39159–39168.
2. **Singh, G.**; Singh, R.; George, N.; Singh, G.; Satija, P.; Kaur, G.; Singh, H.; Singh, J. Selective Recognition of Pb(II) and Cr(III) by Novel Maleic Hydrazide-Based 1,2,3-Triazole Linked Derivatives. *J. Mol. Struct.* **2023**, *1277*, 134823.
3. **Singh, G.**; Singh, R.; George, N.; Singh, G.; Sushma; Kaur, G.; Kaur, G.; Singh, H.; Singh, J. 'Click'-Synthesized PET Based Fluorescent Sensor for Hg(II), Pb(II) and Cr(III) Recognition: DFT and Docking Studies. *J. Photochem. Photobiol. A Chem.* **2023**, *441*, 114741.
4. **Singh, G.**; Lal, B.; Singh, R.; George, N.; Singh, G.; Diksha; Kaur, G.; Singh, H.; Tittal, R. K.; Kaur, G.; Singh, J. Ampyrone appended 1,2,3-triazole as selective fluorescent Cu(II) ion sensor: DFT and docking findings. *Spectrochim. Acta A Mol. Biomol. Spectrosc.* **2023**, 302, 123163.
5. **Singh, G.**; George, N.; Singh, R.; Singh, G.; Sushma; Kaur, G.; Singh, H.; Singh, J. Ion Recognition by 1,2,3-Triazole Moieties Synthesized via "Click Chemistry." *Appl. Organomet. Chem.* **2023**, *37*, e6897.
6. **Singh, G.**; Majeed, A.; Singh, R.; George, N.; Singh, G.; Sophia, N.; Singh, H.; Kaur, G.; Singh, J. CuAAC Ensembled 1,2,3-Triazole Linked Nanogels for Targeted Drug Delivery: A Review. *RSC Adv.* **2023**, *13*, 2912–2936.
7. **Singh, G.**; Saini, P.; Singh, G.; Thakur, Y.; Kaur, G.; Dash, S.; Singh, H.; Kaur, C.; Singh, H.; Singh, J. Click-derived o-cresolphthalein linked 1,2,3-triazole: Pb(II) ion sensing, *in silico* analysis, and aromatase inhibition. *J. Mol. Struct.* **2024**, *1305*, 137740.
8. Mehak, **Singh, G.**; Singh, R.; Singh, G.; Stanzin, J.; Singh, H.; Kaur, G.; Singh, J. Clicking in harmony: exploring the bio-orthogonal overlap in click chemistry. *RSC Adv.* **2024,** 14, 7383-7413.
9. Kumar, S.; **Singh, G.**; Tittal, R. K.; Singh, J.; Ghule, V.; Sharma, R. Selective quinizarin-linked bis-1,2,3-triazoles as probes for Fe(II)/(III): Characterization, metal ion binding, DFT, and antiallergy activity via docking studies. *J. Mol. Struct.* **2024**, 1299, 137142.

10. Singh, R.; **Singh, G.**; George, N.; Singh, G.; Devi, A.; Singh, H.; Kaur, G.; Singh, J. Cu(I)-catalysed 1,2,3-triazole stitched chalcomer assembly as Pb(ii) and Cu(ii) ion sensor: DFT and docking scrutiny. *RSC Adv.* **2023**,13, 32399-32412.
11. Saini, P.; **Singh, G.**; Singh, G.; Kaur, J. D.; Kaur, G.; Singh, J.; Singh, H. 1-Naphtholphthalein Appended 1,2,3-Triazole via CuAAC: A Molecular Assembly for Selective Co(II) Ion Recognition. *Inorganica Chim. Acta* **2023**, 551, 121470.
12. Saini, P.; **Singh, G.**; George, N.; Singh, G.; Kaur, G.; Tiwari, P.; Satija, P.; Singh, J.; Singh, H. α-Naphtholbenzein based heterocyclic sensor for detection of Cu(II) ions. *Inorganica Chim. Acta* **2024,** 568, 122063.
13. George, N.; **Singh, G.**; Singh, R.; Singh, G.; Singh, H.; Kaur, G.; Singh, J. Click Modified Bis-Appended Schiff Base 1,2,3-Triazole Chemosensor for Detection of Pb(II)Ion and Computational Studies. *J. Mol. Struct.* **2023**, *1288*, 135666.
14. George, N.; **Singh, G.**; Singh, R.; Singh, G.; Sushma; Singh, H.; Kaur, G.; Singh, J. Schiff base functionalized 1,2,3-triazole derivative for Fe(III) ion recognition, as N,O,O-Fe-O,O,N sandwich complex: DFT analysis. *Polyhedron*, **2023**, 242, 116496.
15. Singh, R.; **Singh, G.**; George, N.; Singh, G.; Gupta, S.; Singh, H.; Kaur, G.; Singh, J. Copper-Based Metal–Organic Frameworks (MOFs) as an Emerging Catalytic Framework for Click Chemistry. *Catalysts.* **2023**, *13*, 130–159.
16. George, N.; **Singh, G.**; Singh, R.; Singh, G.; Devi, A.; Singh, H.; Kaur, G.; Singh, J. Microwave Accelerated Green Approach for Tailored 1,2,3–Triazoles via CuAAC. *Sustain. Chem. Pharm.* **2022**, *30*, 100824.
17. Kalra, P.; Kaur, R.; **Singh, G.**; Singh, H.; Singh, G.; Pawan; Kaur, G.; Singh, J. Metals as "Click" Catalysts for Alkyne-Azide Cycloaddition Reactions: An Overview. *J. Organomet. Chem.* **2021**, *944*, 121846.
18. Kumar, S.; Lal, B.; Tittal, R. K.; **Singh, G.**; Ghule, V.; Sharma, R.; Sabane, J. A selective chemosensor via click chemistry for Cu^{2+} and Hg^{2+} ions in organic media. *Sens. diagn.* **2023**, 2, 1267-1276.
19. Lal, B.; Kumar, S.; Tittal, R. K.; **Singh, G.**; Singh, J.; Ghule, V.; Mathpati, R.; Sabane, J. 4-aminoantipyrine linked bis-1,2,3-triazole based probes for Cu(II) sensing. *J. Mol. Struct.* **2024**, 1297, 136995.
20. Singh, G.; Sushma; Priyanka; Khurana, S.; **Singh, G.**; Singh, J.; Angeles Esteban, M.; Espinosa-Ruíz, C.; González-Silvera, D. Thiosemicarbazone-Triazole Bearing Siloxy Framework for the Detection of Hg^{2+} and Cu^{2+} Ions and Their Potent Cytotoxic Activity. *Inorganica Chim. Acta.* **2022**, 542, 121087.

21. Singh, G.; Malik, S.; Devi, A.; Kaur, H.; Diskit, T.; Singh, J.; **Singh, G**.; Vandana; Kaur, A. Carbohydrazide-Based schiff bases for selective Hg(II) ion sensing and computational analysis of cholesterol lowering activity. *Inorg. Chem. Commun.* **2024,** 163, 112297.
22. Singh, G.; Diksha; Mohit; Priyanka; Devi, A.; Devi, S.; Kaur, H.; Singh, J.; **Singh, G**. Heterocycle-derived organosilatranes as naked eye sensors for Sn^{2+} ions and their potential inhibiting activity against HIV-1 protease via a computational approach. *New J. Chem.* **2023**, 47, 2608-12619.
23. Singh, G.; Sushma; Priyanka; Devi, A.; Tamana; Kaur, H.; Mithun; Singh, J.; **Singh, G**. A dual response UV-vis and fluorescence receptor based on acetylenic-indole conjoined silatrane for selective recognition of Co^{2+} and Cu^{2+} ions, and *in silico* antidiabetic activity. *New J. Chem.*, **2023**, 47, 22441-22455.

List of conference presentations

1. Paper presented in the **International Conference on Materials for Emerging Technologies (ICMET-21)** held on February 18-19, 2022, organized by Department of Research Impact and Outcome, Division of Research and Development, Lovely Professional University, Punjab, India.

2. Paper presented in the **9th HSCA International Conference on Recent Trends in Bio and Material Sciences** held on September 23-24, 2022, organized by the Him Science Congress Association in collaboration with Sardar Patel University, Mandi, Himachal Pradesh, India.
3. Paper presented in the **International Conference on Advances in Smart Materials, Chemical and Biochemical Engineering (CHEMSMART-22)** held on December 16-18, 2022, organized by the Department of Chemical Engineering, National Institute of Technology (NIT), Rourkela, Odhisha, India.
4. Poster presented in the **International Conference on Molecules and Materials Technology (MMT-2023)** held on April 21-22, 2023, organized by the Department of Chemistry National Institute of Technology (NIT) Kurukshetra, Haryana, India.

Short term courses and Workshops

1. Completed one-week workshop on **'Spectroscopic, Chromatographic, Bioanalytical & Imaging Techniques'** held from 28th November - 04th December 2022, conducted by Central University of Punjab in association with Amity University under the auspices of Department of Science and Technology, Government of India, under Synergistic Training Program Utilizing Scientific and Technological Infrastructure (STUTI).

Published papers and Certificates

ACS OMEGA

http://pubs.acs.org/journal/acsodf

Article

CuAAC-Derived Selective Fluorescent Probe as a Recognition Agent for Pb(II) and Hg(II): DFT and Docking Studies

Gurleen Singh, Nancy George, Riddima Singh, Gurjaspreet Singh, Jashan Deep Kaur, Gurpreet Kaur, Harminder Singh,* and Jandeep Singh*

Cite This: *ACS Omega* 2022, 7, 39159−39168

Read Online

ACCESS | Metrics & More | Article Recommendations | Supporting Information

ABSTRACT: Copper(I)-catalyzed alkyne−azide cycloaddition (CuAAC) is a resourceful and stereospecific methodology that has considerably yielded promising 1,2,3-triazole-appended "click" scaffolds with the potential for selective metal ion recognition. Based on "click" methodology, this report presents a chemosensor probe (TCT) based on 4-*tert*-butylcatechol architecture, via the CuAAC pathway, as a selective and efficient sensor for Pb(II) and Hg(II) ions, categorized as the most toxic and alarming environmental contaminants among the heavy metal ions. The synthesized probe was successfully characterized by spectroscopy [IR and NMR (^{1}H and ^{13}C)] and mass spectrometry. The chemosensing study performed in acetonitrile/water (4:1) solvent media, via UV−vis and fluorescence spectroscopy, established its selective sensitivity for Pb(II) and Hg(II) species among the list of explored metal ions with the limits of detection being 8.6 and 11 μM, respectively. Additionally, the ^{1}H NMR and IR spectra of the synthesized TCT−metal complex also confirmed the metal−ligand binding. Besides, the effect of time and temperature on the binding ability of TCT with Pb(II) and Hg(II) was also studied via UV−vis spectroscopy. Furthermore, density functional theory studies put forward the structural comprehension of the sensor by availing the hybrid density functional (B3LYP)/6311G++(d,p) basis set of theory which was subsequently utilized for investigating its anti-inflammatory potential by performing docking analysis with human leukotriene b4 protein.

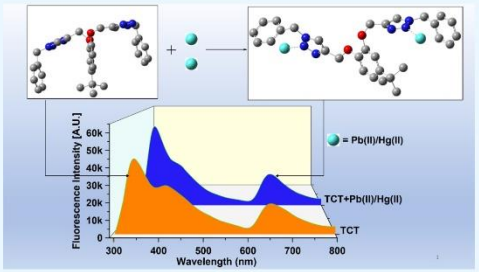

1. INTRODUCTION

The consistent search for efficient and suitable scaffolds for toxic heavy metal ion(s) recognition has been the core idea of ongoing research among the various researchers worldwide owing to their potential deleterious effects on humans and their ecotoxicological presence in the environment.[1−3] The presence of toxic ions such as Pb(II), Hg(II), and so forth above the permissible threshold value can alter the biomolecules mainly via oxidative damage and diminishing of enzymatic activities,[4,5] thereby interfering with the vital processes occurring inside the body to sustain life. Lead has become a ubiquitous heavy metal globally.[6] On accumulation in significant quantities in the soft tissues such as the brain, kidneys, heart, and so forth, it can interact with the physiologically active groups of different proteins and hence incapacitate their biological functions, which result in serious health hazards such as hematological effects (anemia), nephrotoxicity (interstitial nephritis), cardiovascular effects (hypertension), neurological effects (lead encephalopathy), and so forth.[7−11] Mercury in its inorganic form [Hg(II)] is severely toxic to living organisms, and the startling consideration that other forms of mercury are convertible to the insidiously toxic divalent form via "biomethylation" keeps the researchers on their toes for controlling mercury accretion in the environment.[12] Significant concentrations of mercury in the body impairs enzymatic activity and causes mitochondrial dysfunction and increased oxidative stress, thereby resulting in complications such as hypertension, cardiac arrhythmia, coronary heart disease, atherosclerosis, and so forth.[12−16] Therefore, a constant need to confirm the presence of such toxic and non-biodegradable heavy metal ions in the environment becomes indispensable to keep their accumulation in the environment well within the permissible limits.

The archetypal click reaction, that is, CuAAC[17] methodology, provides a well-organized, robust, and efficient pathway to synthesize 1,2,3-triazole-based compounds for addressing the research problem of metal ion toxicity in addition to other sensing devices such as supramolecular polymers.[18−20] The development of new 1,2,3-triazole-linked compounds by

Received: August 8, 2022
Accepted: October 4, 2022
Published: October 20, 2022

https://doi.org/10.1021/acsomega.2c05050
ACS Omega 2022, 7, 39159−39168

Journal of Molecular Structure 1277 (2023) 134823

Contents lists available at ScienceDirect

Journal of Molecular Structure

journal homepage: www.elsevier.com/locate/molstr

Selective recognition of Pb(II) and Cr(III) by novel maleic hydrazide-based 1,2,3-triazole linked derivatives

Gurleen Singh[a], Riddima Singh[a], Nancy George[a], Gurjaspreet Singh[b], Pinky Satija[c], Gurpreet Kaur[d], Harminder Singh[a,*], Jandeep Singh[a,*]

[a] School of Chemical Engineering and Physical Sciences, Lovely Professional University, Phagwara 144411 Punjab, India
[b] Department of Chemistry and Centre of Advanced Studies in Chemistry, Panjab University, Chandigarh 160014, India
[c] School of Advanced Chemical Sciences, Shoolini University, Solan 173212, India
[d] Department of Chemistry, Gujranwala Guru Nanak Khalsa College, Civil lines, Ludhiana 141001 Punjab, India

ARTICLE INFO

Article history:
Received 28 June 2022
Revised 13 December 2022
Accepted 18 December 2022
Available online 20 December 2022

Keywords:
Click chemistry
1,2,3-triazole
Ion recognition
UV–Vis spectroscopy
DFT
Docking studies

ABSTRACT

The present report describes the application of versatile and stereospecific Copper(I) catalyzed alkyne-azide cycloaddition (CuAAC) reaction to synthesize two novel maleic hydrazide appended 1,2,3-triazole based chemosensors (**5** and **6**) as selective probes for Pb(II) and Cr(III) recognition. Maleic hydrazide is a plant growth regulator known to prevent cell division. The probes were characterized via IR, NMR (^{1}H and ^{13}C) spectroscopy and mass spectrometry; and subsequently explored for their ion sensing behavior in DMSO as solvent media via UV–Vis spectroscopy. The probe **5** displayed peak at 312 nm accompanied by a smaller peak at 258 nm; whereas the probe 6 exhibited peaks at 274 nm, 284 nm and 294 nm. Furthermore, the association constants for probe **5** were determined to be 0.61×10^{5} M^{-1} and 0.20×10^{6} M^{-1} for Pb(II) and Cr(III) respectively; and for probe **6** the association constant values for Pb(II) and Cr(III) were 0.46×10^{6} M^{-1} and 0.76×10^{6} M^{-1} respectively. Structural optimization of both the probes was carried out using DFT with hybrid density functional (B3LYP)/6–311G++(d,p)basis set of theory and LANL2DZ basis set was utilized to optimize the representative **5**+metal complex . Subsequent docking analysis of **5** and **6** was carried out with leukotriene b4 via AutoDock Vina to get perceptions about their potential anti-inflammatory properties, wherein the binding energies of the probes **5** and **6** were observed to be -8.3 and -9.6 kcal/mol respectively.

1. Introduction

Selective recognition of biologically relevant metal ions is of paramount interest among the research community at present owing to their importance in diverse physiological processes and environmental toxicity [1–3]. Transition elements present in living systems in trace amounts and other heavy metal ions, in particular, have received great attention in modern-day research [4–6] due to their involvement and/or interference in various metabolic, enzymatic, and redox reactions taking place in the human body [7,8]. In addition to that, fluctuations in their levels from the prescribed levels lead to health complications [9]. Lead is a significant element that has no known function in the human body but in its divalent form is insidiously toxic, affecting almost every organ and system in the body, with the most affected systems being the central nervous system, cardiovascular system, liver, kidneys and reproductive systems [10–12]. Since the twentieth century has witnessed an exponential increase in the use of leaded gasoline and other lead-based products, therefore environmental accretion of lead [13] has posed a great health hazard. Among trivalent ions, Cr(III) is known to perform an imperative part in certain biotic events viz glycometabolism improvement [14] and carbohydrates, proteins, fats and nucleic acid metabolism [15]. Deficiency of Cr(III) is related to increased risks of cardiovascular diseases and diabetes [16] whereas its overabundance is linked with carcinogenicity [17]. Industrial utilization of metallic chromium is also widespread [18] and hence its improper disposal poses a potential threat of its environmental accumulation and subsequent oxidation to the immensely toxic hexavalent state [19]. Hence, there is a constant need of developing new methodologies for quantitative as well as qualitative recognition of such metal ions. Scheme 1

Imposing advantages over other reported methodologies for ion recognition such as atomic absorption spectroscopy (AAS) and inductively coupled plasma-mass spectrometry (ICPMS) [20–22], development of highly selective and sensitive chemosensors as metal ion recognition ensembles has been immensely explored

* Corresponding authors.
E-mail address: singhjandeep@gmail.com (J. Singh).

https://doi.org/10.1016/j.molstruc.2022.134823
0022-2860/

Journal of Photochemistry & Photobiology, A: Chemistry 441 (2023) 114741

Contents lists available at ScienceDirect

Journal of Photochemistry & Photobiology, A: Chemistry

journal homepage: www.elsevier.com/locate/jphotochem

'Click'-synthesized PET based fluorescent sensor for Hg(II), Pb(II) and Cr (III) recognition: DFT and docking studies

Gurleen Singh [a], Riddima Singh [a], Nancy George [a], Gurjaspreet Singh [b], Sushma [c], Gagandeep Kaur [d], Gurpreet Kaur [e], Harminder Singh [a], Jandeep Singh [a,*]

[a] School of Chemical Engineering and Physical Sciences, Lovely Professional University, Phagwara 144411, Punjab, India
[b] Department of Chemistry and Centre of Advanced Studies in Chemistry, Panjab University, Chandigarh 160014, Punjab, India
[c] Chitkara College of Pharmacy, Chitkara University, Punjab 140401, India
[d] Material Application Research Lab. (MARL), Department of Nano Science and Materials, Central University of Jammu, Jammu 181143, Punjab, India
[e] Department of Chemistry, GGN Khalsa College, Civil Lines, Ludhiana 141001, Punjab, India

ARTICLE INFO

Keywords:
Click Chemistry
1,2,3-triazole
p-Rosolic acid
Metal ion recognition
Fluorescence spectroscopy
DFT

ABSTRACT

In this study, a novel photoinduced electron transfer (PET) based 1,2,3-triazole appended chemosensor probe (PRT) for the recognition of toxic heavy metal ions has been developed via Cu(I)-catalyzed alkyne-azide cycloaddition (CuAAC), a quintessential example of 'click chemistry' for which the 2022 Nobel prize in chemistry was awarded to Prof. K.B. Sharpless, Prof. M. Meldal and Prof. C. Bertozzi. The synthesized probe was successfully characterized via IR spectroscopy, NMR (^{1}H and ^{13}C) spectroscopy, and mass spectrometry; and additionally demonstrated to selectively sense the highly toxic Hg(II), Pb(II), and the biologically essential Cr(III) ions via absorption and fluorescence spectroscopy. The Job plot of PRT suggested the stoichiometric ratio of 1:1 with the sensed metal ions, whereas the association constant values determined through Benesi-Hildebrand (B-H) equation indicated the strongest binding of PRT with Cr(III) followed by Pb(II) and Hg(II) respectively, even though the competitive metal ion titration revealed the selectivity of PRT for Pb(II) over the other metal ions. The density functional theory (DFT) approach as implemented in the Gaussian 09 package with B3LYP/6-311G++(d, p) and B3LYP/LANL2DZ was used to perform geometry optimization and quantum chemical computations. Above and beyond, PRT was also docked with Interleukin (IL)-6 protein, thereby providing glimpses of its anti-inflammatory potential.

1. Introduction

The notion of environmental contamination, an exponentially augmenting threat to nature as well as all life forms, has grabbed the attention of the global research community due to its distressing state [1–3]. Laying a special emphasis on this contamination factor by the non-biodegradable and persistent entities such as the heavy metal ions, researchers have significantly ventured to resolve this menace via discrete methodologies [4,5]. However, the ever-evolving challenges such as bioaccumulation and the need for real-time analysis consistently require researchers to find contemporary and sturdy courses of action to curb such hazards. Due to the protein binding potential and enzyme inactivation capabilities of heavy metal ions [6,7] resulting in detrimental effects on the vital body metabolic processes [8], their accumulation in the environment is one such problem that has posed a serious threat since the industrial revolution, largely due to their upsurged release as a result of anthropogenic activities like mining, metallurgy, pesticide production, nuclear and thermal power plants, etc. [9]. Out of the various heavy metals, mercury and lead are two of the most pernicious elements having no biological function but capable of earnest subversance [10,11]. Both the elements in their divalent form are reported to cause impairment of several biological functions like enzymatic and redox reactions; and soft tissues such as the brain, kidneys, heart, etc. [12–15] leading to pervasive and irreversible toxic effects. Also, chromium in its trivalent form is essential for the human body to perform multiple functions including glucose metabolism regulation, facilitation of macronutrient metabolism, stimulation of insulin synthesis, etc. However, its overabundance is linked with irritation of the respiratory tract, irritant dermatitis, carcinogenicity, etc. whereas lower levels in the body tend to induce peripheral neuropathy,

* Corresponding author.
E-mail addresses: harminder_env@yahoo.com (H. Singh), singhjandeep@gmail.com (J. Singh).

https://doi.org/10.1016/j.jphotochem.2023.114741
Received 14 January 2023; Received in revised form 27 March 2023; Accepted 28 March 2023
Available online 1 April 2023

Spectrochimica Acta Part A: Molecular and Biomolecular Spectroscopy 302 (2023) 123163

Contents lists available at ScienceDirect

Spectrochimica Acta Part A:
Molecular and Biomolecular Spectroscopy

journal homepage: www.journals.elsevier.com/spectrochimica-acta-part-a-molecular-and-biomolecular-spectroscopy

Ampyrone appended 1,2,3-triazole as selective fluorescent Cu(II) ion sensor: DFT and docking findings

Gurleen Singh [a, 1], Bajrang Lal [a,b,1], Riddima Singh [a], Nancy George [a], Gurjaspreet Singh [c], Diksha [c], Gagandeep Kaur [d], Harminder Singh [a], Ram Kumar Tittal [b], Gurpreet Kaur [e,*], Jandeep Singh [a,*]

[a] School of Chemical Engineering and Physical Sciences, Lovely Professional University, Phagwara 144411, Punjab, India
[b] Department of Chemistry, National Institute of Technology, Kurukshetra, Haryana 136119, India
[c] Department of Chemistry and Centre of Advanced Studies in Chemistry, Panjab University, Chandigarh 160014, India
[d] Material Application Research Lab. (MARL), Department of Nano Science and Materials, Central University of Jammu, Jammu 181143, India
[e] Department of Chemistry, Gujranwala Guru Nanak Khalsa College, Civil Lines, Ludhiana 141001, Punjab, India

HIGHLIGHTS

- Synthesis of ampyrone based 1,2,3-triazole appended derivative (APT).
- Characterization of the synthesized compound via spectroscopic techniques.
- Ion sensing analysis of APT via UV–visible and fluorescence spectroscopy.
- DFT simulations to obtain energy-minimized structures of APT and APT-Cu(II) complex.
- Molecular docking analysis of APT with synaptic vesicle protein (SV2A).

GRAPHICAL ABSTRACT

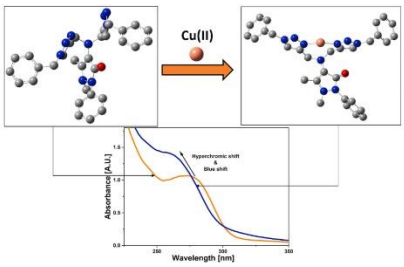

ARTICLE INFO

Keywords:
Click chemistry
1,2,3-triazole
4-aminoantipyrine
Fluorescent probe
DFT
CHEQ

ABSTRACT

The present report describes the application of the 'Click Chemistry' pathway to synthesize a fluorescent probe (APT) based on ampyrone (4-aminoantipyrine), entailing two benzyl groups as the fluorophores coupled to the antipyrine structure through 1,2,3-triazole moieties. Infrared spectroscopy (IR), nuclear magnetic resonance (^{1}H and ^{13}C), and mass spectrometry were the standard spectroscopic methods used to characterize APT. The ion recognition potential of the probe was analyzed through absorption and emission spectroscopy employing a 4:1 combination of CH_3CN and H_2O, which demonstrated APT to be an efficient sensing agent for Cu(II) ions, wherein the absorption spectrum of the probe displayed a hypsochromic shift with a hyperchromic shift on gradually adding the metal ion solution of Cu(II), whereas quenching of the probe's fluorescence emission on Cu (II) addition was attributed to the chelation-enhanced fluorescence quenching (CHEQ), induced by the d^9 electronic configuration of Cu(II). The stoichiometry of the complexation of APT with Cu(II) is indicative of a 1:1 ratio, while the detection limit (LOD) and quantification limit (LOQ) as estimated from the fluorescence titration

* Corresponding authors.
E-mail addresses: chemgurpreet5@gmail.com (G. Kaur), singhjandeep@gmail.com (J. Singh).
[1] The authors contributed equally to this work.

https://doi.org/10.1016/j.saa.2023.123163
Received 5 April 2023; Received in revised form 10 July 2023; Accepted 15 July 2023
Available online 17 July 2023

Received: 28 April 2022 | Revised: 21 June 2022 | Accepted: 10 July 2022

DOI: 10.1002/aoc.6897

REVIEW

Applied Organometallic Chemistry WILEY

Ion recognition by 1,2,3-triazole moieties synthesized via "click chemistry"

Gurleen Singh[1] | Nancy George[1] | Riddima Singh[1] | Gurjaspreet Singh[2] | Sushma[2] | Gurpreet Kaur[3] | Harminder Singh[1] | Jandeep Singh[1]

[1]School of Chemical Engineering and Physical Sciences, Lovely Professional University, Phagwara, Punjab, India

[2]Department of Chemistry and Centre of Advanced Studies in Chemistry, Panjab University, Chandigarh, India

[3]Department of Chemistry, Gujranwala Guru Nanak Khalsa College, Ludhiana, Punjab, India

Correspondence
Jandeep Singh and Harminder Singh, School of Chemical Engineering and Physical Sciences, Lovely Professional University, Phagwara 144411, Punjab, India.
Email: jandeep.19394@lpu.co.in, singhjandccp@gmail.com and harminder_env@yahoo.com, harminder.singh@lpu.co.in

Funding information
There is no funding for this project.

1,2,3-Triazole-based ligands obtained through copper(I)-catalyzed azide-alkyne cycloaddition (CuAAC) have been exploited in vast array of research domains owing to the stitching of simpler molecules through a needle of Cu(I) catalyst. The numerous reports on ion(s) detection capabilities of synthesized 1,4-disubstituted 1,2,3-triazole ligands using absorption and fluorescence spectroscopy are accessible. This review enlists substituted 1,2,3-triazole-based sensor probes, since 2010, synthesized selectively by CuAAC, having the ability to sense either a single ion or multiple ions under specific set of conditions along with their detection limits. The review also apprehends the different techniques and sensing mechanisms involved in the detection of ions by chemosensor probes.

KEYWORDS
alkyne-azide cycloaddition, chemosensor, fluorescence spectroscopy, ion sensing, UV–Vis spectroscopy

1 | INTRODUCTION

Click chemistry is a vital synthetic tool that facilitates an efficient and relatively simple method for construction of large fragments using smaller molecules. The term "click chemistry" was first coined by Karl Barry Sharpless in 1998, in lieu for the discovery of Cu(I)-catalyzed alkyne-azide cycloaddition (CuAAC) reaction on account of the high efficiency, excellent yields, and regioselective product, with inoffensive by-products.[1] The series of "click reactions," which share common trajectories,[2] include metal-catalyzed azide-alkyne cycloaddition,[3–12] strain-promoted azide-alkyne cycloaddition (SPAAC),[13–15] strain-promoted alkyne-nitrone cycloaddition,[16,17] inverse electron demand Diels–Alder reaction (IEDDA),[18,19] and Staudinger ligation,[20–22] as the most widely performed and studied reactions. Amidst the aforementioned reactions, CuAAC (categorized under metal-catalyzed azide-alkyne cycloaddition) has been extensively utilized in pursuit of synthesis of wide variety of complexes attributable to its exceptional thermodynamic and kinetic profile,[23] in addition to high functional group tolerance[24] wherein an azide binds irreversibly with an alkynyl group in a highly regioselective manner[25] to give a five-membered 1,4-disubstituted 1,2,3-triazole ring,[26,27] as illustrated in Figure 1. Cu(I) catalyst[28] enhances the reaction rate by almost 10^7 times in comparison with uncatalyzed Huisgen cycloaddition wherein no regioselective control yields 1,4- and 1,5-triazoles in nearly equal proportions.[29–31] Click chemistry has been extensively exploited in drug discovery and delivery,[32–34] photodynamic therapy,[35,36] solid-

RSC Advances

REVIEW

View Article Online
View Journal | View Issue

Check for updates

Cite this: RSC Adv., 2023, 13, 2912

CuAAC ensembled 1,2,3-triazole linked nanogels for targeted drug delivery: a review

Gurleen Singh,[a] Ather Majeed,[a] Riddima Singh,[a] Nancy George,[a] Gurjaspreet Singh,[b] Sofia Gupta,[b] Harminder Singh,[a] Gurpreet Kaur*[c] and Jandeep Singh*[a]

Copper(I) catalyzed alkyne azide cycloaddition (CuAAC), the quintessential example of 'click chemistry', provides an adaptable and adequate platform for the synthesis of nanogels for sustained drug release at targeted sites because of their better biocompatibility. The coupling of drugs, carried out *via* various synthetic routes including CuAAC, into long-chain polymeric forms like nanogels has exhibited considerable assurance in therapeutic advancements and intracellular drug delivery due to the progression of water solubility, evacuation of precocious drug release, and improved upthrust of the pharmacokinetics of the nanogels, thereby rendering them as better and efficient drug carriers. The inefficiency of drug transmission to the target areas due to the resistance of complex biological barriers *in vivo* is a major hurdle that impedes the therapeutic translation of nanogels. This review compiles the data of nanogels synthesized specifically *via* CuAAC 'click' methodology, as scaffolds for targeted drug delivery and their assimilation into nanomedicine. In addition, it elaborates the ability of CuAAC to graft specific moieties and conjugating biomolecules like proteins and growth factors, onto orthogonally functionalized polymer chains with various chemical groups resulting in nanogels that are not only more appealing but also more effective at delivering drugs, thereby enhancing their site-specific target approach and initiating selective therapies.

Received 5th September 2022
Accepted 11th January 2023

DOI: 10.1039/d2ra05592a

rsc.li/rsc-advances

1. Introduction

In the domains of biomedicine, bio-nanotechnology, and pharmaceutics, polymer-based drug nanocarriers have always been fascinating drug therapies for targeted site-specific drug delivery.[1–3] A wide range of diseases including neurological disorders, cardiovascular diseases, and malignancies can be treated and healed in a better and more efficient manner using polymeric drug delivery systems owing to the targeted and controlled release of therapeutics,[4–6] thereby reducing the side effects of drugs, especially those for cancer which is a major threat to human health after cardiovascular diseases which are the leading cause of human fatality.[7–10] It was reported by the International Agency for Research on Cancer (IARC), in 2018, that there were 18.1 million cancer diagnoses globally, with a projected increase to 29.5 million by 2040.[10] Cancer therapy still has high side effects of anti-cancerous drugs, while damaging the fast-growing cells of the body as well as the tumor sites in adequate immune responses resulting in adverse side effects,[11,12] To tackle such issues, researchers have focused on the development of nanocarriers to transport the drugs for high intracellular drug delivery.[13,14]

The design and expansion of nanocarriers play a key role in the development of new advanced therapeutic ways as the nanotechnology implied for their synthesis additionally empowers the drugs of concern to enhance their vital properties like solubility and increased concentration at the target site for higher potency and reduced side effects.[15] These desirable traits of drugs in consideration with the stealth behavior of the nanocarriers towards the immune system are being explored for the treatment of many chronic and acute disorders, as the nanoparticles potentially improve the therapeutic index, decrease off-target toxicity, and change the pharmacokinetic profile of pharmaceuticals[16] so that the desirable drug gets incorporated into the body and accumulates at the required site while exhibiting pharmacophoric properties exclusively towards the target cells, known as 'targeted drug delivery'. A variety of nanocarriers have been reported in the literature for applications in targeted drug delivery such as mesoporous nanocarriers, dendrimers, carbon nanotubes, gold nanoparticles, quantum dots, nanogels, *etc.*, and are represented in Fig. 1.[17]

Nanogels have proved to be apt agents for targeted drug delivery due to their high biocompatibility and beneficial dimensions ranging from human organs, and cells to viruses.[18,19] Nanogels essentially are submicron-sized hydrogels

[a]School of Chemical Engineering and Physical Sciences, Lovely Professional University, Phagwara 144411, Punjab, India. E-mail: singhjandeep@gmail.com
[b]Department of Chemistry and Centre of Advanced Studies in Chemistry, Panjab University, Chandigarh 160014, India
[c]Department of Chemistry, Gujranwala Guru Nanak Khalsa College, Civil Lines, Ludhiana 141001, Punjab, India. E-mail: chemgurpreet5@gmail.com

Journal of Molecular Structure 1305 (2024) 137740

Contents lists available at ScienceDirect

Journal of Molecular Structure

journal homepage: www.elsevier.com/locate/molstr

Click-derived o-cresolphthalein linked 1,2,3-triazole: Pb(II) ion sensing, *in silico* analysis, and aromatase inhibition

Gurleen Singh [a,1], Parveen Saini [a,1], Gurjaspreet Singh [b], Yamini Thakur [b], Gurpreet Kaur [c], Shubham Dash [d], Harneet Singh Khurana [e,*], Charanjit Kaur [d,*], Harminder Singh [a,*], Jandeep Singh [a,*]

[a] School of Chemical Engineering and Physical Sciences, Lovely Professional University, Phagwara, Punjab 144411, India
[b] Department of Chemistry and Centre of Advanced Studies in Chemistry, Panjab University, Chandigarh 160014, India
[c] Department of Chemistry, Gujranwala Guru Nanak Khalsa College, Civil lines, Ludhiana 141001, India
[d] School of Pharmaceutical Sciences, Lovely Professional University, Phagwara, Punjab 144411, India
[e] Department of Anaesthesia, Dayanand Medical College & Hospital, Ludhiana, Punjab 141001, India

ARTICLE INFO

Keywords:
Click chemistry
Chemosensor
Metal ion sensing
Environmental
Aromatase inhibitor

ABSTRACT

The present study demonstrates the synthesis, characterization, and multifaceted applications of a 1,2,3-triazole derivative synthesized via Copper(I)-Catalyzed Azide-Alkyne Cycloaddition (CuAAC). The design of the probe was carried out using o-cresolphthalein moiety, owing to its substantial absorption and emission behaviour, which was connected to a benzyl group (which acted as the transducer group) via a 1,2,3-triazole bridge. This bridge, in addition to serving as the spacer unit, also had the potential to provide the receptor sites for the metal ions due to the presence of N atoms having lone pairs of electrons. The compound's structural integrity was confirmed through Infrared (IR) Spectroscopy, Nuclear Magnetic Resonance (NMR) Spectroscopy, and Mass Spectrometry analyses. Its selective responsiveness to Pb(II) ions, established by UV–vis spectroscopy, revealed its potential as a robust Pb(II) ion sensor with a limit of detection of 11.2 μM and binding constant (K_a) value of 3.2×10^4 M^{-1}, thereby facilitating applications in environmental monitoring and analytical chemistry. Additionally, the compound's versatility extends to the realm of biology, as indicated by the *in silico* pharmacological studies and molecular docking simulations. These investigations underscored its significant potency as aromatase inhibitor, suggesting opportunities for therapeutic interventions and drug development, as the compound's molecular architecture and distinctive binding interactions offer promise in addressing intricate biological processes.

1. Introduction

The field of chemical synthesis has witnessed remarkable advancements over the years, driven by the quest for efficient and versatile methodologies to construct complex molecular architectures [1–3]. Among these methodologies, the Copper(I)-catalyzed azide-alkyne cycloaddition (CuAAC) reaction stands out as a pivotal methodology that has revolutionized the field of organic synthesis. The significance of CuAAC arises from its ability to synthesize 1,4-disubstituted 1,2,3-triazole linked compounds, which are valuable motifs in medicinal chemistry, materials science, and bioconjugation [4,5]. In this context, the utilization of 1,2,3-triazole derivatives as molecular probes for metal ion sensing has emerged as a promising avenue as the unique electronic and structural properties of 1,2,3-triazoles confer them with the ability to coordinate with metal ions, leading to distinctive changes in their physicochemical properties, such as fluorescence, absorbance, and electrochemical behavior [6,7]. The toxic heavy metal ions such as lead (Pb), mercury (Hg), cadmium (Cd), and arsenic (As) have garnered significant attention due to their widespread occurrence in the environment and their detrimental impact on human health and ecosystems, as they pose a grave threat due to their persistent presence, bioaccumulative nature, and ability to interfere with biological processes at the cellular and molecular levels, thereby resulting in a spectrum of acute and chronic health consequences, ranging from neurological

* Corresponding authors.
E-mail addresses: harminder_env@yahoo.com (H. Singh), singhjandeep@gmail.com (J. Singh).
[1] The authors contributed equally to this work

https://doi.org/10.1016/j.molstruc.2024.137740
Received 7 October 2023; Received in revised form 15 January 2024; Accepted 6 February 2024
Available online 7 February 2024

RSC Advances

REVIEW

View Article Online
View Journal | View Issue

Cite this: *RSC Adv.*, 2024, **14**, 7383

Clicking in harmony: exploring the bio-orthogonal overlap in click chemistry

Mehak,†[a] Gurleen Singh, †[a] Riddima Singh, [a] Gurjaspreet Singh,[b] Jigmat Stanzin,[b] Harminder Singh, [a] Gurpreet Kaur*[c] and Jandeep Singh *[a]

In the quest to scrutinize and modify biological systems, the global research community has continued to explore bio-orthogonal click reactions, a set of reactions exclusively targeting non-native molecules within biological systems. These methodologies have brought about a paradigm shift, demonstrating the feasibility of artificial chemical reactions occurring on cellular surfaces, in the cell cytosol, or within the body – an accomplishment challenging to achieve with the majority of conventional chemical reactions. This review delves into the principles of bio-orthogonal click chemistry, contrasting metal-catalyzed and metal-free reactions of bio-orthogonal nature. It comprehensively explores mechanistic details and applications, highlighting the versatility and potential of this methodology in diverse scientific contexts, from cell labelling to biosensing and polymer synthesis. Researchers globally continue to advance this powerful tool for precise and selective manipulation of biomolecules in complex biological systems.

Received 19th January 2024
Accepted 19th February 2024

DOI: 10.1039/d4ra00494a

rsc.li/rsc-advances

1. Introduction

Biological systems are accompanied by delicate networks of native biomolecules, vital for conventional functioning. For scrutinizing and modifying the biological systems, scientists have introduced a fresh set of reactions, namely bio-orthogonal click reactions, which exclusively alter non-native target molecules in the biological system, heretofore introduced, making it an ideal reaction for employing *in vitro*.[1–3] Bio-orthogonal chemistry enables the execution of organic synthesis typically conducted in a laboratory within living organisms and cells.[4] In contrast to numerous laboratory reactions, bio-orthogonal reactions are not designed for the bulk production of materials. Rather, their purpose is to covalently modify biomolecules with non-native functional groups under biological conditions, facilitating their examination and manipulation.[5,6] The roots of bio-orthogonal chemistry can be traced way back to the Huisgen 1,3-dipolar cycloaddition of organic azide and terminal alkyne to yield a racemic mixture of 1,4-disubstituted and 1,5-disubstituted 1,2,3-triazoles (Fig. 1).[7] The versatility of this reaction

[a]*School of Chemical Engineering and Physical Sciences, Lovely Professional University, Phagwara-144411, Punjab, India. E-mail: singhjandeep@gmail.com*
[b]*Department of Chemistry and Centre of Advanced Studies in Chemistry, Panjab University, Chandigarh-160014, India*
[c]*Department of Chemistry, Gujranwala Guru Nanak Khalsa College, Civil Lines, Ludhiana–141001, Punjab, India*
† The authors contributed equally to this work.

Mehak

Mehak received her Bachelor of Science from GGDSD College, Panjab University, Chandigarh. She is currently pursuing her Masters of Science in the School of Chemical Engineering and Physical Sciences, Lovely Professional University, Phagwara under the guidance of Dr Jandeep Singh and her research field is based on the synthesis of 1,4-disubstituted-1,2,3 triazoles as potential ion sensors.

Gurleen Singh

Gurleen Singh received his Master of Science from the Department of Chemistry, University of Jammu. He is pursuing PhD in the School of Chemical Engineering and Physical Sciences, Lovely Professional University, Phagwara under the guidance of Dr Jandeep Singh and his research is focused on the synthesis of 1,2,3 triazoles utilizing 'Click Chemistry' and their subsequent exploration as potential chemosensors.

Journal of Molecular Structure 1299 (2024) 137142

Contents lists available at ScienceDirect

Journal of Molecular Structure

journal homepage: www.elsevier.com/locate/molstr

Selective quinizarin-linked bis-1,2,3-triazoles as probes for Fe(II)/(III): Characterization, metal ion binding, DFT, and antiallergy activity via docking studies

Sachin Kumar [a,b,1], Gurleen Singh [c,1], Ram Kumar Tittal [a,*], Jandeep Singh [c], Vikas D. Ghule [a], Renu Sharma [b]

[a] Department of Chemistry, National Institute of Technology, Kurukshetra, Haryana 136119, India
[b] School of Applied Sciences, Om Sterling Global University, Hisar, Haryana 125001, India
[c] School of Chemical Engineering and Physical Sciences, Lovely Professional University, Phagwara, Punjab 144411, India

ARTICLE INFO

Keywords:
Quinizarin
Bis-1,2,3-triazole
Fe(II)/(III) sensor
Molecular docking
DFT and Molecular electrostatic potential

ABSTRACT

Herein, two new molecular probes of quinizarin-linked bis-1,2,3-triazoles have been synthesized *via* CuAAC reaction to detect transition metal(s), such as iron (Fe). FTIR, ^{1}H & ^{13}C-NMR, and HRMS spectroscopy fully characterized the synthesized probes. Absorption spectroscopy showed selective binding of probes with Fe(II) and Fe(III) ions. Job's plot suggested a 1:1 stoichiometric ratio of ligand and metal ion. Both probes **3a** and **3b** showed association constant of 4.42×10^3 M^{-1} and $4.35 \times 10^3 M^{-1}$ for Fe(II) and 4.35×10^3 M^{-1} and 4.59×10^3 M^{-1} for Fe(III), through Benesi-Hildebrand (B-H) plots. The DFT was performed for geometrical optimization of probes and their complexes, supported by Mulliken charges and Molecular electrostatic potential. Above and beyond, probes and their complexes were also docked with human histamine H1 receptor (PDB ID: 3RZE) protein, providing foretastes of its anti-allergic activity.

1. Introduction

In recent years, the design and development of effective molecular sensors for the selective and sensitive detection of metal ions have garnered significant attention in analytical chemistry, monitoring environmental issues, materials science, etc. Iron (Fe) holds a central position among the myriad metals of interest due to its vital roles in biological, environmental, and industrial processes. Iron is one of the most crucial transition metals found in living organisms that perform many physiological functions, like red blood cells as hemoglobin, muscle cells as myoglobin, DNA synthesis, and storing and transporting oxygen in the human body [1–4]. Both deficiency and an excess of iron level in the human body can trigger several physiological disorders. A low iron level due to blood loss or lack of dietary iron causes anemia. People with anemia may experience itchy skin (pruritis) that can become red, bumpy, and sore when scratched, i.e., allergic sensitization. Many epidemiological studies have connected allergy with deficient iron status in the last decade [5]. Some studies have suggested that Fe(II) complexes may have anti-allergic properties due to their ability to modulate the immune system and reduce inflammatory responses. These complexes might inhibit the release of histamine and other inflammatory mediators involved in allergic reactions. Histamine is essential for allergic symptoms such as itching, sneezing, and nasal congestion [6,7].

In contrast, excess iron can cause metabolic imbalance, disrupting cellular processes and leading to hemochromatosis. Iron in the +3 oxidation state is predominant due to its oxidization capacity during aerobic oxidation photosynthesis. However, the simultaneous accumulation of Fe(III) ions can be fatal to humans, causing respiration syndrome, skin ailments, convulsions, dysfunction of organs, Parkinson's and Alzheimer's diseases, and cardiac arrest. Also, it may lead to cancer [8–10]. According to the Food and Nutrition Board (FNB) at the Institute of Medicine (US), the daily iron requirement in adults for males and postmenopausal females is 8 mg/d, and premenopausal females are 18 mg/d [11]. Therefore, the ability to detect and monitor Fe(II) and (III) ions with high precision and selectivity is paramount in understanding their biological implications and the environmental impact of iron-rich pollutants. Most chemosensors reported cannot clearly distinguish between Fe(III) and Fe(II) oxidation states. Subsequently, various

* Corresponding author.
E-mail address: rktittaliitd@nitkkr.ac.in (R.K. Tittal).
[1] These authors contributed equally to this work.

https://doi.org/10.1016/j.molstruc.2023.137142
Received 5 September 2023; Received in revised form 5 November 2023; Accepted 21 November 2023
Available online 22 November 2023
0022-2860/

RSC Advances

PAPER

View Article Online
View Journal | View Issue

Cite this: *RSC Adv.*, 2023, **13**, 32399

Cu(I)-catalysed 1,2,3-triazole stitched chalcomer assembly as Pb(II) and Cu(II) ion sensor: DFT and docking scrutiny†

Riddima Singh,[a] Gurleen Singh,[a] Nancy George,[a] Gurjaspreet Singh,[b] Anita Devi,[b] Harminder Singh,[a] Gurpreet Kaur*[c] and Jandeep Singh*[a]

Herein, a 1,2,3-triazole derivative (CBT), synthesized using the Copper(I) catalyzed Alkyne Azide Cycloaddition (CuAAC) procedure, based on a chalcone skeleton has been reported, that was implemented as an effective sensor for Pb(II) and Cu(II) ions. The synthesized CBT was characterized using spectroscopic techniques such as FTIR, NMR (^{1}H and ^{13}C), and mass spectrometry. The sensing behaviour of CBT was analyzed using UV-Vis spectroscopy, demonstrating selective sensing for Pb(II) and Cu(II) ions, competitively. The correlation plot revealed the detection limit for Pb(II) and Cu(II) ions to be 100 μM and 110 μM respectively. In addition, DFT simulations and molecular electrostatic potential (MEP) studies scrutinized the binding strategy of the free CBT and its orientation towards the metal ions in the metal–ligand complex. The probe CBT was predicted *via* the online platform Way2drug for its pharmacological properties, investigating the possibility to inhibit early atherosclerosis. CBT was subsequently docked to the TRIB1 protein using AutoDock Vina and demonstrated a high binding affinity with a value of −6.2 kcal mol^{-1}.

Received 23rd August 2023
Accepted 30th October 2023

DOI: 10.1039/d3ra05760g

rsc.li/rsc-advances

1. Introduction

The environmental accumulation of metal ions above the permissible concentrations has led to their substantial upsurge, which has put forward the need to explore efficient and robust research alternatives for their instantaneous detection even in low concentrations. The emphasis on analytical cation detection is due to their well-documented pervasive toxic effects on both the terrestrial as well as aquatic living systems,[1–3] thereby rendering their qualitative as well as quantitative recognition as the need of the hour.[4] Due to the unregulated use of lead *via* mining, smelting, ceramics, paint, automobile exhaust emissions, *etc.*, its accumulation in the environment has undergone an exponential ascent since the latter years of the 'bygone century'.[5] Also, exposure to lead can denature DNA and proteins, is detrimental to bone health, and may result in cell transformation, thereby rendering the cells to become malignant.[6] Copper ions, though involved in biological processes in electron and oxygen transport in the body's soft tissues, can be toxic in higher concentrations where they can interfere with biological functioning by altering essential proteins/enzymes.[7–9] This can pose serious health risks like anaemia, interstitial nephritis, oxidative damage, hypertension, cardiovascular disease, severe neurological disease, *etc.*[10,11] Therefore, the detection of these metal ions above the threshold limit needs immediate attention to address environmental pollution and minimize impacts on biological systems.[12,13] This leads to the importance of metal ion sensors based on organic frameworks for selective recognition.

In this pursuit, *O*-chalcones and N-heterocycles have been potential sensors due to their selective cation binding capabilities.[14] The chalcones have a backbone of unsaturated carbonyl groups with conjugation and have the potential to exhibit chemosensing.[15–17] The combination of these motifs with the 1,2,3-triazole moiety *via* 'Click' (CuAAC) methodology has emerged as the most preferred synthetic route to form chalcone appended 1,4-disubstituted-1,2,3-triazole derivatives.[18] There is an increased demand for these moieties owing to their extensive selectivity for ion detection,[19,20] in addition to their significant biological properties such as antibacterial, antioxidative, antifungal activities *etc.*

The ion detecting property of a fluorescent chemosensor is based on a host–guest relationship, wherein the interaction of the receptor with the analyte induces photophysical changes in the fluorophore which indicates successful ion recognition.[21] Besides, exclusivity of a sensor is attributable to the cavity size, wherein the N-rich 1,2,3-triazole ring helps in the recognition

[a]*School of Chemical Engineering and Physical Sciences, Lovely Professional University, Phagwara-144411, Punjab, India. E-mail: singhjandeep@gmail.com*
[b]*Department of Chemistry and Centre of Advanced Studies in Chemistry, Panjab University, Chandigarh-160014, Punjab, India*
[c]*Department of Chemistry, Gujranwala Guru Nanak Khalsa College, Civil Lines, Ludhiana-141001, Punjab, India*

† Electronic supplementary information (ESI) available. See DOI: https://doi.org/10.1039/d3ra05760g

Inorganica Chimica Acta 551 (2023) 121470

Contents lists available at ScienceDirect

Inorganica Chimica Acta

journal homepage: www.elsevier.com/locate/ica

1-Naphtholphthalein appended 1,2,3-triazole via CuAAC: A molecular assembly for selective Co(II) ion recognition

Parveen Saini [a,b], Gurleen Singh [a], Gurjaspreet Singh [c], Jashan Deep Kaur [c], Gurpreet Kaur [d], Jandeep Singh [a,*], Harminder Singh [a,*]

[a] School of Chemical Engineering and Physical Sciences, Lovely Professional University, Phagwara 144411, Punjab, India
[b] Department of Chemistry, Shanti Devi Arya Mahila College, Dinanagar 143531, Punjab, India
[c] Department of Chemistry and Centre of Advanced Studies in Chemistry, Panjab University, Chandigarh 160014, India
[d] Department of Chemistry, Gujranwala Guru Nanak Khalsa College, Civil Lines, Ludhiana 141001, India

ARTICLE INFO

Keywords:
Click chemistry
CuAAC
1-Naphtholphthalein
Ion sensors
Co(II) ion detection

ABSTRACT

Current research work reports the 'Click' generation of a ligand, 1- naphtholphthalein linked 1,2,3-triazole (1-NPT) and its "turn-off" absorbance response on binding with Co(II) ions. Copper(I) catalyzed alkyne-azide cycloaddition reaction (CuAAC), a highly stereoselective reaction of 'Click Chemistry' is employed to synthesize the five membered heterocyclic ring based probe 1-NPT, that has been successfully characterized by spectroscopic techniques like IR, NMR (^{1}H, ^{13}C) and Mass spectroscopy. The chemosensing behavior of 1-NPT was analyzed by performing UV–Visible titrations with different metal ions like Mn(II), Hg(II), Cd(II), Pb(II), Cu(II), Fe(II), Zn(II), Ba(II), Cr(III), Co(II), K(I) and Na(I) in CH_3CN:H_2O (4:1, v/v) solution and the results obtained signify the selectivity of synthesized receptor towards Co(II) ions with minimum detection limit of 1.87 μM and 1:1 stoichiometry of 1-NPT:Co(II) complex with no interference of other metal ions.

1. Introduction

The selective detection of analytes, having no characteristic spectroscopic properties of their own is of great challenge. Organic moieties tailored for analyte binding and having subunits signaling modulations in their spectroscopic behavior on binding with specific analyte are quite effectively and significantly used for their recognition [1–3]. 'Click chemistry' is a wonderful approach of various organic syntheses that includes a family of diverse linking reactions, easy to perform, fast and high yielding with minimal or inoffensive byproducts have been proved as highly promising to generate such type of organic molecules [4–7]. Since its discovery in 2001, by an American Nobel laureate Sir K. B. Sharpless, this approach of organic syntheses gained worldwide popularity. The various categories of click chemistry reactions found in literature are metal catalyzed cycloaddition reactions such as Hetero-Diels-alder reaction, 1,3-dipolar cycloaddition reaction, thiol-ene reactions, photo-click reactions, Michael addition, nucleophilic ring opening of strained heterocycles such as epoxides and aziridines etc. [8–12]. Now a day, the click reactions are being incorporated onto or into biomolecules, including introduction of synthetic amino acids with different reactive sites as well as modifications in DNA and nucleotides. Recently, in 2022, the nobel prize in chemistry was awarded to three scientists C. R. Bertozzi, M. P. Meldel and K. B. Sharpless for the 'Development of Click Chemistry and Bioorthogonal Chemistry' [13–14]. Among the various types of click reactions, the 1,3-dipolar cycloaddition reaction, especially CuAAC resulting into the generation of 1,4-disubstituted 1,2,3-triazole linkers as exclusive product has bagged immense importance due to their wide range of applications in the areas like material science, drug discovery, bioconjugation, chemosensing, fluorescent imaging, catalysis and polymer chemistry [15–20]. 1,2,3-triazole linked molecules are also used as predecessors for the synthesis of mesoionic carbenes, very reactive *N*-heterocyclic carbene intermediates that act as ligands for a category of metal ions. The coordination complexes of transition metals such as Rh, Ir, Pd, Pt, Ni, Ag etc. with mesoionic carbenes are used to catalyze various organic syntheses [21–22].

The CuAAC reaction is a highly stereoselective, [3 + 2] cycloaddition reaction of terminal alkyne with organic azide using catalytic amount of Cu(I) under benign reaction conditions to produce 1,4-disubstituted 1,2,3-triazole as single and pure product as shown in Fig. 1. The

* Corresponding authors.
E-mail addresses: singhjandeep@gmail.com (J. Singh), harminder_env@yahoo.com (H. Singh).

https://doi.org/10.1016/j.ica.2023.121470
Received 3 September 2022; Received in revised form 14 February 2023; Accepted 9 March 2023
Available online 11 March 2023

Inorganica Chimica Acta 568 (2024) 122063

Contents lists available at ScienceDirect

Inorganica Chimica Acta

journal homepage: www.elsevier.com/locate/ica

Research paper

α-Naphtholbenzein based heterocyclic sensor for detection of Cu(II) ions

Parveen Saini [a,b], Gurleen Singh [a], Nancy George [a], Gurjaspreet Singh [c], Gurpreet Kaur [d], Punita Tiwari [e], Pinky Satija [f], Jandeep Singh [a,*], Harminder Singh [a,*]

[a] School of Chemical Engineering and Physical Sciences, Lovely Professional University, Phagwara 144411, (Punjab), India
[b] Department of Chemistry, Shanti Devi Arya Mahila College, Dinanagar 143531, (Punjab), India
[c] Department of Chemistry and Centre of Advanced Studies in Chemistry, Panjab University, Chandigarh 160014, India
[d] Department of Chemistry, Gujranwala Guru Nanak Khalsa College, Civil lines, Ludhiana 141001, India
[e] Department of Chemistry, Khalsa College Amritsar, 143002, India
[f] School of Advanced Chemical Sciences, Shoolini University, Solan 173229, India

ARTICLE INFO

Keywords:
α-Naphtholbenzein
Click chemistry
Chemosensor
Cu(II)-recognition
UV–Vis spectroscopy
Fluorescence spectroscopy

ABSTRACT

Present research work illustrates the 'Click' generation of 4-((1-((1-benzyl-1H-1,2,3-triazol-4-yl) methoxy) naphthalen-4-yl) (phenyl)methylene) naphthalen-1(4H)-one **α-NBT**, a heterocyclic compound analyzed as an optical chemosensor for the selective detection of Cu(II) ions. The molecule is synthesized by [3 + 2] cycloaddition reaction of α-naphtholbenzein based terminal alkyne **2** with 1-(azidomethyl) benzene **3** under Cu(I)-catalyzed conditions (CuAAC) and is further characterized for its structural components by various spectroscopic techniques like IR, NMR (^{1}H, ^{13}C) and Mass spectrometry. Being having significant absorption in UV–Visible region, the receptor molecule **α-NBT** is analyzed for its chemosensing characteristics by UV–Visible and fluorescence spectroscopy and found to be very selective towards Cu(II) ions among a range of metal ions including Na(I), K(I), Ba(II), Cr(III), Mn(II), Fe(II), Fe(III), Co(II), Ni(II), Cu(I), Zn(II), Cd(II), Hg(II), Pb(II), Th(IV) and Ce(III) in CH_3CN:H_2O (4:1, v/v) solvent system. From the recorded spectral responses with change in concentration of Cu(II) ions, the binding ratio of **α-NBT**:Cu(II) complexation is calculated as 2:1 with the limit of detection of Cu(II) ions as 3.12 μM and binding constant for ligand–metal interaction equal to 0.15 x 10^5 M^{-1}.

1. Introduction

The potential to sense and recognize analytes through optical techniques such as UV–Visible and fluorescence spectroscopy is quite easy and highly reliable way of analyte detection [1,2]. Out of a variety of optical signaling units working with different signal transduction mechanisms employed to detect a specific ion, the organic molecules appended with structural units having certain photophysical characteristics are of great concern and demand for analytical chemists working in the field of chemosensing [3–5]. Metal ions are one among such species whose selective recognition is of substantial relevance in the present times mainly owing to their detrimental effects on the vital body metabolic processes in the living systems via protein binding potential and enzyme inactivation capabilities [6,7]. For instance, Cu(II) ion is of great importance in living organisms and is a cofactor of various metalloenzymes, responsible for their proper functioning [8]. However, an overdose of these ions is attributed to cells and organs damaging, Wilson disease, Parkinson disease and Alzheimer disease [9]. Therefore, there has been a significant interest in recent years in investigating diverse techniques for selective sensing of metal ions, wherein chemosensors capable of instantaneous and sensitive detection of trace amounts of Cu(II) in the environment have been developed [10–12]. The designing and development of such organic scaffolds in pure form is another task that becomes very much handy through 'Click Chemistry', a set of reactions which are highly stereospecific with diverse chemical functions to generate a single product with no or inoffensive byproducts that can be extracted out by non-chromatographic techniques [13,14].

Among all the click reactions, the Cu(I)-catalyzed azide-alkyne cycloaddition (CuAAC), is a highly versatile and robust reaction involving the 1,3-dipolar cycloaddition of organic azide with terminal alkyne in the presence of Cu(I) as catalyst to generate 1,4-disubstituted 1,2,3-triazole [15]. The methodology has proved to be a great tool for the researchers to stitch a variety of structural units to develop tailored organic moieties for chemosensing purposes. [16–18]. The resultant 1,2,3-triazole group not only functions as a proficient covalent linker but also serves as a binding site for specific metal ions via the nitrogen

* Corresponding authors.
E-mail addresses: singhjandeep@gmail.com (J. Singh), harminder_env@yahoo.com (H. Singh).

https://doi.org/10.1016/j.ica.2024.122063
Received 8 March 2024; Received in revised form 8 April 2024; Accepted 9 April 2024
Available online 10 April 2024

Journal of Molecular Structure 1288 (2023) 135666

Contents lists available at ScienceDirect

Journal of Molecular Structure

journal homepage: www.elsevier.com/locate/molstr

Click modified bis-appended Schiff base 1,2,3-triazole chemosensor for detection of Pb(II)ion and computational studies

Nancy George [a], Gurleen Singh [a], Riddima Singh [a], Gurjaspreet Singh [b], Priyanka [b], Harminder Singh [a], Gurpreet Kaur [c], Jandeep Singh [a,*]

[a] School of Chemical Engineering and Physical Sciences, Lovely Professional University, Phagwara, Punjab 144411, India
[b] Department of Chemistry and Centre of Advanced Studies in Chemistry, Panjab University, Chandigarh 160014, India
[c] Department of Chemistry, Gujranwala Guru Nanak Khalsa College, Civil lines, Ludhiana, Punjab 141001, India

ARTICLE INFO

Keywords:
Click chemistry
CuAAC
Lead (II) sensor
1,2,3-triazole
Chemosensors
Computational chemistry

ABSTRACT

A novel 1,2,3-triazole linked schiff base chemosensor was stitched via Cu(I) catalyzed click reaction with excellent yield, high selectivity, sensitivity and characterized using fourier transform infrared spectroscopy (FTIR), NMR (^{1}H and ^{13}C), mass spectrometry (MS), CHN analysis, thermal gravimetric analysis (TGA) and differential scanning calorimetry (DSC). The developed chemosensor was investigated for it's optical properties using UV–visible and fluorescent spectroscopy. The detected limit of the synthesized probe was estimated 0.25 μM from fluorescence spectroscopy, which is particularly below the WHO guidelines. The binding stoichiometric (2:1) of ligand was confirmed by the job's plot and the binding constant was determined to be 4.1×10^{6} M^{-1} and 1.4×10^{5} M^{-1} from the B-H plot and the Stern-Volmer curve, respectively. These results establish the developed chemosensor as a potent probe for analytical and practical applications. The optimized geometrical structure of the probe (4) was run on Gaussian 09 program using DFT method with (B3LYP)/6–311G++(d,p) basis set of hybrid density functional theory.

1. Introduction

Metal ion pollution has become a worldwide ecological concern in recent years due to rapid development and increasing industrialization. The pervasive use of lead ions in particular has resulted in massive environmental pollution, posing grave health concern to individuals and biological systems. Petrol, paints, pigments, lead batteries, alloys, ceramics, glass, chemicals, toys, electronics, water pipes, and other consumer items are the most prevalent anthropogenic sources of lead contamination in environmental matrices (water, soil, air, and food). Excessive lead exposure causes a variety of health problems in humans, affecting the kidneys, gastrointestinal, hematological, cardiac, reproductive, and neurological systems. Furthermore, Pb^{2} is far more dangerous than those other metals since it is a neurotoxin that may accumulate in muscles and bones, causing nervous system damage as well as brain and blood disorders [1–5]. The United States Environmental Protection Agency (USEPA) and the World Health Organization (WHO) have precisely specified permitted concentration limits of Pb^{2+} metal ions in drinking water as 16 ppb (16 μg L^{-1}) and 10 ppb (48 nM), respectively. Similarly, the US Food and Drug administration had established an action level of 2.5 μM for Pb^{2+} in goods intended for use by newborns and children. As a result, determining and monitoring the level of the lead metal ion is critical to ensure that heavy metal lead concentrations remain below the designated hazardous limit [6–8].

Schiff bases are widely recognized as tunable compounds with an azomethine bond, and they are developing as a prominent class in chemical and medicinal chemistry due to their distinguishing characteristics and diverse biological activities. Schiff bases have been widely explored as flexible ligands for analyte detection, and their facile interactions with metal due to changes in electrical characteristics have been intensively researched [9–13]. Synthetically achievable and structurally versatile, 1,2,3-triazole derivatives are primarily produced via 1,3-dipolar cycloaddition of organic azides and substituted alkynes [10,14]. Recently, Carolyn R. Bertozzia, Morten Meldal, and K. Barry Sharpless were awarded 2022 Nobel Prize in Chemistry for discovering click chemistry, an ecologically benign approach for swiftly combining molecules to produce cancer treatments and generate materials. The potential of the generated 1,2,3-triazole system to behave as a binding

* Corresponding author.
E-mail address: singhjandeep@gmail.com (J. Singh).

https://doi.org/10.1016/j.molstruc.2023.135666
Received 6 January 2023; Received in revised form 24 April 2023; Accepted 25 April 2023
Available online 29 April 2023

Polyhedron 242 (2023) 116496

Contents lists available at ScienceDirect

Polyhedron

journal homepage: www.elsevier.com/locate/poly

Schiff base functionalized 1,2,3-triazole derivative for Fe(III) ion recognition, as N,O,O-Fe-O,O,N sandwich complex: DFT analysis

Nancy George [a], Gurleen Singh [a], Riddima Singh [a], Gurjaspreet Singh [b], Sushma [c], Harminder Singh [a], Gurpreet Kaur [d,*], Jandeep Singh [a,*]

[a] School of Chemical Engineering and Physical Sciences, Lovely Professional University, Phagwara 144411, Punjab, India
[b] Department of Chemistry and Centre of Advanced Studies in Chemistry, Panjab University, Chandigarh 160014, India
[c] Chitkara College of Pharmacy, Chitkara University, Patiala 140417, Punjab, India
[d] Department of Chemistry, Gujranwala Guru Nanak Khalsa College, Civil Lines, Ludhiana 141001, Punjab, India

ARTICLE INFO

Keywords:
Click Chemistry
CuAAC
1,2,3-Triazole
Iron (III) sensor
Chemosensors

ABSTRACT

The present research aims to synthesize Schiff base tethered 1,2,3-triazole derivative using Cu(I) catalyzed click reaction as a highly sensitive and selective optical chemosensor for the recognition of ferric ions. The synthesized probe was characterized using Fourier transform infrared spectroscopy (FTIR), NMR (^{1}H and ^{13}C), mass spectrometry, CHN analysis, and Thermal gravimetric analysis (TGA). The UV–vis spectroscopy was employed in eco-friendly EtOH:H_2O (9:1 v/v) solvent media to investigate the optical properties of the developed chemosensor **SBT**, the association constant and limit of detection of Fe^{3-} was determined to be 2.6×10^4 M^{-1} and 1.3×10^{-7} M establishing the designed **SBT** as a potent probe for analytical and practical applications. Additionally, the time-dependent study and pH sensitivity of the developed probe **SBT** and metal–ligand complex were also studied via UV–visible spectroscopy. Besides, FTIR spectra and TGA curve of the synthesized (**SBT**-metal complex) confirmed the binding of the metal–ligand complex. Furthermore, the real sample application for detection of Fe^{3+} in spinach (food rich in Iron) was analysed, and the **SBT**-based sensing system yielded a recovery rate of greater than 99.07%. The synthesized probe was also explored for its computational-based DFT studies via Gaussian 09 programs using the DFT method with (B3LYP)/-311G (d,p) basis set of hybrid density functional theory.

1. Introduction

Among the most persistent challenges for scientists is to develop extremely sensitive and selective metal-ion responsive chemosensors for the effective tracking of physiologically and ecologically relevant metal ions. Although, Iron is a substantial transition metal that plays a requisite role in oxygen transport in the human body, and subsequently act as a cofactor in the enzymatic activities involved in biochemical reactions [1]. However, excessive deposition of iron in ferritin proteins can cause metabolic imbalance resulting in the disruption of cellular processes, and hinders the biosynthetic activity. Iron in a trivalent state is predominant owing to its capacity to oxidise during aerobic oxidation photosynthesis [2]. But the concomitant accumulation of Fe^{3+} can be fatal to human beings, causing respiration syndrome, convulsions, skin ailments, dysfunction of organs, Parkinson's and Alzheimer's diseases, cardiac arrest and can lead to cancer [3-5]. Meanwhile, the daily requirement of iron uptake in adult male and the female body is 9.1 and 19.6 (mg/d) respectively as recommended by the World Health Organization (WHO) and exceeding these levels can lead to deterioration of human's health if left untreated [2,6,7]. Therefore, development of versatile, precise and efficient Fe^{3+} ion responsive chemosensor, below the permissible levels, is essential [8-10]. Recently, the development of Fe^{3-} selective sensors feature drawbacks such as turn-off responses and interferences with other metal ions. Additionally, these detectors are structurally intricate and need a tedious multistep chemical synthesis, resulting in excessively expensive costs. Most of the chemosensors reported have the inability to clearly distinguish between Fe^{3+} and Fe^{2+} oxidation states. Subsequently, various oxidation states have distinct features, it is vital to identify one from the other in order to analyse their course of action [11-14].Table 1.Table 2..

'Click chemistry' has allured enormous research attention due to the synthetic simplicity for synthesis of 1,2,3-triazole linkers, that act as binding pockets in diverse applications in chemical biology, agrochemical, dyes, pigments and so forth. The CuAAC Meldal–Sharpless

* Corresponding authors.
E-mail address: singhjandeep@gmail.com (J. Singh).

https://doi.org/10.1016/j.poly.2023.116496
Received 29 March 2023; Accepted 7 June 2023
Available online 20 June 2023

catalysts

MDPI

Review

Copper-Based Metal–Organic Frameworks (MOFs) as an Emerging Catalytic Framework for Click Chemistry

Riddima Singh [1], Gurleen Singh [1], Nancy George [1], Gurjaspreet Singh [2], Sofia Gupta [2], Harminder Singh [1], Gurpreet Kaur [3,*] and Jandeep Singh [1,*]

[1] School of Chemical Engineering and Physical Sciences, Lovely Professional University, Phagwara 144411, India
[2] Department of Chemistry and Centre of Advanced Studies in Chemistry, Panjab University, Chandigarh 160014, India
[3] Department of Chemistry, Gujranwala Guru Nanak Khalsa College, Civil Lines, Ludhiana 141001, India
* Correspondence: chemgurpreet5@gmail.com (G.K.); singhjandeep@gmail.com (J.S.)

Abstract: In the extensive terrain of catalytic procedures for the synthesis of organic molecules, metal–organic frameworks (MOFs) as heterogenous catalysts have been investigated in a variety of chemical processes, including Friedel–Crafts reactions, condensation reactions, oxidations, and coupling reactions, and utilized owing to their specific properties such as high porosity, tuneability, extraordinary catalytic activity, and recyclability. The eminent copper-tailored MOF materials can be exceptionally dynamic and regioselective catalysts for click reactions (1,3-dipolar cycloaddition reaction). Considering the fact that Cu(I)-catalyzed alkyne–azide cycloaddition (CuAAC) reactions can be catalyzed by several other copper catalysts such as Cu (II)-β-cyclodextrin, $Cu(OAc)_2$, Fe_3O_4@SiO_2, picolinimidoamide–Cu(II) complex, and Cu(II) porphyrin graphene, the properties of sorption and reusability, as well as the high density of copper-MOFs, open an efficient and robust pathway for regimented catalysis of this reaction. This review provides a comprehensive description and analysis of the relevant literature on the utilization of Cu-MOFs as catalysts for CuAAC 'click' reactions published in the past decade.

Keywords: metal–organic frameworks (MOF); Cu-MOF; catalyst; 1,4-disubstituted 1,2,3-triazole; click chemistry; heterogenous catalysis

Citation: Singh, R.; Singh, G.; George, N.; Singh, G.; Gupta, S.; Singh, H.; Kaur, G.; Singh, J. Copper-Based Metal–Organic Frameworks (MOFs) as an Emerging Catalytic Framework for Click Chemistry. *Catalysts* **2023**, *13*, 130. https://doi.org/10.3390/catal13010130

Academic Editors: Filippo Bossola and Nicola Scotti

Received: 30 November 2022
Revised: 27 December 2022
Accepted: 4 January 2023
Published: 6 January 2023

1. Introduction

Click chemistry is one of the most robust and versatile methodologies currently known to researchers, capable of synthesizing large complex compounds from relatively smaller moieties [1,2]. Due to its advantageous features and facile pathway of synthesis, the methodology has received significant interest globally. Carolyn R. Bertozzi, Morten Meldal, and K. Barry Sharpless in 2022 were awarded the Nobel Prize in Chemistry for their ground-breaking contribution, which was a big step in advancement. The advent of click chemistry has led to the discovery of nitrogen-rich azole heterocycles, which have been shown to be fascinating compounds with broad potential significantly with their pharmacological [3] and chemosensing [4] properties. 'Click' reactions, specifically Cu(I)-catalyzed cycloaddition involving a terminal alkyne and an organic azide to synthesize 1,4-disubstituted-1,2,3-triazole, have received a large amount of consideration in the fields of material science, polymer science, peptide chemistry [5], and synthetic organic chemistry over the past few decades. However, due to the fact that alkynes are poor 1,3-dipole acceptors, this reaction cannot proceed regioselectively without a suitable catalyst. Significantly, the presence of Cu(I), which forms bonds with terminal alkynes, greatly enhances the pace, selectivity, and overall efficiency of click reactions [6].

The catalysts tailored from transition metals have the potential to act as fabricators in the assemblage of supplementary intricate structures, yielding complex organic structures

Sustainable Chemistry and Pharmacy 30 (2022) 100824

Contents lists available at ScienceDirect

Sustainable Chemistry and Pharmacy

journal homepage: www.elsevier.com/locate/scp

Microwave accelerated green approach for tailored 1,2,3–triazoles via CuAAC

Nancy George [a], Gurleen Singh [a], Riddima Singh [a], Gurjaspreet Singh [b], Anita Devi [b], Harminder Singh [a], Gurpreet Kaur [c,**], Jandeep Singh [a,*]

[a] School of Chemical Engineering and Physical Sciences, Lovely Professional University, Phagwara, 144411, Punjab, India
[b] Department of Chemistry and Centre of Advanced Studies in Chemistry, Panjab University, Chandigarh, 160014, India
[c] Department of Chemistry, Gujranwala Guru Nanak Khalsa College, Civil Lines, Ludhiana, 141001, Punjab, India

ARTICLE INFO

Keywords:
Green chemistry
Microwave–assisted synthesis
1,2,3–triazole
Click chemistry
CuAAC
Sustainability

ABSTRACT

The persistent deterioration of our environmental assets has initiated 'a push' among the scientific community for increased reliance on eco-friendly methodologies minimizing the utilization of hazardous materials. As an outcome, there is a paradigm shift in the synthetic modules of organic reactions from conventional techniques to the parameters of green principles. Therefore, the demand for microwave (μw) tailored reactions has witnessed substantial and exponential growth in the last two decades. In accordance, the employment of green methodology in Cu(I) catalyzed alkyne-azide cycloaddition reaction (CuAAC) for the synthesis of 1,2,3–triazole derivatives have reared fruitful results with the reduction of synthetic time, superior yields without benign solvents. The use of the microwave technique has been amplified with its implementation of a range of green methodologies by contributing to solvent-less, catalyst-free, use of ionic liquids and aqueous medium. This review puts forward the microwave synthesis of 1,2,3–triazoles through Cu(I) mediated click chemistry.

1. Introduction

Heterocyclic compounds have emerged as a special class of compounds owing to their numerous medicinal properties such as DNA-virus inhibitors, anti-hepatotoxic, anti-microbial agents and industrial applications like the synthesis of dyes, cosmetics, weed killers, reprography, antioxidants, and plastics, leading to the advancement in scientific research (Mishra et al., 2021; Dharavath et al., 2020; Ashok et al., 2020a). The stitching of a terminal alkyne with an organic azide in a cycloadditive manner is one of the most extensive techniques for the synthesis of N-heterocycles (Hernández-López et al., 2020; SinghSanchita et al., 2018; M'Hamed, 2015; Kumar et al., 2021). and utilizing this methodology, particularly the 5-membered 1,2,3-triazole linked molecules can be effectively synthesized. Huisgen in the 1960's laid down the path for 1,3 dipolar cycloaddition reaction under uncatalyzed and prolonged thermal conditions giving a mixture of 1,4 and 1,5-disubstituted products. However, the reaction methodology suffered from the serious drawbacks of non-regioselectivity, long reaction time, and poor product yields (Bräse et al., 2005; T.-S. L. and Prusoff, 1978; Singh et al., 2018a; Tiwari et al., 2016; Huisgen, 1963; Huisgen et al., 1967; Kanemasa and Kanai, 2000; Bhuyan et al., 2018; Dheer et al., 2017; Hein and Fokin, 2010).

* Corresponding author.
** Corresponding author.
E-mail addresses: chemgurpreet5@gmail.com (G. Kaur), singhjandeep@gmail.com (J. Singh).

https://doi.org/10.1016/j.scp.2022.100824
Received 4 July 2022; Received in revised form 15 August 2022; Accepted 31 August 2022

Journal of Organometallic Chemistry 944 (2021) 121846

Contents lists available at ScienceDirect

Journal of Organometallic Chemistry

journal homepage: www.elsevier.com/locate/jorganchem

Review

Metals as "Click" catalysts for alkyne-azide cycloaddition reactions: An overview

Pooja Kalra[a], Rupinder Kaur[b], Gurleen Singh[b], Harminder Singh[b], Gurjaspreet Singh[c], Pawan[c], Gurpreet Kaur[d,*], Jandeep Singh[b,**]

[a] Department of Chemistry and Biochemistry, Sharda University, Greater Noida, Uttar Pradesh 201310, India
[b] Department of Chemistry, Lovely Professional University, Phagwara, Punjab 144411, India
[c] Department of Chemistry and Centre of Advanced Studies in Chemistry, Panjab University, Chandigarh, 160014, India
[d] Department of Chemistry, Gujranwala Guru Nanak Khalsa College, Civil lines, Ludhiana, 141001, India

ARTICLE INFO

Article history:
Received 19 February 2021
Revised 1 April 2021
Accepted 16 April 2021
Available online 23 April 2021

Keywords:
Click chemistry
Metal catalysts
Mechanism

ABSTRACT

This review emphasizes on the efficacy of various metals in their diverse oxidation states to efficiently sew terminal alkyne to azide to give triazole ring. The emergence of Alkyne-Azide Cycloaddition reaction as one of the finest tools for the tailoring of two unsaturated fragments has equipped researchers with a methodology to weave in the alkyne-azide groups into either 1,2,3- or 1,2,4-traizole. The use of metal catalysts have efficiency comparative to CuAAC but comes at an expensive cost. The use of different metals involving the mechanistic cycles, reusability studies, solvent system/reacting conditions have been discussed in the review.

1. Introduction

'Click chemistry', a term devised by Sir K. B. Sharpless in 2001 defines a set of high yielding and stereospecific reactions giving off effortlessly separable inoffensive by-products [1]. This modular technique produces clean and efficient reactions at the molecular level from precise and small group of molecules [2]. The term 'Click' mimics the molecular building blocks annotating the 'seat belt-buckle' module that can be easily conjoined but is inseparable. Metal catalyzed alkyne-azide cycloaddition reactions form an incredible synthetic framework which functions as a true chemical click by enabling functional reactions easily regulated joining of readily available but specific fragments [3,4]. In general, 'Click' describe a class of chemical transformation with a variety of attractive features including excellent functional group tolerance, strong

Abbreviations: 2D, Two Dimensional; AAC, Azide alkyne cycloaddition; AAcP, azide-alkyne click polymerization; AcOH, Acetic acid; AEB, N-(4-azidophenyl)-4-ethynylbenzamide; AgAAC, Silver catalyzed alkyne azide cycloaddition; $AgNO_3$, Silver nitrate; AgOTf, Silver trifluoromethanesulfonate; AuAAC, Gold catalyzed azide-alkyne cycloaddition; Au / TiO_2AAC, Gold / Titanium dioxide azide-alkyne cycloaddition; Bu_4NBr, Tetrabutylammonium bromide; BuOH, Butanol; CH_2Cl_2, Dichloromethane; CH_3CN, Acetonitrile; CuAAC, Cu (I) Catalysed Alkyne Azide Cycloaddition.; Cu(I), Copper (I); CuNPs, Copper-based nanoparticles; $Cu(OAc)_2$, Cupric acetate; $Cu(PPh_3)_3Br$, Bromotris(triphenylphosphine)copper(I); $CuSo_4$, Copper(II) sulfate; DA, Diels-Alder; DBU, 1,8-Diazbicyclo[5.4.0]undec-7-ene; DFT, Density functional theory; DIPEA, N,N-Diisopropylethylamine (Hunig's base); DMF, Dimethylformaide; DMSO, Dimethylsulphoxide; EDC, Electron data capture; Et_3N, Ethylenetriamine; EtOH, Ethanol; EWG, Electron withdrawing group; FTIR, Fourier Infrared Spectroscopy; FMO, Frontier Molecular Orbital; ^1H NMR, Proton Nuclear Magnetic Resonance; H_2O, water; HOBt, Hydroxybenzotriazole; HPLC, High pressure liquid chromatography; IEG, iterative exponential growth; IR, Infrared Spectrum; IrAAC, Iridium-catalyzed intermolecular azide-alkyne cycloaddition; K_2CO_3, Potassium carbonate; KOH, Potassium hydroxide; MAAC, Metal catalyzed azide-alkyne cycloaddition; MCRs, Aqeous solvent reaction; MeCN, Methyl cyanide; MNPs, Magnetic Nanoparticles; MW, Microwave; NaN_3, Sodium azide; $NaNO_2$, sodium nitrite; NiAAC, Raney Nickel azide-alkyne cycloaddition; NMI, N-methylimidazole; NPA, Natural Population Analysis; OTES, Organotriethoxysilanes; OTs, O-tosyl; $P(Cy)_3$, Tricyclohexylphosphine; PdAAc, Palladium catalyzed azide-alkyne cycloaddition; $Pd_2(dba)_3$, Tris(dibenzylideneacetone)dipalladium(0); Pd@PR, Polystyrene resin assisted by palladium(0); PED, Performance-enhancing substance; PhMe, Toulene; $PhSiMe_3$, Trimethyl(phenyl)silane; P_2O_5, Phosphorus pentaoxide; $P(Ph)_3$, Triphenylphosphine; Pr_2NET, Diisopropylethylamine; PTA, Purified Terephthalic acid; PTC, Phase transfer catalyst; RD32, Gold Rhombic Dodecahedra; ROS, Reactive oxygen species; RT, Room temperature; RuAAc, Ruthenium-catalyzed azide alkyne cycloaddition; RuAAcP, Ru(II)-catalyzed azide-alkyne click polymerization; SEM, 2-(trimethylsilyl)ethoxymethyl; TBAF, Tetra-n-butylammonium fluoride; TBTA, tris[(1-benzyl-1H-1,2,3-triazol-4-yl)methyl]amine); TEA, Triethanolamine; TEM, Transmission Electon Microscopy; TETA, Triethylenetratramine; THF, Tetrahydrofuran; TiO_2, Titanium dioxide; TLC, Thin Layer Chromatography; TMS, Tetramethylsilane; TMSA, Trimethylsilacetylene; UHV, Ultra-high vacuum; XPS, X-ray photoelectron spectroscopy; ZnAAC, Zinc catalyzed azide-alkyne cycloaddition; Zn/C, Zinc on charcoal; $ZnEt_2$, Diethylzinc; ZnNPs, Zinc nanoparticles; $Zn(OAc)_2$, Zinc acetate.

* Corresponding author.
** Corresponding author.
E-mail addresses: chemgurpreet5@gmail.com (G. Kaur), singhjandeep@gmail.com (J. Singh).

https://doi.org/10.1016/j.jorganchem.2021.121846
0022-328X/

Sensors & Diagnostics

PAPER

View Article Online
View Journal

Cite this: DOI: 10.1039/d3sd00109a

A selective chemosensor *via* click chemistry for Cu^{2+} and Hg^{2+} ions in organic media†

Sachin Kumar, [ab] Bajrang Lal, [a] Ram Kumar Tittal, [*a] Gurleen Singh, [c] Jandeep Singh, [c] Ghule Vikas D., [a] Renu Sharma[b] and Jagjivan K. Sabane[d]

Received 8th May 2023,
Accepted 30th June 2023

DOI: 10.1039/d3sd00109a

rsc.li/sensors

A simple chemosensor, 4-amino antipyrine linked bis-1,2,3-triazole, was synthesized *via* the "click" approach using the CuAAC method and characterized by FTIR, NMR, and ESI-MS spectroscopy. The synthesized chemosensor upon ion sensing study showed a selective and significant detection of Hg(II) and Cu(II) ions, with the LOD being 56 and 63 μM, respectively. Mercury and copper are toxic heavy metals. The quantitative and qualitative detection of these ions is paramount for human health and the environment. The effect of time and temperature on the binding capability of APT with Hg(II) and Cu(II) ions was also studied using UV-Vis spectroscopy. Additionally, DFT studies lay forward the structural optimization of the chemosensor by the (B3LYP)/6-311G(d,p) and B3LYP/LanL2DZ level of theory.

1. Introduction

In recent years, heavy metal exposure has increased due to anthropogenic and agricultural activity and modern industrialization, which negatively impact human health. Worldwide, millions of people are intoxicated by toxic metal contamination in water, air, and food, which are a matter of grave concern for humankind and the complete ecosystem of the environment. Among them, mercury and copper are toxic heavy metals that can cause severe health problems in humans and wildlife. Copper in surface waters occurs predominantly in Cu(II) cupric form. Mercury is a naturally occurring element found in air, water, and soil in various forms: elemental (or metallic) and inorganic (to which people may be exposed through their occupation), and organic (*e.g.*, methylmercury, to which people may be exposed through their diet). Exposure to mercury, even in small amounts, may cause serious health problems. The toxicity and potential of mercury may bio-accumulate and be biomagnified in the food chain, leading to severe health problems such as neurological disorders, renal failure, and congenital disabilities.[1] The permissible limit of Hg and Cu in human physiology according to the World Health Organisation (WHO) and Indian Standard Institutions (ISI) is (0.001 mg l^{-1} and 0.001 mg l^{-1}) and (1.0 mg l^{-1} and 0.05 mg l^{-1}), respectively.[2] Beyond this limit, the aforementioned harmful effects may appear. Therefore, quantitative and qualitative detection of essential trace elements is vital to balance the smooth physiological functioning in biological systems. Developing reliable and sensitive sensors for detecting Hg and Cu ions is crucial.

Various analytical methods have been developed for detecting mercury and copper, including atomic absorption spectroscopy[3] (AAS), inductively coupled plasma mass spectroscopy[4] (ICPMS), and electrochemical sensing.[5] However, these techniques require expensive instrumentation, large sample volume, and trained personnel, and are not always suitable for field applications. Therefore, there is a growing demand to develop a low-cost, portable, and reliable sensing platform for metal ion detection.

One promising approach for developing such a sensing platform is to use 1,2,3-triazole linked with a suitable fluorophore as a sensing molecule[6–8] that allows researchers to develop recognition devices that have distinct advantages like low detection limit, naked eye visual changes, *etc.*, over the other techniques mentioned above. 1,2,3-Triazole is a heterocyclic compound containing a five-membered ring with two carbon atoms and three nitrogen atoms that has been extensively used as a building block in synthetic organic chemistry. The biological importance of 1,4-disubstituted 1,2,3-triazoles includes antimicrobial,[9–11] anticancer,[12] antiviral activities,[13] *etc.* It has also been widely used in developing various analytes due to its unique electronic and structural properties, including its complexation ability with

[a] *Department of Chemistry, National Institute of Technology, Kurukshetra, Haryana 136119, India. E-mail: rktittaliitd@nitkkr.ac.in; Tel: +91 1744 233 542*
[b] *School of Applied Sciences, Om Sterling Global University, Hisar, Haryana 125001, India*
[c] *School of Chemical Engineering and Physical Sciences, Lovely Professional University, Phagwara, Punjab 144411, India*
[d] *Division of Organic Chemistry, CSIR-National Chemical Laboratory, Dr. Homi Bhabha Road, Pune 411008, India*

† Electronic supplementary information (ESI) available. CCDC 2254070. For ESI and crystallographic data in CIF or other electronic format see DOI: https://doi.org/10.1039/d3sd00109a

Journal of Molecular Structure 1297 (2024) 136995

Contents lists available at ScienceDirect

Journal of Molecular Structure

journal homepage: www.elsevier.com/locate/molstr

4-aminoantipyrine linked bis-1,2,3-triazole based probes for Cu(II) sensing

Bajrang Lal [a], Sachin Kumar [a,b], Ram Kumar Tittal [a,*], Gurleen Singh [c], Jandeep Singh [c], Vikas D. Ghule [a], Ramling S. Mathpati [a], Jagjivan K. Sabane [d]

[a] Department of Chemistry, National Institute of Technology Kurukshetra, Haryana, 136119, India
[b] School of Applied Sciences, Om Sterling Global University, Hisar, Haryana, 125001, India
[c] School of Chemical Engineering and Physical Sciences, Lovely Professional University, Phagwara, Punjab, 144411, India
[d] Division of Organic Chemistry, CSIR-National Chemical Laboratory, Dr. Homi Bhabha Road, Pune, 411008, India

ARTICLE INFO

Keywords:
4-aminoantipyrine
Bis-1,2,3-triazole
X-ray crystallography
Cu^{2+} sensor
DFT
and Molecular docking

ABSTRACT

Herein, two molecular probes of 4-aminoantipyrine-linked bis-1,2,3-triazoles have been studied for metal ion sensing applications. The crystal structure of one of the probes named as *4,4'-((4,4'-(((1,5-dimethyl- 3- oxo- 2-phenyl- 2,3- dihydro- 1H- pyrazol- 4-yl) azanediyl) bis(methylene))bis(1H-1,2,3-triazole-4,1-diyl))bis(methylene)) dibenzonitrile* (**3b**) crystalizes in Monoclinic crystal system in P 1 21/n 1 space group. Both probes responded more strongly and selectively to Cu(II) than other tested metal ions (K^+, Na^+, Mg^{2+}, Ba^{2+}, Ca^{2+}, Cr^{3+}, Mn^{2+}, Co^{2+}, Zn^{2-}, Cd^{2+}, Ni^{2+}, Hg^{2+}, and Pb^{2+}). Job's plot suggested a 1:1 stoichiometric ratio of ligand and metal ion. Both probes showed an association constant of 2.48×10^3 M^{-1} and 3.73×10^3 M^{-1} through Benesi-Hildebrand (B-H) plot. The geometries of both probes and their complexes were optimized by DFT using B3LYP/6–311 G(d, p) and B3LYP/LanL2DZ basis sets, and properties were supported by Mulliken atomic charge and Molecular electrostatic potential. Molecular docking on both probes and their complexes with Type-II topoisomerases(PDB ID: 4G0V) protein was conducted to foretastes anticancer activity.

1. Introduction

In recent years, developing highly efficient and sensitive sensors for detecting metal ions has garnered significant attention in various scientific fields, such as monitoring environmental issues, bio-medicinal research, industrial processes, etc. Among heavy transition metals, copper, the 3rd most abundant element, plays a crucial role due to its essential biological systems like the transportation and activation of cellular oxygen and signal transduction [1]. Also, its potential toxicity, when present in excessive amounts, can disrupt cellular functions, which cause neurodegenerative disorders like Alzheimer's disease, Wilson's disease [2], Hodgkin's lymphoma, Parkinson's disease (PD), and Menkes [3,4]. In 1991, as per the Environmental Protection Agency (EPA), the recommended maximum limit of Cu^{2+} ion concentration in drinking water must not exceed 1.3 mg/L [5]. Also, Cu^{2+} ion concentration became a global environmental pollutant due to its extensive large-scale use in chemical industries and agricultural processes [6]. Therefore, the design and development of selective and sensitive Cu^{2+} ion sensors have become paramount.

One promising class of compounds that have emerged in this context is 1,2,3-triazoles [7–9]. These heterocyclic molecules containing five-membered rings have two carbon and three nitrogen atoms, possess various structural features, and exhibit significant potential as a building block for the construction of functional materials in biology and sensors. The ability to modulate their properties by acquiring appropriate functional groups makes 1,2,3-triazole derivatives an attractive platform for sensor development.

Moreover, the development of Cu^{2+} ion sensors hold significant promise for various applications, including environmental monitoring, biological & biomedical research, and industrial quality control. Copper was also involved in antiangiogenic anticancer activity, leading to an interest in copper chelation as a mechanism to decrease the angiogenic activity of cancerous cells [10]. Additionally, 1,2,3-triazoles are nitrogen-containing heterocycles particularly important in life sciences because they are very familiar and also found as subunits in various natural products, including nutrients, hormones, and medications. Also, base pairs of DNA and RNA comprise N-heterocycles, like purines, pyrimidines, etc.

Herein, we focus on the rational design and the synthesis of a metal ion sensor based on 4-amino antipyrine, known for its versatile

* Corresponding author.
E-mail address: rktittaliitd@nitkkr.ac.in (R.K. Tittal).

https://doi.org/10.1016/j.molstruc.2023.136995
Received 12 September 2023; Received in revised form 15 October 2023; Accepted 2 November 2023
Available online 2 November 2023

Inorganica Chimica Acta 542 (2022) 121087

Contents lists available at ScienceDirect

Inorganica Chimica Acta

journal homepage: www.elsevier.com/locate/ica

Research paper

Thiosemicarbazone-triazole bearing siloxy framework for the detection of Hg^{2+} and Cu^{2+} ions and their potent cytotoxic activity

Gurjaspreet Singh [a,*], Sushma [b,*], Priyanka [a], Sumesh Khurana [a], Gurleen Singh [c], Jandeep Singh [c], Maria Angeles Esteban [d,*], Cristóbal Espinosa-Ruíz [d], D. González-Silvera [d]

[a] Department of Chemistry, Panjab University, Chandigarh 160014, India
[b] Department of Applied Sciences and Humanities, School of Engineering and Technology, Ganga Technical Campus, Bahadurgarh 124507, India
[c] Department of Chemistry, Lovely Professional University, Phagwara 144411, India
[d] Department of Cell Biology and Histology, Faculty of Biology, University of Murcia, Murcia 30100, Spain

ARTICLE INFO

Keywords:
Thiosemicarbazone
1,2,3-triazole
Siloxy framework
Hg^{2+} and Cu^{2-} ions
Cytotoxic activity

ABSTRACT

The designing of chemosensors is a fascinating and growing research field among the scientific community. This article emphasizes the synthesis of thiosemicarbazone-triazole bearing siloxy framework (5a-5c) by utilizing an effective and biocompatible Cu(I) catalyzed "Click Silylation" approach. All the newly synthesized compounds (4a-4c and 5a-5c) have been well-characterized by various spectroscopy techniques like Infrared, Nuclear Magnetic Rasonance (^{1}H NMR and ^{13}C NMR), mass spectrometry and Thermogravimetric Analysis. The photophysical properties of 5a and its precursor alkyne 4a were investigated by employing UV-vis spectroscopy, which showed the selective and sensitive recognition of Hg^{2} and Cu^{2} ions with negligible interference from different metal ions. All types of the binding interaction between chemosensors (**4a**/**5a**) and Hg^{2-}/Cu^{2-} ions got reversed upon addition of salt of ethylene diamminetetraacetic acid. The association constant and limit of detection values were also determined by plotting BH-plot and linear calibration curve respectively. Furthermore, the cytotoxic activity results indicate that the siloxy compounds were found to be excellent postulants compared to ascorbic acid and hence can be applied for biological purposes.

1. Introduction

In the realm of science, the identification of heavy and transition metal ions (HTM's) has attained considerable attention as their exposure is extremely harmful to human health and other living systems because they are toxic, even in trace amounts [1–3]. Among HTM's, Hg^{2+} and Cu^{2+} ions are of prime concern due to their adverse effect on living organisms as well as on the environment [4–6]. Hg^{2-} is highly poisonous and non-biodegradable metal ion that can be released in the biosphere in the form of methylmercury from gold mining, caustic soda, mercury lamps and burning of fossil fuels [7,8]. It is famous for Minamata disease and poisoning in Iraq and ranked as the third most toxic substance by Agency for Toxic Substances and Disease Registry (ATSDR) [9,10]. It can enter inside the human body via the food chain and causes severe health problems like various cognitive and motion disorders, cancer, neurotoxic effect, genotoxic effect, immunotoxic effect and damages to DNA, brain, endocrine and central nervous system [11–13]. Cu^{2-} ions are the third most abundant crucial nutrients in humans that help in multiple biochemical processes such as dopamine production, brain functioning, bone development, gene transcription, free radical scavenging, mitochondrial respiration, iron absorption etc. [14–16]. However, disruption of Cu^{2+} homeostasis in the human body commences to several neurodegenerative diseases like Wilson's disease, Parkinson's disease, Alzheimer's disease, Indian Childhood Cirrhosis and also damages liver and kidney [17–19]. In view of the above, the detection and quantification of Hg^{2+} and Cu^{2+} are of vital importance. There are so many traditional instrument-assisted methods like chromatography, voltammetry, atomic absorption spectrometry (AAS), inductively coupled plasma-mass spectroscopy (ICP-MS), inductively coupled plasma-atomic emission spectrometry (ICP-AES) and electrochemical methods that are employed for the detection of Hg^{2+} and Cu^{2+} ions. Although, these methods show acceptable sensitivity but they required sophisticated and expensive instruments, special operators for analysis, pre treatment of samples and are time-consuming [20–22]. Presently the UV-vis absorption spectroscopy method is favoured over these conventionally used techniques for the selective and sensitive recognition of Hg^{2+} and Cu^{2} ions due to their

* Corresponding authors at: Department of Chemistry and Centre of Advanced Studies, Panjab University, Chandigarh 160014, India (G. Singh).
E-mail addresses: gjpsingh@pu.ac.in (G. Singh), sushma.dhanda21@gmail.com (Sushma), gurjaspreet@gmail.com, aesteban@um.es (M. Angeles Esteban).

https://doi.org/10.1016/j.ica.2022.121087
Received 14 June 2022; Received in revised form 11 July 2022; Accepted 11 July 2022
Available online 14 July 2022

Inorganic Chemistry Communications 163 (2024) 112297

Contents lists available at ScienceDirect

Inorganic Chemistry Communications

journal homepage: www.elsevier.com/locate/inoche

Short communication

Carbohydrazide-Based schiff bases for selective Hg (II) ion sensing and computational analysis of cholesterol lowering activity

Gurjaspreet Singh [a,*], Sudha Malik [a], Anita Devi [a,*], Harshbir Kaur [a], Tsering Diskit [a], Jandeep Singh [b], Gurleen Singh [b], Vandana [a], Amarjit Kaur [a,*]

[a] Department of Chemistry, Panjab University, Chandigarh 160014, India
[b] School of Chemical Engineering and Physical Sciences, Lovely Professional University, Phagwara 144411, Punjab, India

ARTICLE INFO

Keywords:
Mercury
Schiff bases
UV–Visible
PASS analysis
Molecular docking

ABSTRACT

The presence of mercury ion (Hg (II)) in the environment is a serious health concern. Therefore, it is essential to measure and monitor the levels of Hg (II) in the environment to safeguard public health. This study focuses on the synthesis of carbohydrazide-based Schiff bases (**4**–**5**) and exhibit a red-shift in absorption upon addition of Hg (II) ion, making them highly selective and sensitive in detecting Hg (II). The confirmation of the synthesized compounds was achieved using (^{1}H and ^{13}C) NMR spectroscopy and mass spectrometry. Additionally, the detection limits towards Hg (II) were determined to be 7.56×10^{-7} M and 1.42×10^{-6} M for compounds **4** and **5**, respectively. The ^{1}H NMR spectra provided evidence of interactions between compounds **4**–**5** and Hg (II) ion. The compounds **4** and **5** were evaluated for Bioactivity, Drug likeness parameters and Prediction of Activity Spectra (PASS) analysis to design a new molecule with a favorable pharmacological profile. Based on the PASS results, molecular docking studies of compounds **4** and **5** were performed with Cholesteryl Ester Transfer Protein (CETP) (PDB ID: 2OBD), revealing inhibitory activity. These findings suggest the potential of these compounds as candidates for antihyperlipidemic or cholesterol-lowering agents.

1. Introduction

The rapid growth of industries and insufficient waste disposal has led to notable chemical pollution in water sources. This contamination introduces harmful elements such as heavy metals, pharmaceuticals, and pesticides from diverse industrial sources, posing risks to both ecosystems and human well-being, while also exacerbating water scarcity problems [1–3]. Therefore, there's an urgent need for effective methods to detect these contaminants. Among these pollutants, mercury stands out as an exceptionally dangerous heavy metal ion [4–7]. Its deadly toxicity primarily stems from its ability to bind with proteins and enzymes, leading to severe health consequences [8,9]. Accumulation of mercury in the biological system, whether through drinking water, the food chain, or other means, can result in a range of severe health problems, including abdominal pain, minamata disease and in extreme cases, even death [10–12]. The inorganic form of mercury, specifically Hg (II), poses significant risks to both the environment and human health, as it readily transforms into methyl mercury through methylation reactions involving aquatic microorganisms [13–15]. As a result, the development of reliable and highly sensitive methods to detect mercury (II) is critical.

Hydrazide derivatives are important organic compounds known for their nitrogen-nitrogen covalent bond and acyl group substituent [16,17]. These compounds possess significant pharmaceutical relevance due to their distinctive functional groups and demonstrate diverse biological properties, including antibacterial, anti-inflammatory, anticancer, antimalarial and antioxidant activities [18–21]. In drug synthesis, hydrazide-hydrazones play a crucial role, offering versatile applications in pharmaceuticals and materials science [22].

Schiff bases are compounds formed through a condensation reaction between primary amines and carbonyl compounds [23]. These compounds are highly valued for their versatility as ligands, making them suitable for applications in chelating agents, catalysts, and corrosion inhibitors [24–26]. Moreover, the integration of hydrazide compounds into Schiff bases enhances their stability in biological environments, leading to improved efficacy in biological applications [27].

Herein, we utilized carbohydrazide to synthesize new Schiff bases. Carbohydrazide play a crucial role in hetero-chemistry and find

* Corresponding authors at: Department of Chemistry & Centre of Advanced Studies Panjab University, Chandigarh, India.
E-mail addresses: gjpsingh@pu.ac.in (G. Singh), anitadevi0025@gmail.com (A. Devi), amarjitk@pu.ac.in (A. Kaur).

https://doi.org/10.1016/j.inoche.2024.112297
Received 19 January 2024; Received in revised form 5 March 2024; Accepted 11 March 2024
Available online 18 March 2024

NJC

ROYAL SOCIETY OF CHEMISTRY

PAPER

View Article Online
View Journal

Cite this: DOI: 10.1039/d3nj01484c

Heterocycle-derived organosilatranes as naked eye sensors for Sn^{2+} ions and their potential inhibiting activity against HIV-1 protease *via* a computational approach†

Gurjaspreet Singh, *[a] Diksha,*[a] Mohit,[a] Priyanka,[b] Anita Devi,[a] Swati Devi,[a] Harshbir Kaur,[a] Jandeep Singh [c] and Gurleen Singh[c]

Nitrogen-based heterocycles are frequently present in active pharmaceutical products. Inspired by this, we design heterocycle-appended organosilatranes having an azomethine linkage using a simple synthetic approach. All the synthesized organosilatranes were well characterized by elemental analysis; FTIR, NMR (^{1}H and ^{13}C) and mass spectrometry. The chemosensor shows high selectivity towards Sn^{2+} metal ions and the transparent solution of the ligand turned to yellow colour in the presence of Sn^{2+} ions. The ligand binds with metal ions with a high binding affinity (K_a = 3.5 × 10^6 M^{-1}). Furthermore, by using fluorometric spectroscopy, the limit of detection was calculated to be 4.5 × 10^{-8} M. In addition, to find the binding mode of the ligand and metal, the complex was synthesized and characterized by ^{1}H NMR spectroscopy and DFT calculations were also performed. Also, the bioavailability of the compounds was confirmed by pharmacological investigations using Molinspiration and PreADMET online servers and the results show that all the synthetic silatranes obey Lipinski's rule and possess acceptable ADMET properties. Moreover, the molecular docking studies provide valuable information regarding the interaction of compound **4a** with the HIV-1 protease protein with a binding energy of −7.00 kcal mol^{-1}.

Received 30th March 2023,
Accepted 27th May 2023

DOI: 10.1039/d3nj01484c

rsc.li/njc

1. Introduction

Medicinal chemistry is science at the junction of chemistry, particularly organic synthesis, pharmaceutics, and various other biological specialities that lead to the design, chemical synthesis, and evolution of bioactive molecules that can be prescribed and purchased.[1] Heterocyclic compounds which are the most significant organic compounds, are commonly found in medicinal chemistry applications.[2] Nitrogen-containing heterocycles are particularly important in life sciences because they are common in nature and may be found as subunits in a variety of natural products, including nutrients, hormones, and medications.[3,4] Base pairs of DNA and RNA are composed of *N*-heterocycles (*i.e.*, purines, pyrimidines).[5,6] Additionally, the electron-rich nitrogen heterocycles may easily create a variety of weak interactions like hydrogen bonding, π-stacking interactions and van der Waals forces and because of their increased solubility, they can interact with a wide range of enzymes and proteins in biologically active compounds with strong potential.[7,8] The pharmaceutical industry relies heavily on the utilization of the morpholine moiety as a building unit because it has been utilized in anti-inflammatory medicines, used to treat diseases such as asthma and migraines.[9,10] Due to their unique characteristics, the heterocyclic rings used in the manufacture of sensors for the detection of metal ions have expanded.[11]

For the time being, a number of analytical and spectrophotometric methods have been created to identify heavy metals in the environment. Various traditional analytical techniques, such as adsorptive stripping voltammetry,[12] high-performance liquid chromatography,[13] atomic absorption/emission spectrometry,[14] electrochemical approaches[15] and spectrophotometry,[16] provide accurate detection and quantification of metal ions but they all have drawbacks, such as high operational costs, complex handling, and the use of hazardous solvents.[17] Therefore, effective methods for measuring metal ions should be created that are inexpensive, easy to use, and quick to react and have excellent sensitivity and selectivity. Researchers have recently started to use optical sensors

[a] *Department of Applied Sciences, Chandigarh group of colleges, Jhanjeri, Mohali-140307, India. E-mail: gjpsingh@pu.ac.in, mehtadiksha49@gmail.com*
[b] *Department of Humanities and Applied Sciences, Echelon Institute of Technology Faridabad, Haryana, 121101, India*
[c] *Department of Chemistry, Lovely Professional University, Phagwara, Punjab, India*
† Electronic supplementary information (ESI) available. See DOI: https://doi.org/10.1039/d3nj01484c

DIVISION OF RESEARCH AND DEVELOPMENT

[Under the Aegis of Lovely Professional University, Jalandhar-Delhi G.T. Road, Phagwara (Punjab)]

Certificate No.240180

Certificate of Participation

This is to certify that **Mr. Gurleen Singh** of **Lovely Professional University, Phagwara, Punjab, India** has presented paper on **Synthesis and characterization of 1,2,3-triazole derivative following 'click' pathway** in the **International Conference on Materials for Emerging Technologies (ICMET-21)** held on February 18-19, 2022, organized by Department of Research Impact and Outcome, Division of Research and Development, Lovely Professional University, Punjab.

Date of Issue: 16-03-2022
Place: Phagwara (Punjab), India

Prepared by
(Administrative Officer-Records)

Dr. Vipul Srivastava
Convener
(ICMET-21)

Dr. Manish Vyas
Organizing Secretary
(ICMET-21)

Dr. Chander Prakash
Co-Chairperson
(ICMET-21)

एसजेवीएन
SJVN

Him Science Congress Association
Promoting Excellence in Sciences

iNSERB DIA

CERTIFICATE

OF PARTICIPATION

International Conference on

Recent Trends in Bio and Material Sciences

This certificate is awarded to

Gurleen Singh

of **Lovely Professional University** for **Oral/Poster Presentation** of research paper titled **CuAAC based 1,2,3-triazole 'click' derivative as selective chemosensor for Cr(III) and Pb(II)** in the **International Conference on Recent Trends in Bio and Material Sciences** October 10 - 11, 2022 organised by **Him Science Congress Association** at **Sardar Patel University**, Mandi, Himachal Pradesh.

Dr. Deepak Pathania
HSCA - President

Dr. Rajesh Kumar Sharma
HSCA - Vice President

Dr. Jagdeep Verma
Conference Chairman

NATIONAL INSTITUTE OF TECHNOLOGY ROURKELA

(An Institution of National Importance)

CHEMSMART-22

Certificate of Participation

This is to Certify that the Paper titled

'Click' based chemosensor as selective recognition probe for toxic Hg2+ and Pb2+

has been presented by the author(s)

Gurleen Singh

from

Lovely Professional University

In one of the technical sessions of An International Conference on ADVANCES IN SMART MATERIALS, CHEMICAL & BIOCHEMICAL ENGINEERING (CHEMSMART-22) organized by the Department of **Chemical Engineering, NIT Rourkela,** during **December 16-18, 2022.**

Dr. Krunal Gangawane
Convener–CHEMSMART-22

Prof. Abanti Sahoo
Chairman –CHEMSMART-22

Under Diamond Jubilee Celebration

International Conference

on

आज़ादी का अमृत महोत्सव

Molecules and Materials Technology (MMT-2023)

21st - 22nd April, 2023

Certificate of Presentation

This is to certify that Dr./Mr./Ms. GURLEEN SINGH

of LOVELY PROFESSIONAL UNIVESITY *has Presented* POSTER

in International Conference on Molecules and Materials Technology (MMT-2023) organized by, Department of Chemistry National Institute of Technology, Kurukshetra held in 21st - 22nd April, 2023.

Conference Secretary
MMT-2023

Chairman
MMT-2023

पंजाब केन्द्रीय विश्वविद्यालय/ਪੰਜਾਬ ਕੇਂਦਰੀ ਯੂਨੀਵਰਸਿਟੀ
Central University of Punjab
A Central University established by an Act of Parliament

विज्ञान एवं प्रौद्योगिकी विभाग
DEPARTMENT OF
SCIENCE AND TECHNOLOGY

AMITY
UNIVERSITY

STUTI

This is to certify that

Mr. Gurleen Singh

has successfully completed the

workshop

On Spectroscopic,Chromatographic, Bioanalytical & Imaging Techniques

(28th November - 04th December, 2022)

conducted by

Central University Of Punjab

in association with

Amity University

under the auspices of

Department of Science and Technology(DST)
Government of India

under

Synergistic Training Program Utilizing Scientific and Technological Infrastructure (STUTI)

Prof. Ramkrishna Wusirika
Dean Incharge Academics
Central University of Punjab

Prof. Anjana Munshi
Director R&D
Central University of Punjab

Dr. Nitin Batra
CEO,
Amity Institute of Training & Development

Dr. W Selvamurthy
President, ASTIF
Chancellor,
Amity University Chattisgarh